Los Alamos
NATIONAL LABORATORY
EST. 1943

General

*From/MS:* Ardyth Simmons, ENV-ECR, MS M992
*Phone/Fax:* (505) 665-3935/(505) 665-4747
*Symbol:* ER2006-0041
*Date:* January 24, 2006

AMS

RECEIVED
FEB 2006

# memorandum

**Environmental Stewardship (ENV)**
**Environmental Remediation & Surveillance Program (ERS)**

**SUBJECT: DISTRIBUTION OF "LOS ALAMOS NATIONAL LABORATORY'S HYDROGEOLOGIC SYNTHESIS REPORT OF THE PAJARITO PLATEAU: A SYNTHESIS OF HYDROGEOLOGIC WORK PLAN ACTIVITIES (1998–2004)"**

Enclosed please find a copy of the report titled "Los Alamos National Laboratory's Hydrogeologic Studies of the Pajarito Plateau: A Synthesis of Hydrogeologic Work Plan Activities (1998–2004)." This report documents sitewide characterization work completed under the Hydrogeologic Workplan. It comprehensively captures the Laboratory's understanding of the geology of the Pajarito Plateau, hydrologic properties and flow in the various groundwater systems, geochemistry of the regional aquifer, flow and transport models, and implications for contaminant transport.

If you have any questons, please contact Charlie Nylander at 665-4681 (nylander@lanl.gov) or me at 665-3935 (asimmons@lanl.gov).

Enclosure: Los Alamos National Laboratory's "Hydrogeologic Studies of the Pajarito Plateau: A Synthesis of Hydrogeologic Workplan Activities (1998 – 2004)" (LA-14263-MS)

AS/jk

Cy (w/enc):
A. Barr, ENV-SWRC, MS K490
R. Beers, ENV-WQH, MS K497
K. Birdsell, EES-6, MS T003
D. Broxton, EES-6, MS T006
L. Bonds-Lopez, ENV-DO, MS J591
B. Carey, EES-6, MS D462
S. Chipera, EES-6, MS D469
G. Cole, EES-6, MS D462
D. Counce, EES-6, MS D469
C. Criswell, ENV-DO, MS M992
J. Dewart, ENV-DO, MS M992

13976

A. Dorries, ENV-ECR, MS M992
J. Ellvinger, ENV-SWRC, MS K490
A. Eddebbarh, EES-6, MS T003
J. Fabryka-Martin, EES-6, MS T003
D. Fuehne, ENV-MAQ, MS M978
C. Gable, EES-6, MS T003
B. Gallaher, ENV-WQH, MS K497
T. George, ENV-DO, MS K591
T. Grieggs, ENV-SWRC, MS K490
A. Groffman, ENV-WQH, MS M992
K. Hargis, ENV-DO, MS J591
D. Hjeresen, ENV-DO, MS M992
D. Hickmott, EES-6, MS D462
D. Janecky, ENV-ECO, MS M887
D. Katzman, EES-9, MS M992
E. Keating, EES-6, MS T003
R. Koch, ENV-WQH, MS K497
E. Kwicklis, EES-6, MS T003
J. Little, ENV-ECO, MS M887
P. Longmire, EES-6, MS D462
G. Lopez-Escobedo, ENV-ERS, MS M992
Z. Lu, EES-6, MS T003
E. Louderbough, LC-ESH, MS A187
C. Mangeng, ADTS, MS A104
J. McCann, ENV-WQH, MS M992
D. McInroy, ENV-ECR, MS M992
S. McLin, ENV-WQH, MS K497
B. Newman, EES-2, MS J495
C. Nylander, ENV-GPP, MS M992
S. Pearson, ENV-WQH, MS M992
P. Reneau, ENV-ECR, MS M992
S. Rae, ENV-WQH, MS K497
B. Robinson, EES-6, MS T003
D. Rogers, ENV-WQH, MS K497
T. Sandoval, ENV-WQH, MS K497
A. Simmons, ENV-ECR, MS M992
E. Springer, STB-UC, MS M701
P. Stauffer, EES-6, MS T003
D. Stavert, ENV-DO, MS J591
B. Stine, ADTS, MS A104
R. Tate, PADNWP, MS F627
D Vaniman, EES-6, MS D462
V. Vesselinov, EES-6, MS T003
M. Witkowski, EES-9, M D452
G. WoldeGabriel, EES-6, MS D462
B. Enz, DOE-LA-AO, MS A316
M. Johansen, DOE-LA-AO, MS A316
T. Whitacre, DOE-LA-AO, MS A316

M. Dale, NMED-DOE-OB, White Rock, NM
J. Keiling, NMED-HWB, Santa Fe, NM
M. Leavitt, NMED-GWQB, Santa Fe, NM
S. Yanicak, NMED-DOE-OB, Santa Fe, NM
J. Young, NMED-HWB, Santa Fe, NM (3c.)
J.D. Campbell, CAB, Santa Fe, NM (3 c.)
Elizabeth Anderson, Science International, Inc., Alexandria, VA
Robert Charles, Robert Charles Products, Ranchester, WY
Charles McLane, McLane Environmental, Inc., Princeton, NJ
Jack Powers, Bloomington, MN
Bob Powell, Powell & Associates, Waterford, MI
David C. Schafer, David Schafer & Associates, North Oaks, MN
R. Warren, Comprehensive Volcanic Petrographics, Grand Junction, CO
K. A. Collins, CDM, Albuquerque, NM
Neil Weber, San Ildefonso Pueblo, NM
Joni Ahrens, CCNS, Santa Fe, NM
Pete Padilla, Los Alamos County, Los Alamos, NM
Andy Manning, US Geological Survey, Denver, CO
S-7, MS F674
IM-9, MS A150 (w/o enclosure)
ENV-GPP-File, MS M992
RPF MS M992
ENV-ECR-File, MS M992

LA-14263-MS
Issued: December 2005

# Los Alamos National Laboratory's Hydrogeologic Studies of the Pajarito Plateau:

## A Synthesis of Hydrogeologic Workplan Activities (1998–2004)

Edited by:
Kelly A. Collins
Ardyth M. Simmons
Bruce A. Robinson
Charles L. Nylander

Los Alamos
NATIONAL LABORATORY
EST. 1943

The World's Greatest Science Protecting America

**Acknowledgments**

This report culminates the implementation of the Hydrogeologic Workplan, approved by the New Mexico Environment Department in March 1998. The Workplan was sponsored by the U.S. Department of Energy and the University of California. It was written by an interdisciplinary group of contributing authors representing various Los Alamos National Laboratory divisions, programs, and projects. Many of these individuals were also contributing authors of this Hydrogeologic Synthesis Report. These authors were members of the Groundwater Integration Team (GIT) that was created to implement the Hydrogeologic Workplan.

Over the past eight years, many individuals, too numerous to mention, contributed to studies performed under the Workplan. In particular, contributions made by the GIT members were significant and are much appreciated. The leadership of Charles Nylander as Program Manager throughout the history of the Workplan is appreciated, as is the technical oversight provided by Bruce Robinson. The Hydrogeologic Synthesis Report was much improved by reviews by Alice Barr, Al Eddebbarh, June Fabryka-Martin, Don Hickmott, Ellen Louderbough, Everett Springer, and Ardyth Simmons. In addition, significant peer review of the Hydrogeologic Synthesis Report was provided by External Advisory Group (EAG) members, who were professionally involved in implementation of the Hydrogeologic Workplan, and their contributions are appreciated. The EAG members are Robert Charles, Elizabeth Anderson, Charles McLane, David Schafer, Robert Powell, and Jack Powers. We thank the staff of the Daniel B. Stephens and Associates Visual Resources Group for improving the quality of figures. Finally, the professional contributions made by Ardyth Simmons and Kelly Collins in completing the compilation and editing of this document are appreciated.

# TABLE OF CONTENTS

**EXECUTIVE SUMMARY** ..... **xxi**

**ABSTRACT** ..... **1-1**
**1.0 INTRODUCTION** ..... **1-5**
1.1 Technical Objectives of the Hydrogeologic Workplan ..... 1-7
1.2 Hydrogeologic Characterization Overview ..... 1-7
1.3 Topical Organization ..... 1-11

**2.0 HYDROGEOLOGY** ..... **2-1**
2.1 Geologic Conceptual Model ..... 2-1
2.1.1 Goals of the Geologic Model ..... 2-5
2.1.2 Site-Wide Geology ..... 2-5
2.1.2.1 Regional Setting ..... 2-5
2.1.2.2 Structural Geology of the Pajarito Plateau ..... 2-7
2.1.2.3 Volcanic Setting of the Pajarito Plateau ..... 2-9
2.2 Stratigraphic Framework of the Pajarito Plateau ..... 2-10
2.2.1 Tesuque Formation ..... 2-19
2.2.2 Miocene Basalts ..... 2-19
2.2.3 Older Fanglomerate ..... 2-19
2.2.4 Totavi Lentil ..... 2-20
2.2.5 Pumice-Rich Volcaniclastic Rocks ..... 2-21
2.2.6 Tschicoma Formation ..... 2-23
2.2.7 Puye Formation ..... 2-23
2.2.8 Basaltic Rocks of the Cerros del Rio Volcanic Field ..... 2-24
2.2.9 Bandelier Tuff ..... 2-25
2.2.9.1 Otowi Member, Bandelier Tuff ..... 2-26
2.2.9.2 Tephra and Volcaniclastic Sediments of the Cerro Toledo Interval ..... 2-27
2.2.9.3 Tshirege Member, Bandelier Tuff ..... 2-28
2.2.10 Alluvium and Colluvium ..... 2-29
2.3 Geologic Conceptual Model Cross-Sections ..... 2-30
2.3.1 Geology at the Water Table ..... 2-30
2.3.2 Representative Cross-Sections ..... 2-33
2.3.2.1 Los Alamos Canyon Cross-Section ..... 2-43
2.3.2.2 Mortandad Canyon Cross-Section ..... 2-43
2.3.2.3 Pajarito Canyon Cross-Section ..... 2-44
2.3.2.4 Water Canyon Cross-Section ..... 2-44
2.3.2.5 Western Boundary Cross-Section ..... 2-45
2.3.2.6 West-Central Cross-Section ..... 2-45
2.3.2.7 East-Central Cross-Section ..... 2-46
2.3.2.8 Eastern Cross-Section ..... 2-46
2.4 Hydrologic Properties ..... 2-46
2.4.1 Vadose Zone Hydrologic Properties ..... 2-47

2.4.2 Regional Aquifer Hydrologic Properties ..... 2-49
2.4.2.1 Expected Lithologic Controls on Regional Aquifer Hydrologic Properties ..... 2-50
2.4.2.2 Contact between Units ..... 2-55
2.4.2.3 Regional Aquifer Hydraulic Conductivity ..... 2-57
2.4.2.4 Anisotropy ..... 2-69
2.4.2.5 Porosity ..... 2-70
2.4.2.6 Storage Properities ..... 2-72
2.4.3 Summary of Hydrologic Properties ..... 2-72
2.4.4 Uncertainties in the Relationship between Geologic and Hydrogeologic Units ..... 2-73
2.4.4.1 Extent and Nature of the Cerros del Rio Hydrogeologic Unit ..... 2-74
2.4.4.2 Unassigned Pumice-Rich Volcaniclastic Rocks ..... 2-74
2.4.4.3 Totavi Variants ..... 2-74
2.4.4.4 Disposition of Santa Fe Group Sediments ..... 2-75
2.4.4.5 Spatial Variation in Permeability within Sedimentary Rocks ..... 2-75
2.4.4.6 Influence of Structure on Groundwater Flow ..... 2-76
2.5 Alluvial Groundwater Conceptual Model ..... 2-76
2.5.1 Physical Setting ..... 2-77
2.5.2 Hydrology ..... 2-77
2.5.2.1 Alluvial Recharge ..... 2-78
2.5.2.2 Alluvial Aquifer Properties ..... 2-84
2.5.2.3 Cerro Grande Fire Effects ..... 2-85
2.6 Vadose Zone Conceptual Model ..... 2-85
2.6.1 Climate and Infiltration ..... 2-88
2.6.2 General Description of Conceptual Models ..... 2-88
2.6.2.1 Mesas ..... 2-89
2.6.2.2 Canyons ..... 2-90
2.6.3 Vadose Zone Flow and Transport Mechanisms ..... 2-91
2.6.4 Alternative Hypotheses ..... 2-94
2.7 Perched Water ..... 2-95
2.7.1 Perched Water Occurrence ..... 2-95
2.7.2 Interpretation of Perched Water Observations ..... 2-97
2.7.2.1 Surface Water Conditions for Perched Water ..... 2-97
2.7.2.2 Geologic and Hydrostratigraphic Controls on Perched Water Occurrence ..... 2-98
2.7.2.3 Subsurface Extent of Zones of Saturation ..... 2-99
2.7.2.4 Flow Conditions Upstream and Within Intermediate Perched Groundwater Zones ..... 2-99
2.8 Regional Aquifer Conceptual Model ..... 2-101
2.8.1 Regional Hydrologic Setting ..... 2-101
2.8.2 Hydrology Beneath the Pajarito Plateau ..... 2-103
2.8.3 Water Budget ..... 2-104
2.8.3.1 Recharge ..... 2-104

2.8.3.2 Discharge ..... 2-108
2.8.3.3 Interbasin Flow ..... 2-109
2.8.4 Aquifer Hydrologic Properties ..... 2-110
2.8.5 Anisotropy and Scale Dependence ..... 2-111
2.8.6 Hydraulic Heads and Flow Directions ..... 2-115
2.8.6.1 Water Level Map ..... 2-115
2.8.6.2 Shallow and Deep Flow Paths ..... 2-115
2.8.6.3 Influence of Water Supply Well Pumping ..... 2-116
2.8.7 Aquifer Hydrodynamics ..... 2-118
2.8.8 Velocities and Travel Times ..... 2-124

**3.0 GROUNDWATER GEOCHEMISTRY, CONTAMINANT DISTRIBUTIONS, AND IMPLICATIONS FOR FLOW AND TRANSPORT ..... 3-1**
3.1 Geochemical Conceptual Model ..... 3-1
3.1.1 Natural Chemical Composition of Groundwater ..... 3-2
3.1.1.1 Geochemistry of the Recharge Zone ..... 3-3
3.1.1.2 Aqueous Geochemistry along the Flow Path ..... 3-3
3.1.1.3 Geochemistry of the Discharge Zone ..... 3-7
3.1.2 Residence Times ..... 3-8
3.1.3 Reactive Minerals Controlling Groundwater Composition and Solute Mobility ..... 3-9
3.1.4 Adsorption and Precipitation Reactions ..... 3-10
3.1.4.1 Adsorption and Precipitation of Uranium(VI) Species ..... 3-12
3.1.5 Redox Conditions ..... 3-16
3.1.6 Uranium Speciation ..... 3-17
3.1.7 Summary of Geochemical Conceptual Model ..... 3-19
3.2 Contaminant Distributions and Transport ..... 3-22
3.2.1 Contaminant and Constituent Sources ..... 3-27
3.2.2 Water Inputs ..... 3-27
3.2.3 Hydrogeologic Controls ..... 3-28
3.2.3.1 Infiltration Rate and Transport in Alluvial Groundwater ..... 3-29
3.2.3.2 Vadose Zone Pathways and Transport in Intermediate Groundwater ..... 3-36
3.2.3.3 Flow Field Modification and Transport in Regional Aquifer Groundwater ..... 3-43
3.2.4 Off-Site Transport ..... 3-44
3.2.5 Summary of Contaminant and Transport ..... 3-47

**4.0 NUMERICAL MODELS ..... 4-1**
4.1 Site-Wide Vadose Zone Flow and Transport Model ..... 4-1
4.1.1 Model Development ..... 4-1
4.1.1.1 Flow and Transport Processes ..... 4-2
4.1.1.2 Infiltration Rate ..... 4-2
4.1.1.3 Numerical Model Implementation ..... 4-3
4.1.2 Model Results ..... 4-5

4.1.2.1 Base-Case Results ..... 4-5
4.1.2.2 Uncertain Infiltration Rate ..... 4-6
4.1.2.3 Perched Water Conceptual Uncertainty ..... 4-8
4.1.3 Contaminant Transport Model Predictions—Representative Canyon and Mesa Sites ..... 4-10
4.1.3.1 MDA G Model ..... 4-10
4.1.3.2 Los Alamos Canyon Model ..... 4-13
4.2 Numerical Models of Flow and Transport in the Regional Aquifer ..... 4-19
4.2.1 Previous Numerical Models ..... 4-19
4.2.2 Overview of LANL Model Development ..... 4-21
4.2.3 Numerical Framework ..... 4-22
4.2.4 Hydrostratigraphy ..... 4-23
4.2.5 Boundary Conditions ..... 4-25
4.2.6 Recharge ..... 4-25
4.2.7 Discharge at Rivers and Interbasin-Flow ..... 4-27
4.2.8 Lateral Boundaries of the Site-Scale Model ..... 4-27
4.2.9 Data Used in Model Development and Testing ..... 4-29
4.2.10 Flow Model Parameters ..... 4-29
4.2.11 Transport Model Methods and Parameters ..... 4-30
4.2.12 Model Applications ..... 4-35
4.2.12.1 Category A: Integrate and interpret 3-D site-wide hydrologic and hydrostratigraphic data, to provide a more quantitative basis for testing site-wide conceptual models than was previously possible. ..... 4-35
4.2.12.2 Category B: Predict fate and transport of contaminants in the regional aquifer, in order to optimally place monitoring wells and inform risk assessment studies. ..... 4-50
4.2.12.3 Category C: Provide guidance in prioritization of data collection activities, highlighting the importance of those data that could most reduce numerical and conceptual model uncertainty. ..... 4-55

**5.0 CONCLUSIONS ..... 5-1**
5.1 Summary ..... 5-1
5.1.1 Presence of Contaminants ..... 5-1
5.1.2 Water Inputs ..... 5-3
5.1.3 Vadose Zone Hydrogeologic Controls ..... 5-4
5.1.4 Regional Aquifer Transport ..... 5-6
5.2 Relation of Hydrogeologic Workplan Results to Risk Assessment ..... 5-8
5.3 Implications of Hydrogeologic Workplan Findings for Monitoring ..... 5-10
5.3.1 Alluvial Groundwater ..... 5-11
5.3.2 Vadose Zone ..... 5-12
5.3.3 Regional Aquifer ..... 5-15

**6.0 REFERENCES ..... 6-1**

# LIST OF TABLES


Table 1-1. Crosswalk Between HSWA Permit Requirements* and Synthesis Report Section ..... 1-9
Table 1-2. Los Alamos National Hydrogeologic Characterization Wells ..... 1-12

Table 2-1. Summary of Geologic Data ..... 2-2
Table 2-2. Inferred Properties of Hydrostratigraphic Units, Based on Field-Scale Testing, Model Calibration, and Head Gradients. ..... 2-54
Table 2-3. Estimates of Hydraulic Conductivity from Well Tests on the Pajarito Plateau ..... 2-58
Table 2-4. Summary Table of Hydraulic Conductivity for Each Hydrostratigraphic Unit ..... 2-65
Table 2-5. Summary of Formation Micro-Image (FMI) Data Derived from Borehole Geophysics ..... 2-66
Table 2-6. Summary of Effective Porosity Estimates based on Borehole Geophysics. 2-71
Table 2-7. Groundwater Velocities in Alluvial Aquifers on the Pajarito Plateau ..... 2-86
Table 2-8. Saturated hydraulic conductivity values for Alluvial Groundwater on the Pajarito Plateau. ..... 2-86
Table 2-10. Water-Level Data Used to Create the Revised Piezometric Water-Level Contours for the Top of the Regional Aquifer ..... 2-119

Table 3-1. Summary of Factors Influencing Contaminant Distributions in Groundwater at Los Alamos National Laboratory ..... 3-23

Table 4-1. Determination of Net Infiltration Index and Net Infiltration Rates Used in the Model ..... 4-4
Table 4-2. Infiltration Rates (mm/year) Used as Upper Boundary Conditions for MDA G Performance Assessment Simulations ..... 4-12
Table 4-3. Example Recharge Models, Shown in Figure 4-13. ..... 4-29
Table 4-4. Regional Aquifer Model Parameters ..... 4-31
Table 4-5. Travel Times Calculated Using Ten Different Models of Hydraulic Conductivity within the Puye Formation ..... 4-52

# LIST OF FIGURES


Figure 1-1. Location of Los Alamos National Laboratory. ..... 1-6
Figure 1-2. Groundwater components at LANL. ..... 1-10
Figure 1-3. Locations of the hydrogeologic workplan characterization wells. ..... 1-17

Figure 2-1. Locations of major structural and geologic elements near LANL.. ..... 2-6
Figure 2-2. Location map of the central Pajarito Plateau. Yellow-shaded area is the Los Alamos National Laboratory. ..... 2-8
Figure 2-3. Pajarito Plateau stratigraphy and hydrogeologic units as used in this report ..... 2-12
Figure 2-4. Structure contour and isopach map for the Cerro Toledo interval. ..... 2-13
Figure 2-5. Structure contour and isopach map for the Otowi Member of the Bandelier Tuff.. ..... 2-14
Figure 2-6. Isopach and structure contour map of the Guaje Pumice Bed. ..... 2-15
Figure 2-7. Structure contour for the top of Cerros del Rio basalt and western dacite on the Pajarito Plateau. ..... 2-16
Figure 2-8. Structure contour for the base of Cerros del Rio basalt with isopachs showing the cumulative thickness of flows ..... 2-17
Figure 2-9. Topography at the upper surface of the pumiceous deposits underlying Puye fanglomerates, with pumiceous deposit thicknesses ..... 2-18
Figure 2-10. Map showing distribution of geologic units at the top of the regional saturated zone beneath the Pajarito Plateau. ..... 2-32
Figure 2-11. Lines of cross-section for Figures 2-12 through 2-19 ..... 2-34
Figure 2-12. Conceptual cross-section for Los Alamos Canyon ..... 2-35
Figure 2-13. Conceptual cross-section for Mortandad Canyon ..... 2-36
Figure 2-14. Conceptual cross-section for Pajarito Canyon. ..... 2-37
Figure 2-15. Conceptual cross-section for Water Canyon ..... 2-38
Figure 2-16. Conceptual north-south cross-section for the western portion of the Laboratory. ..... 2-39
Figure 2-17. Conceptual southwest-northeast cross-section from TA-16 through the west-central portion of the Laboratory. ..... 2-40
Figure 2-18. Conceptual southwest-northeast cross-section from TA-49 through the central portion of the Laboratory ..... 2-41
Figure 2-19. Conceptual north-south cross-section through the eastern portion of the Laboratory. ..... 2-42
Figure 2-20. Permeability as a function of measurement scale for Bandelier Tuff (units 1g, 1v, and 2) and basalts. ..... 2-48
Figure 2-21. (a) Outcrop of the Puye Formation, Rendija Canyon (north of LANL); (b) Outcrop of the Santa Fe Group, lower Los Alamos Canyon (east of LANL); (c) Outcrop of the Santa Fe Group, near Española (provided by Gary Smith, UNM Dept. of Earth and Planetary Sciences). ..... 2-51
Figure 2-22. Outcrop of Totavi Lentil along SR 304 (D. Vaniman in foreground). ..... 2-51
Figure 2-23. Outcrop of Cerros del Rio basalt at White Rock Overlook (east of LANL). ..... 2-53
Figure 2-24. Regional aquifer water table map. ..... 2-56

Figure 2-25. Distribution of hydraulic conductivity estimates, derived from tests of 59 wells on the plateau ..... 2-62
Figure 2-26. Hydraulic conductivity estimates in the regional aquifer. ..... 2-62
Figure 2-27-a. Hydraulic conductivity within the Santa Fe Group ..... 2-64
Figure 2-27-b. Variation of hydraulic conductivity in volcanic rocks of the Pajarito Plateau. ..... 2-64
Figure 2-28. Comparison of the percentage of clay present in a hydrostratigraphic unit to the spatial variation in permeability ..... 2-68
Figure 2-29. Distribution of effective porosity measured within the Puye Formation beneath the regional aquifer water table. ..... 2-71
Figure 2-30. Schematic cross section of complex stratigraphy within the alluvial package in Ancho Canyon ..... 2-79
Figure 2-31. LAO-0.3 water level with streamflow and precipitation. ..... 2-80
Figure 2-32. PAO-4 water level with streamflow and precipitation. ..... 2-81
Figure 2-33. Los Alamos Canyon alluvial water level depths and stream flows. ..... 2-83
Figure 2-34. Estimated infiltration on the Pajarito Plateau ..... 2-84
Figure 2-35. Contours of water content constructed from the neutron log data during and after the wellbore injection test ..... 2-93
Figure 2-36. Low head weir monitoring well setup. ..... 2-94
Figure 2-37. Conceptual model of groundwater occurrences beneath the Pajarito Plateau. ..... 2-96
Figure 2-38. Locations of wells and boreholes that have penetrated perched groundwater systems in bedrock. ..... 2-98
Figure 2-39. The Española Basin and vicinity, with basin-scale numerical model outline shown in red, site-scale model outline shown in green. ..... 2-102
Figure 2-40. Approximation to present-day water table elevations (m). ..... 2-102
Figure 2-41. The Pajarito Plateau, with major wellfields indicated by enclosures in red. ..... 2-104
Figure 2-42. Idealized radius of influence of PM-2 on surrounding wells ..... 2-112
Figure 2-43. Drawdown at wells R-20 (a) and R-32 (b) in response to pumping at PM-2 ..... 2-113
Figure 2-44. Idealized representation of the aquifer near PM-2 during the pumping test. ..... 2-114
Figure 2-45. Annual water level decline due to municipal water supply well pumping. ..... 2-117
Figure 2-46. Map view showing the location of (a) a cross-section of the plateau ..... 2-120
Figure 2-47. Piezometric water levels in different screens in well CdV-R-15-3. ..... 2-120
Figure 2-48. Piezometric water levels in different screens in well R-16. ..... 2-121
Figure 2-49. Piezometric water levels in different screens in well R-19. ..... 2-121
Figure 2-50. Piezometric water levels in different screens in well R-20. ..... 2-122
Figure 2-51. Piezometric water levels in different screens in well R-31. ..... 2-122
Figure 2-52. Diagram of the locations of "young" and "old" water at different locations. ..... 2-125

Figure 3-1. Average spatial distributions (n = 6) for key analytes in LANL background wells and springs ..... 3-4

Figure 3-2. Stable isotope results for wells R-9, R-12, R-15, R-19, R-25, R-26, CdV-R-15-3, and CdV-R-37-2, and for other springs in the Jemez Mountains. ..... 3-5
Figure 3-3. Average dissolved concentrations of selected natural trace elements in a represenative well or spring within alluvial and perched intermediate groundwater and the regional aquifer. ..... 3-5
Figure 3-4. Activity diagram of log activity [$H_4SiO_4$] versus log activity $Ca^{2+}/[H^+]^2$ at 25°C for wells Otowi-4, R-9, R-12 (screen #3), and LAOI(A)-1.1 and La Mesita Spring ..... 3-6
Figure 3-5. Saturation indices for calcite versus calcium and bicarbonate concentrations (millimoles/liter) at springs and wells representing different aquifer types at LANL (perched, intermediate, and regional). ..... 3-11
Figure 3-6. Calculated distributions of adsorbed and dissolved uranyl species for well R-9 (275 ft perched zone) (HFO concentration = 1.46 g/L and total dissolved uranyl [$UO_2^{2+}$] = 0.054 ppm, 25°C) ..... 3-14
Figure 3-7. Calcium/sodium (meq/L) versus uranium concentrations, Pojoaque water fair, June 2004. ..... 3-15
Figure 3-8. Saturation indices for several solid phases in alluvial (LAO-B) and perched intermediate groundwater (LAOI(A)-1.1) and the regional aquifer. ..... 3-16
Figure 3-9. Selected oxidation-reduction couples in water at pH 7 and 25°C for the Pajarito Plateau and surrounding areas. ..... 3-18
Figure 3-10. Results of speciation calculations for Spring 9B in White Rock Canyon using the computer program MINTEQA2. ..... 3-19
Figure 3-11. Total alkalinity (as carbonate) versus uranium concentrations in groundwater samples collected from the Rio Grande Valley and the Pajarito Plateau. ... 3-20
Figure 3-12. Major liquid release sources that have potentially affected groundwater at Los Alamos National Laboratory. ..... 3-28
Figure 3-13. Tritium histories in Pueblo Canyon surface water and alluvial and intermediate groundwater zones. ..... 3-31
Figure 3-14. Tritium histories in DP and Los Alamos Canyon surface water and alluvial groundwater. ..... 3-31
Figure 3-15. Location of inferred past extent of groundwater contamination by tritium above the 20,000 pCi/L EPA MCL. ..... 3-32
Figure 3-16. Tritium histories in Mortandad Canyon alluvial groundwater and the regional aquifer. ..... 3-33
Figure 3-17. Nitrate histories in Pueblo Canyon surface water, alluvial and intermediate groundwater zones, and the regional aquifer. ..... 3-33
Figure 3-18. Location of inferred past extent of groundwater contamination by nitrate (as nitrogen) above the 10 mg/L EPA MCL. ..... 3-34
Figure 3-19. Nitrate histories in DP and Los Alamos Canyon surface water, alluvial groundwater, and the regional aquifer. ..... 3-35
Figure 3-20. Nitrate histories in Mortandad Canyon alluvial groundwater and the regional aquifer. ..... 3-35
Figure 3-21. Location of groundwater contamination by perchlorate above the 3.7 ppb EPA Region VI risk level. ..... 3-37
Figure 3-22. Perchlorate histories in Mortandad Canyon alluvial groundwater. ..... 3-38

Figure 3-23. Strontium-90 histories in Acid and Pueblo Canyon surface water..... 3-38
Figure 3-24. Strontium-90 histories in DP and Los Alamos Canyon surface water and alluvial groundwater.. ..... 3-39
Figure 3-25. Plutonium-239, -240 histories in DP and Los Alamos Canyon surface water, alluvial groundwater, and the regional aquifer..... 3-39
Figure 3-26. Strontium-90 histories in Mortandad Canyon aluval groundwater and the regional aquifer..... 3-40
Figure 3-27. Location of groundwater contamination by plutonium-238; plutonium-239,-240; and americium-241 above the 4-mrem DOE DCG for drinking water. ..... 3-41
Figure 3-28. Low-detection-limit tritium data from wells and springs sampling intermediate perched groundwater. ..... 3-42
Figure 3-29. Low-detection-limit tritium data from wells and springs sampling the regional aquifer..... 3-44
Figure 3-30. Anion concentrations in Springs 3 and 3A. ..... 3-46

Figure 4-1. Predicted vadose zone travel times (years) to the water table: base case, full scale of travel times..... 4-5
Figure 4-2. Predicted vadose zone travel times (years) to the water table, showing only travel times of 100 years or less..... 4-7
Figure 4-3. Predicted vadose zone travel times (years) to the water table, showing only travel times of 100 years or less..... 4-9
Figure 4-4. Study area for the performance assessment of MDA G, an active low-level, solid radioactive waste site located at LANL (from Birdsell et al. 2000)..... 4-11
Figure 4-5. Approximate locations of the four waste classes and the 100-m compliance boundary used for the MDA G performance assessment..... 4-12
Figure 4-6. Location of Los Alamos, New Mexico (a), Los Alamos Canyon study area, and the flow and transport model domain(b)..... 4-14
Figure 4-7. Three-dimensional flow model results, showing fluid saturation predictions (%) through the model domain (full model view). ..... 4-16
Figure 4-8. Fence diagram showing fluid saturation predictions (%) along one north-south and three east-west cross-sections. ..... 4-17
Figure 4-9. Three-dimensional model predictions of the tritium concentration of fluid reaching the water table in the year 1999..... 4-18
Figure 4-10. Geologic map of the Española Basin. ..... 4-21
Figure 4-11. The Española Basin, with the basin-scale numerical model outline shown in red, and the site-scale model outline shown in green..... 4-24
Figure 4-12. Basin model grid (plan view) with site-model boundaries indicated..... 4-26
Figure 4-13. Examples of three recharge models, all imparting the same total flux. ..... 4-28
Figure 4-14. For the basin-scale model, comparison between measured and simulated (a) fluxes; (b) heads..... 4-33
Figure 4-15. Comparison of simulated and measured hydrographs for representative wells on the plateau..... 4-34
Figure 4-16. Location of predicted transition between significant areal recharge and negligible areal recharge (2195 m), and uncertainty bounds..... 4-36

Figure 4-17. Fluxes across lateral site-model boundaries predicted by the calibrated basin model. 4-37
Figure 4-18. Results of predictive analysis, compared to two calibrated models. 4-38
Figure 4-19. Model-predicted horizontal component of pore-water velocity at the water table, in m/yr. 4-39
Figure 4-20. Comparison of simulated groundwater carbon-14 ages at nodes within the screened depths of wells with the corrected and uncorrected groundwater ages estimated from measured carbon-14 activities. 4-40
Figure 4-21. Predicted steady-state capture zones for wellfields in the vicinity of Los Alamos. 4-42
Figure 4-22. Predicted transient capture zones for wellfields in the vicinity of Los Alamos from Vesselinov and Keating (2003). 4-42
Figure 4-23. Simulated discharge to the Rio Grande, and estimated proportion of production in local wellfields that originates as storage and as captured recharge. 4-43
Figure 4-24. Heterogeneity within the Puye Formation; one realization of a stochastic Markov-chain model of the Totavi Lentil. 4-45
Figure 4-25. Cross-section through hydrostratigraphic framework model, showing location of layer selected to perform a sensitivity analysis exploring the uncertainty in the geologic framework. 4-45
Figure 4-26. Predicted steady-state capture zones for wellfields in the vicinity of Los Alamos, using two different alternative models of hydrostratigraphy. 4-46
Figure 4-27. Heterogeneity within the Puye Formation; three realizations of a stochastic Gaussian model. 4-47
Figure 4-28. Heterogeneity within the Puye Formation, fanglomerate; two realizations of a stochastic Markov-chain model. 4-48
Figure 4-29. Two representations of the north-south trending trough in the upper Santa Fe Group. 4-49
Figure 4-30. Predicted paths for particles released at TA-16 and beneath Cañon de Valle and captured at PM-4 and PM-2. 4-51
Figure 4-31 Breakthrough curves for particles released at TA-16 and beneath Cañon de Valle at PM-4 and PM-2. 4-51
Figure 4-32. Results of predictive analysis, showing the possible range of flow directions (farthest northward and farthest southward) for sources at TA-16. 4-53
Figure 4-33. Predicted plume migration for sources released at the water table below Mortandad Canyon, based on a steady-state, with pumping, flow field. 4-54
Figure 4-34. Predicted total dissolved salts in the groundwater at steady state, using a simple model of mineral dissolution. 4-56
Figure 4-35. Location of hypothetical wells used to evaluate the potential value of head data in reducing uncertainty in flow directions. 4-57
Figure 4-36. Mean flowpath for three simulations of plume migration away from Mortandad Canyon. 4-58
Figure 4-37. Illustration of plume migration for minimum capture by PM-5 (0%). 4-58
Figure 4-38. (a) Hydrostratigraphic units in the vicinity of well O-1, interpolated onto radial grid; (b) predicted drawdowns at the top of the aquifer, for eight cases. 4-60

# APPENDICES

**APPENDIX 1**

APPENDIX 1-A. REGULATORY FRAMEWORK ..... 1-A-1
1-A-1. Hydrogeologic Workplan Background ..... 1-A-1
1-A-1.1. DOE Orders ..... 1-A-1
1-A-1.2. RCRA Permit and HSWA Requirements ..... 1-A-1
1-A-1.3. RCRA Monitoring Requirements ..... 1-A-1
1-A-2. Technical Objectives of the Hydrogeologic Workplan ..... 1-A-4
1-A-3. Hydrogeologic Workplan Data Collection Approach ..... 1-A-8
1-A-3.1 Revision to Hydrogeologic Workplan Data Collection Approach ..... 1-A-9
1-A-3.2 Alluvial Groundwater Investigations ..... 1-A-9
1-A-4. Independent Peer Review of the Hydrogeologic Workplan ..... 1-A-11
1-A-5. Outreach Activities ..... 1-A-11

APPENDIX 1-B. WELL COMPLETION FACT SHEETS ..... 1-B-1

**APPENDIX 2**

APPENDIX 2-A. GEOLOGIC INFORMATION USED TO DEFINE THE CONTROLS ON HYDROLOGY ..... 2-A-1
2-A.1 Lithologic Information from Cuttings and Core ..... 2-A-1
2-A.2 Borehole Geophysical Data ..... 2-A-2
2-A.3 Borehole Video Logs ..... 2-A-3
2-A.4 Surface Geophysical Data ..... 2-A-3
2-A.5 Drilling Information ..... 2-A-4
2-A.6 Data Generated by Other Projects ..... 2-A-5
APPENDIX 2-B. PERCHED WATER OCCURRENCES ..... 2-B-1

**APPENDIX 3**

APPENDIX 3-A. WATERSHED DESCRIPTIONS ..... 3-A-1
APPENDIX 3-B. ALTERNATIVE CONCEPTUAL MODELS OF CONTAMINANT TRANSPORT ..... 3-B-1
3-B-1. Colloid-Facilitated Transport ..... 3-B-1
3-B-1.1 Strengths and Limitations of the Colloid-Facilitated Transport Model ..... 3-B-2
3-B-1.2 Effect on Current Conceptual Model and Assessment of Risk ..... 3-B-2
3-B-2. Cs-137 "Groundwater Transport" to the Rio Grande ..... 3-B-3
3-B-2.1 Strengths and Limitations of Cs-137 Groundwater Transport Alternative Model ..... 3-B-3
3-B-2.2 Effect on Current Conceptual Model and Assessment of Risk ..... 3-B-4

**APPENDIX 4**

APPENDIX 4-A. METHOD FOR ESTIMATING INFILTRATION RATE IN CANYONS ..... 4-A-1
APPENDIX 4-B. MDA G MODEL ..... 4-B-1
4-B-1. Introduction and Motivation ..... 4-B-1
4-B-2. Hydrostratigraphy and Hydraulic Properties ..... 4-B-1
4-B-3. Infiltration ..... 4-B-3
4-B-4. Radionuclide Releases ..... 4-B-3
4-B-5. Computational Grids ..... 4-B-4
4-B-6. Model Implementation ..... 4-B-4
4-B-7. Representative Transport Result ..... 4-B-7
4-B-8. Discussion ..... 4-B-9
APPENDIX 4-C. LOS ALAMOS CANYON MODEL ..... 4-C-1
4-C.1. Introduction and Motivation ..... 4-C-1
4-C.2. Hydrostratigraphy ..... 4-C-1
4-C.3. Infiltration Rates and Water Budget Model ..... 4-C-6
4-C.4. Contaminant Sources ..... 4-C-7
4-C.5. Numerical Grids ..... 4-C-9
4-C.6. Model Implementation ..... 4-C-11
4-C.7. Fluid Saturation Model Results ..... 4-C-12
4-C.7.1 Moisture Comparisons to Data ..... 4-C-14
4-C.7.2 Sensitivity Analysis ..... 4-C-14
4-C.8. Tritium Modeling Results ..... 4-C-18
APPENDIX 4-D. REGIONAL AQUIFER MODEL DEVELOPMENT ..... 4-D-1
4-D.1. Grid Information ..... 4-D-1
4-D.2. Recharge Model ..... 4-D-6
4-D.3. Flux Estimates. ..... 4-D-10
APPENDIX 4-E. ESTIMATING AQUIFER DISCHARGE USING STREAMFLOW DATA ..... 4-E-1

# LIST OF APPENDIX TABLES


Table 1-A-1. RCRA Groundwater Monitoring Programs for Regulated units ..... 1-A-3
Table 1-A-2. Drilling Methods Used for Hydrogeologic Characterization Wells at Los Alamos National Laboratory ..... 1-A-10
Table 1-A-3. Documents Relevant to the Hydrogeologic Workplan ..... 1-A-13

Table 2-A-1. Typical Wire-Line Geophysical Logging Tools ..... 2-A-7
Table 2-B-1. Characteristics of Deep Perched Groundwater Zones Encountered in Wells on the Pajarito Plateau ..... 2-B-3

Table 3-A-1. Guaje Canyon Watershed Description ..... 3-A-1
Table 3-A-2. Los Alamos Canyon Watershed Description ..... 3-A-5
Table 3-A-3. Sandia Canyon Watershed Description ..... 3-A-21
Table 3-A-4. Mortandad Canyon Watershed Description ..... 3-A-24
Table 3-A-5. Pajarito Canyon Watershed Description ..... 3-A-31
Table 3-A-6. Water Canyon Watershed Description ..... 3-A-36
Table 3-A-7. Ancho Canyon Watershed Description ..... 3-A-44
Table 3-A-8. Chaquehui Canyon Watershed Description ..... 3-A-47
Table 3-A-9. Frijoles Canyon Watershed Description ..... 3-A-49
Table 3-A-10. White Rock Canyon Watershed Description ..... 3-A-51
Table 3-B-1. Colloid Facilitated Alternative Transport Model ..... 3-B-2
Table 3-B-2. Groundwater Transport Alternative Model ..... 3-B-3

Table 4-A-1. Determination of Net Infiltration Index for Sections of Canyons on the Pajarito Plateau ..... 4-A-3
Table 4-B-1. Infiltration Rates (mm/year) Used as Upper Boundary Conditions for MDA G Performance Assessment ..... 4-B-8
Table 4-B-2. Maximum Ground Water and All Pathways Doses for the PA and CA Wastes, Base Case Flow Field (mrem/yr) MDA G Performance Assessment ..... 4-B-10
Table 4-C-1. Stratigraphic Units Present in the Vicinity of Los Alamos Canyon ..... 4-C-3
Table 4-C-2. Hydrologic Property Values in the Los Alamos Canyon Model ..... 4-C-5
Table 4-C-3. Infiltration Rates for Various Portions of the Canyon ..... 4-C-8
Table 4-D-1. Hydrostratigraphic Units in Site-Scale Model ..... 4-D-6
Table 4-D-2. Flux Estimates Derived from Previous Models, in AFY ..... 4-D-10
Table 4-E-1. Comparison of Gain/Loss Calculations to Other Studies ..... 4-E-3
Table 4-E-2. Estimates of Long-Term Average Flow at Small Tributaries ..... 4-E-5
Table 4-E-3. Water Budget Components Estimated for Watersheds within the Española Basin, Expressed as Fraction of Total Precipitation ..... 4-E-6

# LIST OF APPENDIX FIGURES

Figure 1-A-1. Flow chart used for hydrogeologic characterization decisions ..... 1-A-7

Figure 1-B-1. Completion diagram for well R-1 ..... 1-B-1
Figure 1-B-2. Completion diagram for well R-2 ..... 1-B-2
Figure 1-B-3. Completion diagram for well R-4 ..... 1-B-3
Figure 1-B-4. Completion diagram for well R-5 ..... 1-B-4
Figure 1-B-5. Completion diagram for well R-6 ..... 1-B-5
Figure 1-B-6. Completion diagram for well R-7 ..... 1-B-6
Figure 1-B-7. Completion diagram for wells R-8 and R-8a ..... 1-B-7
Figure 1-B-8. Completion diagram for well R-9 ..... 1-B-8
Figure 1-B-9. Completion diagram for well R-11 ..... 1-B-9
Figure 1-B-10. Completion diagram for well R-12 ..... 1-B-10
Figure 1-B-11. Completion diagram for well R-13 ..... 1-B-11
Figure 1-B-12. Completion diagram for well R-14 ..... 1-B-12
Figure 1-B-13. Completion diagram for well R-15 ..... 1-B-13
Figure 1-B-14. Completion diagram for well R-16 ..... 1-B-14
Figure 1-B-15. Completion diagram for well R-18 ..... 1-B-15
Figure 1-B-16. Completion diagram for well R-19 ..... 1-B-16
Figure 1-B-17. Completion diagram for well R-20 ..... 1-B-17
Figure 1-B-18. Completion diagram for well R-21 ..... 1-B-18
Figure 1-B-19. Completion diagram for well R-22 ..... 1-B-19
Figure 1-B-20. Completion diagram for well R-23 ..... 1-B-20
Figure 1-B-21. Completion diagram for well R-25 ..... 1-B-21
Figure 1-B-22. Completion diagram for well R-26 ..... 1-B-22
Figure 1-B-23. Completion diagram for well R-28 ..... 1-B-23
Figure 1-B-24. Completion diagram for well R-31 ..... 1-B-24
Figure 1-B-25. Completion diagram for well R-32 ..... 1-B-25
Figure 1-B-26. Completion diagram for well R-33 ..... 1-B-26
Figure 1-B-27. Completion diagram for well R-34 ..... 1-B-27

Figure 3-A-1. Map of watersheds on the Pajarito Plateau in the vicinity of Los Alamos National Laboratory. ..... 3-A-3
Figure 3-A-2. Map of Guaje Canyon watershed. ..... 3-A-4
Figure 3-A-3. Map of Los Alamos Canyon watershed, including Los Alamos Canyon, Bayo Canyon, Acid Canyon, Pueblo Canyon, and DP Canyon. ..... 3-A-20
Figure 3-A-4. Map of Sandia Canyon watershed ..... 3-A-23
Figure 3-A-5. Map of Mortandad Canyon watershed including Mortandad Canyon and Cañada del Buey. ..... 3-A-30
Figure 3-A-6. Map of Pajarito Canyon watershed. ..... 3-A-35

Figure 3-A-7. Map of Water Canyon watershed including Pajarito Canyon, Cañon de Valle, Potrillo Canyon, and Fence Canyon. ..... 3-A-43
Figure 3-A-8. Map of Ancho Canyon watershed. ..... 3-A-46

Figure 3-A-9. Map of Chaquehui Canyon watershed. ..... 3-A-48
Figure 3-A-10. Map of Frijoles Canyon watershed. ..... 3-A-50
Figure 3-A-11. Map of White Rock Canyon. ..... 3-A-56

Figure 4-A-1. Infiltration on the Pajarito Plateau ..... 4-A-2
Figure 4-B-1. Conceptual model of hydrostratigraphy of the unsaturated zone for the MDA G performance Assessment Model. ..... 4-B-2
Figure 4-B-2. Comparison of site data to calculated steady-state saturation profiles for several infiltration rates. ..... 4-B-6
Figure 4-B-3. Iodine-129 plumes (concentration, moles/liter) in the vadose zone at 1000 years for the four different source regions, base-case flow field. ..... 4-B-8
Figure 4-B-4. Total flux of the 1988–1995 $^{129}I$ inventory from the unsaturated zone to the saturated zone for various flow cases. ..... 4-B-9
Figure 4-C-1. Cross-section of stratigraphy in the vicinity of Los Alamos Canyon. ..... 4-C-4
Figure 4-C-2. Three-dimensional depiction of the stratigraphic framework model used to construct the flow and transport model for Los Alamos Canyon. ..... 4-C-4
Figure 4-C-3. Three-dimensional model grid. ..... 4-C-10
Figure 4-C-4. Three-dimensional view of the Los Alamos Canyon model numerical grid. ..... 4-C-11
Figure 4-C-5. Full model three-dimensional flow results showing fluid saturation predictions through the model domain. ..... 4-C-13
Figure 4-C-6. Fence diagram showing one north-south and three east-west cross-sections. ..... 4-C-13
Figure 4-C-7. Comparison of data and three-dimensional model predictions for water contents in well LADP-3. ..... 4-C-15
Figure 4-C-8. Comparison of data and three-dimensional model predictions for water contents in well LADP-4. ..... 4-C-16
Figure 4-C-9. Two-dimensional model predictions for the water content in response to transient episodes of enhanced infiltration ..... 4-C-17
Figure 4-C-10. Three-dimensional model predictions of the tritium concentration of fluid reaching the water table in the year 1999 ..... 4-C-19
Figure 4-D-1. Top view of basin-scale model grid with side view ..... 4-D-2
Figure 4-D-2. Boundary conditions along top surface of basin scale model ..... 4-D-3
Figure 4-D-3. Plan view of site-scale grid. ..... 4-D-4
Figure 4-D-4. Boundary conditions along top surface of site-scale model. ..... 4-D-5
Figure 4-D-5. Three-dimensional representation of the major hydrostratigraphic units in the basin, scale model. ..... 4-D-8
Figure 4-D-6. Site-scale model grid, colored according to major hydro-stratigraphic units. ..... 4-D-9
Figure 4-D-7. (a) Average annual precipitation in the vicinity of the Española Basin. ... 4-D-11
Figure 4-D-8. Average annual precipitation verses elevation ..... 4-D-12
Figure 4-E-1. Measured January flow at the Otowi gage. ..... 4-E-4

# Los Alamos National Laboratory's Hydrogeologic Studies of the Pajarito Plateau: A Synthesis of Hydrogeologic Workplan Activities (1998–2004)

edited by

Kelly A. Collins, Ardyth M. Simmons, Bruce A. Robinson, and Charles L. Nylander

## ABSTRACT

This report provides a comprehensive description of the hydrogeologic setting beneath the Pajarito Plateau and Los Alamos National Laboratory (LANL). It is based on interpretative synthesis of hydrogeologic and geochemical data collected through December 2004. Since 1998, twenty-five regional aquifer wells and six intermediate-zone wells have been completed for hydrogeologic characterization. Characterization of the hydrogeologic setting was undertaken in order to fulfill regulatory requirements for characterization and monitoring. This report provides the data and information necessary to evaluate the existing monitoring network and, if necessary, to design an enhanced monitoring network.

Los Alamos National Laboratory (LANL) is situated on the Pajarito Plateau, located within the Española Basin section of the Rio Grande Rift. The Española Basin, as well as the Pajarito Plateau on its western edge, is filled with Miocene and Pliocene-age sediments and volcanic rocks. The topographic plateau is formed by Pleistocene Bandelier Formation ash-flow tuffs from the Jemez volcanic field, which cover the basin-fill sediments.

Groundwater occurs in three settings beneath the Pajarito Plateau: alluvial groundwater, intermediate-perched saturated zones, and the regional aquifer. Alluvial groundwater occurs to a limited and variable extent in the alluvium lining canyon bottoms. Alluvial groundwater provides pathways for LANL-derived contamination introduced into canyons to migrate to significant lateral distances and infiltrate to greater depths.

Flow and transport of water in the vadose zone varies by rock type. Most of the plateau is covered with nonwelded to moderately welded Tshirege and Otowi Member ash-flow tuffs of the Bandelier Tuff. Unsaturated flow and transport through these nonwelded to moderately welded tuffs occurs predominantly through the porous matrix. On the western edge of the plateau, both fracture and matrix-dominated flow can occur, depending on the degree of welding (or matrix conductivity) of the tuff. In contrast to the flow behavior in the Bandelier Tuff units, much of the vadose zone flow through the basalt units is almost certainly fracture dominated. Beneath the Pajarito Plateau, perched water bodies in the vadose zone may be important components of subsurface pathways that facilitate movement of contaminated fluids from the ground surface to the water table of the

regional aquifer. Perched water is most often found in Puye fanglomerates, the Cerros del Rio basalt, and in units of the Bandelier Tuff.

The regional aquifer beneath the Pajarito Plateau is part of an aquifer which extends throughout the Española Basin (an area roughly 6000 km2). This aquifer is the primary source of water for the Laboratory, the communities of Santa Fe, Española, Los Alamos, and numerous pueblos. The sources of recharge to the regional aquifer are diffuse recharge in the Sierra de los Valles and focused recharge from wet canyons on the Pajarito Plateau. Natural discharge from the regional aquifer is primarily into the Rio Grande directly or to springs that flow into the Rio Grande. The aquifer is under water-table conditions across much of the Plateau, but exhibits more confined aquifer behavior near the Rio. Hydraulic properties are highly anisotropic, with vertical hydraulic conductivities much smaller than horizontal hydraulic conductivites, resulting in a muted response at the water table to supply-well pumping at greater depths. Flow modeling simulations suggest that flow beneath the Rio Grande (west to east) has been induced by production at the Buckman wellfield just east of the Rio Grande, which supplies the city of Santa Fe. Because of the heterogeneous nature of the aquifer, groundwater velocity varies considerably over short distances. The fastest velocities are in the basalts where fracture flow is assumed.

Imprinted on the natural variations in chemistry along flowpaths is the presence of contaminants historically released since the early 1940s when Laboratory operations commenced. The impacts to groundwater at the Laboratory have occurred mainly where effluent discharges have caused increased infiltration of water. The movement of groundwater contaminants is best seen through the distribution of conservative (that is, non-reactive) chemical species. Under many conditions, compounds like RDX, tritium, perchlorate, and nitrate move readily with the groundwater. In many settings, chemical reactions do not retard the movement of these compounds or decrease their concentrations, although the activity of tritium does decrease due to radioactive decay. For some compounds or constituents (uranium, strontium-90, barium, some HE compounds, and solvents), movement is slowed or their concentrations are decreased by adsorption or cation exchange, precipitation or dissolution, chemical reactions like oxidation/reduction, or radioactive decay. Other constituents (americium-241, plutonium, and cesium-137) are nearly immobile because they are strongly adsorbed onto sediment particles.

The distribution of tritium in the regional aquifer supports the conceptual model that surface effluent discharges have caused the cases where Laboratory contaminants are found at depth. In most cases, the highest regional aquifer tritium values are found near where effluent discharges have occurred, but are much lower than values observed in overlying alluvial or intermediate perched groundwater. The lower regional aquifer values may be due to dilution of recharge by other groundwater sources as well as radioactive decay due to recharge times of decades.

The conceptual models of the hydrologic system beneath the Pajarito Plateau have been translated into numerical models. A site-wide model for performing first-order analysis of travel time through the vadose zone across the entire Pajarito Plateau was used to identify areas where contaminant pathways are likely to exist. Results indicated that the predicted travel times on mesas are variable, but for the

most part are greater than 1000 years, ranging from 1000–5000 years in the eastern portions of the Laboratory to 20,000 to 30,000 years in the western region. Two factors control these results: infiltration rate and hydrostratigraphy. Generally, travel times less than 100 years are predicted in the portions of canyons with net infiltration of 300 mm/yr to 1000 mm/yr, especially in locations where the Bandelier Tuff is thin.

The regional aquifer model has been applied to predict fate and transport of contaminants in the regional aquifer, in order to optimally place monitoring wells and inform risk assessment studies; and to provide guidance in prioritization of data collection activities.

Armed with the understanding gained from the Hydrogeologic Workplan activities, it is now possible to develop improved groundwater monitoring strategies or conduct more cost-effective detailed studies of individual canyons where initial studies have suggested that groundwater risk may exist.

# 1.0 INTRODUCTION

This report provides a comprehensive description of the hydrogeologic setting beneath the Pajarito Plateau and Los Alamos National Laboratory (LANL). It is based on interpretative synthesis of hydrogeologic data collected through December, 2004. Characterization of the hydrogeologic setting was undertaken in order to fulfill regulatory requirements for characterization and monitoring. This report provides the data and information necessary to evaluate the existing monitoring network and, if necessary, to design an enhanced monitoring network. Monitoring network evaluation and design are not addressed in this report. Recommendations included in this report are for scientific interest only, and are not necessary to comply with the regulatory requirements.

LANL is located in Los Alamos, Santa Fe, and Sandoval counties of north-central New Mexico, roughly 25 mi northwest of Santa Fe (Figure 1-1). It is owned by the Department of Energy (DOE) and co-operated by DOE and the University of California (UC). Work at LANL began in 1943 with the mission to design, develop, and test nuclear weapons.

Beginning in 1945, the US Geological Survey (USGS) became involved in various studies to develop the water supply at LANL (LANL 1995). Special studies to protect and monitor groundwater quality were initiated by LANL in 1949. Thus, groundwater monitoring has been conducted at LANL for over 50 years. The first monitoring network was limited to the water supply wells, a handful of test wells, and springs. The monitoring network evolved as environmental programs, such as those managed by LANL's Environmental Restoration (ER) organization (now Environmental Stewardship—Environmental Remediation & Surveillance Program [ENV-ERS]), added more wells, primarily in the shallow alluvial systems, as potential monitoring points.

In 1997, LANL personnel began a site-wide hydrogeologic characterization program, which is described in the Hydrogeologic Workplan (LANL 1998). The primary objective of the characterization program was to sufficiently refine the understanding of the hydrogeologic systems so that, if appropriate, an enhanced monitoring network could be designed. The Hydrogeologic Workplan was implemented, resulting in installation of 25 regional aquifer wells. Data from sampling and measurements taken at these wells have provided information about the subsurface geologic environment, including the vadose zone and intermediate perched and regional aquifer groundwater. This report is a synthesis of data from Hydrogeologic Workplan activities and all other groundwater-related investigations conducted at LANL since 1997. Collection and analysis of groundwater data is ongoing at LANL, associated with site-specific (not site-wide) investigations. It is considered unlikely that information from wells drilled after December 2004 will significantly change the understanding of the site-wide hydrogeologic setting described in this report. In some cases, analysis and interpretation of data lags behind data collection, and what is presented here does not include analysis of all data collected up to December 2004. Analysis of the data collected as part of the site-wide characterization has sufficiently improved the understanding of the hydrogeologic system and the ability to design and implement an integrated site-wide groundwater monitoring program.

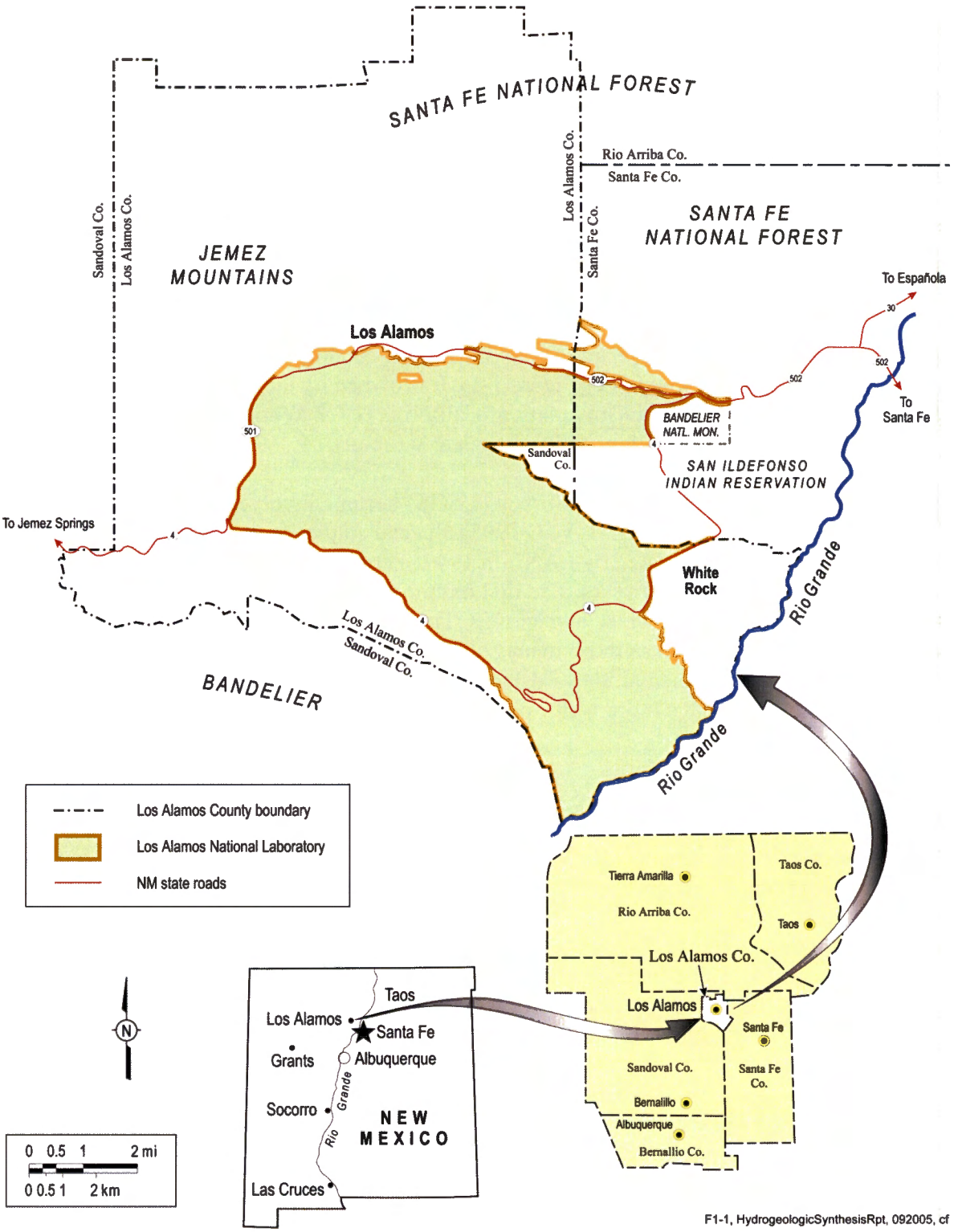


**Figure 1-1.** Location of Los Alamos National Laboratory.

## 1.1 Technical Objectives of the Hydrogeologic Workplan

The primary technical objective of the Hydrogeologic Workplan was to collect data necessary to evaluate and, if necessary, enhance the groundwater monitoring network at LANL. The technical objectives of the Hydrogeologic Workplan were intended to be comprehensive with respect to groundwater regulatory requirements for characterization and monitoring, described in Appendix 1-A. The regulatory requirements included

- Resource Conservation and Recovery Act (RCRA) operating permit which requires monitoring for RCRA units, unless a groundwater monitoring waiver is demonstrated.
- New Mexico Environment Department (NMED) letters requiring a better understanding of the hydrogeologic regime in order evaluate groundwater monitoring waivers submitted by LANL.
- RCRA permits Hazardous and Solid Waste Amendments (HSWA) module requirements to characterize the hydrogeologic setting.

Specifically, NMED identified four issues that needed to be resolved in order to evaluate the groundwater monitoring waivers submitted by LANL (Appendix 1-A):

- Individual zones of saturation beneath LANL had not been adequately delineated and the "hydraulic interconnection" between these was not understood.
- The recharge area(s) for the regional and intermediate aquifers and any associated effects of fracture-fault zones with regard to contaminant transport and hydrology had not been identified.
- The groundwater flow direction(s) of the regional aquifer and intermediate aquifers, as influenced by pumping of production wells, were unknown.
- Aquifer characteristics could not be determined without additional monitoring wells installed within specific intervals of the various aquifers beneath the facility.

Table 1-1 is a crosswalk of HSWA module requirements for groundwater characterization, how they have been addressed, and which sections of this report contain that information.

## 1.2 Hydrogeologic Characterization Overview

In order to establish the data quality objectives that guided the development of the Hydrogeologic Workplan (LANL 1998), the information needed to evaluate and design a monitoring network was articulated. Groundwater at LANL occurs in three modes: alluvial, perched intermediate groundwater in the vadose zone, and the regional aquifer. Figure 1-2 shows the relationship between the Pajarito Plateau topography and modes of groundwater. In general, to monitor the quality of water that has the potential to be impacted by releases of hazardous or radioactive wastes, there must be an understanding of the following:

## Table 1-1.
## Crosswalk Between HSWA Permit Requirements* and Synthesis Report Section

| HSWA Permit Reference | Permit Requirement | Synthesis Report Sections |
|---|---|---|
| Task III.A.1.a | A description of the regional and facility specific geologic and hydrogeologic characteristics affecting groundwater flow beneath the facility | Section 2.2, Section 2.4 |
| Task III.A.1.b | An analysis of any topographic features that might influence the groundwater flow system | Section 2.1.3 |
| Task III.A.1.c | An analysis of fractures within the tuff, addressing tectonic trend fractures versus cooling fractures | Section 2.5.4 |
| Task III.A.1.d | Based on field data, tests, (gamma and neutron logging of existing and new wells, piezometers, and borings) and cores, a representative and accurate classification and description of the hydrogeologic units which may be part of the migration pathways at the facility (e.g., the aquifers and any intervening saturated and unsaturated units) | Section 2.3; Section 4.2.12 |
| Task III.A.1.e | Based on field studies and cores, structural geology and hydrogeologic cross sections showing the extent (depth, thickness, lateral extent) of hydrogeologic units which may be part of the migration pathway identifying<br>Unconsolidated sand and gravel deposits<br>Zones of fracturing or channeling in consolidated and unconsolidated deposits<br>Zones of high or low permeability that might direct and restrict the flow of contaminants | Section 2.3; Section 4.1.2; Section 4.2.12 |
| Task III.A.1.f | Based on data obtained from groundwater monitoring wells and piezometers installed upgradient and downgradient of the potential contaminant source, a representative description of water level or fluid pressure monitoring | Section 2.4.2 |
| Task III.A.1.g | A description of manmade influences that may affect the hydrogeology of the site | Section 2.7.6 |
| Task III.A.1.h | Analysis of available geophysical information and remote sensing information such as infrared photography and Landsat imagery | Appendix 2-A |
| Task III.A.2.d | Characterize rock and soil units above the water table including saturated hydraulic conductivity | Section 2.2, Section 2.3, Section 2.4.1 |
| Task III.A.2.e | Characterize rock and soil units above the water table including porosity | Section 2.2, Section 2.3, Section 2.4.1 |
| Task III.A.2.j | Characterize rock and soil units above the water table including depth of water table | Section 2.2, Section 2.3, Section 2.4.1 |
| Task III.A.2.k | Characterize rock and soil units above the water table including moisture content | Section 2.2, Section 2.3, Section 2.4.1 |
| Task III.A.2.l | Characterize rock and soil units above the water table including effect of stratification on unsaturated flow | Section 2.4.1 |

**Table 1-1.**
**Crosswalk Between HSWA Permit Requirements* and Synthesis Report Section (continued)**

| HSWA Permit Reference | Permit Requirement | Synthesis Report Sections |
|---|---|---|
| Task III.A.2.m | Characterize rock and soil units above the water table including infiltration | Section 2.4.1 |
| Task III.A.2.n | Characterize rock and soil units above the water table including evapotranspiration | Section 2.4.1; Section 2.4.2 |
| Task III.A.2.o | Characterize rock and soil units above the water table including residual contaminants in soil | Section 2.4.1, Appendix 3-A |
| Task III.A.2.r | Characterize rock and soil units above the water table including water balance scenarios | Section 2.4.1 |
| Task III.C.1.a | A description of horizontal and vertical extent of any immiscible or dissolved groundwater plume(s) originating from the facility | Appendix 3-A |
| Task III.C.1.b | The horizontal and vertical direction of contaminant movement in groundwater | Section 3.2; Section 4.1; Section 4.2.11; Section 4.2.12 |
| Task III.C.1.c | The velocity of contaminant movement in groundwater | Section 4.1; Section 4.2.11; Section 4.2.12 |
| Task III.C.1.d | The horizontal and vertical concentration profiles of any 40 CFR Part 264 Appendix IX constituents and radiochemical constituents in the groundwater plume(s) | Section 3.2; Appendix 3-A |
| Task III.C.1.e | An evaluation of factors influencing the plume movement | Section 3.1, Section 3.2, Section 4.1, Section 4.2.12 |
| Task III.C.1.f | An extrapolation of future plume movement | Section 4.1, Section 4.2.12 |

* LANL, 1995.

- Potential sources of contaminants: contaminant character, inventory, and locations
- Release mechanisms that introduce contaminants to the environment
- Contaminant transport mechanisms from the location of the release to groundwater
- Transport of contaminants through the groundwater system: direction and velocity of groundwater and of contaminants

Monitoring data needs were identified for each component of the groundwater system: alluvial, intermediate perched groundwater in the vadose zone, and regional aquifer and the connections between the components. Figure 1-2 shows the overall hydrogeologic conceptual model. In wet canyons, where surface water is present, the water infiltrates the alluvium in the canyon bottoms and forms alluvial groundwater. Dry canyons and mesas do not have alluvial groundwater. Alluvial groundwater flows down the canyon until it reaches an area where infiltration is enhanced by thin or absent Bandelier Tuff, highly fractured rock below the alluvium, or anthropogenic alterations (e.g. sediment traps). In areas with enhanced infiltration, alluvial groundwater percolates through the vadose zone and collects in relatively more permeable units, if there are any present beneath the canyon, e.g. fractured basalt. Alluvial groundwater and perched intermediate groundwater continue to percolate through the deeper vadose zone until they reach the regional

aquifer. The interconnected nature of the hydrogeologic system may allow anthropogenic constituents that are present in surface water to be transported into alluvial groundwater, the vadose zone and to the regional aquifer.

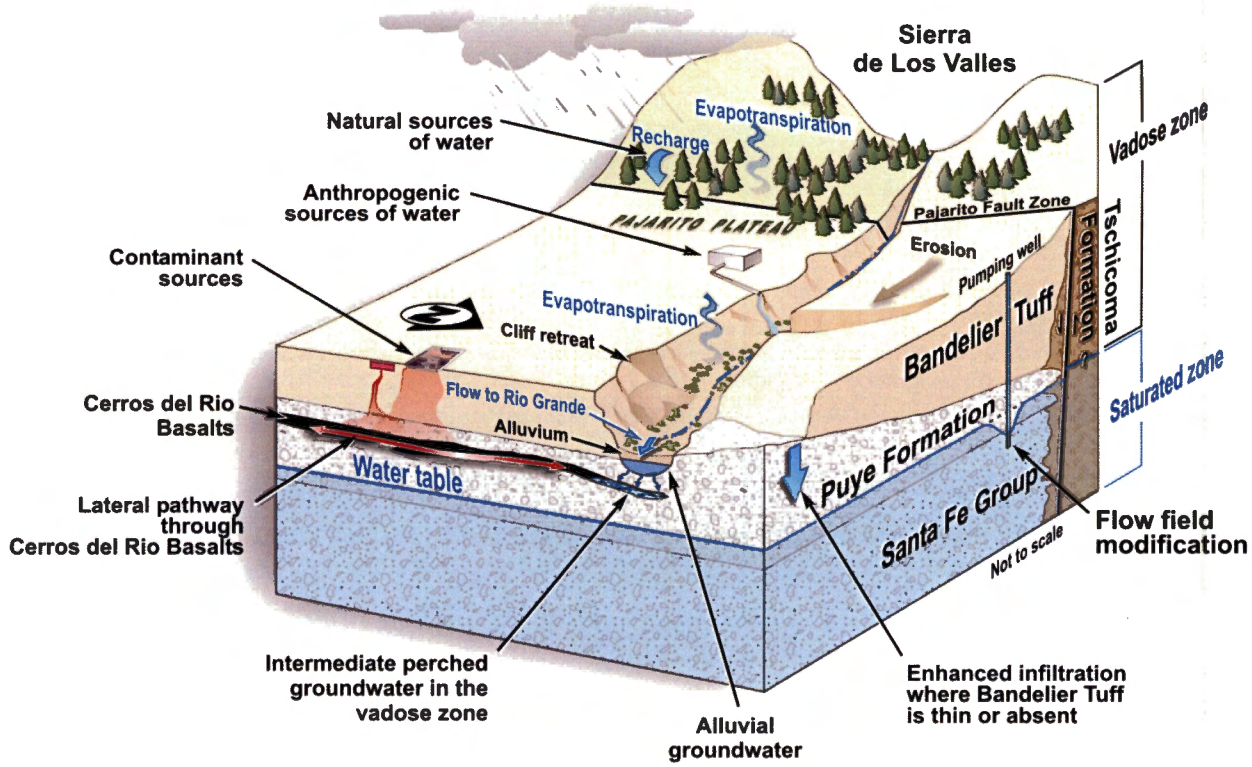


**Figure 1-2.** Groundwater components at LANL.

The data collection articulated in the Hydrogeologic Workplan considered elements of risk assessment, e.g. sources, release mechanisms, and transport, because these same elements are important in establishing a monitoring network capable of detecting releases. Thus, the data collected under the auspices of the Hydrogeologic Workplan are considered adequate to support risk assessment, but are not intended to serve as a risk assessment. Characterizing the source terms and release mechanisms or other chemical phenomena is the subject of ongoing investigations and information from those investigations was used in developing the Hydrogeologic Workplan (LANL 1998). Characterizing the alluvial component of the hydrologic system was undertaken in conjunction with investigating source terms and the results of the alluvial investigations are reported here (Section 2.4) because of the importance of alluvial groundwater in the hydrogeologic system. The primary focus of the Hydrogeologic Workplan (LANL 1998) activities was on the deeper groundwater components and to understand the movement of contaminants through the vadose zone and in the regional aquifer.

Since 1998, twenty-five regional aquifer wells and six intermediate-zone wells have been completed for hydrogeologic characterization (Table 1-2). The locations of the hydrogeologic characterization wells are shown on Figure 1-3. Well completion fact sheets (Appendix 1-B) and well completion reports document the drilling, well construction, well completion, testing, and

sampling for each characterization well. A description and analysis of the characterization sampling for many wells are documented in geochemistry reports.

## 1.3. Topical Organization

The most basic control on the movement of water and contaminants through the system is the rocks through which the water moves. The conceptual model of the site is built from surface and subsurface geologic data (Appendix 2-A). Section 2.1 describes the regional geologic setting as a context for understanding the stratigraphic framework of the Pajarito Plateau presented in Section 2.2. Cross sections that illustrate the relationship between the stratigraphic units are critical for understanding how groundwater flows (Section 2.3).

The hydrologic properties of stratigraphic units in the vadose zone and regional aquifer are described in Section 2.4. This section quantifies the properties of the hydrologic units and explains the sources of data, including the uncertainties in the properties. The hydrologic properties and processes are combined to create conceptual models of the alluvial, vadose zone, and regional aquifer components in Sections 2.5, 2.6 and 2.7, respectively.

The natural groundwater geochemistry of the Pajarito Plateau is important to understand in order to identify and quantify contaminants added to the system. The background groundwater chemistry is integrated with geochemical processes to provide the comprehensive geochemical model described in Section 3.1. Overprinted on the natural water chemistry are the contaminants potentially released by LANL activities. Section 3.2 synthesizes the contaminant distribution data with respect to hydrologic processes and explores the contaminant transport implications.

Numerical modeling is an analytical tool that can be used to integrate and synthesize the sometimes widely-spaced point hydrogeologic field data and that predicts how the hydrologic system will behave at different times and under different conditions in the future. However, before models can be used for prediction, they must adequately reproduce the current conditions. The vadose zone and regional aquifer models that have been developed adequately reproduce current conditions beneath the Pajarito Plateau are described in Sections 4.1 and 4.2. These sections include the underlying assumptions, hydrologic processes, calibration, and predictions for flow and transport.

Section 5 summarizes the information presented in Sections 2, 3 and 4 and highlights how the refined understanding of the hydrogeologic systems can be applied to evaluating the adequacy of the existing the monitoring system and, if necessary, the design of an enhanced monitoring network.

## Table 1-2.
## Los Alamos National Laboratory Hydrogeologic Characterization Wells

| Well | Location | Date Completed | Primary Drilling Methods | Type of Drilling Fluid Used | Total Depth (ft bgs*) | Number of Screens[1] | Reference |
|---|---|---|---|---|---|---|---|
| R-1 | Mortandad Canyon | November 2003 | Conventional-circulation fluid-assisted air-rotary methods with casing advance to 90 ft followed by conventional-circulation fluid-assisted air-rotary drilling in an open hole to[2] TD at 1165 ft. | Air and municipal water mixed with Quik-FOAM, EZ-MUD | 1165 | 1–R | Kleinfelder, 2004e |
| R-2 | Pueblo Canyon | October 2003 | Conventional-circulation fluid-assisted air-rotary drilling in an open hole to 403 ft followed by conventional-circulation mud rotary drilling to TD at 943 ft. | Air and municipal water mixed with Quik-FOAM, EZ-MUD in the upper part and municipal water mixed with bentonite, soda ash, PAC-L in the lower part | 943 | 1–R | Kleinfelder, 2004b |
| R-4 | Pueblo Canyon | October 2003 | Conventional-circulation fluid-assisted air-rotary drilling in an open hole to 266 ft followed by conventional-circulation mud rotary drilling to TD at 844 ft. | Air and municipal water mixed with Quik-FOAM, EZ-MUD in the upper part and municipal water mixed with bentonite, soda ash, PAC-L in the lower part | 844 | 1–R | Kleinfelder, 2004a |
| R-5 | Pueblo Canyon | June 2001 | A combination of reverse- circulation fluid-assisted air-rotary methods in open hole and with casing advance to 870 ft followed by reverse-circulation fluid-assisted air-rotary drilling in an open hole to TD at 902 ft. | Air and municipal water mixed with Quik-FOAM, EZ-MUD | 902 | 2–I<br>2–R | LANL, 2003a |
| R-6 | Los Alamos Canyon | December 2004 | Conventional-circulation air-rotary and fluid-assisted air-rotary drilling methods in an open hole to 945 ft followed by conventional-circulation mud rotary drilling in a cased hole (casing set to 815 ft depth) to TD at 1303 ft. | Air and municipal water mixed with Quik-FOAM, EZ-MUD in the upper part and municipal water mixed with bentonite (Max-Gel and Quik-Gel), N-seal, Drispac, and soda ash in the lower part | 1303 | 1–R | Well completion report unavailable |
| R-7 | Los Alamos Canyon | February 2001 | Reverse-circulation fluid-assisted air-rotary methods with casing advance to 290 ft followed by reverse-circulation fluid-assisted air-rotary drilling in an open hole to TD at 1097 ft. | Air and municipal water mixed with Quik-FOAM, EZ-MUD | 1097 | 2–I<br>1–R | Stone et al. 2002 |
| R-8 | Los Alamos Canyon | February 2002 | A combination of reverse- circulation fluid-assisted air-rotary methods in open hole and with casing advance to 809 ft followed by reverse-circulation fluid-assisted air-rotary drilling in an open hole to TD at 880 ft. | Air and municipal water mixed with Quik-FOAM, EZ-MUD | 880 | 2–R | LANL, 2003b |

**Table 1-2.**
**Los Alamos National Laboratory Hydrogeologic Characterization Wells (continued)**

| Well | Location | Date Completed | Primary Drilling Methods | Type of Drilling Fluid Used | Total Depth (ft bgs*) | Number of Screens[1] | Reference |
|---|---|---|---|---|---|---|---|
| R-9 | Los Alamos Canyon | October 1999 | A combination of reverse-circulation air-rotary methods in open hole to 175 ft, coring to 419 ft, and with casing advance and reverse-circulation air-rotary methods TD at 771 ft. | Air in upper part of the borehole and air with municipal water mixed with Quik-FOAM, EZ-MUD in the lower part | 771 | 1–R | Broxton et al. 2001a |
| R-11 | Sandia Canyon | August 2004 | Conventional-circulation fluid-assisted air-rotary drilling in an open hole to TD at 927 ft. | Air and municipal water mixed with Quik-FOAM, EZ-MUD | 927 | 1–R | Kleinfelder, 2004c |
| R-12 | Sandia Canyon | January 2000 | A combination of reverse- circulation air-rotary methods in open hole and with casing advance to 710 ft followed by reverse-circulation fluid-assisted air-rotary drilling in an open hole to TD at 886 ft. | Air and municipal water in the upper part and air with municipal water mixed with TORKEASE, Quik-FOAM, EZ-MUD in the lower part | 886 | 2–I<br>1–R | Broxton et al. 2001 |
| R-13 | Mortandad Canyon | September 2001 | A combination of reverse- circulation fluid-assisted air-rotary methods in open hole and with casing advance to TD at 1133 ft. | Air and municipal water mixed with Quik-FOAM, EZ-MUD | 1133 | 1–R | LANL 2003c |
| R-14 | Mortandad Canyon | July 2002 | Reverse-circulation fluid-assisted air-rotary methods in open hole to 1225 ft with hole cased to 1050 ft; conventional-circulation mud rotary drilling in open hole from 1225-1285 ft; reverse-circulation fluid-assisted air-rotary methods with casing advance from 1285 ft to TD at 1327 ft. | Air and municipal water mixed with EZ-MUD in the upper part and municipal water mixed with soda ash, bentonite, LIQUI-TROL, in the lower part | 1327 | 2–R | LANL, 2003d |
| R-15 | Mortandad Canyon | February 2000 | Reverse-circulation fluid-assisted air-rotary methods with casing advance to TD at 1107 ft. | Air and municipal water mixed with TORKEASE, Quik-FOAM, EZ-MUD | 1107 | 1–R | Longmire et al. 2000 |
| R-16 | White Rock Overlook | August 2002 | A combination of reverse- circulation fluid-assisted air-rotary methods in open hole and with casing advance to 729 ft followed by reverse-circulation fluid-assisted air-rotary drilling in an open hole to 867 ft. Hole completed using conventional-circulation mud rotary methods from 867 ft to TD at 1287 ft. | Air and municipal water mixed Quick-gel, liqui-trol, Quick-FOAM, and soda ash in the upper part and municipal water mixed Quick-gel, EZ-MUD, liqui-trol, magma-fiber, n-seal in the lower part | 1287 | 4–R | LANL, 2003e |
| R-18 | Mesa above Pajarito Canyon | December 2004 | Conventional-circulation fluid-assisted air-rotary drilling methods in an open hole to TD at 1440 ft. | Air and municipal water mixed with Quik-FOAM and EZ-MUD | 1440 | 1–R | Well completion report unavailable |

**Table 1-2.**
**Los Alamos National Laboratory Hydrogeologic Characterization Wells (continued)**

| Well | Location | Date Completed | Primary Drilling Methods | Type of Drilling Fluid Used | Total Depth (ft bgs*) | Number of Screens[1] | Reference |
|---|---|---|---|---|---|---|---|
| R-19 | Mesa above Potrillo Canyon | April 2000 | Reverse-circulation fluid-assisted air-rotary methods with casing advance to 227 ft followed by reverse-circulation fluid-assisted air-rotary drilling in an open hole to TD at 1902 ft. | Air and municipal water mixed with TORKEASE, Quik-FOAM, EZ-MUD | 1902 | 2–I<br>5–R | Broxton et al. 2001d |
| CdV-R-15-3 | Cañon de Valle | September 2000 | Reverse-circulation fluid-assisted air-rotary methods with casing advance to 722 ft; install casing; complete hole by reverse-circulation fluid-assisted air-rotary drilling in an open hole to TD at 1722 ft. | Air and municipal water mixed with Quik-FOAM, EZ-MUD plus polymers | 1722 | 3–I<br>3–R | Kopp et al. 2002 |
| CdV-R-37-2 | Cañon de Valle | October 2001 | A combination of reverse- circulation fluid-assisted air-rotary methods in open hole and with casing advance to 825 ft followed by reverse-circulation fluid-assisted air-rotary drilling in an open hole to TD at 1664 ft. | Air and municipal water mixed with Quik-FOAM, EZ-MUD | 1664 | 1–I<br>3–R | Kopp et al. 2003 |
| R-20 | Pajarito Canyon | January 2003 | Conventional-circulation mud rotary drilling to TD at 1365 ft. | Municipal water mixed Quick-gel, liqui-trol, Quik-FOAM, soda ash, PAC-L, n-seal (mineral fiber) | 1365 | 3–R | LANL, 2003f |
| R-21 | Cañada del Buey | January 2003 | Conventional-circulation air-rotary drilling in an open hole to 237 ft followed by conventional-circulation fluid-assisted air-rotary drilling in an open hole to TD at 995 ft. | Air and municipal water mixed with Quik-FOAM, EZ-MUD | 995 | 1–R | Kleinfelder, 2003f |
| R-22 | Mesa above Pajarito Canyon | December 2000 | A combination of reverse- circulation fluid-assisted air-rotary methods in open hole and with casing advance to 1345 ft followed by reverse-circulation fluid-assisted air-rotary drilling in an open hole to TD at 1489 ft. | Air and municipal water mixed with Quik-FOAM, EZ-MUD | 1489 | 5–R | Ball et al. 2002 |
| R-23 | Pajarito Canyon | January 2003 | A combination of conventional mud-rotary drilling, reverse-circulation fluid-assisted air-rotary drilling in open hole, and reverse-circulation fluid-assisted air-rotary drilling with casing advance to TD of 935 ft. | Municipal water mixed with bentonite, Quick-gel, liqui-trol, Quik-FOAM, soda ash, magna-fiber, PAC-L, n-seal and air with municipal water mixed with Quick-gel, liqui-trol, Quik-FOAM, and soda ash | 935 | 1–R | LANL, 2003g |
| R-25 | Mesa above Cañon de Valle | February 1999 | Reverse-circulation fluid-assisted air-rotary drilling with casing advance to TD of 1942 ft. | Air and municipal water mixed with TORKEASE, Quik-FOAM, EZ-MUD | 1942 | 4–I<br>5–R | Broxton et al. 2001e |

**Table 1-2.**
**Los Alamos National Laboratory Hydrogeologic Characterization Wells (continued)**

| Well | Location | Date Completed | Primary Drilling Methods | Type of Drilling Fluid Used | Total Depth (ft bgs*) | Number of Screens[1] | Reference |
|---|---|---|---|---|---|---|---|
| R-26 | Cañon de Valle | October 2003 | Conventional-circulation fluid-assisted air-rotary drilling in an open hole to 1000 ft; casing installed to 1000 ft; borehole completed by conventional-circulation mud-rotary drilling in an open hole to TD at 1490.5 ft. | Air and municipal water mixed with Quik-FOAM, EZ-MUD | 1490.5 | 1–I<br>1–R | Kleinfelder, 2004f |
| R-28 | Mortandad Canyon | December 2003 | Conventional-circulation fluid-assisted air-rotary methods with casing advance to 80 ft followed by conventional-circulation fluid-assisted air-rotary drilling in an open hole to TD at 1005 ft. | Air and municipal water mixed with Quik-FOAM, EZ-MUD | 1005 | 1–R | Kleinfelder, 2004d |
| R-31 | Ancho Canyon | March 2000 | A combination of reverse- circulation fluid-assisted air-rotary methods in open hole and with casing advance to 787 ft followed by reverse- circulation fluid-assisted air-rotary methods with casing advance to TD at 1103 ft. | Air and municipal water mixed with Quik-FOAM, EZ-MUD | 1103 | 1–I<br>4–R | Vaniman et al. 2002 |
| R-32 | Pajarito Canyon | January 2003 | Reverse-circulation fluid-assisted air-rotary drilling in open hole to 908; install casing; complete hole by conventional-circulation mud rotary drilling in an open hole to TD at 1008 ft. | Air and municipal water mixed with Quick-gel, liqui-trol, Quik-FOAM, and soda ash in the upper part and municipal water mixed with Quick-gel, liqui-trol, EZ-MUD, magma-fiber, PAC-L, n-seal in the lower part | 1008 | 3–R | LANL, 2003h |
| R-33 | Ten Site Canyon | October 2004 | Conventional-circulation air-rotary and fluid-assisted air-rotary drilling methods in an open hole to 1030 ft followed by reverse-circulation fluid-assisted air-rotary drilling methods in an open hole to TD at 1140 ft. | Air and municipal water mixed with Quik-FOAM, EZ-MUD | 1140 | 1–R | Completion report not available |
| R-34 | Cedro Canyon | August 2004 | Conventional-circulation air-rotary and fluid-assisted air-rotary drilling methods in an open hole to TD at 1065 ft. | Air and municipal water mixed with Quik-FOAM and EZ-MUD | 1065 | 1–R | Completion report not available |
| MCOB T-4.4 | Mortandad Canyon | June 2001 | Reverse-circulation fluid-assisted air-rotary drilling using casing advance to 130 ft followed by reverse-circulation fluid-assisted air-rotary drilling in an open hole to TD at 767 ft. | Air and municipal water mixed with Quik-FOAM, EZ-MUD | 767 | 1–I | Broxton et al. 2002 |

**Table 1-2.**
**Los Alamos National Laboratory Hydrogeologic Characterization Wells (continued)**

| Well | Location | Date Completed | Primary Drilling Methods | Type of Drilling Fluid Used | Total Depth (ft bgs*) | Number of Screens[1] | Reference |
|---|---|---|---|---|---|---|---|
| MCOB T-8.5 | Mortandad Canyon | June 2001 | Reverse-circulation fluid-assisted air-rotary drilling using casing advance to 130 ft followed by reverse-circulation fluid-assisted air-rotary drilling in an open hole to TD at 740 ft. | Air and municipal water mixed with Quik-FOAM, EZ-MUD | 740 | — | Broxton et al. 2002 |
| R-6i | Los Alamos Canyon | December 2004 | Conventional-circulation air-rotary and fluid-assisted air-rotary drilling in an open hole to TD at 660 ft. | Air and municipal water mixed with Quik-FOAM | 660 | 1–I | Completion report not available |
| R-9i | Los Alamos Canyon | March 2000 | Reverse-circulation fluid-assisted air-rotary drilling in an open hole to TD at 322 ft. | Air and municipal water mixed with EZ-MUD | 322 | 2–I | Broxton et al. 2001c |
| CdV-16-1(i) | Cañon de Valle | November 2003 | Conventional-circulation fluid-assisted air-rotary drilling in an open hole to TD at 683 ft. | Air and municipal water mixed with Quik-FOAM, EZ-MUD | 683 | 1–I | Completion report not available |
| CdV-16-2(i) | Cañon de Valle | December 2003 | Conventional-circulation fluid-assisted air-rotary drilling in an open hole to TD at 1063 ft. | Air and municipal water mixed with Quik-FOAM, EZ-MUD | 1063 | 2–I | Completion report not available |
| CdV-16-3(i) | Cañon de Valle | January 2004 | Conventional-circulation fluid-assisted air-rotary drilling in an open hole to TD at 1405 ft. | Air and municipal water mixed with Quik-FOAM, EZ-MUD | 1405 | — | Completion report not available |

* bgs = below ground surface
[1] R = screen(s) in regional groundwater; I = screen(s) in intermediate-depth (perched) groundwater
[2] TD = total depth

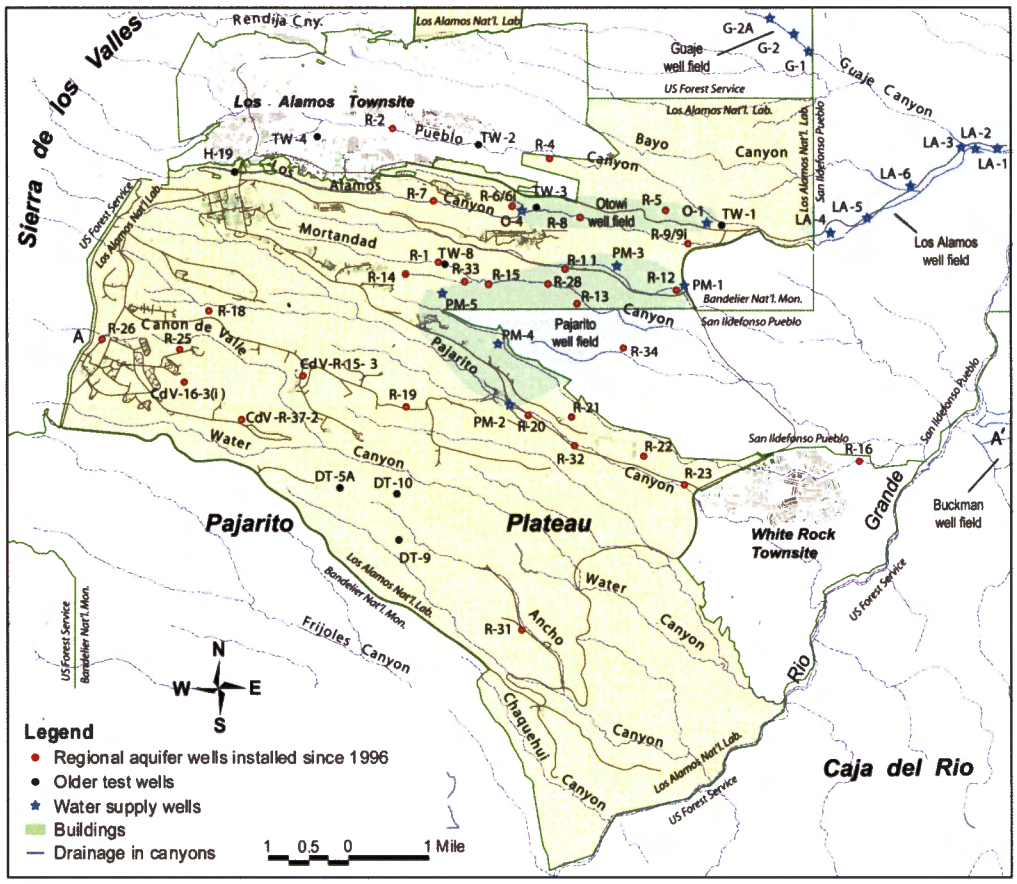


**Figure 1-3.** Locations of the Hydrogeologic Workplan characterization wells.

# 2.0 HYDROGEOLOGY

Groundwater occurs in three settings beneath the Pajarito Plateau: alluvium, intermediate perched saturated zones, and the regional aquifer. The major source of recharge to the regional aquifer is precipitation within the Sierra de los Valles. However, alluvial groundwater on the Pajarito Plateau is a source of recharge to underlying intermediate perched saturated zones and to the regional aquifer.

This section describes the conceptual understanding of the hydrogeology beneath the Pajarito Plateau. The conceptual models of the hydrogeologic system described here are based on empirical observations combined with knowledge of geologic and hydrologic processes. These conceptual models are the foundation of the numerical models described in Section 4. First, the geologic conceptual model is described to provide an understanding of the geologic units that are present. Second, the connection between geology and hydrology is discussed because the geology is the first-order control on the Pajarito Plateau hydrology. Finally, the conceptual models for the alluvial groundwater, perched intermediate groundwater, and the regional aquifer are described.

## 2.1 Geologic Conceptual Model

The geologic conceptual model for the LANL site is developed from (1) past studies of site and regional geology that predate implementation of the Hydrogeologic Workplan, including over 50 years of mapping, drilling, and regional geophysical studies; (2) borehole data collected specifically for the Hydrogeologic Workplan; and (3) integration of results from current Hydrogeologic Workplan studies with other studies in the region, particularly those that are brought together by the Española Basin Technical Advisory Group. Table 2-1 provides a summary of the types of information used to develop the geologic conceptual model and Appendix 2-A contains a detailed description of the geologic types of data used to develop the conceptual model.

There are localized subsurface geologic data associated with drilling boreholes and regional geologic data, surface and subsurface, which are obtained by aerial surveys and work done by others on a regional scale. The localized subsurface geologic data are obtained from:

- Cuttings and core
- Borehole geophysical data
- Borehole video logs
- Drilling rates and character

.

**Table 2-1.**
**Summary of Geologic Data**

| Data Type | Purpose | Data Collection | Data Records | Archives |
|---|---|---|---|---|
| Lithologic Information from Cuttings | Direct measurements of the top and bottom and character of the hydrogeologic units at each borehole. Correlations of rock units among boreholes are key components of the site-wide 3-D geologic model for the plateau. | Approximately 500 to 700 ml of bulk drill cuttings were collected every 5 ft, as conditions permitted, to the total depth (TD) of each boring.<br>Cuttings were visually examined and a small subset of core and cuttings was selected for additional characterization: X-ray diffraction for mineralogy, X-ray fluorescence for rock chemistry, thin-section petrography, and $^{40}Ar/^{39}Ar$ age dating. | Lithologic logs summarize rock lithologies, alteration features, and stratigraphic contacts from visual examination and interpretations of borehole geophysical logs. | Core and cuttings are currently archived at the ENV Division Sample Management Facility located at Technical Area 3, building 03-0271-101. All borehole materials are stored in core boxes labeled with the well name, box number, and footage range for the box. |
| Lithologic Information from Core | Core was collected to fulfill a number of characterization objectives, including:<br>• geology of perched saturated zones and aquitards<br>• hydrologic and chemical analyses of vadose-zone samples (e.g. moisture, anions)<br>• hydraulic properties of selected hydrogeologic units. | Core was collected from dedicated core holes and from selected intervals in some regional aquifer boreholes. | Same as for cuttings above. | Same as for cuttings above |

**Table 2-1.**
**Summary of Geologic Data (continued)**

| Data Type | Purpose | Data Collection | Data Records | Archives |
|---|---|---|---|---|
| Drilling Information | Observations about drilling characteristics by the drillers and on-site geologists contributed to understanding the hydrogeology of the boreholes. | Major lithologic and stratigraphic contacts were commonly marked by significant changes in drill penetration rates. Drilling rates are primarily affected the competency of the rocks being penetrated. Hard rock units have slow drilling rates, whereas less-competent rocks were drilled more rapidly. Important information about water-bearing strata was obtained when drillers noted changes in the drilling fluids circulating through the borehole. | These observational data were recorded in field logs, and they provided supplemental information that aided the interpretation of hydrogeologic data from other sources such as cuttings and geophysical logs. | N/A |
| Borehole Geophysical Data | Determine the geologic and hydrologic characteristics of the vadose zone, perched saturated zones, and regional aquifer. Preliminary logs were used by contractor, DOE, and LANL personnel to help select well screen locations and to evaluate borehole conditions prior to well construction. | *LANL*: caliper, spontaneous potential, single-point resistance and induction, and natural gamma radiation logs.<br>*Contractor:* wire-line logging service was contracted to obtain a more extensive suite of borehole geophysical logs once the borehole reached total depth | Preliminary results of geophysical logs were generated in the logging truck at the time the geophysical services were performed.<br>Contractor reprocessed the field measurements to correct them and to combine the logs into a single presentation enabling integrated interpretation. | Results of contractor geophysical logging and analysis are summarized in an interpretive report that is included in each well completion report. |

**Table 2-1.**
**Summary of Geologic Data (continued)**

| Data Type | Purpose | Data Collection | Data Records | Archives |
|---|---|---|---|---|
| Borehole Video Logs | To obtain lithologic information and to help determine stratigraphic contacts; visual examination of borehole walls for evidence of perched saturation; document water levels in the boreholes; document the as-built condition of installed well components; assess the effectiveness of well development techniques; to assess problematic borehole conditions and to guide fishing operations for tools and equipment lost downhole. | Borehole video was used in each borehole or completed well. The videos were viewed by geologists to assess geologic conditions. Often used in conjunction with geophysical logs to determine the locations of perched zones in some boreholes and the presence and nature of fractures. | Video logs were collected during installation of workplan wells. | N/A |
| Regional Airborne Surveys | Focus groundwater investigations by defining the conductivity structure beneath the plateau. Gravity data were used to help define regional structure beneath the Pajarito Plateau. | A total of 762 line kilometers of MegaTEM® time domain EM data and magnetic data were collected (80% of LANL area). Flight lines spaced at 105 m within the laboratory boundaries, and at 210 m in buffer zones. Lines oriented N20E, with tie lines about 2000-meter spacing. | Maps of Residual Magnetic Intensity (RMI), apparent conductance and conductivity depth slices at various depths, multiparameter profiles with conductivity-depth-transform (CDT) sections for flight lines and digital archives of line and grid data. | All of the processing assumed a "layered-earth" model, and inversions were: single points/multiple depths (1-D), multiple depths along individual flight lines (2-D), or a constant depth on multiple flight lines (2-D). The results of all three models, for each flight line are available as Adobe PDF files. |

Note: N/A = not applicable

Geologic data derived from regional-scale studies were obtained from multiple sources, including:

- Surface geophysical data were used to help constrain the site-wide geologic model (Appendix 2-A). These data include regional gravity data, airborne electromagnetic data, high resolution resistivity, and magnetotellurics. Gravity data were used to help define regional structure beneath the Pajarito Plateau. Airborne electromagnetic data, high resolution resistivity, and magnetotelluric data were used to focus groundwater investigations by defining the conductivity structure beneath the plateau
- Numerous local and regional mapping projects and geological studies have provided important information supporting development of geologic conceptual models and digital realizations of these models.
- Española Basin workshops were hosted annually by the Española Basin Technical Advisory Group and sponsored by the U.S. Geological Survey, the New Mexico Bureau of Geology and Mineral Resources, Los Alamos National Laboratory, and the city of Santa Fe.
- The Seismic Hazards program at LANL was an important source of information about faults and fractures in the vicinity of the Laboratory.
- Students and their advisors from the graduate programs from the University of New Mexico and New Mexico State University, New Mexico Institute of Mining and Technology, and the University of Texas have provided additional hydrogeologic information for the Jemez volcanic field, the Espanola Basin, and the Puye Formation.

### 2.1.1 Goals of the Geologic Model

- Define the geologic setting of the groundwater system beneath the Pajarito Plateau
- Relate lithologic properties of rocks to groundwater flow characteristics and rock/water interactions
- Provide a benchmark for comparing new data to predicted geology
- Improve selection of new well sites based on iterative evaluation of hydrogeologic information
- Provide a framework for numerical flow and transport models of the vadose and saturated zones

### 2.1.2 Site-Wide Geology

The discussion of site-wide geology presented here is condensed from a summary by Broxton and Vaniman (2005). More detailed, fully referenced information is available in that publication. The deep characterization wells drilled in the time period from 1997 to 2004 have provided the foundation for constructing the geologic framework surfaces presented in this section.

#### 2.1.2.1 Regional Setting

The Pajarito Plateau lies at the volcanically and seismically active boundary between the Colorado Plateau and the Rio Grande Rift in north-central New Mexico (Figure 2-1). The Rio Grande rift is a major geologic feature that consists of north-trending, fault-bounded basins

extending from central Colorado to northern Mexico. The local area of subsidence, termed the Española Basin, lies between two larger basins—the Albuquerque Basin to the south and San Luis Basin to the north (Kelley, 1978). The Española Basin is about 70 km (44 mi) long and 60 km (37 mi) wide. The plateau overlies the deepest part of the west-tilted Española Basin adjacent to the highlands of the Jemez volcanic field. Geologic units consist of Miocene and Pliocene basin-fill deposits and interfingering volcanic rocks from the Jemez and Cerros del Rio volcanic fields. Miocene and Pliocene sedimentary and volcanic rocks are covered by Pleistocene ash-flow tuffs making up the Pajarito Plateau.

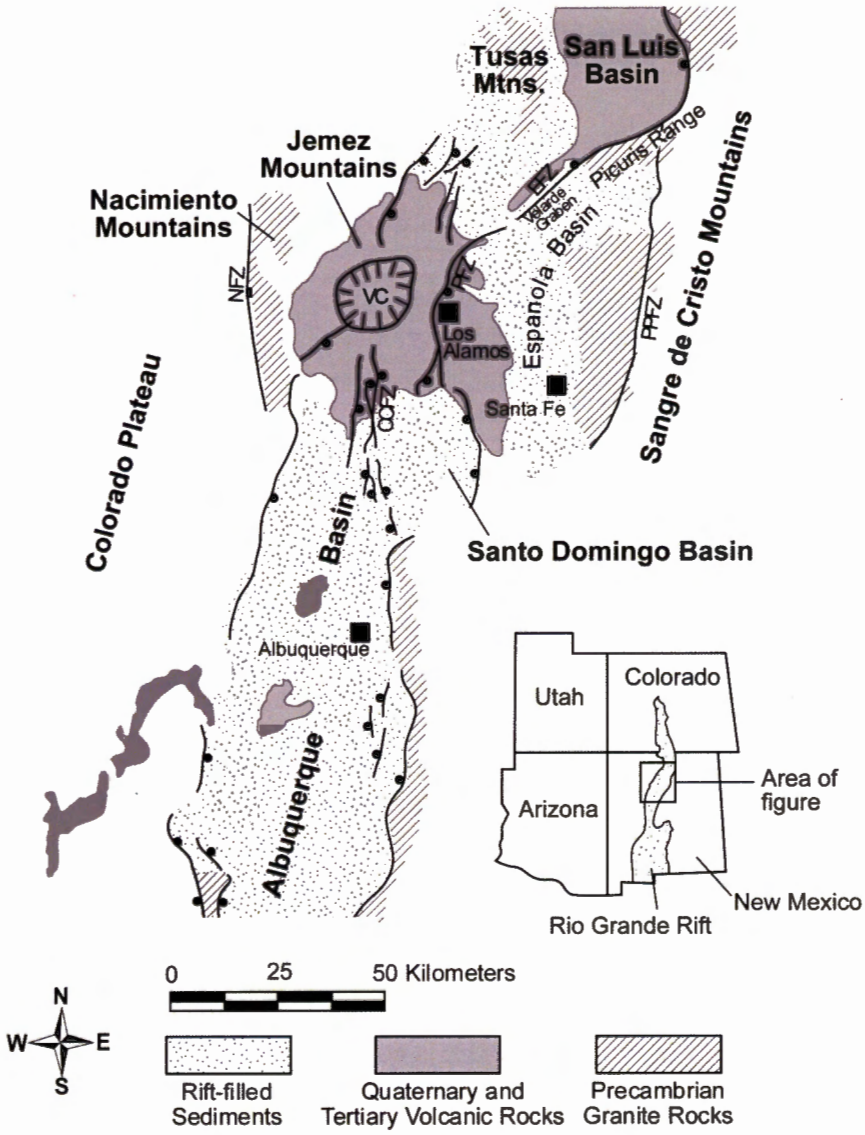


**Figure 2-1.** Locations of major structural and geologic elements near LANL. Major fault systems are shown with ball on downthrown side. VC is the Valles Caldera complex; NFZ is the Nacimiento fault zone; CCFZ is the Cañada del Cochiti fault zone; PFZ is the Pajarito fault zone; and PPFZ is the Picuris-Pecos fault zone.

The western structural margin of the Española Basin is partly covered by rocks of the Jemez volcanic field, but probably includes a broad zone of north-trending faults such as the Cañada de Cochiti fault zone (Figure 2-1) that cut older volcanic units in the south-central part of the volcanic field (Gardner and Goff, 1984). The present active western boundary of the Española Basin is the Pajarito fault zone, a narrow band of north- and northeast-trending normal faults that delineate the western margin of the Pajarito Plateau. Neogene displacement along the Pajarito fault zone is dominantly down to the east with episodic faulting indicated by progressively larger offsets in older rock units.

Gravity data (Biehler et al., 1991; Ferguson et al., 1995) indicates the deepest part of the Española Basin coincides with three deep, intrabasinal grabens arrayed along the Pajarito and Embudo fault systems. From north to south, these subbasins include the Velarde graben (Manley, 1979, 1984), a north-northeast trending basin beneath Santa Clara pueblo, and a north-trending basin near Los Alamos. The Pajarito fault zone forms the western boundary of the Los Alamos subbasin (Biehler et al., 1991; Ferguson et al., 1995; Smith, 2004). Gravity data suggest that the eastern boundary is bounded by buried faults that lie east of the southern projections of the Rendija Canyon and Guaje Mountain (Ferguson et al., 1995), but the location and size of faults in this area are not well known.

The basement of the Española Basin is an eroded terrane of Eocene-Precambrian aged rocks uplifted during the Laramide mountain-building episode (orogeny, approximately 65 million years ago (m.y.a.). One of these uplifted areas, the Pajarito uplift, is bounded on the east by the Picuris-Pecos fault in the Sangre de Cristo Range and on the west by the Pajarito fault (Cather, 2004; Smith, 2004). At the time of Laramide uplift, the Pajarito fault was a westward-verging reverse fault, but it was reactivated as a down-to-the-east normal fault during Neogene (within the last 24 m.y.) subsidence of the Española Basin.

#### 2.1.2.2. Structural Geology of the Pajarito Plateau

The Pajarito fault zone and its associated structures are the most prominent tectonic features of the LANL site (Figure 2-2). The fault, which forms a 120-m (400-ft) high escarpment on the western margin of the plateau, has the surface expression of a large, north-trending, faulted monocline. Along strike the fault varies from a simple normal fault to broad zones of small faults, faulted monoclines, and unfaulted monoclines. These varied styles of deformation are all considered expressions of deep-seated normal faulting. The amount of fault displacement for older rock units is not known because thick deposits of Bandelier Tuff cover critical relations. Stratigraphic separation on the Tshirege Member of the Bandelier Tuff (1.22 Ma) ranges between 80 and 120 m (260 to 400 ft) along the segment of the fault west of LANL (Gardner et al., 1999). Holocene movements (within the last 10,000 years) and historic seismicity indicate this fault system is still active.

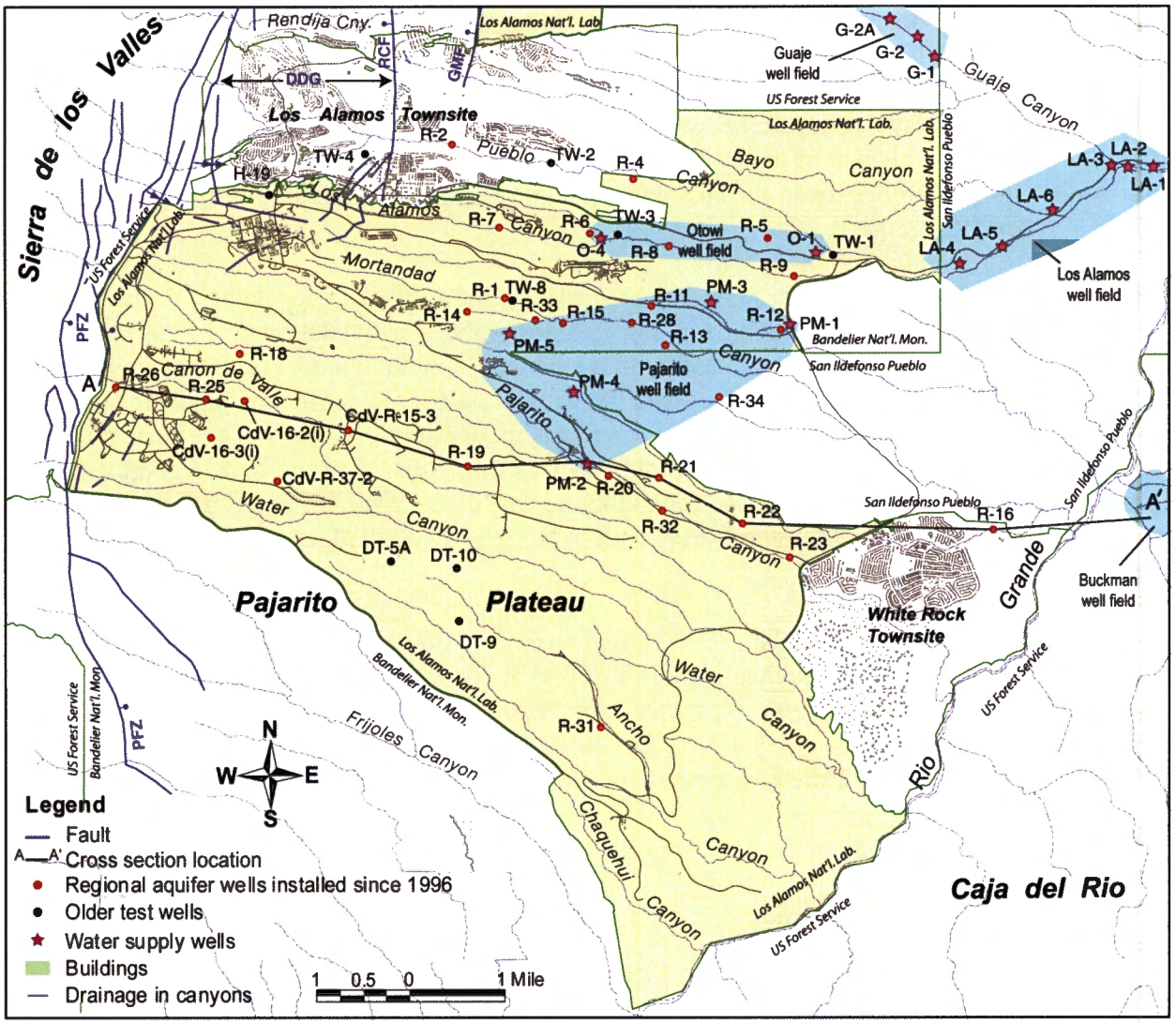


**Figure 2-2.** Location map of the central Pajarito Plateau.

Yellow-shaded area is the Los Alamos National Laboratory. Also shown are the municipalities of Los Alamos and White Rock. East- and southeast-trending canyons are incised into the plateau. Water supply wells are shown as blue stars and the water-supply well fields are indicated in blue shading; additional wells of Guaje well field extend north of this map. The Buckman well field provides water to Santa Fe. Water supply wells LA-1 through LA-6 are no longer used for municipal water production. New regional aquifer wells installed since 1998 are shown as red dots. Older test wells are shown as black dots. Line A-A' shows the location of the cross-section in Figure 2-5. Main elements of the Pajarito fault zone are shown in blue. PFZ is the main trace of the Pajarito fault zone; RCF is the Rendija Canyon fault; GMF is the Guaje Mountain fault; and DDG is the Diamond Drive graben. Faults modified from Gardner et al. (2001) and Lewis et al. (2002).

Other major faults on the Pajarito Plateau include the Rendija Canyon and Guaje Mountain faults. The Rendija Canyon fault, located in the northern part of the plateau, is a north-trending normal fault with down-to-the-west displacement. The Rendija Canyon fault dies out as a simple normal fault on the north side of LANL. Southward across LANL it is replaced by a broad arc of small-displacement faults that trend in a southwesterly direction towards the main trace of the Pajarito fault. The Guaje Mountain fault lies east of and is generally parallel to the Rendija Canyon fault. It is also a north-trending normal fault with down-to-the-west displacement. Surface traces of the Guaje Mountain fault die out north of LANL.

Additional faults are probably buried beneath the cover of Bandelier Tuff on the Pajarito Plateau. Where exposed along the east side of the basin, Santa Fe Group rocks are cut by numerous north-trending normal faults. Similar fault densities and orientations are probably present in the basin-fill sediments beneath the Pajarito Plateau. Unfortunately, existing well data are of limited use in defining these structures because of the complex depositional patterns and interfingering relations of Pre-Bandelier rock units beneath the plateau.

#### 2.1.2.3 Volcanic Setting of the Pajarito Plateau

The Pajarito Plateau overlaps two volcanic fields whose activities were coeval with rifting. The plateau is bounded on the west by the Jemez volcanic field, a nearly circular volcanic field 72 km (45 mi) in diameter that includes the Valles caldera (Figure 2-1). The plateau is bounded on the southeast by the smaller Cerros del Rio volcanic field. The Jemez volcanic field was an important source of sediments during basin subsidence and the basin-fill sediments interfinger laterally with rocks of both volcanic fields.

**Cerros del Rio Volcanic Field**

The Cerros del Rio volcanic field is mainly exposed as the Caja del Rio basalt plateau on the east side of the Rio Grande. The surface of the basalt plateau ranges in elevation from 6000 to 7396 ft. The exposed part of the volcanic field extends about 26 mi in a north-south direction and is up to 12 mi wide. The volcanic field extends an additional 7 mi to the west beneath the Pajarito Plateau, where Bandelier Tuff covers it. The exposed portion of the volcanic field is made up of about a dozen volcanoes and >70 vents of cinder cones, plugs, and tuff rings. Basalts and related intermediate-composition lavas are the predominant rock types, and most were erupted between 2.3 and 2.8 Ma. The Rio Grande cuts a south-southwesterly course through the northwestern part of the basalt plateau, forming White Rock Canyon (Broxton and Vaniman 2005).

**Jemez Volcanic Field**

The Jemez volcanic field lies at the intersection of the northeast-trending Jemez lineament, a major crustal structure of Precambrian ancestry, and north-trending faults of the Rio Grande Rift. Volcanism over the last 14 million years (m.y.) built up the Jemez Mountains, while contemporaneous tectonic rifting resulted in subsidence of the Española Basin, the area extending from the Valles caldera to the western margin of the Sangre de Cristo Mountains. The Jemez volcanic highlands were a major source of Miocene and Pliocene volcaniclastic sediments that were deposited as alluvial fans in the western part of the Española Basin. Eastward, these volcaniclastic deposits interfinger with arkosic basin-fill sands and gravels derived predominantly from Precambrian–cored uplifts on the east side of the Española Basin.

The Jemez volcanic field began to develop between ~14 and 10 Ma with the eruption of predominantly basaltic and rhyolitic rocks of the Keres Group. Major rock units of the Keres Group include:

- **~14.5 to 7.6 Ma:** Basalts that were erupted predominantly in the southern and northeastern parts of the volcanic field.
- **~12.4 to 8.8 Ma:** The Canovas Canyon Rhyolite of the Keres Group, made up of rhyolite domes and associated pyroclastic deposits that were erupted from vents aligned along faults of the Cañada de Cochiti fault zone.
- **~10.6 to 7.1 Ma:** 1000 $km^3$ of andesite and subordinate basalt and rhyodacite that were erupted as part of the Paliza Canyon Formation.
- **7.1 to 6.0 Ma:** High-silica rhyolite plugs, domes, and tuffs of the Bearhead Rhyolite, including thick tuffaceous deposits of the Peralta Canyon Member, that were erupted from along faults of the Cañada de Cochiti fault zone.

The period from 6 to 7 Ma also coincided with a transition to predominantly dacitic volcanism throughout the volcanic field (Gardner et al., 1986). Porphyritc dacitic lavas of the Tschicoma Formation of the Polvadera Group were erupted primarily between 5 and 3 Ma (Goff and Gardner, 2004; G. WoldeGabriel, personal communication) from large, overlapping dome complexes typified by the extensive exposures of this formation in the highlands of the Sierra de los Valles west of the Pajarito fault zone.

Volcanism in the Jemez volcanic field reached a climax with eruption of the Bandelier Tuff from the Toledo and Valles calderas. The Bandelier Tuff has two members, each consisting of a basal pumice fall overlain by a petrologically related succession of ash-flow tuffs. Eruption of the two members was accompanied in each case by caldera collapse. The Otowi Member (1.61 Ma) was erupted from an earlier caldera that was nearly coincident with, and was largely destroyed by, the younger Valles caldera. The Valles caldera formed during the eruption of the Tshirege Member (1.22 Ma). About 300 $km^3$ of high-silica rhyolite magma was erupted for each of the two Bandelier Tuff members. Deposits of Bandelier Tuff form radially distributed flat-topped tuff plateaus that dip away from the central volcanic highlands. The Pajarito Plateau at LANL is made up of Bandelier Tuff that flowed more than 21 km across the western Española Basin.

An interval of about 400,000 years separated the eruptions of the two Bandelier Tuff members. During this interval, domes of Cerro Toledo Rhyolite were emplaced northeast and southeast of the earlier Toledo caldera. Tephras from these domes were deposited as ash and pumice falls over the Sierra de los Valles and Pajarito Plateau. The Cerro Toledo interval is a mixture of reworked Cerro Toledo Rhyolite tephras and Tschicoma dacite sediments eroded from the Sierra de los Valles.

## 2.2 Stratigraphic Framework of the Pajarito Plateau

A generalized diagram showing the stratigraphic sequence of rock units of the Pajarito Plateau is shown in Figure 2-3. Rock units are described below from oldest to youngest. The stratigraphy, lithology, and geochronology of the Santa Fe Group beneath the Pajarito Plateau are known primarily through drillhole data because Bandelier Tuff covers these older rock units. Based on

exposures near the Rio Grande and new drillhole data, the Santa Fe Group beneath the Pajarito Plateau is believed to include, in ascending order, the Tesuque Formation, older fanglomerate deposits of the Jemez volcanic field, the Totavi Lentil and older river gravels, pumice-rich volcaniclastic rocks, and the Puye Formation. Recent mapping of basin sediments north and east of Los Alamos suggests that the Tesuque Formation, as used in this report, may include rocks of the Chamita Formation (Koning et al., 2005). The older fanglomerate and pumice-rich volcaniclastic rocks are new units that are given provisional informal names. These units are generally similar to the Puye and Cochiti Formations, but are older than rocks normally assigned to them. Redefining the Puye and Cochiti Formations is beyond the scope of this report, and the older fanglomerates and pumice-rich volcaniclastic rocks are treated as informal units until they can be incorporated into the new stratigraphic framework being developed for the Española Basin (see discussion in Smith, 2004). In the vicinity of the Pajarito Plateau, Santa Fe Group deposits interfinger with or are overlain by volcanic rocks of the Jemez and Cerros del Rio volcanic fields. Rock units older than the Santa Fe Group (e.g., early Tertiary and older rocks) are not described here because they underlie the Laboratory at considerable depth and have not been penetrated by deep drillholes. These prebasin rock units are described in papers by Biehler et al. (1991), Cather (1992 and 2004), Ferguson et al. (1995), and Smith (2004).

The total thickness of the Santa Fe Group in the eastern and northern part of the Española Basin is as much as 1450 m (4800 ft) (Galusha and Blick, 1971). The Yates La Mesa no. 2 exploration well penetrated 1200 m (3966 ft) of Tesuque Formation in the south-central part of the basin (Meyer and Smith, 2004). However, the thickest Santa Fe Group deposits are believed to occur in the western Española Basin beneath the Pajarito Plateau (Kelly, 1978; Biehler et al., 1991; Ferguson et al., 1995; Smith, 2004). The thickness of these deposits is not well known because the deepest wells on the plateau (e.g., PM-5 with a depth 950 m; 3110 ft) do not fully penetrate the basin-fill sediments. Biehler et al. (1991) estimate that the Santa Fe Group in the central basin might be as much as 2000 m (6650 ft) thick based on gravity data. Cross sections by Kelly (1978) and Koning and Maldonado (2001) show up to 2750 to 3300 m (9000 to 10000 ft) of Santa Fe Group deposits in the central and western parts of the basin. Drillhole data and outcrops indicate that Santa Fe Group deposits are considerably thinner (<500 m; <1640 ft) west of the Pajarito fault (Goff and Gardner, 2004).

This section includes structure contour maps (contoured elevations at the top or bottom of a hydrogeologic unit) and isopach maps (contoured maps showing the unit thickness). These maps, which are prepared by interpolation between points of one-dimensional drillhole data, provide information on the extent of a unit beneath the site and the relative contribution of each unit to the hydrostratigraphy at any given point. Isopach and structure-contour figures representing key hydrostratigraphic units include:

- Cerro Toledo interval (Figure 2-4),
- Otowi Member ash flows (Figure 2-5),
- Guaje Pumice Bed at the base of the Otowi Member (Figure 2-6),
- Cerros del Rio lavas (Figures 2-7 and 2-8),
- Pumiceous volcaniclastic rocks (Figure 2-9).

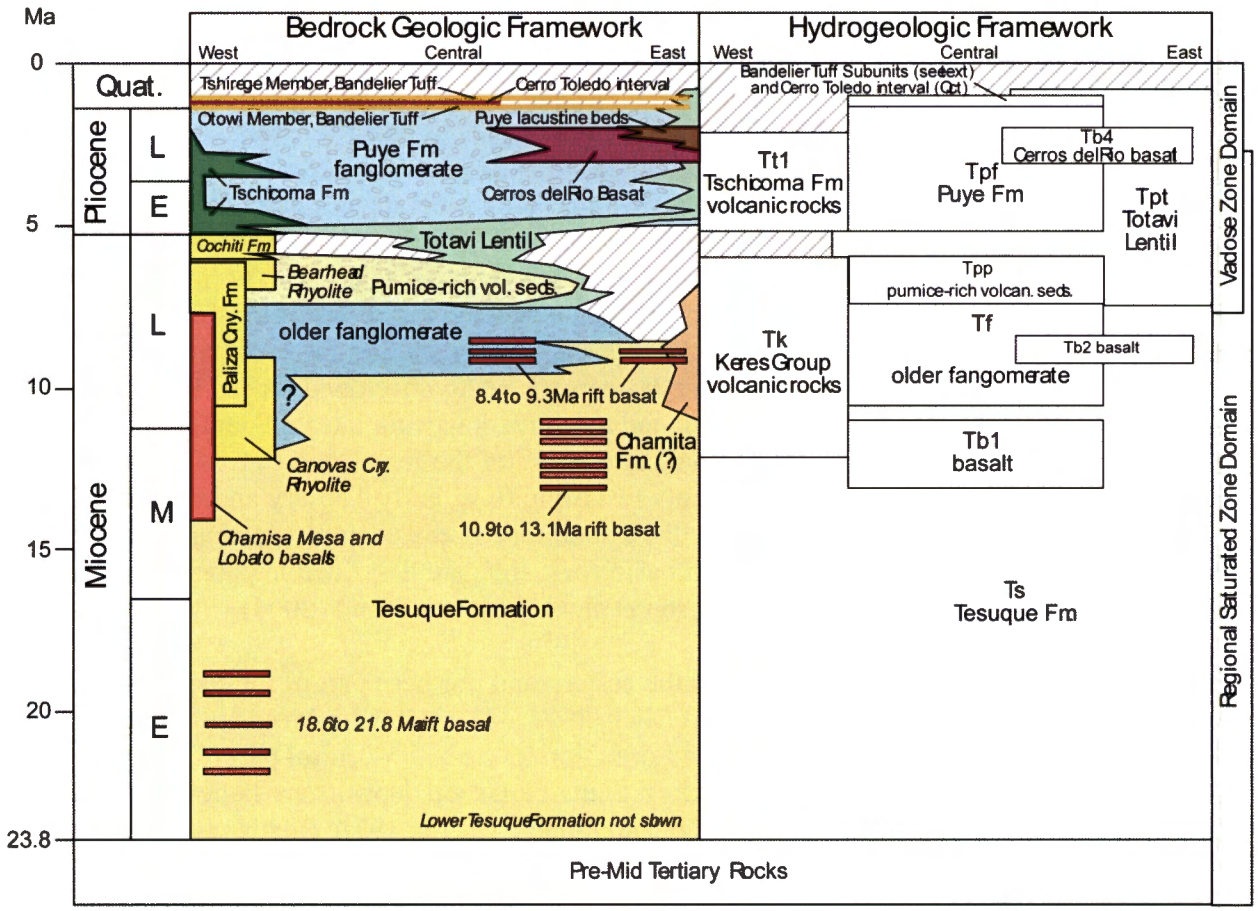


**Figure 2-3.** Pajarito Plateau stratigraphy and hydrogeologic units as used in this report. The bedrock geologic framework shows the stratigraphy of the plateau and the adjacent Sierra de los Valles. Units with italicized names are not exposed or penetrated by boreholes in the immediate vicinity of the plateau, but they are coeval units of the Jemez volcanic field that may be important source rocks for plateau deposits. The hydrogeologic framework shows units that are defined for site-wide numerical modeling (Broxton and Vaniman, 2005).

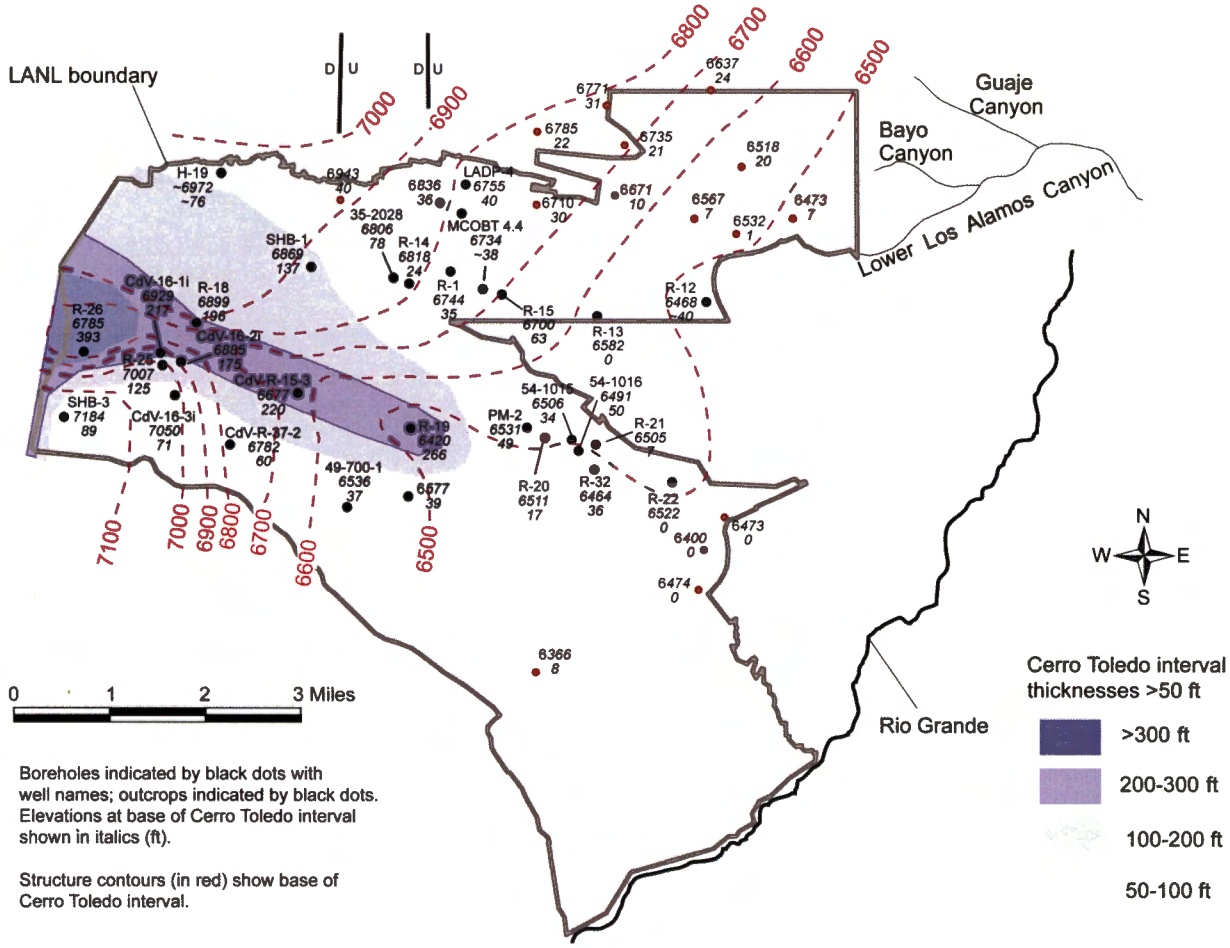


**Figure 2-4.** Structure contour and isopach map for the Cerro Toledo interval. Structure contours for base of unit indicate that Cerro Toledo filled a broad southeast-trending paleovalley incised into the Otowi Member (see isopach map for Otowi Member in Figure 2-5). The thickest Cerro Toledo deposits coincide with the axis of the paleovalley.

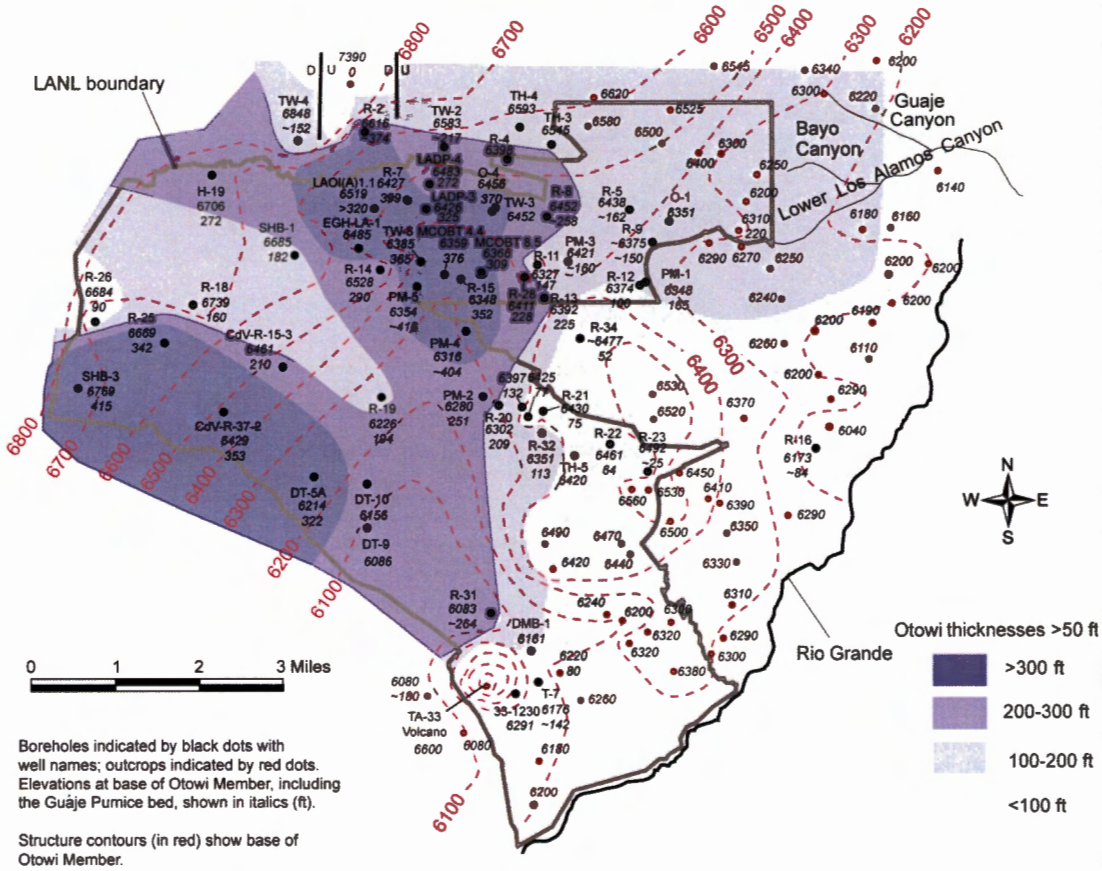


**Figure 2-5.** Structure contour and isopach map for the Otowi Member of the Bandelier Tuff. Structure contours are for base of Guaje Pumice Bed and show the paleotopography prior to eruption of the Otowi Member. Otowi ash-flow tuffs filled a broad north-trending paleovalley bounded by the Sierra de los Valles highlands on the west and the Cerros del Rio basaltic highland on the east. The variable thickness of the Otowi Member on the western side of the plateau represents deep erosion of these poorly consolidated nonwelded tuffs prior to eruption of the Tshirege Member.

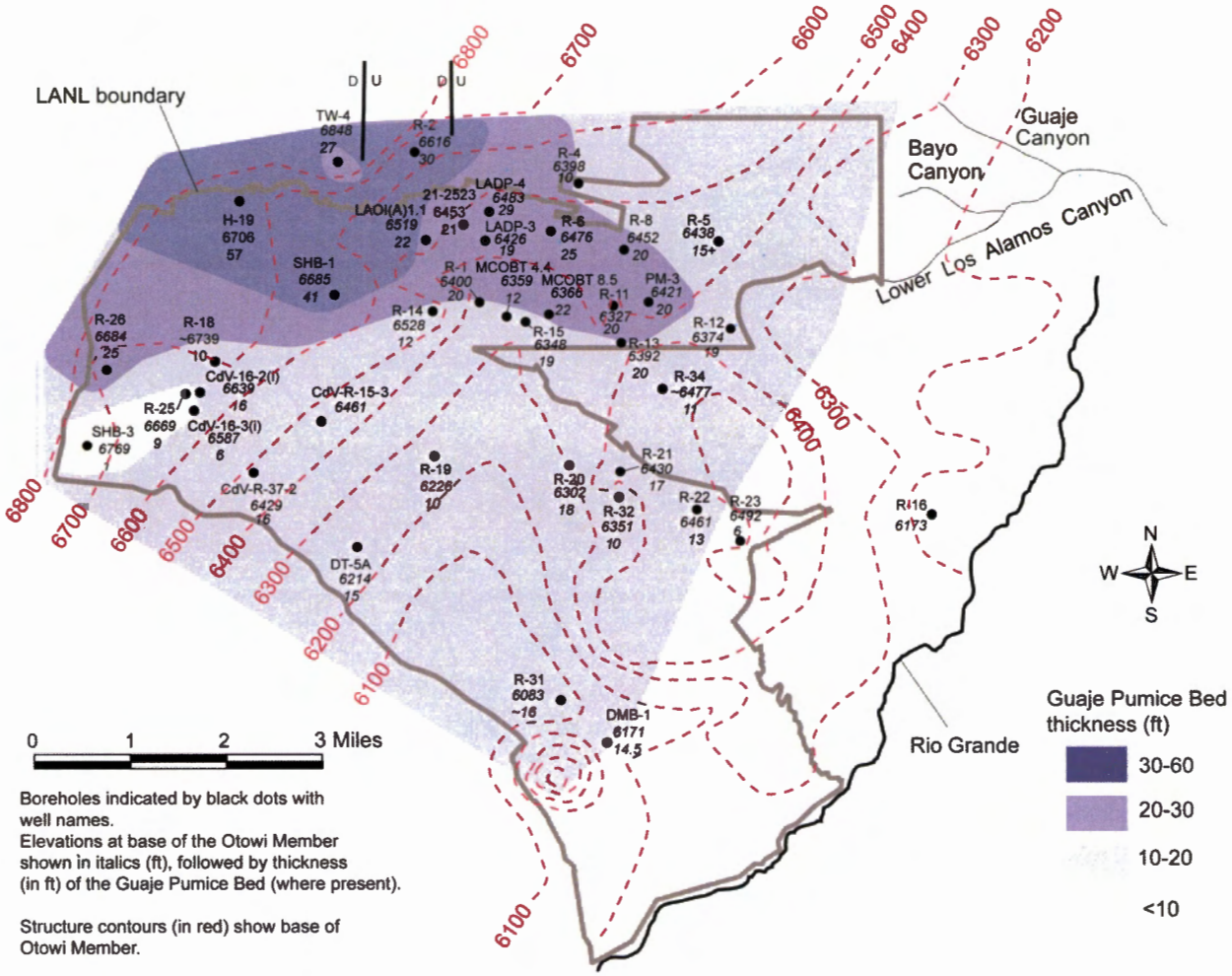


**Figure 2-6.** Isopach and structure contour map of the Guaje Pumice Bed.

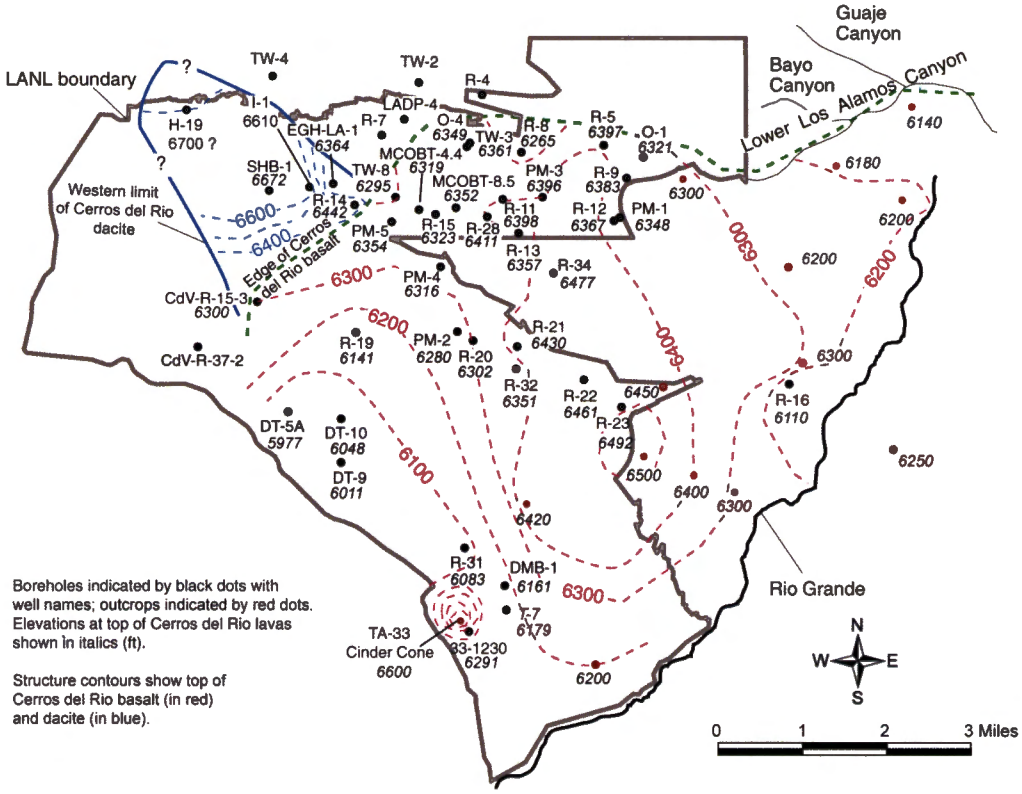


**Figure 2-7.** Structure contour for the top of Cerros del Rio basalt and western dacite on the Pajarito Plateau. Green dashed line indicates the northern and western extent of the Cerros del Rio volcanic field. Blue line indicates western extent of dacitic lavas that were contemporaneous with the basalts. Top of Cerros del Rio basalts formed broad north-trending highland on east side of plateau. This highland is now covered by Bandelier Tuff.

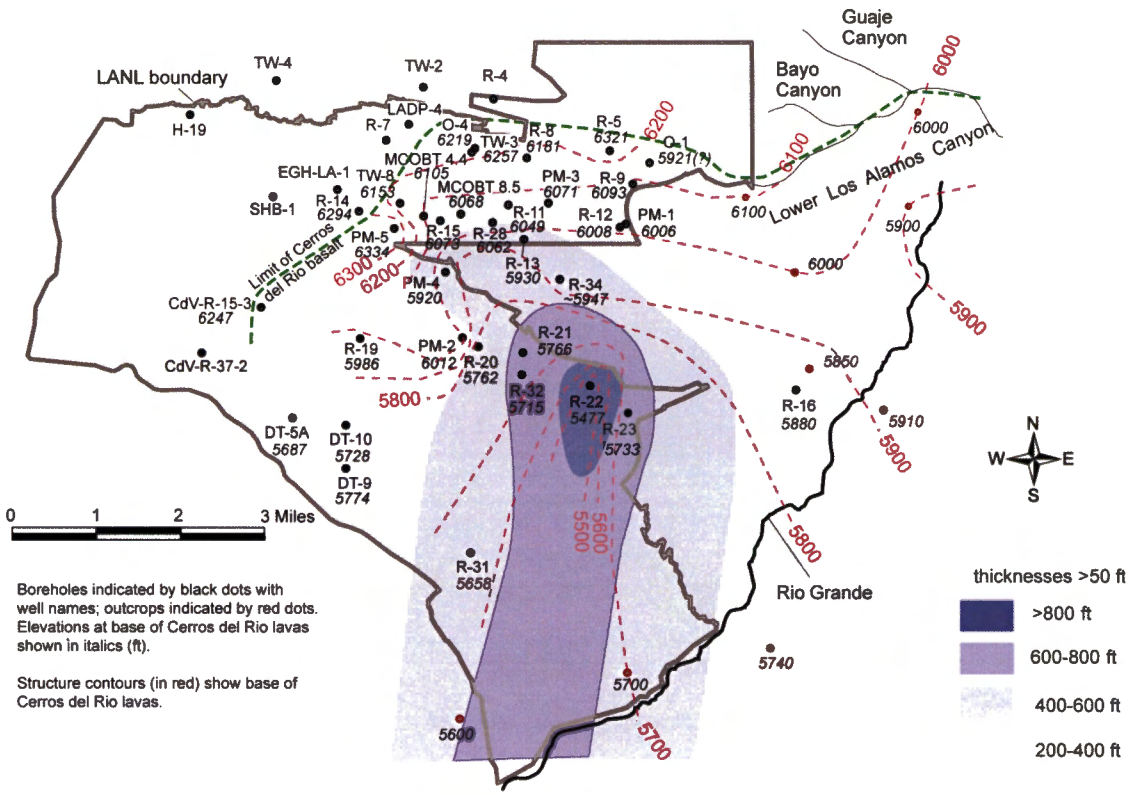


**Figure 2-8.** Structure contour for the base of Cerros del Rio basalt with isopachs showing the cumulative thickness of flows. Green dashed line indicates the northern and western boundary of the Cerros del Rio volcanic field. The maximum thickness of basalt corresponds with structural-contour lows, suggesting that the basalts accumulated in topographic basins.

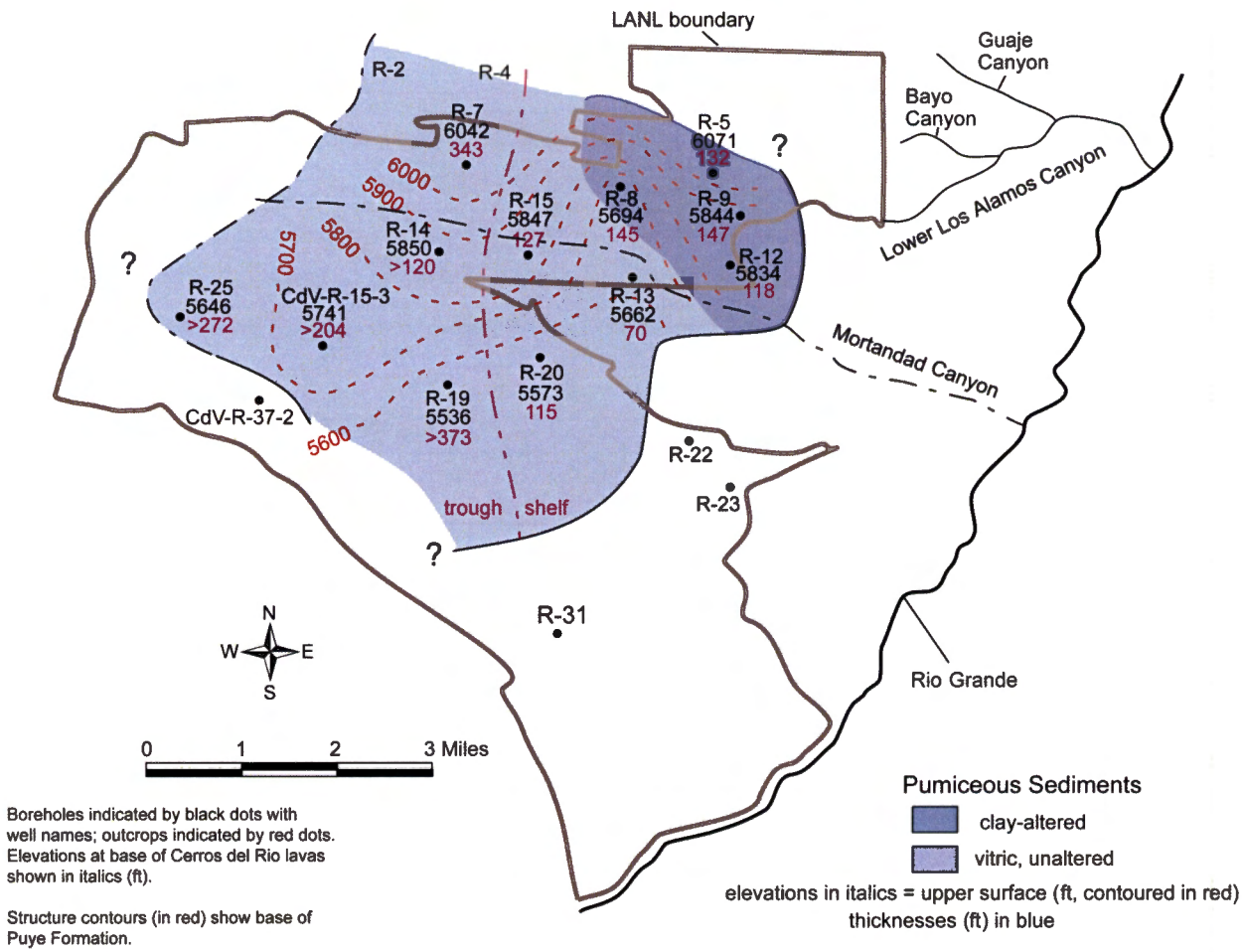


**Figure 2-9.** Topography at the upper surface of the pumiceous deposits underlying Puye Formation fanglomerates, with pumiceous deposit thicknesses (ft) indicated in blue. Color shading is used to distinguish vitric unaltered pumiceous deposits from those that are clay-altered.

Each of these figures is based on the interpretations of cuttings, geophysical logs, and in some cases borehole video data to determine the elevations of the upper and lower stratigraphic contacts for individual stratigraphic units. Isopach maps for shallow units that crop out in canyon walls, such as the Cerro Toledo interval and the Otowi Member, are corrected for the effects of the modern canyon incision. Each point on the figure represents either a borehole (with borehole name listed) or an outcrop location (without a borehole label). The data points list the elevation of the basal contact in ft above sea level (asl) and the unit thickness in ft. Dashed red contours are hand-generated and indicate an interpretation of the topology of the geologic contact; increasingly darker shades of blue indicate increasing unit thickness above this topologic surface.

### 2.2.1 Tesuque Formation

The Miocene Tesuque Formation is partially penetrated by wells in the eastern part of the Pajarito Plateau where it makes up a significant portion of the aquifer for local communities and LANL (Purtymun, 1995). It is primarily made up of thick fluvial deposits consisting of partly lithified, arkosic sediments derived from Precambrian granite, pegmatite, and sparse sedimentary rocks of the Sangre de Cristo Range and from Tertiary intermediate to felsic volcanic rocks from northern New Mexico and possibly southern Colorado (Cavazza, 1989). Individual beds are generally less than 3 m (10 ft) thick and consist of massive to planar- and cross-bedded light pink-to-buff siltstone and sandstone, with minor lenses of pebbly conglomerate. Exposures near the Rio Grande (Koning and Maldonado, 2001) indicate that the Tesuque Formation beneath the plateau probably consists primarily of the Pojoaque Member. In well PM-5, a 110-m (360-ft) thick series of basalt flows within the Tesuque Formation yielded a $^{40}Ar/^{39}Ar$ date of 11.39 ± 0.40 Ma (WoldeGabriel et al., 2001).

Based on Formation Microimager (FMI) logs for well R-16, bedding in the Tesuque Formation on the east side of the plateau dips predominantly towards the west-northwest (LANL, 2003). The mean dip is 11° but dips tend to be greater in the lower part of the well (median dip 14° below 1170 ft) than in the upper part (median dip 9°). Tesuque beds just east of the Rio Grande dip westward mainly at angles of 3° to 10° (Koning and Maldonado, 2001).

### 2.2.2 Miocene Basalts

Miocene basalts are intercalated with Santa Fe Group deposits in the east-central part of the Pajarito Plateau. WoldeGabriel et al. (1996) divided these basalts into two age groups based on $^{40}Ar/^{39}Ar$ dates. The older group ranges in age from 10.9 to 13.1 Ma and is largely found in the vicinity of Guaje Canyon. The younger group ranges in age from 8.4 to 9.3 Ma and is found over a wide area that extends from Bayo Canyon on the north to Ancho Canyon on the south and from PM-1 on the east to PM-5 to the west.

### 2.2.3 Older Fanglomerate

The informal term "older fanglomerates" refers to a thick sequence of late Miocene fan deposits that were shed from the Jemez volcanic field into the western Española Basin. These deposits, which are found only in deep boreholes, are important for the development of high-yield,

low-draw-down municipal and industrial water supply wells on the Pajarito Plateau (Purtymun, 1995). Purtymun (1995) called these deposits the "Chaquehui Formation" and assigned them a post-Chamita and pre-Puye age. From borehole observations, the Chaquehui Formation consisted of up to 1500 ft of gravels, cobbles, and boulders derived from the Jemez volcanic field and volcanic, metamorphic, and sedimentary rocks derived from highlands to the north and east. However, the Miocene deposits identified as Chaquehui Formation in deep wells are more appropriately called "older fanglomerates" because recent stratigraphic studies indicate the Chaquehui Formation type section consists of younger (late Pliocene) phreatomagmatic deposits (Heiken et al., 1996).

The older fanglomerates are widespread beneath the Pajarito Plateau, based on borehole observations. These deposits are mostly made up of volcanic detritus derived from Keres Group rocks and possibly from early Tschicoma Formation centers. They are characterized by dark, lithic sandstones and gravel and cobble deposits dominated by fresh to silicified, subangular to rounded andesite, latite, and porphyritic dacite. Subordinate clasts (<10%) include subangular to rounded rhyolite and basalt, and rounded quartzite. Rounded granite and angular chert clasts are generally rare (<1%) (Broxton and Vaniman 2005).

Precambrian quartzite, granite, and chert clasts are persistent, but in low abundance in the older fanglomerates. The source of Precambrian clasts may be Santa Fe Group rocks that were exposed within the Jemez volcanic field at the time of Keres volcanism. Stratigraphic relationships described by Gardner and Goff (1996) indicate that Santa Fe Group deposition interfingered with Keres volcanism in the caldera area. Additionally, rounded quartzite and granitic gneiss pebbles are found in lag gravels on the resurgent dome of the Valles caldera where they presumably weathered out of Santa Fe Group rocks in megabreccia blocks that slumped into caldera during caldera collapse (Goff et al., 2003).

The maximum thickness of older fanglomerate penetrated by wells is 1650 ft in well Otowi-4. However, thicknesses could be greater to the west where drillholes did not fully penetrate the unit. The westward thickening wedge of volcaniclastic sedimentary deposits corresponds to the zone of thick, highly productive aquifer rocks that extend northeastward across the central plateau as described by Purtymun (1995). The western boundary of this thick sequence of sediments is poorly defined, but recent drilling results suggest that these rocks probably extend to the Pajarito fault zone. The older volcaniclastic deposits abruptly thin eastward between east-west pairs of wells such as R-23/R-22 and Otowi-1/Otowi-4. The transition zone generally corresponds to the eastern boundary of the gravity low beneath the Pajarito Plateau described by Ferguson et al. (1995).

### 2.2.4 Totavi Lentil

The Totavi Lentil is made up of river-channel sands and gravels that crop out along the Puye escarpment, in lower Los Alamos and Guaje Canyons, and along White Rock Canyon. These rocks are also penetrated by a number of wells on the Pajarito Plateau. These axial-channel deposits were named the Totavi Lentil of the Puye Formation for a type section in Los Alamos Canyon (Griggs, 1964). Griggs recognized their importance as ancestral Rio Grande deposits,

and he used them to delineate the base of the Puye Formation with which they are conformable in outcrops.

The Totavi Lentil is a poorly consolidated conglomerate containing well-rounded cobbles and gravels of Precambrian quartzite, granite, and pegmatite with subrounded to subangular cobbles and boulders of silicic to intermediate and rarer basaltic volcanic rocks. Precambrian clasts typically make up >80% of the clasts in the deposits. Though commonly subordinate in abundance, clasts of volcanic rocks from the Jemez volcanic field make up to 50% of the deposit in some interbedded horizons. Lenses of loose, well sorted, fine to coarse sands containing abundant quartz and microcline are intercalated with the conglomerate. Totavi deposits are generally ~50 ft thick near the Rio Grande and thicken to the northwest (Griggs, 1964). An unusually thick sequence of quartzite-rich conglomerate (>323 ft) was penetrated in well R-31, located in Ancho Canyon. A number of wells (e.g. R-5, R-9, R-12, R-32) did not encounter the Totavi Lentil, indicating that these channel conglomerates may form lenticular deposits of limited lateral extent.

Based on new well data, it is evident that ancient river deposits in the Pajarito Plateau area are coeval with variety of stratigraphic units that span a longer time interval than previously recognized. River gravels occur beneath the pumice-rich volcaniclastic rocks (described below) in wells R-13, R-15, R-20, R-33, R-34, PM-1, PM-2, and PM-5. These river gravel deposits are generally 10- to 30-m (30- to 100-ft) thick and include abundant well-rounded gravels of quartzite, angular to subangular basalt, andesite, and dacite, and minor metavolcanics. Granitic clasts are rare to absent. Radiometric ages indicate the overlying pumice-rich volcaniclastic rocks are late Miocene in age. In well H-19, river gravels 3-m (10-ft) thick occur as rounded quartzite pebbles between two Tschicoma lava flows (Griggs, 1955, 1964). The quartzite-dominated clast compositions suggest these gravels were derived from the Tusas Mountains and were transported southward by the ancestral Rio Chama, with tributaries draining the Jemez volcanic field. A late Miocene age for the early riverine deposits is consistent with geologic interpretations that through-going rivers were established in the Española Basin prior to about 6.96 Ma (Smith et al., 2001; Smith, 2004).

### 2.2.5 Pumice-Rich Volcaniclastic Rocks

The pumice-rich volcaniclastic rocks (pumiceous deposits) are characterized by well-bedded horizons of light-colored, reworked, tephra-rich sedimentary deposits and subordinate primary ash- and pumice-fall deposits. These rocks consist mainly of tuffaceous sandstones and contain a few beds of lava-rich gravels. The underlying older fanglomerate and overlying Puye Formation contain higher percentages of gravel and cobble beds. In a number of wells, pumice-rich volcaniclastic rocks are separated from the older fanglomerate by the Totavi Lentil (axial deposits of the ancestral Rio Grande).

The pumice-rich deposits typically contain 10 to 30% subangular to rounded, rhyolitic lapilli mixed with 70 to 90% ash and lithic sands. Gravels contain porphyritic dacite, rhyolite, and lesser andesite and basalt. Some intervals contain as much as 90% subangular to angular pumice lapilli that represent primary fall deposits or reworked deposits that underwent minimal transport. In most areas, pumice lapilli are vitric and show little effect from submergence within

the regional saturated zone except for oxidation on clast surfaces and minor clay development in vesicles.

However, these deposits are diagenetically altered where most of the volcanic glass is replaced by smectite in the northeastern portion of the Laboratory, an area defined by wells R-5, R-8, R-9, and R-12. Shadings of blue in Figure 2-9 distinguish vitric unaltered pumiceous deposits (pale blue) from those that are heavily clay-altered and retain little or no glass (dark blue). The formation of clay in this area is locally accompanied by abundant calcite and variable amounts of zeolite alteration. Because of the extent of alteration, the lack of preservation of glass, and the loss of many petrographic clues for individual pumice bed correlation, it is difficult to determine whether the heavily altered pumices are related to the unaltered pumice or represent an earlier pumice unit and an earlier alteration event.

Most lapilli in the pumice-rich volcaniclastic rocks are aphyric or contain sparse phenocrysts of quartz, sanidine, and plagioclase, but the presence of some biotite-, hornblende-, and pyroxene-phyric varieties indicates that multiple volcanic sources supplied tephra to these deposits. Seven recent $^{40}Ar/^{39}Ar$ feldspar ages between 6.8 and 7.5 Ma were obtained from crystal-poor pumice falls in six wells that penetrate into this unit. The younger ages overlap the 6.01 to 7.1 Ma range of ages reported for the Bearhead Rhyolite (Justet, 1996; Smith, 2001) and the older ages are slightly older. Additional work is taking place to investigate the relation between the pumice-rich volcaniclastic rocks and Keres Group silicic volcanism with the goal of assigning the pumiceous sediments to either the Puye or Cochiti Formations or delineating them as a separate formation.

The pumice-rich volcaniclastic rocks thin northeastward across the central part of the plateau and are absent north of Pueblo Canyon. Borehole geophysical logs indicate that these deposits dip 5° to 15°, primarily towards the southwest and west. Figure 2-9 illustrates structure contours and thickness of pumiceous deposits that occur over a broad region beneath the central portion of the Laboratory where multiple pumice beds have been encountered. Observations from boreholes suggest that the structure of these pumiceous deposits is complex, including both primary and reworked pumiceous units intermixed with fanglomerates. Nevertheless, the pumiceous unit is predictably encountered in the area shown in Figure 2-9. Drilling experience shows that this unit is highly transmissive, providing a difficult drilling horizon where injected fluids are likely to be lost. Hydrologic testing shows that the pumiceous deposits have relatively high transmissivity (Section 2.3.4.2).

In Figure 2-9 the structure contours represent the top, rather than the bottom of the pumiceous deposits. This is done because the bottom of this unit is poorly constrained in R-series drillholes to the south and west, where this unit was seldom penetrated. The structure contours at the top of the pumiceous unit show that it slopes to the south and shows evidence of incision of a broad south-trending paleocanyon, filled by Puye fanglomerate, in the central portion of the Laboratory. This broad canyon is somewhat similar to that seen at the base of the Bandelier Tuff (Figure 2-6) and at the base of the Cerros del Rio volcanic rocks (Figure 2-8), suggesting that broadly south-trending canyons have been a common feature for over 5 m.y. prior to the eruption of the Bandelier Tuff. The present west-northwest/east-southeast drainages on the plateau may be a relatively recent drainage pattern that developed on the thick east-sloping tuff ash flows emplaced after 1.6 Ma.

### 2.2.6 Tschicoma Formation

The Tschicoma Formation of the Polvadera Group consists of thick, predominantly dacite to low-silica rhyolite lava flows erupted from large overlapping dome complexes. Major peaks in the Sierra de los Valles, including Cerro Grande, Pajarito Mountain, Caballo Mountain, and Tschicoma Mountain, are compositionally distinct lava domes that represent separate volcanic source areas for detritus that was shed to form the Puye fanglomerates. Low-silica rhyolite erupted from a deeply eroded dome complex in the upper Rendija Canyon and Guaje Mountain area yielded three ages between 4.95 and 5.32 Ma. Dacites of the Cerro Grande, Pajarito Mountain, and Caballo Mountain centers have closely overlapping ages of 2.91 Ma to 3.34 Ma (Broxton and Vaniman, 2005).

Outcrops of the Tschicoma Formation in the Sierra de los Valles are primarily gray to purplish-gray lavas characterized by pronounced jointing and flow foliation. The interflow zones between flow units are commonly marked by blocky breccias. Flow interiors consist of dense, massive rock that is commonly devitrified to form a microcrystalline groundmass, giving the rocks a stony appearance. Chilled volcanic glass is sometimes preserved in flow tops and bottoms. Fragmental deposits of ash and lava debris occur in the distal parts of the formation.

The Tschicoma Formation is at least 2,500 ft thick in the Sierra de los Valles, but has a variable thickness due to the lenticular shapes of its lava flows. The Tschicoma Formation thins eastward under the western Pajarito Plateau where it interfingers with the Puye Formation. The Tschicoma Formation was encountered in wells TW-4, H-19, CDV-16-3(i) and CDV-R-37-2 in the western part of the Pajarito Plateau, but is absent in boreholes to the east, with the possible exception of thick dacite lava in boreholes EGH-LA-1, SHB-1, and I-1. These lavas may be assigned to the Tschicoma but their source and distribution is presently unknown.

### 2.2.7 Puye Formation

The Puye Formation is a large apron of overlapping alluvial and pyroclastic fans that were shed eastward from the Jemez volcanic field into the western Española Basin (Griggs, 1964; Turbeville et al., 1989). The Puye Formation unconformably overlies rocks of the Santa Fe Group (Tesuque Formation), and the Otowi Member of the Bandelier Tuff unconformably overlies it. Turbeville et al. (1989) estimated its areal distribution at 200 $mi^2$ and its volume at ~3.6 $mi^3$. Because its primary source area was volcanic domes in the Sierra de los Valles, the Puye Formation overlaps and post-dates the Tschicoma Formation in age. The Puye Formation is subdivided into fanglomerate and lacustrine facies.

The fanglomerate facies, the dominant unit of the Puye Formation, is a heterogeneous assemblage of clast- to matrix-supported conglomerates, and of gravels and lithic-rich sandstones. Clasts in the coarsest deposits consist of subangular to subrounded cobbles and boulders of latite, dacite, rhyolite, and tuff in a poorly sorted matrix of ash, silts, and sands. Consolidated mudflow deposits are common throughout the unit, and tend to be cliff-forming. At least 25 ash beds of dacitic to rhyolitic composition are interbedded with the conglomerates and gravels (Turbeville et al., 1989).

The lacustrine facies includes lake and riverine deposits in the upper part of the Puye Formation. These deposits are characterized by lacustrine fine sand, silt, and clay up to 30 ft thick. Basaltic ash beds (maar deposits) up to 10 ft thick are locally present above or below the lacustrine deposits. The lacustrine facies includes some well-rounded riverine gravels of Precambrian quartzite and gneiss that fill channels cut into the underlying fanglomerates. The lacustrine facies crops out in lower Los Alamos Canyon and extends both northward and southward in discontinuous outcrops for several miles. Apparently, their extent is limited to the eastern side of the plateau because they are found only in wells R-9, R-12, and R-16. Because of their spatial and temporal association with palagonitic basalt flows and maar deposits, these lacustrine deposits probably represent periods of damming and diversion of the Rio Grande caused by the eruptions of lavas within the Cerros del Rio volcanic field.

The Puye Formation reaches a maximum thickness of >1000 ft in well R-25 on the western side of the Laboratory but thins to 50 ft in areas north of the Pajarito Plateau. In the central and eastern portions of LANL, it is about 600 ft thick and the upper Puye is interbedded with basaltic lavas of the Cerros del Rio volcanic field.

### 2.2.8 Basaltic Rocks of the Cerros del Rio Volcanic Field

Cerros del Rio basalts typically form thick sequences of stacked lava flows separated by interflow breccia, scoria, sediment, and ash. These rocks are mostly basalts and basaltic andesites, but subordinate dacite is present within thick basalt stacks in the east and central plateau (e.g. Ball et al., 2002) or is found as isolated flows on the western side of the volcanic field. Cerros del Rio lavas were erupted from vents located both east and west of the Rio Grande (Smith et al., 1970; Aubele, 1978; Kelley, 1978).

In major-element composition the dacitic components are very similar to partially contemporaneous dacitic lavas that occur within the highlands of the Tschicoma Formation to the west. However, dacites are less abundant than basalts within the Cerros del Rio and these thin dacitic lavas have relatively few of the common hydrous minerals (amphibole and biotite) that characterize most of the Tschicoma lavas. These distinctions are important because they strongly affect the hydrogeologic character of the lavas. Lavas of the Cerros del Rio lie within suites of relatively thin (a few tens of feet), largely basaltic lava flows with laterally extensive flow-boundary rubble zones that provide pathways for flow. Lavas of the Tschicoma Formation are far more massive, up to hundreds of feet thick, and are generally poorly transmissive (Griggs, 1964).

Individual flows typically range in thickness from about 3 ft to more than 100 ft. The internal structures of flows show some similarities to those described for the Columbia River Basalt Group in Washington, Oregon, and Idaho and for Snake River basalts in Idaho (Swanson et al., 1979; Whiteman et al., 1994; Faybishenko et al., 2000). In ascending order, the flows are characterized by: (1) a flow base characterized by vesicular basalt with clinker and scoria, (2) a colonnade zone made up of vertical, large-diameter columns bound by cooling joints, (3) a thin zone of complexly-overlapping fractures, and (4) a flow top of vesicular basalt with scoria and clinker. In addition to highly porous clinker zones associated with flow tops and bottoms, interflow zones include cinder deposits and sedimentary deposits. Interflow cinder deposits are

fairly common, and their thickness is highly variable (0 to 100 ft), depending on proximity to source vents. The thickest cinder deposits are as much as 300 ft thick on or near source vents (e.g. R-34). Interflow sedimentary deposits are generally thin (<20 ft) where present and consist mostly of reworked basaltic rocks. In the eastern part of the plateau, where the basalts interacted with surface water, flow bases commonly include porous, pillow-palagonite complexes.

The basaltic rocks of the Cerros del Rio volcanic field include buried remnants of maar volcanoes in White Rock Canyon. The aprons of fragmental debris surrounding these buried craters consist of thin layers of basaltic ash and sediments. The maar deposits resulted from steam explosions that occurred where basalt erupted through an aquifer or standing body of water. Thin maar deposits were identified at the base of the Cerros del Rio basalt in R-9 and R-12.

The distribution, form, and thickness of the Cerros del Rio volcanic field beneath the plateau are illustrated in Figure 2-7, which shows the topography at the top of the Cerros del Rio and Figure 2-8, which shows structure contours (red dashed lines) at the base of the Cerros del Rio. In Figure 2-8 shadings of purple represent the variation in thickness of the total Cerros del Rio deposits that lie between the two contoured surfaces in these figures.

Figure 2-7 shows that the upper surface of the Cerros del Rio is irregular, with a broad highland that extends from north to south under the east-central portion of the Laboratory. This highland is largely buried beneath the Bandelier Tuff, but remnants of the eastern slope extending from the highland are exposed beneath the town of White Rock. The highland represents distributed volcanic centers that produced most of the basaltic and dacitic lavas that underlie the Laboratory. Direct evidence of these eruptive centers is found in thick cinder deposits that were encountered in drillholes R-22 and especially R-34, and a low cinder-covered volcanic center exposed just south of R-23 in TA-36. These cinder deposits are extremely porous and generally provide highly transmissive media, but they are localized around volcanic centers so that enhanced groundwater flow is likely to extend for less than one mile, based on the extent of the TA-33 cinder cone (Figure 2-7).

Figure 2-8 shows the topography at the base of the Cerros del Rio volcanic series and the exceptional thickening of these deposits beneath R-22 and (probably) extending along a paleocanyon extending to the south. The extent of this deep trough to the north and south is not well defined by current drillhole locations. Based on the absence of Totavi-like deposits within this channel at R-22 and the lack of evidence to the northeast in the canyon walls of lower Los Alamos Canyon, it is likely that the head of the canyon rose steeply to the northwest and drained the Sierra de los Valles. This thick keel of lavas and intercalated rubble zones occurs largely beneath the regional aquifer water table and hosts an important part of the regional aquifer beneath the southeast portion of the Laboratory. It is possible that this feature could affect the flow direction and head distributions at depth.

### 2.2.9 Bandelier Tuff

The Laboratory facilities are located almost entirely on mesa and canyon outcrops of Bandelier Tuff. The Bandelier Tuff consists of ash flows and minor airfall pyroclastic deposits with ages of

1.61 Ma for the Otowi Member and 1.22 Ma for the Tshirege Member (Izett and Obradovich, 1994). The two Bandelier Tuff members are separated by the Cerro Toledo interval, which is a stratified sequence of volcaniclastic sediments and tephra of mixed provenance. Although it occurs between the ash-flow members of the Bandelier Tuff, the Cerro Toledo interval is not considered part of the Bandelier Tuff, a usage consistent with the original definition by Bailey et al. (1969).

#### 2.2.9.1 Otowi Member, Bandelier Tuff

The Otowi Member crops out in several canyons but is best exposed in Los Alamos Canyon and in canyons to the north. It consists of moderately consolidated, porous, nonwelded ash-flow tuffs that form colluvium-covered slopes along the base of canyon walls. The Otowi ash-flow tuffs are vitric and contain light gray-to-orange pumice supported in a white to tan ashy matrix of glass shards, broken pumice, crystals, and rock fragments. The Otowi Member is made up of multiple ash flows, but individual ash-flow deposits cannot be traced in the subsurface using core and cuttings from widely spaced boreholes. The base of the member is called the Guaje Pumice Bed (Figure 2-6), and is discussed below. In some drillholes, a shift in borehole gamma measurements in the central part of the unit provides a useful datum for correlations between drillholes. The nonwelded ash-flow tuffs of the Otowi Member collectively form a relatively homogenous rock unit throughout the plateau. Transport through this hydrogeologic unit appears to occur primarily by matrix flow, although open fractures may contribute to transport locally (e.g., R-25). Although made up of multiple flow units, the combined Otowi ash flows are massive, and borehole geophysical logs show only minor variations in density and porosity.

The present maximum thickness of Otowi Member occurs in two areas in the western part of the plateau where the deposits are about 350 to 400 ft thick. Otowi deposits are only <100 to 300 ft thick between these two areas. The thin deposits are overlain by unusually thick Cerro Toledo sediments that apparently accumulated in a broad east-southeast-trending drainage incised into the top of the Otowi Member. On the eastern side of the plateau, the Otowi Member is 0 to 100 ft thick. Thinning of the deposits eastward reflects both the general thinning of the Otowi Member away from its caldera source and thinning of the ash-flow tuffs over the Cerros del Rio highland on the east side of the plateau. Structure contours indicate that Otowi ash-flow tuffs filled a broad south-draining paleovalley west of the Cerros del Rio basaltic highland.

Figure 2-5 shows structure contours (red dashed lines) at the base of the Otowi Member of the Bandelier Tuff and color shading in purple that represents relative overall thickness of the unit. The Otowi Member thickens from the central portion of the Laboratory toward the west, with the exception of a paleocanyon that is aligned with and filled by the thick Cerro Toledo deposits shown in Figure 2-5. To the east, south of PM-1 where Otowi deposits ramp up onto the Cerros del Rio basaltic volcanic centers with little or no Puye sediment cover, the Otowi deposits are thinner than to the northeast where they are underlain mostly by eastward-sloping Puye fans. In the south-central portion of the Laboratory the Otowi deposits fill a broad south-trending valley formed by low terrain between Puye fans sloping down from the west and Cerros del Rio highlands to the east, such as the TA-33 volcano.

The Guaje Pumice Bed occurs at the base of the Otowi Member and is an extensive marker horizon in outcrop and wells. The Guaje Pumice Bed contains layers of sorted pumice fragments

whose mean size varies between 2 and 4 cm. It has an average thickness of ~15 ft over much of the plateau, but thickens considerably to the northwest (Figure 2-6). Geophysical logs show that the Guaje Pumice Bed has a higher porosity than overlying Otowi ash-flow tuffs and underlying Puye Formation. The Guaje Pumice Bed appears consistently as a zone of higher porosity and elevated moisture content in CMR geophysical logs. Because of this property the Guaje Pumice Bed can provide a relatively thin (a few feet to a few tens of feet) but laterally continuous horizon capable of local saturation.

Figure 2-6 uses color shading to represent the thickness of the Guaje Pumice Bed. Because the Guaje Pumice Bed formed as a pumice fall rather than an ash flow, the tendency to thin away from the source (the Valles caldera) is much less pronounced except for the area underlying the northwestern corner of the Laboratory. The distribution of pumice fall deposits is more strongly influenced by prevailing wind direction at the time of eruption, compared with the largely internal energy sources that distribute ash flows. A general lack of incision and weathering at the top of the Guaje Pumice Bed indicates that little time elapsed before it was buried by magmatically related ash flows of the Otowi Member. Locally, however, the Guaje Pumice is unusually thin compared to surrounding areas and may have been partially eroded before or during the passage of the earliest Otowi ash flows. In the eastern portion of the Laboratory the Guaje Pumice Bed is seldom more than a few feet thick and is locally absent.

#### 2.2.9.2 Tephra and Volcaniclastic Sediments of the Cerro Toledo Interval

The Cerro Toledo interval crops out in Los Alamos Canyon and in canyons to the north, and it occurs in many of the wells on the plateau. It unconformably overlies the deeply eroded Otowi Member and its thickness is highly variable (3 to 390 ft). Figure 2-4 shows structure contours at the base of the Cerro Toledo interval and a colored representation of relative overall thickness of the unit. Structure contours for the base of the Cerro Toledo indicate that this unit fills a broad southeast-draining valley fed by one or more canyons exiting the Sierra de los Valles. The thickest Cerro Toledo deposits coincide with the axis of this paleovalley.

The predominant rock type in the Cerro Toledo interval is rhyolitic tuffaceous sandstone and tephra. These deposits contain abundant crystal-poor ash and pumice, and clasts of vitric to devitrified rhyolite lava and minor obsidian. They represent the reworked equivalents of Cerro Toledo Rhyolite tephra erupted from the Cerro Toledo and Rabbit Mountain dome complexes located northeast and southeast of the Valles caldera, respectively. Primary pumice-and ash-falls are interbedded with these sedimentary deposits in most locations.

Clast-supported gravel, cobble, and boulder deposits of porphyritic Tschicoma dacite derived from the Tschicoma Formation are also interbedded with the tuffaceous rocks. In some deposits, the dacitic detritus is volumetrically more important than the tuffaceous detritus. These coarse dacitic deposits commonly define the axial portions of channels incised into the underlying Otowi Member.

In the western part of the plateau, the Cerro Toledo interval contains a large component of crystal-rich tuffaceous detritus. These tuffaceous sediments represent reworked Otowi tuff that accumulated in drainages incised into the Otowi Member prior to emplacement of the Tshirege

Member. These reworked Otowi deposits are interbedded with other volcaniclastic deposits derived from Cerro Toledo and Tschicoma sources.

Data from boreholes R-19, CdV-R-15-3, CdV-16-1(i), R-18, and R-26 revised the conceptual model for the Cerro Toledo interval, which was a general thinning from Cerro Toledo age volcanic sources in the caldera to the northwest of the Laboratory to distal deposits toward the east-southeast (Broxton and Vaniman, 2005). These boreholes, however, showed that the thickening is not uniform and the Cerro Toledo sediments fill a deep and broad east-southeast draining paleocanyon in the middle western portion of the Laboratory. This paleocanyon is incised into the top of the Otowi ash flows; the overlying base of the Tshirege Member of the Bandelier Tuff and the underlying base of the Otowi Member (Figure 2-5) show no such canyon development. The structure contours that show the base of the Cerro Toledo interval in Figure 2-4 show the topology of the canyon eroded into the top of the Otowi ash flows. The exact width and the orientation of this canyon, whether it is one canyon or several, and where this canyon connected to paleodrainages toward the Rio Grande to the east are relatively unconstrained points that allow a certain amount of latitude in the way that Figure 2-4 is constructed.

#### 2.2.9.3 Tshirege Member, Bandelier Tuff

The Tshirege Member is the upper member of the Bandelier Tuff and is the most widely exposed bedrock unit of the Pajarito Plateau. It is a multiple-flow, ash-and-pumice sheet that forms the prominent cliffs throughout the plateau. It also underlies canyon floors in all but the middle and lower reaches of Los Alamos Canyon and in canyons to the north. The Tshirege Member is generally over 200 ft thick in the north-central part of LANL and over 600 ft thick near the southern edge of LANL.

The Tshirege Member differs from the Otowi Member most notably in its generally greater degree of welding compaction. Time breaks between the successive emplacements of ash-flow units caused the tuff to cool as several distinct cooling units. For this reason the Tshirege Member is a compound cooling unit, consisting of at least four cooling subunits that display variable physical properties vertically and horizontally. These variations in physical properties reflect zonal patterns of varying degrees of compaction, welding, and glass crystallization. The welding and crystallization zones in the Tshirege Member produce vertical variations in properties such as density, porosity, hardness, composition, color, and surface weathering patterns. The degree of welding in each of the cooling units generally decreases from west to east, reflecting higher emplacement temperatures and thicker deposits closer to the Valles caldera.

The Tsankawi Pumice Bed forms the base of the Tshirege Member. Where exposed, it is commonly 2 to 3 feet in thickness. This pumice-fall deposit contains sorted pumice lapilli (diameters reaching about 2.5 in) in a crystal-rich matrix. Several thin ash beds are interbedded with the pumice-fall deposits.

Because the thick Tshirege ash flow tuffs make up a significant portion of the upper vadose zone, brief descriptions are provided below for the major subunits of the member, from bottom to top:

- **Qbt 1g** is the lowermost subunit above the Tsankawi Pumice Bed. It consists of porous, nonwelded, and poorly sorted ash-flow tuffs. The "g" in this designation stands for "glass" because none of the glass in ash shards and pumices shows crystallization by devitrification or vapor phase alteration. The tuffs of Qbt 1g are nonwelded and have an open, porous structure.
- **Qbt 1v** forms alternating cliff-like and sloping outcrops composed of porous, nonwelded, but crystalline tuffs. The "v" stands for vapor-phase crystallization that together with crystallization of glass in shards and pumices (devitrification) transformed the rock matrix into microcrystalline aggregates of silica polymorphs and sanidine. The tuffs of Qbt 1v are generally nonwelded to slightly welded, and have an open, porous structure.
- **Qbt 2** forms a distinctive, medium brown, vertical cliff that stands out in marked contrast to the slope-forming, lighter colored tuffs above and below. A series of laminated and cross-bedded deposits commonly mark its base in the eastern part of the Laboratory. In the central and western part of the Laboratory, the boundary between Qbt 2 and Qbt 1v is gradational and the distinction between the two units is somewhat arbitrary. Qbt 2 is typically the most strongly welded tuff in the Tshirege Member. Vapor-phase crystallization of flattened shards and pumices is extensive in this subunit.
- **Qbt 3** is a nonwelded to partly welded, vapor-phase altered tuff that forms the cap rock of mesas in the central part of the Pajarito Plateau. Qbt 3 becomes moderately to densely welded in the western part of the plateau.
- **Qbt 4** is a complex unit consisting of nonwelded to densely welded ash-flow tuffs and thin intercalated surge deposits. Devitrification and vapor-phase alteration are typical in this unit, but thin zones of vitric ash-flow tuff occur locally. The occurrence of Qbt 4 is limited to the western part of the Pajarito Plateau.

### 2.2.10 Alluvium and Colluvium

Holocene and late Pleistocene canyon-floor alluvium consists of stratified, lenticular deposits of unconsolidated fluvial sands, gravels, and cobbles (Reneau et al., 1996). Smaller canyons whose headwaters are located on the plateau contain detritus exclusively of Bandelier Tuff. Larger canyon systems that head in the Sierra de los Valles contain Bandelier detritus mixed with dacite detritus derived from the Tschicoma Formation. Active and inactive channels and floodplains form complex, cross-cutting deposits. These fluvial sediments interfinger laterally with colluvium derived from canyon walls. In Pueblo Canyon alluvium is about 11 ft thick on the west side of the plateau and about 18 ft thick near the confluence with Los Alamos Canyon. Mortandad Canyon has 1 to 2 ft of alluvium near its headwaters and more than 100 ft of alluvium (plus colluvium) near the eastern LANL boundary.

Alluvium of probable early Pleistocene age overlies Bandelier Tuff on mesas throughout the plateau (Reneau and McDonald, 1996). The alluvial deposits form fairly continuous deposits on the western side of the plateau, but only remnants of these deposits are preserved further east. These alluvial deposits are primarily made up of coarse dacitic detritus from the Sierra de los Valles, but some locations also contain Valles Rhyolite (Cerro del Medio and El Cajete) fall deposits or their reworked equivalents. These deposits record the locations post-Tshirege alluvial fans and streams that predate incision of canyons on the plateau (Reneau and McDonald, 1996).

Colluvium consists of slope or cliff detritus shed gravitationally into canyons. In most instances only large blocks of colluvium can be distinguished from locally derived alluvium, where the colluvial blocks are identified with material in adjacent cliffs. Colluvial blocks are commonly overlain by alluvium, as in the wider reaches along Mortandad Canyon where blocks of upper devitrifed units of the Tshirege Member, often several feet in diameter, are found beneath alluvial sands and gravels in drillhole MCOBT-8.5.

## 2.3 Geologic Conceptual Model Cross-Sections

The geologic conceptual model is based on the accumulated geologic, geophysical, and hydrogeologic data described in Section 2.1. Regional and local data sources are used to constrain possible visualizations of the thickness and extent of major hydrogeologic units beneath the Laboratory. Of all data sources, the principal sources for building the subsurface components of the geologic conceptual model are obtained through the R-hole drilling program conducted under the Hydrogeologic Workplan. These data are supplemented by drilling data collected from boreholes that were drilled for other purposes. Because samples and geophysical logs from earlier boreholes are largely unavailable, and earlier wells were not drilled with the goal of obtaining a sitewide hydrogeologic model, the R-series wells provide the best available dataset for subsurface geology at the Laboratory. The various types of stratigraphic data from R-series wells and from other boreholes used to support the geologic conceptual model are summarized in Appendix 2-A.

### 2.3.1 Geology at the Water Table

The distribution of bedrock units at the top of regional saturation is shown in Figure 2-10. Regional groundwater enters the Pajarito Plateau by underflow through the rocks that underlie the Sierra de los Valles (Griggs, 1964; Purtymun, 1984). This underflow is supplemented by recharge from drainages that cross the plateau (Kwicklis et al., 2005). Hydrogeologic conditions beneath the Sierra de los Valles west of the Pajarito fault zone are largely unknown because there are no deep wells in this area. Groundwater probably flows through Tschicoma lavas and underlying geologic units at depth, based on stratigraphic cross-sections (see Section 2.3.2). The geologic units beneath the Tschicoma Formation are poorly constrained but probably consist of Keres Group volcanic rocks, Santa Fe Group sediments, Eocene sedimentary rocks, Paleozoic and Mesozoic sedimentary rocks, and Precambrian crystalline rocks (Smith et al., 1970; Goff and Gardner, 2004; Smith, 2004). In the western part of the plateau, in the vicinity of Pueblo and Water Canyons, the water table is straddled by two lobes of down-faulted Tschicoma lavas that extend up to 3 km (2 mi) east of the Pajarito fault zone. Based on the physical characteristics of the rocks, groundwater flow through dacite most likely occurs as fracture flow in the lava interiors and as porous flow in interflow zones and interbedded clastic deposits.

In the central part of the plateau, the regional water table occurs within basin-fill deposits that become progressively older to the east. These basin-fill deposits consist of the Puye Formation, pumice-rich volcaniclastic rocks, older fanglomerates, and the Tesuque Formation (Figure 2-10). The most productive municipal supply wells on the plateau occur in this area where long well

screens (500 m [1600 ft]) span the Puye Formation, pumiceous deposits, Totavi deposits, older fanglomerates, and Tesuque sedimentary rocks and basalts.

Basalt straddles the water table in two areas. The most extensive is located in the south-central part of the plateau where as much as 195 ft of saturated Pliocene Cerros del Rio basalt occurs at the top of the regional zone of saturation in well DT-10 and 290 ft occurs in well R-22 (Figure 2-10). A smaller region of older Miocene basalts straddles the water table in a north-trending zone extending between wells R-12 to R-5. The southern extent of this zone is poorly constrained.

The Tesuque Formation is the primary rock unit making up the regional aquifer in the eastern part of the plateau and in the Buckman well field east of the Rio Grande (Figure 2-10). Miocene basalts are interbedded with the Tesuque Formation beneath parts of the plateau, but are absent in wells drilled to depths of 300 to 575 m (1000 to 1900 ft) in the Buckman well field (Shomaker, 1974). Most of the production from municipal supply wells in Guaje Canyon and in lower Los Alamos Canyon comes from the Tesuque Formation.

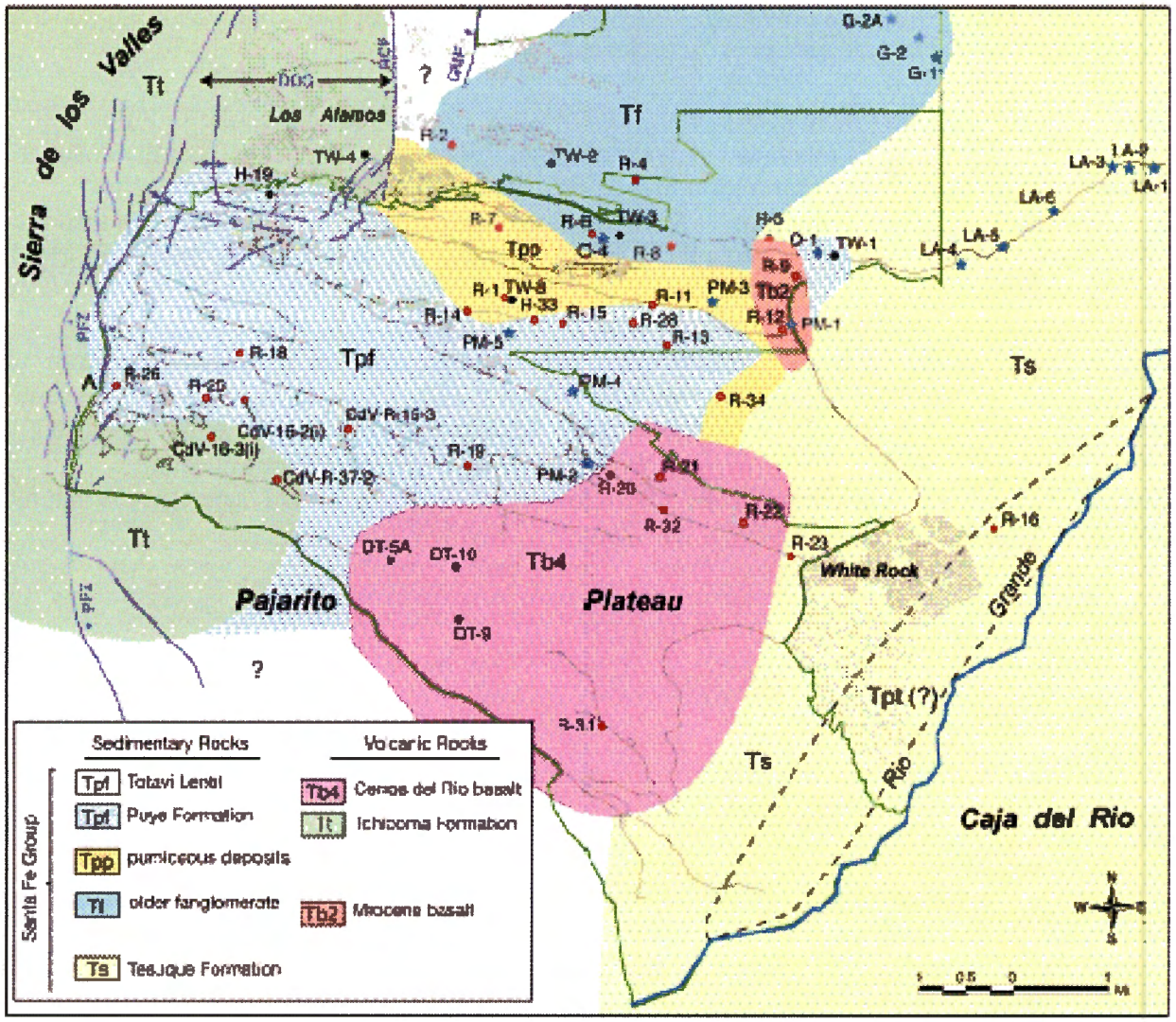


**Figure 2-10.** Map showing distribution of geologic units at the top of the regional saturated zone beneath the Pajarito Plateau. The wells that provided geologic control for this map are indicated by dots using the same color schemes as Figure 2-2. The LANL boundary is shown by the green outline, and the Pajarito fault zone is shown in blue. The map portrays the dominant rock unit in the upper 50 ft of the regional saturated zone.

### 2.3.2 Representative Cross-Sections

The full three-dimensional implementation of the geologic model is discussed in Section 4.1. The 3D model is tested against conceptual cross-sections that incorporate time-stratigraphic constraints, structural considerations, and correlations and limitations that take into account source regions and settings beyond the boundaries of the 3D model. The development of a manageable 3D model is time-intensive and requires treatment of geologic units on a large scale, where some details must necessarily be incorporated into larger units or ignored. Conceptual cross-sections help to test ideas concerning site geology, present details that may not be manageable in the 3D model, and provide a means of rapid testing of new borehole data against existing concepts.

Figure 2-11 shows alignments for eight conceptual geologic cross-sections that cover the Laboratory area. Included are four conceptual cross-sections for principal drainages:

- Los Alamos Canyon (Figure 2-12),
- Mortandad Canyon (Figure 2-13),
- Pajarito Canyon (Figure 2-14), and
- Water Canyon (Figure 2-15).

In addition, four cross-sections of approximately southwest-northeast alignment cross the grain of drainage at the Laboratory from western to eastern portions of the site (Figures 2-16, 2-17, 2-18, 2-19). Each geologic section is presented here at a vertical exaggeration of 10:1 in order to permit appropriate labeling and allow a level of detail that would not be possible at true vertical scale. Each geologic section is described separately below.

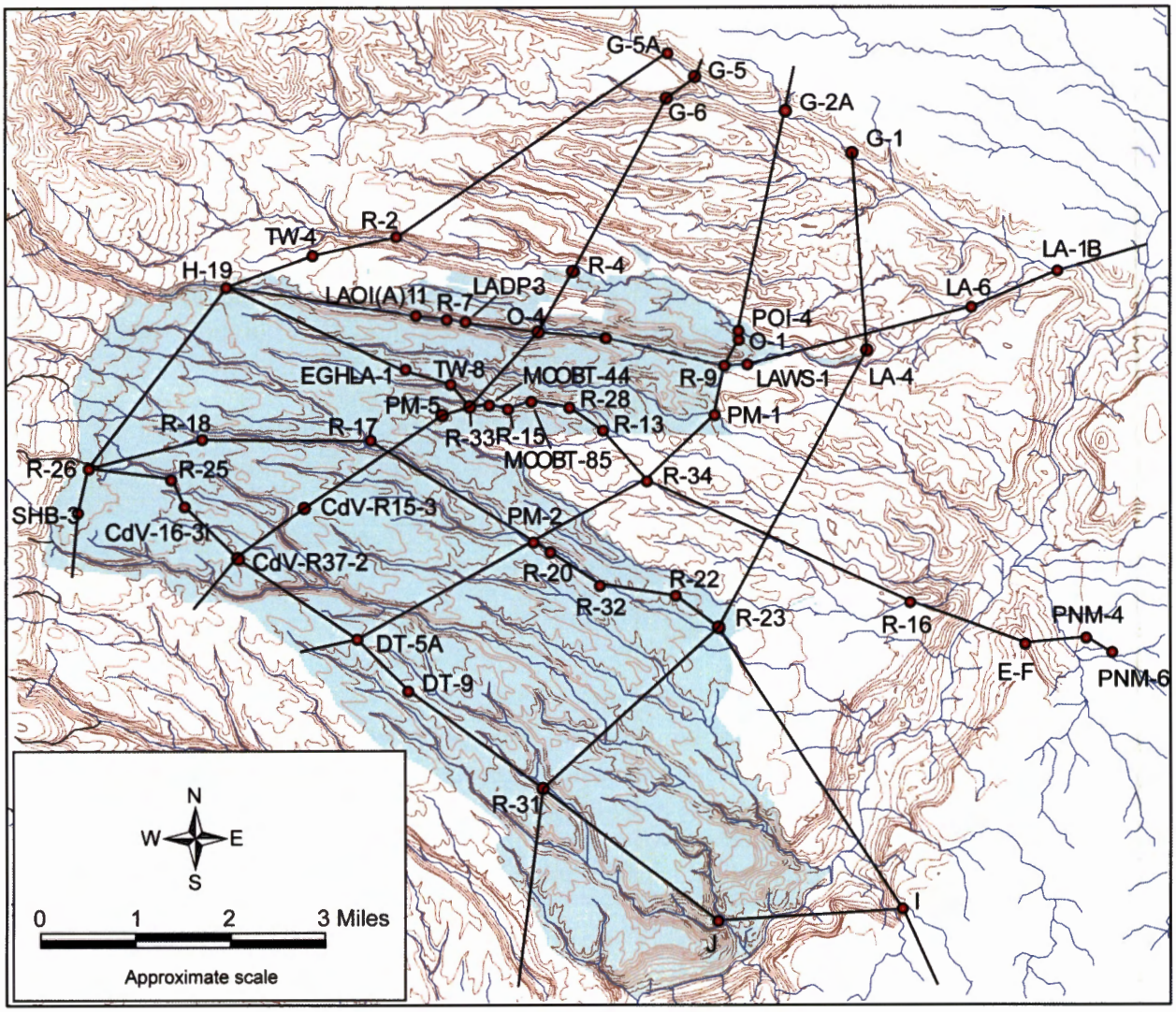


**Figure 2-11.** Lines of cross-section for Figures 2-12 through 2-19.

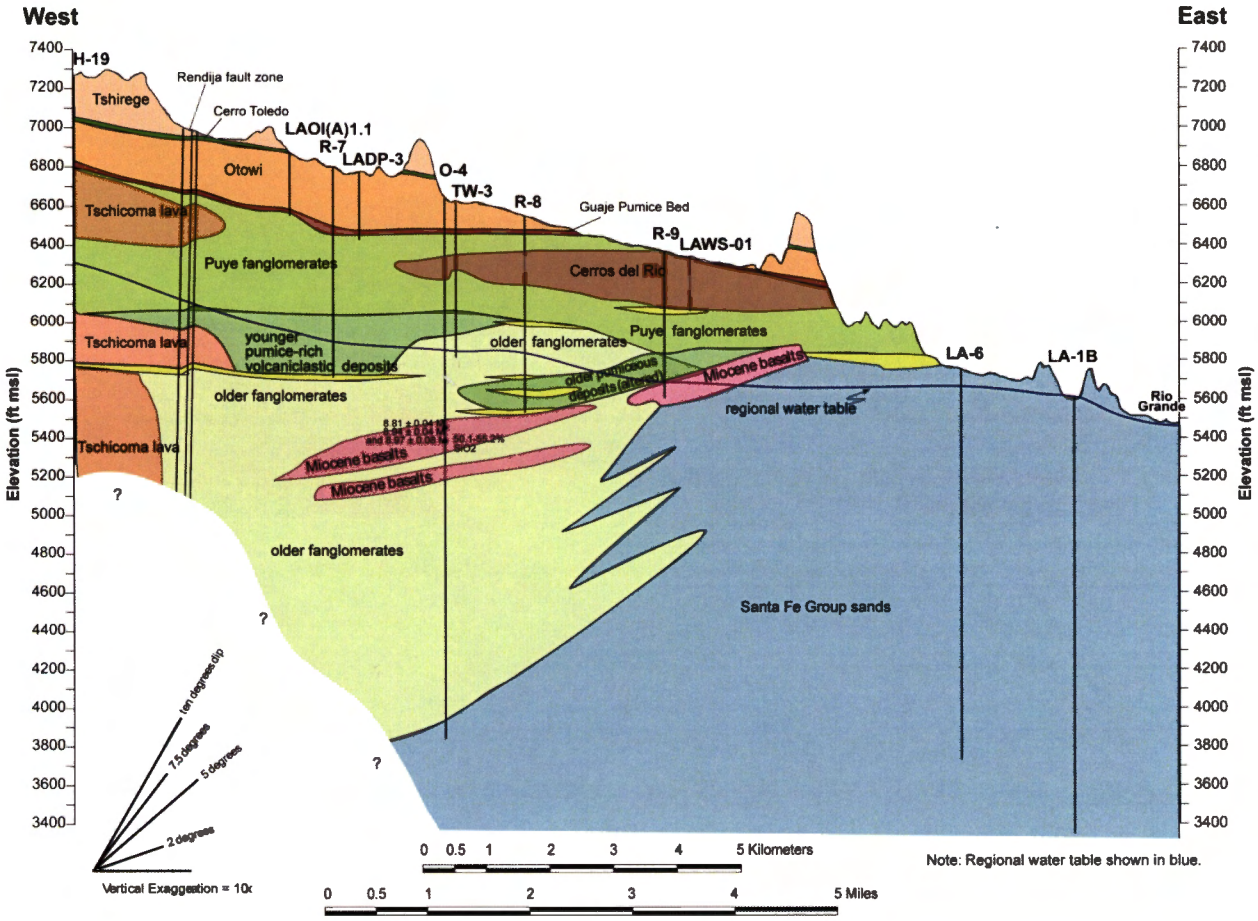


**Figure 2-12.** Conceptual cross-section for Los Alamos Canyon. Blue line is regional water table.

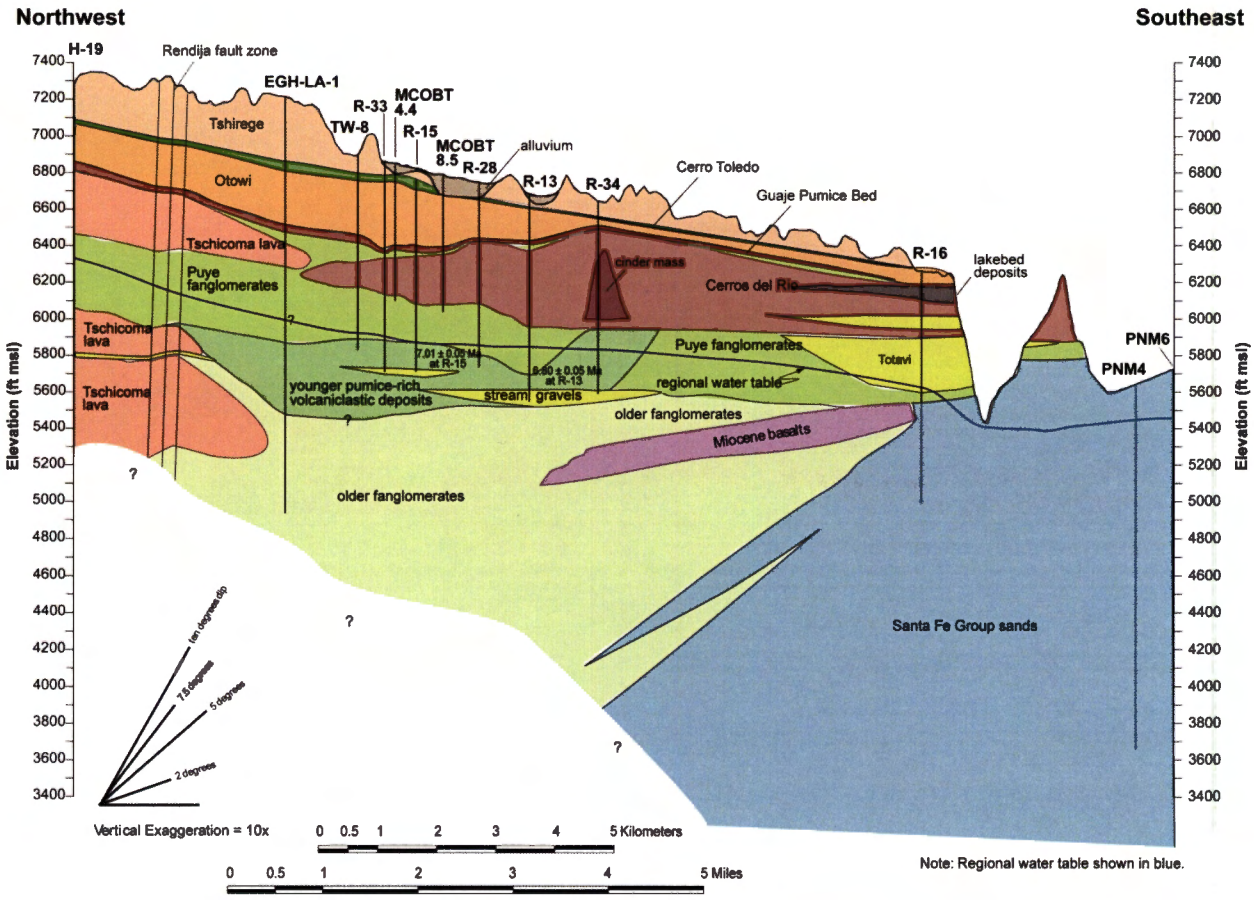


**Figure 2-13.** Conceptual cross-section for Mortandad Canyon. Regional water table is shown in blue.

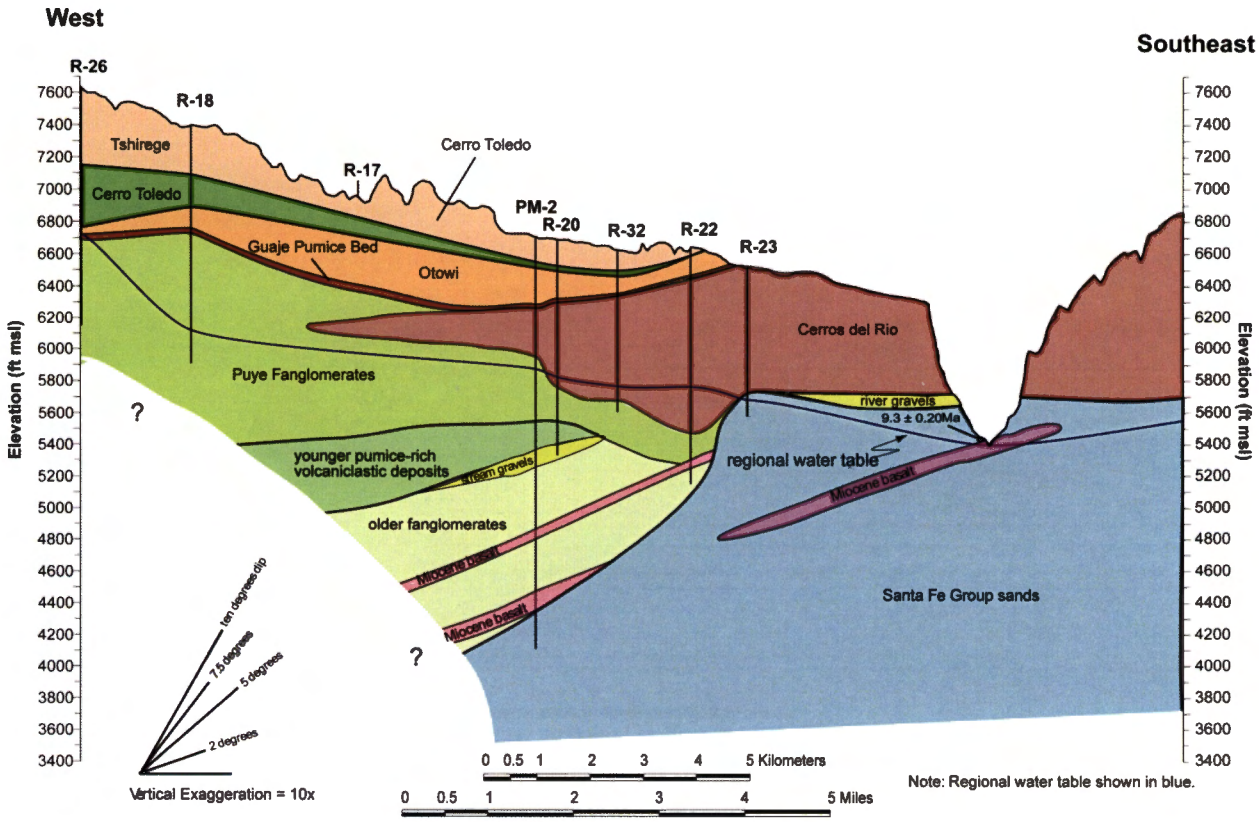


**Figure 2-14.** Conceptual cross-section for Pajarito Canyon. Water table is shown in blue.

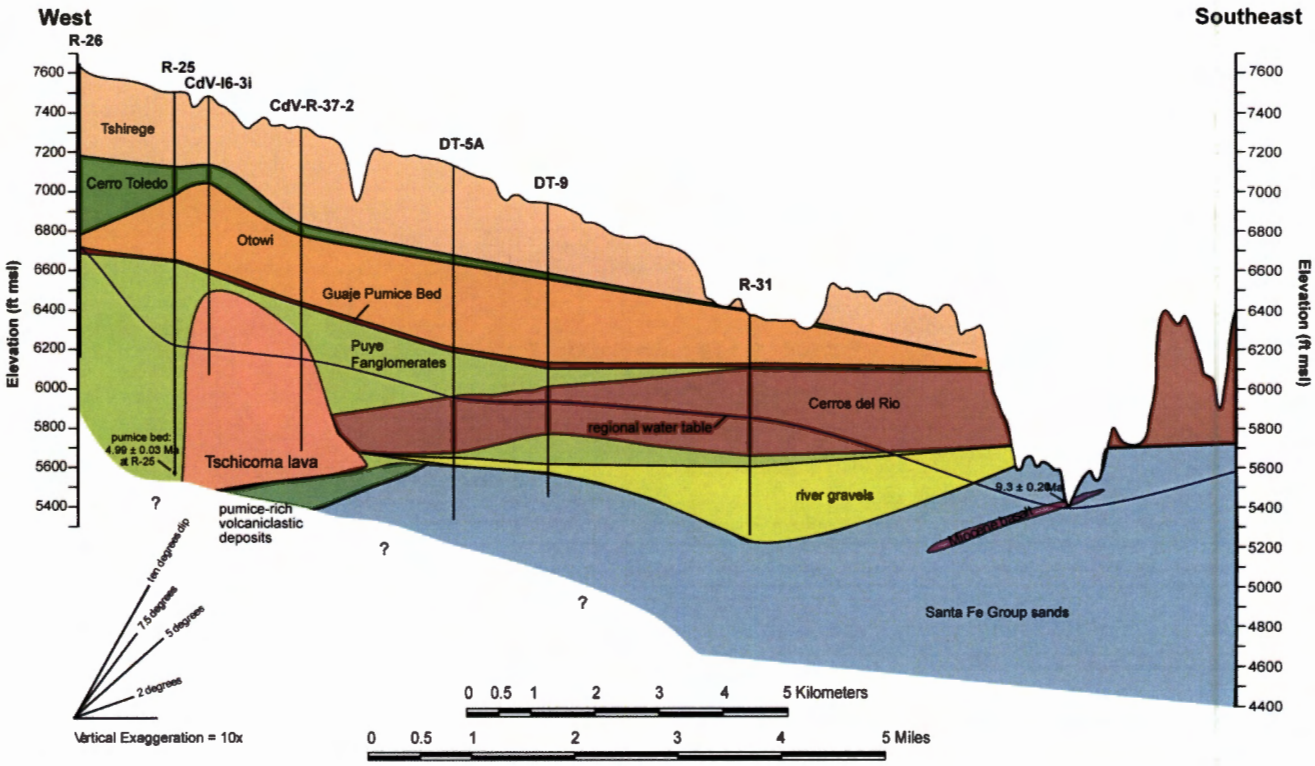


**Figure 2-15.** Conceptual cross-section for Water Canyon. Water table is shown in blue.

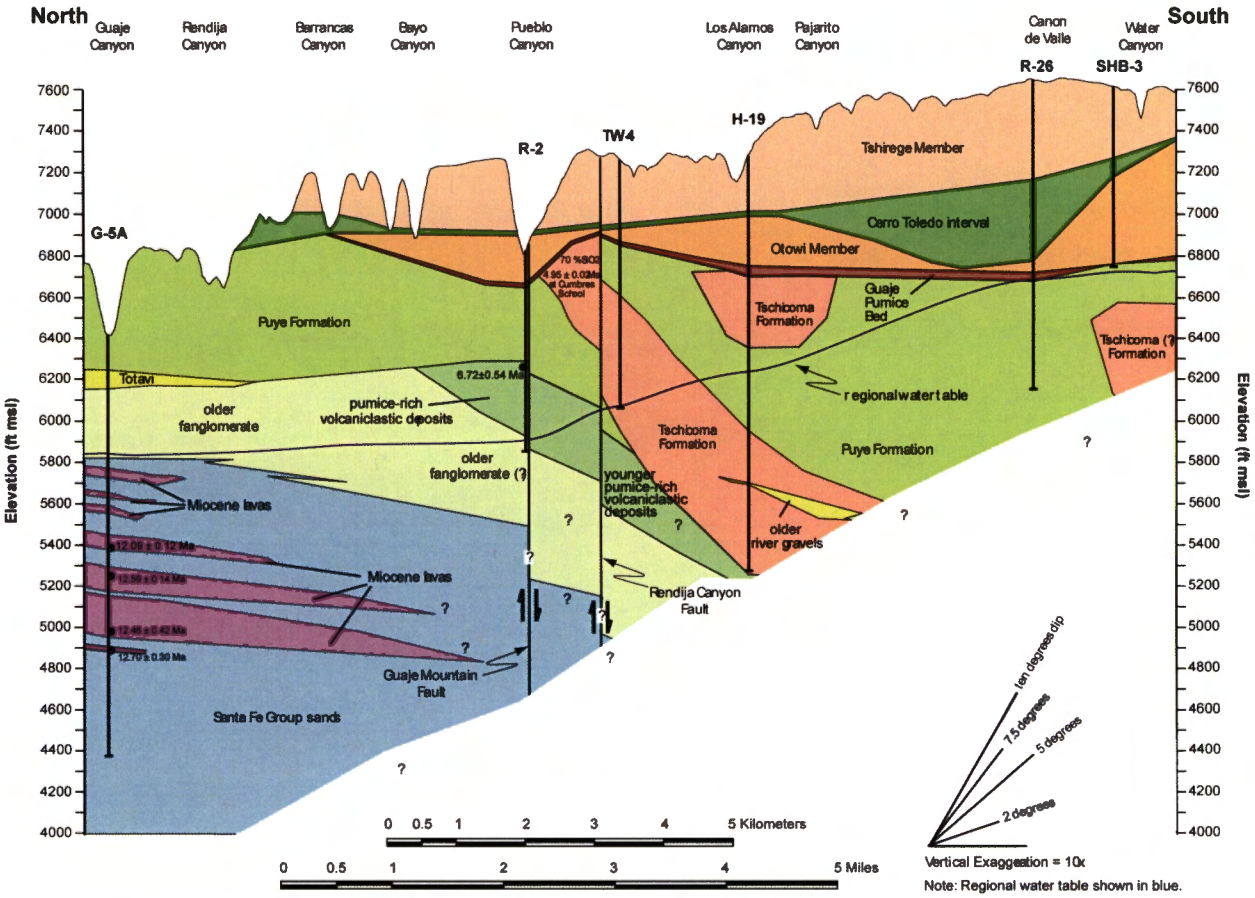


**Figure 2-16.** Conceptual north-south cross-section for the western portion of the Laboratory.

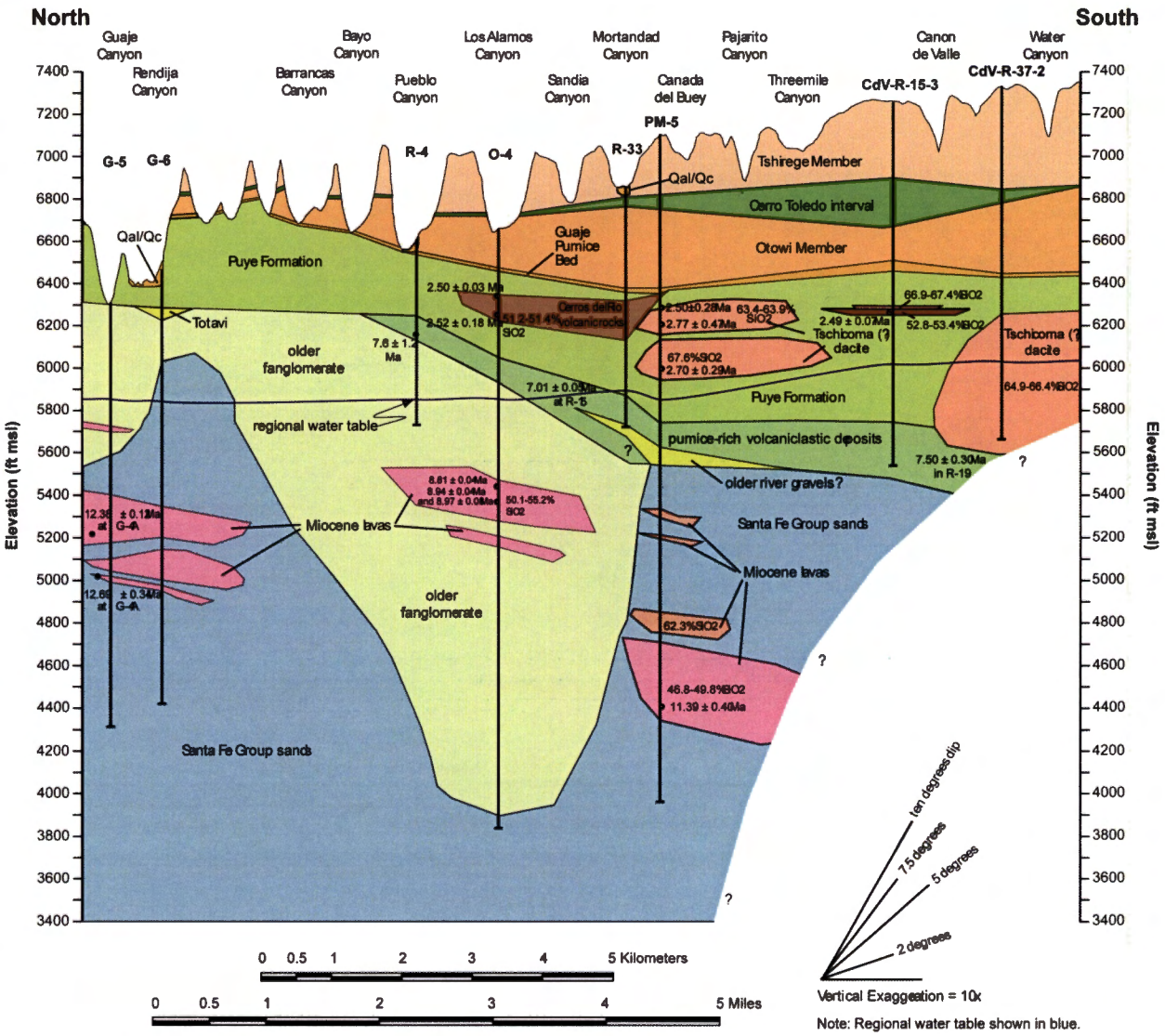


**Figure 2-17.** Conceptual southwest-northeast cross-section from TA-16 through the west-central portion of the Laboratory.

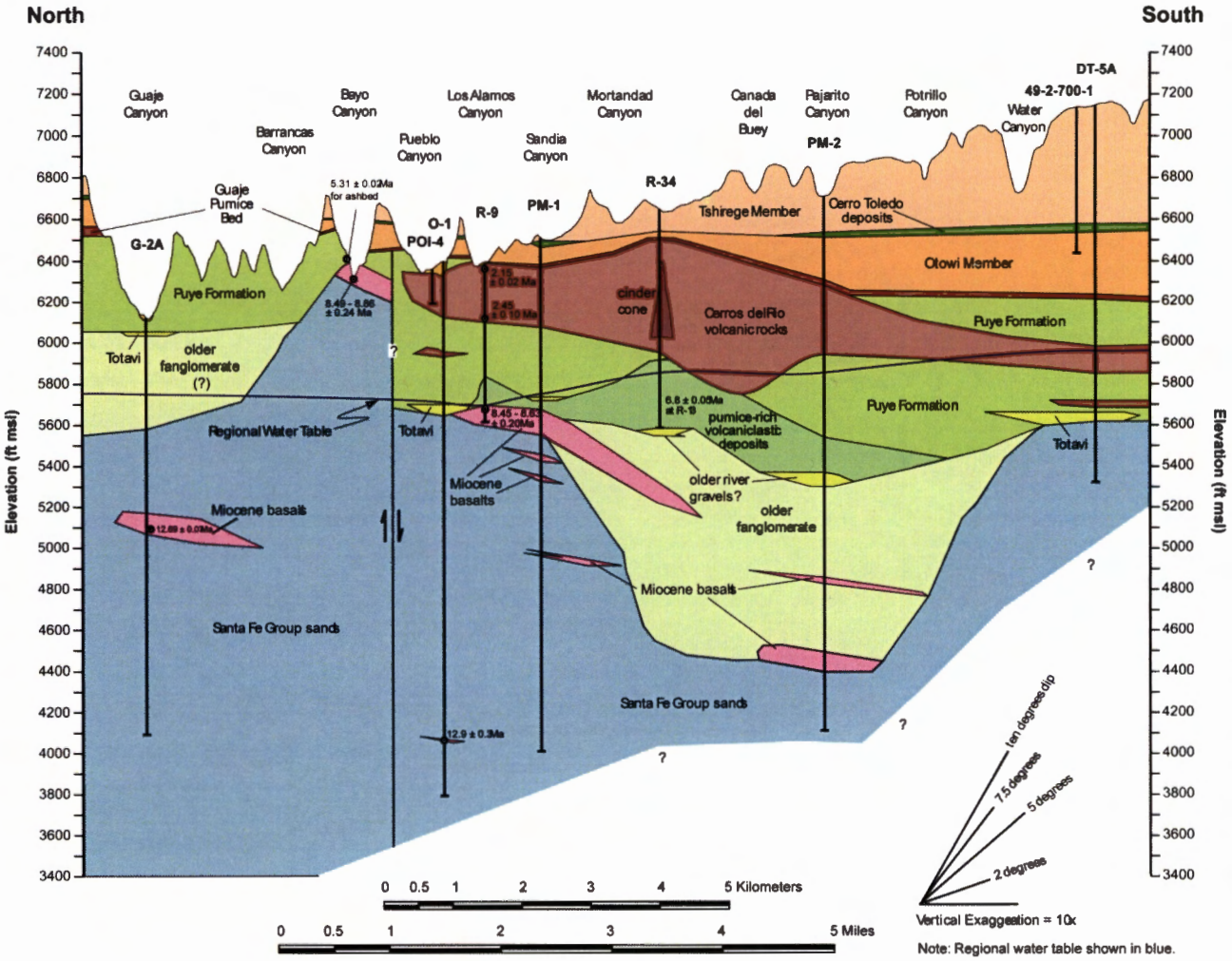


**Figure 2-18.** Conceptual southwest-northeast cross-section from TA-49 through the central portion of the Laboratory.

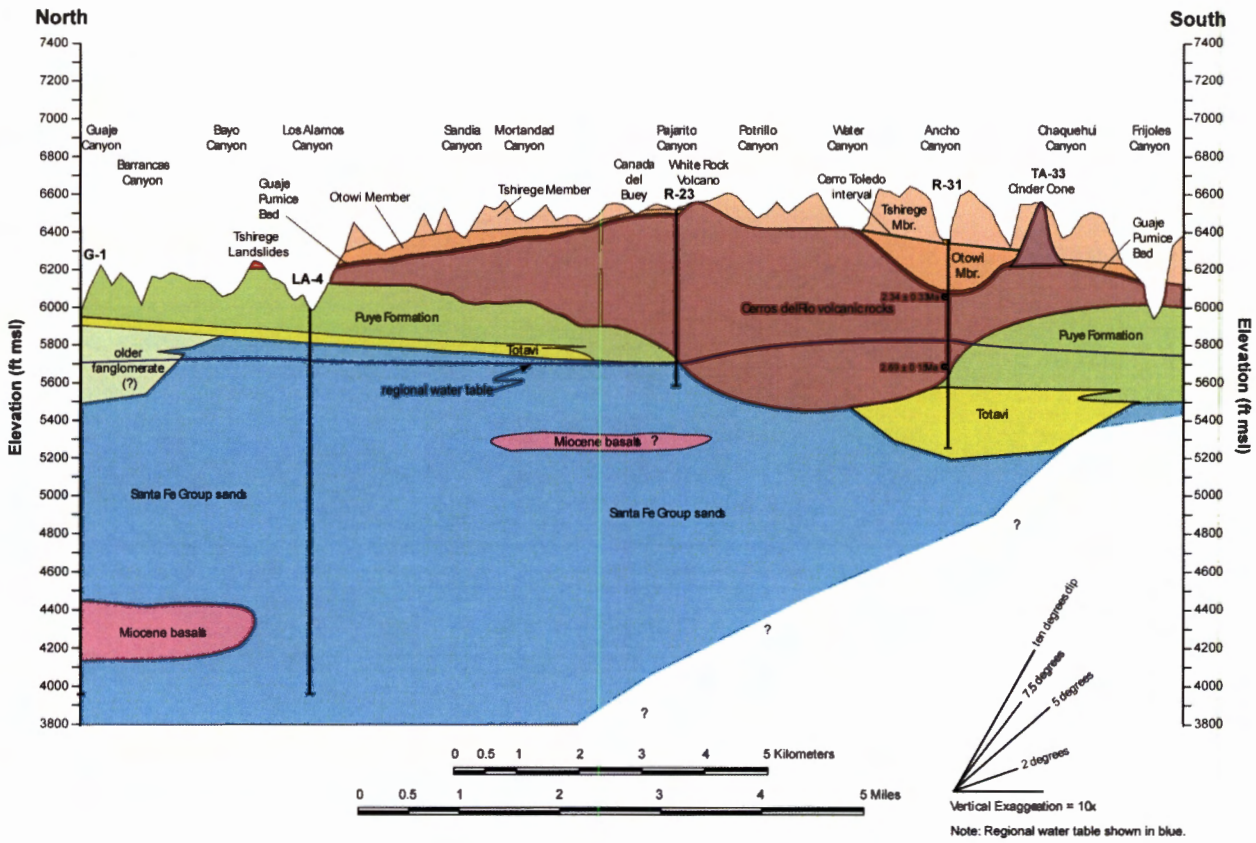


**Figure 2-19.** Conceptual north-south cross-section through the eastern portion of the Laboratory.

#### 2.3.2.1 Los Alamos Canyon Cross-Section

Figure 2-12 shows a cross-section based on boreholes along the length of Los Alamos Canyon, from H-19 to the Rio Grande. At the western margin of this section, thick Tschicoma lava flows are shown extending almost to the Rendija fault zone or slightly beyond. The lack of dacitic lavas in R-7 suggests that the lavas do not extend this far to the east; however, lithologic homogeneity of dacitic lithologies in thick Puye fanglomerate sequences at R-7 may indicate that the dominant lava sources are not far away. From the opposite direction, Cerros del Rio lavas extend from exposures in lower Los Alamos Canyon to O-4 but not to R-7. The "lava gap" at R-7 provides a section of more homogeneous lithology (Bandelier, Puye, and pumice-rich volcaniclastic rocks) from canyon bottom to regional water table without interference from low-porosity dacitic or basaltic lava flow.

Pumice-rich volcaniclastic rocks at R-7 occur in a series of primary or reworked pumice beds intercalated with fanglomerates. In this cross-section these are referred to as "younger pumiceous deposits" to distinguish them from heavily clay-altered and possibly older pumice deposits observed at greater depth in O-4, R-8, and in R-9. In reality these may be unaltered and altered variants of a single unit and the distinction shown here may be abandoned if future studies provide a link between these deposits. The lenses and thin layers labeled as "river gravels" refer to well-rounded gravels that contain at least 10% Precambrian lithologies (quartzite, with and without granite and schists, etc.). As noted in Section 2.2.4, relationships between these gravels and the Totavi are uncertain.

Dips on hydrostratigraphic units in this cross section vary with age; the youngest units dip to the east and older units dip to the west. This variation in dip reflects in part the progressive drop in structural elevation along the Pajarito fault zone, just west of H-19. Younger contributions of Tschicoma lavas, steep fanglomerate slopes shed from these fans, and proximally thick Bandelier ash flows provide the east-dipping masses at higher stratigraphic levels.

#### 2.3.2.2 Mortandad Canyon Cross-Section

Figure 2-13 shows a cross-section beginning at borehole H-19, dropping into Mortandad Canyon at TW-8 and extending along Mortandad Canyon, then to R-16 and across the Rio Grande to well PNM6 in the Buckman well field. This cross section begins in the west where Tschicoma dacitic lavas were found in drillhole H-19, but here the uppermost lavas are extended to borehole EGH-LA-1. The implied relationship between dacitic lavas in these two drillholes is speculative because there are no samples from H-19 to test similarity. If there is continuity of dacitic lavas between H-19 and EGH-LA-1 to the west as shown, then there is likely little or no "lava gap" between Tschicoma dacites and Cerros del Rio basalts as seen in the vicinity of R-7 in Figure 2-12.

The top of the pumiceous deposits, beneath Puye fanglomerates, is well defined in boreholes from TW-8 to R-13. The data from EGH-LA-1 and R-34 are largely inferred due to poor sample returns in these drillholes. There is also a lack of information to indicate whether or not there is a series of clay-altered and possibly older pumiceous deposits, as shown in Figure 2-12, on top of the Miocene basalts shown here. As in the previous cross-section for Los Alamos Canyon, dips on most units vary from easterly in upper horizons to westerly in lower horizons. The evidence for westerly dips in Santa Fe Group sands for this section is based largely on extrapolation from

the FMI dips recorded in drillhole R-16 (see Table 1-A-1). The pumice-rich volcaniclastic deposits dip 5-7° to the southwest at R-1 and R-33 and 6° to the southeast at R-28.

The south-trending paleocanyon at the base of the Bandelier Tuff is more evident in this section than in the more northerly section along Los Alamos Canyon (Figure 2-12). In Figure 2-13 the axis of the paleocanyon is clearly transected in the vicinity of drillholes R-33 to MCOBT-8.5. Evidence for a comparable canyon, offset to the east, may be seen in the depth to pumiceous deposits at R-13, but the paucity of deep cuttings from R-34 make this interpretation somewhat speculative. Evidence for the cinder mass within the Cerros del Rio at R-34 however is very good, and it is likely that a buried basaltic vent source is close to the R-34 drill site, although the distance and direction to the vent are not constrained.

#### 2.3.2.3 Pajarito Canyon Cross-Section

Figure 2-14 shows a cross-section beginning at borehole R-26, extending to the location of well R-18 and planned well R-17, then along Pajarito Canyon to well R-23 and across the Rio Grande to a measured section on the eastern canyon wall (Dethier, 1997). In this cross section the deep erosion into the Otowi ash flows and filling of this eroded canyon by Cerro Toledo deposits is evident (compare with Figures 2-4 and 2-5). As in the Mortandad Canyon cross section, the broad south-trending valley filled by Bandelier Tuff is visible west of PM-2, although placement of the valley axis will depend on observations yet to be obtained from future drillhole R-17.

The deepest point filled by Cerros del Rio lavas in this section is at R-22. This point is the principal evidence for the south-trending paleocanyon seen in Figure 2-8, although the exact trend and the head of the canyon are poorly constrained by current borehole data. The west-dipping Miocene basalts are suggested by dips seen in other drillholes to the north, in outcrop along White Rock Canyon (Dethier, 1997), and by suggested correlations between Miocene basaltic lavas in PM-2 and R-22 and between PM-2 and basalt outcrops in White Rock Canyon. At R-20, FMI logs show that the pumice-rich volcaniclastic deposits dip about 5° to the southwest.

#### 2.3.2.4 Water Canyon Cross-Section

The cross-section shown in Figure 2-15 runs approximately parallel to the southern boundary of the Laboratory, from borehole R-26 to two measured sections on the western and eastern walls of White Rock Canyon (Dethier, 1997). Here the axis of the paleocanyon at the base of the Bandelier Tuff is less evident because the eastern wall of that paleocanyon is essentially flat, from borehole DT-9 to White Rock Canyon. An older and more prominent paleocanyon is shown in the vicinity of borehole R-31, filled by accumulation of largely Precambrian sands and gravels marking a previous channel of the ancestral Rio Grande. The depth of this paleochannel is poorly known because borehole R-31 was unable to penetrate completely through the gravel deposit.

Boreholes CdV-16-3(i) and CdV-R-37-2 were both completed within thick sequences of Tschicoma Formation dacitic lavas. These lavas do not occur in borehole R-25; moreover, lavas encountered in boreholes DT-5A and DT-9 are poorly characterized but are believed to be flows within the Cerros del Rio volcanic field that are likely younger than these thick dacitic lavas, although no samples of these lavas are available for dating. Completion of planned drillhole

R-27 within Water Canyon north of DT-5A will address this question by providing samples of these lavas. Specifically, the well will provide additional information about the composition of lavas in the vicinity of TA-49 and their possible relationship with the lavas encountered in CdV-16-3(i) and CdV-R-37-2. In this cross-section the dacitic lavas in CdV-16-3i and CdV-R-37-2 are shown as being limited in lateral extent. The flow base for these lavas is speculated to be at the top of the older fanglomerates, but actual stratigraphic relations are unknown at this time.

#### 2.3.2.5 Western Boundary Cross-Section

Figure 2-16 shows a cross-section from south of borehole SHB-3 extending up along the western boundary of the Laboratory, northeast to borehole G-5A in Guaje Canyon. This section shows in cross-section the depth and width of the paleocanyon cut into the Otowi Member and filled by deposits of the Cerro Toledo interval in the vicinity of borehole R-26. To the north the Otowi Member has been eroded away and the sediments of the Cerro Toledo interval are deposited on fanglomerates of the Puye Formation. Fanglomerates of the Puye Formation are considerably thicker beneath the Laboratory than to the north. The pumice-rich volcaniclastic and older fanglomerate are believed to occur beneath the western part of LANL but their presence is speculative because boreholes do not fully penetrate the thick Puye Formation in that area. The correlation of dacitic lavas in TW-4 and H-19 is based on lithologic descriptions of phenocryst minerals, but the lack of available cuttings from these boreholes means that this correlation cannot be tested.

#### 2.3.2.6 West-Central Cross-Section

Figure 2-17 shows a cross-section from south of borehole CdV-R-37-2 and extending northeast across the Laboratory to borehole G-5 in Guaje Canyon. In this section the chemical composition of the lavas (wt% $SiO_2$) and available radiometric ages are shown to indicate how the lavas can be used as a guide in stratigraphic interpretation. In general, the ages of lavas assigned to the Cerros del Rio volcanic field or to the older Miocene sequences correlate with stratigraphic depth. The Tschicoma intermediate-composition lavas at the margins of the Laboratory, as in borehole CdV-R-37-2, have not been fully penetrated by any boreholes and the nature of their basal contacts is not known.

As in Figure 2-15, the pumiceous deposits and the underlying river gravels (Totavi) are shown with a southern component of dip, consistent with FMI dip information described earlier. The river gravels can be extended as a continuous unit between boreholes R-33 and PM-5. However, another interpretation would be as unconnected river channels at different elevations, as seen in the east-central cross-section to the east (Figure 2-18).

The cross-section suggests that there is considerable incision into the top pf the Santa Fe Group sands prior to deposition of the older fanglomerate in the vicinity of O-4. This interpretation is supported by the presence of younger Miocene basalts at O-4 that occur at the same structural levels as older Miocene basalts beneath Guaje Canyon. The orientation of possible paleovalleys incised into Santa Fe Group sands cannot be determined because most boreholes in the central and western part of the plateau are not deep enough to penetrate the base of the older fanglomerates. Relations described by Griggs (1964) for wells in the Guaje Canyon areas suggest that some uppermost Santa Fe Group sands interfinger with the older fanglomerate.

#### 2.3.2.7 East-Central Cross-Section

Figure 2-18 shows a cross-section from southwest of borehole DT-5A extending northeast across the Laboratory to drillhole G-2A in Guaje Canyon. This section crosses a high point in the Cerros del Rio volcanic field at borehole R-34. As in the western-boundary and west-central cross-sections (Figures 2-16 and 2-17) the stratigraphy beneath the Bandelier Tuff at the southern Laboratory boundary is speculative. If the lavas penetrated by borehole DT-5A are attributed to the Cerros del Rio (see Figure 2-8) rather than the Tschicoma Formation, the distinction from Cerros del Rio volcanic rocks shown as a contact here may unnecessary. The lack of samples for analysis from borehole DT-5A allows either interpretation, but this problem should be resolved when borehole R-27 is completed in Water Canyon north of DT-5A.

Petrographic and radiometric data from lavas outcropping in Bayo Canyon and comparable data from lavas in borehole R-9 suggest an offset of several hundred feet down to the south, interpreted in this cross section as a normal fault between Bayo and Pueblo canyons, covered by and not offsetting the Bandelier Tuff. Other explanations are possible but fault offset is supported by observed offset of exposures in Bayo Canyon. The number and distribution of faults beneath the Laboratory remains largely unknown, but continuity in many younger units, particularly the Bandelier Tuff and Cerros del Rio volcanic rocks, limits the amount of significant fault offset in the central and eastern Laboratory area to units older than about 3 Ma. As in Figure 2-17, the cross section shows a paleovally incised into the top of Santa Fe Group sands filled by older fanglomerate. These relationships are based on descriptions of the pre-Puye rock units described in the lithologic logs for PM-1, PM-2, and DT-5A, and they cannot be verified because drill cuttings for these wells are not available.

#### 2.3.2.8 Eastern Cross-Section

Figure 2-19 shows a cross-section from south of borehole R-31 extending northeast and then north across the eastern portion of the Laboratory to drillhole G-1 in Guaje Canyon. This figure illustrates the thinning and local absence of the Otowi Member of the Bandelier Tuff over highlands of Cerros del Rio volcanic rocks. The very thick sequence of Cerros del Rio volcanic rocks between boreholes R-23 and R-31 has a total depth that is poorly constrained but likely to have filled a paleocanyon (see Figure 2-8). Continuity of Totavi river gravels from north to south is shown as disrupted in the vicinity of this paleocanyon, for such gravels are missing in several boreholes near this feature. At greater depth the stratigraphic sequence is dominated by Santa Fe Group sands, based on evidence from boreholes in lower Los Alamos Canyon (e.g., LA-4), boreholes to the east (R-16), and exposures mapped in White Rock Canyon (Dethier, 1997).

## 2.4 Hydrologic Properties

The geologic units of the Pajarito Plateau are organized into more generalized hydrogeologic units that form the framework for flow and transport numerical models (Section 4). Hydrogeologic units are subdivided based on lithologic characteristics believed to result in different hydrologic properties. A comparison of geologic and hydrologic frameworks for the plateau region is provided in Figure 2-3.

### 2.4.1 Vadose Zone Hydrologic Properties

The vadose zone, the region between the ground surface and the regional aquifer, consists of variably saturated rocks, and locally saturated zones. The hydrologic properties controlling the flow of water from the surface to the regional aquifer are the saturated hydraulic conductivity (ksat) and the unsaturated hydraulic properties. As explained in basic hydrology texts and in references related to the vadose zone beneath the Pajarito Plateau such as Rogers and Gallaher (1995), when rocks are not completely saturated, the moisture retention curve defines the relationship between the volumetric water content of a soil or rock and its capillary pressure (sometimes referred to as the matric suction or matric potential). As the pores fill with water, capillary forces result in the small-diameter pores filling first, and at progressively larger water contents, the larger pores fill. The resistance to flow is much lower for the large-diameter pores, so that the unsaturated hydraulic conductivity increases as a strong function of the water content, reaching a maximum when the medium is saturated. Under unsaturated conditions, the local water content and matric potential are controlled by the percolation flux; the local values of these variables modulate themselves in response to changes in the local percolation rate, in order that fluid may pass through the rock under gravity-driven or capillary-flow conditions. For unsaturated conditions flux and water content are related and flow is in response to a gradient that is composed of capillary and gravitational terms.

Although most contaminants of concern associated with past LANL operations travel in the liquid phase, gas-phase transport is an important mechanism for radon and also for various volatile organic chemicals present in the subsurface. Furthermore, vadose zone observations used to estimate permeability at larger scales tend to be pneumatic, that is, based on the response of gas-phase pressures to changes in the air pressure exerted at the surface. When treating vapor transport, the permeability to the gas phase is the relevant property. Although in principle the permeability of the medium should be independent of the fluid (air or water), the role of fractures and issues of scale dependence come into play. Given that open fractures are most likely to be air-filled under ambient conditions, fractures dominate the behavior for gas-phase contaminant transport and the interpretation of pneumatic data.

To quantify the scale dependence of permeability of the Bandelier Tuff and to demonstrate the role of fractures, permeability estimates across all scales from laboratory samples to the scale of a mesa have been compiled. For the Laboratory scale, the geometric mean values of saturated hydraulic conductivity reported by Rogers and Gallaher (1995) are used, and water properties at standard conditions are used to convert conductivities to permeabilities. Parameter estimates for larger scales include gas-phase permeability estimates from Neeper (2002) for the tuff, and hydraulic conductivity measurements for the basalts from Stauffer and Stone (2005). In that study, Neeper (2002) presents field-scale results of pneumatic testing using straddle packers, and larger scale estimates based on the interpretation of the pressure responses to barometric cycles. The packer tests are termed "intermediate scale," and the estimates based on response to barometric cycles are called the "large scale."

Figure 2-20 compares the permeability estimates for the three scales. The laboratory scale values represent matrix permeability and discount the role of fractures, as unfractured samples were typically tested. Permeability values are at least one order of magnitude smaller than the

Intermediate-scale estimates. The large-scale values are similar to the intermediate scale, except in certain highly fractured regions, where even higher estimates of permeability are made. The most striking difference with scale is for the Cerros del Rio basalt, where core samples represent competent, low-permeability rock, whereas the field scale is dominated by large, open fractures or cavities that transmit air with virtually no resistance. Field observations in the basalts indicate that pressure changes at the surface are transmitted rapidly to depth (Neeper, 2002).

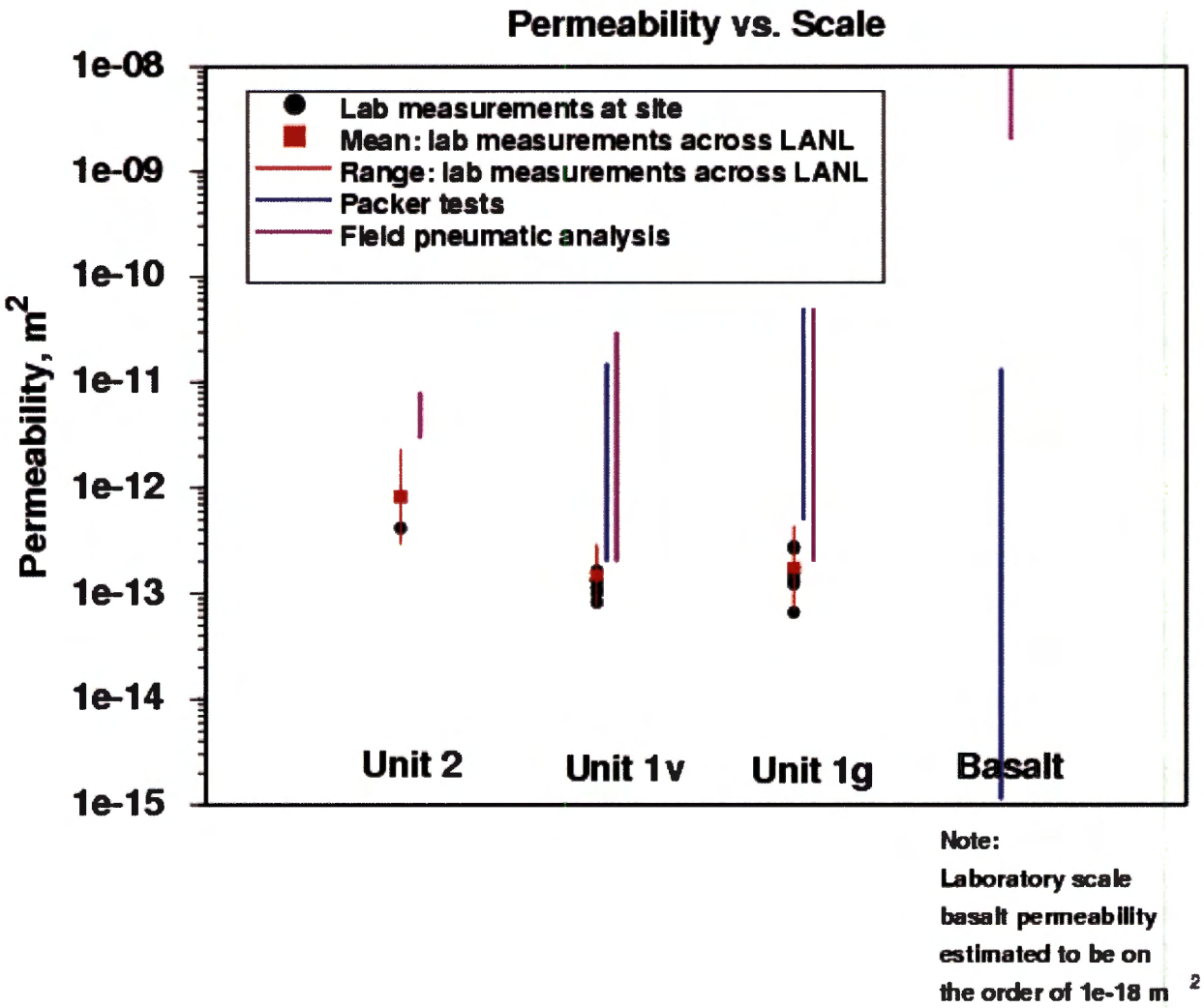


**Figure 2-20.** Permeability as a function of measurement scale for Bandelier Tuff (units 1g, 1v, and 2) and basalts.

These results illustrate the role of measurement scale and rock type on estimating the effective permeability of the rocks in the vadose zone. Clearly, fractures, faults, or other large-scale features exert control on the properties of the rock as scale increases. In this comparison, we have mixed the results of water and air flow observations to examine the role of scale. While it is apparent that the role of fractures in transmitting air through the vadose zone must be considered, the question of water flow and the role of fractures must also be considered. Robinson et al. (2005) provide field evidence and numerical model results that suggest that the Bandelier Tuff transmits water through the porous and permeable matrix even for cases in which water is injected at very high percolation rates. Furthermore, the hydrologic properties measured in samples collected from boreholes suffice to describe the percolation of water through the Bandelier Tuff under unsaturated conditions. That study concluded that as long as the percolation rate is lower than the local saturated hydraulic conductivity, water initially present in fractures is imbibed into the rock matrix. Therefore, rock properties of the matrix are most important, except perhaps near the surface where high-fracture-density zones may coincide with regions of high local infiltration rate. Matrix flow is an important simplification that makes vadose-zone characterization in individual canyons a more tractable problem.

In contrast to the Bandelier Tuff, the basaltic rocks clearly exhibit rapid flow through fractures and other fast pathways, and the permeability of the rock matrix is essentially irrelevant to the rates of water percolation (Stauffer and Stone, 2005). The difference is the orders of magnitude lower matrix permeabilities of these rocks, compared to the Bandelier Tuff.

### 2.4.2 Regional Aquifer Hydrologic Properties

Aquifer properties that are relevant to issues of groundwater quality and quantity are hydraulic conductivity, specific yield (unconfined aquifer) or storativity (confined aquifer), and effective porosity. This subsection summarizes all available information, both recent data collected in R-wells and older estimates from water supply wells. No new information on storage properties of the rocks has been collected in R-wells; this discussion, therefore, will rely entirely on older data.

There are inherent uncertainties associated with any particular estimate of aquifer properties, and there are two particularly important issues to consider when assessing these estimates. First, at the field-scale, these are quantities that are virtually impossible to measure directly. They can only be measured indirectly, via measuring the response of the aquifer to stress, then applying a theoretical model to that response. In a particularly complex aquifer such as the one beneath the Pajarito Plateau, the models used to interpret aquifer tests are necessarily much simpler than the actual aquifer and this will affect the accuracy of the test interpretation. Second, in a complex aquifer, hydraulic conductivity will vary substantially depending on the scale over which it is measured. Tests conducted in wells with long screens (such as water supply wells) and/or tests conducted over long time periods will sample large portions of the aquifer and the results will be average properties of the aquifer, including possible structural features such as faults. Short-term tests and/or tests in wells with short screens will sample small-scale features. The results from such tests will tend to show much greater variability than those in the first category. Only field-scale test results are considered here, since these are most pertinent to field-scale flow and transport in the regional aquifer. Borehole geophysics and bench-scale test approaches to

estimating hydraulic conductivity are not summarized here, although borehole geophysics-based estimates of effective porosity are discussed.

#### 2.4.2.1 Expected Lithologic Controls on Regional Aquifer Hydrologic Properties

The two major types of aquifer rocks beneath the Pajario Plateau are sedimentary and volcanic rocks. The hydrologic properties of sedimentary and volcanic rocks can be very different and they are discussed separately.

**Sedimentary units** include the Puye Formation, pumice-rich volcaniclastic rocks, Totavi Lentil, older fanglomerate, Santa Fe Group sands, and sedimentary deposits between basalt flows. Based on outcrop and borehole observations, all these units are expected to be highly heterogeneous and strongly anisotropic, with a much higher conductivity parallel to sedimentary beds than perpendicular to these beds. Figure 2-21 shows photographs of the Puye Formation and the Santa Fe Group showing the typical nature of bedding. Figure 2-22 shows an outcrop of the Totavi Lentil, a unit found at the base of the Puye in some locations, containing cobble beds with abundant quartzite.

The Puye Formation is heterogeneous, containing a variety of sedimentary lithologies. Based on previous studies by Waresback et al. (1984) and Turbeville (1991) significant heterogeneity is expected to occur at scales from kilometers to meters (laterally) and meters to centimeters (vertically).

Due to lack of drill core, it is generally not possible to identify the depositional environments penetrated by R-wells within the Puye. Cuttings and borehole geophysics were used to distinguish between Puye fanglomerate (dacite detritius and sparse to absent pumice fragments), pumice-rich volcaniclastic rocks (abundant pumiceous fragments), Totavi Lentil (rounded clasts of abundant quartzite and other Precambrian lithologies), and older fanglomerate (volcanic detritus and sparse quartzite). The pumic-rich volcaniclastic rocks are expected to have a relatively high porosity, given the abundance of fairly coarse vitric pumice fragments. This high porosity *may* translate to high permeability. In some areas the pumiceous rocks are extensively clay-altered and permeability may be greatly reduced. The Totavi Lentil, an ancestral Rio-Grande alluvial deposit, is possibly the most transmissive of the sedimentary units due to the abundance of unconsolidated sands and gravels (see Figure 2-22). Fine-grained sediments, which may have low permeability, are also present in this unit.

Purtymun (1995) identified a thick zone of highly productive aquifer rocks that extends northeastward across the central plateau. Recent revisions to the plateau stratigraphy (Section 2.1) suggest that this zone includes older fanglomerate deposits, pumiceous volcaniclastic rocks, and lower portions of the Puye Formation. As will be shown below, both high and low permeability rocks are present within this zone.

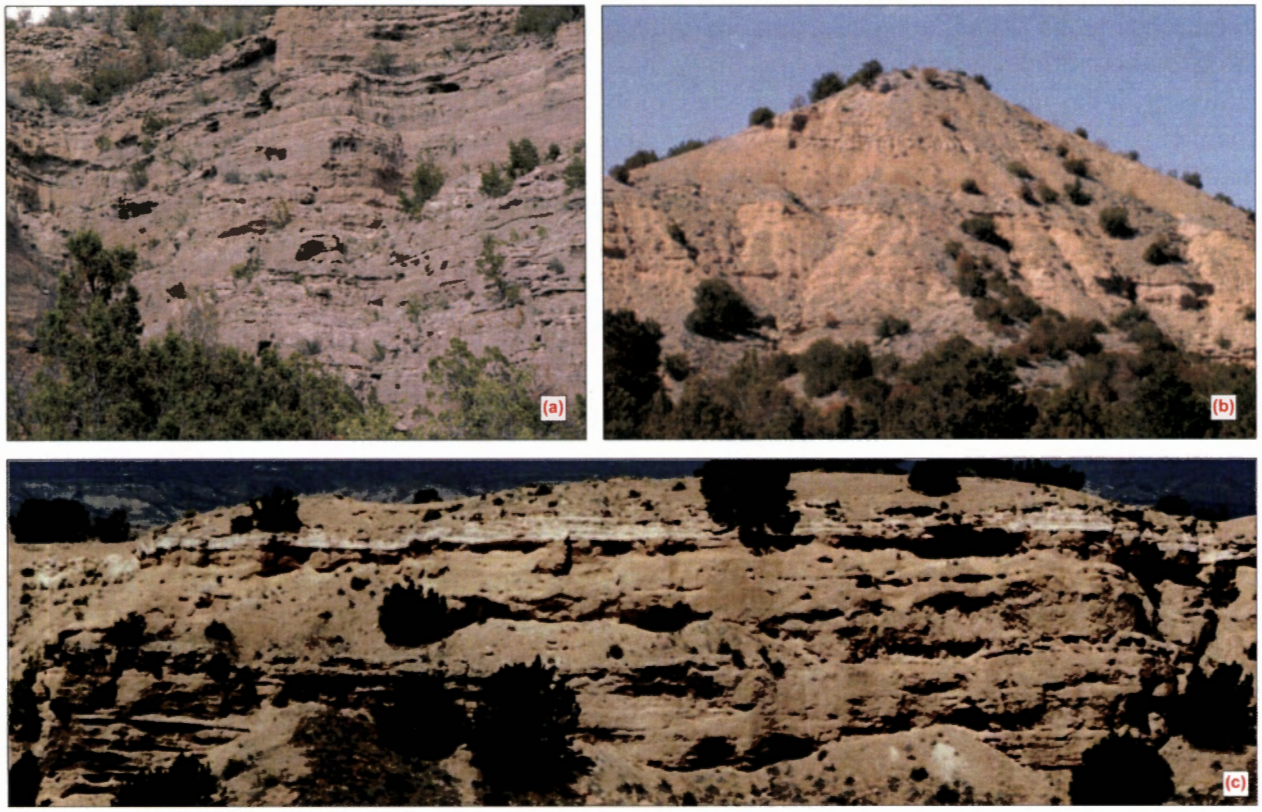


**Figure 2-21.** (a) Outcrop of the Puye Formation, Rendija Canyon (north of LANL); (b) Outcrop of the Santa Fe Group, lower Los Alamos Canyon (east of LANL); (c) Outcrop of the Santa Fe Group, near Española (provided by Gary Smith, UNM Dept. of Earth and Planetary Sciences).

**Figure 2-22.** Outcrop of Totavi Lentil along SR 304 (D. Vaniman in foreground).

In heterogeneous units like these sedimentary deposits, it is particularly important to determine the lateral continuity of the high-permeability facies such as coarse stream channel deposits. However, it has not been possible to correlate individual beds in the Puye Formation because channel and overbank deposits in alluvial fan settings form complex, cross-cutting deposits, many of which are channelized or of limited lateral extent. Because of similar source rocks, clast compositions fail to provide distinct criteria for discriminating individual beds, particularly for boreholes spaced as far apart as the R-wells.

The storage properties of these rocks are expected to be within the normal range for sedimentary aquifers: specific yield (Sy) between 0.01 and 0.3 and storativity (S) between 5.E-3 and 5E-5. Likewise, effective porosity values are expected to be in the normal range for sedimentary rocks from 0.1 to 0.3 (Freeze and Cherry, 1979).

**Volcanic rocks** on the Pajarito Plateau include intermediate-composition lavas of the Tschicoma Formation and basalts (Cerros del Rio, Bayo Canyon, and Miocene basalts within the Santa Fe Group). These volcanic rocks consist of stacked lava flows separated by interflow zones. Figure 2-23 shows an example of Cerros del Rio basalt. Flow interiors are made up of dense impermeable rock that is variably fractured. The interflow zones contain highly porous breccias, clinker, cinder deposits, and sedimentary deposits. Groundwater flow in lava interiors is controlled by fractures, with hydraulic conductivity determined by aperture dimensions, fracture density, interconnectivity, and the presence or absence of fracture-filling minerals. Porous flow is expected to dominate groundwater flow in the interflow zones. Both nonfractured flow interiors and clay-filled fractured zones are expected to have very low permeability; zones with significant, connected open fractures, lava tubes, and interflow zones are expected to have higher permeability and low porosity, a combination of properties which can lead to very fast travel times (Stauffer and Stone, 2005).

The lava interiors presumably have very low effective porosity (<<0.1) and negligible storativity. Highly fractured zones and interflow zones may have larger porosity and storativity values, comparable to values expected for sedimentary rocks. Moderately fractured zones may have low effective porosity ($10^{-3}$–$10^{-4}$). Table 2-2 summarizes qualitative expectations of aquifer properties based on lithology and on the available data, augmented by field-scale testing, model calibration, and head gradients.

**Fault zones.** There are several faults on the plateau, including the Pajarito fault zone and the Rendija Canyon and Guaje Canyon faults (Figure 2-2). These are primarily oriented north-south, with local deviations. There are numerous north-south trending faults in the Santa Fe Group within the larger Española Basin; these types of faults are presumably present beneath the plateau, but they are covered by younger rocks. In general, faults can be conduits to flow (if open) or barriers to flow (if cemented or clay-filled). Field hydrologic evidence has been interpreted based on both of these occurrences. For example, Griggs and Hem (1964) postulated the presence of a fault acting as a flow barrier based on pumping tests in the Guaje Canyon wells. By contrast, Purtymun (1977) and Blake et al. (1995) observed evidence of faults acting as conduits for upward flow of deep thermal waters in the Santa Fe Group, based on geochemical and thermal evidence in lower Los Alamos Canyon wells and San Ildefonso wells. More recently, Keating et al. (2003), suggested that the large-scale effective permeability of the

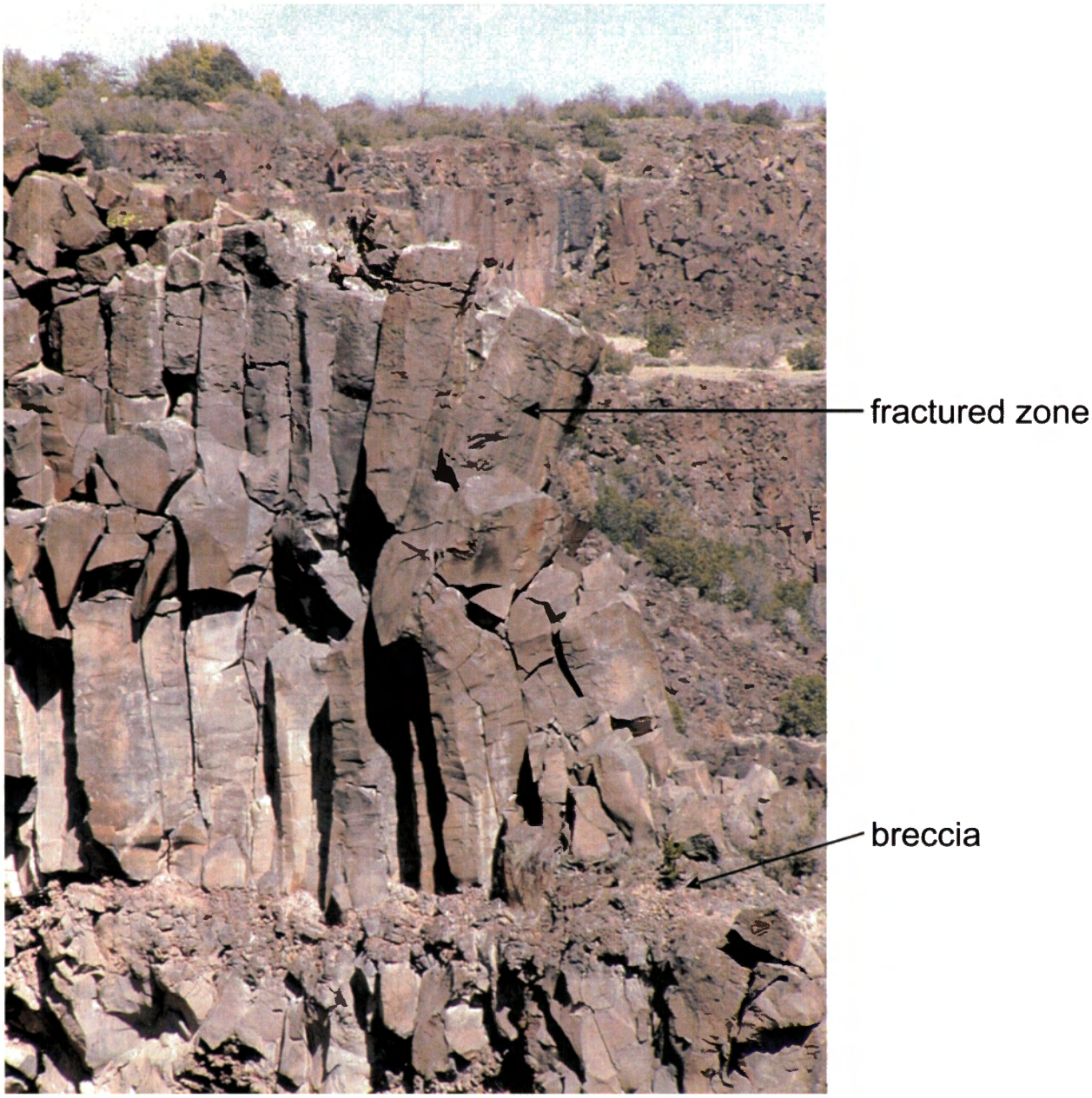


**Figure 2-23.** Outcrop of Cerros del Rio basalt at White Rock Overlook (east of LANL).

**Table 2-2.**
**Inferred Properties of Hydrostratigraphic Units,**
**Based on Field-Scale Testing, Model Calibration, and Head Gradients**

| Stratigraphic Unit | Sub-Unit | Description | Hydraulic Conductivity | Effective Porosity | Storage |
|---|---|---|---|---|---|
| Puye | Fanglomerate | Stream channel, overbank, colluvium, and lahar deposits | Extremely variable(0.007–45 m/day), both the highest and lowest K estimates on the plateau occur within this unit | 0.07–0.2 | No data |
| | Pumiceous | Ash and pumice-rich layers, both air fall and reworked | Extremely variable (0.3–6 m/day) | 0.15–0 .2 | No data |
| Lava flows (Tb1, Tb2, Tb4, Tt) | Massive | Pore space (vesicles) is not connected | <0.15 m/day | No data | No data |
| | Fractured | In flow interiors, fractures tend to be vertical; near flow tops and bottoms, many fracture orientations are observed, including sub-horizontal | 1–9 m/day | No data | No data |
| | Breccia zones | Highly fractured rock, either open or clay-filled | No data | No data | No data |
| Santa Fe Group | Sandy | Alluvial fan deposits (stream channel, colluvium, overbank) | Relatively uniform (0.3 m/day); faults may decrease large scale effective K | No data | Log10 [$m_{-1}$] ~ –3.8 to–4.8 |
| | Fanglomerate | Stream channel, overbank, and colluvium, | Variable (0.1–5.3 m/day), no evidence of very high permeability | No data | Log10 [$m_{-1}$] ~ –5.5 |

Pajarito fault zone is lower than surrounding rocks, based on observations of large horizontal gradients and model interpretations of these gradients. They also concluded that the large-scale effective permeability of the Santa Fe Group is lower than that indicated by individual pump test results (summarized below). These results indicate that faults in the Santa Fe Group, which tend to be north-south trending (transverse to the hydraulic gradient), may act as flow barriers in the direction perpendicular to their orientation, lowering the large-scale effective permeability of the aquifer.

#### 2.4.2.2 Contact between Units

Depths to contacts between the major geologic units are generally well established, but their physical characteristics must be inferred from cuttings and geophysical logs. Outcrop data provide additional information about these contacts. Intra-formational and between-unit sedimentary contacts are generally conformable but are frequently disrupted by facies transitions and channel incisions. Individual beds can be traced laterally over the scale of meters to hundreds of meters. Major erosional unconformities between principal units, such as the Puye and Tesuque Formations, probably occur beneath the Pajarito Plateau, but the nature and orientations of features such as paleocanyons are unknown. Features such as clay-rich soils occur internally within some units like the Puye Formation, but do not appear to be important along intraformational contacts.

The contacts between coarse-grained units, such as the Puye Formation or the older fanglomerate, and fine-grained sediments of the Tesuque Formation may have hydrologic significance because of the juxtaposition of fundamentally different lithologies. Where exposed in the eastern part of the plateau, the contact between Puye rocks and Tesuque strata is a slight angular unconformity. Hydraulic gradients are generally easterly/southeasterly on the plateau (Figure 2-24). Within the Puye Formation, this driving force is parallel to the east-dipping beds. In contrast, within the Tesuque Formation, beds tilt to the west. This anisotropic condition will result in larger flow resistance and possible local deviations in flow direction within the Tesuque rocks.

The contact between the older fanglomerate and the Tesuque Formation may also be hydrologically important. In Guaje Canyon, thick sequences of older fanglomerate interfinger laterally for several kilometers with the Tesuque Formation (see Griggs, 1964 for discussion of these relations). The effect of these interfingering relations on groundwater flow is not known but could include changes in potentiometric surface gradients and partial confinement of groundwater in older fanglomerate enclosed by less permeable Tesuque strata. In Los Alamos and Pueblo Canyons, lateral infingering between the older fanglomerate and the Tesuque Formation appears to be more abrupt. The lithologic difference between the older fanglomerate in Otowi-4 and the Tesuque Formation in Otowi-1 is striking, and the lateral hydraulic conductivity should decrease eastward. The presence of altered Miocene basalts in the Tesuque Formation in wells R-9 and R-12 should also contribute to a decrease in hydraulic conductivity eastward.

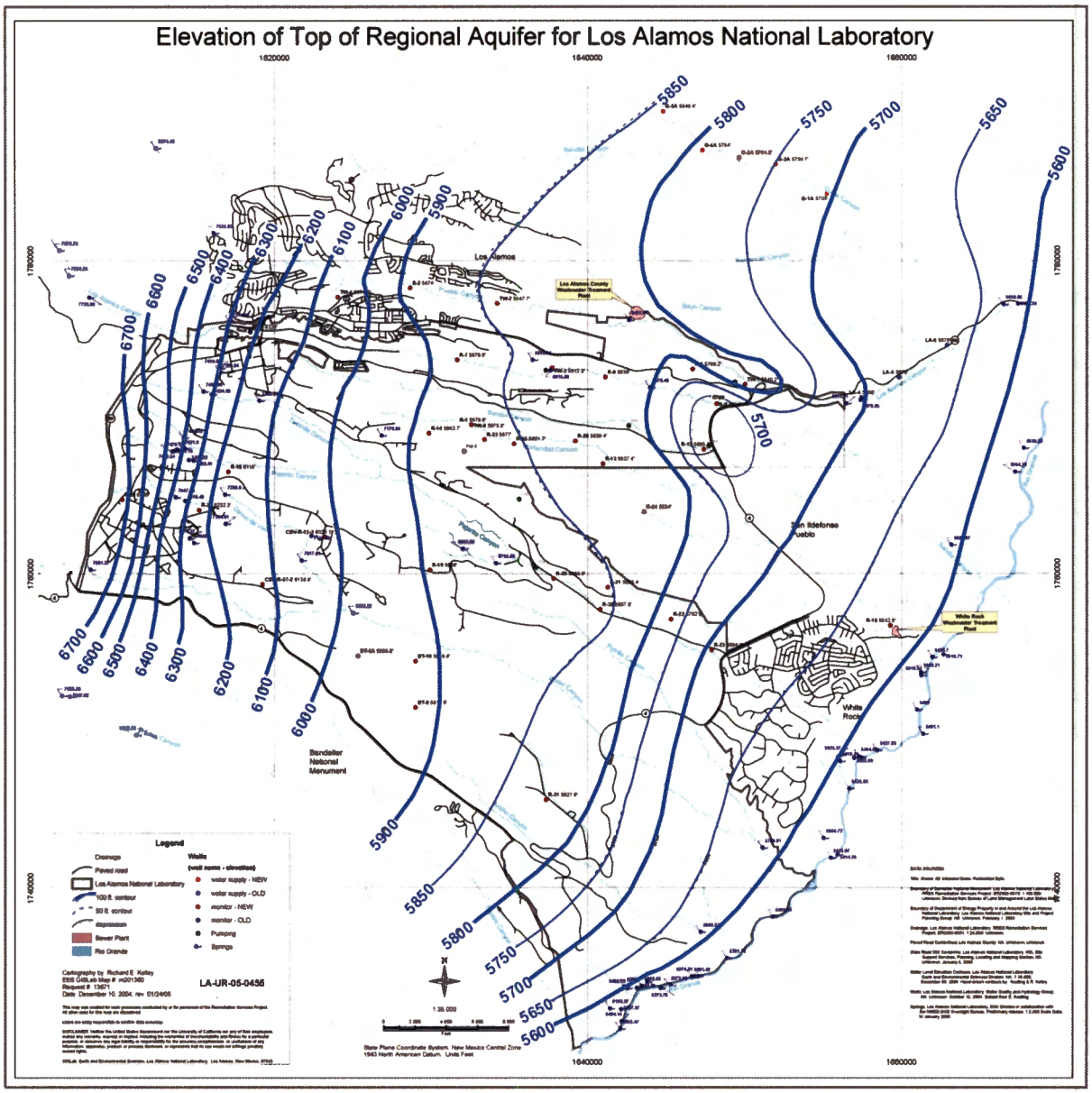


**Figure 2-24.** Regional aquifer water table map.

We note again that the sedimentary rocks themselves are highly stratified, and so contrasts between layers within these rocks may be as hydrologically significant (or more so) than the contacts between major geologic units described above. Contacts within volcanic units can have significant hydrologic impact. The contacts between lava flows are generally represented by interflow zones that can be very transmissive or, if clay-filled, barriers to flow. One example of a low-permeability, clay-filled interflow zone was that encountered in screen 2 of R-9i. This zone appears to act as a confining bed; water levels rose significantly in the borehole after the well penetrated this zone. Contacts between sedimentary and volcanic rocks can be structurally complex, as in the inferred paleovalley in the eastern part of the plateau that is filled by Cerros

del Rio basalt (Section 2.2.8; Figure 2-8). Groundwater flow from west to east may be more tortuous and possibly diverted when encountering such large-scale structures.

#### 2.4.2.3 Regional Aquifer Hydraulic Conductivity

**Inferences based on field-scale testing.** Over the last 40 years, hydraulic conductivity has been measured using pump tests and straddle-packer injection tests in 61 locations within the Pajarito Plateau; some locations have been measured multiple times. Table 2-3 presents a compilation of these test results (86 in all). For those wells tested multiple times, or for which multiple interpretations of a single test are available, we selected one representative value for the discussion and analyses below (these are indicated with an asterisk in Table 2-3). All these tests are within the regional aquifer, with the exception of a perched zone in R-9i that is included because it represents a test of saturated basalt. If the screened interval for a test contained at least 50% of a single stratigraphic unit, the test was categorized as representing that unit. Some wells (all the PM wells, for example) are screened across too many rock units and are labeled as "mixed" in Table 2-3.

Figure 2-25 shows a histogram of the 61 hydraulic conductivity values, which range from 0.007 m/day (R-26, screen 2) to 45 m/day (R-28). The geometric mean of these estimates is 0.6 m/day, and the distribution appears to be lognormal, although we ascribe no special significance to this fact, other than to point out that it is a convenient distribution for modeling purposes. Based on the distribution, the standard deviation of the lognormal distribution is 0.76 in units of ln(m/d).

Figure 2-26 illustrates the spatial variation in hydraulic conductivity on the plateau. There are two areas with relatively high hydraulic conductivity (K > 3 m/day): the north-central aquifer beneath LANL (TW-2, R-4, TW-3, R-11, R-28, and R-13) and the south-central aquifer beneath LANL (R-19, screen 6, DT-10, DT-9). The location of these zones overlaps the zone of high-yield wells identified by Purtymun (1984). However, based on new geologic data and interpretations, the rocks making up this zone consist of a variety of sedimentary and volcanic units in addition to those attributed to the "Chaquehui Formation" by Purtymun. Also, it is clear that lower conductivity zones also exist within Purtymun's proposed northeast-trending high-production trough, indicating that it is a heterogeneous portion of the aquifer, with locally high and low permeability zones.

**Table 2-3.**
**Estimates of Hydraulic Conductivity from Well Tests on the Pajarito Plateau**

| Well | Source | Method | m/day | ft/day | Unit | Screen | | Comments |
|---|---|---|---|---|---|---|---|---|
| | | | | | | Top | Bottom | |
| DT-10 | Purtymun (1995) | Pump test | 4.53 | 14.87 | Tb4 | 472 | 475 | Tf, Tpt, and Tpf also |
| R-22-2 | McLin and Stone (2004) | Injection | 0.01 | 0.04 | Tb4 | 289 | 301 | Could be a breccia zone |
| R-31-3 | McLin and Stone(2004) | Injection | 0.15 | 0.48 | Tb4 | 203 | 206 | 0 |
| R-9i-1 | McLin and Stone (2004) | Injection | 2.16 | 7.10 | Tb4 | 331 | 429 | Fractured |
| R-9i-2 | McLin and Stone (2004) | Injection | 0.03 | 0.11 | Tb4 | 82 | 85 | Massive |
| G-3A | Shomaker (1999) | Pump test | 0.45 | 1.48 | Tb1 | 180 | 604 | |
| G-5A | Shomaker (1999) | Pump test | 0.23 | 0.75 | Tb1 | 228 | 604 | |
| R-22-4 | McLin and Stone (2004) | Injection | 0.16 | 0.54 | Tb1 | 420 | 422 | Fractured basalt with alteration |
| CDV-R-15-3-5 | Well completion report | Injection | 0.08 | 0.25 | Tpf | 411 | 413 | 0 |
| R-13 | McLin and Stone (2004) | Pump test | 5.36 | 17.60 | Tpf | 292 | 311 | Straddles Tpf/Tpp contact |
| R-22-3 | McLin and Stone (2004) | Injection | 0.10 | 0.32 | Tpf | 388 | 390 | High glass to clay ratio |
| R-26-2 | Shafer (personal communication) | Pump test | 0.00 | .002 | Tpf | 433 | 440 | |
| R-28 | Kleinfelder (2004) | Pump test | 45.42 | 149.00 | Tpf | 285 | 292 | Tpf according to cuttings, Tpp/Tpf mixture according to geophysics |
| R-32-3 | McLin and Stone (2004) | | 0.37 | 1.20 | Tpf | | | |
| R-11 | Kleinfelder (2004) | Pump test | 35.51 | 116.50 | Tpp | 261 | 268 | Assigned by Broxton and Vaniman |
| R-19-7 | McLin and Stone (2004) | Injection | 6.71 | 22.00 | Tpp | 558 | 561 | 0 |
| R-19-6 | McLin and Stone (2004) | Injection | 5.67 | 18.60 | Tpp | 526 | 529 | 0 |
| R-1 | Kleinfelder (2004) | Pump test | 1.19 | 3.90 | Tpp | 314 | 322 | Assigned by Broxton and Vaniman |

**Table 2-3.**
**Estimates of Hydraulic Conductivity from Well Tests on the Pajarito Plateau (continued)**

| Well | Source | Method | m/day | ft/day | Unit | Screen | | Comments |
|---|---|---|---|---|---|---|---|---|
| | | | | | | Top | Bottom | |
| R-34 | Shafer (personal communication) | Pump test | 1.07 | 3.5 | Tpp | 269 | 276 | |
| TW-8 | Purtymun (1995) | Pump test | 1.02 | 3.35 | Tpp | 290 | 325 | 0 |
| R-15 | McLin (2004) | Pump test | 0.67 | 2.20 | Tpp | 292 | 311 | Small portion is Tpf |
| R-14-2 | McLin and Stone(2004) | Injection | 0.30 | 1.00 | Tpp | 390 | 404 | 0 |
| CDV-R-15-3-6 | Well completion report | Injection | 0.03 | 0.10 | Tpp | 499 | 501 | 0 |
| R-4 | Kleinfelder (2004) | Pump test | 5.30 | 17.40 | Tf | 242 | 249 | 0 |
| O-4* | Purtymun (1995) | Pump test | 1.23 | 4.02 | Tf | 340 | 791 | Basalt and Tsf, as well |
| O-4 | Stoker et al. (1992) | Pump test | 2.18 | 7.15 | Tf | 340 | 791 | |
| O-4 | Purtymun et al. (1995) | Pump test | 2.88 | 9.46 | Tf | 340 | 791 | |
| G-6 | Purtymun (1995) | Pump test | 0.27 | 0.90 | Tf | 213 | 460 | And basalt and a little Tsf |
| R-2 | Kleinfelder (2004) | Pump test | 0.09 | 0.31 | Tf | 277 | 284 | Very fine grained with fine-scale bedding |
| R-22-5 | McLin and Stone (2004) | Injection | 0.08 | 0.27 | Tf | 441 | 443 | High glass to clay ratio |
| G-1* | Purtymun (1995) | Pump test | 0.29 | 0.94 | Tsf | 86 | 604 | Also Tf and basalt |
| G-1 | Griggs (1964) | Pump test | 0.40 | 1.31 | Tsf | 86 | 604 | |
| G-1 | Griggs (1964) | Pump test | 0.55 | 1.79 | Tsf | 86 | 604 | |
| G-1A | Purtymun (1995) | Pump test | 0.37 | 1.22 | Tsf | 83 | 461 | Significant Tf? |
| G-2* | Purtymun (1995) | Pump test | 0.37 | 1.22 | Tsf | 86 | 597 | Significant Tf? |
| G-2 | Griggs (1964) | Pump test | 0.05 | 0.16 | Tsf | 86 | 597 | |
| G-2 | Griggs (1964) | Pump test | 0.54 | 1.78 | Tsf | 86 | 597 | |
| G-2A | Shomaker (1999) | Pump test | 0.21 | 0.70 | Tsf | 172 | 431 | 0 |
| G-3* | Griggs (1964) | Pump test | 0.27 | 0.90 | Tsf | 134 | 544 | Also Tf and basalt |
| G-3 | Purtymun (1995) | Pump test | 0.22 | 0.71 | Tsf | 134 | 544 | |
| G-4* | Purtymun (1995) | Pump test | 0.46 | 1.51 | Tsf | 130 | 587 | Also Tf and basalt |

**Table 2-3.**
**Estimates of Hydraulic Conductivity from Well Tests on the Pajarito Plateau (continued)**

| Well | Source | Method | m/day | ft/day | Unit | Screen | | Comments |
|---|---|---|---|---|---|---|---|---|
| | | | | | | Top | Bottom | |
| G-4 | Griggs (1964) | Pump test | 0.63 | 2.05 | Tsf | 130 | 587 | |
| G-4 | Griggs (1964) | Pump test | 0.91 | 3.00 | Tsf | 130 | 587 | |
| G-4A | Shomaker (1999) | Pump test | 0.36 | 1.17 | Tsf | 200 | 604 | 0 |
| G-5* | Purtymun (1995) | Pump test | 0.36 | 1.17 | Tsf | 141 | 558 | 0 |
| G-5 | Griggs (1964) | Pump test | 0.50 | 1.65 | Tsf | 141 | 558 | |
| G-5 | Griggs (1964) | Pump test | 0.72 | 2.35 | Tsf | 141 | 558 | |
| LA-1B | Purtymun (1995) | Pump test | 0.38 | 1.25 | Tsf | 99 | 516 | 0 |
| LA-3* | Theis and Conover (1962) | Pump test | 0.16 | 0.51 | Tsf | 32 | 264 | 0 |
| LA-3 | Theis and Conover (1962) | Pump test | 0.08 | 0.25 | Tsf | 32 | 264 | |
| LA-3 | Purtymun (1995) | Pump test | 0.13 | 0.44 | Tsf | 32 | 264 | |
| LA-3 | Theis and Conover (1962) | Pump test | 0.14 | 0.46 | Tsf | 32 | 264 | |
| LA-3 | Theis and Conover (1962) | Pump test | 0.22 | 0.72 | Tsf | 32 | 264 | |
| LA-2 | Purtymun (1995) | Pump test | 0.14 | 0.47 | Tsf | 32 | 264 | |
| LA-2* | Purtymun et al. (1995) | Pump test | 0.20 | 0.66 | Tsf | 32 | 264 | |
| LA-2 | Purtymun et al. (1995) | Pump test | 0.36 | 1.17 | Tsf | 32 | 264 | |
| LA-4 | Purtymun (1995) | Pump test | 0.23 | 0.76 | Tsf | 230 | 599 | 0 |
| LA-5* | Theis and Conover (1962) | Pump test | 0.20 | 0.67 | Tsf | 134 | 530 | 0 |
| LA-5 | Purtymun (1995) | Pump test | 0.12 | 0.40 | Tsf | 134 | 530 | |
| LA-6* | Purtymun, (1977) | Pump test | 0.29 | 0.96 | Tsf | 128 | 542 | 0 |
| LA-6 | Purtymun (1977) | Pump test | 0.22 | 0.73 | Tsf | 128 | 542 | |
| LA-6 | Purtymun (1995) | Pump test | 0.37 | 1.22 | Tsf | 128 | 542 | |

## Table 2-3.
## Estimates of Hydraulic Conductivity from Well Tests on the Pajarito Plateau (continued)

| Well | Source | Method | m/day | ft/day | Unit | Screen | | Comments |
|---|---|---|---|---|---|---|---|---|
| | | | | | | Top | Bottom | |
| **O-1*** | Purtymun (1995) | Pump test | 0.19 | 0.63 | Tsf | 310 | 755 | Thin basalt |
| **O-1** | Purtymun et al. (1993) | Pump test | 0.25 | 0.81 | Tsf | 310 | 755 | |
| **R-16-2** | McLin (2005; personal communication) | Pump test | 0.49 | 1.6 | Tsf | 187 | 187 | |
| **R-16-3** | McLin (2005; personal communication) | Pump test | 0.61 | 2.0 | Tsf | 306 | 314 | |
| **R-16-4** | McLin (2005; personal communication) | Pump test | 0.49 | 1.6 | Tsf | 367 | 392 | |
| **TW-2** | Purtymun (1995) | Pump test | 9.84 | 32.29 | Tpt | 234 | 251 | 0 |
| **TW-3** | Purtymun (1995) | Pump test | 4.90 | 16.08 | Tpt | 245 | 248 | 0 |
| **R-31-4** | McLin and Stone (2004) | Injection | 3.38 | 11.10 | Tpt | 252 | 255 | 0 |
| **R-31-5** | McLin and Stone (2004) | Injection | 2.53 | 8.30 | Tpt | 307 | 310 | 0 |
| **TW-1** | Purtymun (1995) | Pump test | 0.16 | 0.54 | Tpt | 193 | 196 | 0 |
| **R-32-1** | McLin and Stone (2004) | Injection | 1.28 | 4.20 | Tpt | | | |
| **CDV-R-37-4** | Well completion report | Injection | 3.46 | 11.36 | Tt | 472 | 475 | 0 |
| **CDV-R-37-3** | Well completion report | Injection | 2.14 | 7.01 | Tt | 472 | 475 | 0 |
| **TW-4** | Purtymun (1995) | Pump test | 0.78 | 2.55 | Tt | 364 | 367 | 0 |
| **PM-1** | Purtymun (1995) | Pump test | 1.26 | 4.15 | Mixed | 288 | 756 | |
| **PM-2** | Purtymun (1995) | Pump test | 1.14 | 3.75 | Mixed | 306 | 695 | |
| **PM-3** | Purtymun (1995) | Pump test | 7.31 | 23.99 | Mixed | 291 | 772 | |
| **PM-4** | Purtymun (1995) | Pump test | 0.98 | 3.22 | Mixed | 384 | 870 | |
| **PM-5** | Purtymun (1995) | Pump test | 0.22 | 0.71 | Mixed | 439 | 936 | |
| **DT-5A** | Purtymun (1995) | Pump test | 0.69 | 2.28 | Mixed | 357 | 555 | |
| **DT-9** | Purtymun (1995) | Pump test | 4.98 | 16.35 | Mixed | 317 | 457 | |

An asterisk (*) after a well number indicates inclusion in statistical summaries.

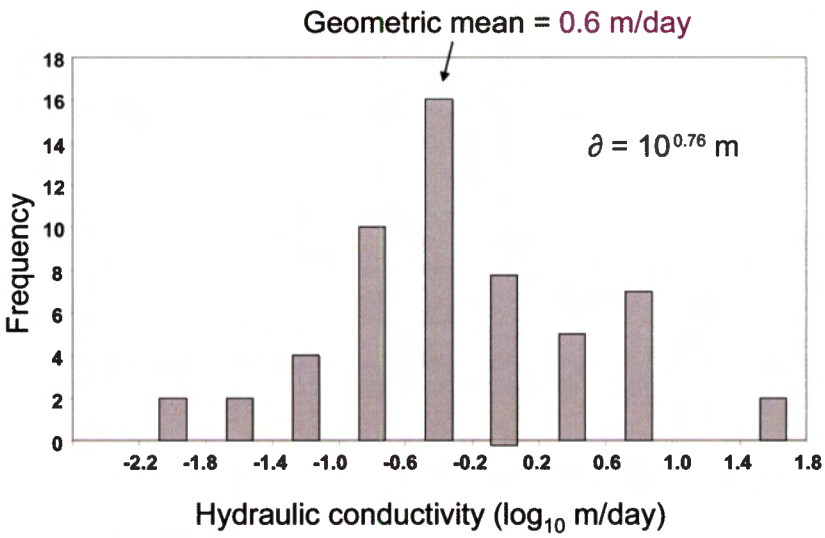


**Note:** Field scale testing (61 tests) - pump tests, slug tests, and tracer test

**Figure 2-25.** Distribution of hydraulic conductivity estimates, derived from tests of 59 wells on the plateau; N = 59; geometric mean = 0.6 m/day.

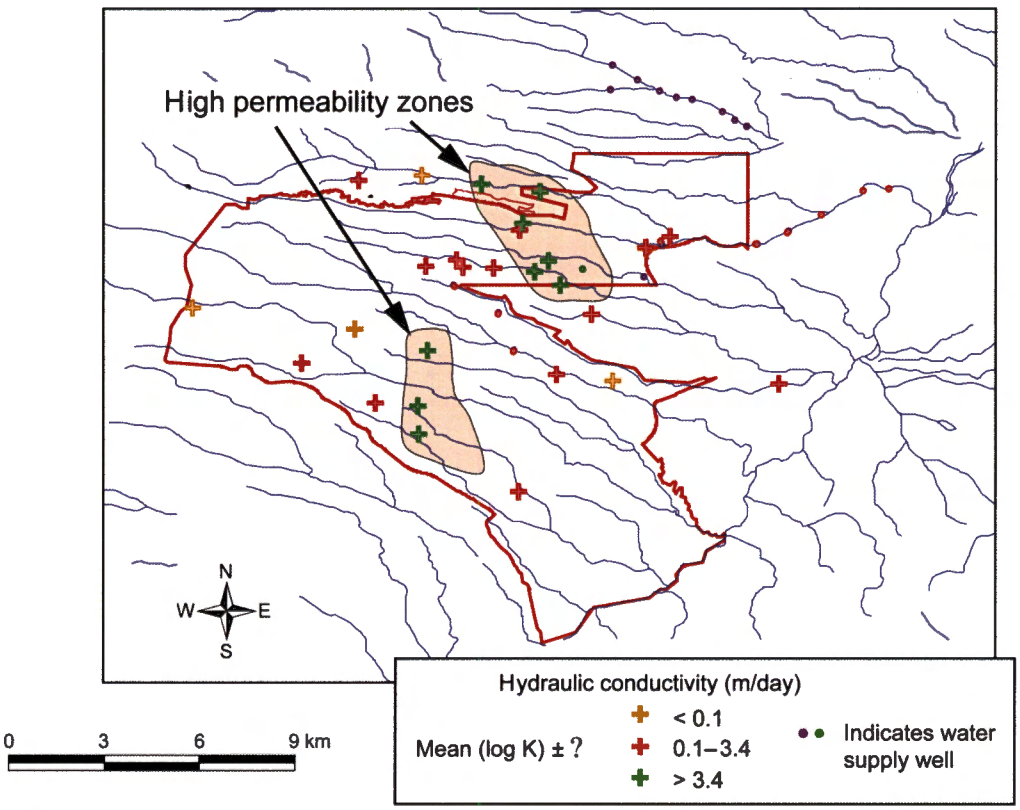


**Figure 2-26.** Hydraulic conductivity estimates in the regional aquifer. If multiple screens have been tested at a single location, the uppermost result is shown. Red line is the outline of the Laboratory.

In several wells there are multiple estimates of hydraulic conductivity at different depths (R-22, CDV-R-15-3, CDV-R-37-2, R-16, R-31, R-19, R-9i); in these cases we show the uppermost screen result in Figure 2-26. Only two of these wells, R-9i and R-31, show significant difference in hydraulic conductivity with depth. R-31, screen 3 (uppermost regional aquifer screen), completed in basalt, is very poorly conductive. The two lower screens, 4 and 5, completed in the Totavi Lentil, are very conductive. For this reason, they are shown in Figure 2-26 as connected to the southern high permeability zone. Both screens in R-9i are completed in basalt. The upper conductive screen is located in an interval that includes highly fractured basalt and an interflow zone, and the lower nonconductive screen is located within clay-filled interflow breccia at the base of the basalt sequence. The other wells (R-22, CDV-R-15-3, CDV-R-37-2, and R-19) show consistent results in all screens. This is particularly interesting in the case of R-22 and CDV-R-15-3, where the screens are located in a variety of rock units.

The hydraulic conductivity values for major rock units of the regional aquifer are shown in Figure 2-27 and summarized in Table 2-4. Cerros del Rio basalt, Puye Formation, pumiceous volcaniclastic rocks, Totavi Lentil, older fanglomerate, and Santa Fe Group sands are clearly heterogeneous. The Santa Fe Group sandy unit (Tesuque Formation) appears to be more uniform, although many of the wells representing this unit have very long screens (>300 m), which would tend to smooth the effect of small-scale heterogeneity. Nonetheless, the short screens within Tesuque sands tested at R-16 gave results similar to those obtained from wells with long screens.

The variation within the Cerros del Rio basalt may be related to whether the tested interval contains abundant open fractures (as reported at R-9i, screen 1) or is a clay-filled interflow zone (reported at R-9i, screen 2). All three tests within the Tschicoma Formation represent interflow zones and/or breccia and show relatively high permeability. Both outcrop and borehole observations suggest that much of the Tschicoma Formation is, in fact, massive and so these tests of breccia zones may not be representative of the larger aquifer unit. Some of the low permeability measurements in the Cerros del Rio basalt may represent clay-filled fractures in flow interiors or clay-filled interflow breccia zones.

A number of factors could explain the variability of hydraulic conductivities within the Puye, the Totavi, and the Santa Fe Group fanglomerate, including different degrees of alteration (clay content) and intraformational depositional facies (e.g., stream channel versus overbank deposits). Depositional facies are characterized by different grain sizes and degrees of sorting, but bedding characteristics and rock fabric are needed to evaluate the depositional setting. Bedding and rock fabric cannot be identified from drill cuttings, however borehole geophysical tools such as FMI logs can provide information that may be relevant (Table 2-5). In some cases, depositional environments inferred from FMI logs (Table 2-5) appear to be related to measured hydraulic conductivities. For example, the coarse-grained, poorly sorted gravels and cobbles in CdV-R-15-3, screens 5 and 6, are consistent with deposits expected in proximal alluvial fan deposits. The K values measured here (0.08 and 0.03 m/day, respectively) are lower than most on the plateau. The four highest conductivity zones in Tpf or Tpp, measured in R-28, R-11, R-4, and R-13, are associated with well-bedded sands and gravels with sparse cobbles located in the medial portion of the Puye alluvial fans. Fractures are visible in the screened intervals of the R-11 and R-13 wells.

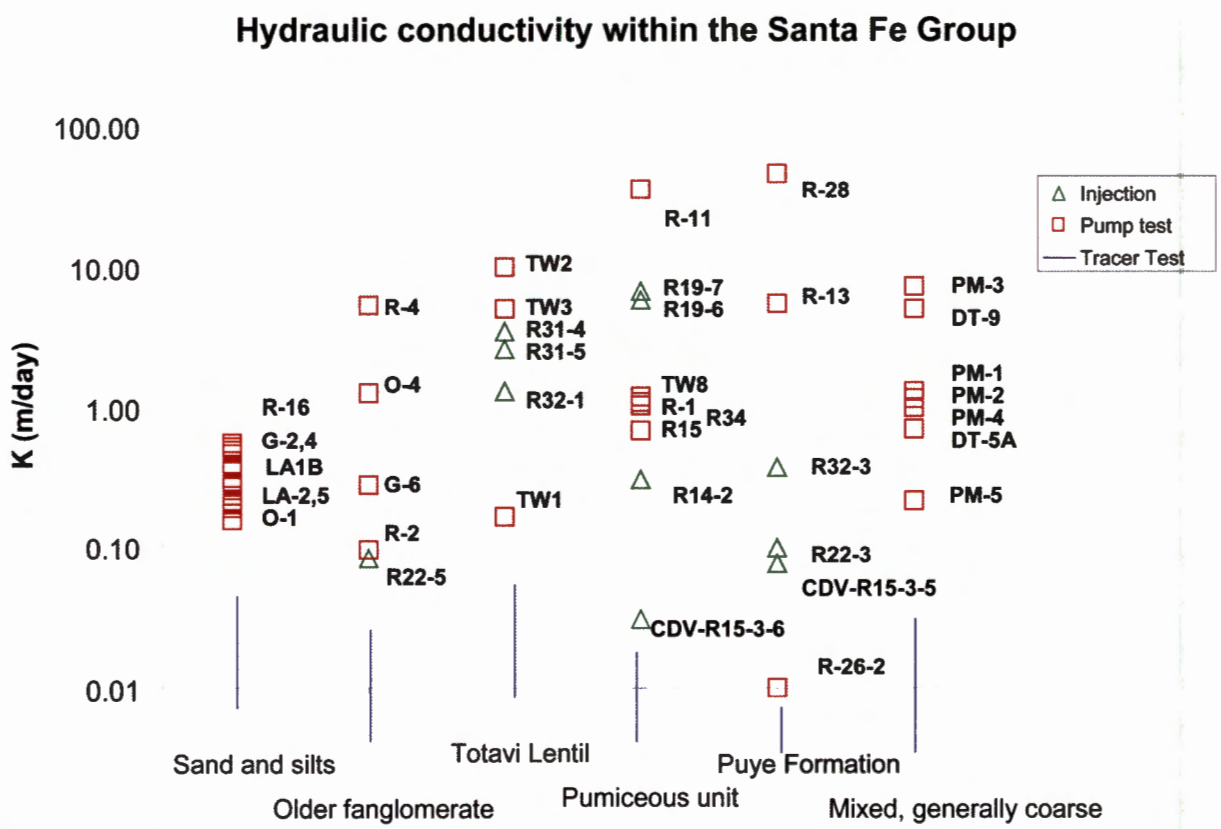


**Figure 2-27-a.** Hydraulic conductivity within the Santa Fe Group. (See Table 2-3 for a list of wells.)

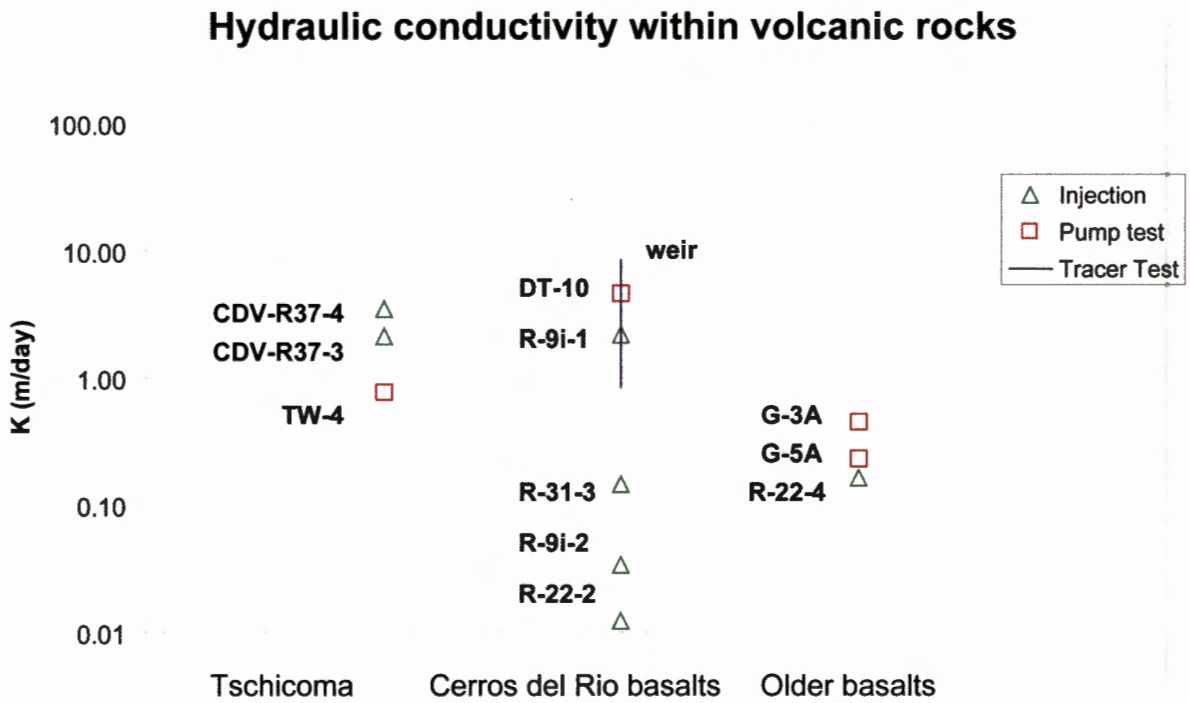


**Figure 2-27-b.** Variation of hydraulic conductivity in volcanic rocks of the Pajarito Plateau.

**Table 2-4.**
**Summary Table of Hydraulic Conductivity for Each Hydrostratigraphic Unit**

| Unit | | Number of Wells | m/day | Max m/day | Geometric Mean |
|---|---|---|---|---|---|
| Cerros del Rio | | 5 | <0.1 | 4.5 | 0.2 |
| | Older | 3 | 0.2 | 0.6 | 0.3 |
| Puye | fanglomerate | 6 | .007 | 45 | 0.4 |
| | pumiceous | 9 | 0.3 | 36 | 1.3 |
| Totavi | | 5 | 0.2 | 9.8 | 2.1 |
| Santa Fe Group | Fanglomerate | 5 | 0.1 | 5.3 | 0.4 |
| | Sandy | 18 | 0.2 | 0.5 | 0.3 |
| | (off plateau data)* | 15 | <0.1 | 4.4 | 0.1 |
| Tschicoma | | 3 | 0.2 | 9.8 | 0.9 |

Source: Daniel B. Stephens (1994)
Note: An asterisk (*) means reported in the literature by numerous workers.

There are exceptions to these trends, however. For example, screen 3 of R-32 is also completed in the medial portion of Puye Formation alluvial fans, but has lower conductivities than the wells listed above. The screened interval in R-28 does not show evidence of fractures, yet it has a higher conductivity than does R-11, which is screened across an interval containing several fractures.

The possible influence of alteration can be examined by comparing the percentage of clay present in a hydrostratigraphic unit to the spatial variation in permeability. As shown in Figure 2-28a, there is a tendency for the Puye Formation and pumice-rich volcaniclastic rocks to be more altered in the southeastern portion of the plateau, which may explain the low K values estimated for R-22, screen 3 and R-32, screen 3. However, low clay content is not necessarily associated with higher conductivity. R-26, screen 2 in the western part of the plateau has low clay content and a low K value. Presumably a combination of facies distributions and post-depositional alteration are contributing to the complex patterns evident in Figure 2-26. Data on which to base these results are somewhat limited, and additional data collection could shed light on this issue.

There is no readily apparent correlation between alteration trends in the pumiceous unit (Figure 2-28b) and hydraulic conductivity. In fact, the lowest K values reported for this unit (CDV-R-15-3, screen 6, and R-14, screen 2) are both in regions of lowest clay content. With the limited data available, it appears that alteration within the pumiceous unit is not the only factor controlling hydraulic conductivity.

**Table 2-5.**
**Summary of Formation Micro-Image (FMI) Data Derived from Borehole Geophysics**

| Drillhole | K m/day | Unit | Texture | Bed thickness | Orientation | Fractures | Effective porosity | Comments |
|---|---|---|---|---|---|---|---|---|
| R-26 | 0.002 | Tpf | Very coarse, crude bedding, boulders 2 ft tall | Most are 5–10 ft (some are 0.5 ft) | 10–40° | nd | 2–0% | Similar to outcrops in upper Guaje, vertical k should be large, probably is colluvium (like at the bottom of a fault scarp) |
| CDV-R15-3-5 | nd | nd | Discrete packages of coarse and fine layers, 1520% is boulder beds, rest is sand and gravels, perhaps thin clay beds, overlapping channel deposits and some overbank | 1–5 ft (sand beds are 1 ft) | nd | nd | nd | Coarse layers are comparable to R-26 |
| CDV-R15-3-6 | nd | nd | Coarser than screen 5, mostly discrete sand bodies (above screen in sandpack are gravel and coarse sands) | 0.5–5 ft | nd | nd | nd | Similar to outcrops in upper Rendija Canyon |
| R-13 | 17.6 | Tpf (upper half of screen) | Sand and gravel beds, a few cobbley lenses | 1 ft–3 ft | nd | One 8' vertical, another dipping, intersecting 2 ft of screen | >60% | Medial fan |
| | nd | Tpp (upper half of screen) | Fine bedding, intercolated in coarser beds of gravels and cobbles | 2-6 in. | nd | nd | nd | |
| R-11 | 116.5 | Tpp | No fine-grained beds, very stratified | 0.5 ft (up to 3 ft) | <10° | Fractures visible (one 2 ft long) | 5–10% | |
| R-28 | 149 | Tpf | Very similar to R-11, very stratified, perhaps can correlate beds | nd | 5–10° (S and E) | None visible | 15–60% | |

**Table 2-5.**
**Summary of Formation Micro-Image (FMI) Data Derived from Borehole Geophysics (continued)**

| Drillhole | K m/day | Unit | Texture | Bed thickness | Orientation | Fractures | Effective porosity | Comments |
|---|---|---|---|---|---|---|---|---|
| R-4 | 17.4 | Tf | Mostly sands and gravels, very sparse cobbles, very stratified | Few tenths up to 1 ft | 5–0° (30° max) | nd | | |
| R-2 | 0.31 | Tf | Coarser, 15% cobbles, the rest is sand and gravels | Most are 1–2 ft (range 0.5–3 ft) | Many dips are to the west | nd | 5–10% | |
| R-16-2 | 1.6 | Tsf | Sands and silts, a little gravel (10% or less) | 0.1–1.5 ft | 2–10° variable direction | nd | nd | |
| R-16-3 | 1.8 | Tsf | Sands and silts, sand beds are massive (2' thick) | nd | 10–5° dip, strongly westerly | nd | nd | |
| R-16-4 | 1.7 | Tsf | Fine laminar bedding, silts sands, perhaps some cross-bedding | 0.1 ft or less (max of 0.5 ft) | 10–0° (to the west) | nd | nd | |
| R-34 | 3.5 | Tpp | Fairly coarse, gravels with some cobble beds, lesser amount of sand | Mostly 3 ft (0.5 to 4 ft) | Not many data, 5–10° | Most commonly 35% (10–60) | nd | Pumice looks mostly reworked, possibly one fall bed |

Note: nd = no data

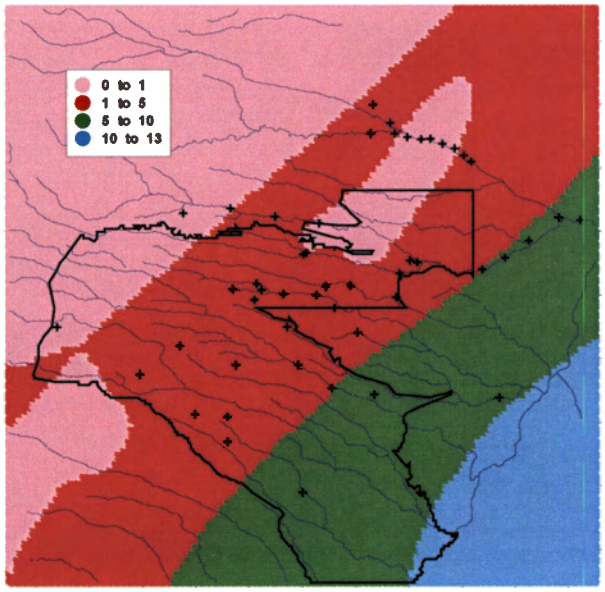


(a) Percentage of clay within Puye Pumiceous Unit

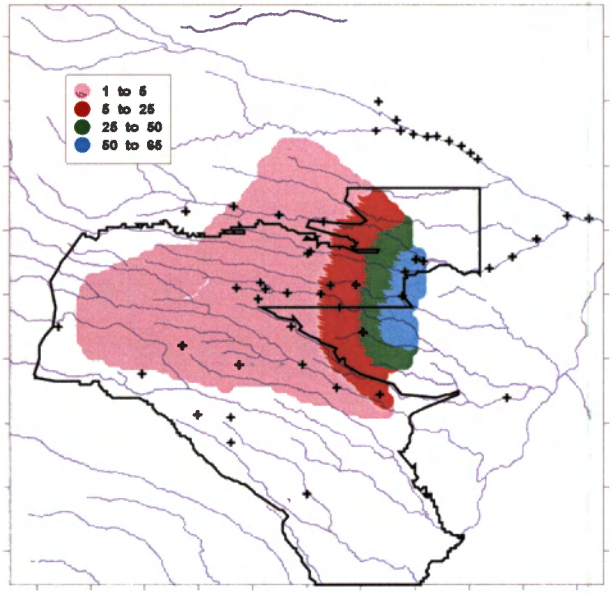


(b) Percentage of clay within Puye Fanglomerate Unit

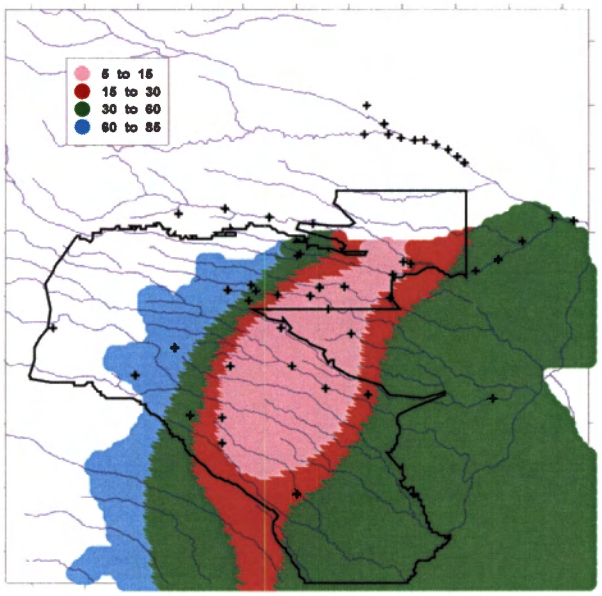


(c) Percentage of clay-filled breccia within the Cerros del Rio Basalt

**Figure 2-28.** Comparison of the percentage of clay present in a hydrostratigraphic unit to the spatial variation in permeability: (a) percentage of clay within the Puye pumiceous unit; (b) percentage of clay within Puye fanglomerate unit; (c) percentage of clay-filled breccia within the Cerros del Rio basalt.
Note: + = well locations

The percent of clay-filled breccia within the Cerros del Rio basalts (Figure 2-28c) is relatively high to the southeast and this factor may explain the low K value estimated for R-22, screen 2 and R-31, screen 3. These areas coincide with the topographically-highest part of the Cerros del Rio basalts on the Pajarito Plateau, and they probably are proximal volcanic vent areas. The low values for K and high degrees of alteration here, both within the basalts and within the Puye, suggest that hydrothermal alteration may have affected the rocks in this area.

Despite the evident variability in most of the rock types, the average properties of the rocks derived from our limited data sets show a few distinctions. The geometric mean hydraulic conductivity of the pumice-rich unit and Totavi Lentil appear to be significantly greater than the other rock types (Table 2-4). At large scales, this trend may be important for flow and transport calculations. At small scales, however, the variability evident in both these rock types will be very important to consider. Local flow directions in the vicinity of release locations and water supply wells are likely to depend strongly on these small-scale differences in hydrologic properties.

**Inferences based on hydraulic gradients.** Head gradients will tend to be larger in low permeability rocks, and so head data can be used, at least in a qualitative way, to infer information about permeability. Other controls on head gradients, such a recharge and pumping, complicate this approach. It is evident from the water table map (Figure 2-24) that there is large spatial variation in head gradients at the top of the aquifer. If these variations were entirely or mostly due to variations in permeability, we might conclude that rocks and structures on the western portion of the plateau (Tschicoma Formation, Pajarito Fault zone) have relatively low permeability. However, mountain-front recharge creates hydrologic conditions that lead to larger gradients, even if the rocks were homogeneous. In addition, there is an increase in permeability towards the center of the plateau (older fanglomerate, pumiceous rocks, Puye Formation and Cerros del Rio basalts). The gradient is relatively steep in the vicinity of R-22, where hydraulic testing indicates very low permeability (locally) in the Cerros del Rio basalts.

#### 2.4.2.4 Anisotropy

As mentioned above, bedding within the Santa Fe Group and the Puye Formation is likely to cause higher permeability parallel to beds than perpendicular to beds. Large vertical head gradients measured in R wells are evidence of anisotropy; persistent vertical gradients are presumably caused by intermittent low-permeability strata that provide resistance to vertical flow. The beds within the Puye Formation range from centimeters to meters in thickness. Most are very low angle, dipping to the east. In contrast, beds within the pumiceous volcaniclastic rocks tend to dip to the southwest (R-20, R-2, R-7, R-19, and R-33). Beds within the Santa Fe Group exposed on the eastern margin of the plateau dip approximately 2–5° to the west (Golombek et al. 1983). Data from R-16 suggest that shallow layers are very low-angle, but deeper layers dip as much as 14° to the west. Hydrologic modeling and pump test analysis suggests that vertical permeability is 100 to 1000 times lower than horizontal permeability in the Santa Fe Group silts and sands (Hearne, 1985; McAda and Wasiolek, 1988; Keating et al., 2003).

If the north-south trending fault zones on the plateau tend to be barriers to flow, this would cause horizontal anisotropy, with north-south permeability higher than east-west permeability. Multiple-well pump tests on the plateau could be used to test this hypothesis.

#### 2.4.2.5 Porosity

Tracer tests, which provide the most valuable information about effective porosity, have not been conducted in the saturated zone at this site. The only available data come from interpretations of borehole geophysical logs, using the combined magnetic resonance (CMR) tool. Using only data from the Puye Formation and the pumice-rich volcaniclastic rocks within the saturated zone, estimates of total porosity based on geophysical logs from R-7, R-19, and CDV-R-15-3 have been compiled. Figure 2-29 shows the distribution of these estimates, with data collected at 0.5 ft intervals. Table 2-6 summarizes the data. The mean effective porosity for these units as estimated from these logs (0.01–0.2) are somewhat low for sedimentary rocks (0.1–0.3, from Freeze and Cherry 1979). There is some indication that these values relate to hydraulic conductivity. For example, CDV-R-15, which has a high proportion of very low effective porosity measurements, also has a relatively low hydraulic conductivity (0.03–0.08 m/day; Table 2-6). R-19 has higher mean effective porosities and higher K values (5.7–6.7 m/day). However, there are significant differences in effective porosities between screens 5 and 6 in CDV-R-15 that do not correlate with differences in hydraulic conductivity.

**Table 2-6.**
**Summary of Effective Porosity Estimates based on Borehole Geophysics**

| Well | Mean Effective Porosity | N | Formation | Hydraulic Conductivity (m/day) |
|---|---|---|---|---|
| CDV-R-15[a] | 0.07 | 744 | Tpf, Tpp | - |
| CDV-R-15-4 | 0.06 | 87 | Tpf | - |
| CDV-R-15-5 | 0.01 | 13 | Tpf | 0.08 |
| CDV-R-15-6 | 0.16 | 15 | Tpp | 0.03 |
| R19[a] | 0.1 | 1466 | Tpf, Tpp | - |
| R19-6 | 0.2 | 14 | Tpp | 5.7 |
| R19-7 | 0.2 | 15 | Tpp | 6.7 |
| R7[a] | 0.09 | 293 | Tpf, Tpp | - |

[a] all depths within Puye Formation
Note: - = no data
Note: For comparison, hydraulic conductivity values derived from in situ testing (Table 2-3) are also shown.

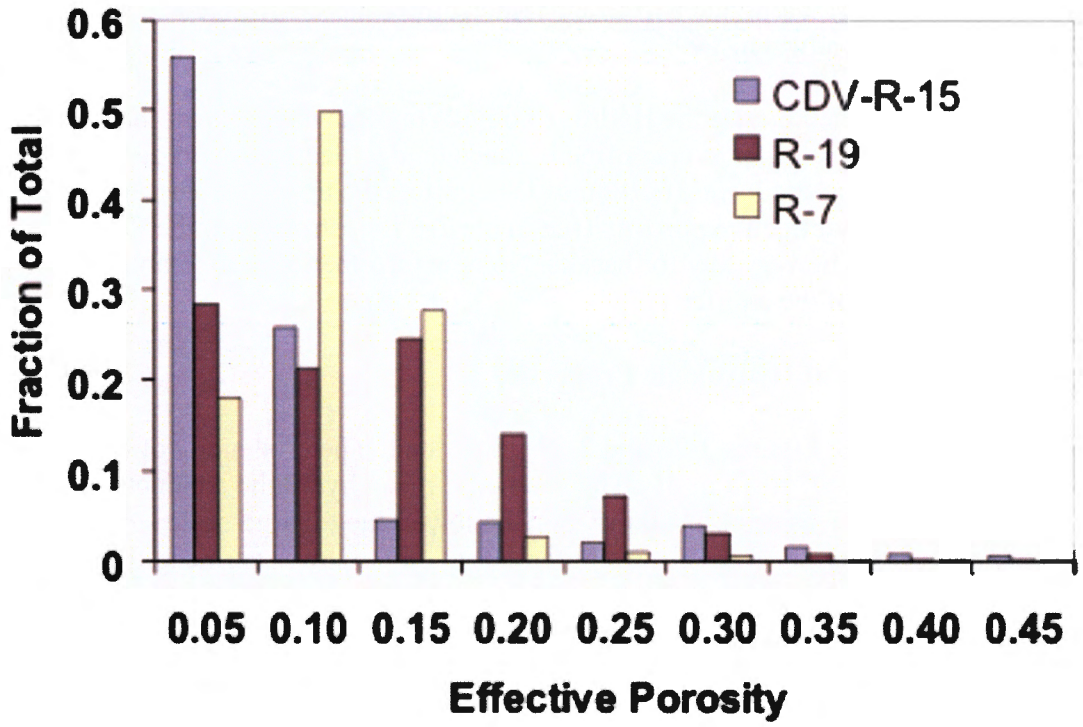


**Figure 2-29.** Distribution of effective porosity measured within the Puye Formation beneath the regional aquifer water table.

#### 2.4.2.6 Storage Properties

Storage properties of rocks will depend on whether the aquifer is unconfined or confined; delineating these two conditions beneath the plateau has been difficult. There are a number of interpretations in the literature about the degree and extent of confined conditions on the Parjarito Plateau. Based on limited data, Cushman (1965) concluded that the aquifer is under water table conditions beneath the plateau, with the exception of the vicinity of the Rio Grande where water table conditions exist in shallow layers and confined conditions exist at depth. Purtymun (1974) suggested that water table conditions exist on the western margin of the plateau and artesian conditions exist along the eastern edge and along the Rio Grande. Recent drilling has confirmed the existence of water table conditions at many locations beneath the plateau. Pump test results for water supply wells, drilled to depths up to 2000 ft below the water table on the plateau, suggest that the deeper portions of the aquifer behave as either:

- "Leaky confined" in the Los Alamos well field, specific storage $S_s \sim 10^{-4.8}$/m (Theis and Conover, 1962); and in O-4, $S_s \sim 10^{-5.5}$/m (Purtymun et al., 1995a and 1995b) or
- Unconfined in O-1, $S_s \sim 10^{-3.8}$/m (Purtymun et al., 1990, Purtymun and McLin, 1990).

In the LA wellfield, Theis and Conover (1962) expanded on the "leaky confined" interpretation by stating that there are, in fact, several aquifers and several semiconfining beds in this well field. Just to the southeast, along the Rio Grande, the aquifer has been called "partially confined" (Balleau Groundwater, 1995).

Drilling activities conducted during the Hydrogeologic Workplan have shown that in most R-wells, at all screens, the aquifer is unconfined. Heads tend to decrease with depth (see Figure 2-45, Section 2.7.7). In the shallowest portion of the aquifer (the upper 150 m), specific yield is presumably dominated by effective porosity (see Table 2-6 for estimates in the Puye Formation). Specific yield is likely to be very low for basalts. No new information is available for the deeper, leaky-confined portions of the aquifer.

### 2.4.3 Summary of Hydrologic Properties

Pump test data (Table 2-3, Figures 2-26 and 2-27) illustrate the heterogeneity of the aquifer, with K values ranging from 0.007 to 45 m/day The geometric mean hydraulic conductivity is 0.6 m/day; the larger-scale effective permeability may be lower due to large-scale structures and/or untested, low-permeability portions of the aquifer, based on the lower permeability values obtained in regional aquifer model calibrations (Section 4.2). Table 2-2 presents a summary of inferred properties of each of the lithologies present in the regional aquifer.

Heterogeneity tends to be particularly significant in the Puye Formation, pumiceous volcaniclastic rocks, Totavi Lentil, and older fanglomerate. The wide variety of depositional environments within the Puye Formation are consistent with this observation. However, it is difficult to go beyond this general statement to develop a predictive relationship between facies and hydrologic properties. On average, the permeabilities of the Puye Formation, pumiceous volcaniclastic rocks, Totavi Lentil, and older fanglomerate are similar and ranges of permeability overlap one another.

As shown in Figure 2-26, there appear to be two zones near the top of the aquifer that are particularly conductive (>3 m/day). These zones are not correlated with hydrostratigraphy, suggesting that structure or alteration may be the controlling factor. No high permeability zones occur east of R-13. Large-scale trends in alteration (Figure 2-28) do not explain the location of these zones; although alteration may be an important factor in the location of a low-conductivity zone in the southeast (R-31 and R-22).

The older fanglomerate unit is also heterogeneous, consistent with its probable depositional history. The Tesuque sandy unit appears to be less heterogeneous, due to the dominance of relatively well-sorted sand and silt layers (Section 2.2.1). Discrepancies between pump test data and model-calibrated values suggest the possibility that large-scale structures such as north-south trending faults may lower the large-scale effective permeability of this unit.

Permeabilities of volcanic rocks appear to be bimodal, presumably a function of whether the groundwater is associated with fractures in flow interiors or is found in interflow zones between lavas. The amount of clay filling pore space in these settings can also affect permeability. Permeabilities of the fractured Tschicoma and Cerros del Rio lava flows are of the order of 1 to 9 m/day; permeability of poorly fractured flow interiors or clay-filled fractured units is much lower (<0.15 m/day). Limited data on Bayo Canyon basalts suggest an intermediate permeability.

Based on the depositional environment (Figure 2-21) of the Puye Formation and the Santa Fe Group, strong anisotropy (horizontal K >> vertical K) is predicted. This is confirmed by modeling studies, pump test analyses, and by the presence of large vertical gradients in many R-wells. The ratio of horizontal to vertical K may be as large as 1000 (see Section 2.4.2.3). If north-south trending low-permeability faults exist within these units (as modeling results suggest; Keating et al., 2003), this would tend to cause horizontal anisotropy.

Although porosity data are limited, geophysical logs indicate that the effective porosity of the sedimentary rocks is relatively low (0.07–0.2). Small-scale data from these geophysical logs need to be augmented by interwell tracer tests to obtain larger scale, transport-related porosity values that can be used in numerical models and transport-velocity estimates.

### 2.4.4 Uncertainties in the Relationship between Geologic and Hydrogeologic Units

This section describes uncertainties and sources of error in defining the relationships between hydrogeologic properties and lithology. Three of the uncertainties described here are large scale, in that they reflect the reliability of stratigraphic assignments. The large-scale uncertainties are:

- Extent and hydrogeologic nature of the Cerros del Rio unit
- Unassigned pumiceous sediments of uncertain age
- Totavi variants (see Section 2.4.4.3 below)

The remaining two uncertainties are small scale, in that they address uncertainties in the composition within a single stratigraphic unit or of a single property. The small-scale uncertainties are:

- Disposition of Santa Fe Group sediments
- Spatial variation in permeability within sedimentary rocks

#### 2.4.4.1 Extent and Nature of the Cerros del Rio Hydrogeologic Unit

The Cerros del Rio hydrogeologic unit straddles the top of regional saturation across much of the southeastern portion of the LANL site (Figure 2-10). The thickness of the unit has proved difficult to predict in critical areas (e.g., drillhole R-22 within TA-54) because multiple flows from different source areas accumulated as stacked sequences in topographically low areas. The nature of the volcanic deposits is highly variable and has led to difficult drilling, as at R-34 where the drill site appears to have been located above a buried cinder cone with no surface expression and unknown shape and lateral extent (Figure 2-14). Data from the basalt field in the Snake River Plain indicate that permeability in basaltic volcanic sequences can vary by 10 orders of magnitude from the laboratory to the field scale, and the flow field can be strongly anisotropic (Whelan and Reed, 1997). Drilling experience in this unit at LANL shows that air permeability can be very high; open boreholes generally "breathe" with diurnal barometric variation as soon as they penetrate into the Cerros del Rio deposits. All of these features indicate significant importance of the Cerros del Rio in flow and transport. At present the 3-D geologic model allows for estimation of relative percent of flow interior, open breccia, and clay-filled breccia for each borehole, but such distributed percentages may not be sufficient for adequate hydrogeologic characterization where stochastic flow simulation may require knowledge of volcanic stratigraphy (Whelan and Reed, 1997). In addition, a conceptual model describing the characteristic length scales of the basalt subunits would also be required.

#### 2.4.4.2 Unassigned Pumice-Rich Volcaniclastic Rocks

The extent of clay alteration in pumiceous sediments can be a critical hydrogeologic parameter, for the unaltered deposits are highly transmissive whereas local zones of extensive clay alteration transform the pumice-rich intervals into aquitards. Extensive pumiceous sediments (Figure 2-9) are widely distributed beneath Puye fanglomerates in the central portion of the LANL site. This unit is not known in outcrop and was not anticipated when drilling for the Hydrogeologic Workplan began. Radiometric dates of 6.8 and 7.5 Ma from pumice in this unit suggest a possible relationship with Peralta Tuff to the south, but petrographic variation and stratigraphic occurrence indicate that multiple volcanic sources supplied tephra to these deposits. The pumiceous sediments in R-9 and R-12 are completely altered to smectite, whereas other occurrences have little clay and are essentially unaltered. It is uncertain whether the altered and unaltered pumice units are related. This uncertainty can have considerable impact on how the pumiceous deposits are represented in cross-section for the conceptual geologic model (see Figure 2-12) and in 3-D for the numerical geologic model, as well as having an impact on flow and transport properties.

#### 2.4.4.3 Totavi Variants

The Totavi may be an important transmissive unit at the site, providing a significant flowpath where laterally contiguous, making the treatment of this unit in the 3-D numerical geologic model particularly important. The axial deposits left by paleochannels of the Rio Grande are well defined in outcrop by their high abundance of Precambrian lithologies derived from northern sources. Dethier (1997) provides extensive data for these deposits exposed along the eastern margin of the LANL site; his definition of the Totavi notes that it contains "generally >80%

quartzite and other resistant lithologies from northern New Mexico, but clasts from the southern Sangre de Cristo range are common locally." The high quartzite abundance is distinctive. Previous conceptual models of the LANL site geology have extended these axial gravels in a continuous unit beneath the site as a horizon underlying Puye fanglomerates. More recent drilling has provided evidence of many stream gravels at varied stratigraphic levels, most with a smaller abundance of Precambrian stream gravels (generally <25% Precambrian gravel) and with more gravels from volcaniclastic sources. Furthermore, new radiometric dates on pumice-rich volcaniclastic rocks indicate that underlying river gravels are considerably older than the Totavi deposits exposed on the east side of the plateau. The construction of a Totavi unit is thus problematic, with some areas where the stream gravels are moderately extensive and other areas with isolated channels (e.g., cross-sections in Figures 2-12 and 2-13). Therefore, the representation of the Totavi unit within the geologic framework model is illustrative.

#### 2.4.4.4 Disposition of Santa Fe Group Sediments

The impact of distinguishing different lithologies of Santa Fe Group sediments can be of hydrogeologic significance in defining the extent of more productive gravels and in construction of hydrogeologic unit boundaries. The Santa Fe Group sediments exposed in outcrop along the eastern margin of the LANL site consist of sands and lesser stream gravels, commonly with some amount of carbonate cement, that are derived predominantly from plutonic and metamorphic Precambrian sources. The 1997 conceptual geologic model for the site projected extensive amounts of Santa Fe Group sediments beneath the site that were predicted to be encountered by most drillholes deeper than ~1000–1500 ft. Furthermore, the central and most hydrologically productive zone was interpreted as consisting of deposits of equivalent age that contained more abundant volcaniclastic material. More recent drillholes have found that this deeper volcaniclastic material is predominantly of Jemez-derived lithologies and is distinct from the generally arkosic deposits of the Tesuque Formation. Recent work in the Española Basin suggests that "lithosomes" of the Santa Fe Group grade laterally and interfinger, as fault displacements episodically dropped the western margin of the basin. However, the downdropping western margin of the basin, which is beneath the LANL site, may also have been the locus of past flow for major drainages. At this time it is uncertain whether the lithologic variations in these older sediments beneath the site reflect interfingered facies of similar age or unconformable, younger channel deposits in paleocanyons cut into the older Santa Fe Group sands. Resolution of this uncertainty could confirm or rule out the existence of long-distance, high-permeability pathways in the regional aquifer.

#### 2.4.4.5 Spatial Variation in Permeability within Sedimentary Rocks

With the exception of the relatively uniform sandy sub-unit of the Santa Fe Group, variability within hydrostratigraphic units tends to be much larger than variability between hydrostratigraphic units. To understand intra-unit variability, using limited data the possible role of texture (Table 2-5) and alteration (Figure 2-28) have been examined and no consistent relationships were found. There does not appear to be a method to deterministically interpolate the spatial variation in permeability within these sedimentary rocks, given the available data. It is possible that a larger dataset and better information about sedimentary facies (if cores were available, for example) would allow a better understanding of the mechanisms controlling hydraulic conductivity. Even so, local variation may be sufficiently great that accurately

interpolating point data (tests at wells) within a deterministic 3-D framework model from known point estimates may not be feasible.

For the purposes of modeling flow and transport through sedimentary rocks in the saturated zone, it may be more appropriate to use a probabilistic approach based on the statistical properties of the hydraulic conductivity dataset rather than a deterministic approach based on defined geometries of hydrostratigraphic units (Section 4.2.10). Another promising method may be to use head data directly to infer heterogeneities in the aquifer (Doherty et al., 1994).

Although the data suggest there are no large differences in permeability between the volcanic and sedimentary rocks, differences in porosity and storage characteristics are likely to be large. For this reason, it is important to delineate the extent of the volcanic rocks in a 3-D framework model of the site for the purposes of flow and transport modeling.

Available porosity data are very limited; more data could be derived from existing borehole geophysical logs and perhaps a geostatistical model of porosity could be built from those logs.

#### 2.4.4.6 Influence of Structure on Groundwater Flow

The influence of structures on groundwater flow is uncertain, but the evidence suggests that structure plays a role in groundwater flow beneath the Pajarito Plateau. First, the large head gradients across the Pajarito fault zone indicate that the faults exert control on flow. Associated modeling results described in Section 4.2.10 suggest that the Pajarito fault zone and north-south trending faults in the Santa Fe Group may act as flow barriers at large scales. Zones of high permeability in the center portion of the plateau (Figure 2-26), which cross hydrostratigraphic boundaries, suggest that perhaps large-scale features such as faults play an important role here.

Further interdisciplinary work combining geophysics, geochemistry, hydrology, and geology investigations would be required to better understand the processes controlling variability in aquifer properties at this site. Given the large heterogeneities in flow and transport properties and the complexities of the hydrogeologic formations, it is unlikely that transport models can ever be based purely on a deterministic hydrogeologic framework. Rather, models should be based on a blend of deterministic (e.g., 3-D hydrogeologic framework models) and geostatistical approaches.

## 2.5 Alluvial Groundwater Conceptual Model

The alluvial groundwater conceptual model is based on data collected during investigations of alluvial groundwater systems at LANL that have been conducted to meet various objectives not specific to the Hydrogeologic Workplan (Appendix 1-A). Most of the early investigations were driven by alluvial groundwater contamination concerns in canyons with persistent alluvial saturation along significant segments of the canyon, and most of the early investigations were conducted in Mortandad Canyon. Examples of these studies include those conducted by Purtymun (1974), Purtymun et al. (1983), and Stoker et al. (1992). Many of these investigations were conducted in collaboration with the United States Geological Survey. Additional investigations conducted in the mid-1990s measured alluvial aquifer properties (Koening and Guevara, 1992) and calculated bulk groundwater flow velocity (Gallaher, 1995). Purtymun

(1995) contains a significant body of additional information and references pertaining to alluvial groundwater investigations conducted at the Laboratory up to the mid-1990s.

### 2.5.1 Physical Setting

Average annual precipitation across the Pajarito Plateau ranges from over 0.5 m along the western boundary near the Jemez Mountains to less than 0.36 m to the east at the Rio Grande (Bowen, 1990). Most precipitation occurs either as winter/spring snow or as summer "monsoonal" rains. As a result, most infiltration occurs episodically during spring snowmelts or during the intense summer thunderstorm season.

Surface-water flow in the canyons is generally ephemeral or intermittent, although a few canyons have short stretches with perennial surface flow. Anthropogenic discharges from water treatment outfalls can be a significant source of water in some canyons. Infiltration of these surface sources forms near-surface perched alluvial groundwater systems in many of the canyons (Stone et al., 2001). These alluvial groundwaters are not sufficiently extensive for domestic use. Nevertheless, these waters are an important component of the subsurface hydrologic system. In addition, laboratory contaminants introduced into the canyons can affect shallow groundwaters. Therefore, alluvial groundwaters provide pathways for contamination to migrate to significant lateral distances and potentially to greater depths.

The deposits that comprise alluvial groundwater aquifers are confined to the bottoms of canyons and are composed of axial fluvial deposits interbedded with deposits of alluvial fans, colluvium, and rock fall from adjacent mesa slopes. For watersheds that head on the Pajarito Plateau (e.g., Mortandad and Sandia Canyons), the source of sediment is primarily Bandelier Tuff and, to a much lesser extent, other formations such as the Cerro Toledo interval. Tschicoma dacite and Bandelier Tuff are primary sources of sediment for watersheds that head in the Sierra de los Valles. Canyons that have Bandelier Tuff as the primary source of sediment tend to have predominantly sand-sized alluvial fill with some interbedded coarser-grained side-slope deposits, including colluvium, whereas canyons that head in the Sierra de los Valles have alluvial fill that contains a wide range of grain sizes including dacitic boulders and gravels. Available data indicate that the thickness of alluvium and colluvium in the canyons ranges from a few feet up to approximately 100 feet.

### 2.5.2 Hydrology

The presence and extent of saturation within the canyons is dependent on a number of variables including source(s) of water, volume and persistence of water sources, the magnitude and location of infiltration of groundwater from the alluvial system to underlying bedrock units (i.e., loss to underlying vadose zone), and evapotranspiration.

These controls on variability of saturation are difficult to quantify, but are based largely on observations made during drilling for installation of alluvial monitoring wells and piezometers in several canyons, including, Los Alamos and Mortandad Canyons, and Cañon de Valle. Adjacent boreholes commonly show different saturated conditions and sometimes a borehole with substantial saturation will be adjacent to one or more boreholes with no or minimal saturation.

This phenomenon is likely related to juxtaposition of facies with highly variable hydrologic properties, such as porosity, permeability, or hydrologic conductivity (Figure 2-30; Reneau and McDonald, 1996).

#### 2.5.2.1 Alluvial Recharge

Recharge to alluvial groundwater systems on the Pajarito Plateau occurs via infiltration from three primary sources: storm-water runoff, anthropogenic effluents, and snowmelt. Each of these recharge sources produces a characteristic groundwater response. The conceptual model for alluvial system recharge on the Pajarito Plateau is based on continuous stream flow, precipitation, and water-level data collected within the Los Alamos and Pueblo Canyon watersheds (including DP Canyon). Three example plots (Figures 2-31, 2-32, and 2-33) show the relations of precipitation, stream flow, and groundwater hydrographs for several representative alluvial monitoring wells in Los Alamos and Pueblo Canyons. The precipitation data shown in the plots are values of average daily precipitation estimated using Theissen weighted averages of precipitation measured within and near the watershed (Dunne and Leopold, 1978). This approach is described in greater detail in LANL (2004) and in Reneau and Kuyumjian (2005). These examples are believed to be representative of canyons across the plateau.

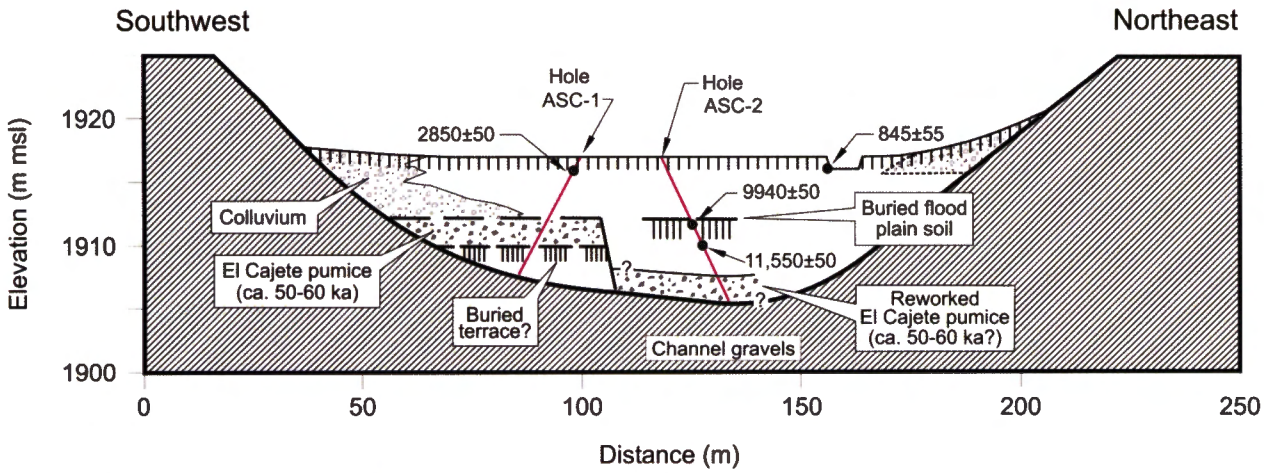


Note: The numbers shown at the dots are radiocarbon dates in years before the present.
Source: Reneau and McDonald (1996).

**Figure 2-30.** Schematic cross section of complex stratigraphy within the alluvial package in Ancho Canyon.

Examples of recharge via infiltration of storm water are shown in Figure 2-31. The water-level record for monitoring well LAO-0.3 in Los Alamos Canyon is plotted against precipitation data and the stream flow record at gaging stations E025, E030, and E042. The water-level data show generally rapid rises in response to summer and fall precipitation events and associated storm water runoff. Good examples are the large precipitation events in mid-August 2001 and late June 2002. These water-level rises occur instantaneously and generally correlate well with the stream flow record, indicating infiltration into the streambed during floods. The duration of the recessional limb varies between events. Several small but distinct increases in the water-level recorded during late spring and summer months are not related to precipitation events, but rather are related to draining of the Los Alamos Reservoir for dredging and maintenance following the Cerro Grande fire. Storm-water runoff can be generated from precipitation in upland portions of watersheds, directly onto the plateau, or on impervious surfaces in developed areas within the Laboratory or in the Los Alamos townsite.

Effluent-supported recharge results in more sustained and consistent water levels, as shown in Figure 2-32. Groundwater levels observed in monitoring well PAO-4 are dominated by infiltration of effluent discharged from the Bayo wastewater treatment plant (WWTP) to the stream channel in Pueblo Canyon (Figure 2-2). The variation in water-level elevations down canyon of the WWTP is controlled primarily by seasonal rerouting of effluent for "downstream" uses such as watering at the Los Alamos County golf course. Other examples of canyon reaches with similar effluent-supported recharge include effluent/upper Mortandad Canyon (TA-50 outfall) and upper Sandia Canyon (power-plant outfall). These sources represent relatively consistent sources of recharge to alluvial groundwater creating stable alluvial groundwater levels. During dry periods in drier canyons that have little natural runoff, anthropogenic sources provide the majority of groundwater recharge.

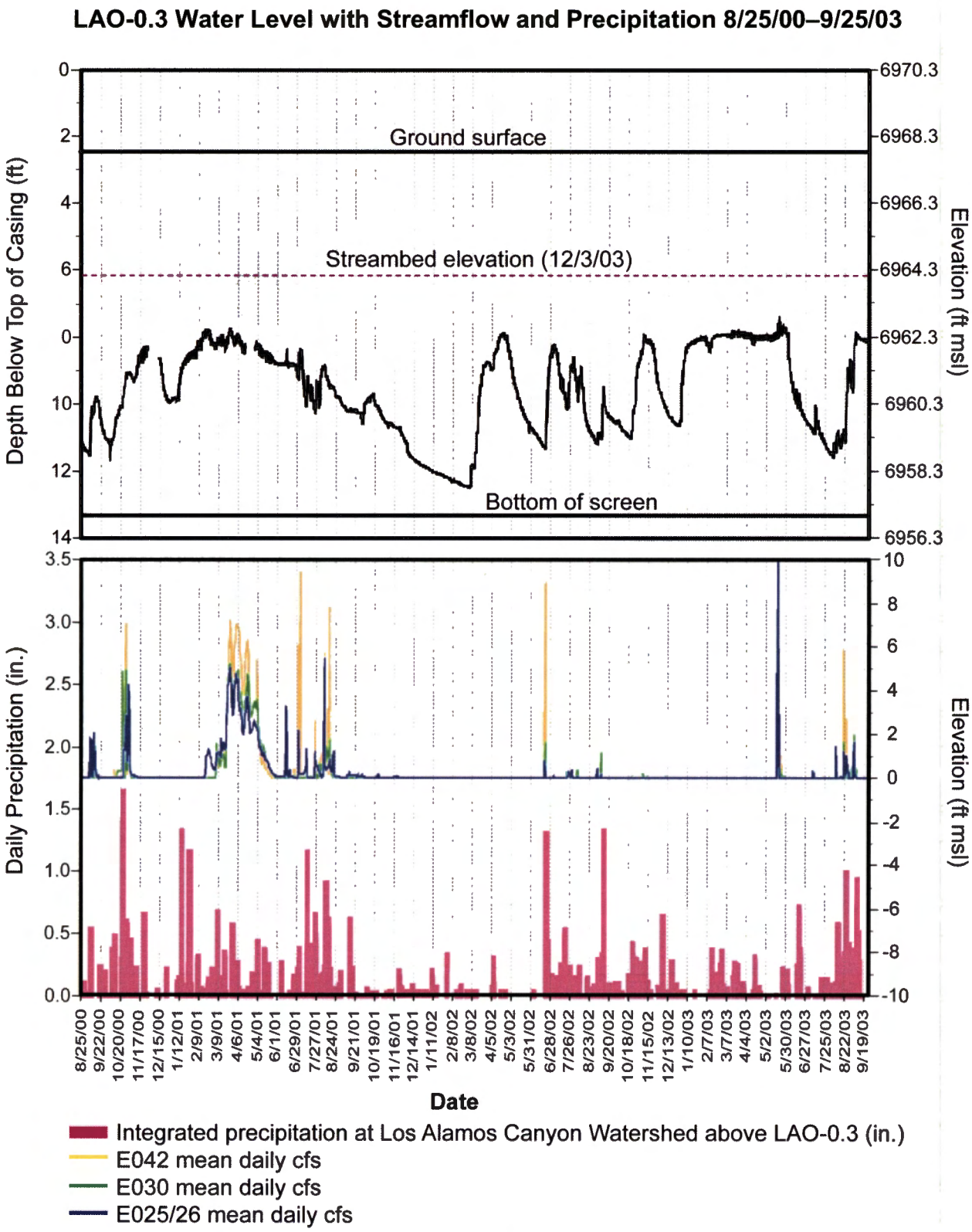


**Figure 2-31.** LAO-0.3 water level with streamflow and precipitation.

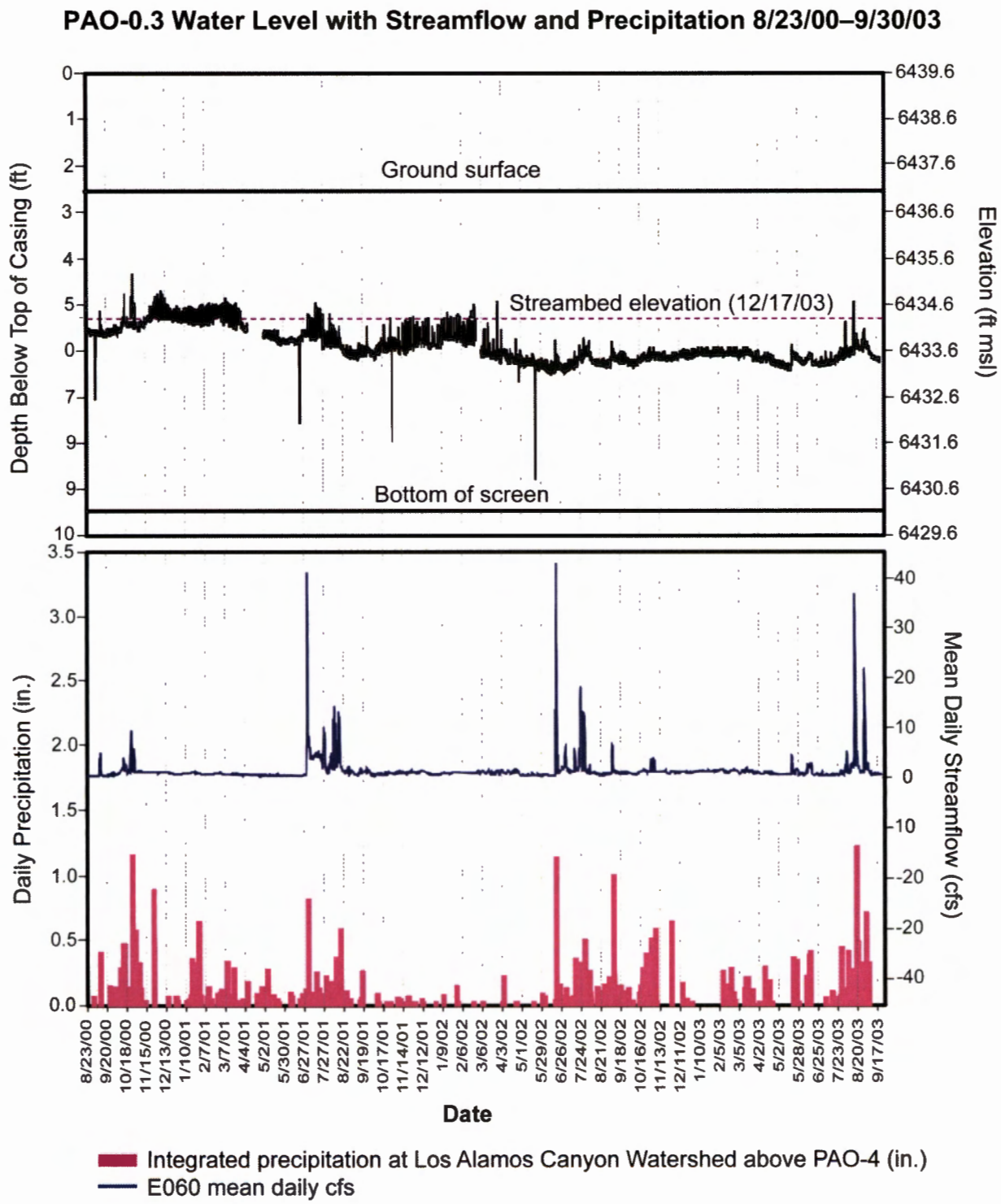


**Figure 2-32.** PAO-4 water level with streamflow and precipitation.

Recharge also occurs in response to winter/spring snowmelt. Figure 2-31 shows rising alluvial groundwater levels during the late winter to early spring of each of the years represented on the plot. All three winter/spring periods show alluvial-groundwater-level responses prior to initiation of sustained streamflow at even the most up-canyon gaging station, E025. The winter and spring

of 2000–2001 alluvial-groundwater-level shows a substantial response to snowmelt runoff from an appreciable winter snowpack. The alluvial-groundwater-level response occurs over one month prior to initiation of stream flow at E025. The conceptual model for this type of response is that recharge within the alluvium is associated with early-season snowmelt that infiltrates into alluvium in the upper canyon and creates an underflow recharge front that advances down canyon. Once the aquifer saturation has reached capacity (i.e., the elevation of the adjacent stream channel), stream flow is initiated, suggesting that stream flow during these periods represents discharge from the aquifer to the channel.

Figure 2-33 shows groundwater-level data from four alluvial groundwater monitoring wells in Los Alamos Canyon. Initiation of the alluvial-groundwater-level rise in the winter/spring of 2001 at each well occurs prior to the onset of sustained surface water flow. This suggests that the persistent baseflow conditions associated with snowmelt infiltration may actually be sustained largely from discharge of groundwater to the channel. Long-duration snowmelt runoff is most significant in watersheds with upland drainage basin areas, although watersheds that drain developed areas with pavement and storm-drain systems can provide short-duration, pulsed snowmelt runoff associated with melt from individual events.

The down-canyon extent of alluvial groundwater saturation varies significantly from year to year and seasonally. During dry years, and especially during years with limited spring snowmelt runoff, saturation may not extend far from the upland sources of snowmelt recharge.

Gray (1997; 2000) and LANL (2004) investigated alluvial groundwater in Los Alamos Canyon, creating a numerical model that calculated infiltration of alluvial groundwater to the underlying vadose zone. Results indicate that the alluvial groundwater infiltrates into the underlying vadose zone at variable rates along the length of the canyon with a higher rate of loss estimated for a portion of the canyon coincident with the projected trace of the Guaje Mountain fault (mapped to the north but not evident in the walls of Los Alamos Canyon). Nested piezometer data from Los Alamos Canyon (LANL 2004) corroborate modeling results indicating greater infiltration rates in the vicinity of the projected Guaje Mountain fault. The variability in infiltration rates is interpreted to be caused by either loss into permeable units underlying the alluvium or loss within zones of relatively greater fracture size or density.

In addition to the watershed-scale investigation of alluvial groundwater responses to various recharge sources, site-specific alluvial groundwater investigations have been conducted in DP Canyon and in Cañon de Valle. A potassium bromide tracer study was conducted in DP Canyon in 2003 to investigate alluvial groundwater travel times, surface water/groundwater exchange, hydrologic linkage from reach DP-2 to DP Spring, and to measure vertical hydraulic gradients and seepage velocity into the underlying Bandelier Tuff. The primary conclusions regarding alluvial recharge from this study were that surface water/groundwater exchange is an important recharge mechanism and that groundwater flow is transient, primarily controlled by episodic recharge from townsite runoff. For a detailed description of these findings, see LANL (2004) and LANL (2003a).

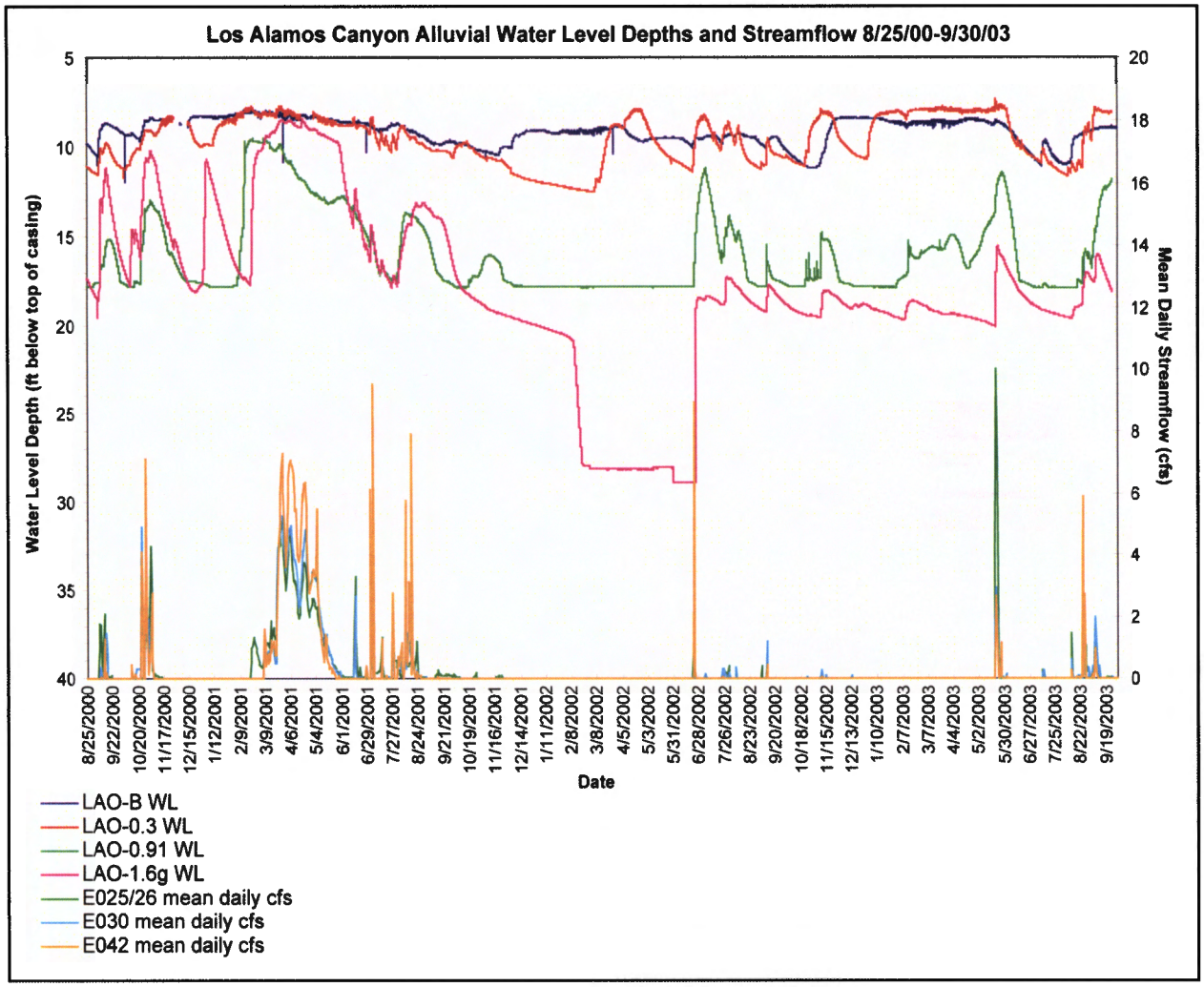


**Figure 2-33.** Los Alamos Canyon alluvial water level depths and stream flows.

To quantify infiltration, Kwicklis et al. (2005) developed a map of average annual "net infiltration" in the Los Alamos area, based on physical features such as elevation, vegetation, surface geology and stream flow (Figure 2-34). They define net infiltration as that water remaining after accounting for evapotranspiration in the shallow subsurface (i.e., the root zone). They estimate the highest net infiltration rates in canyons, especially those that head in the mountains, with magnitudes of up to a few hundred millimeters per year caused by channelized runoff. In contrast, much lower net infiltration rates occur across mesas and in the smaller canyons that head on the plateau (see Section 4.1 for a site-wide numerical model employing these concepts).

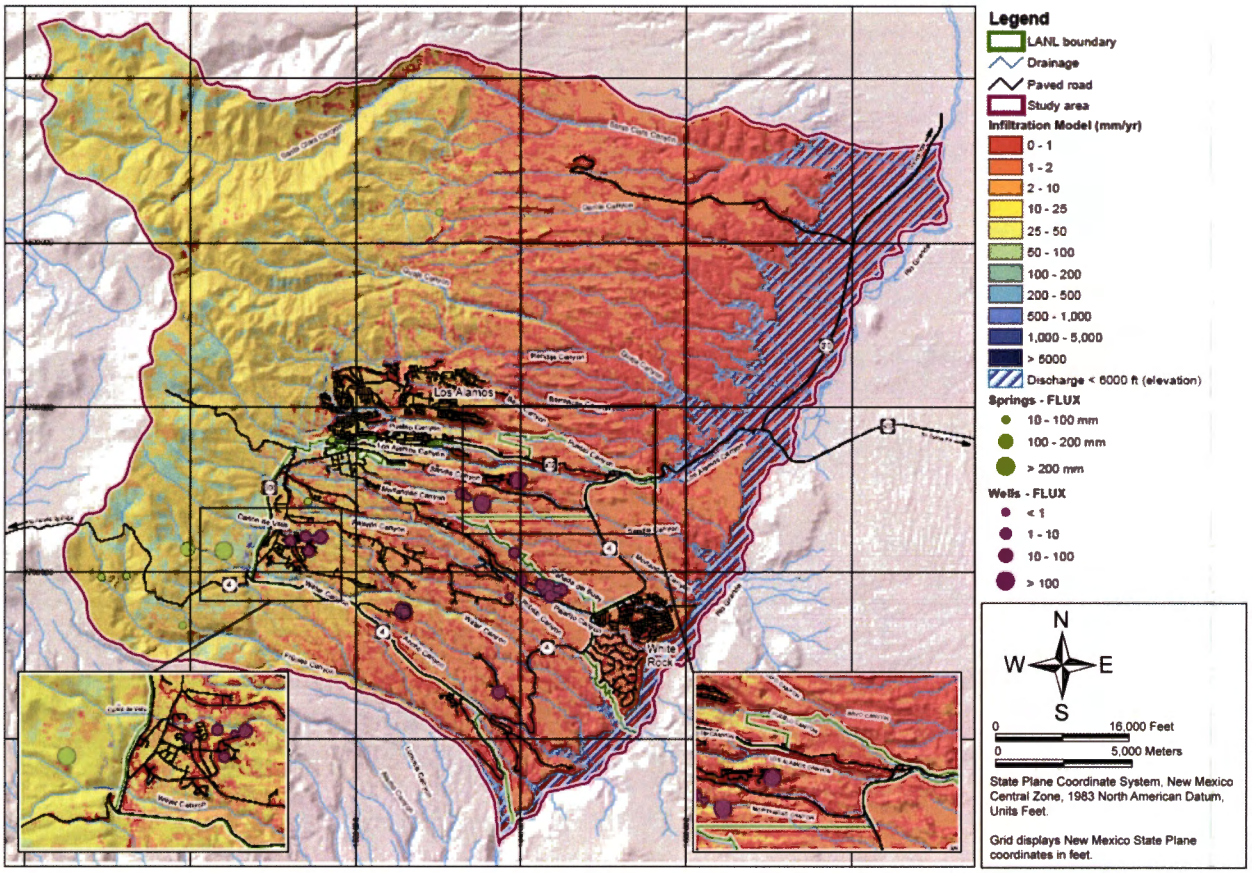


**Figure 2-34.** Estimated infiltration on the Pajarito Plateau (reproduced from Kwicklis et al., 2005).

### 2.5.2.2 Alluvial Aquifer Properties

Observations of alluvial groundwater were initially focused on understanding the distribution of contaminants. Purtymun (1974) performed one of the first quantitative investigations where groundwater velocities were calculated from a tritium release in Mortandad Canyon. The release from the TA-50 outfall was a planned event staged to discharge wastewater containing elevated tritium. Groundwater velocities calculated from travel time of the tritium centroid showed values ranging from 20 meters/day in the upper canyon, where alluvium is thin and the alluvial aquifer volume is small, to approximately 2 meters/day in the lower canyon where the canyon widens and alluvium thickens to approximately 30 meters (Table 2-7). These observations indicate that alluvial groundwater flow can be highly variable along the length of a canyon. Other factors influencing system-scale groundwater velocity include aquifer sediment textures, stratigraphic complexity, and hydraulic gradient.

Gallaher (1995) calculated Darcy velocity (Table 2-7) from mean saturated hydraulic conductivities (Table 2-8) and water table gradients in Los Alamos Canyon. Using the results from slug tests conducted by Koening and Guevara (1992), Gallaher estimated the rate of groundwater movement in alluvium at 0.75 meters/day. Additional saturated conductivity values for Los Alamos and Mortandad Canyons are presented in Table 2-8. Slightly lower hydraulic

conductivities in middle Mortandad Canyon may be due to an overall fining of the alluvial material in that portion of the canyon.

Gray (1997, 2000) measured aquifer parameters, calculated a hydrologic budget and performed numerical modeling of groundwater flow in Los Alamos Canyon. Hydraulic conductivity measurements from these studies are included in Table 2-9.

#### 2.5.2.3 Cerro Grande Fire Effects

The May 2000 Cerro Grande fire produced significant hydrologic changes in the watersheds west of the Laboratory (BAER 2000). Loss of vegetation and forest litter, development of ash covers, and extreme hydrophobic soil conditions, primarily in the upland portions of watersheds, greatly reduced the capacity for infiltration and storage of precipitation. Rapid surface-water runoff in the first two summer monsoon seasons following the fire contained high ash content with a complex mixture of inorganic and organic compounds. Calcium, magnesium, silica, potassium, sodium, and carbonate were among the constituents concentrated in the ash (Longmire et al., 2002).

A detailed water-level and water-quality record was obtained from Los Alamos and Pueblo Canyons using dedicated multiparameter pressure transducers installed in a series of alluvial monitoring wells. Hydrologic system effects were manifested as rapid water-level response to numerous post-fire floods and possibly also earlier-than-typical onset of a snowmelt runoff response. Reduced or eliminated forest canopy is thought to have allowed winter snow to melt shortly after individual precipitation events and early in the spring. There were stormwater related excursions in water-quality parameters, including increases in pH in the alluvial groundwater and elevated concentrations of several constituents in alluvial groundwater due to infiltration of ash-rich storm water. A detailed discussion is presented in Chapter 7 and Appendix B of the Los Alamos and Pueblo Canyons Investigation Report (LANL, 2004). It is not known how long such perturbations will persist, although the effects of the fire are expected to progressively decrease over time as the upper watershed recovers.

## 2.6 Vadose Zone Conceptual Model

The vadose zone is the section of soil and rock material between the alluvial groundwater or the ground surface (where alluvial groundwater is not present) and the regional aquifer water table. Beneath the Pajarito Plateau, the thickness of the vadose zone ranges from about 600 feet to over 1,200 feet. Intermediate-depth perched groundwaters are present within the vadose zone. Specific intermediate perched zones that occur beneath major canyons and in the western portion of the Laboratory are described in Section 2.7.

## Table 2-7.
## Groundwater Velocities in Alluvial Aquifers on the Pajarito Plateau

| Measure Locations | Source | Distance between Measurement Points (m) | GW Velocity (m/d) | Test Type |
|---|---|---|---|---|
| Upper Los Alamos Canyon | A | Approximately 7000 | 0.75 | Calculated from (mean $K_s^A$), average gradient of stream channel (0.027), and an estimated porosity of 0.3. |
| **Mortandad Canyon** | | | | |
| MCO-5 to MCO-6 | B | 393 | $^3$H 16<br>Cl 25 | Tritium ($^3$H) and chloride (Cl) TA-50 discharge tracer test |
| MCO-6 to MCO-7 | B | 320 | $^3$H 4.2<br>Cl 5.1 | Tritium ($^3$H) and chloride (Cl) TA-50 discharge tracer test |
| MCO-7 to MCO-7.5 | B | 290 | $^3$H 4.4<br>Cl 5.6 | Tritium ($^3$H) and chloride (Cl) TA-50 discharge tracer test |
| MCO-7.5 to MCO-8 | B | 185 | $^3$H 1.7<br>Cl 2.3 | Tritium ($^3$H) and chloride (Cl) TA-50 discharge tracer test |

Note: Calculated groundwater velocity using mean saturated hydraulic conductivity from LAO-C, LAO-1, LAO-2, LAO-3, LAO-3A, LAO-4, LAO-4.5A, LAO-4.5C, LAO-5.

A Gallaher (1995)

B Purtymun (1974)

## Table 2-8.
## Saturated Hydraulic Conductivity Values for Alluvial Groundwater on the Pajarito Plateau

| Well/Piezometer | Location | Mean Ksat (cm/sec) | Test Type |
|---|---|---|---|
| **Los Alamos Canyon** | | | |
| Piezometer | LAP-1-#1a | 4.67E-04 | Rising head slug test; Bouwer-Rice solution |
| Piezometer | LAP-1-#2a | 1.32E-03 | Rising/falling head slug test; Bouwer-Rice (1976) |
| Piezometer | LAP-1-#3a | 2.71E-03 | Rising/falling head slug test; Bouwer-Rice (1976) |
| Piezometer | LAP-1.5-#1a | 2.62E-03 | Rising/falling head slug test; Bouwer-Rice (1976) |
| Piezometer | LAP-1.5-#2a | 4.43E-03 | Rising/falling head slug test; Bouwer-Rice (1976) |
| Piezometer | LAP-1.5-#3a | 9.42E-03 | Rising/falling head slug test; Bouwer-Rice (1976) |
| Piezometer | LAP-3a | 3.10E-03 | Rising/falling head slug test; Bouwer-Rice (1976) |
| Piezometer | LAP-3.5-#1a | 2.660E-03 | Rising/falling head slug test; Bouwer-Rice (1976) |
| Piezometer | LAP-3.5-#2a | 1.27E-03 | Rising/falling head slug test; Bouwer-Rice (1976) |
| Piezometer | LAP-3.5-#3a | 2.82E-05 | Rising/falling head slug test; Bouwer-Rice (1976) |
| Piezometer | LAP-4-#1a | 2.58E-05 | Rising/falling head slug test; Bouwer-Rice (1976) |
| Piezometer | LAP-4-#2a | 2.20E-05 | Rising/falling head slug test; Bouwer-Rice (1976) |
| observation well | LAO-Bb | 7.01E-03 | slug tests; Bouwer-Rice (1976) |
| observation well | LAO-Cc | 1.16E-03 | slug tests; Bouwer-Rice (1976) |
| observation well | LAO-0.3b | 1.25E-02 | slug tests; Bouwer-Rice (1976) |
| observation well | LAO-0.6b | 7.58E-03 | slug tests; Bouwer-Rice (1976) |
| observation well | LAO-0.91b | 3.56E-02 | slug tests; Bouwer-Rice (1976) |
| observation well | LAO-1c | 1.58E-02 | slug tests; Bouwer-Rice (1976) |
| observation well | LAO-1.6(g)b | 4.82E-03 | slug tests; Bouwer-Rice (1976) |
| observation well | LAO-2c | 1.01E-02 | slug tests; Bouwer-Rice (1976) |
| observation well | LAO-3c | 1.34E-02 | slug tests; Bouwer-Rice (1976) |
| observation well | LAO-3ac | 1.22E-02 | slug tests; Bouwer-Rice (1976) |

## Table 2-8.
## Saturated Hydraulic Conductivity Values for Alluvial Groundwater on the Pajarito Plateau (continued)

| Well/Piezometer | Location | Mean Ksat (cm/sec) | Test Type |
|---|---|---|---|
| observation well | LAO-4c | 2.41E-02 | slug tests; (1976) |
| observation well | LAO-4.5b | 2.55E-03 | slug tests; (1976) |
| observation well | LAO-4.5ac | 2.33E-03 | slug tests; (1976) |
| observation well | LAO-4.5cc | 2.77E-03 | slug tests; (1976) |
| observation well | LAO-5c | 3.35E-03 | slug tests; (1976) |
| **Mortandad Canyon** | | | |
| observation well | MCO-3c | 3.72E-02 | slug tests; (1976) |
| observation well | MCO-4c | 7.13E-04 | slug tests; (1976) |
| observation well | MCO-4Cc | 3.47E-04 | slug tests; (1976) |
| observation well | MCO-4.9c | 2.88E-05 | slug tests; (1976) |
| observation well | MCO-5c | 5.41E-05 | slug tests; (1976) |
| observation well | MCO-6c | 7.08E-04 | slug tests; (1976) |
| observation well | MCO-7.5c | 9.63E-04 | slug tests; (1976) |
| observation well | MCO-7Ac | 1.06E-04 | slug tests; (1976) |
| observation well | MCO-7c | 5.11E-04 | slug tests; (1976) |
| observation well | MT-3c | 2.93E-05 | slug tests; (1976) |

a Results have been published in the Los Alamos and Pueblo Canyons Investigation Report (LANL, 2004b).
b Results from 1998 slug tests (Los Alamos and Pueblo Canyons Investigation Report (LANL, 2004b).
c Results from 1995 slug tests.

### 2.6.1 Climate and Infiltration

Arid and semi-arid regions often exhibit thick vadose zones. Infiltration is often focused in topographic lows or beneath surface water bodies, rather than being diffuse, as is common in wetter climes (e.g. Sanford, 2002). The average annual potential evapotranspiration (PET) rates far exceed precipitation rates. Under these conditions, infiltration events that propagate beneath the root zone are sporadic and occur only when the short-term infiltration rate exceeds the ET rate, such as during snowmelt or after large rainstorms. Consequently, the rates for deeper infiltration are difficult to quantify through traditional water balance studies because this component of the water-balance can be orders of magnitude smaller than the other components (Devries and Simmers, 2002; Scanlon et al., 2002; Sophocleous, 2002; Sanford, 2002; Flint et al., 2002). These generalities apply to the near-surface hydrology of the Pajarito Plateau, which has a semiarid climate.

The infiltration rate estimates from canyon bottom alluvium and mesa top sites developed by Kwicklis et al. (2005) (Figure 2-34) can be tested for consistency against the estimated infiltration rates inferred from moisture content profiles. In Section 4.1.3.2, a set of numerical models for wells LADP-3 and LADP-4 in Los Alamos Canyon are presented showing that moisture profiles reflect the conceptual model of high infiltration in canyons and low infiltration in mesas. That analysis also shows that the uncertainties associated with such estimates are quite high (in the range of a factor of 3). However, by combining moisture content, tracer or contaminant profiles, and water budget information, a more constrained estimate can be achieved. One of the purposes of the vadose zone numerical models being developed is to provide the additional constraints afforded by the use of multiple, independent data sets (Robinson et al. 2005a).

### 2.6.2 General Description of Conceptual Models

Conceptual models for vadose zone flow and transport on the Pajarito Plateau are based on observations from a variety of data sources, including both mesa-top and canyon sites under both natural conditions and disturbed conditions resulting from Laboratory operations. The key conceptual-model elements describe percolation of water through both fractured and relatively unfractured volcanic tuffs, buried sedimentary formations, and basalts. The types of data incorporated into the development of the conceptual models include water content and pore-water chemical compositions from borehole samples for naturally occurring tracers, introduced tracers, and Laboratory contaminants.

The conceptual models differentiate the rate of percolation by their location and surface hydrologic setting, including wet and dry canyons, and wet, dry, and disturbed mesas. Perched water is often found beneath wetter canyons, either associated with near-surface alluvial systems or at intermediate depths, along low-permeability interfaces such as buried soils and unfractured or clay-filled horizons of basalt flows. Alluvial groundwater is discussed in Section 2.4, while perched water is addressed in Section 2.6. The generalized view of the role of wet and dry canyons on vadose zone flow and transport is quantified in the numerical model section of this report (Section 4).

#### 2.6.2.1 Mesas

Dry finger mesas constitute most of the mesa area on the plateau. The hydrologic conditions on the surface and within these dry mesas lead to slow unsaturated flow and transport. The mesas shed precipitation as surface runoff to the surrounding canyons such that most deep infiltration occurs episodically following snowmelt (Section 2.4.2.1). Much of the water that does enter the soil zone is lost through evapotranspiration (ET). As a result, annual net infiltration rates for dry mesas are less than ten mm/yr and are more often estimated to be on the order of one mm/yr or less (Kwicklis et al., 2005). Since the dry mesas are generally comprised of nonwelded to moderately welded tuffs with low water content, flow is likely to be matrix dominated. Wetter mesas, supporting ponderosa forest above densely welded and fractured tuff in the western portion of the plateau, may provide fracture flow to a few meters to tens of meters depth but evidence of fracture infiltration usually diminishes at the depth of the first nonwelded horizon. For most of the LANL site, travel times for contaminants migrating through mesas to the regional aquifer are expected to be several hundred to thousands of years (Newman, 1996; Newman et al., 1997b; Birdsell et al., 2000; and Section 4.1.1 of this report).

The topographic relief of these steep-sided mesas influences their internal hydrologic conditions as well. High solar radiation, strong winds, and fluctuations in barometric pressure cause temperature and pressure gradients between the surface of the mesa and its interior. These gradients enhance air circulation through the mesas, which is thought to enhance deep evaporation (Neeper 2002; Neeper and Gilkeson, 1996; Newman, 1996; and Newman et al., 1997b). This additional drying in the mesa-top units further slows downward water flow and transport of dissolved species. However, these same conditions enhance vapor transport of volatile species (Stauffer et al., 2005).

Anthropogenic discharges and surface disturbances due to laboratory operations can drive infiltration rates higher in usually dry mesas. In some cases, multiple disturbances of mesa sites through liquid waste disposal, asphalt covers, and/or devegetation have caused mesa infiltration rates to temporarily increase to near wet canyon levels (representative values are given in Section 4.1). Even with elevated infiltration, at most sites flow remains matrix dominated. Fracture flow has occurred in a few instances beneath long-term liquid disposal sites with ponded conditions. However, fracture flow ceases once liquid disposals stop. Infiltration rates are expected to return to low, near-background levels when the surface and vegetation return to natural conditions.

An exception to the general concepts just discussed occurs for mesas along the mountain front of the plateau. Due to their higher elevation, these mesas receive higher precipitation and higher infiltration than the drier mesas in the central and eastern portions of the plateau (Birdsell et al., 2005). Mountain-front areas also have units of the Tshirege Member that are more strongly welded, yielding rocks with more fracturing and lower matrix permeabilities. Under these conditions, infiltrating water travels laterally through fractures and other fast pathways, often issuing at springs that feed the canyons in this area. These near-surface processes can be thought of as sources for deeper vadose zone transport from canyon bottoms, although the possibility of deeper vertical migration from the mesa source without first entering the canyon is also possible.

#### 2.6.2.2 Canyons

This section summarizes the hydrologic conditions present in canyons characterized as either wet or dry. Several features characterize naturally wet canyons on the Pajarito Plateau. Their headwaters are in the mountains, they have large catchment areas (13 to 26 $km^2$), surface flow occurs frequently, and alluvial groundwater systems exist in the canyon floors. In some cases, anthropogenic sources can elevate flows sufficiently in smaller dry canyons that head on the plateau so that they act as wet canyons. In addition, springs issuing from the sides of mesas are a water source in the mountain front canyons; these springs are a characteristic of wet canyons in the western portion of the plateau. Often, deeper, intermediate perched zones are associated with wet canyons. The geometry of wet canyons promotes hydrologic conditions that yield relatively fast, unsaturated flow and transport.

Wet canyons such as Los Alamos Canyon receive large runoff volumes, either through channeling of precipitation or through wastewater discharges. This runoff, in turn, creates surface-water flow along canyon bottoms, which subsequently infiltrates to form near-surface, alluvial water bodies (Section 2.4.2.1). Lateral flow and transport through surface water and in the alluvial systems are rapid with respect to other subsurface hydrologic processes on the plateau. Rates of lateral transport are even higher during surface flow events, which occur more frequently in the larger wet watersheds than in other areas of the plateau. Sorbing species transport slowly in alluvial waters and more commonly migrate down the canyon floor by sediment transport (LANL, 2004; Lopes and Dionne, 1998; Solomons and Forstner, 1984; and Watters et al., 1983).

It has been suggested that trace quantities of strongly sorbing contaminants can travel via colloid-facilitated transport in the alluvial groundwater (Penrose et al. 1990), although this interpretation of the data from Mortandad Canyon has been called into question (Marty et al., 1997). Since some of the wet canyons that cross Laboratory land have received liquid-waste discharges from outfalls, the alluvial systems act as line sources for both water and contaminants to the deeper vadose zone beneath such canyons (Birdsell et al., 2005). The term "line source" denotes that infiltration is likely at any location along the region defined by the alluvial groundwater; there are probably preferential zones of enhanced infiltration at certain locations that will yield larger than average travel velocities through the deeper vadose zone. The net percolation rates beneath the alluvial systems of wet canyons to the underlying unsaturated zone are expected to be among the highest across the plateau, approaching meters per year (100 - 1000 mm/yr) (Kwicklis et al., 2005).

In addition, the vadose-zone thickness decreases with increasing distance down canyon, due to thinning of the Bandelier Tuff (Section 2.2.9). This is especially true for the deep wet canyons because their canyon bottom elevations are 45 to 60 m lower than smaller canyon systems on the plateau. Contaminants transported down canyon via surface flow or through the alluvial groundwater system often percolate through a geologic column consisting primarily of basalt and fanglomerate with little or no overlying tuff. Downward percolation is believed to be more rapid in the basalt than through moderately welded tuff (Section 2.2.8). Thus, these wet canyons have thinner vadose zones and a smaller portion of the flow path with matrix-dominated flow.

These stratigraphic factors, compounded by the relatively high deep-percolation rate in wet canyons, likely yield the fastest vadose-zone travel times for contaminants from the land surface of the plateau to the regional aquifer. Transport to the regional aquifer beneath wet canyons is predicted to be on the order of decades to hundreds of years (see Section 4.1 for details).

In contrast to wet canyons, dry canyons such as Potrillo Canyon and Cañada del Buey head on the plateau, have smaller catchment areas (less than 13 square km), experience infrequent surface flows, and have limited or no saturated alluvial systems in their floors. If anthropogenic sources are present, they are small volume sources. These hydrologic factors yield little lateral near-surface contaminant migration and slower unsaturated flow and transport from the surface to the regional aquifer. For example, because surface and alluvial waters are less common, contaminants remain close to their original source locations. Pathways through the vadose zone tend to be longer in the shallow dry canyons that have thicker sections of nonwelded to moderately welded tuff than the deeper-cut wet canyons. Net infiltration beneath dry canyons is much slower, with rates generally believed to be less than tens of millimeters per year and commonly on the order of 1 mm/yr. Finally, transport times to the aquifer beneath dry canyons are expected to be much longer than travel times from the bottom of wet canyons.

### 2.6.3 Vadose Zone Flow and Transport Mechanisms

Given the description in the previous section of surface and near-surface hydrologic conditions, the next step is to consider the flow and transport mechanisms for water that infiltrates into the subsurface. Most of the plateau is covered with nonwelded to moderately welded Tshirege and Otowi Member ash-flow tuffs (Section 2.2.9). Unsaturated flow and transport through these nonwelded to moderately welded tuffs is thought to occur predominantly through the porous matrix. These units are quite porous, with typical porosities of 40 to 50%, moderate saturated hydraulic conductivities (e.g., $10^{-4}$ cm/sec), and water contents that are generally far below saturated conditions (2 to 25%) (Abrahams et al., 1961; Rogers et al., 1996a; Birdsell et al., 2000; Springer, 2005).

Although the tuff units are often fractured, flow is expected to be matrix dominated unless conditions approach full saturation due to the presence of a high-flow-rate, constant water source (Soll and Birdsell, 1998), such as beneath liquid-waste disposal pits or outfalls. This result is a consequence of the difference in capillary pressure behavior in a porous matrix versus within a fracture. Even if water is injected into a fracture, capillary forces tend to pull water into the rock matrix over a relatively short flow distance. This concept has been established for a wide variety of fracture and matrix hydrologic properties (e.g., Nitao and Buscheck, 1991; Robinson and Bussod, 2000; Soll and Birdsell, 1998; Robinson et al., 2005a, 2005b).

Field observations and analyses support the matrix-flow hypothesis. Robinson et al. (2005b) modeled a vadose-zone, wellbore injection test that was performed in the Tshirege Member of the Bandelier Tuff (Section 2.2.9.3) and reported by Purtymun et al. (1989). Their analysis examined different numerical representations for the fractured porous medium, including a discrete fracture model, a matrix-dominated continuum model, and a dual-permeability representation. Figure 2-35 shows the field-measured moisture profiles at different times during the injection. Water diffused laterally downward, and upward in a relatively uniform fashion,

rather than percolating rapidly through a fracture network. The agreement between the matrix-dominated model and the observations was acceptable, both qualitatively and quantitatively (Robinson et al. 2005b). They estimated an equivalent infiltration rate during the injection phase of about $2.7 \times 10^4$ mm/yr, which is greater than any estimates of infiltration across the plateau. They concluded that if matrix-dominated flow is observed at the high effective infiltration rate of this injection test, then it is even more likely to be the case under natural conditions on the plateau.

As discussed in Section 2.6.2.1, this general picture that applies in the eastern portion of the Pajarito Plateau must be modified for areas near the mountain front on the western edge, where some of the Tshirege units of the Bandelier Tuff have densely welded intervals as a result of being closer to the volcanic source (Section 2.2.9.3). These more welded units are less porous, with porosities ranging from 17 to 40%, and have low saturated hydraulic conductivities (e.g., $10^{-6}$ to $10^{-9}$ cm/sec) (LANL, 2003b). They are also more fractured and can support fracture flow and transport when sufficient water is present. A bromide tracer test and high explosives contaminant distributions suggest that both fracture and matrix-dominated flow can occur near the mountain front depending on the degree of welding (or matrix conductivity) of the tuff (LANL, 1998b; LANL, 2003b). Therefore, the location and degree of welding of the tuff units affects the degree to which fracture flow will be sustained.

In contrast to the behavior of the Bandelier Tuff units, much of the vadose zone flow through the basalt units is almost certainly fracture dominated (flow-base rubble and scoria may also be highly permeable, but these are stratified components of generally limited vertical extent). Under ponded conditions, rapid flow through fractured basalt has been observed (Stauffer and Stone, 2005). The Laboratory fielded an experiment on the upstream side of a low-head weir located in Los Alamos Canyon (Stone and Newell, 2002). Figure 2-36 is a schematic of the field experimental setup. The objective of the experiment was to monitor flow and bromide tracer transport through fractured basalt under typical unsaturated and periodically ponded conditions using three observation boreholes. Following three ponding events, the bromide tracer advanced quickly downward to a depth of several tens of meters in 10 to 14 days after the first ponding event (Stauffer and Stone, 2005). These observations confirm that fracture flow and transport occurs through basalts under ponded conditions. Model calibration of the bromide transport yields an effective fracture porosity in the range of $10^{-2}$ to $10^{-3}$ and saturated hydraulic conductivity in the range of $10^{-2}$ to $10^{-3}$ cm/sec (Stauffer and Stone, 2005). In fact, the data and simulations both indicate that the bromide continued to advance through the fractured system even after the all the ponded water had infiltrated.

However, under drier conditions no direct observations have been made of vadose-zone flow and transport in these deeper locations. For this reason, the conceptual model for unsaturated flow and transport through basalts is still evolving.

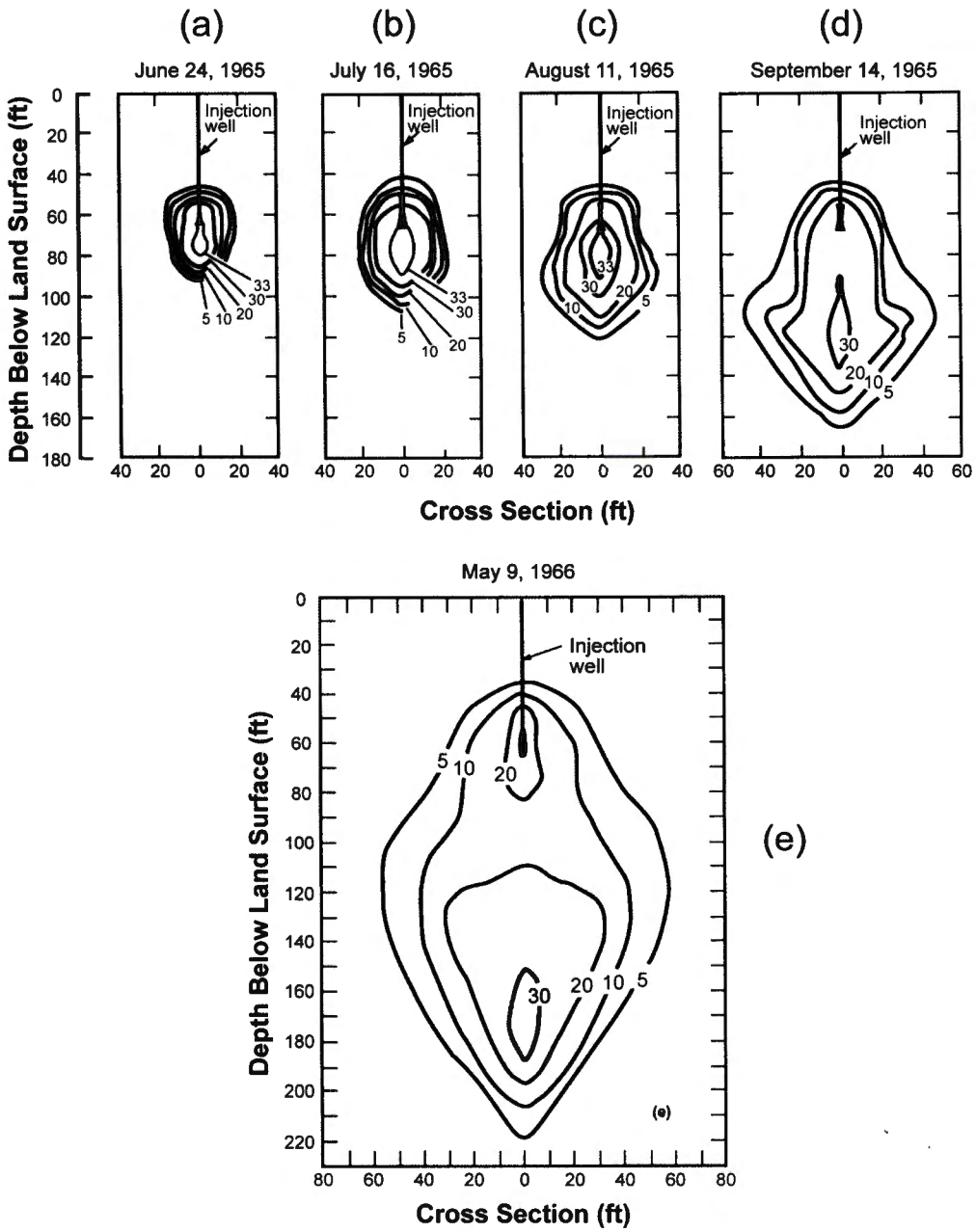


**Figure 2-35.** Contours of water content constructed from the neutron log data during and after the wellbore injection test: (a) Day 7 after injection; (b) Day 29; (c) Day 55; (d) Day 89 (end of injection phase); (e) Day 327 (post-injection phase). From Purtymun et al. (1989).

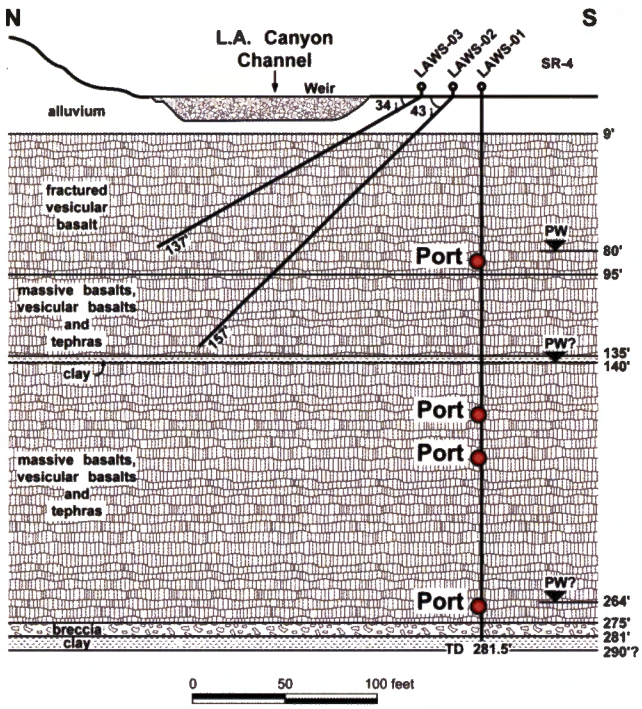


(a)

(b)

**Figure 2-36.** Low head weir monitoring well setup; (a) schematic; (b) north-south photograph.

### 2.6.4 Alternative Hypotheses

Although the basic processes outlined in the preceding sections are supported by the available data and observations and form the best current conceptual model, alternative hypotheses are possible and cannot be completely ruled out by the available information. This section briefly discusses the potential alternative conceptual model of fracture flow. In addition, alternative conceptual models for the mechanisms of flow within perched water zones are described in Section 2.7.

Fracture flow through the Bandelier Tuff is a conceptual model that is often proposed, in contrast to the conceptual model of matrix-dominated flow and transport discussed earlier. Although the available information is consistent with matrix flow, it is possible that in certain situations, fracture flow is important, including the examples related to mountain front processes described earlier. Despite the fact that water input into fractures tends to imbibe into the rock matrix, the observations presented earlier may capture the flow behavior of most, but not all of the water flow. It is possible that preferential flow paths through Bandelier Tuff fractures allow a small portion of the infiltrating fluid to travel to significant depths, even though most water imbibes into the matrix. Alternatively, unstable fingering flow through heterogeneous matrix rock could also lead to preferential downward flow. Regarding the TA-50 water injection test, it is possible that a small amount of fast-moving water could have escaped detection and traveled to greater depths via these mechanisms. The implication of this uncertainty is that small quantities of contamination could potentially be observed at some point in the future at greater depths than

"expected." If this occurs, then we will need to assess whether a relatively small, fast-moving fraction of a released contaminant, combined with a center of mass that travels much more slowly, poses a significant threat to groundwater.

## 2.7 Perched Water

A common feature of vadose zone flow systems is the presence of perched water. Perching can occur for a number of reasons, including capillary barriers and low-permeability barriers coupled with complex stratigraphic structures in the subsurface (e.g., Bagtzoglou, 2003a, 2003b). Beneath the Pajarito Plateau, perched waters may be important components of subsurface pathways that facilitate movement of contaminated fluids from the ground surface to the water table of the regional aquifer. These perched groundwater bodies are generally too small for use as municipal water supplies. Nonetheless, they are of interest because (1) they represent natural groundwater resources that are protected under State law, (2) their chemical and isotopic characteristics help constrain groundwater transport rates through the vadose zone, (3) their presence may divert, slow, or stop the vertical migration of groundwater through the vadose zone, or they may indicate the presence of a fast subsurface pathway, depending on the characteristics of the perched zone, and (4) they can be used as vadose zone monitoring points that provide early warning of contaminants approaching the regional aquifer.

Characterization of these groundwater bodies is challenging because of the thickness of the vadose zone, the heterogenous nature of bedrock geologic units that serve as host rocks and perching horizons, and the depths of groundwater occurrences. Despite these limitations, substantial new information has been gathered about intermediate perched zones on the plateau. This section summarizes information about the location, depth to water, saturated thickness, and geologic setting of perched water occurrences beneath the Pajarito Plateau. This summary includes data from historical investigations and much new information collected as part of the Hydrogeologic Workplan characterization program.

### 2.7.1 Perched Water Occurrence

The different modes of groundwater occurrence beneath the Pajarito Plateau are shown conceptually in Figure 2-37. Contaminant distributions in groundwater strongly suggest that groundwater of the plateau alluvial systems is in communication with intermediate perched and regional aquifer groundwater to varying degrees. The focus of this section is the intermediate perched groundwater; a description of the alluvial groundwater is presented in Section 2.5, and the regional aquifer is described in Section 2.8.

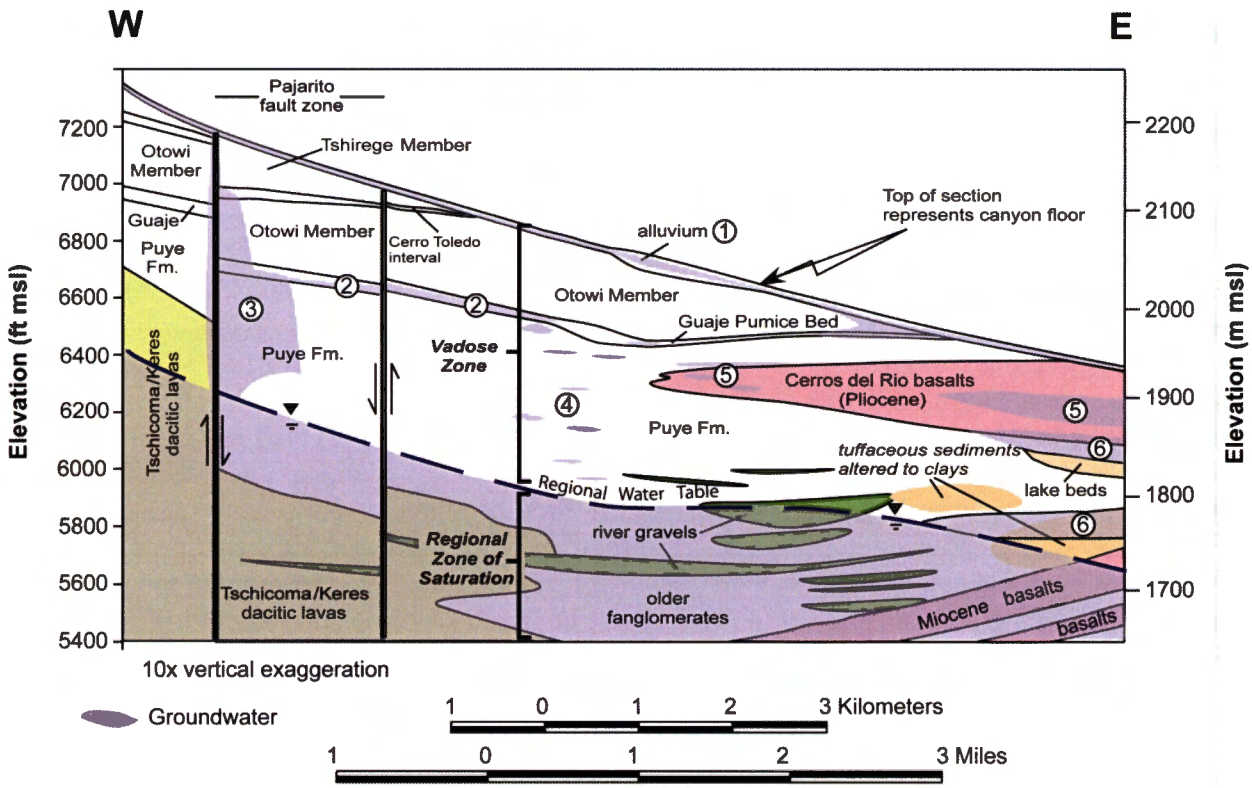


1. Canyon-floor alluvial groundwater—most commonly found in large, wet watersheds with significant snow and storm run off or in smaller watersheds that receive liquid effluent from wastewater treatment plants. Saturated thickness and down-canyon extent varies seasonally.
2. Perched ground water is associated with the Guaje Pumice Bed in Los Alamos Canyon. This perched water body has a lateral extent of up to 3.7 mi Guaje Pumice Bed has a high moisture content but is not fully saturated in most other locations.
3. Cañon de Valle area in the southwest part of LANL. This is the largest perched zone identified on the plateau. A deep-sounding surface-based magnetotelluric survey suggest that this perched zone is discontinuous laterally, occurring as vertical pipe-like groundwater bodies. One interpretation of this zone is that it represents groundwater record(s) formed in response to local recharge beneath a wet cany9on floor. Recharge may be enhanced across the Pajarito fault zone where shallow, densely-welded tuffs rocks are highly fractured.
4. Small zones of perched water formed above stratigraphic traps in Puye fanglomerate. these perched zones tend to be more numerous beneath large wet canyons and less frequent beneath dry mesa tops.
5. Perched groundwater associated with Cerros del Rio basalt. Saturation occurs in fractured basalt flows and in interflow breccias and sediments.
6. Perched zones form in response to local geologic conditions on the eastern side of the plateau. These include perched zones within clay-altered tuffaceous sediments and above lake deposits.

**Figure 2-37.** Conceptual model of groundwater occurrences beneath the Pajarito Plateau.

Identification of perched groundwater systems beneath the Pajarito Plateau comes mostly from direct observation of saturation in boreholes, wells, or piezometers or from borehole geophysics. Additional information is provided by surface-based electrical geophysics, although these types of investigations are generally limited by their relatively shallow depths of investigation and poor vertical resolution. Identification of larger perched groundwater bodies in boreholes is generally reliable, but use of drilling fluids, which is necessary in most boreholes, may mask smaller or relatively unproductive zones. Defining the lateral extent of saturation is more problematical because of the costs associated with installing deep wells. One geophysical method, a deep-sounding surface-based magnetotelluric survey, has been conducted in the Cañon de Valle/Water Canyon area. The survey results suggest that perched groundwater is

discontinuous laterally, occurring instead as vertical, finger-like groundwater bodies. These geophysical interpretations are currently being tested by additional drilling. Despite these limitations, substantial new information has been gathered about deep perched zones on the plateau during the Hydrogeologic Workplan investigations.

This section briefly summarizes the observed occurrences of perched water. Appendix 2-B contains a comprehensive description of the 33 occurrences of perched groundwater detected in boreholes across the Pajarito Plateau. Perched groundwater is widely distributed across the northern and central part of the plateau (Figure 2-38) with depth to water ranging from 36 to 272 m (118 to 894 ft). The principal occurrences of perched groundwater occur in (1) the large, relatively wet Los Alamos and Pueblo Canyon watersheds, (2) the smaller watersheds of Sandia and Mortandad Canyons that receive significant volumes of treated effluent from LANL operations, and (3) in the Cañon de Valle area in the southwestern part of LANL. Perched water is most often found in Puye fanglomerates (Section 2.2.7 ), the Cerros del Rio basalt (Section 2.2.8), and in units of the Bandelier Tuff (Section 2.2.9) (Figure 2-38). There are few reported occurrences of perched water in the southern part of LANL, but few deep boreholes are located there and additional perched zones are likely beneath the large wet watersheds of Pajarito and Water Canyons.

### 2.7.2 Interpretation of Perched Water Observations

General conclusions about the nature of perched groundwater beneath the Pajarito Plateau are based on the observations summarized above. The conclusions pertain to surface hydrologic conditions necessary to support perched groundwater, geologic and hydrostratigraphic controls on perched water occurrence, the lateral and vertical extent of perched zones, and alternative hypotheses about the role of perched zones in contaminant transport.

#### 2.7.2.1 Surface Water Conditions for Perched Water

A requirement for deep perched water to exist is a surface water source (natural or anthropogenic) that supplies water to alluvial systems. The alluvial groundwater systems act as storage for groundwater entering underlying bedrock units at high infiltration rates (Section 2.5). This interpretation is supported by the observation of perched groundwater in wet canyons. In addition, ponding associated with anthropogenic sources is another possible water source that could lead to subsurface perched water.

A special situation also exists in the western portion of the Laboratory, in the mountain-front mesa area at TA-16. In contrast to the dry mesas prevalent further east, these mesas receive greater precipitation (e.g., 500 mm/yr) and increased runoff and infiltration. The wet, mountain-front mesas contain numerous perennial and ephemeral springs. Such springs are rare in the dry mesas of the eastern part of the plateau, except where the regional groundwater aquifer discharges along the Rio Grande.

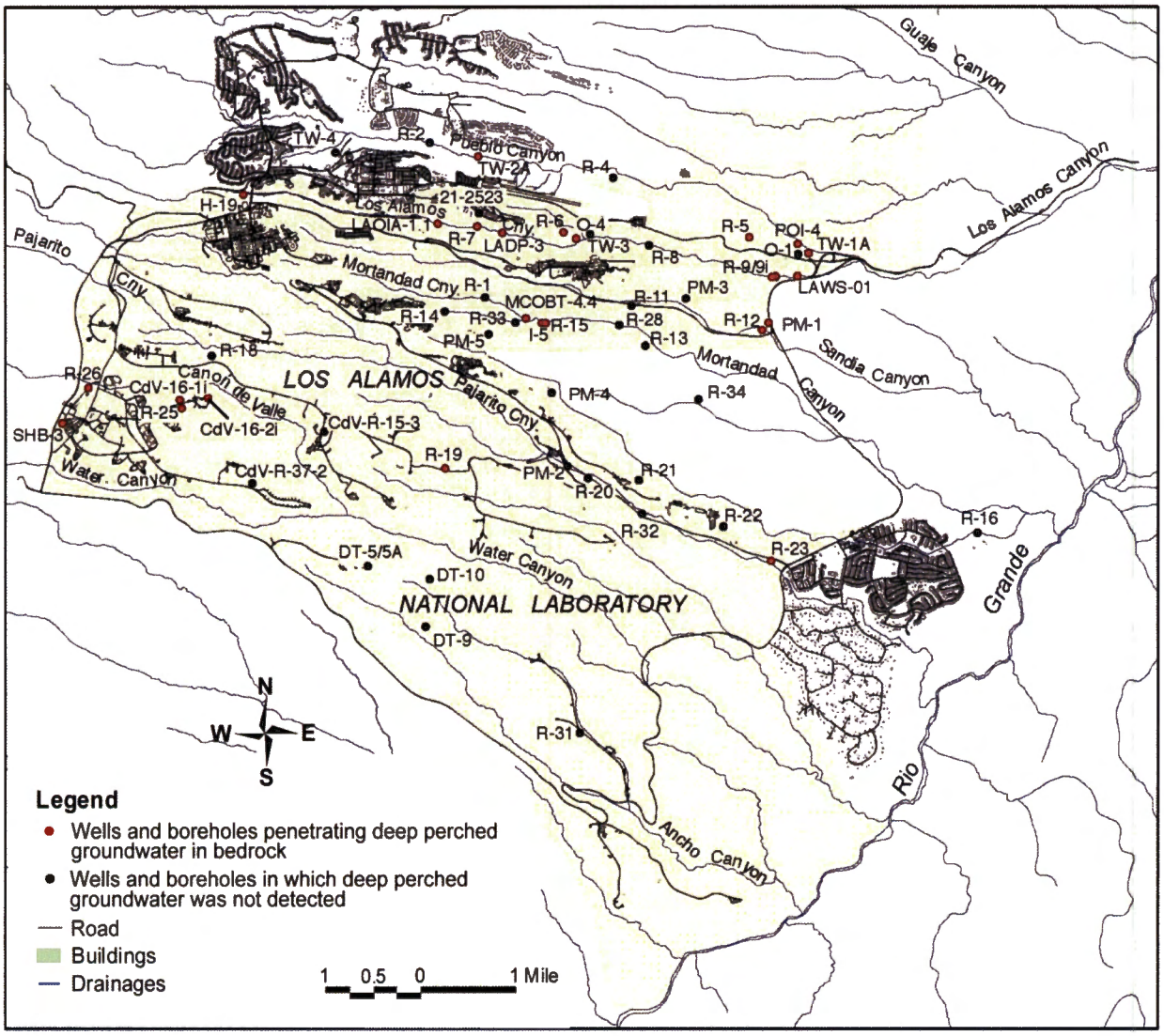


**Figure 2-38.** Locations of wells and boreholes that have penetrated perched groundwater systems in bedrock.
Note: The area shown in yellow is LANL.

### 2.7.2.2 Geologic and Hydrostratigraphic Controls on Perched Water Occurrence

Deep perched groundwater occurs most frequently in the Puye Formation (Section 2.2.7) and Cerros del Rio basalt (Section 2.2.8), but some of the thickest and/or most laterally extensive zones involve units of the Bandelier Tuff (Section 2.2.9). Perching horizons include a wide variety of layered geologic lithologies including

- Unfractured basalt flows
- Clay-rich interflow zones in basalt
- Buried soils and other fine-grained deposits in fanglomerate,

- Clay-altered tuffaceous sediments
- Lake deposits.

Therefore, in addition to high local infiltration rates, low-permeability barriers to downward vertical flow appear to be required to induce perched groundwater (Robinson et al., 2005b). In contrast, there have been no observations of perched groundwater caused by a capillary barrier effect, despite the presence of layered stratigraphy with units of contrasting unsaturated flow properties.

An alternative hypothesis is that the deepest perched water occurrences are a manifestation of complex groundwater flow within the phreatic zone at the top of the regional aquifer. Localized heterogeneities, such as the clay-rich alteration zones in the Puye Formation at well R-9, combined with high recharge, may give rise to a complex flow structure that includes mounding, interconnected saturated zones, and locally confined conditions (Robinson et al., 2005b). However, the complexity of the alteration and the depth of these groundwater zones make detailed characterization prohibitively expensive. Hydrologic testing of the regional aquifer could be conducted to discriminate between alternatives.

With respect to the western portion of the Laboratory, Duffy (2004) discusses the importance of mountain-front processes and hydrologic conditions in semiarid landscapes and suggests that the mountain block and mountain-front areas are the dominant recharge zones in semiarid landscapes. An important hydrostratigraphic feature in this area is that the upper tuff units along the mountain front are often moderately to strongly welded because of close proximity to the caldera source. Welding results in increased fracturing during cooling, and because the mountain-front mesas lie within the Pajarito fault zone, additional fracturing and minor faulting of the tuff units has resulted. The welded tuffs create a hydraulic condition where matrix hydraulic conductivities are low (e.g., $10^{-7}$ to $10^{-9}$ cm/sec), but fracture densities are relatively high. Thus, there is a possibility for significant fracture flow. Fracturing appears to control locations of springs along the mountain-front mesas and fracture flow is suggested by water content and contaminant distributions in the tuff proximal to outfalls and wastewater lagoons (LANL, 2003b).

#### 2.7.2.3 Subsurface Extent of Zones of Saturation

Observed saturated thicknesses of perched zones vary from 1 to 128 m (3 to 421 ft). The lateral extent of saturation in these zones is less well understood because costs associated with installing deep wells are high. However, perched groundwater generally is more likely to be present beneath wet canyons, based on observations of both occurrences and nearby absences of perched groundwater in adjacent wells. The extent that perched groundwater flows along dipping geologic strata into areas beneath adjacent mesas is not fully known. However, the few paired canyon/mesa wells such as R-7 and 21-2523 in Los Alamos Canyon and R-22 and R-23 in Pajarito Canyon suggest that perched zones are much less common beneath dry mesas.

#### 2.7.2.4 Flow Conditions Upstream and Within Intermediate Perched Groundwater Zones

The presence of mobile (nonsorbing) anthropogenic chemicals in some perched groundwater zones indicates a connection with surface and alluvial groundwater (e.g., Robinson et al., 2005

and references therein). The travel time of groundwater moving from the surface to perched groundwater systems is on the order of several decades, based on the age of facilities that are potential sources of contaminants. Within the perched zones themselves, the topography of the perching horizon, the bedding features, and the orientation of interconnected fracture systems probably control local groundwater flow velocity. However, direct evidence such as single-well or multiple-well hydrologic and tracer testing, is not available. Therefore, the following discussion is based on reasonable hydrologic principles rather than direct measurements.

Flow conditions can, in principle, be categorized with the following two end-member conceptual models for flow within a perched water zone:

- *Low-velocity, virtually stagnant water resting in a perching horizon within a local structural or stratigraphic depression.* Water percolates very slowly out the bottom of this zone, or spills over the sides of the depression. This configuration views perching horizons as barriers that slow the downward percolation of water. In several wells, intermediate saturated zones thought to represent perched groundwater were screened but failed to produce significant water (Robinson et al., 2005). These occurrences may represent cases where zones of limited extent were substantially drained when the perching horizon was penetrated during drilling. Once the stagnant water is depleted in an initial round of sampling, there is insufficient recharge to keep the zone saturated.
- *High-velocity, laterally migrating fluid that travels on top of the perching horizon.* This conceptualization suggests that once groundwater reaches a perched zone, it rapidly percolates laterally along high-permeability pathways until the perching horizon pinches out or is breached by high-permeability features such as fractures or lateral changes in lithology. In this scenario, water could move in stairstep fashion from one perching horizon to another. There are no confirmed instances of large-scale, lateral vadose zone pathways beneath the Pajarito Plateau at depths greater than the alluvial groundwater. The case of lateral flow through the wet, mountain-front mesas at TA-16 suggests that this possibility exists at greater depths. Although we categorize the TA-16 observations as shallow for the purposes of this discussion because they discharge via springs in the local canyons, it could be argued that deep pathways with flow geometries similar to those of the mountain-front mesa or today's alluvial groundwater zones are evidence for the possibility of deeper fast pathways elsewhere.

Tracer experiments in alluvial and mountain-front mesa perched zones have been used to measure transport velocities. However, fluid velocity in the deeper perched groundwater zones is unknown due to the lack of direct measurements. The two end-member conceptual models, relatively stagnant fluid in a local subsurface depression, or lateral diversion in the hydrologic unit overlying the perching horizon, cannot be ruled out with existing data. Hydrologic, tracer, or remote geophysical techniques would be required to shed light on this question. Given the complexity and cost of such field campaigns, they should be performed only if model sensitivity analyses indicate that sorting out this issue is important to study impacts, or if remediation of a perched zone is to be conducted.

## 2.8 Regional Aquifer Conceptual Model

This section summarizes the current understanding of flow and transport in the regional aquifer beneath the plateau. This work builds on results obtained from earlier hydrologic studies in the region (Griggs and Hem, 1964; Purtymun, 1984; Purtymun and Johansen, 1974; Rogers et al., 1996b). The previous literature is supplemented with interpretations of new data collected by the LANL Groundwater Protection Program. These new data, combined with previous studies, provide the foundation for the flow and transport model development presented in Section 4.2

### 2.8.1 Regional Hydrologic Setting

This section briefly summarizes the regional hydrologic setting before focusing on the regional aquifer beneath the Pajarito Plateau (Section 2.7.2), which is the subject of this report. The Española Basin (see Figure 2-39) is one of a series of basins located within the Rio Grade Rift zone, a tectonic feature that extends from northern Colorado to the south into Mexico. Elevations within the basin range from more than 3,800 m along peaks in the surrounding mountain ranges to about 1,700 m at the basin surface water outlet. Vegetation is predominantly ponderosa pine forest at higher elevations and piñon pine/ juniper at lower elevations (Spiegel and Baldwin 1963).

The Española Basin and surrounding areas receive annual total precipitation ranging from 18 to 86 cm/yr. Precipitation is strongly elevation dependent (Spiegel and Baldwin 1963). The largest streams in the basin are the Rio Grande and Rio Chama. Median monthly flow, calculated using USGS average monthly flow data for the past 80 years, is 26.0 $m^3/s$ along the Rio Grande (at Otowi Bridge) and 10.0 $m^3/s$ along the Rio Chama (at Chamita) (U.S. Geological Survey, 2001). Numerous tributaries enter these rivers; many of these are ephemeral and many are ungaged. The Rio Grande and the lower reaches of many tributaries comprise the regional groundwater discharge zone.

In most parts of the basin, the water table is 0–60 m below ground surface; but on the Pajarito Plateau the water table is much deeper (up to 350 m below the surface). Throughout much of the basin, the water table appears to intersect the surface at the Rio Grande (Purtymun, 1984). Perched waters exist on the Pajarito Plateau (Robinson et al., 2005) where the unsaturated zone is much thicker than in other parts of the basin (Section 2.7). Contours of predevelopment water level data (Purtymun et al., 1995a, 1995b; U.S. Geological Survey, 1997) indicate that hydraulic gradients are generally towards the Rio Grande (Figure 2-40).

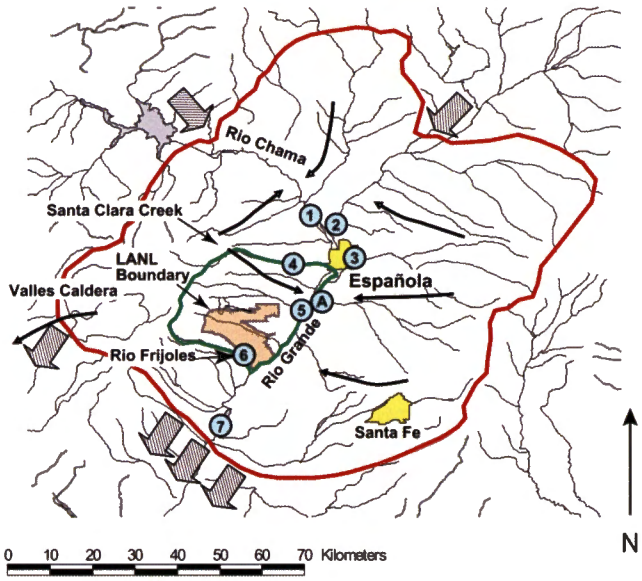


**Figure 2-39.** The Española Basin and vicinity, with basin-scale numerical model outline shown in red, site-scale model outline shown in green. Black arrows are generalized groundwater flow directions, based on regional water level data (Keating et al., 2003). The striped arrows indicate groundwater flow between the Española Basin and adjacent basins. Circled numbers refer to USGS stream gages: (1) Rio Chama at Chamita; (2) Rio Grande at San Juan; (3) Santa Cruz River; (4) Santa Clara Creek; (5) Rio Grande at Otowi; (6) Rio Frijoles; (7) Rio Grande at Cochiti. Circled "A" indicates the mouth of the Pojoaque Creek.

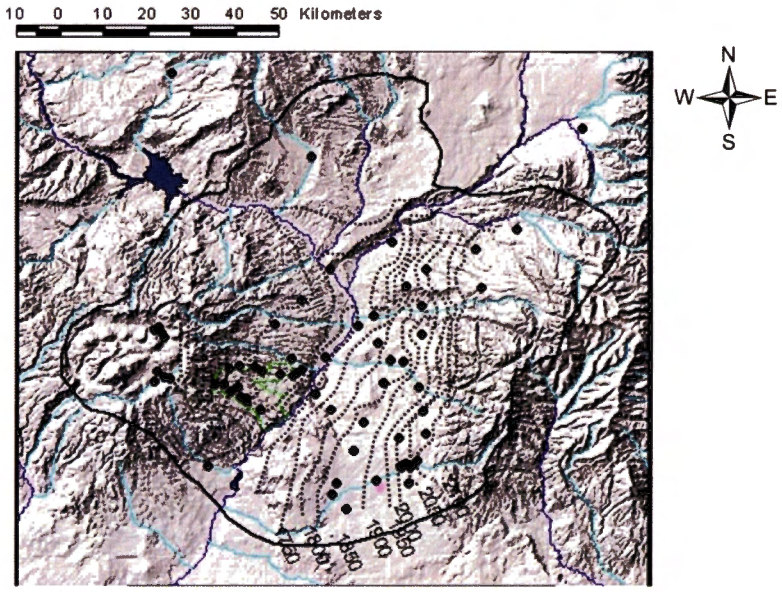


**Figure 2-40.** Approximation to present-day water table elevations (m).
Note: Some older head data are used to improve the spatial distribution.

The regional aquifer is a major source of drinking water and agricultural water supply for northern New Mexico. The largest cities in the basin are Santa Fe, Española, and Los Alamos; these all rely primarily on groundwater for municipal supply. In addition to discharges to water supply wells, the aquifer discharges to the Rio Grande, the lower reaches of its tributaries, and to numerous springs. There are additional withdrawals for municipal and agricultural supply. Recharge is thought to occur primarily in the higher elevations—estimates based on water budget and chloride mass balance methods range from 7–26% of total precipitation (Anderholm, 1994; Wasiolek, 1995). Little or no recharge occurs at lower elevations other than along stream channels due to low precipitation rates and high evapotranspiration demand (Anderholm, 1994).

The aquifer is predominantly composed of Santa Fe Group rocks, which are weakly consolidated basin-fill sediments reaching over 3,000 m in thickness near the basin axis (Cordell 1979). Groundwater also occurs in older crystalline rocks along the eastern and northern basin margin and in younger volcanic lavas and volcaniclastic sedimentary rocks in the vicinity of the Pajarito Plateau to the west (Purtymun and Johansen, 1974; Coon and Kelly, 1984; Daniel B. Stephens & Associates, 1994).

### 2.8.2 Hydrology Beneath the Pajarito Plateau

Groundwater beneath the Pajarito Plateau is part of a regional aquifer which extends throughout the Española Basin (an area roughly 6000 $km^2$; Figure 2-39). This aquifer is the primary source of water for the Laboratory, the communities of Santa Fe, Española, Los Alamos, and numerous pueblos. Four water supply wellfields exist on the plateau (Figure 2-41); one additional wellfield that supplies the city of Santa Fe (Buckman) sits just to the east of the Rio Grande, close to the plateau. As is the case for many aquifers in the semiarid southwest, there is concern that current withdrawal rates may not be sustainable over long periods of time and current drought conditions might have significant impacts on both surface water and groundwater quantity and quality.

Of more direct relevance to the Hydrogeologic Workplan studies are concerns about water quality, due to a variety of anthropogenic contaminants. Beneath the Pajarito Plateau, there is contamination from various LANL sources in shallow groundwaters in some locations (primarily alluvial aquifers). Some of the LANL-derived contamination has been observed in the regional aquifer at trace concentrations much below the EPA drinking water standards (see Section 3 for a complete discussion of this point). The regional aquifer is the groundwater zone most directly accessible to humans through municipal water-supply wells or springs issuing to the Rio Grande. Therefore, a solid foundation of understanding of the hydrogeologic conditions and controls on flow and transport in the regional aquifer must be obtained in order to make risk-based decisions, to design the required groundwater monitoring network, or to design treatment and remediation systems.

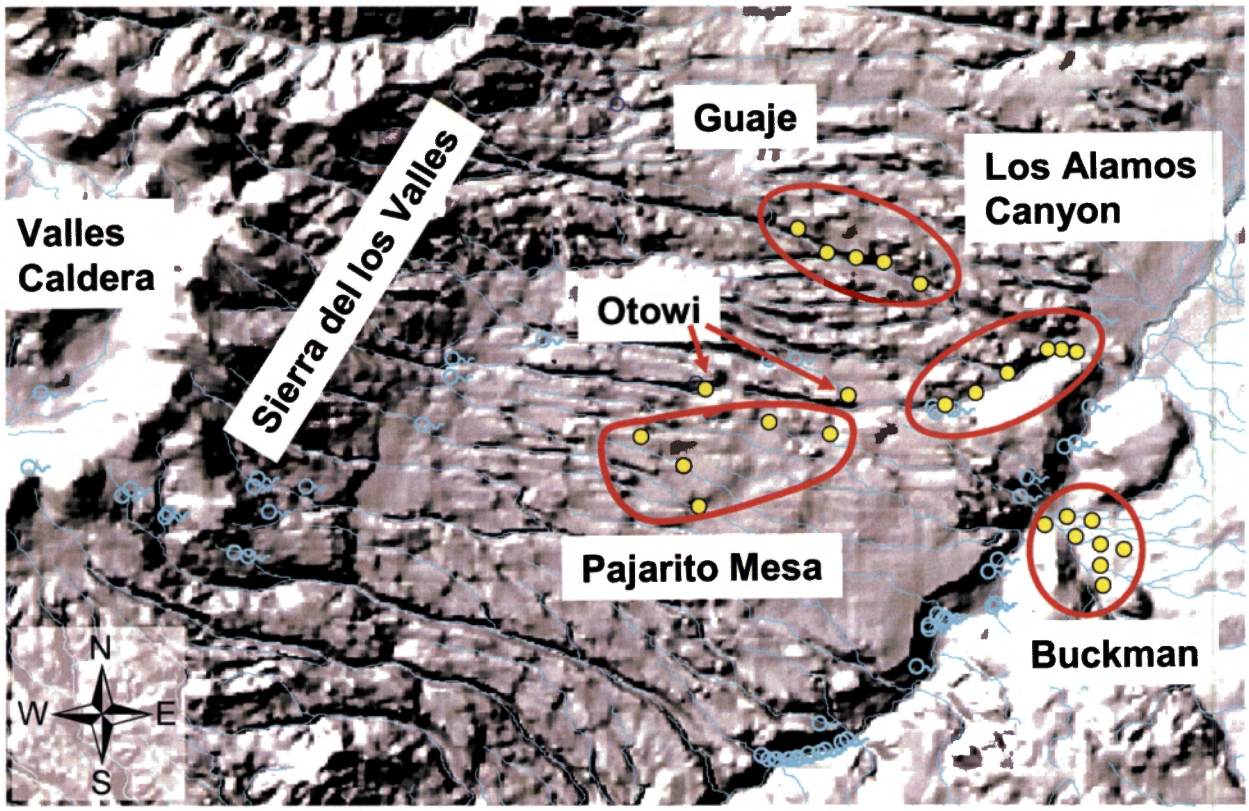


Water supply well
Springs

**Figure 2-41.** The Pajarito Plateau, with major wellfields indicated by enclosures in red.

### 2.8.3 Water Budget

The water budget for the regional aquifer defines the sources and sinks of water to and from the Española Basin and, on a smaller scale, under the Pajarito Plateau. This section summarizes the state of knowledge and addresses uncertainties in the quantities and spatial distribution of recharge, discharge, and interbasin flow.

#### 2.8.3.1 Recharge

As the water source term, recharge to the regional aquifer provides the driving force for fluid movement through the system. Furthermore, water recharging on the Pajarito Plateau on LANL property can carry with it liquid-borne contamination. This subsection addresses both basin-scale and local recharge, addressing the spatial distribution and quantity of recharge.

##### 2.8.3.1.1 Recharge Distribution

Various theories have been proposed regarding the locations of recharge zones for this aquifer. Griggs (1964) suggested that most of the recharge occurred in the Sierra del los Valles and along stream channels in the western edge of the Pajarito Plateau (Figure 2-41). Purtymun and Johansen (1974) proposed that the major portion of the recharge occurs in the Valles Caldera, with smaller amounts recharging through stream channels in the Sierra del los Valles. However, Blake et al., (1995) argued that recharge could not originate in the Valles Caldera, since the

chemistry of geothermal waters in the western Valles Caldera is clearly distinct from the groundwaters on the Pajarito Plateau (Blake et al., 1995; Goff and Sayer, 1980). These authors also proposed, on the basis of stable isotope values in groundwaters beneath the plateau, that recharge areas for the aquifer beneath the plateau were either to the north and/or to the east (Sangre de Cristo Mountains) and not to the west. They hypothesized that the two flow systems are separated by the Pajarito fault acting as a flow barrier (Blake et al., 1995).

In contrast, other lines of evidence indicate that the majority of recharge to the basin aquifer occurs in the mountains along the basin margin where precipitation rates are relatively high. This has been shown using water-budget and chloride-mass balance analyses in the eastern portion of the basin (Anderholm, 1994; Wasiolek, 1995). In the course of the Hydrogeologic Workplan studies, inverse modeling using head and streamflow data (Keating et al., 2003) demonstrated that the elevation above which significant recharge occurs at the basin-scale is very well constrained (2195m ± 177m). Modeling results such as this are to some extent a function of the model conceptualization and structure, and therefore do not provide a precise indication of the recharge elevation. Nevertheless, the modeling result agrees with the conclusion on the elevation above which recharge occurs, as determined from those other lines of evidence.

Isotope geochemical information can also be brought to bear on the question of recharge distribution. Distributions of $\delta D$ and $\delta^{18}O$ ratios are consistent with the conclusion that the mountain front recharge supplies most of the groundwater beneath the Pajarito Plateau (Longmire, 2002a; Longmire, 2002b; Longmire, 2002c; Longmire, 2002d; Longmire, 2002; Longmire and Goff, 2002). Lighter or more negative $\delta D$ and $\delta^{18}O$ ratios indicate both a cooler climate for precipitation and/or a higher elevation of recharge (Clark and Fritz, 1997). Heavier or less negative $\delta D$ and $\delta^{18}O$ ratios are representative of a warmer climate for precipitation and/or recharge that occurs at lower elevations. Groundwater samples collected within the Sierra de los Valles have lighter $\delta D$ and $\delta^{18}O$ ratios relative to those collected beneath the Pajarito Plateau and along the Rio Grande. Precipitation of meteoric water at higher elevations, for example near the Sierra de los Valles, is characterized by cooler temperatures relative to other waters found at lower elevations on the Pajarito Plateau. Long-term temperatures (paleotemperatures) and seasonal variations in temperature also influence $\delta^{18}O$ and $\delta D$ values because of enrichment or depletion of oxygen-18 and deuterium (Clark and Fritz, 1997).

A plot of $\delta D$ versus $\delta^{18}O$ (average values) for numerous groundwater samples collected from wells R-9, R-12, R-15, R-19, R-25, R-26, CdV-R-37-2, and CdV-R15-3 and springs within the Valles caldera and Sierra de los Valles is shown in Section 3.1.1.1. In this figure, the Jemez Mountains meteoric line (upper) ($\delta D = 8\delta^{18}O + 12$) (Vuataz et al., 1986) and the mean worldwide meteoric water line (lower) (($D = 8\delta^{18}O + 10$) (Clark and Fritz, 1997) are denoted by JMML and MWL, respectively. Analytical uncertainties of $\delta^{18}O$ and $\delta D$ are ± 0.1 and ± 1‰ (per mil), respectively. Results of stable isotope analyses for the R wells and springs indicate a meteoric source in which the samples plot close to both the JMML and MWL (Section 3.1.1.1). The distribution of isotopic ratios suggests that evaporation of groundwater has not taken place to a significant extent prior to recharge.

The Sierra de los Valles is the likely recharge source for wells R-25, R-26, CdV-R-15-3, CdV-R-37-2 because the Sierra de los Valles springs have similar $\delta^{18}O$ and $\delta D$ ratios (Blake et al. 1995).

The less negative stable $\delta^{18}O$ and $\delta D$ values (relative to well R-25) in wells R-9, R-12, R-15, and R-19 are consistent with additional recharge at lower elevations (Section 3.1.1.1). This interpretation is consistent with the concept of local recharge on the plateau as the source for water at shallow depths in the regional aquifer beneath the Laboratory.

Although analyses such as these can be useful in identifying the elevation of recharge, Keating et al. (2005) point out that uncertainties due to variability in isotopic composition of precipitation and potential differences in precipitation and infiltration elevations complicate the use of these isotopic tracers. For example, stable isotope ratios may actually be tracing the *timing* of recharge for very old waters (Phillips et al., 1986), as opposed to the location. Very low $\delta^{18}O$ values (< -14), significantly lower than average modern precipitation signatures at all elevations in the basin, have been measured in groundwaters near the Rio Grande (Anderholm, 1994; Blake et al., 1995). These ratios are indicative of paleorecharge during a cooler climate (Phillips et al., 1986) and were interpreted by Anderholm (1994) and Newman (1996) to indicate recharge during the Pleistocene (with age in order of 8,000 – 17,000 years). These age estimates are consistent with $^{14}C$ observations suggesting a component of old fluid (Rogers et al., 1996b). Note however that some of these same waters also clearly contain a component of young water, as indicated in Section 3.1.1.3.

A quantitative assessment of the spatial distribution of recharge on the Plateau was recently published by Kwicklis et al. (2005). The goal of the study was to provide a summary of the current state of knowledge on amount and spatial distribution of infiltration. The study was intended to provide quantitative estimates for use in other studies, as well as to provide a baseline that can be tested and improved upon as more data are collected. The study uses streamflow gain and loss data along canyon bottoms from the Pajarito Plateau, along with point infiltration estimates based on moisture content profiles interpreted using the Richards equation, the chloride mass-balance method, transport rates of tritium in canyons on the Plateau, and numerical modeling. The infiltration rates estimated with these techniques were extrapolated to uncharacterized parts of the study area using maps of environmental variables that are correlated with infiltration (such as topography, vegetation cover, and surficial geology and structure) and spatial algorithms implemented with GIS software that use the mapped variables.

The map of estimated infiltration is presented in Figure 2-34. The large-scale characteristics of these estimates are in line with the discussion presented above. Infiltration rates throughout most of the plateau are generally less than 2 mm/yr, whereas infiltration rates in the mixed conifer-dominated areas of the Sierra de los Valles are typically greater than 25 mm/yr and, in the aspen-dominated areas, greater than 200 mm/yr. Thus, at lower elevations, recharge occurs primarily along arroyos and canyons, and infiltration rates are estimated to be low on mesas except near the mountain front (Anderholm, 1994; Birdsell et al., 2005). Despite the low flux, the total quantity of infiltration associated with the mesas is small but not negligible, due to the large area associated with these parts of the plateau.

The Kwicklis et al. (2005) study estimates that of the total infiltration of about 8600 acre-ft/yr (336 kg/sec), about 23% of the infiltration occurs from canyon bottoms on the plateau at lower elevations. This canyon-bottom infiltration includes about 14% of the total from streams that flow at least partly within LANL boundaries. The inserts in Figure 2-34 indicate regions for

which localized, high-infiltration zones are expected to exist on the plateau. Focused infiltration is expected in the faulted regions associated with the Pajarito fault zone within Cañon de Valle and Water Canyon (see lower left insert in Figure 2-34). Local infiltration at rates up to 1000 mm/yr is estimated. For the insert showing the confluence of Los Alamos and Pueblo Canyons (lower right), rates of 1500–2000 mm/yr are estimated in this region. These high values are a consequence of infiltration directly onto Puye fanglomerates or fractured basalts. In other canyons with similar characteristics, such as Pajarito Canyon, similarly high local infiltration values are expected.

Although relatively small volumetrically compared to mountain recharge to the west, aquifer recharge occurring locally on the plateau is important to the assessment of flow paths of potentially contaminated water. Tritium data confirm that relatively young water is present in the aquifer (Rogers et al., 1996b), indicating fast pathways through the vadose zone beneath LANL. Quantitative estimation of recharge using $^{3}H$ data is complicated by the sometimes confounding influences of bomb-pulse atmospheric $^{3}H$ and locally derived $^{3}H$ related to on-site LANL activities. Elevated $^{3}H$ in regional aquifer samples has been observed at O-1, TW-1, TW-3, TW-8, LA-1A and LA-2 (Rogers et al., 1996b), as well as in several wells drilled during the more recent characterization drilling program (see Section 3.3).

Kwicklis et al. (2005) used vadose zone occurrences of $^{3}H$ to estimate the time-dependent transport velocities, from which they derived infiltration rates to the regional aquifer. They found that in Mortandad Canyon, infiltration rates are as high as 2000 mm/yr occur during periods of large volumes of effluent discharge. This infiltration rate has apparently decreased to 100-200 mm/yr once effluent discharge flow rates were reduced. These observations and analysis confirm that local recharge in canyons is an important component of the recharge distribution for the plateau.

#### 2.8.3.1.2 Total Recharge

Estimates of total recharge provide important constraints on flow and transport models of the regional aquifer by tying model calibrations to measured or estimated water balance components. Therefore, various techniques and data sets have been examined to estimate total recharge. Griggs (1964) estimated the total recharge to the aquifer beneath the Plateau to be between 168 and 216 kg/s. McLin et al. (1996) estimated an upper bound of 192 kg/s, based on recovery of water levels in supply wells rested for a period of several months to several years. Using a variety of methods and considering a larger area, the Kwicklis et al. (2005) study discussed above estimates total average annual recharge to the Pajarito Plateau of 336 kg/sec.

A number of researchers have used baseflow gain to the Rio Grande to estimate total aquifer discharge, from beneath both the plateau and the eastern basin. These estimates presumably approximate the total aquifer recharge before significant pumping began. However, total gain must be combined with an estimate of the proportion of the gain that originates beneath the plateau. Long-term average aquifer discharge between the Otowi Bridge gage and the now-submerged Cochiti gage, a reach which bounds the southern portion of the plateau, was estimated by Spiegel and Baldwin (1963) to be 710 kg/sec and more recently by the U.S. Department of Justice to be 400 kg/sec (U.S. Department of Justice and New Mexico State Engineer Office, 1996). The former estimate is significantly higher because the authors did not

include years of record that indicated the reach to be losing, which was attributed to measurement error. Keating et al. (2005) present an analysis of data from this reach as well as the reach immediately to the north (Española to Otowi), which bounds the northern portion of the plateau. This analysis estimates the total gain to the Rio Grande adjacent to the Pajarito Plateau (Santa Clara Creek to Rio Frijoles) to be approximately 911 kg/sec (+/– 30%). The modeling study of Hearne (1985) assumes 316 kg/sec recharge to the Pajarito Plateau; McAda and Wasiolek (1988) assume 291 kg/sec lateral inflow from the Jemez Mountains.

Aquifer modeling studies can also shed light on the recharge quantities and distribution. Keating et al. (2003) performed basin-scale inverse modeling as part of the Hydrogeologic Workplan, using both streamflow data and transient head data. That study indicated that approximately 253 kg/sec of the gain to the river along this reach originated on the Pajarito Plateau and the Sierra de los Valles. This analysis probably underestimated total recharge on the plateau, in part because the basin model was calibrated to a lower estimate of aquifer discharge north of Otowi Bridge than is indicated by the streamflow analysis subsequently performed by Keating et al. (2005). Part of the reason for the differences between these various estimates of total recharge is that several of the smaller estimates (McLin et al., 1996; Speigel and Baldwin, 1963; and Griggs 1964) emphasized the southern portion of the plateau (including LANL) which, according to the streamflow analysis in Keating et al. (2005), is discharging less water than the northern portion of the plateau.

In summary, although these various estimates span a range and reflect some uncertainty, they are extremely valuable as bounding values for flow and transport modeling in that they constrain the total quantity of water flowing through the aquifer beneath the Pajarito Plateau.

#### 2.8.3.2 Discharge

Data constraining quantity of discharge for the regional aquifer were discussed in Section 2.8.3.1 in the context of estimating recharge. Regarding discharge locations, many authors have identified the Rio Grande as the principal discharge point for the regional aquifer (Cushman, 1965; Griggs and Hem, 1964; Hearne, 1985; McAda and Wasiolek, 1988; Purtymun and Johansen, 1974; Theis and Conover, 1962). Previous reports have cited a variety of evidence to support this, including:

- Streamflow gain along the Rio Grande (Balleau Groundwater, 1995; Purtymun and Johansen, 1974; Spiegel and Baldwin, 1963)
- Measured vertical upward gradients in the vicinity of the Rio Grande (Cushman, 1965; Griggs and Hem, 1964)
- The presence of flowing wells (McAda and Wasiolek, 1988; McLin et al., 1996; Spiegel and Baldwin, 1963)
- Springs along the river (McLin et al., 1996).

Discharge to the river may occur as lateral flow, upward flow, or as flow from springs in White Rock Canyon. Purtymun (1966) suggested that all the springs, which collectively flow approximately 85 kg/sec, discharge water from the upper surface of the main aquifer. Stone (1996) suggested that many of these springs may be discharging perched aquifers rather than the regional aquifer; unfortunately it is difficult to test these alternative hypotheses, although stable

isotopes may provide some discrimination. It has been emphasized that although discontinuous, low-permeability beds produce confining conditions in the aquifer locally near the Rio Grande and elsewhere in the basin, flow is able to cross the low permeability beds in some locations as water discharges to the river (Hearne, 1985; Spiegel and Baldwin, 1963).

The degree of connection between the aquifer and the Rio Grande has been investigated by Balleau Groundwater (1995), who drilled 16 wells in the alluvial aquifer of the Rio Grande near the Buckman wellfield and conducted pumping tests. They found that head in the alluvium is generally 0.1 to 0.2 feet higher than the Rio Grande, indicating discharge from the alluvium to the Rio Grande. Head in the regional aquifer below the alluvium, at a depth of 59 feet, is about 2.8 feet higher than the Rio Grande. From pumping tests, they concluded that the hydrogeologic system at the site behaves as a layered water-table system in hydraulic contact with the river with delayed yield from pore-water storage and an adjacent river boundary source.

#### 2.8.3.3 Interbasin Flow

Overall groundwater fluxes between the regional aquifer beneath the plateau and the basin and flow between the Española Basin and adjoining basins are not well constrained. It is possible that virtually all the groundwater flowing beneath the Pajarito Plateau flows easterly/southeasterly and discharges to the Rio Grande, and that interbasin flow to the south is small. An alternative possibility, that deep flow discharges instead to the basins to the south, is difficult to confirm or refute because of the lack of hydraulic data collected at discrete intervals at great depths within the aquifer. This could have a large impact on flow conditions at and near the site and thus will be the subject of future study.

The Española Basin is separated from the Albuquerque and Santo Domingo basins to the south by a structural high, a prong of older sedimentary rocks, and several major fault zones (Golombek et al., 1983). The Santa Fe Group aquifer thins significantly at this boundary (Shomaker, 1974). If these structures impede flow to the south, this might enhance both regional aquifer and interflow discharge to the surface. We have not evaluated the possible interflow component to streamflow gain in the southern portion of the basin; if it were significant our estimate of groundwater discharge would be erroneously high.

Numerical models of groundwater flow in the basin have generally predicted the interflow component of flow to the south to be small. The model of Hearne (1985) has no groundwater flow to the south by assumption; the McAda and Wasiolek (1988) and Keating et al. (2003) models allow interflow, but the models predict much larger discharge within the basin (to the Rio Grande) than to basins to the south. For example, Keating et al. (2003) estimated southerly flow from the Pajarito Plateau aquifer to the south to be approximately 9 kg/sec. Uncertainty analysis showed a possible range of values + 34 kg/sec or – 62 kg/sec. All of these values are relatively small compared to the total flow to the Rio Grande.

Regarding basin boundaries to the north and west, fluxes entering the region beneath the plateau were estimated by Keating et al. (2003), using basin-scale head and streamflow data and inverse modeling analysis. They estimated that flow into the plateau from the north was very small or zero, with a relatively large degree of certainty. Inflow from the west (Valles caldera) and outflow to the south is more uncertain, and could be as low as zero or as high as 94 or 34 kg/s,

respectively. These fluxes are relatively small compared to estimates of total recharge for the plateau.

These modeling results, when combined with recharge and streamflow estimates, result in a self-consistent mass balance on water moving through the aquifer. Given the uncertainties in the individual flow estimates and the inherent difficulty of defining the appropriate structural features for a large-scale model, it is possible that other conceptualizations would provide equally valid representations of the available information. For example, it is possible that a conceptualization in which more water flows from the Española Basin to the adjoining Albuquerque Basin, rather than discharging at the Rio Grande, would prove valid. Elements of such a model conceptualization are (1) less flow restriction to the south; (2) more restricted flow from the deeper, confined aquifer to the Rio; and (3) southerly flow of a fraction of the deeper aquifer from the Sierra de los Valles and the Sangre de Cristo Mountains to the south. Of course, such a conceptualization would also need to be consistent with the available water budget information. The point here is that alternate conceptualizations such as this cannot be unequivocally ruled out and thus should be considered in future numerical models developed for the plateau and the basin.

### 2.8.4 Aquifer Hydrologic Properties

This subsection briefly summarizes the hydrologic properties of the regional aquifer rocks. A more detailed treatment of this critical topic, including statistical and spatial distributions of hydraulic conductivities measured in aquifer tests, is presented in Section 2.4. The aquifer beneath the plateau consists of the fractured crystalline rocks of the Tschicoma Formation, Cerros del Rio basalts, and older basalt flows, as well as the sedimentary rocks of the Puye Formation and the Santa Fe Group. These units are described in detail in Section 2.1, as well as by Broxton and Vaniman (2005). Both the Santa Fe Group and the Puye Formation are alluvial fan deposits with alternating beds of high and low permeability, with north-south trending faults associated with basin-scale rifting (Kelley, 1978).

Permeability estimates for the Santa Fe Group are primarily derived from pumping tests in water supply wells screened over large intervals; estimates range from $10^{-11}$ to $10^{-12.8}$ $m^2$ (Griggs and Hem, 1964; Purtymun, 1995; Purtymun et al., 1995a; Theis and Conover, 1962). Testing of monitoring wells, with relatively short screens completed within the Puye Formation, has shown very large variability ($10^{-11}$ to $10^{-13.5}$ $m^2$). The basalt flows beneath the plateau include massive, fractured lava units, breccia zones, and inter-flow zones with significant clay content. Permeability within the Cerros del Rio basalts ranges from $10^{-11.2}$ to $10^{-13.8}$ $m^2$ (Nylander et al., 2002). Testing at R-28 shows the upper bound of permeability to be between $10^{-10.5}$ and $10^{-10.2}$ $m^2$ (Kleinfelder, 2004b).

Several estimates of specific storage (Ss) have been derived from various pumping tests: $10^{-4.8}$ /m in the Los Alamos Canyon wellfield (Theis and Conover, 1962); $10^{-5.5}$/m and $10^{-3.8}$/m in the Otowi wellfield (Purtymun et al., 1990; Purtymun et al., 1995b). These relatively low values are indicative of confined or leaky-confined conditions at the depth that these observations were made. This point is expanded upon in the next subsection, along with more recent estimates of specific storage based on a pumping test conducted as part of the Hydrogeologic Workplan.

### 2.8.5 Anisotropy and Scale Dependence

Both the Santa Fe Group and the Puye Formation are, at least locally, strongly anisotropic. Pumping tests have confirmed that permeability normal to bedding is much lower than permeability parallel to bedding, both on the Pajarito Plateau (McLin et al., 2005; Purtymun et al., 1990; Purtymun et al., 1995b; Stoker et al., 1989) and elsewhere in the basin (Hearne, 1980). Estimates of anisotropy (ratio of vertical to horizontal hydraulic conductivity) vary from 0.00005 (Hearne (1980), pumping test analysis) to 0.04 (Hearne (1980), hydraulic gradient analysis), to 0.01 (McAda and Wasiolek, 1998).

Effective permeability and anisotropy at large spatial scales are difficult to estimate. Many authors have noted the lack of spatial continuity of low or high permeability beds with the Santa Fe Group (Hearne, 1980; Spiegel and Baldwin, 1963; Theis and Conover, 1962) and the difficulty of correlating geophysical or lithologic logs between even closely spaced wells (Cushman, 1965; Shomaker, 1974). Hearne (1980) notes that because of limited spatial continuity in low or high permeability rocks, under a regional pressure gradient vertical flow will occur through circuitous routes and thus effective anisotropy may be less pronounced at large spatial scales than that measured at small scales during pumping tests.

Large-scale, multiple-observation-well aquifer pumping tests are invaluable to examine scale effects and to estimate the impacts of water supply well pumping on pressure gradients in the aquifer. As part of the characterization program, a 25-day aquifer test was conducted at municipal water supply well PM-2 from February 3–28, 2003 (McLin, 2005). The pumping phase was conducted at a constant discharge rate of 1,249 gpm, followed immediately by a 25-day recovery period. Surrounding observation wells were used to record both drawdown and recovery in response to pumping at PM-2. The PM-2 well draws water from a continuous louvered screen between 1,004 and 2,280 ft below ground surface (bgs). Prior to the start of the test, production wells in the vicinity were completely shut down so that hydrostatic conditions in the regional aquifer could recover and a static baseline could be established. Except for the test pumping at PM-2, all of the surrounding water supply wells remained off throughout the test period. Continuous water-level responses to pumping at PM-2 were recorded by transducers that were placed in municipal wells PM-2, PM-4, and PM-5 and in characterization wells R-20 (three separate screens) and R-32 (three separate screens). Periodic responses to pumping were also recorded in characterization wells R-15 (one screen), R-21 (one screen), and R-22 (five separate screens); however, no significant drawdown values were recorded in these latter wells.

Figure 2-42 (from McLin, 2005) shows a layout of PM-2 and nearby monitoring locations during the test. Individual drawdown and recovery water levels in responsive wells demonstrate that the regional aquifer surrounding PM-2 is vertically anisotropic with pronounced resistance to vertical propagation of drawdown at shallower depths. Hydraulically, the aquifer behaves like a semiconfined aquifer at depth with leaky units located above (and perhaps below) a highly conductive layer that averages about 850 ft in thickness. Drawdown in this highly permeable unit was recorded more than 8,800 ft away in well PM-5, while drawdown only 1,225 ft away at the R-20 multiple-screened well was directly related to individual screen depth (Figure 2-43a, from McLin, 2005); the shallowest screen at R-20 showed little drawdown, while the deepest screen

showed a dramatic response to pumping at PM-2. Similar but more subdued behavior was also recorded 4,457 feet away in the R-32 multiple screened well (Figure 2-43b). In contrast, no recordable drawdown was recorded 8,900 feet away in the R-22 multiple screened well, suggesting that an idealized radius of influence for pressure responses due to pumping at PM-2 was at least 8,800 feet after 25 days of continuous pumping. The idealized radius of influence shown in Figure 2-42 is schematic, based on the available data and is not meant to imply that the pressure response spreads uniformly in all directions.

A schematic diagram proposed by McLin (2005) to interpret the aquifer-pumping test and to estimate hydrologic parameters is reproduced in Figure 2-44. Clearly, this aquifer configuration is highly idealized, in that a single, well-defined semi-confining layer has not been identified, and layered heterogeneities certainly exist within the zone depicted as the deeper aquifer (for example, see the geologic cross section of Figure 3 in McLin, 2005). Nevertheless, using this idealized aquifer configuration, McLin (2005) estimated hydraulic conductivity at the scale of this test to be about 5.0 ft/day (based on an assumed aquifer thickness of 850 ft), with a storage coefficient ranging from about 0.00032 to 0.002. Finally, the observations of muted drawdown at observation points near the water table (significantly above the pumping elevation) suggest that the horizontal-to-vertical anisotropy ratio of hydraulic conductivities is highly variable: McLin (2005) suggests that the ratio of vertical to horizontal hydraulic conductivity may be on the order of 0.01 in some locations within the regional aquifer.

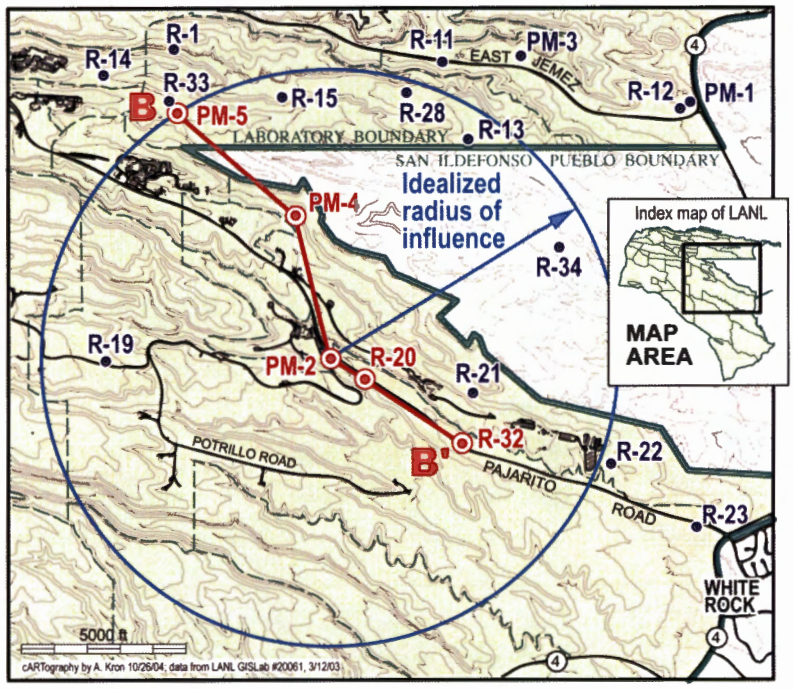


**Figure 2-42.** Idealized radius of influence of PM-2 on surrounding wells (McLin, 2005).

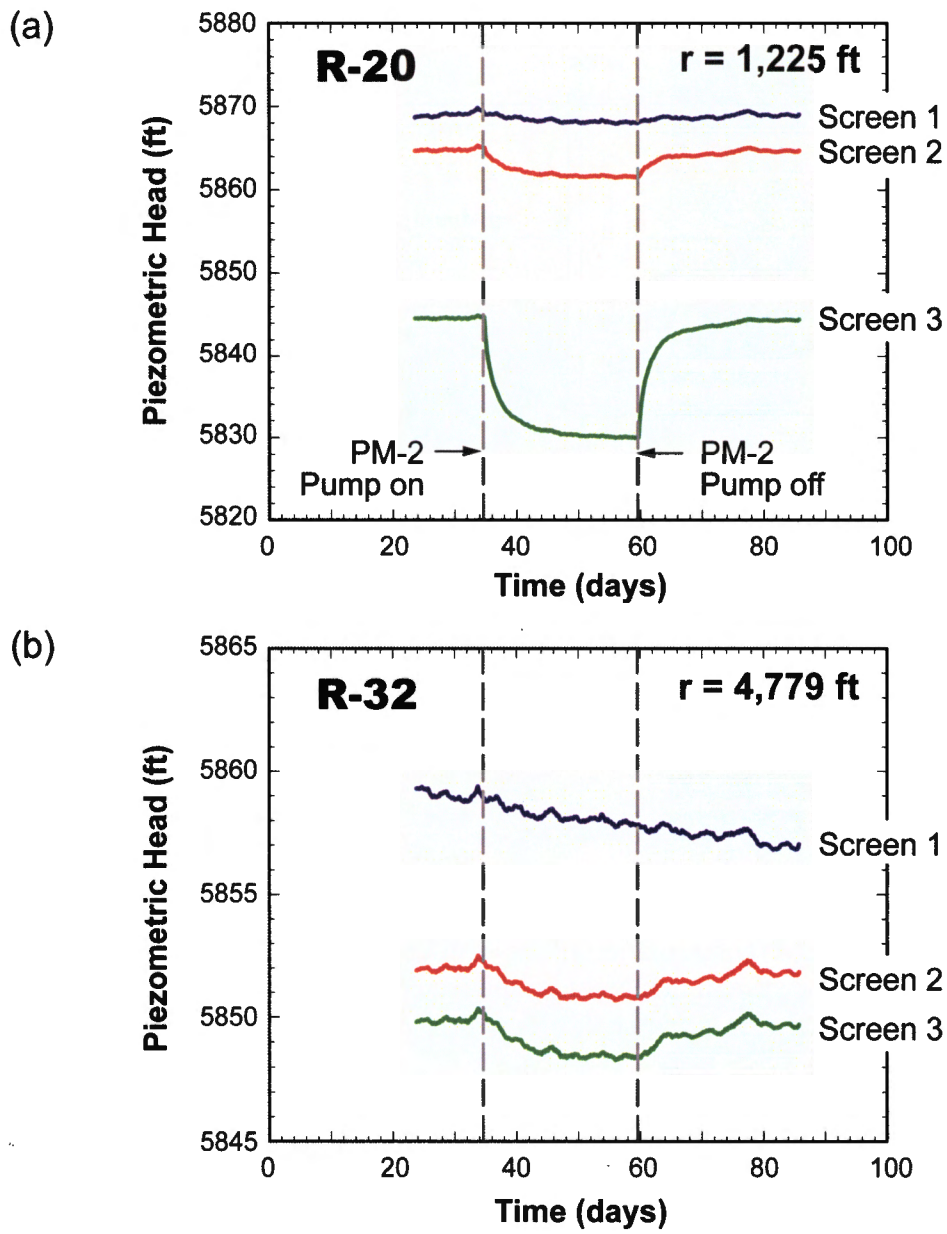


**Figure 2-43.** Drawdown at wells R-20 (a) and R-32 (b) in response to pumping at PM-2 (McLin, 2005).

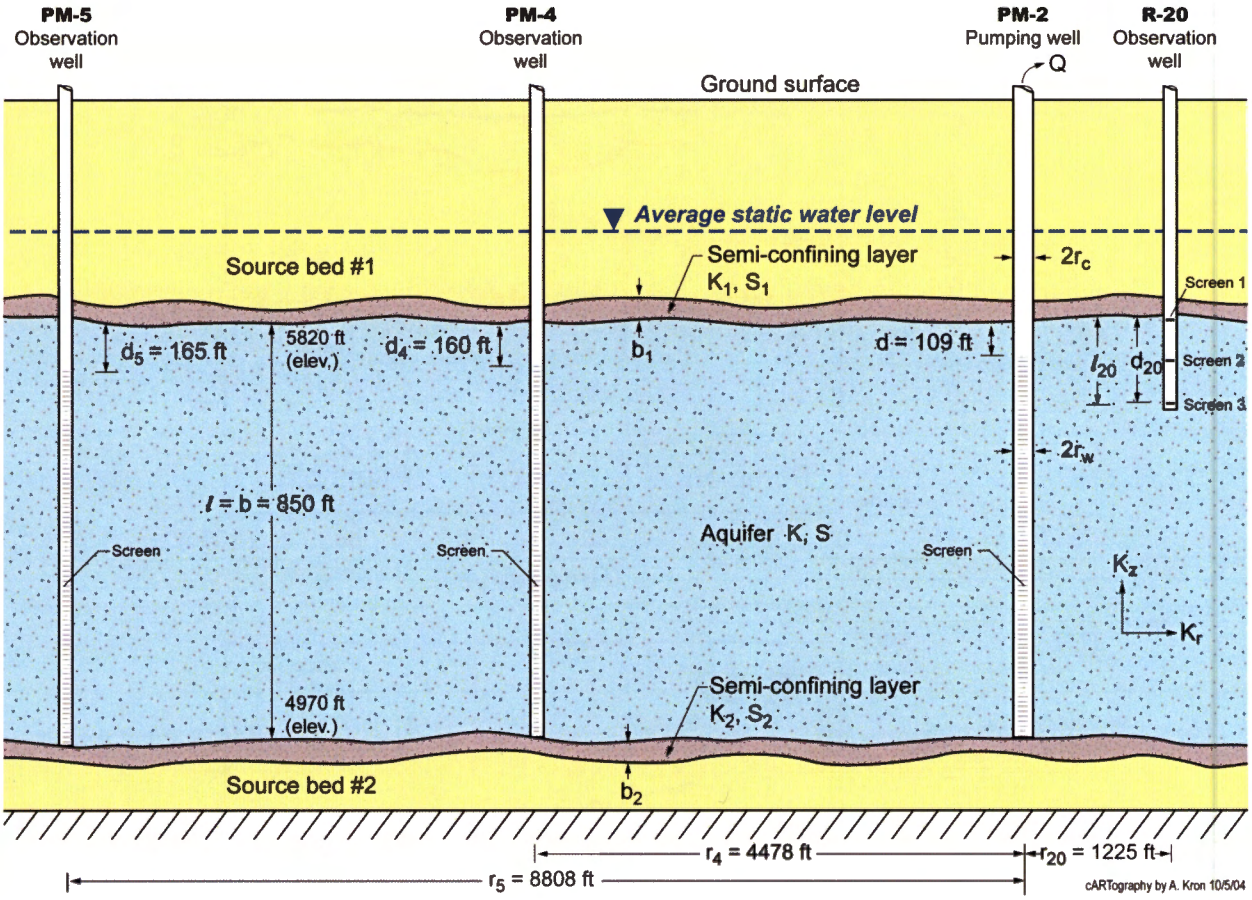


**Figure 2-44.** Idealized representation of the aquifer near PM-2 during the pumping test. A shallow system that includes the water table is separated from a deeper system by a semiconfining layer of low permeability (McLin, 2005).

The analysis of McLin (2005) suggested an aquifer that behaves as a confined system at early stages in the test, transitioning to a behavior characteristic of leaky-confined aquifer behavior when the long-term drawdown behavior is interpreted. Although the behavior of the pumping test has the signature of a leaky-confined aquifer, with a temporal stabilization of drawdown relative to a confined aquifer, other aquifer flow mechanisms can give rise to similar behavior. For example, either leakage from low-permeability aquitards within a confined aquifer or interception of the cone of depression with a recharge boundary is an alternative explanation. The pumping test illustrated the importance of conducting tests of long enough duration to discern the large-scale behavior of the aquifer at progressively larger scales. Additional tests at other municipal water supply wells are planned to probe the hydrodynamic conditions of the aquifer at different locations. By combining the results of several such tests, we should be able to sort out the various flow mechanisms, thereby uncovering a more detailed picture of flow paths and mechanisms in the aquifer.

### 2.8.6 Hydraulic Heads and Flow Directions

The principal reason for studying the regional aquifer in the Hydrogeologic Workplan activities is to determine the direction and rate of movement of water and contaminants. Historically, easterly/southeasterly flow directions in the regional aquifer have been proposed, based on data available to Purtymun and Johansen (1974) and Rogers et al. (1996b). Data collected as part of the Hydrogeologic Workplan confirm this result with a much larger number of wells than were available to earlier studies, particularly wells completed with short screens near the water table.

#### 2.8.6.1 Water Level Map

The potentiometric surface for the regional aquifer is shown in Figure 2-24 (from LANL, 2005). Data used to construct this map are given in Table 2-10 for wells under water table conditions. In addition, data from wells under leaky-confined conditions in lower Los Alamos Canyon were included to augment the spatial coverage of the data because observations at the water table are not available at that location. The analysis of the data used to construct this and other maps of water levels and trends with time is discussed in detail in LANL (2005). The lateral component of gradients along the top of the aquifer beneath the plateau varies over one order of magnitude, from a low of 0.0026 (TW-3 to R-5) to a high of 0.04 (CDV-R-37 to CDV-R-15). Even higher gradients are evident west of R-25 (0.162; R-26 to R-25).

A simple conceptual model for these trends is that gradients are high to the west where significant recharge is occurring and gradients are low in the central plateau where lower recharge rates are occurring and higher permeability rocks are present (Purtymun, 1995). The general easterly-southeasterly flow direction suggested by these gradients is consistent with radiocarbon ages of water from deep wells beneath the Pajarito Plateau, which increase from west to east. Age estimates for groundwaters beneath the plateau range between about one to six thousand years, increasing to several tens of thousands of years near the Rio Grande (Rogers et al., 1996b). However, as will be discussed below, interpretation of these data is complicated by the fact that the flow patterns within the aquifer are complex, and mixing of fluids of different ages is likely. The presence of anthropogenic tritium in the regional aquifer demonstrates that mixed waters of vastly different ages are present in the aquifer.

#### 2.8.6.2 Shallow and Deep Flow Paths

The nature of the measured head gradients suggests that flow in the shallow portion of the aquifer (less than 150 m) below the upper surface of the saturated zone is primarily easterly-southeasterly. The tendency for aquifer rocks to be strongly anisotropic will cause water to move in large part horizontally, despite the strong driving force of vertical head gradients. As described in the previous subsection, the degree to which the uppermost phreatic zone and the deeper, leaky-confined aquifer are hydrologically connected is not known with certainty. Nevertheless, hydrologic testing indicates that there is considerable resistance to vertical flow relative to horizontal flow; this phenomenon is likely to be widespread throughout the aquifer, but the magnitude of the anisotropy ratio at small scales probably varies considerably across the plateau. One interesting observation is that the amount of recharge estimated by Kwicklis et al. (2005) to occur in canyon bottoms on the plateau (77 kg/sec) is close to the total discharge from the springs of 85 kg/sec estimated by Purtymun (1966). This observation is consistent with a

compartmentalized aquifer with plateau recharge traveling laterally in the phreatic zone, partially isolated from deeper groundwater flow.

In general, the direction of flow in deeper portions of the aquifer (at depths greater than the deepest water supply wells) is unknown because of sparse data, and is likely to be different under pumping conditions than under pre-development conditions. Purtymun (1995) suggested that heads at deeper intervals of the aquifer also have a westerly gradient. It is conceivable that the predominant flow direction under natural gradient conditions could be different from what is found at shallower depths, but data to constrain the direction are insufficient. The conceptual model for the nature of flow discharging to the Rio Grande or flowing to the Albuquerque Basin to the south will likely influence the predicted flow direction deeper in the aquifer. A model with significant flow to the Albuquerque Basin (described in Section 2.8.3.3 as an alternate conceptual model) would lead to more southerly flow paths in the deep aquifer.

#### 2.8.6.3 Influence of Water Supply Well Pumping

Despite evidence for compartmentalized flow with significant flow resistance between the shallower and deeper zones, it is likely that some downward movement of water and contaminants does occur due to pumping of water supply wells at depth. Occurrences of tritium and perchlorate in well O-1 show that flow paths between the shallow and deep aquifer water can exist during production. However, the extent of vertical transport is undoubtedly a function of the local permeability structure between the water table and the pumping interval in the water supply well, which may vary spatially across the plateau. Finally, pumping-induced upward movement of deeper water has been observed in the Los Alamos Canyon wellfield (Gallaher et al., 2004; Purtymun, 1977).

Although our understanding of the impact of water production on aquifer storage and discharge to the Rio Grande is incomplete, there is a clear trend of decreasing water levels over the time period of production from major wellfields on the plateau. Pumping rates increased from near zero in 1945 to 183 kg/sec in 1971 and have been relatively stable since then (171 kg/sec in 2001) (Koch et al., 2004); although year-to-year variability in pumping rates at individual wells has been large. Figure 2-45 (from LANL, 2005) shows the rate of water level decline in ft/yr estimated from long-term monitoring of water levels in wells on the plateau. Details of this map, constructed using a combination of test wells with a long (greater than 10 year) record and more recent characterization wells, are described in LANL (2005). The main features of the map are an area of high water-level decline rate (over 1 ft/yr) along Pueblo Canyon, which lies at the northern edge of data coverage, and an elongated zone of high decline rate (up to 0.8 ft/yr) that runs north to south, just east of and including PM-5, PM-4, and PM-2. This zone then extends east along Pajarito Canyon to R-23.

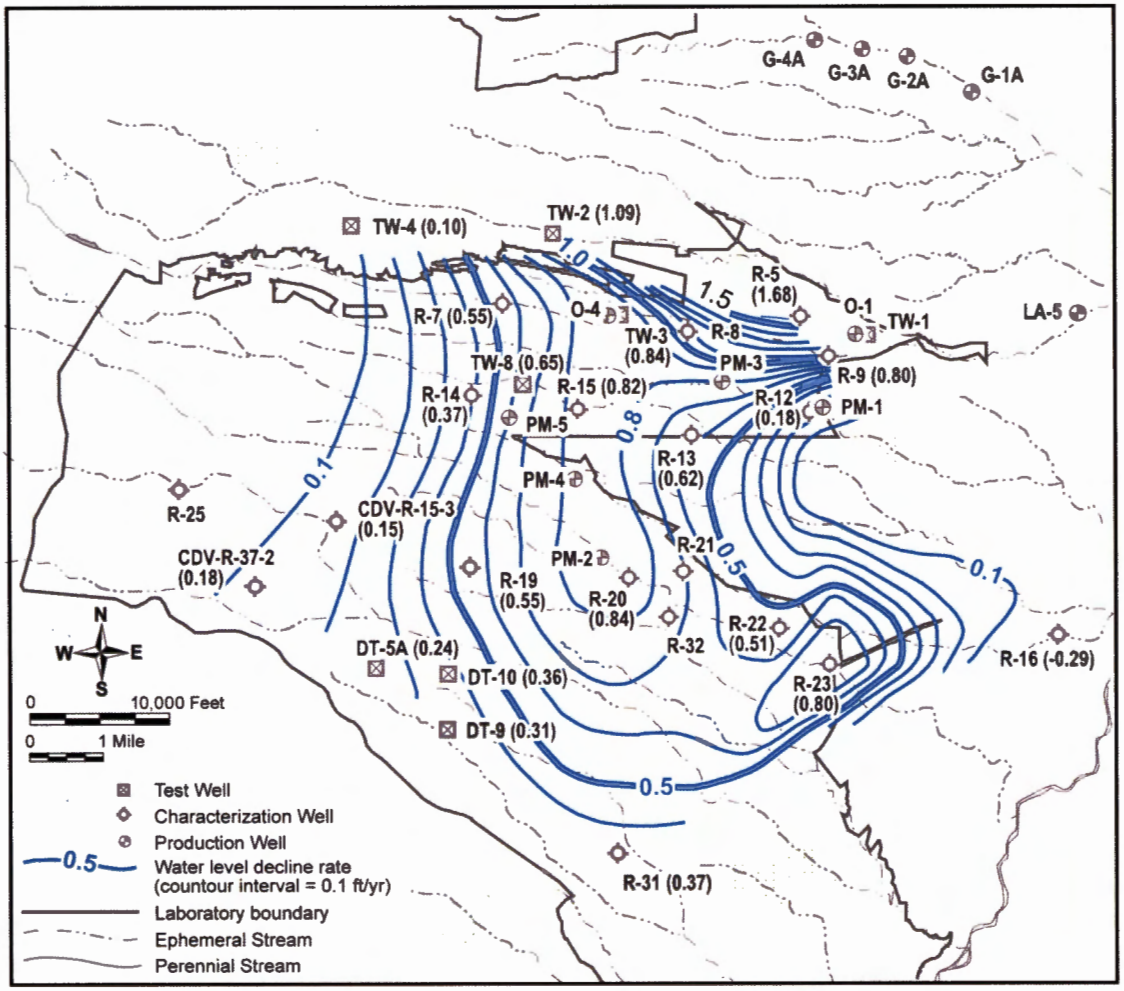


**Figure 2-45.** Annual water level decline due to municipal water supply well pumping (from LANL, 2005).

In the Los Alamos Canyon wellfield, after substantial water level declines when pumping initiated in the late 1940s, water levels rose and fell in response to inter-annual pumping variability. When the wells were retired in the late 1980s to early 1990s, water levels rapidly increased. Similarly, water levels in the Guaje wellfield decreased initially in response to pumping in the early 1950s and then stabilized until the 1970s; this was interpreted by Koch et al. (2004) to suggest that the aquifer had reached equilibrium. Water levels began to decline gradually again in the 1990s, perhaps due to pumping in nearby wellfields. Pumping in the Pajarito Mesa (PM) wellfield has produced less water level decline than pumping in the Guaje or Los Alamos Canyon wellfields, despite heavy usage. Nevertheless, water levels in PM-1 and PM-3, which have been pumped more consistently than other PM wells, have shown a long, steady decline. Test wells, which are much shallower than water supply wells, have also shown long, steady, declining water levels; before 1970 declines were very small (~1 m); since 1970 declines have increased to a total of ~5 m.

The impact of production on storage in the aquifer was estimated by Rogers et al. (1996b). They calculated storage depletion by estimating the volume of the combined cones of depression observed in all the wellfields on the plateau, assuming drainage under water table conditions, and by assuming uniform aquifer properties (porosity = 0.1). They concluded that the total storage loss has been approximately equal to total production in the time period 1949 – 1993, and thus perhaps that there has been no significant net recharge to the wellfields during this period. In contrast, McLin et al. (1996) suggested that significant recharge has occurred, since water levels have recovered in wells that were allowed to rest a period of several months or several years. Flow modeling is one approach to estimate the proportion of storage loss that has been replaced by recharge. Simulations suggest that flow beneath the Rio Grande (west to east) has been induced by production at the Buckman wellfield. Calculations show that this flux may have increased from zero (pre-1980) to approximately 45 kg/s at present, or ~20% of the total annual production at Buckman (Keating et al. 2003).

### 2.8.7 Aquifer Hydrodynamics

The hydrodynamics in various portions of the aquifer beneath the plateau is critical to determining the potential pathways of contaminant transport. There have been numerous theories proposed in the literature on the degree and extent of confined conditions of the plateau. This is not too surprising considering the extremely complex geologic structure of the plateau and the inherent limitations of short-term pumping tests. Based on limited data, Cushman (1965) concluded that the aquifer is under water-table conditions beneath the plateau, with the exception of the vicinity of the Rio Grande, where water-table conditions exist in shallow layers and confined conditions exist at depth. Purtymun (1974) suggested that water-table conditions exist on the western margin of the plateau and artesian conditions exist along the eastern edge and along the Rio Grande.

Drilling associated with the characterization program has confirmed existence of water-table conditions at many locations beneath the plateau. Table 2-10 shows the water levels in wells (or, for wells with multiple screens, in the uppermost screen below the water table) used to construct the water table map discussed in Section 2.8.6. Clearly, the characterization program has revealed the presence of unconfined conditions locally over most regions of the plateau, with the exception of locations near the Rio Grande, where confined conditions are generally observed.

**Table 2-10.**
**Water-Level Data Used to Create the Revised Piezometric Water-Level Contours for the Top of the Regional Aquifer**

| Well Name-Screen Zone | Water Elevation (ft) | Data Vintage | | Well Name-Screen Zone | Water Elevation (ft) | Data Vintage |
|---|---|---|---|---|---|---|
| CDV-R15-3-4 | 6020.1 | 2004 | | R-14-1 | 5883.7 | 2005 |
| CDV-R-37-2-2 | 6138.8 | 2004 | | R-15 | 5851.7 | 2005 |
| DT-10 | 5919.8 | 2003 | | R-16-2 | 5642.9 | 2004 |
| DT-5A | 5958.8 | 2003 | | R-18 | 6118.0 | 2004 |
| DT-9 | 5917.9 | 2002 | | R-19-3 | 5888.0 | 2005 |
| G-1A | 5705.0 | 2001 | | R-20-1 | 5865.9 | 2003 |
| G-2A | 5750.7 | 2001 | | R-21 | 5853.4 | 2004 |
| G-3A | 5704.5 | 2001 | | R-22-1 | 5762.9 | 2004 |
| G-4A | 5784.0 | 2001 | | R-23 | 5696.6 | 2004 |
| G-5A | 5848.4 | 2001 | | R-25-5 | 6232.3 | 2004 |
| H-19 | 6228.0 | 1949 | | R-26-1 | 7034.8 | 2003 |
| LA-4 | 5706.0 | 1987 | | R-28 | 5839.4 | 2005 |
| LA-5 | 5673.0 | 1987 | | R-31-3 | 5827.9 | 2002 |
| LA-6 | 5678.0 | 1995 | | R-32-1 | 5857.8 | 2005 |
| R-1 | 5879.9 | 2005 | | R-33 | 5877.0 | 2004 |
| R-2 | 5874.0 | 2004 | | R-34 | 5834.0 | 2004 |
| R-5-3 | 5769.2 | 2004 | | TW-1 | 5840.2 | 2003 |
| R-7-3 | 5879.6 | 2004 | | TW-2 | 5847.7 | 2000 |
| R-8 | 5836.0 | 2004 | | TW-3 | 5812.5 | 1999 |
| R-9 | 5691.0 | 2004 | | TW-4 | 6071.5 | 2003 |
| R-12-3 | 5695.9 | 2004 | | TW-8 | 5875.5 | 2003 |
| R-13 | 5837.4 | 2005 | | | | |

Source: LANL (2005) and references therein

Significant new information on the relationship of the shallow and deeper regional aquifer hydrodynamics has also been obtained. Potentiometric measurements at several new multiple-screened wells have revealed that decreasing head with depth is a pervasive feature of the aquifer. Head data (in meters) along a vertical cross-section in the southern portion of the plateau, where there are several wells with multiple completions, are presented in Figure 2-46. Decreasing head with depth has been observed in wells in the western portion of the Laboratory (see Figure 2-47 for well CdV-R-15-3) away from pumping well influence, but in a region where increased recharge is expected; near the Rio Grande (see Figure 2-48 for well R-16); in the central portion of the Laboratory (R-19, Figure 2-49); and in locations expected to be more strongly influenced by water supply well pumping (R-20, Figure 2-50). One counter example, well R-31 (Figure 2-51) located in the southern portion of the Laboratory away from municipal water supply wells and the region of expected high recharge, shows a very small (note the expanded scale of the y-axis compared to the other plots) decrease in head with screen depth between screens 2 and 3, but head increases with depth in the lower two screens 4 and 5.

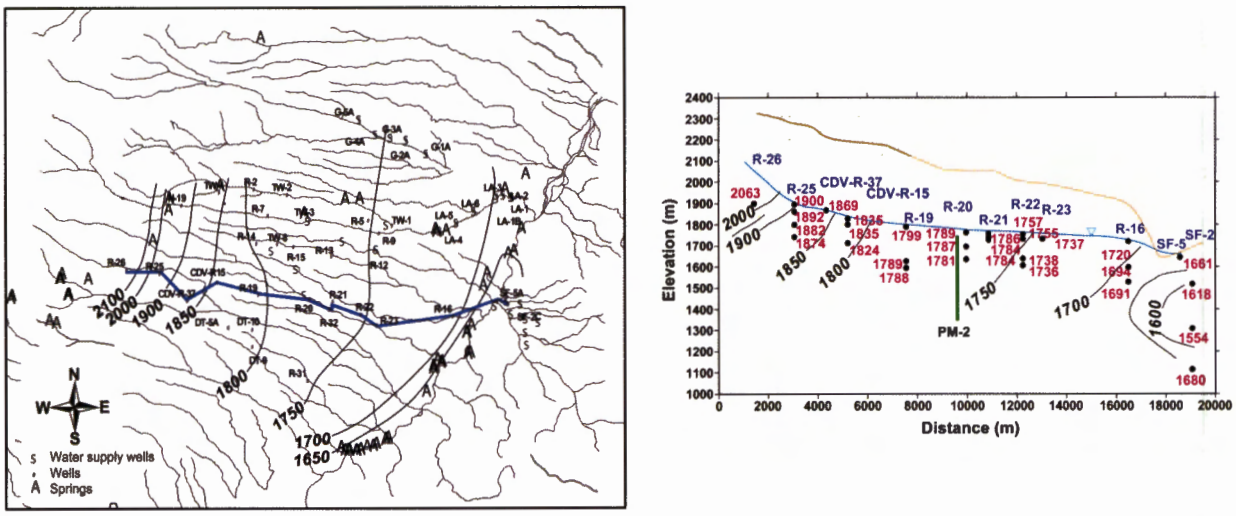


(a) (b)

**Figure 2-46.** (a) Map view showing the location of a cross-section of the plateau. (b) Head data from a vertical cross-section across the southern portion.

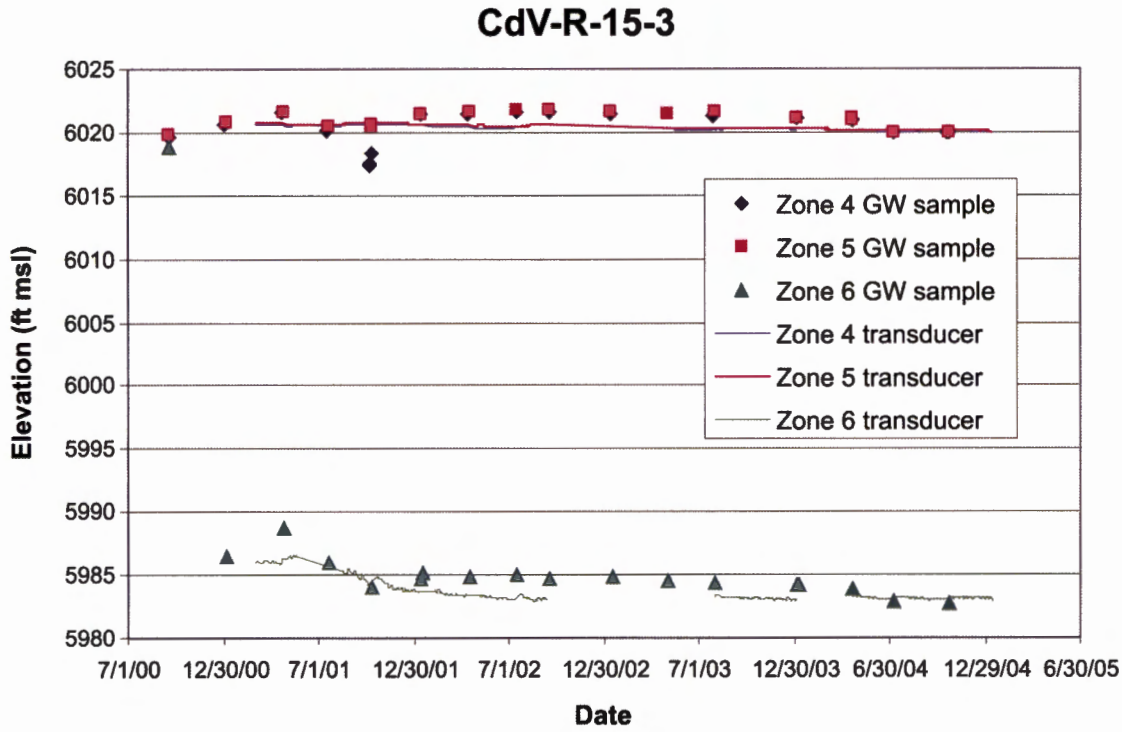


**Figure 2-47.** Piezometric water levels in different screens in well CdV-R-15-3.

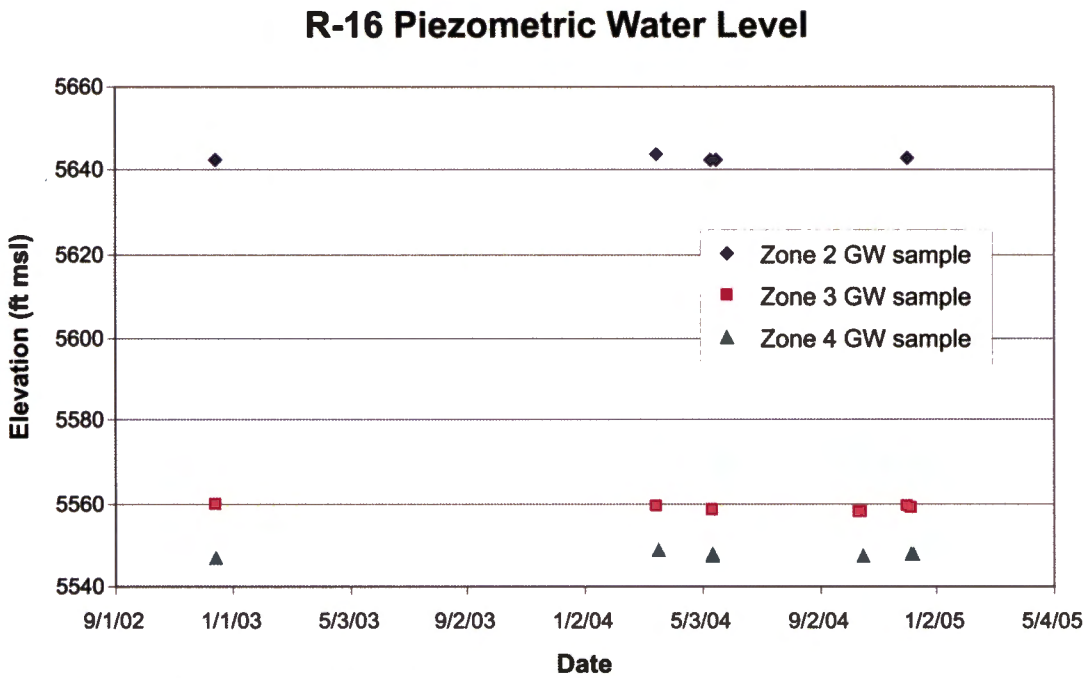


**Figure 2-48.** Piezometric water levels in different screens in well R-16.

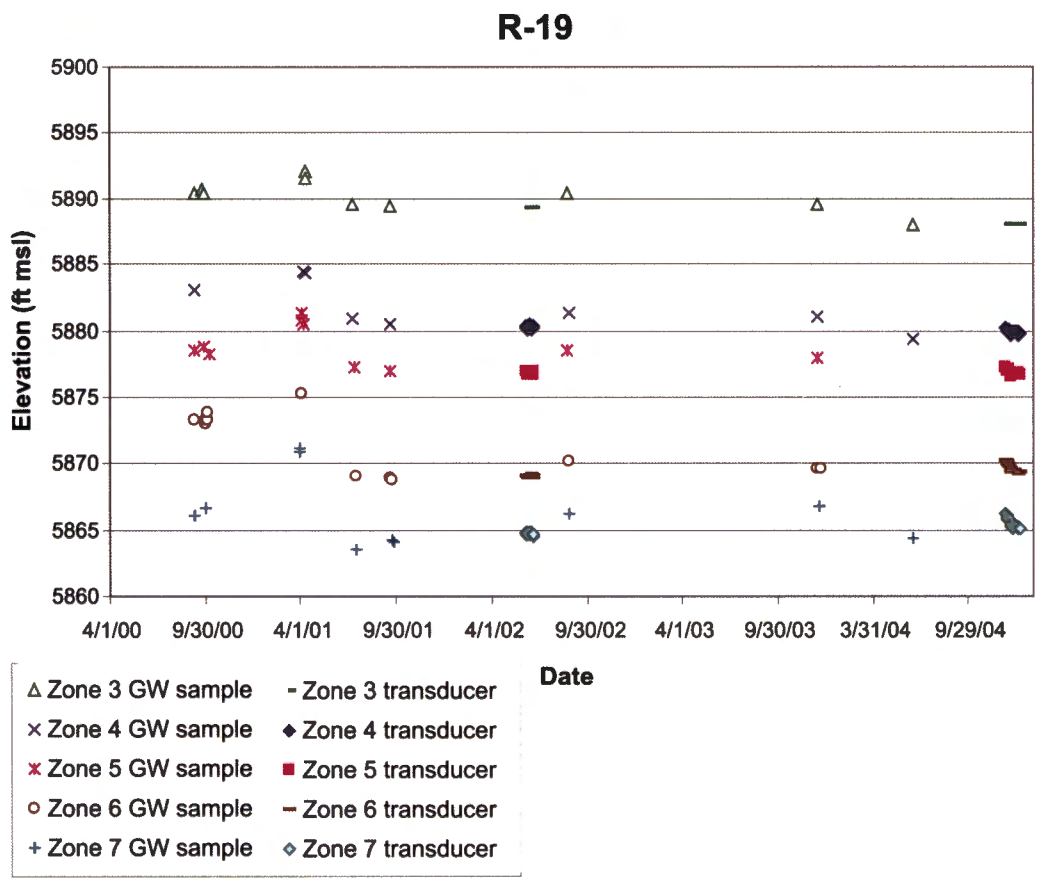


**Figure 2-49.** Piezometric water levels in different screens in well R-19.

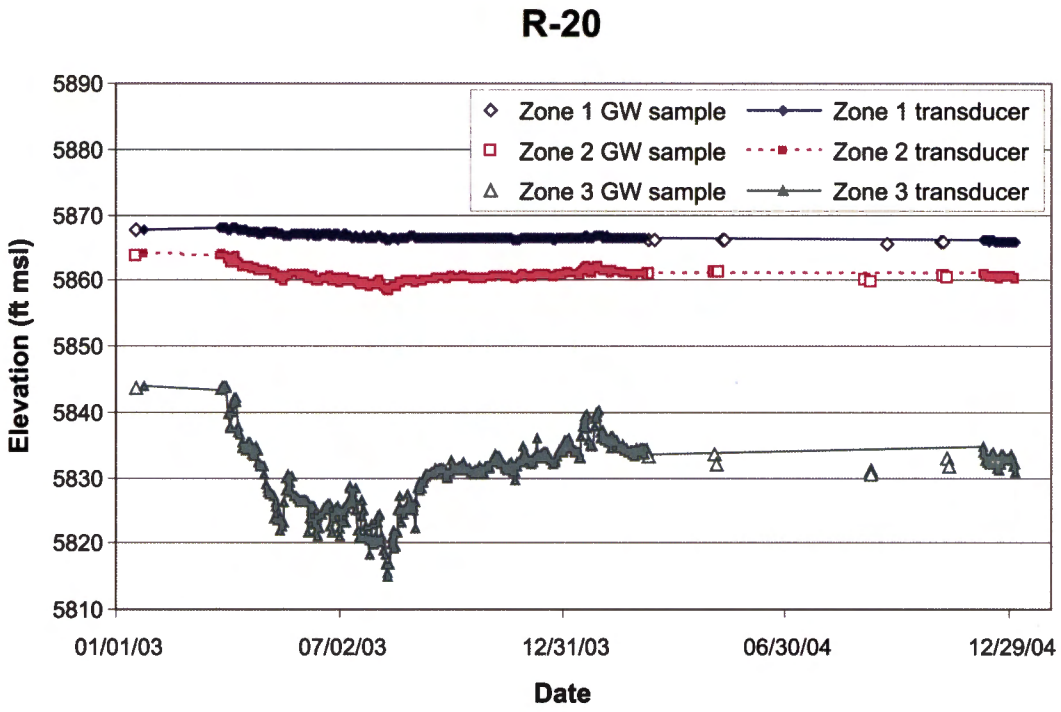


**Figure 2-50.** Piezometric water levels in different screens in well R-20.

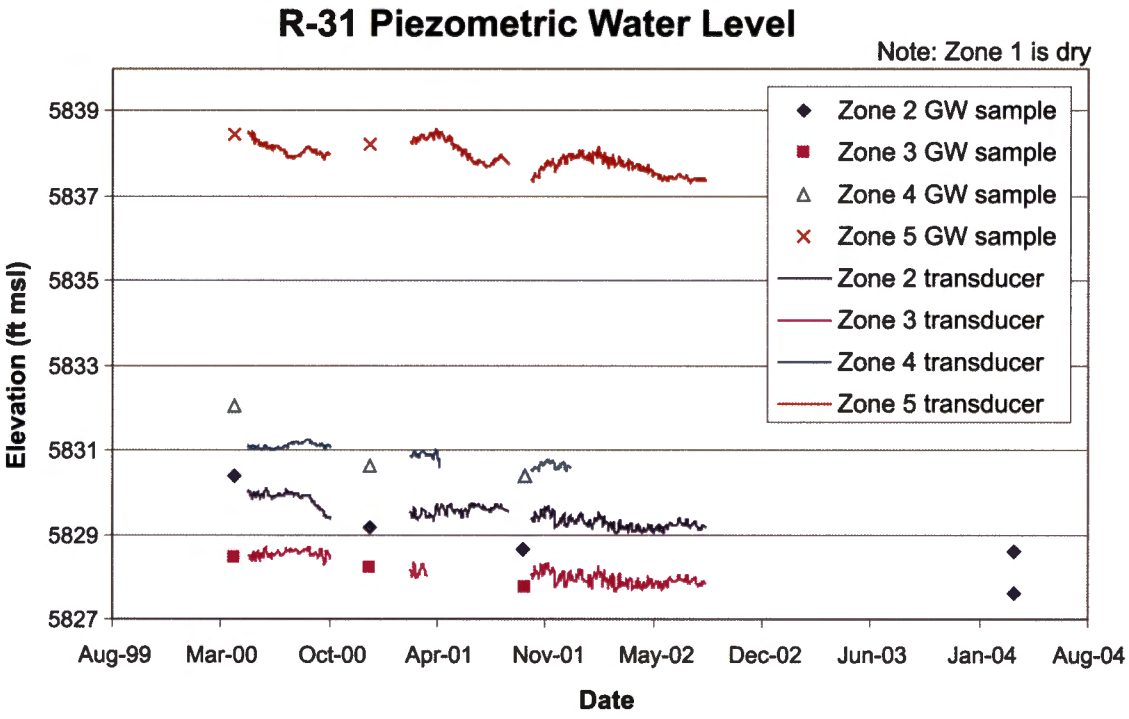


**Figure 2-51.** Piezometric water levels in different screens in well R-31.

There are several hydrologic mechanisms that can give rise to the observed data. First, note that in a region with a sloping water table, with recharge at high elevation and discharge at lower elevations, the theoretical result for a uniform medium is lower heads with depth, except close to the discharge zone. This explanation alone is consistent with the uppermost screens of R-31. At greater depths in R-31, the higher heads are perhaps due to a zone that is hydrologically separated from the upper zone, with higher head due to recharge to the west and deep, confined flow beneath the plateau. The reasons for the larger downward head drops in well CdV-R-15-3 (as well as other wells in the vicinity, such as R-25) are uncertain, but are probably due to a combination of high local and mountain front recharge, combined with an extremely complex hydrostratigraphic and structural condition in which poorly connected, compartmentalized flow zones are encountered with depth. The wells in the vicinity of water supply wells on the plateau are clearly influenced by water extraction. It is possible that relatively small head differences with depth before water withdrawal have grown substantially because of pumping. Although data on shallow and deep head declines due to long-term pumping are sparse, it is likely that drawdown at the elevation of pumping is highest, and a more muted drawdown exists at the water table. Finally, for R-16, the lower head with depth is probably caused by pumping at the Buckman wellfield.

The critical element that appears to be necessary to explain the observations from both pumping tests and information from multiple-screened wells is the presence of different hydrodynamic conditions at depth than are present at the top of the regional aquifer. The observations (unconfined conditions and a muted response to pumping at depth) suggest a phreatic zone under water-table conditions that is weakly connected hydrologically to a deeper zone that behaves as a leaky-confined aquifer.

The nature of the aquifer heterogeneities giving rise to this compartmentalized system remains an open question. Two conceptual models appear to be possible. One is that the strongly anisotropic characteristic of the aquifer, which limits vertical movement of groundwater at virtually all depths within the Puye Formation and Santa Fe Group, produces the observed trends with depth. Cushman (1965) noted that this aquifer characteristic can cause an unconfined aquifer to appear confined in a short-term pumping test. This explanation is consistent with the observation of McLin (2005) described in Section 2.8.5 of a hydrograph that transitions from confined to leaky-confined behavior at later times. This conceptual model is implemented in the numerical models of McAda and Wasiolek (1988) and Hearne (1980). The McAda and Wasiolek (1988) model places the majority of water supply wells in the basin within the upper 600-ft-thick unconfined layer of the model.

Another conceptual model is that a laterally extensive low permeability zone exists within the aquifer separating the shallow phreatic zone from a deeper confined aquifer. This is the conceptualization depicted in Figure 2-44. A single, laterally extensive zone of low permeability has not yet been identified in boreholes on the plateau. This fact, combined with observations indicating vertical resistance at all elevations in basalts, the Puye Formation, and the Santa Fe Group, strongly favor the former conceptual model. Either model would be expected to give rise to lateral transport of contaminants reaching the water table, especially at locations relatively unaffected by municipal water well pumping. The anisotropic model would allow for vertical

contaminant pathways to water supply wells in locations where continuous high-permeability pathways are present.

### 2.8.8 Velocities and Travel Times

Transport velocities and travel times through the regional aquifer are poorly understood, because of the lack of tracer tests and in-situ measurements of effective porosity. Data concerning the spatial distribution of anthropogenic contaminants in the regional aquifer have been difficult to use to constrain regional aquifer travel times because of the exceptionally thick and complex vadose zone, which makes it impossible to define the location and timing of contaminant entry to the regional aquifer. Transport over significant distances in the alluvial aquifers is known to occur, and complex vadose zone lateral pathways are also possible, though they have not been directly observed, except for the shallow subsurface pathways identified in the mountain front portion of the plateau (See Section 2.6.2.1). Despite these limitations, we note that no evidence of larger-scale migration of contaminant plumes has been observed, although the presence of anthropogenic chemicals at low levels in springs discharging to the Rio Grande at White Rock Canyon has been suggested by some to be due to regional aquifer transport (Section 3.2). Lack of evidence of migrating plumes may indicate that they travel too slowly to be observed over the relatively short period of study, or that sampling locations are not present in the right locations in sufficient density to track a migrating plume.

In principle, isotopic data can constrain possible transport velocities. These data clearly demonstrate that some waters beneath the plateau and discharging to the Rio Grande are thousands of years old, similar to ages of groundwaters measured in the Albuquerque Basin to the south (Plummer et al., 2004). Tritium data, described in Section 2.8.3, clearly demonstrate that young waters are present as well. These young and old waters may co-mingle at numerous locations within the aquifer including the discharge zone at the Rio Grande.

Therefore, there is no single answer to the question: How old is the groundwater? Mixing between older and younger waters is the norm for the waters sampled from the regional aquifer. Figure 2-52 illustrates that in many instances, both younger and older components are present. Tritium measurements at wells tapping the top of the regional aquifer near Los Alamos Canyon and Mortandad Canyon (among others), as well as isolated observations that include some of the springs discharging at White Rock Canyon, indicate a component of the water is young (less than 60 years old). Reconciling these observations with age estimates of several thousand years based on C-14 requires a model in which fluids of vastly different ages mix, yielding disparate age estimates from the different groundwater tracers.

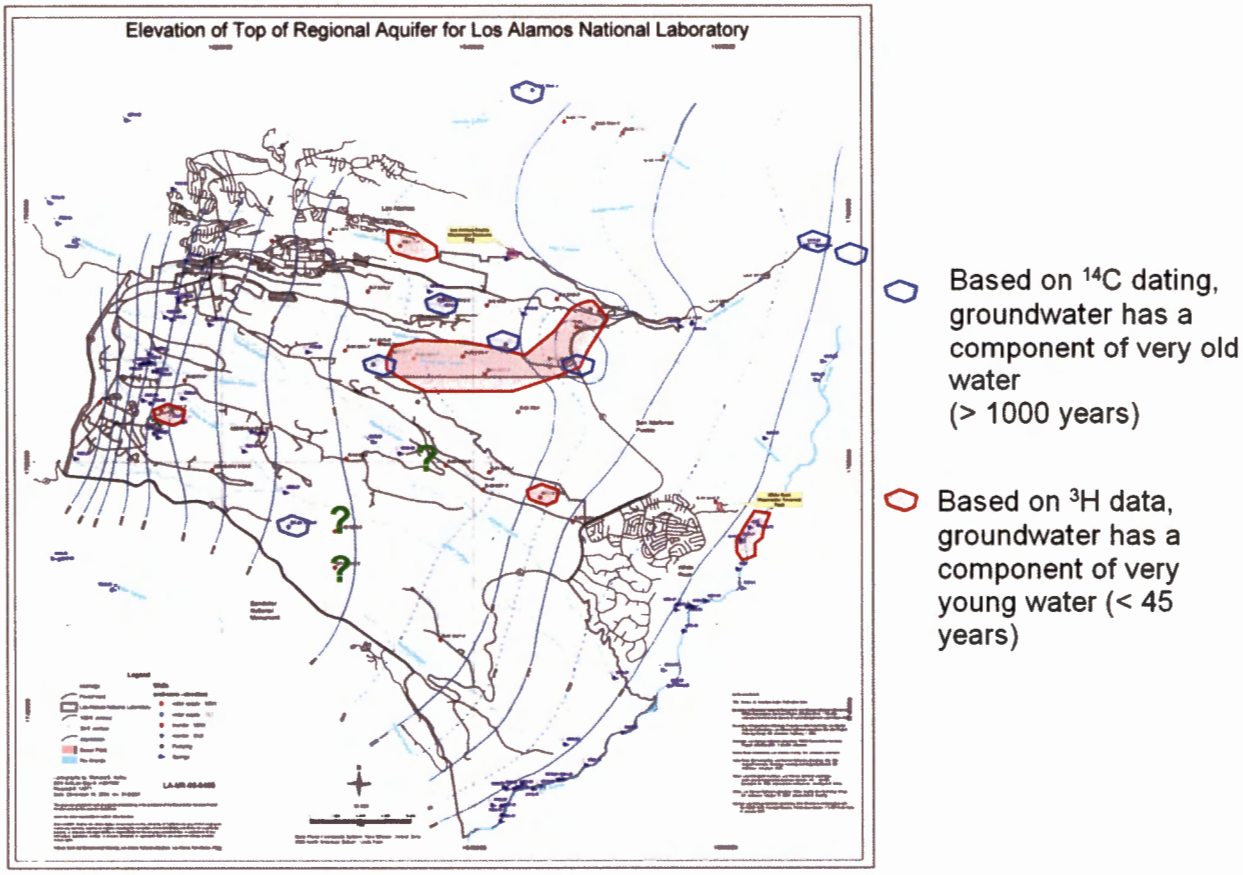


**Figure 2-52.** Diagram of the locations of "young" and "old" water at different locations. The figure shows that waters with different apparent ages, based on different geochemical indicators, can co-exist at the same location.

The model prediction of transport velocity and ultimate point of discharge of a contaminant in the regional aquifer is intimately tied to, even controlled by, the conceptual model used to develop the numerical model. If the picture emerging from the data described above of a compartmentalized aquifer is valid, then contaminants would travel laterally in the phreatic zone and arrive at springs discharging at the Rio Grande. These flow paths would be predominantly within the Puye Formation and the Cerros del Rio basalts, the geologic units commonly present at the water table of the regional aquifer (Figure 2-10). Travel times through these rocks might be expected to be relatively short. For example, taking the hydraulic conductivity of 1 m/d, a gradient of 0.02, and a porosity of 0.1, the computed velocity of a contaminant moving with the water (with no adsorption to the rock) is about 70 m/yr. Travel times on the order of 100 years would therefore be predicted to the springs from the most easterly zones of contaminated waters in the alluvial aquifers on LANL property.

The role of supply-well pumping in altering these directions and points of discharge is a function of the conceptual model and the water usage scenario chosen for examination. Section 4.2.12. presents a capture zone analysis suggesting that contaminants reaching the regional aquifer beneath canyons on the plateau will be largely captured by the PM wells. Anisotropic conditions in the regional aquifer that tend to keep transport pathways shallow are overcome by induced

downward gradients, and contaminants are drawn to the depths of the screens of the water supply wells, where they are captured. Implicit in these results is the conceptualization of discrete pathways leading to downward transport, perhaps through tortuous "windows" of high-permeability rock in between discontinuous low-permeability layers. A more continuous low-permeability zone between the contaminant residing at the water table and the water supply well would create two disconnected zones at the scale of a contaminant plume. Under this scenario, contaminants would be isolated to the phreatic zone and travel to a down-gradient supply well or the Rio Grande, despite pumping near the contaminant source.

Another important consideration is that steady-state capture-zone results require the assumption of constant pumping for a long enough time for a water particle to arrive at the well. This water usage scenario maximizes the induced downward gradient, exaggerating the downward gradients and leading to flow paths in which capture by the water supply wells is favored over lateral transport at shallow depths. If transport velocities are low enough, water supply wells are likely to be taken out of service before this theoretical arrival at the well would occur. In this case, the actual transport problem is inherently transient, and predictions are intimately tied to the actual water withdrawal scenario. In summary, these complexities render the predictions model- and scenario-dependent. Interpretations based on such models must keep this fact in mind. In the future, a broader range of water-usage scenarios and transient capture zone analyses should be used to fully explore these alternatives.

# 3.0 GROUNDWATER GEOCHEMISTRY, CONTAMINANT DISTRIBUTIONS, AND IMPLICATIONS FOR FLOW AND TRANSPORT

It is important to understand geochemical processes and the natural water quality beneath the Pajarito Plateau, so that anthropogenic perturbations to the natural system can be identified and quantified. The natural geochemistry of groundwater is the result of physiochemical interactions between air, water, soil, biota, and aquifer material. Geochemical processes are influenced by several factors, including the composition of the groundwater, groundwater temperature, microbial populations, the mineralogical composition of the aquifer material(s), and the length of time the water is in contact with aquifer material(s). Section 3.1 describes the conceptual model of geochemical processes and reactions for the Pajarito Plateau and surrounding area. It also describes the "background" water chemistry, that is, the water chemistry not affected by Laboratory activities.

Imprinted on the natural variations in chemistry is the presence of contaminants historically released since the early 1940s when Laboratory operations commenced. While most of the contaminants are at concentrations largely below regulatory standards, they demonstrate the presence of pathways for groundwater flow and contaminant transport from the surface to deeper groundwater. The impacts to groundwater at the Laboratory have occurred mainly where effluent discharges have caused increased infiltration of water. The depth to which chemical constituents move in the subsurface is determined partly by their chemical behavior: non-reactive constituents move readily with groundwater, while reactive or adsorbing constituents move a shorter distance.

In most cases where effluent sources have been eliminated, groundwater concentrations of non-reactive discharged contaminants have decreased far below past levels (e.g., RDX, nitrate, tritium, and perchlorate) in alluvial groundwater. These mobile contaminants readily move through the subsurface and are detected within perched intermediate zones and at the regional water table beneath several canyons, including Pueblo Canyon, Los Alamos Canyon, Sandia Canyon, Mortandad Canyon, and Cañon de Valle (HE in Cañon de Valle is an exception to this). In the case of reactive or adsorbing chemicals, the concentrations remain elevated significantly above background levels after elimination of discharges or other contaminant source terms (e.g., excavation and removal of contaminated sediments). These include constituents such as strontium-90 and the actinides (americium-241, plutonium-238, and plutonium-239,-240). A discussion of observed contaminant distributions within alluvial and perched intermediate zones and the regional aquifer is provided in Section 3.2. Many of the characterization wells and their chemical data are not included because characterization sampling conducted as part of the Hydrogeologic Workplan is not complete.

## 3.1 Geochemical Conceptual Model

A geochemical conceptual model that describes the geochemical environment beneath the Pajarito Plateau combines knowledge of geochemical processes with observations of water chemistry at sampling locations and mineralogy of aquifer materials. The components that contribute to the geochemical conceptual model include

- natural chemical compositions of groundwater,

- residence time,
- reactive minerals controlling groundwater composition and solute mobility,
- adsorption and precipitation reactions,
- redox conditions controlling solubility, and
- chemical speciation.

The following subsections discuss these conceptual model components and describe the observations and data that are the basis of each component.

### 3.1.1 Natural Chemical Composition of Groundwater

Groundwater occurs in three hydrostratigraphic settings beneath the Pajarito Plateau, which include the alluvium, perched intermediate zones (Bandelier Tuff, Cerros del Rio basalt, and the Puye Formation), and the regional aquifer (Puye Formation, Cerros del Rio basalt, older basalts, and the Santa Fe Group). As a result of geochemical processes, the natural composition of groundwater in the three hydrostratigraphic settings varies along flow paths from recharge areas in the Sierra de los Valles, west of the Laboratory, to the discharge areas along the Rio Grande to the east. Recharge also occurs along canyon reaches that contain saturated alluvium.

A hydrochemical investigation was conducted from 1997 to 2000 to define the background chemical composition of groundwater beneath the Pajarito Plateau. Based on the data and information compiled, the statistical properties of natural (background) distributions of stable isotopes ($\delta D$, $\delta^{15}N$, and $\delta^{18}O$), tritium, and major and trace solutes in groundwater were established. A complete description of the background study is available in LANL (2005a).

Natural groundwater (alluvial, intermediate, and regional aquifer) ranges from calcium-sodium bicarbonate composition within the Sierra de los Valles to a sodium-calcium bicarbonate composition east and northeast of the Laboratory. Sodium bicarbonate groundwater occurs within the regional aquifer in lower Los Alamos Canyon and at several White Rock Canyon springs near Otowi Bridge (Blake et al. 1995; LANL, 2001a; LANL, 2002; LANL, 2004b). Figure 3-1 shows average background concentrations of specific conductance, major cations and anions, silica, tritium, and several trace elements including barium and uranium analyzed during six sampling rounds (LANL 2005a).

Concentrations of trace elements increase from alluvial groundwater to perched intermediate zones to the regional aquifer. They also increase from west to east within the regional aquifer due to increasing solute residence times and water/rock interactions, including recipitation/dissolution and adsorption/desorption reactions. The highest natural solute concentrations are associated with older groundwater within the regional aquifer. Concentrations of dissolved bicarbonate, sodium, calcium, and uranium increase from west to east. The following subsections discuss the evolution of natural groundwater chemistry from the recharge zone, along the flow paths, and out to the discharge zone.

#### 3.1.1.1 Geochemistry of the Recharge Zone

Groundwater generally has the lowest total dissolved solids (TDS) in the recharge area and increases in TDS along flow paths (Figure 3-1, where TDS is approximated by specific conductance). The Sierra de los Valles provides most of the recharge to groundwater beneath the Pajarito Plateau, based on distributions of stable isotopes, including δD and $\delta^{18}O$ ratios (Figure 3-2). This interpretation was presented in Section 2.8.3.1.1. Recharge water derived from precipitation near the Sierra de los Valles contains natural tritium (19 to 71 pCi/L), which decays to less than 3 pCi/L along groundwater flow paths within non-contaminated perched intermediate zones and the regional aquifer beneath the central and eastern parts of the Laboratory (Figure 3-1).

#### 3.1.1.2 Aqueous Geochemistry along the Flow Path

This subsection evaluates or describes solutes or dissolved species occurring along groundwater flow paths, which show variation among the three types of saturated zones. Variation in solute concentration results from the mixing of groundwaters, mineral precipitation (solute sink), mineral dissolution (solute source), and adsorption/desorption reactions. Natural groundwater quality in the regional aquifer beneath the Pajarito Plateau is excellent and, with the exception of arsenic in Guaje Canyon groundwater, does not exceed federal and state drinking water standards.

The occurrence of reactive minerals within aquifer material controls the composition of groundwater chemistry along flow pathways. Calcium, sodium, and bicarbonate are the dominant major ion solutes in natural groundwater beneath the Pajarito Plateau and surrounding areas. Bicarbonate is the dominant anion in groundwater at Los Alamos (LANL 2005a). This solute increases in background concentrations from shallow alluvial groundwater to the regional aquifer (Figure 3-3). Bicarbonate forms complexes with several trace metals, which has a direct influence on the metal's mobility or transport in the subsurface. Low concentrations of natural bicarbonate and calcium within the alluvium and perched intermediate zones within the Bandelier Tuff and the Puye Formation are insufficient to precipitate calcium carbonate (calcite) (Figure 3-4). Calcite is not typically observed within these saturated zones under natural conditions. In contrast occurrences of calcite within the Santa Fe Group basalt and sediments are reflective of higher concentrations of both calcium and bicarbonate.

Silica is the next most abundant solute found in surface water and groundwater within the Los Alamos area (Figure 3-1) because of hydrolysis reactions taking place between soluble silica volcanic glass and water. All groundwater sampled as part of the background investigation (LANL 2005) are oversaturated with respect to quartz, which is the most stable mineral of the silica phases (Lindsay 1979). Dissolved silica concentrations, however, are not controlled by quartz because this mineral is less reactive than volcanic and sedimentary glass found within the different hydrostratigraphic units. Groundwater within the three groundwater zones is calculated to be in equilibrium with silica glass. In some instances, dissolved silica can be used as a tracer to evaluate groundwater flow from the silica-rich (pumice-rich) Puye Formation to the underlying Santa Fe Group basalt encountered at wells R-9 and R-12. Groundwater flowing through the Bandelier Tuff (well LAOI(A)-1.1) and some sections of the pumiceous-rich Puye

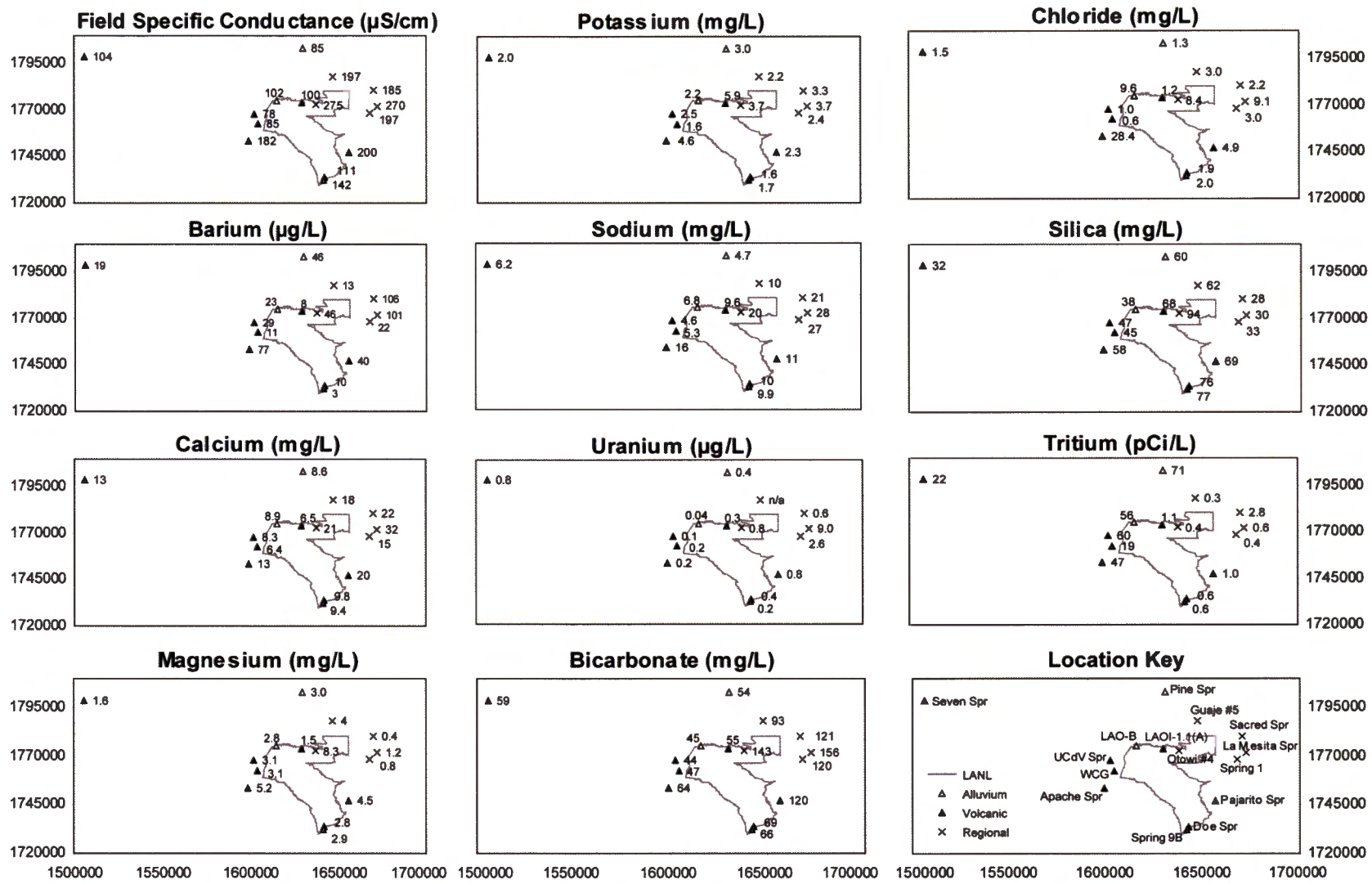


**Figure 3-1.** Average spatial distributions (n = 6) for key analytes in LANL background wells and springs (LANL, 2005a).

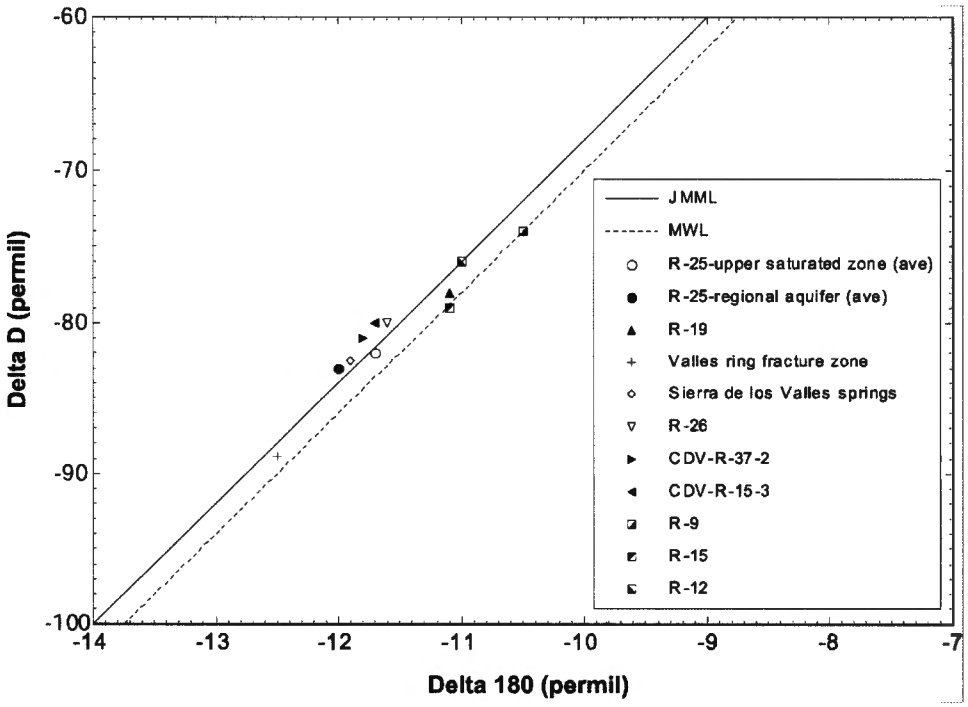


**Figure 3-2.** Stable isotope results for wells R-9, R-12, R-15, R-19, R-25, R-26, CdV-R-15-3, and CdV-R-37-2, and for other springs in the Jemez Mountains. (The upper line is the Jemez Mountains meteoric line and the lower is the mean worldwide meteoric line.)

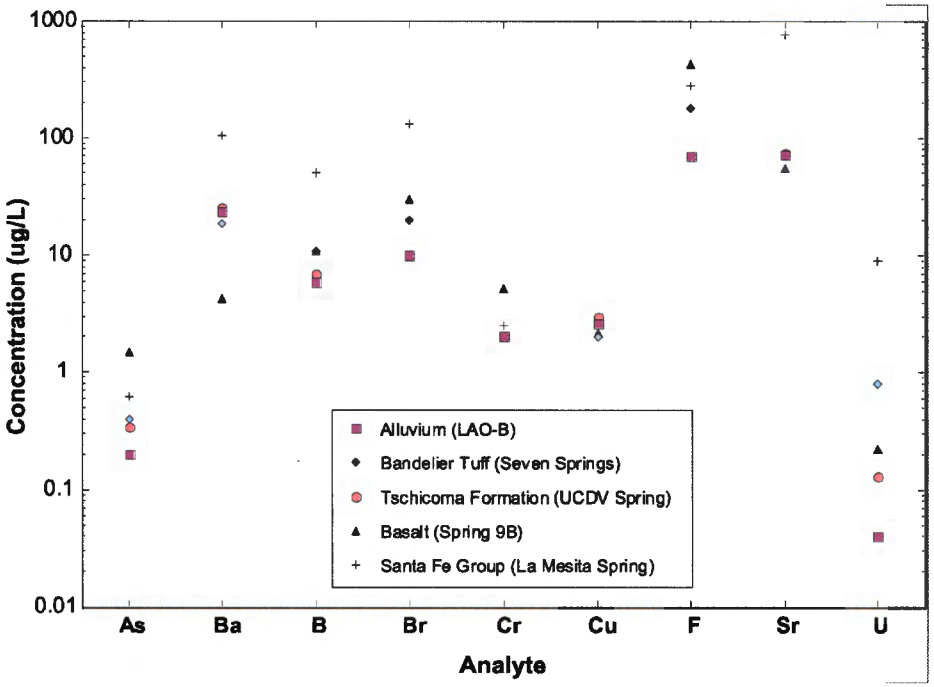


**Figure 3-3.** Average dissolved concentrations of selected natural trace elements in a represenative well or spring within alluvial and perched intermediate groundwater and the regional aquifer. Note: Average of six rounds.

Formation (wells R-7 and R-15) is characterized by higher dissolved silica concentrations than groundwater flowing through the Cerros del Rio basalt (well R-9i and Spring 9-B) (Figure 3-4). This contrast is attributable to the fact that the volcanic glass within the basalt is both less abundant and less reactive than the ubiquitous glass within the Otowi Member of the Bandelier Tuff and pumiceous-rich Puye Formation.

Figure 3-3 shows average dissolved concentrations of several natural trace elements within alluvial and perched intermediate groundwater and the regional aquifer. Average concentrations of natural arsenic, chromium, and fluoride were the highest within the Cerros del Rio basalt (Spring 9B). Variations in groundwater trace element concentrations depend on solute residence time, speciation, and extent of water-rock interactions. Many trace elements show considerable variations, even in young recharge water. For example, average concentrations of barium, boron, bromide, strontium, and uranium are the highest within the regional aquifer in the Santa Fe Group at La Mesita Spring. Average concentrations of dissolved natural uranium were 9.1 µg/L at La Mesita Spring, which is 300 times greater than that observed at well LAO-B in alluvium (Figure 3-3).

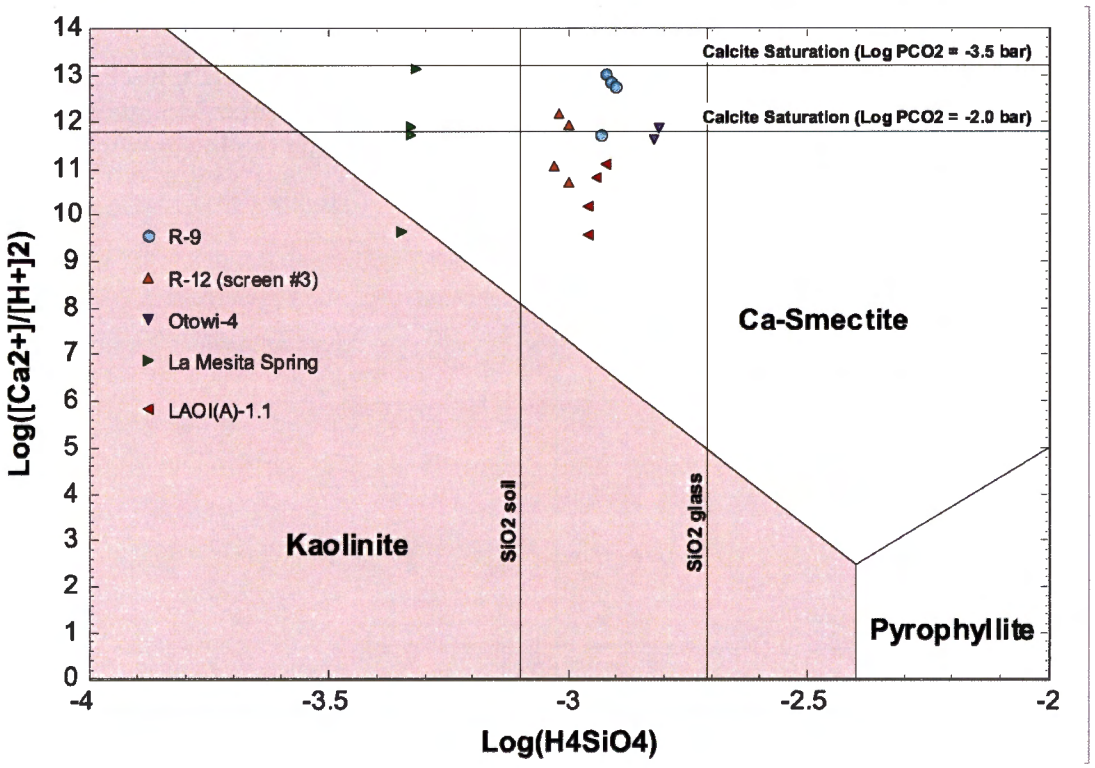


**Figure 3-4.** Activity diagram of log activity $[H_4SiO_4]$ versus log activity $Ca^{2+}/[H^+]^2$ at 25°C for wells Otowi-4, R-9, R-12 (screen #3), and LAOI(A)-1.1 and La Mesita Spring.
Note: These were selected because of observed smectite in x-ray diffraction of core and cuttings.

Naturally occurring solid organic matter containing carbon, oxygen, nitrogen, and hydrogen is an important component of alluvial sediments within and surrounding the Laboratory. Dissolved organic carbon (DOC) is derived from leaching of solid organic matter and concentrations of DOC are typically less than 2 mg carbon (C)/L within perched intermediate zones and the regional aquifer. Higher concentrations of DOC (up to 20 mg C/L) are found in soil, surface water, and alluvial groundwater within the upper reaches of Los Alamos Canyon where runoff through grasslands and forests takes place. The DOC contains dissociated carboxylic acids that are stable as anions above pH 4.5 (Thurman, 1985). The anions are mobile in the groundwater. Dissolved organic carbon mainly occurs in the forms of humic and fulvic acids (Vilks and Bachinski, 1996). These acids occur as anions and can complex with calcium and magnesium, which can influence precipitation reactions involving calcite.

Leaching of ash produced from the Cerro Grande fire in May 2000 resulted in the generation of elevated concentrations of total organic carbon (TOC), consisting of both DOC and suspended organic carbon (SOC). Shortly after the Cerro Grande fire, increased concentrations of TOC were observed in surface water and alluvial groundwater within Pueblo Canyon, Los Alamos Canyon, Pajarito Canyon, and other watersheds. Since 2002, concentrations of TOC have decreased in surface water, but remain elevated in alluvial and perched-intermediate groundwater. Total organic carbon provides an excellent tracer for tracking movement of recent water (post Cerro Grande fire) in the subsurface. For example, concentrations of TOC have exceeded 300 mg C/L in perched zones within the Cerros del Rio basalt at the Los Alamos Canyon weir (Stone et al., 2004).

#### 3.1.1.3 Geochemistry of the Discharge Zone

Groundwater chemistry within discharge zones can significantly differ from that characteristic of recharge zones. Total dissolved solids generally increase along groundwater flow paths. Specific conductance provides an indirect measurement of TDS and both parameters increase from west to east along groundwater flow paths. For example, groundwater within the Sierra de los Valles contains specific conductance values typically less than 100 µS/cm (Figure 3-1). Springs discharging within White Rock Canyon, however, have specific conductance greater than 100 µS/cm. Concentrations of sodium also increase relative to calcium and magnesium at selected White Rock Canyon springs. This change in major cation chemistry most likely results from cation exchange processes with reactive minerals along flow paths, including smectite, kaolinite, and volcanic glass (discussed in Section 3.1.3).

Groundwater within a discharge zone, at the end of groundwater flow paths, generally has the highest mineral or solute content and also represents the oldest water, provided that mixing with younger groundwater has not taken place. The main groundwater discharge zone for the Sierra de los Valles and the Sangre de Cristo Mountains occurs as springs and gaining reaches along the Rio Grande. Older groundwater within the regional aquifer tends to have higher concentrations of trace elements due to a combination of mineral dissolution and desorption processes. Many trace elements, including arsenic(III, V) and uranium(VI), form anions and tend to desorb from mineral surfaces under basic pH conditions (Langmuir, 1997). Dissolved concentrations of major cations and anions, arsenic, uranium, and other trace elements are higher in groundwater east of the Rio Grande based on water quality/geochemical data collected by the New Mexico

Environment Department (NMED) and most recently by LANL. Based on water samples brought in to the Pojoaque water fair in 2004, concentrations of natural uranium in groundwater are generally in the range from up to 0.2 ppm along the Rio Grande and eastward toward the Sangre de Cristo Mountains. In contrast, uranium concentrations in the regional aquifer beneath the Pajarito Plateau rarely exceed 0.1 ppm.

In the discharge zone, as well as along flow paths, tritium is an excellent tracer that can be used to qualitatively date or bound the age of groundwater less than 61 years old, with a few exceptions. Background springs discharging within White Rock Canyon typically have tritium concentrations less than 1 pCi/L, indicating that groundwater is greater than 61 years old. This pre-dates historic discharges associated with the Laboratory and atmospheric fallout that may provide sources of recharge. These springs are characterized by groundwater flow paths that are of variable lengths and differing groundwater residence times.

### 3.1.2 Residence Times

Residence times of groundwater and chemical solutes increase both with depth and from west to east across the Pajarito Plateau within each groundwater zone. Groundwater flow paths within the regional aquifer generally are from west to east based on water level measurements. Accordingly, the concentrations of natural major ions and trace elements increase with distance along flow paths.

In the Sierra de los Valles, a known recharge area west of the Laboratory, a component of groundwater is less than 61 years old, based on measurable activities of tritium observed in springs. Movement of groundwater through fractured volcanic rock within the Sierra de los Valles is rapid in most cases (Water Canyon Gallery, Apache Spring, upper Cañon de Valle Spring, and Pine Spring). With a few exceptions, most springs in the discharge zone in White Rock Canyon, however, do not contain tritium, and the age of groundwater probably ranges between 3,000 and 10,000 years and possibly even older (Rogers et al. 1996b).

The oldest groundwater residence times within the regional aquifer are on the order of several to tens of thousands of years, based on carbon-14 dating (Rogers et al, 1996b). The carbon-14 dates provide a reasonable estimate of the maximum age of groundwater within the regional aquifer, provided that mixing with more recent water or older water with lower alkalinity has not taken place. Groundwater within the regional aquifer becomes progressively older from west to east (Rogers et al, 1996b). Presence of tritium near the water table and within the regional aquifer beneath the Laboratory, however, confirms that a much younger component of groundwater is present in the regional aquifer. Small concentrations of anthropogenic tritium (less than 100 pCi/L) at some locations are suggestive of mixing of a majority of old water with a component of young water at the regional water table. Mixing ratios using chloride or bromide are needed as additional information to more precisely determine fractions of young and old groundwater.

### 3.1.3 Reactive Minerals Controlling Groundwater Composition and Solute Mobility

Because there are variations in pH, temperature, and major ion and trace element chemistry within shallow and deep saturated zones, different reactive minerals and amorphous solids precipitate or dissolve. In some instances, they control the major ion composition of groundwater. Some of these phases, including hydrous ferric oxide, manganese (oxy)hydroxide, smectite, calcite, and zeolites, have a high adsorptive capacity for trace elements including chromium, lead, strontium, and thorium, and radionuclides including americium-241, cesium-137, and plutonium-238, -239, -240. Reactive minerals and amorphous solids approach equilibrium with groundwater when the residence time exceeds the reaction half time (amount of time required for 50% of reactant A to form product B assuming there is no B initially present). This condition is usually met within perched intermediate zones and the regional aquifer based on observed mineralogy, because hydrous ferric oxide is present in all the groundwater zones.

Calcite and smectite are two important minerals that have been observed in core samples collected from several R wells. The stability of reactive phases, including $CaCO_3$ (calcite) and calcium smectite, can be evaluated by considering concentrations of major dissolved ions, chemical composition of minerals, and equilibrium concepts. Figure 3-4 is a log activity diagram showing the stability of several minerals including kaolinite, pyrophyllite, silica soil, silica glass, and calcium smectite. Groundwater samples collected from selected wells R-9, Otowi-4, R-12 (screen #3), and LAOI(A)-1.1 and La Mesita Spring are also plotted on the figure. Important points from this figure are as follows:

- Most groundwater is oversaturated with respect to calcium smectite, as the groundwater samples plot within that stability field.
- One sample collected from La Mesita Spring plots within the stability field for kaolinite due to a lower pH measurement.
- Groundwater is oversaturated with respect to $SiO_2$ soil (amorphous silica) and undersaturated with $SiO_2$ glass, which suggests that some of the silica could be formed from pedogenic (soil-forming) processes.
- La Mesita Spring (representative of young recharge water) is undersaturated with respect to silica soil and silica glass and has lower concentrations of silica relative to those measured in groundwater samples collected at wells R-9, Otowi-4, R-12, and LAOI(A)-1.1.

Under equilibrium conditions, calcite controls dissolved concentrations of calcium and bicarbonate within the regional aquifer. Beneath the western and central portions of the Laboratory, however, calcite is relatively rare in most of the lithologies characterized at the regional aquifer water table (Figure 2-10) except for the pre-Puye Formation Santa Fe Group sediments. These sediments have variable amounts of dispersed calcite cement (0-20 wt%). There is also a zone of post-depositional alteration centered in the northeastern portion of the Laboratory where calcite alteration is common in the Puye fanglomerate and the pumiceous sediments. Calcite precipitation is observed in Santa Fe Group sediments near the Rio Grande.

As groundwater flows through perched intermediate zones and the regional aquifer, chemical and mineralogical compositions of reactive phases, including silica glass, change over time. For example, silica glass is the most soluble component of the aquifer material (Puye Formation and unassigned pumiceous unit) and reacts with groundwater to form clay minerals, such as kaolinite and smectite. These alteration phases have been observed at wells R-5, R-8A, R-9, and R-12. Calcium-sodium smectite has been observed in core and cutting samples collected from R-9 (Broxton et al., 2001a). Smectite has also been observed in rock samples collected from Santa Fe Group sediments in lower Los Alamos Canyon (Vaniman, unpublished data). The presence of smectite enhances natural attenuation of anthropogenic metals stable as cations, including strontium and barium, because this phase increases the adsorption capacity of the aquifer material under circumneutral pH conditions (discussed in more detail in Section 3.1.4).

The saturation index (SI) is an indicator of whether a mineral is likely to precipitate or dissolve under particular groundwater conditions. The SI is defined as the $\log_{10}$(activity product/solubility product). Precipitation of reactive minerals, including calcite, occurs in groundwater under near neutral pH conditions. Figure 3-5 shows saturation indices for calcite versus calcium and bicarbonate concentrations (millimoles/liter) at selected background springs and wells. The computer program MINTEQA2 (Allison et al., 1991) was used to perform SI calculations. For a given solid phase at equilibrium, the SI is equal to $0 \pm 0.05$. Oversaturation (positive SI) implies precipitation, whereas undersaturation (negative SI) implies dissolution. Native alluvial and perched intermediate groundwaters are calculated to be undersaturated with respect to calcite, and dissolution of this mineral takes place. This is consistent with the absence of calcite within the natural alluvium at the Laboratory. Groundwater samples collected at wells R-9, R-12, and Otowi-4 and La Mesita Spring generally are saturated with respect to calcite, whereas LAOI(A)-1.1 is not. Activities of dissolved calcium and bicarbonate at well LAOI(A)-1.1 are not sufficient to precipitate calcite. Calcite typically is not observed in native groundwater within the alluvium and Bandelier Tuff. The regional aquifer (Santa Fe Group sediments) is slightly undersaturated, but within thermodynamic uncertainty, with respect to calcite.

### 3.1.4 Adsorption and Precipitation Reactions

Adsorption occurs when dissolved species interact with surfaces of aquifer material coated with hydrous ferric oxide, manganese dioxide, clay minerals, or other adsorbents. Adsorption is usually reversible with the net effect being that the transport of the absorbed species is much slower than that of the water. Hydrous ferric oxide is an important adsorbent present in different aquifer materials beneath the Pajarito Plateau. Other adsorbents of metals include smectite, calcite, manganese oxide, and solid organic carbon, which can provide additional adsorption sites on aquifer material and within the unsaturated zone. Hydrous ferric oxide has a specific surface area of 600 $m^2/g$, which is much higher than quartz or silica gel that have specific surface areas of 0.14 and 53 to 292 $m^2/g$, respectively (Langmuir, 1997). Many metals and radionuclides including barium, chromium, nickel, uranium, strontium-90, americium-241, plutonium-238, and plutonium-239, -240 typically adsorb onto hydrous ferric oxide-coated particles between pH values 5 and 8.

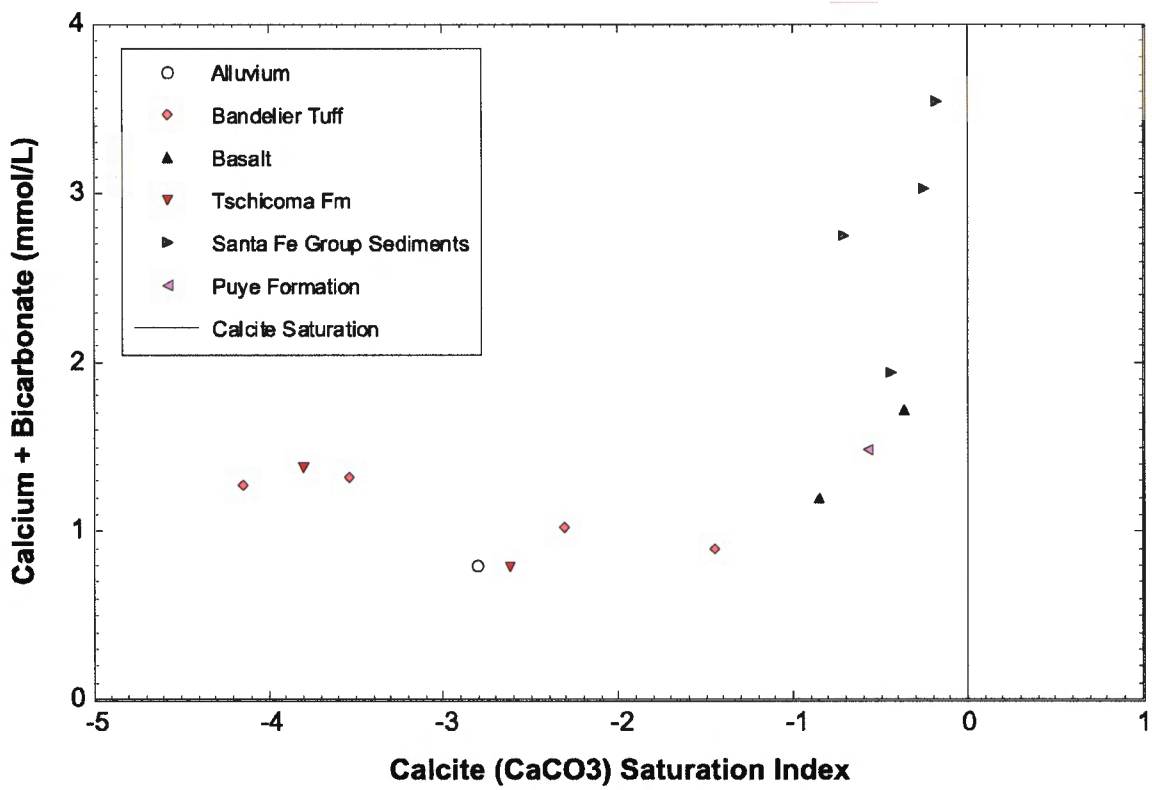


**Figure 3-5.** Saturation indices for calcite versus calcium and bicarbonate concentrations (millimoles/liter) at springs and wells representing different aquifer types at LANL (perched, intermediate, and regional).

Concentrations of inorganic contaminants (actinides, fission products, and trace elements) remaining within treated effluents are too small to be removed from solution through precipitation, based on results of computer simulations. Downgradient from Laboratory discharge points, adsorption processes are considered to dominate over mineral precipitation for continual removal of metals and radionuclides from alluvial groundwater. As a result, concentrations of adsorbing radionuclides and inorganic species generally decrease downgradient along the groundwater flow path. Alluvial material provides the largest reservoir for constituents from treated Laboratory effluent, including strontium-90, cesium-137, plutonium-238, plutonium-239, -240, and americium-241 because the constituents readily adsorb onto clay- and silt-sized material. For example, it is hypothesized that strontium-90 has been reversibly adsorbed on alluvial sediments by cation exchange, and the sediments provide a continuing source of this constituent to the alluvial groundwater. Eventually, strontium-90 will decay to stable zirconium-90 (via short-lived yttrium-90), reducing its remaining radioactivity by a factor of two approximately every 29 years.

Based on numerous studies reported in the literature, and supported by field observations documented in LANL Surveillance Reports (e.g. LANL, 1996a, 2000a, 2001a, 2002) and

experimental results, the relative adsorption of HE compounds, radionuclides and inorganic species decreases at circumneutral pH (6 to 8) conditions as follows:

cesium-137 (highest adsorption) = americium-241 > barium > strontium-90 > uranium > nitrate = molybdate = sulfate = chloride = perchlorate = TNT > RDX = tritium (lowest adsorption).

Cations adsorb more strongly than anions under acidic to circumneutral pH conditions because adsorbents, including hydrous ferric oxide, smectite, and silica glass, are characterized by a net-negative surface charge (Langmuir, 1997). (Oxy)anions, including molybdate, nitrate, and perchlorate, are mobile in groundwater under circumneutral to basic pH conditions due to the net-negative surface charge on the adsorbent. Neutral species including TNT, RDX, and tritium do not adsorb to any significant extent onto inorganic mineral surfaces. Characterization and surveillance data collected within Pueblo Canyon, Los Alamos Canyon, Mortandad Canyon, and Cañon de Valle support the observed mobilities of anions (chloride, molybdate, nitrate, perchlorate, sulfate, and uranium) and neutral species (RDX, TNT, and tritium). High explosive compounds undergo hydrophobic sorption with solid organic matter present in alluvial channels, including Cañon de Valle, but such material is not present in significant concentrations in the regional aquifer.

Other variables that influence adsorption processes include precipitation and dissolution of the adsorbent, adsorption capacity, and changes in aqueous chemistry. Adsorption capacities of unsaturated and saturated material may change over time due to changes in solution composition, contaminant speciation and reactive phase mineralogy. In isolated cases where effluent discharges have changed alluvial groundwater alkalinity or pH, trace elements such as strontium and barium may precipitate as $SrCO_3$, $BaCO_3$, and coprecipitate as $(Sr\text{-}Ba)SO_4$. These precipitation processes are considered to be important within the upper reaches of Cañon de Valle and Mortandad Canyon.

Cation exchange reactions typically influence major cation compositions of groundwater. This influence is especially true for older groundwater with a long residence time characteristic of the regional aquifer east of the Rio Grande. Cation exchange between divalent, magnesium and calcium and monovalent sodium results in increasing water hardness (increased calcium and magnesium) in which calcium typically dominates over magnesium as the dominant dissolved cation. Softening of water occurs when calcium and magnesium are removed from groundwater and sodium becomes the dominant cation. This water-softening process is observed northeast of the Laboratory (former lower Los Alamos wellfield) and along sections of the Rio Grande.

#### 3.1.4.1 Adsorption and Precipitation of Uranium(VI) Species

Uranium is a naturally occurring trace element found in groundwater and it is also processed at the Laboratory. This subsection provides a summary of the aqueous chemistry and adsorptive characteristics of this actinide because of its importance to background conditions and Laboratory effluents.

Uranium is a naturally occurring actinide found essentially in all soils, sediments, rocks, surface waters, and groundwaters worldwide. Whole rock concentrations of uranium within the Bandelier Tuff, Cerros del Rio basalt, and Puye Formation range from less than 1 to over 10 mg/kg or ppm (Longmire et al. 1996a, Broxton et al. 2001a). Silica-rich rocks, including the Bandelier Tuff, contain higher concentrations of uranium than do the less siliceous rocks, including the Cerros del Rio basalt and Puye Formation.

Background concentrations of dissolved uranium within alluvium, perched intermediate zones, and the regional aquifer are generally detectable but at concentrations less than 1 μg/L in groundwater beneath the Pajarito Plateau (Longmire et al., 1996b, LANL 2005a). These naturally low concentrations of dissolved uranium are probably controlled by aqueous solubilities of minerals containing uranium. For example, zircon ($ZrSiO_4$) is a trace mineral found within the Bandelier Tuff. Concentration of uranium in a zircon crystal within a sample of the Bandelier Tuff was 1180 ppm (Stimac et al. 1996). This highly refractory mineral has an aqueous solubility of $10^{-15.4}$ M at pH 7. Uranium does not significantly leach out of this mineral at circumneutral pH values (6 to 9) based on its low aqueous solubility. Some uranium concentrated within the Bandelier Tuff is associated with volcanic glass, which has an aqueous solubility of $10^{-2.71}$ M at pH 7. Consequently, there is higher occurrence of uranium in groundwater within the Bandelier Tuff because it is more susceptible to leaching from glass due to its higher aqueous solubility. The rate of uranium leaching from glass, however, is slow, as indicated by the low dissolved concentrations of uranium (<0.5μg/L) measured in perched groundwater within the Bandelier Tuff (well LAOI(A)-1.1).

The uranyl ($UO_2^{2+}$) cation is analogous to other divalent metal species that significantly adsorb onto hydrous ferric oxide under acidic pH conditions. Increasing concentrations of hydrous ferric oxide result in increasing the adsorption capacity of uranium(VI) complexes because more binding sites are present. Concentrations of hydrous ferric oxide vary between alluvial groundwater, perched intermediate zones, and the regional aquifer. This variation is dependent on chemical weathering of primary iron-rich minerals and iron-rich volcanic glass. Iron-rich glass and minerals within the Cerros del Rio basalt enhance precipitation of increasing amounts of hydrous ferric oxide compared to the Bandelier Tuff, which contains iron-depleted glass and smaller amounts of iron-bearing minerals.

The computer program MINTEQA2 (Allison et al., 1991) was used to model adsorption (surface complexation) of uranium(VI) onto hydrous ferric oxide for perched intermediate groundwater characterized at well R-9. The double layer model (DLM) was selected for the simulation because it takes into account adsorbent characteristics (specific surface area, charge density, and adsorbent concentration) and aqueous chemistry parameters (pH, ionic strength, and solution composition).

Figure 3-6 shows both calculated distributions of adsorbed uranium(VI) complexes onto hydrous ferric oxide and dissolved complexes as a function of pH. Results of the calculation suggest that maximum adsorption takes place at pH 5.5 and decreasing adsorption occurs with increasing pH, which is due to the formation of uranyl carbonate complexes. Uranyl dicarbonate and uranyl tricarbonate complexes do not significantly adsorb onto negatively charged surface sites present

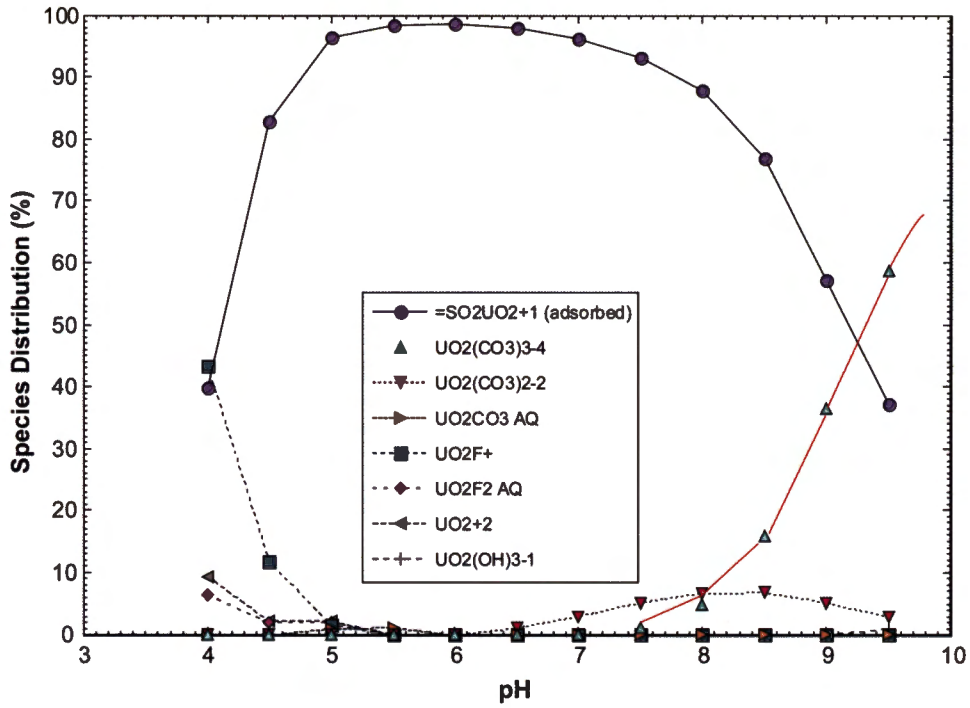


**Figure 3-6.** Calculated distributions of adsorbed and dissolved uranyl species for well R-9 (275 ft perched zone) (HFO concentration = 1.46 g/L and total dissolved uranyl $[UO_2^{2+}]$ = 0.054 ppm, 25°C). Calculation was made for R-9 because uranium was measured in groundwater whithin the Cerros del Rio basalt.

on hydrous ferric oxide. There is a sharp rise in uranium(VI) adsorption onto hydrous ferric oxide between pH values of 4.0 and 5.0 (Figure 3-6), where uranyl cation species dominate.

Other divalent cations compete with uranyl species in both natural and contaminated groundwater. Calcium ($Ca^{2+}$) strongly competes with $UO_2^{2+}$ for adsorption sites present on hydrous ferric oxide, based on experimental results, including DLM intrinsic stability constants provided by Langmuir (1997). Concentrations of dissolved calcium are much higher (in the mg/L range) than dissolved uranium (less than 1 µg/L), which allows for more calcium binding onto hydrous ferric oxide.

Similar competition between calcium and the uranyl cation may take place with clay minerals. This has relevance to groundwater chemistry east of the Rio Grande that is characterized by higher concentrations of calcium and uranium compared to groundwater beneath the Pajarito Plateau. This exchange reaction results in concentrations of natural uranium within the regional aquifer ranging from 0.5 µg/L (Los Alamos) to over 1800 µg/L (west of Nambé).

Exchange reactions between calcium and sodium are of importance based on inverse relationships between dissolved calcium, sodium, and uranium. Figure 3-7 shows calcium/sodium ratios (milliequivalents/L) versus uranium concentrations for 127 groundwater samples collected at Pojoaque, New Mexico during June 2004. The highest concentrations of uranium in groundwater occur at lower calcium/sodium ratios. This relationship suggests that

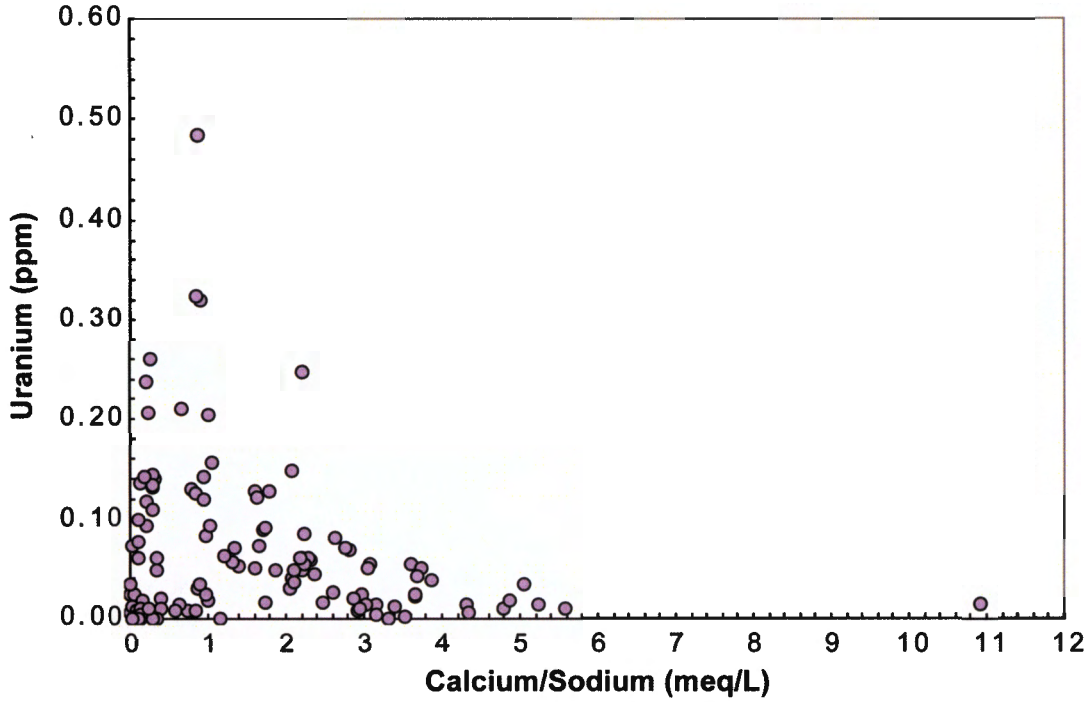


**Figure 3-7.** Calcium/sodium (meq/L) versus uranium concentrations, Pojoaque water fair, June 2004.

calcium is removed from groundwater, whereas uranium is added to groundwater through cation exchange. Alternatively, the relationship between uranium and sodium/calcium rations could be due to bulk compositional effects rather than cation exchange. In some groundwater samples, calcium is removed to a greater extent than sodium.

Precipitation reactions serve as a sink for removing uranium from solution. There are numerous uranium (VI) minerals that are naturally occurring and are found in aquifers (ore deposits) within sedimentary and igneous rocks. Several uranyl silicate minerals including $(UO_2)_2SiO_4 \cdot 2H_2O$ (soddyite) and $Ca(UO_2)_2(Si_2O_5)_3 \cdot 5H_2O$ (haiweeite) are potentially important within silica-rich groundwater beneath the Pajarito Plateau. Figure 3-8 shows a plot of saturation indices for several reactive minerals including silica solids, carbonate minerals, soddyite, and haiweeite for several groundwater sampling stations including Spring 2B, alluvial well LAO-B, perched intermediate groundwater (well LAOI(A)-1.1), and regional aquifer groundwater (wells Otowi-4, TW-3, R-9, and TW-1). The computer program MINTEQA2 (Allison et al., 1991) was used to perform the saturation calculations.

Temperature, pH, redox potential, and dissolved activities of calcium, uranium(VI), bicarbonate, and silicic acid influence the precipitation/dissolution of soddyite and haiweeite. As bicarbonate concentrations increase, dissolved uranium(VI) reacts to form complexes, which decreases the amount of uranyl cation ($UO_2^{2+}$) available for precipitation of soddyite and haiweeite. This is counter balanced, however, by increasing concentrations of dissolved calcium that enhances precipitation of haiweeite at Otowi-4, R-9, TW-1, and Spring 2B (Figure 3-8). This assessment is

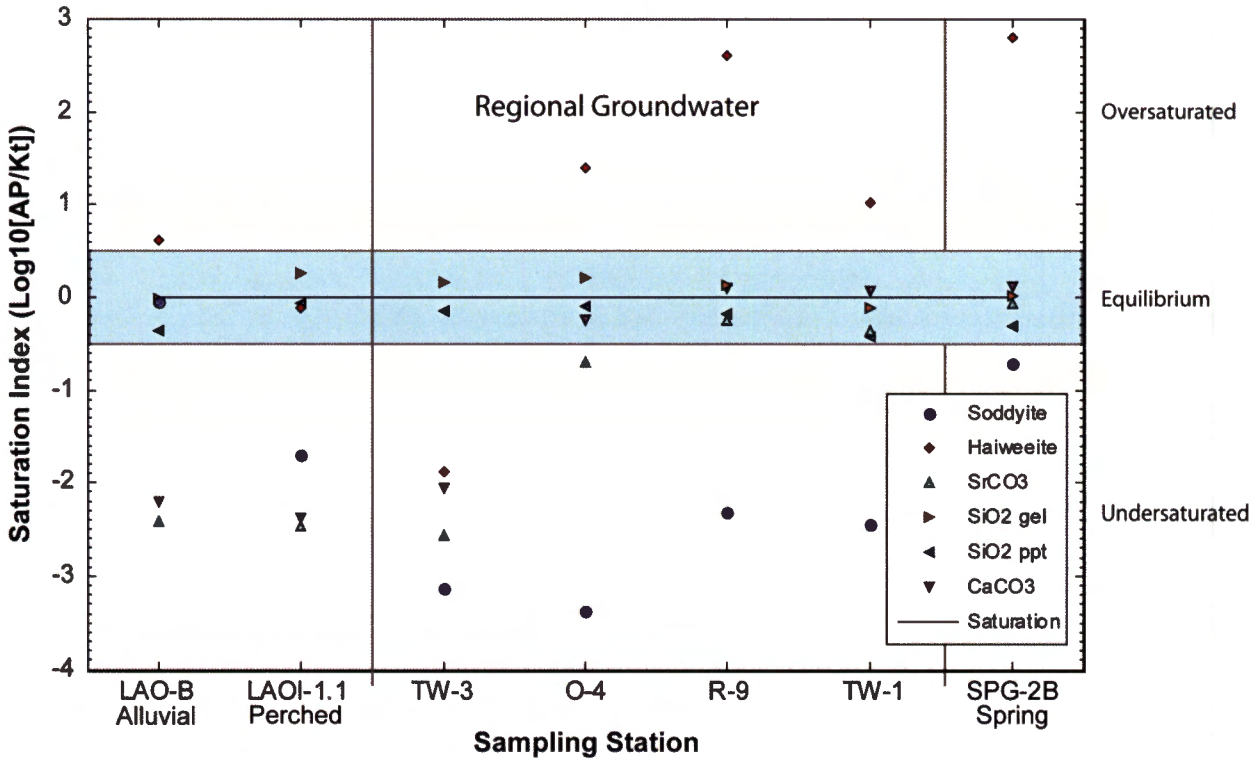


**Figure 3-8.** Saturation indices for several solid phases in alluvial (LAO-B) and perched intermediate groundwater (LAOI(A)-1.1) and the regional aquifer (Otowi-4, TW-3, R-9 and TW-1) within Los Alamos Canyon, Pueblo Canyon, and Spring 2B. The computer program MINTEQA2 was used to perform the calculations. Note: These wells were selected because they show hyrochemical snapshot of the three aquifer types within the Los Alamos Canyon and a spring.

based on geochemical calculations and the overall oxidizing conditions characteristic of natural groundwater beneath the Pajarito Plateau.

While it is useful to perform saturation index calculations to evaluate mineral equilibrium, most of the deep groundwaters are not in equilibrium with respect to either soddyite or haiweeite. Based on results of the calculations presented, adsorption processes involving uranium(VI) appear to control dissolved concentrations of this actinide in groundwater beneath the Pajarito Plateau.

### 3.1.5 Redox Conditions

This subsection presents a brief discussion on oxidation-reduction concepts with application to groundwater chemistry characterized during this investigation. Contaminants associated with treated Laboratory effluents that are stable in more than one oxidation state include plutonium(III, IV, V, and VI), uranium(IV and VI), technetium(IV and VII), iron(II and III), and chromium(III and VI). Other contaminants that can undergo reduction include perchlorate,

molybdate, nitrate, RDX, and TNT. A group of contaminants that is stable in one oxidation state under the geochemical conditions that prevail in groundwater includes americium(III)-241, cesium(I)-137, strontium(II)-90, barium(II), boron(III), and tritium(I). Adsorption and precipitation reactions involving redox-sensitive contaminants are directly influenced by oxidation and reduction reactions. Under oxidizing conditions, species including uranium(VI), sulfate, nitrate, and perchlorate form soluble anions that are mobile in groundwater. Under reducing conditions, however, these species either precipitate from solution (uranium and sulfide minerals), transform (perchlorate) and/or adsorb onto aquifer materials (nitrogen-ammonium).

Oxidation-reduction (redox) reactions are very important in groundwater systems for controlling distributions of trace elements and are quite often mediated by a wide variety of microbes. Redox conditions for groundwater most often cannot be quantified with a single redox couple and oxidation-reduction potential (ORP) (Langmuir, 1997) because numerous couples are present and they differ with respect to kinetic reaction rates (Figure 3-9). Some couples are electrochemically reversible, including the iron(III)/iron(II) and hydrous ferric oxide/iron(II) pairs. However, most pairs are not reversible under normal groundwater conditions in the absence of microbes, including: dissolved oxygen/water, nitrogen (V)/nitrogen(0), nitrogen(V)/nitrogen(III), uranium(VI)/uranium(IV), sulfur(VI)/sulfur(-II), and carbon(IV)/carbon(0, -IV). General trends in redox chemistry, however, can be inferred based on distribution and concentration of redox-sensitive solutes such as iron and manganese, mineralogy of aquifer material, presence or absence of dissolved oxygen, knowledge of microbial populations, and presence of electron donors (reducing agents, reductants), and electron acceptors (oxidizing agents, oxidants).

Under natural or baseline conditions, groundwater under the Pajarito Plateau within perched intermediate zones and the regional aquifer is oxidizing. This is also generally true for alluvial groundwater, although DOC may enhance localized reducing conditions within wetlands occupying some canyon reaches. Naturally occurring and measurable concentrations of dissolved oxygen (DO) (1 to 9 ppm), sulfate (>2 ppm), and nitrate (typically 0.5 ppm) are characteristic of oxidizing conditions. Low concentrations of dissolved iron (<0.5 ppm) and manganese (<0.05 ppm) are also characteristic of oxidizing conditions. Under reducing conditions, concentrations of reduced forms of carbon (methane, hydrocarbons, carbohydrates), nitrogen (ammonium), and sulfur (hydrogen sulfide) would exceed concentrations of the oxidized forms. Iron and manganese reduction would also be observed under reducing conditions. Reducing conditions do not occur in normal groundwater beneath the Pajarito Plateau although they have been encountered in several R wells as a highly localized consequence of residual drilling fluids, as described by Longmire and Goff (2002) and Longmire (2002a, 2002b, 2002d, and 2002e) and Bitner et al. (2004) in detail.

### 3.1.6 Uranium Speciation

Chemical speciation has a direct control on mineral precipitation and adsorption processes. Special attention is given to uranium in this report because this actinide occurs naturally in groundwater and has also been processed at the Laboratory. Large variations in natural uranium concentrations are observed beneath the Pajarito Plateau and to the east in the Rio Grande Valley.

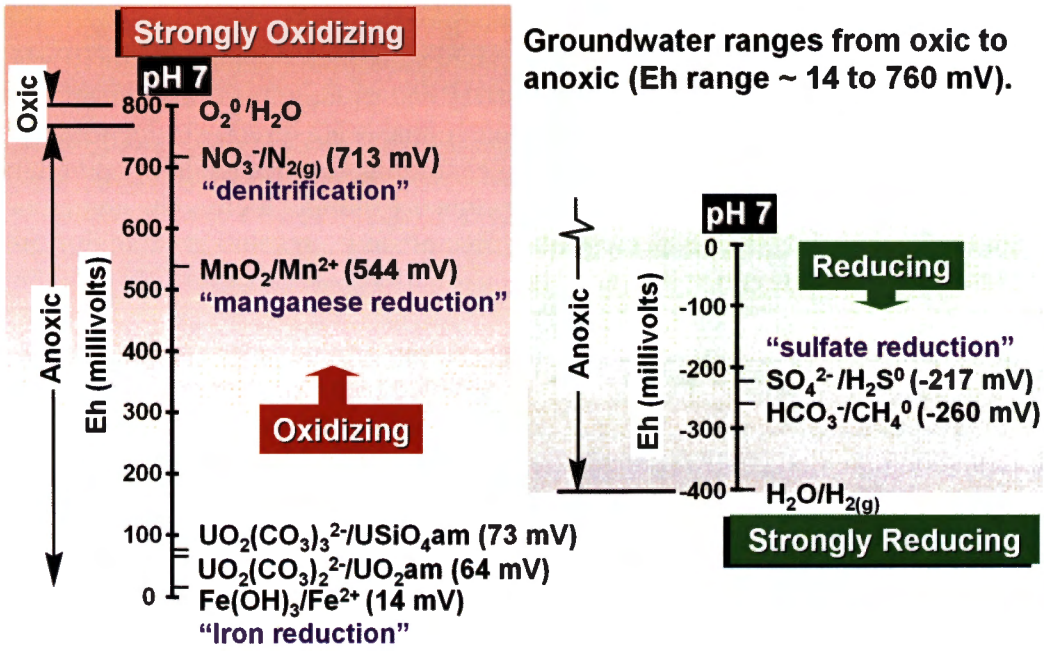


**Figure 3-9.** Selected oxidation-reduction couples in water at pH 7 and 25°C for the Pajarito Plateau and surrounding areas.

As uranium leaches from minerals and glass, it is stable as uranium(VI) under oxidizing conditions characteristic of aquifer systems beneath the Pajarito Plateau. Uranium(VI) forms strong complexes with bicarbonate and carbonate including $UO_2CO_3^0$, $UO_2(CO_3)_2^{2-}$, and $UO_2(CO_3)_3^{4-}$ (Langmuir 1997) above pH 6.

Figure 3-10 shows calculated distribution of uranium(VI) at Spring 9B discharging from the Cerros del Rio basalt east of the Laboratory. Dissolved concentrations of uranium are typically less than 0.2 µg/L at Spring 9B (LANL 1996a, 2000a, 2001a, 2002).The computer program MINTEQA2 (Allison et al., 1991) was used for the speciation calculations of Spring 9B. The aqueous complex, $UO_2(CO_3)_3^{4-}$ dominates above pH 8.4, whereas $UO_2(CO_3)_2^{2-}$ dominates between pH values of 6.6 and 8.4 at Spring 9B (Figure 3-10). Dissolved uranyl carbonate ($UO_2CO_3^0$) dominates between pH values of 5.0 and 6.6. Spectroscopic evidence has shown that $Ca_2UO_2(CO_3)_3^0$ significantly influences uranium(VI) speciation between pH values of 6 to 10 in calcium-rich uranium-mining waters (Bernhard et al., 2001). This complex may have relevance to groundwater east of the Rio Grande characterized by high calcium and carbonate alkalinity.

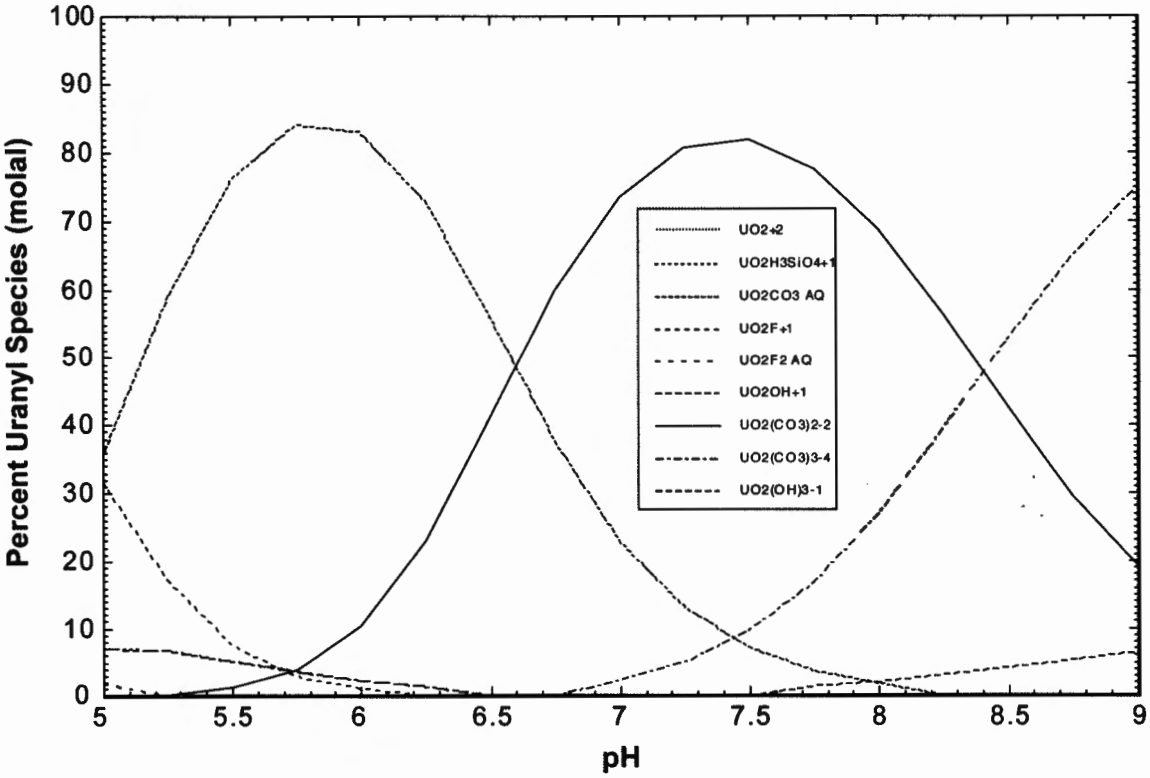


**Figure 3-10.** Results of speciation calculations for Spring 9B in White Rock Canyon using the computer program MINTEQA2. Log U(VI) = -9.26 molal (m), log F = -4.69 m, log $H_4SiO_4$ = -2.92 m, and log $CO_3^{2-}$ = -3.07 m at 20.5°C.

Figure 3-11 shows total alkalinity versus uranium concentrations for 127 groundwater samples collected within the Rio Grande Valley near Pojoaque, New Mexico, contrasted with samples from the Pajarito Plateau. Formation of uranyl carbonate complexes has a direct control on the solubility of uranium(VI), leading to dissolved concentrations of uranium much greater than 10 µg/L observed in the Rio Grande Valley.

Uranium(IV) is stable in strongly reducing groundwater containing dissolved sulfide and reduced forms of DOC (Langmuir 1997). Calculations show that uranium(IV) in the form of $U(OH)_4^0$ is stable under reducing conditions below an Eh of –225 millivolts (mV) at pH 7, 25°C, and $10^{-3.0}$ M (61 mg/L) bicarbonate. Formation of uranium(IV) complexes is very unlikely to occur because natural groundwater at Los Alamos, New Mexico is oxidizing and uranium(VI) species are stable. However, in groundwater near Pojoaque uranium(IV) is inferred to be stable in the presence of hydrous ferric oxide reduction.

### 3.1.7 Summary of Geochemical Conceptual Model

It is important to understand geochemical processes and the natural water quality beneath the Pajarito Plateau, so that anthropogenic perturbations to the natural system can be identified and quantified. While the contaminants are at concentrations largely below regulatory standards or

risk levels, they demonstrate the presence of pathways for groundwater flow and contaminant transport from the surface to deeper groundwater.

Natural groundwater (alluvial, intermediate, and regional aquifer) ranges from calcium-sodium bicarbonate composition within the Sierra de los Valles to a sodium-calcium bicarbonate composition east and northeast of the Laboratory. The Sierra de los Valles provides most of the recharge to groundwater beneath the Pajarito Plateau and groundwater in the recharge area has the lowest TDS of the overall flow system.

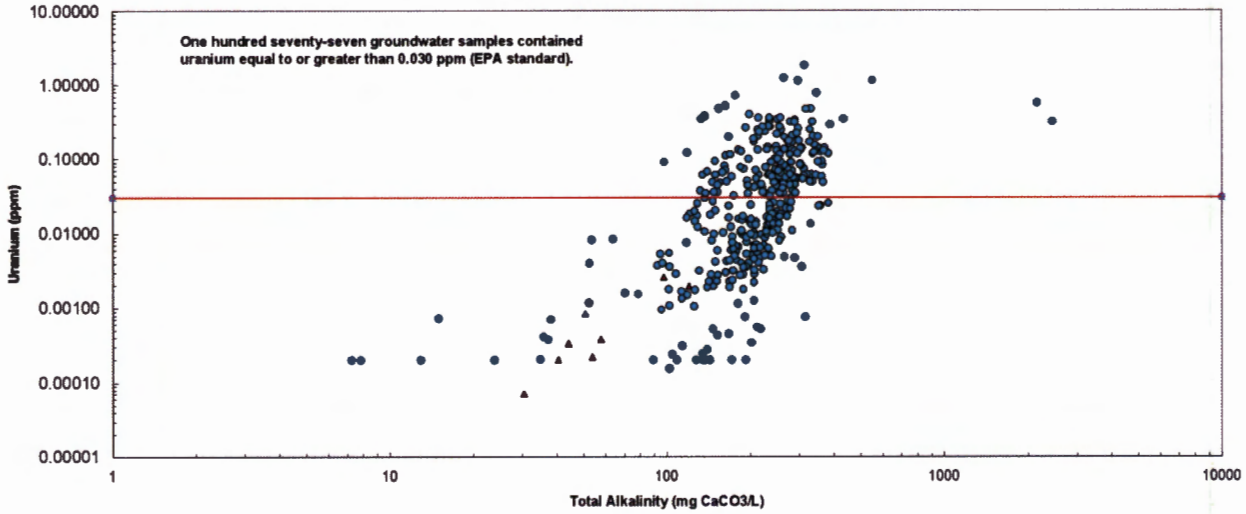


**Figure 3-11.** Total alkalinity (as carbonate) versus uranium concentrations in groundwater samples collected from the Rio Grande Valley and the Pajarito Plateau. Red triangles are from Pajarito Plateau and blue dots are from the Rio Grande Valley.

Along flow paths variation in solute concentration results from mixing of groundwaters, mineral precipitation (solute sink), mineral dissolution (solute source), and adsorption/desorption reactions. Calcium, sodium, and bicarbonate are the dominant major ion solutes in natural groundwater beneath the Pajarito Plateau and surrounding areas. Silica is the second most abundant solute found in surface water and groundwater within the Los Alamos area because of hydrolysis reactions taking place between soluble silica volcanic glass and water. Variations in groundwater trace element concentrations depend on solute residence time, speciation, and extent of water-rock interactions.

All of the mobile chemicals measured in perched intermediate zones and in the regional aquifer are stable as anions (perchlorate, nitrate, sulfate, chloride, uranium) or as neutral species (RDX, TNT, HMX, boron). Contaminants stable as cations (barium, americium-241, plutonium(V)-238, -239, -240, strontium-90, cesium-137) have migrated within alluvial groundwater and are infrequently detected in deeper groundwater.

Groundwater within a discharge zone, at the end of groundwater flow paths, generally has the highest mineral or solute content and also represents the oldest water. Residence times of groundwater and chemical solutes increase both with depth and from west to east across the Pajarito Plateau within each groundwater zone. The oldest groundwater residence times within the regional aquifer are on the order of several thousand to tens of thousands of years, based on carbon-14 dating and on flow and transport models.

Geochemical processes that affect the groundwater chemistry include the following:

- ***Precipitation/Dissolution***: Different reactive minerals and amorphous solids precipitate or dissolve and can control the major ion composition of groundwater. As groundwater flows through perched intermediate zones and the regional aquifer, chemical and mineralogical compositions of reactive phases including silica glass change over time. For example, silica glass is the most soluble component of the aquifer material reacting with groundwater to form clay minerals, including kaolinite and smectite. Precipitation reactions serve as a sink for removing uranium from solution.
- ***Adsorption:*** Dissolved species interact with surfaces of aquifer material coated with hydrous ferric oxide, manganese dioxide, clay minerals, or other adsorbents, often resulting in the release of adsorbed species via replacement reactions. Hydrous ferric oxide is an important adsorbent present in different aquifer materials beneath the Pajarito Plateau. Other common adsorbents of metals include smectite, calcite, manganese oxide, and solid organic carbon. Downgradient from Laboratory discharge points, adsorption processes are considered to dominate over mineral precipitation for continual removal of metals and radionuclides from alluvial groundwater. Adsorption processes involving uranium(VI) appear to control dissolved concentrations of this actinide in groundwater beneath the Pajarito Plateau.
- ***Redox Conditions***: Under natural or baseline conditions, groundwater under the Pajarito Plateau within alluvial, perched intermediate zones, and the regional aquifer is oxidizing. Adsorption and precipitation reactions involving redox-sensitive contaminants are directly influenced by oxidation and reduction reactions. Under oxidizing conditions, species including uranium(VI), sulfate, nitrate, and perchlorate form soluble anions that are semimobile in groundwater. Uranium(VI) partly adsorbes onto ferric oxyhydroxide and is semimobile in groundwater between a pH range of 7 to 8.5, typically observed in groundwaters of the Pajarito Plateau. Under reducing conditions, however, these species either precipitate from solution (uranium and sulfide minerals), transform (perchlorate) and/or adsorb onto aquifer materials (nitrogen-ammonium).
- ***Chemical Speciation***: has a direct control on mineral precipitation and adsorption processes. Formation of uranium(IV) complexes is very unlikely to occur because natural groundwater at Los Alamos, New Mexico is oxidizing and uranium(VI) species are stable.

## 3.2 Contaminant Distributions and Transport

This section describes the sources, presence, and trends through time of chemical constituents in groundwater originating from anthropogenic (principally LANL) sources. The movement rates and distribution of these chemical constituents give an indication of groundwater flow paths and flow mechanisms over time. Appendix 3-A provides a description and map of each canyon, arranged by watershed, because this framework highlights the connection between surface liquid discharge sources and their effects on shallow and deeper groundwater chemistries.

In this section anthropogenic chemical constituents found in groundwater are divided into two classes: contaminants and other anthropogenic chemical constituents. Contaminants in groundwater are chemicals found at concentrations near or exceeding either regulatory standards or, where no standards exist, exceeding EPA screening levels of either hazard index (HI) of 1 or excess cancer risk of $10^{-5}$. For chemicals with no standards, the EPA Region VI tap water screening levels were used (http://www.epa.gov/earth1r6/6pd/rcra_c/pdn/screen.htm). For cancer-causing substances, the Region VI tap water screening levels are at a risk level of $10^{-6}$, therefore, 10 times these values were used to screen for a risk level of $10^{-5}$. A hazard index value of 1 or less indicates that no (noncancer) adverse human health effects are expected to occur.

Anthropogenic chemical constituents other than contaminants are found at lower concentrations, although some of these constituents may have been contaminants (that is, at higher concentrations) in the past.

Table 3-1 summarizes the anthropogenic constituent observations in alluvial, intermediate, and regional aquifer groundwater. Information on Table 3-1 indicates that most canyons with anthropogenic constituents in alluvial groundwater also have anthropogenic constituents in the intermediate (if present) and the regional aquifer. The water quality impacts of effluent releases on alluvial groundwater extend to perched groundwater at depths of a few hundred feet beneath these canyons. The contaminated perched groundwater bodies are separated from the regional aquifer by hundreds of feet of dry rock, and in these wet canyons recharge from the shallow perched groundwater occurs in a time frame of decades. Nevertheless, the magnitude of water quality impacts on the regional aquifer are quite low.

**Table 3-1.**
**Summary of Factors Influencing Contaminant Distributions in Groundwater at Los Alamos National Laboratory**

| Canyon | Presence of Contaminant Sources | Water Inputs | | Hydrogeologic Controls | | | Observed Contaminants in Groundwater | | |
|---|---|---|---|---|---|---|---|---|---|
| | | Natural | Anthropogenic | Enhanced Infiltration | Potential Lateral Pathways | Flow Field Modification | Alluvial | Intermediate | Regional Aquifer |
| Guaje | Minor dry sources | Low | None | Puye Formation exposed in canyon bottom | None | Near Guaje wellfield | None | No intermediate groundwater | None |
| Bayo | Previous sources removed; little present source | Low | Low | None, basalts not present in vadose zone | None, basalts not present in vadose zone | | No alluvial groundwater present | No intermediate groundwater present | None |
| Pueblo (including Acid Canyon) | Multiple, liquid sources | Low | High, POTW effluent-supported stream | Yes, associated with faults | No, basalts not present in vadose zone | O-1 located in Pueblo Canyon | Nitrate, boron, tritium (past); Strontium-90 | Tritium (TW-2A); nitrate (TW-1A) | Perchlorate (O-1), tritium (O-1, R-4), nitrate (TW-1, O-1, R-4) |
| Los Alamos (including DP) | Multiple liquid sources | Moderate | High, effluent discharges | Yes, Cerros del Rio basalt exposed in canyon bottom at R-9 | Yes, Cerros del Rio basalt present in vadose zone | O-4 located in Los Alamos Canyon | Strontium-90; molybde-num, tritium, plutonium-239, -240, -248 | Tritium (LADP-3, R-9i,R-6i); nitrate (R-6i) | Tritium (TW-3, R-9, R-6) |
| Sandia | Multiple liquid sources | Low | High, effluent discharges | Yes, Cerro Toledo Member exposed in canyon bottom near PM-1 | Yes, Cerros del Rios basalts within shallow vadose zone | PM-1 and PM-3 located in Sandia Canyon | Alluvial groundwater not present | Tritium (R-12, R-7), nitrate (R-12) | Tritium (R-12, R-11), nitrate (R-12, R-11) |

**Table 3-1.**
**Summary of Factors Influencing Contaminant Distributions in Groundwater at Los Alamos National Laboratory (continued)**

| Canyon | Presence of Contaminant Sources | Water Inputs | | Hydrogeologic Controls | | | Observed Contaminants in Groundwater | | |
|---|---|---|---|---|---|---|---|---|---|
| | | Natural | Anthropogenic | Enhanced Infiltration | Potential Lateral Pathways | Flow Field Modification | Alluvial | Intermediate | Regional Aquifer |
| Mortandad | Multiple liquid sources | Low | High, effluent discharges | Thick pockets of alluvium; sediment ponds | Extensive Cerros del Rio basalt in vadose zone | Within PM wellfield | Americium-241, plutonium-238, plutonium-239, -240, strontium-90, tritium, nitrate, perchlorate, fluoride | Tritium (MCOBT-4.4, R-15), nitrate (MCOBT-4.4), perchlorate (MCOBT-4.4, R-15) | Tritium (R-15, R-28), nitrate (R-15, R-28), perchlorate (R-15) |
| Canada del Buey | Major dry sources; minor liquid sources | None | None on LANL property; effluent from White Rock POTW | No, canyon bottom underlain by Bandelier Tuff | Extensive Cerros del Rio basalt close to surface | Within PM wellfield | Gross alpha, gross beta | No intermediate perched groundwater is present | None |
| Pajarito Canyon | Major dry sources | High | Moderate | Yes, Cerros del Rio basalt exposed at the surface from west of R-23 to Rio Grande | Yes, extensive Cerros del Rio basalt | Yes, within PM wellfield | Metals, radio-nuclides, HE, VOCs and anions | HE (springs) | None |
| Water | Multiple dry and liquid sources in upper part of canyon | High | High | Yes, Cerros del Rio basalt exposed in lower part of canyon | Yes, extensive Cerros del Rio basalts in lower canyon | None | HE, barium | | |

**Table 3-1.**
**Summary of Factors Influencing Contaminant Distributions in Groundwater at Los Alamos National Laboratory (continued)**

| Canyon | Presence of Contaminant Sources | Water Inputs | | Hydrogeologic Controls | | | Observed Contaminants in Groundwater | | |
|---|---|---|---|---|---|---|---|---|---|
| | | Natural | Anthropogenic | Enhanced Infiltration | Potential Lateral Pathways | Flow Field Modification | Alluvial | Intermediate | Regional Aquifer |
| Cañon de Valle | Multiple dry and liquid sources in upper part of canyon | High | High | No, underlain by thick Bandelier Tuff | Yes, Cerro Toledo interval in vadose zone | None | Barium, HE, perchlorate | HE, barium, | Tritium (R-25), HE(?) (R-25) |
| Potrillo/ Fence | Minor dry sources | Low | None | No, underlain by Bandelier Tuff | Yes, extensive Cerros del Rio basalt in vadose zone | None | No, alluvial groundwater not present | No, intermediate perched groundwater not present | None |
| Ancho | Minor dry and liquid sources | Low in upper portion; moderate in lower portion | Minor, septic systems | No, underlain by Bandelier Tuff | No | None | None | No, intermediate perched groundwater is not expected | HE(?) (Ancho Spring) |
| Chaquehui | Minor dry and liquid sources | Low in upper portion; moderate in lower portion | Low | Yes, basalts exposed at surface in canyon | Yes, extensive Cerros del Rio basalts present in vadose zone | None | No, alluvial groundwater not present | No, perched intermediate groundwater not expected | |
| Frijoles | No LANL sources | High | None | Yes, basalts exposed in canyon bottom | Yes, basalts in vadose zone | None | No data | No data | |
| White Rock | No LANL sources | High | Low | Yes, basalts exposed in canyon bottom | Yes, basalts in vadose zone | None | No alluvial groundwater present | No intermediate groundwater is present | Tritium, nitrate (Springs 1, 3, 3A, 4, 5); |

**Table 3-1.**
**Summary of Factors Influencing Contaminant Distributions in Groundwater at Los Alamos National Laboratory (continued)**

| Canyon | Presence of Contaminant Sources | Water Inputs | | Hydrogeologic Controls | | | Observed Contaminants in Groundwater | | |
|---|---|---|---|---|---|---|---|---|---|
| | | Natural | Anthropogenic | Enhanced Infiltration | Potential Lateral Pathways | Flow Field Modification | Alluvial | Intermediate | Regional Aquifer |
| | | | | | | | | | perchlorate, uranium (Spring 2B) |

### 3.2.1 Contaminant and Constituent Sources

Table 3-1 indicates the factors that have primary influence on distribution of anthropogenic constituents in groundwater. The first factor is the presence of upgradient sources of these constituents. The sources affecting groundwater at the Laboratory are mainly liquid effluents rather than solid waste disposal or other activities. Since the 1940s, liquid effluent disposal by the Laboratory has degraded water quality in the shallow perched groundwater that underlies a few canyons (Figure 3-12). Drainages that received significant radioactive effluent discharges are Mortandad Canyon and Pueblo Canyon from its tributary Acid Canyon, and Los Alamos Canyon from its tributary DP Canyon. Rogers (2001) and Emelity (1996) summarize radioactive effluent discharge history at the Laboratory. Water Canyon, its tributary Cañon de Valle, and Pajarito Canyon have received effluents produced by HE processing and experimentation (Glatzmaier 1993, Martin 1993, LANL, 1998a). Over the years, Los Alamos County has operated three sanitary treatment plants in Pueblo Canyon (LANL, 1981). Only the Bayo plant is currently operating. The Laboratory has also operated numerous sanitary wastewater treatment plants, as shown in Figure 3-12.

Solid waste disposal has less potential to affect groundwater. Most solid waste disposal sites are located on mesa tops where there is little natural or artificial percolation to carry anthropogenic constituents to groundwater. Canyons that have little or no source of anthropogenic constituents (Guaje, Bayo, Potrillo, Fence, Ancho, Chaquehui, and Frijoles) have no anthropogenic constituents in groundwater (Table 3-1). Canyons that had small volume liquid sources or major dry sources are Cañada del Buey and Pajarito Canyon (Table 3-1).

### 3.2.2 Water Inputs

The second factor influencing anthropogenic constituent distribution in groundwater shown on Table 3-1 is water input, either natural or anthropogenic. The amount of water in a canyon system is a determining factor for transporting anthropogenic constituents. In most cases where Laboratory anthropogenic constituents are found at depth, the setting is one of the following:

- canyons where natural water input is high (Pajarito Canyon, Water Canyon, and Cañon de Valle);
- canyons where anthropogenic water input is high (Pueblo, Los Alamos, Sandia, Mortandad Canyons); or
- mesa-top sites where large amounts of liquid effluent have been discharged (such as retention ponds or outfalls) (mesa tops bounded by Cañon de Valle and Water Canyon).

The presence of water, either natural or from the discharge of effluents to canyons or mesa-top locations in the Laboratory's semiarid setting initiates or increases downward percolation of water. Even under unsaturated flow conditions, this percolation may move significant volumes of water to the regional aquifer within a few decades.

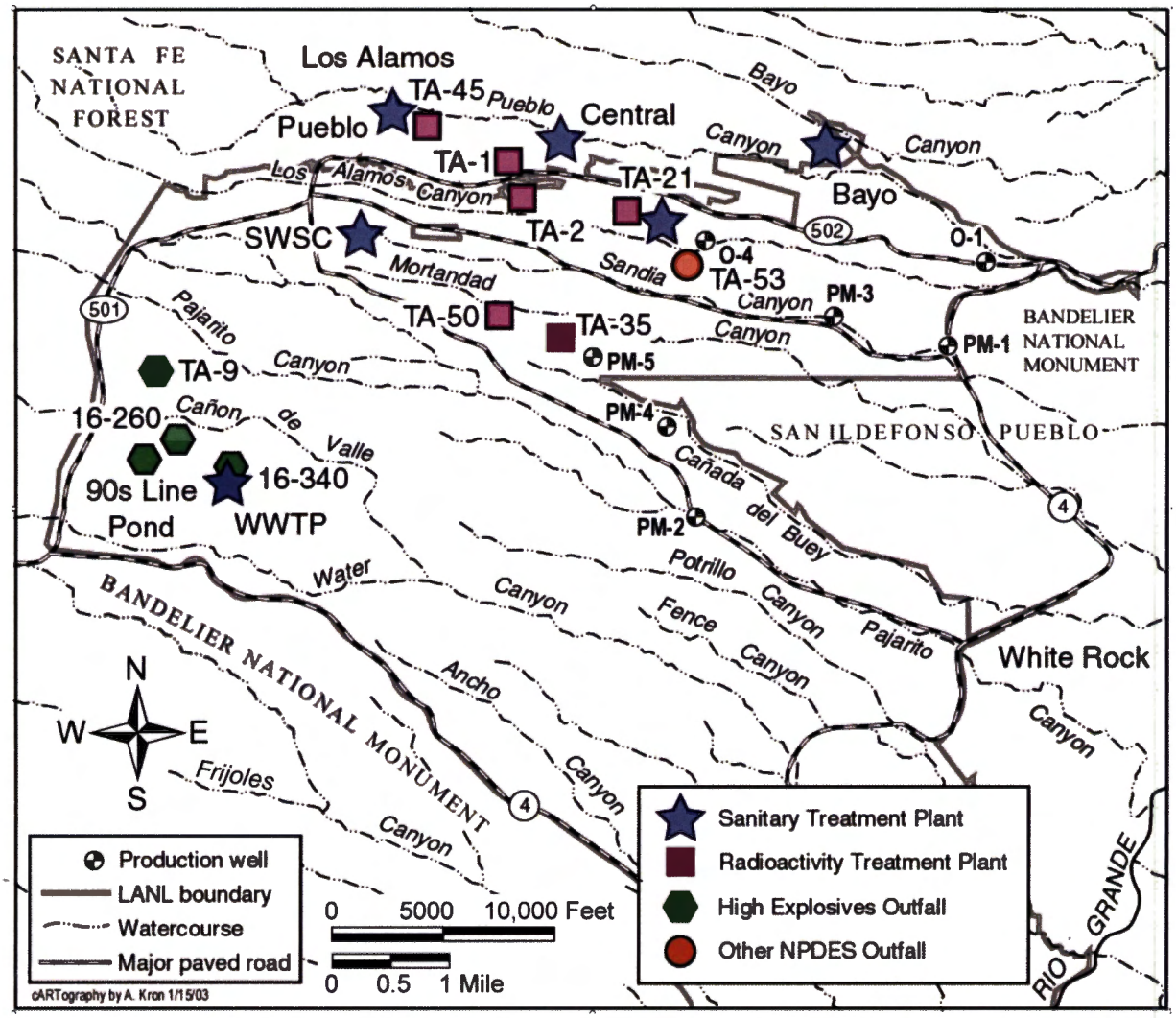


**Figure 3-12.** Major liquid release sources that have potentially affected groundwater at Los Alamos National Laboratory. Most of these sources are now inactive.

### 3.2.3 Hydrogeologic Controls

The third factor that contributes to anthropogenic constituent distribution consists of hydrogeologic controls on groundwater pathways and travel rates (Table 3-1). The controls considered most important in influencing contaminant distribution and transport are infiltration at the surface and transport of contaminants in alluvial groundwater, pathways in the vadose zone and transport through intermediate perched groundwater, and flow field modification in the regional aquifer.

The movement of groundwater contaminants is best seen through the distribution of conservative (that is, non-reactive) chemical species. Under most conditions, compounds like RDX, tritium, perchlorate, and nitrate move readily with the groundwater. In many settings, chemical reactions do not retard the movement of these compounds or decrease their concentrations, although the

activity of tritium does decrease due to radioactive decay. For some compounds or constituents (uranium, strontium-90, barium, some HE compounds, and solvents) movement is slowed or their concentrations are decreased by adsorption or cation exchange, precipitation or dissolution, chemical reactions like oxidation/reduction, or radioactive decay. Other constituents (americium-241, plutonium, and cesium-137) are nearly immobile because they are strongly adsorbed onto sediment particles.

#### 3.2.3.1 Infiltration Rate and Transport in Alluvial Groundwater

The first hydrogeologic control, infiltration rate, affects the movement of anthropogenic constituents from the surface to groundwater. As described in Section 2.5.3, undisturbed Bandelier Tuff has a very low infiltration rate. Areas that have other geologic units (particularly basalt units) exposed in the canyon bottom have higher, or enhanced, infiltration rates. Anthropogenic alterations can also enhance infiltration, for example sediment ponds in Mortandad Canyon and ponds in the Cañon de Valle watershed.

The alluvial groundwater present in several canyons has a small volume relative to the annual volume of runoff or effluents, does not extend beyond the LANL boundary, and is generally completely refreshed by recharge on a time scale of about a year (Section 2.4.1). This rapid turnover of groundwater volume means that, rather than increasing over time, the groundwater concentrations of conservative compounds are controlled by concentrations in recharge sources such as effluent. The principal compounds that accumulate or persist in alluvial groundwater are those, such as strontium-90, that are not highly mobile. Strontium-90 has accumulated mainly in the canyon floor sediments, from which it slowly but continually leaches into the groundwater due to cation exchange, maintaining a nearly steady concentration. In some cases, such as RDV in Cañon de Valle, mobile contaminants also persist, possibly due to their continuing presence in water source regions.

A study by Purtymun et al. (1977) documented this rapid turnover of groundwater and solutes in Mortandad Canyon. Purtymun showed that the mass of various solutes in Mortandad Canyon alluvial groundwater was a fraction of the total solute mass that had been discharged into the canyon over the history of effluent releases. To a first approximation, the entire body of alluvial groundwater in Mortandad Canyon is chemically well mixed, and variations in concentrations of specific sources propagate throughout the groundwater system in times of about a year. Concentrations are at times higher for wells nearest to the outfall, partly because of variable mixing of effluent with ground and surface water. Concentrations appear to decrease downstream from the outfall due to mixing and the occasional higher values in upstream wells. While concentrations vary between wells, overall concentrations of the constituents are generally similar throughout the alluvial groundwater body at a given time.

Rather than a contaminant plume existing within the alluvial groundwater, a relatively small volume of groundwater (with a volume of about 20,000 cubic meters) is completely replenished annually by recharge water (with a volume of about 90,000 to 160,000 cubic meters) which includes the discharges from RLWTF at TA-50. Purtymun et al. (1977) attributed the losses of water to evapotranspiration and infiltration into the underlying tuff. The composition of the alluvial groundwater is a combination of input from the TA-50 facility and other sources such as

runoff and other Laboratory discharges. The groundwater composition nearest the TA-50 discharge point shows short term (weekly or daily) variations related to the TA-50 outfall, but over the longer term (annually), these variations are spread throughout the alluvial groundwater body.

Data for conservative constituents (tritium, nitrate) in alluvial groundwater support the conceptual model that this groundwater has a short residence time and conservative contaminants do not accumulate in alluvial groundwater. The time trend pattern for these contaminants shows a high level when they were being released, followed by a sharp decline in concentration to nearly nondetectable levels when the source is eliminated. Past values of tritium and nitrate in alluvial groundwater in DP, Los Alamos, Pueblo, and Mortandad Canyons exceeded the 20,000 pCi/L MCL (Rogers 1998). Such high values do not occur today in these locations because of improvement in effluent quality, and also possibly because of deeper infiltration of older effluents.

In Pueblo Canyon, tritium activity in alluvial groundwater was 15,000 pCi/L in the early 1970s, nearly a decade after effluent discharges ceased; today it is barely detectable (Figure 3-13). Similarly, alluvial groundwater tritium values in DP and Los Alamos Canyons exceeded 300,000 pCi/L in the late 1960s, but have been barely detectable for the past decade (Figure 3-14). TA-21 effluent caused tritium levels in surface water and alluvial groundwater in and downstream of DP Canyon to reach values up to 5,000,000 pCi/L, or 250 times the MCL (Figure 3-14, Figure 3-15). The tritium levels decreased greatly after discharges ceased. In Los Alamos Canyon above the mouth of DP Canyon, the Omega West Reactor cooling line leaked water containing tritium from 1956 to 1993. As a result of this leak, tritium activity in alluvial groundwater remained at values around 10,000 pCi/L or half of the MCL. Once the leak was discovered and shut off, tritium levels in Los Alamos Canyon water returned to background. In Mortandad Canyon alluvial groundwater tritium activities often exceeded 300,000 pCi/L and even reached 2,000,000 pCi/L, but have fallen below the MCL since the RLWTF adopted effluent limits in 2001 (Figure 3-15, Figure 3-16). At the end of 2000, the RLWTF adopted a voluntary goal of having tritium activity in its effluent below 20,000 pCi/L, and tritium activity in the effluent dropped below that in 2001 and was 10,400 pCi/L in 2003. Tritium activity in alluvial groundwater downgradient of the facility has dropped correspondingly, with a maximum value of 8,770 pCi/L in 2003.

Nitrate levels in Pueblo Canyon surface water and groundwater follow a strong downward trend similar to those for tritium. Nitrate has been discharged from Laboratory radioactive liquid waste effluents and Los Alamos County sanitary wastewater effluent (Figure 3-17, Figure 3-18). The highest values were found in surface water in the 1950s and 1960s, related to both types of sources. With decommissioning of the radioactive outfall in 1964 and moving the sanitary discharge downstream to the Bayo treatment plant, less water and less nitrate have been present in the upper portion of the drainage in recent years. Nitrate in discharges into DP Canyon from TA-21 caused surface water and alluvial groundwater concentrations to exceed 100 mg/L (nitrate as nitrogen), or 10 times the MCL, until discharges ceased in 1986 (Figure 3-18, Figure 3-19). Nitrate concentrations have returned to background since discharges ended. In Mortandad Canyon nitrate (as N) concentrations in alluvial groundwater have generally mirrored the concentration in RLWTF effluent (Figure 3-18, Figure 3-20). The nitrate concentration in the

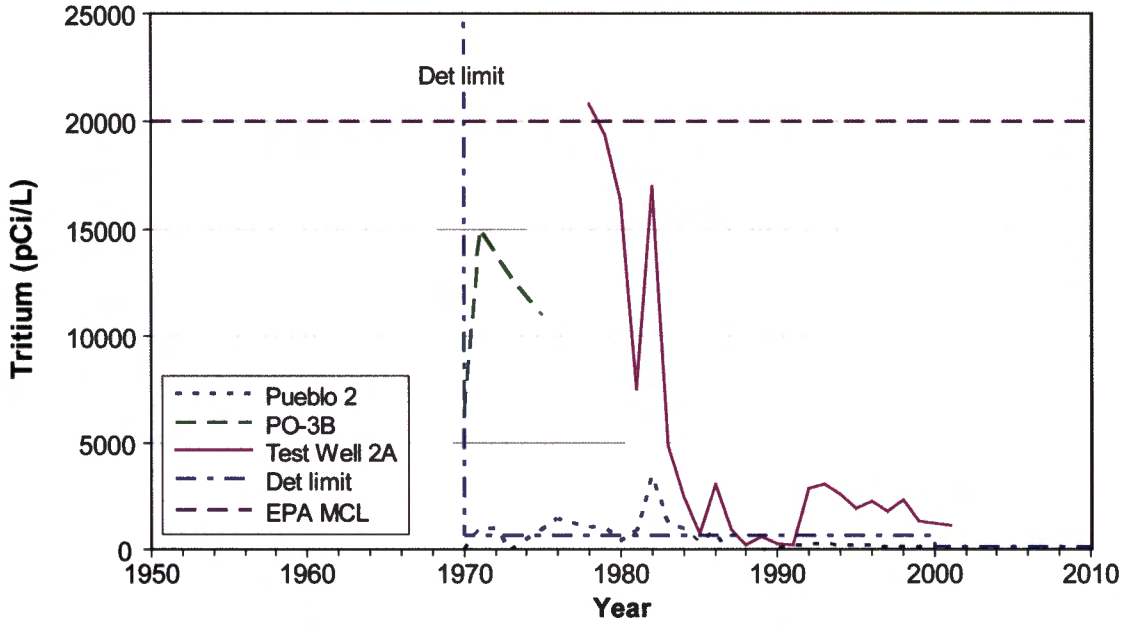


**Figure 3-13.** Tritium histories in Pueblo Canyon surface water and alluvial and intermediate groundwater zones. Data are annual averages of all results including nondetects; note that detection limits have varied greatly through time.

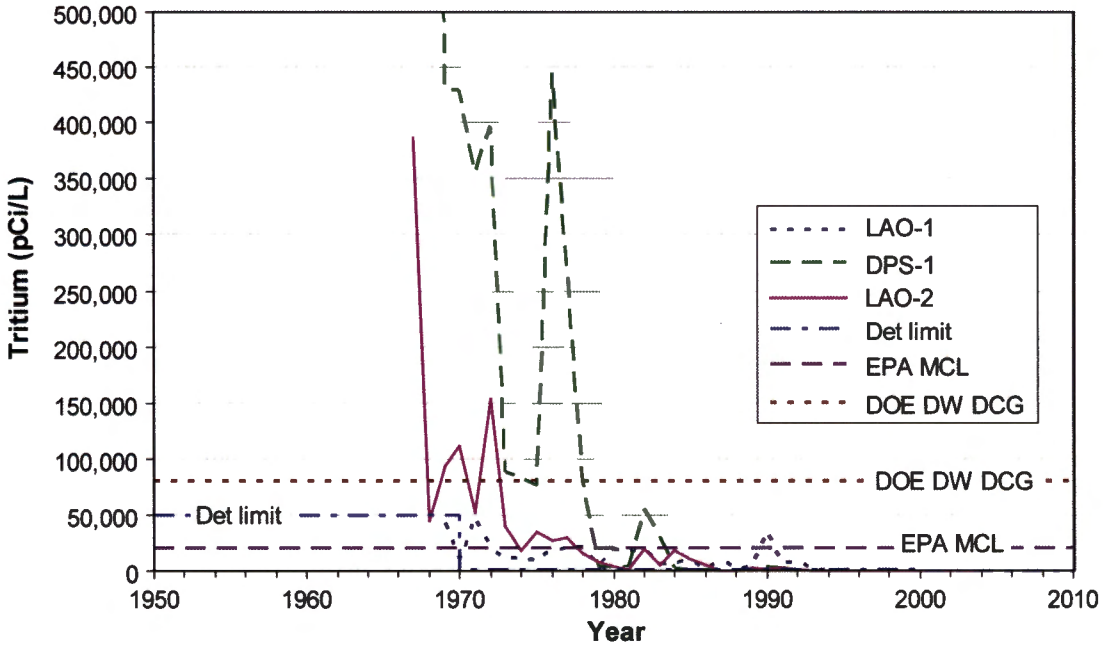


**Figure 3-14.** Tritium histories in DP and Los Alamos Canyon surface water and alluvial groundwater. Data are annual averages of all results including nondetects; note that detection limits have varied greatly through time.

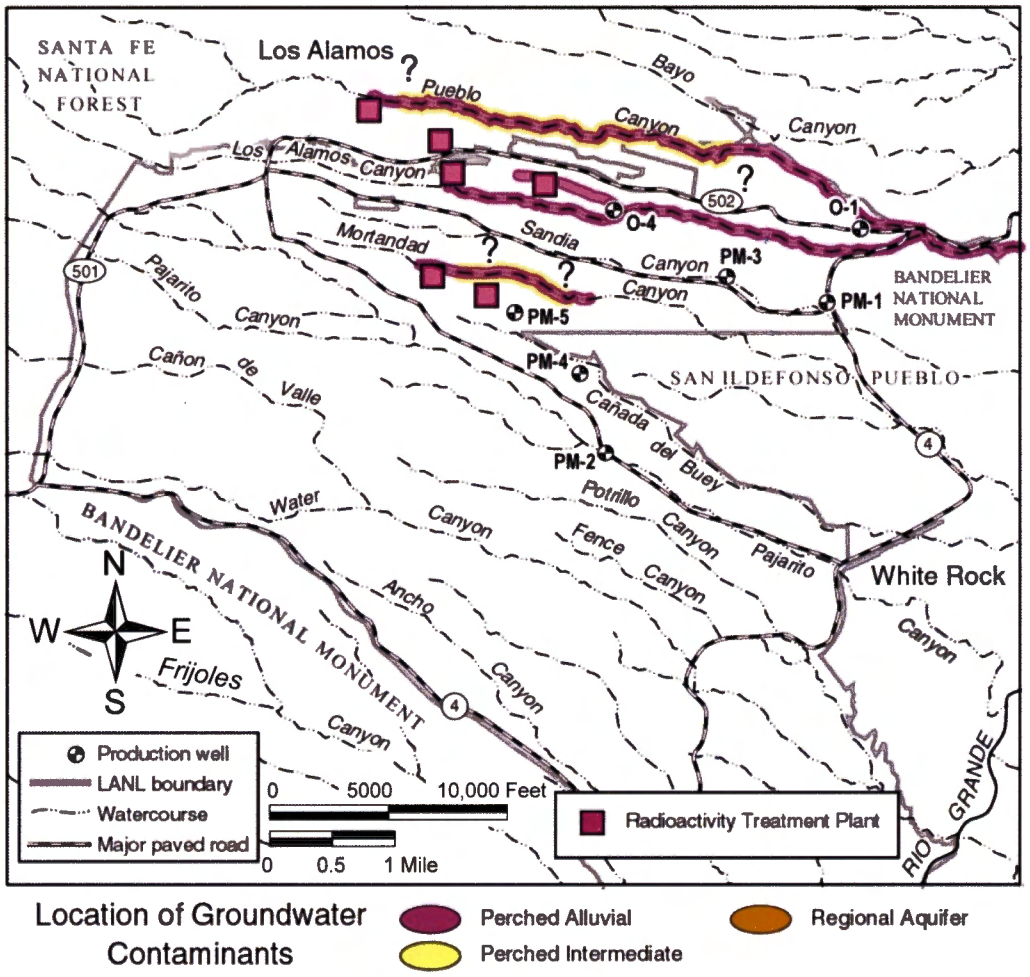


**Figure 3-15.** Location of inferred past extent of groundwater contamination by tritium above the 20,000 pCi/L EPA MCL. No groundwater tritium exceeded this value in 2003. Different colors indicate the affected groundwater zones. The extent of intermediate groundwater and regional aquifer contamination is based on a limited number of wells; question marks on the maps indicate where contaminant extent is inferred, not necessarily substantiated.

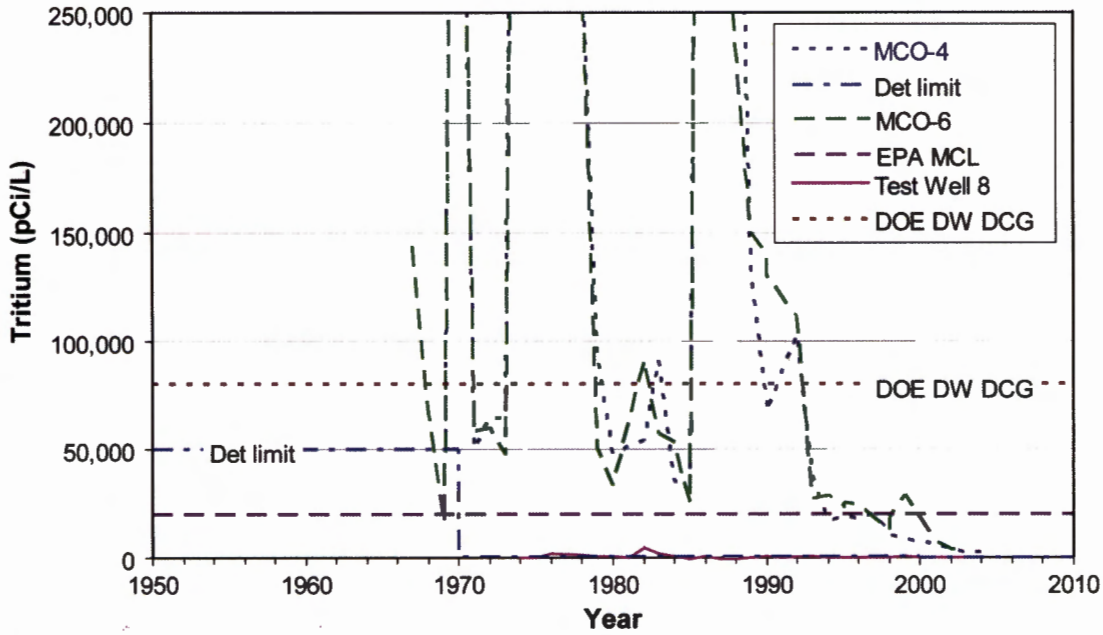


**Figure 3-16.** Tritium histories in Mortandad Canyon alluvial groundwater and the regional aquifer. Data are annual averages of all results including nondetects; note that detection limits have varied greatly through time.

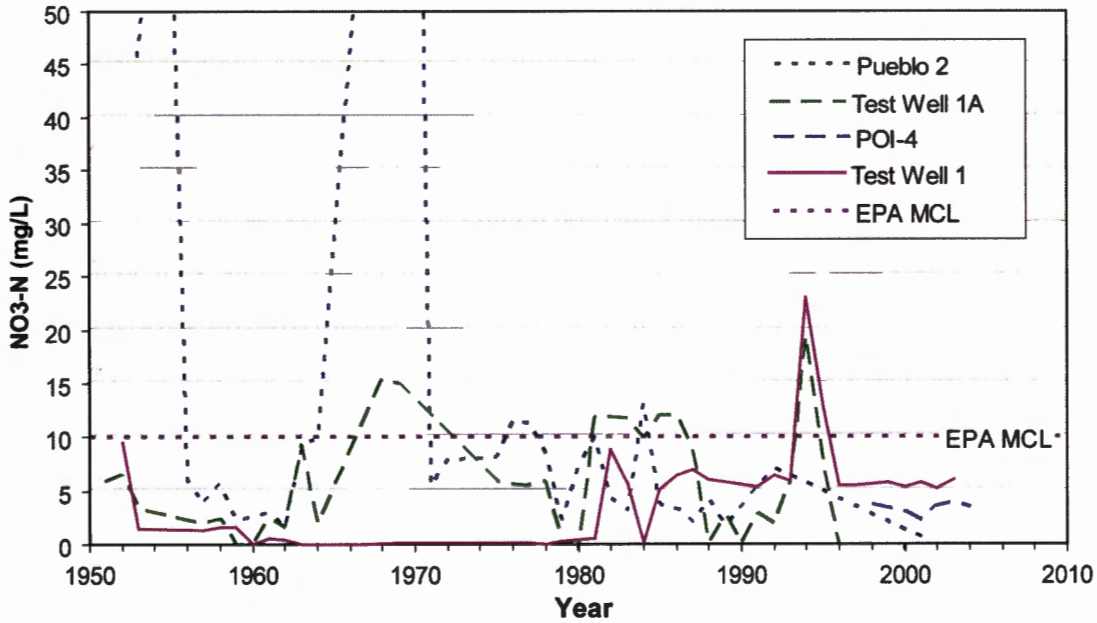


**Figure 3-17.** Nitrate histories in Pueblo Canyon surface water, alluvial and intermediate groundwater zones, and the regional aquifer. Data are annual averages of all results.

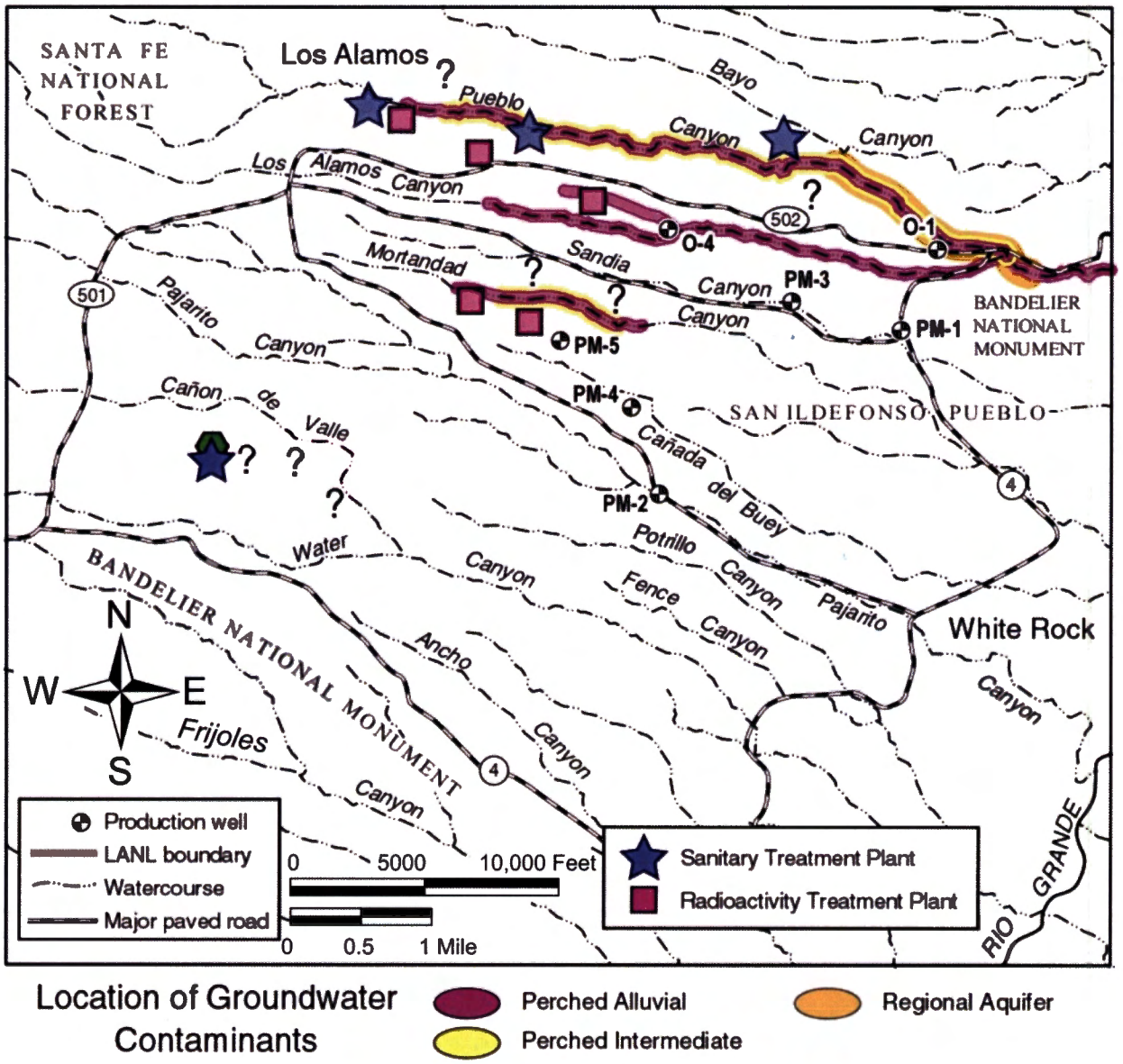


**Figure 3-18.** Location of inferred past extent of groundwater contamination by nitrate (as nitrogen) above the 10 mg/L EPA MCL. Only intermediate perched groundwater in Mortandad Canyon exceeded this level in recent years. Different colors indicate the affected groundwater zones. Along canyons, the extent of alluvial groundwater contamination lateral to the canyon is not to scale: contamination is confined to the alluvium within the canyon bottom and is narrow at the map scale. The extent of intermediate groundwater and regional aquifer contamination is based on a limited number of wells; question marks on the maps indicate where contaminant extent is inferred, not necessarily substantiated.

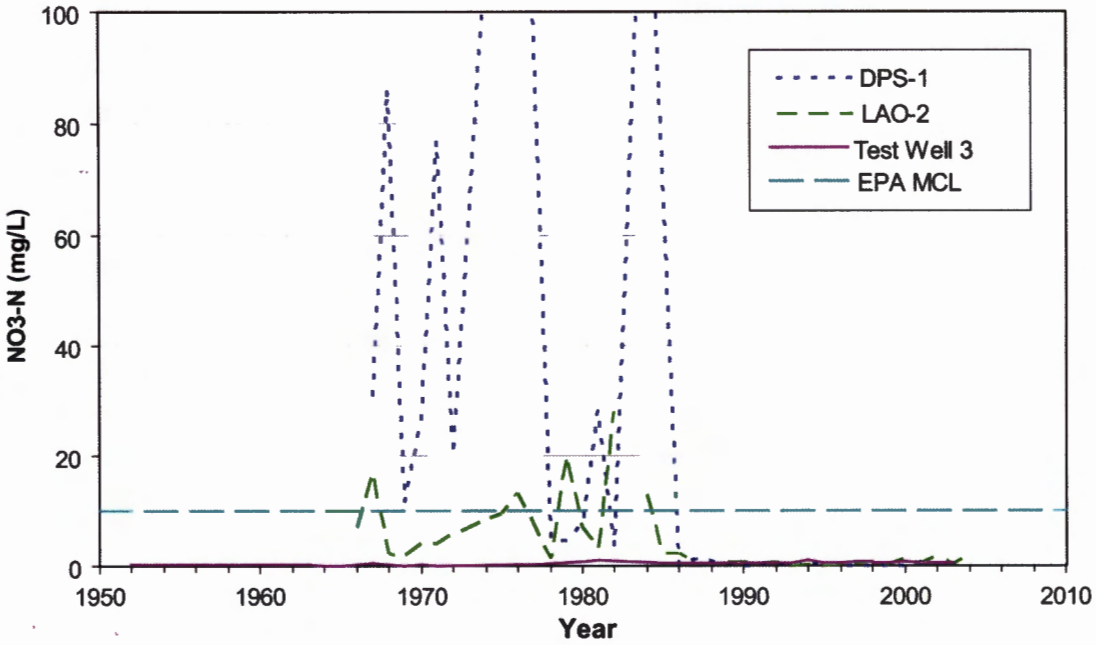


**Figure 3-19.** Nitrate histories in DP and Los Alamos Canyon surface water, alluvial groundwater, and the regional aquifer. Data are annual averages of all results.

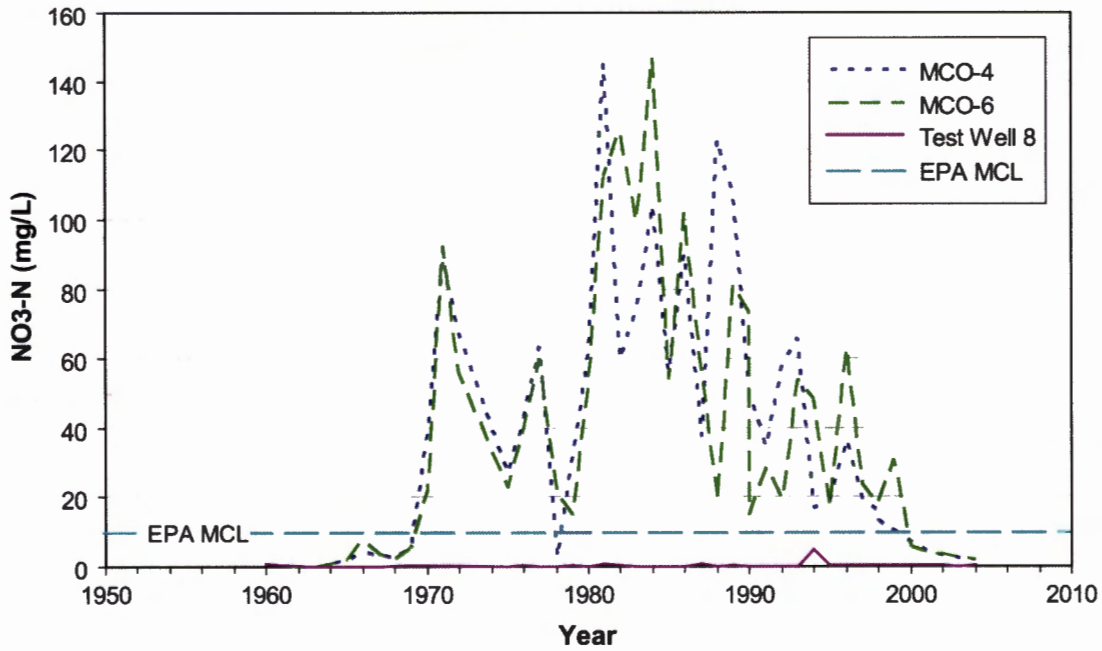


**Figure 3-20.** Nitrate histories in Mortandad Canyon alluvial groundwater and the regional aquifer. Data are annual averages of all results.

effluent decreased in 1999 due to improved treatment in the RLWTF, and alluvial groundwater concentrations have fallen below the New Mexico Groundwater Standard of 10 mg/L as a result.

The distribution of perchlorate indicates where effluent releases have occurred in canyons (Figure 3-21). Perchlorate history in Mortandad Canyon shows the rapid decrease in perchlorate after the source was eliminated (Figure 3-22). The perchlorate concentration in the effluent decreased in 2002 due to improved treatment in the RLWTF, and alluvial groundwater concentrations have fallen significantly as a result.

Data for adsorbing constituents (strontium-90, plutonium-239, -240) support the conceptual model of contaminant adsorption onto alluvial sediments. The adsorbing contaminants decline in concentration when the source is cut off, followed by maintenance of a fairly constant low concentration in the groundwater due to cation exchange. The highest measured strontium-90 activity was about 500 pCi/L in Acid Canyon surface water in 1960. With no present source, levels have dropped dramatically and strontium-90 is now seen only at low activities, below 1 pCi/L in alluvial groundwater (Figure 3-23).

In Los Alamos Canyon is strontium-90 contamination in surface water and alluvial groundwater derived from reactor sources at TA-2 and effluent discharges from TA-21 (Figure 3-24). The strontium-90 activity in DP Canyon surface water reached 28,600 pCi/L. There is no present source, and activities dropped greatly after discharges ceased. However, strontium-90 persists in alluvial groundwater at levels above the EPA MCL of 8 pCi/L due to the large inventory in alluvial sediment, which moves to the groundwater by cation exchange (Figure 3-24). Effects of Manhattan Project releases in upper Los Alamos Canyon cause plutonium-239, -240 activity in alluvial groundwater to remain at about 25% of the DOE 4 mrem drinking water derived concentration guide (DCG) of 1.2 pCi/L (Figure 3-25). Discharges from TA-21 resulted in plutonium-239, -240 activity in surface water much above the DOE 4 mrem DCG, even exceeding the 100 mrem DCG of 30 pCi/L in the late 1960s. Plutonium activity decreased substantially with the end of discharges in 1986, but is still occasionally detected in surface water and alluvial groundwater below the former outfall. In Mortandad Canyon the discharge from the RLWTF creates a localized area of alluvial groundwater where strontium-90 persists at levels above the 8-pCi/L EPA drinking-water MCL (Figure 3-26). The radionuclides plutonium-238; plutonium-239, -240; and americium-241 are also present above the 4-mrem DOE DCG for drinking water (Figure 3-27).

#### 3.2.3.2 Vadose Zone Pathways and Transport in Intermediate Groundwater

A hydrogeologic control on movement of anthropogenic constituents through the vadose zone is the presence of geologic units that can act as pathways. In general, these are units that are conducive to perching groundwater and forming intermediate perched groundwater. The water quality impacts from effluent releases extend in a few cases to intermediate perched groundwater at depths of a few hundred feet beneath these canyons. Because the contaminated alluvial groundwater bodies are separated from the intermediate perched groundwater by hundreds of feet of dry rock, pathways within the vadose zone are likely present in those canyons.

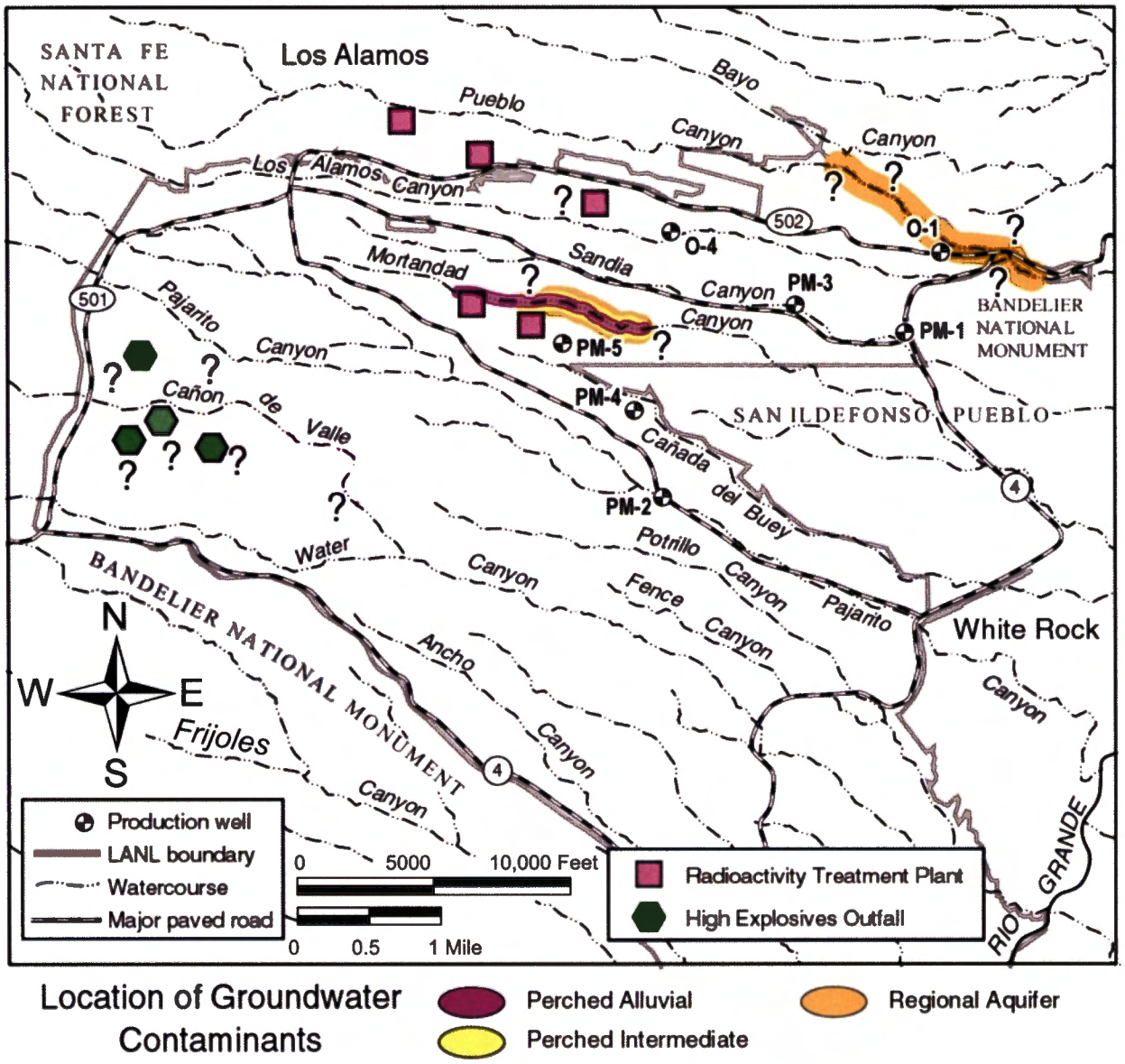


**Figure 3-21.** Location of groundwater contamination by perchlorate above the 3.7 ppb EPA Region VI risk level. Different colors indicate the affected groundwater zones. The extent of intermediate groundwater and regional aquifer contamination is based on a limited number of wells: question marks on the maps indicate where contaminant extent is inferred, not necessarily substantiated.

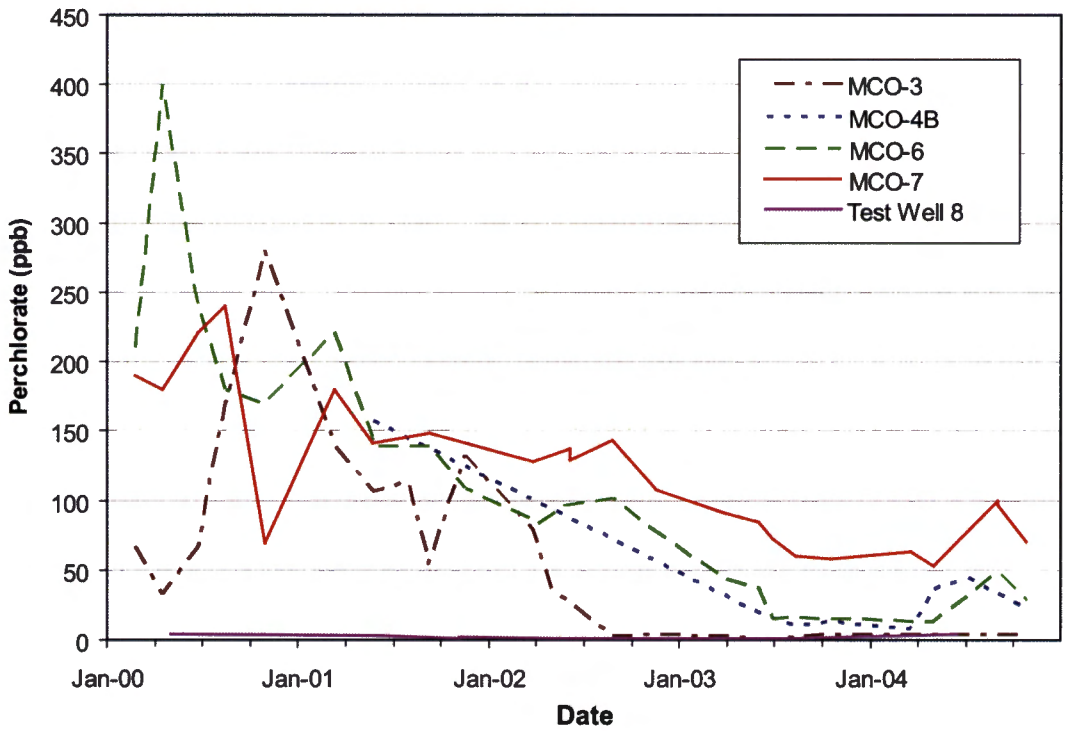


**Figure 3-22.** Perchlorate histories in Mortandad Canyon alluvial groundwater. All data points are shown.

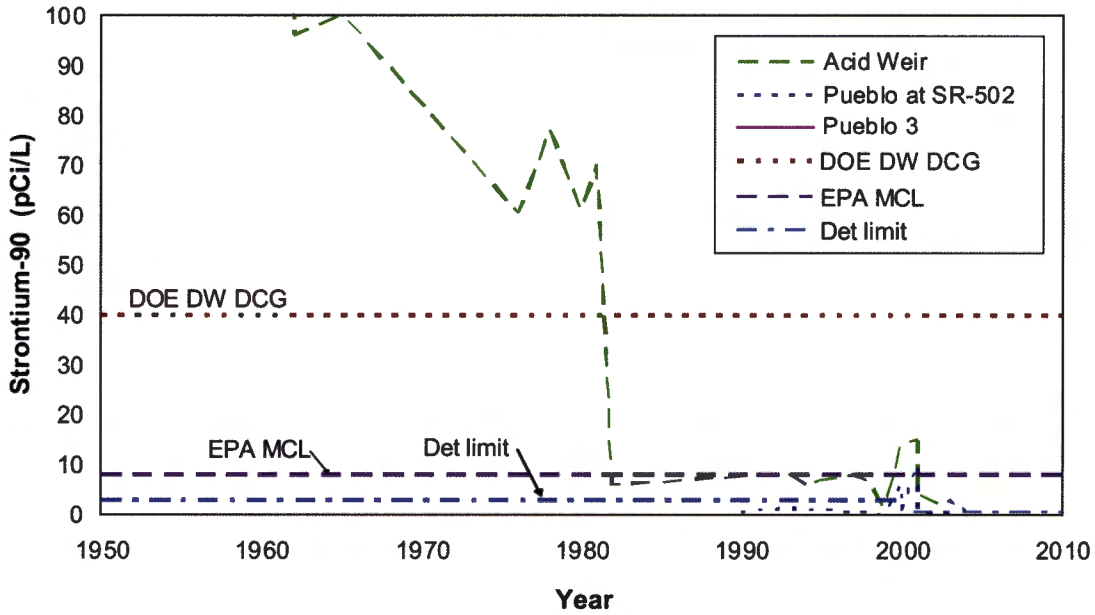


**Figure 3-23.** Strontium-90 histories in Acid and Pueblo Canyon surface water. The surface water data incorporate the longest record of strontium-90 and the highest values in these canyons; few strontium-90 detections have occurred in groundwater in these canyons. Data are annual averages of all results including nondetects; note that detection limits have varied greatly through time.

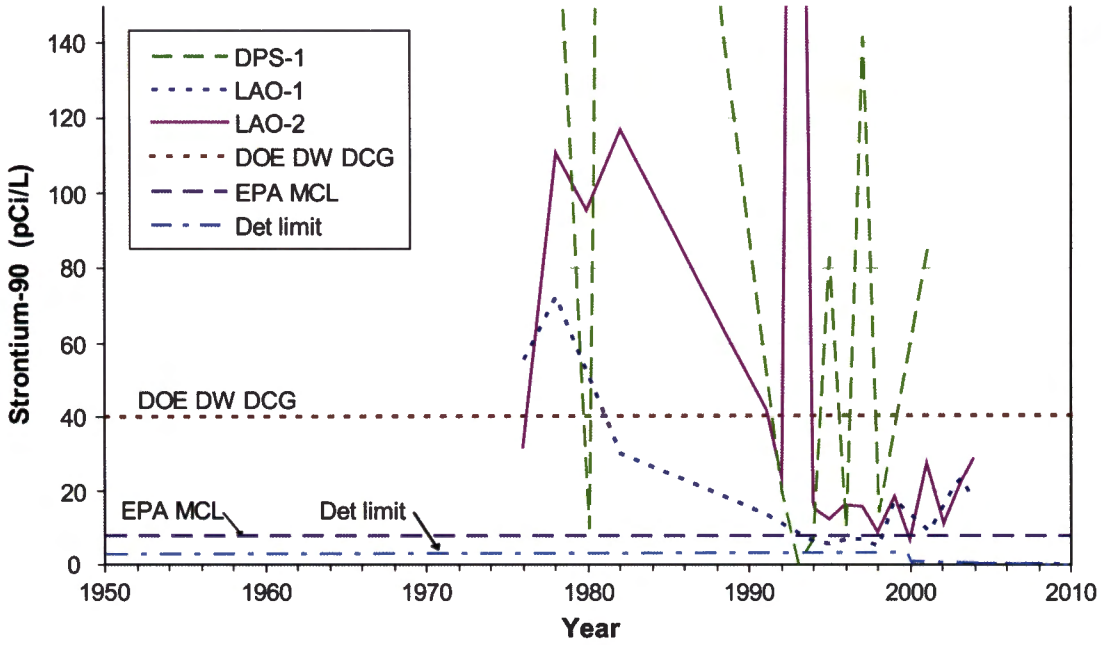


**Figure 3-24.** Strontium-90 histories in DP and Los Alamos Canyon surface water and alluvial groundwater. Data are annual averages of all results including nondetects; note that detection limits have varied greatly through time.

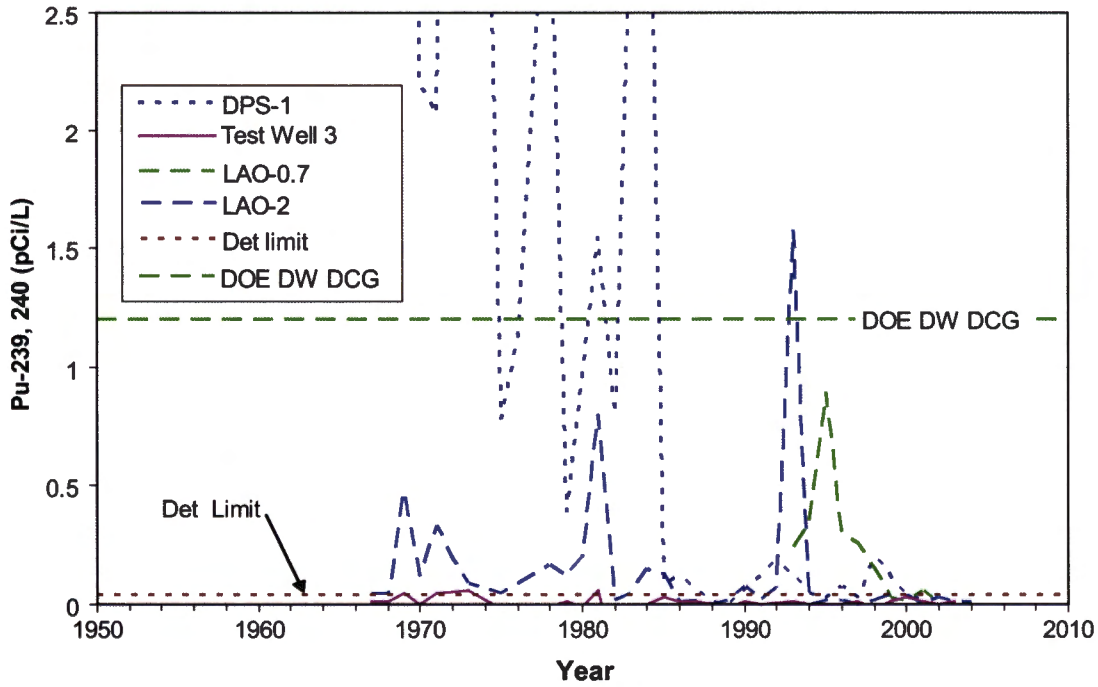


**Figure 3-25.** Plutonium-239, -240 histories in DP and Los Alamos Canyon surface water, alluvial groundwater, and the regional aquifer. Data are annual averages of all results including nondetects; note that detection limits have varied greatly through time.

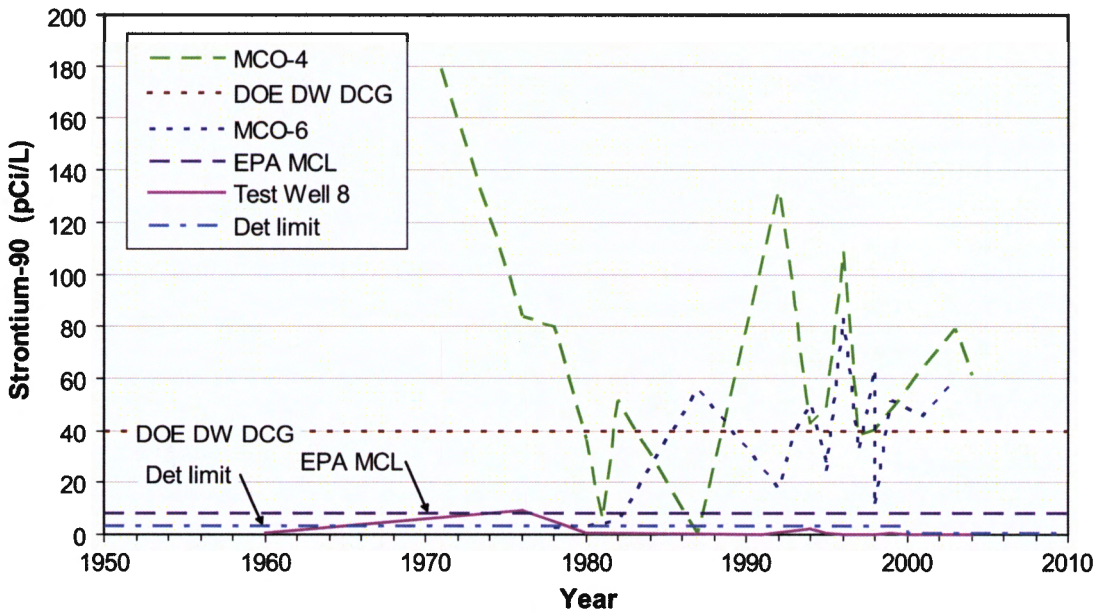


**Figure 3-26.** Strontium-90 histories in Mortandad Canyon alluvial groundwater and the regional aquifer. Data are annual averages of all results including nondetects; note that detection limits have varied greatly through time.

In Mortandad Canyon, Purtymun et al. (1977) estimated that, on average, about 15% of the surface water and shallow alluvial groundwater was lost to evapotranspiration. Because surface water or alluvial groundwater rarely flows beyond the Laboratory boundary, the remaining 85% of the water that enters the canyon must be lost by infiltration into the underlying tuff. Core profiles (Longmire 2001a) indicate a significant inventory of perchlorate and nitrate within the 400 ft of unsaturated Bandelier Tuff underlying the canyon floor.

Concentrations of contaminants such as nitrate, perchlorate, and tritium in Mortandad Canyon intermediate perched groundwater lie between current and past values in the alluvial groundwater. This banded range of observed concentrations suggests that the alluvial groundwater is a significant source of recharge to the intermediate groundwater; that this recharge requires on the order of decades; and that the solutes in the infiltrating water may be diluted by uncontaminated water already in the vadose zone or in the intermediate perched zone.

Low-level tritium data in intermediate perched groundwater support the conceptual model that alluvial groundwater affected by effluent discharges is a principal source of recharge and contaminants for the intermediate perched groundwater (Figure 3-28). The highest values are found where effluent discharges have occurred, but are much lower than values observed in alluvial groundwater. The lower values may be due to mixing of recharge with other groundwater sources as well as radioactive decay due to recharge time of decades. Higher-than-background tritium values occur in

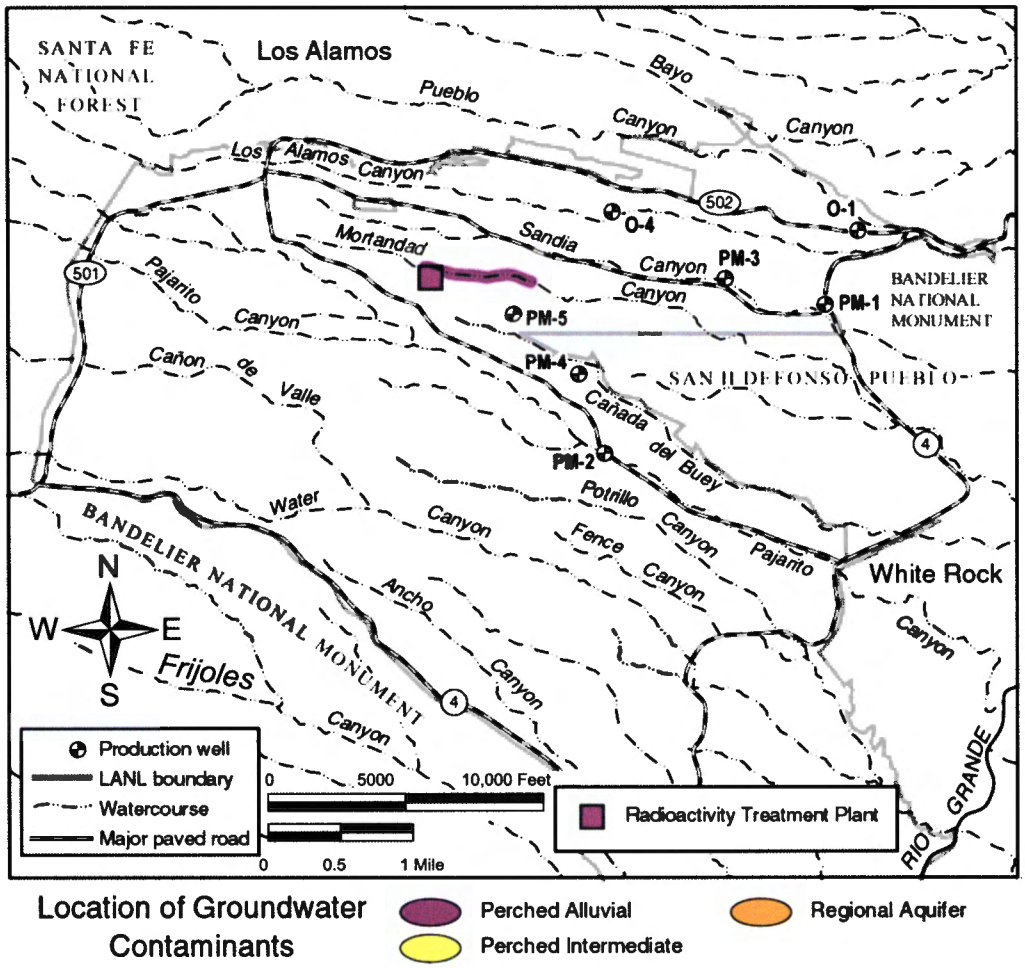


**Figure 3-27.** Location of groundwater contamination by plutonium-238; plutonium-239, -240; and americium-241 above the 4-mrem DOE DCG for drinking water. The 2003 maximum values in Mortandad Canyon alluvial groundwater for plutonium-238; plutonium-239, -240; and americium-241 were 1.4, 1.3, and 1.4 times the 4-mrem limit, respectively. Different colors indicate the affected groundwater zones.

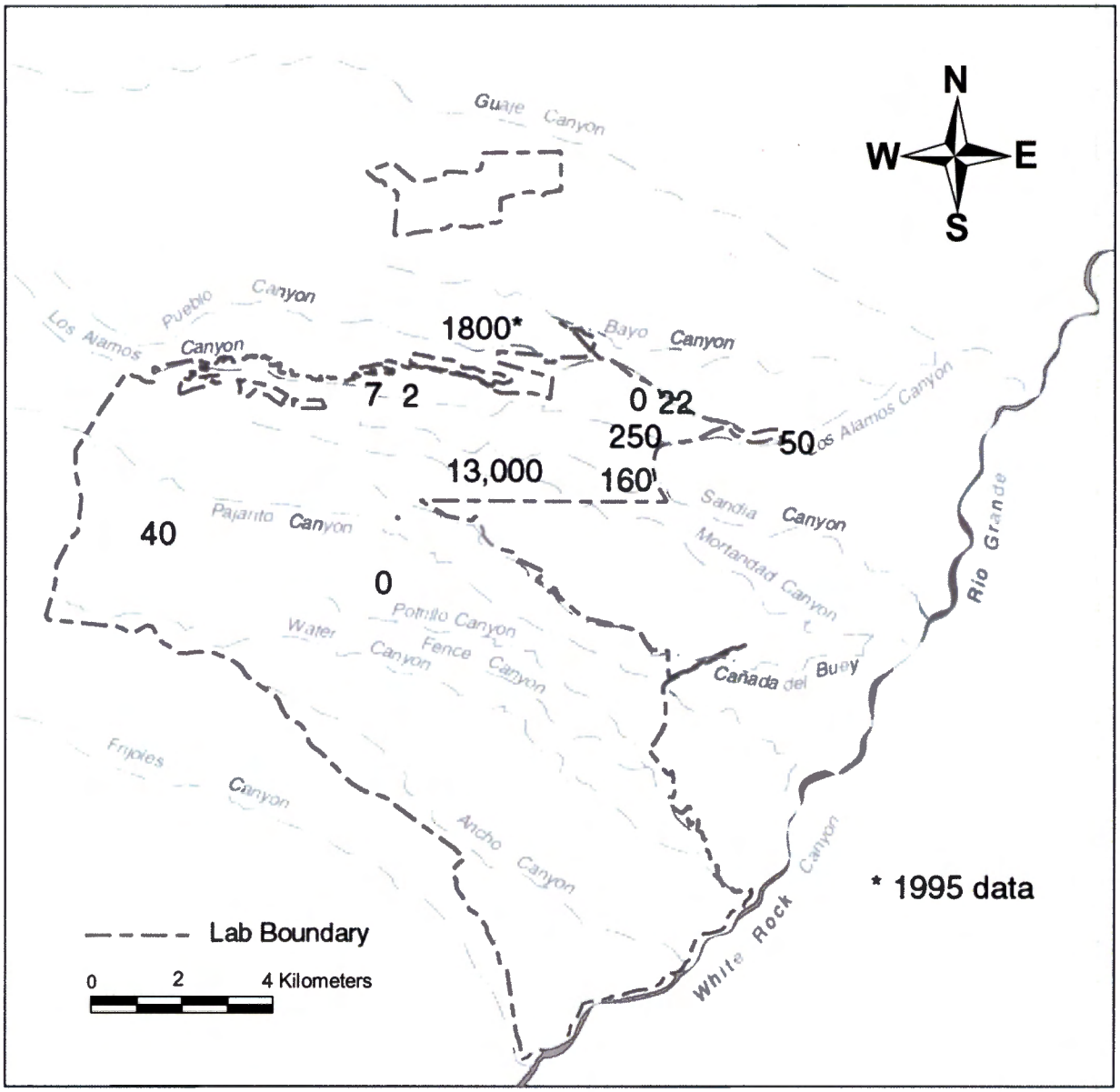


**Figure 3-28.** Low-detection-limit tritium data from wells and springs sampling intermediate perched groundwater. Data are mainly from 2002 to 2004 and do not include borehole data. The highest values occur where effluent discharges have occurred.

- R-25 near the 260 outfall and other discharges in TA-16,
- below the former TA-45 discharge in Pueblo Canyon,
- downstream from the Omega West reactor site and TA-21 discharges in Los Alamos Canyon, and
- below the sanitary effluent discharge site in Sandia Canyon, and the RLWTF in Mortandad Canyon.

Tritium time-series data also support a conceptual model that groundwater in the intermediate perched zones may have short residence times. Following cessation on effluent discharge from TA-45 into Acid Canyon in 1964, tritium in the intermediate perched zone sampled by TW-2A fell rapidly during the 1980s (Figure 3-13). Analysis of water samples from TW-2A show that this perched zone continues to contain elevated activities of tritium (2,228 pCi/L). This suggests that tritium associated with the former TA-45 treatment plant has infiltrated the canyon floor and migrated vertically, at least to the depth of the intermediate perched zone at TW-2A. Elsewhere in intermediate perched groundwater tritium has been detected mainly at trace levels (Figure 3-13). Although these incomplete data sets begin 15 years after discharges ceased, they support the conceptual model of short groundwater residence time.

In LADP-3 in Los Alamos Canyon, tritium activities fell rapidly over the decade after the Omega West reactor cooling line leak was stopped. Tritium was initially found in LADP-3 at 5500 pCi/L (Broxton et al. 1995) but activity has declined greatly since then, related to cessation of the Omega West reactor cooling line leak in 1993. Tritium in the two intermediate perched zones at R-9i was about 233 pCi/L at 180 ft and 110 pCi/L at 275 ft.

#### 3.2.3.3 Flow Field Modification and Transport in Regional Aquifer Groundwater

Relatively little contamination reaches the regional aquifer from the alluvial groundwater bodies, and water quality impacts on the regional aquifer, though present, are low. The last hydrogeologic control, flow field modification, is considered important in controlling anthropogenic constituent distribution in the regional aquifer. Anthropogenic constituents that enter the regional aquifer near pumping wells are predicted to have much travel times than those outside the influence of pumping (Section 4).

The distribution of tritium in the regional aquifer supports the conceptual model that surface effluent discharges are the source of Laboratory contaminants at depth (Figure 3-29). The map shows low-level tritium values from 2002-2004 and includes springs and wells.

In most cases, the highest regional aquifer tritium values are found near where effluent discharges have occurred, but are much lower than values observed in overlying alluvial or intermediate perched groundwater. The lower regional aquifer values may be due to dilution of recharge by other groundwater sources as well as radioactive decay due to recharge times of decades. The locations of the highest values in Figure 3-29 are near the recharge sources described in Appendix 3-A, with two additional locations that have high tritium values. One is at R-22 near MDA G, which may be due to past tritium disposal at that site. The second is at

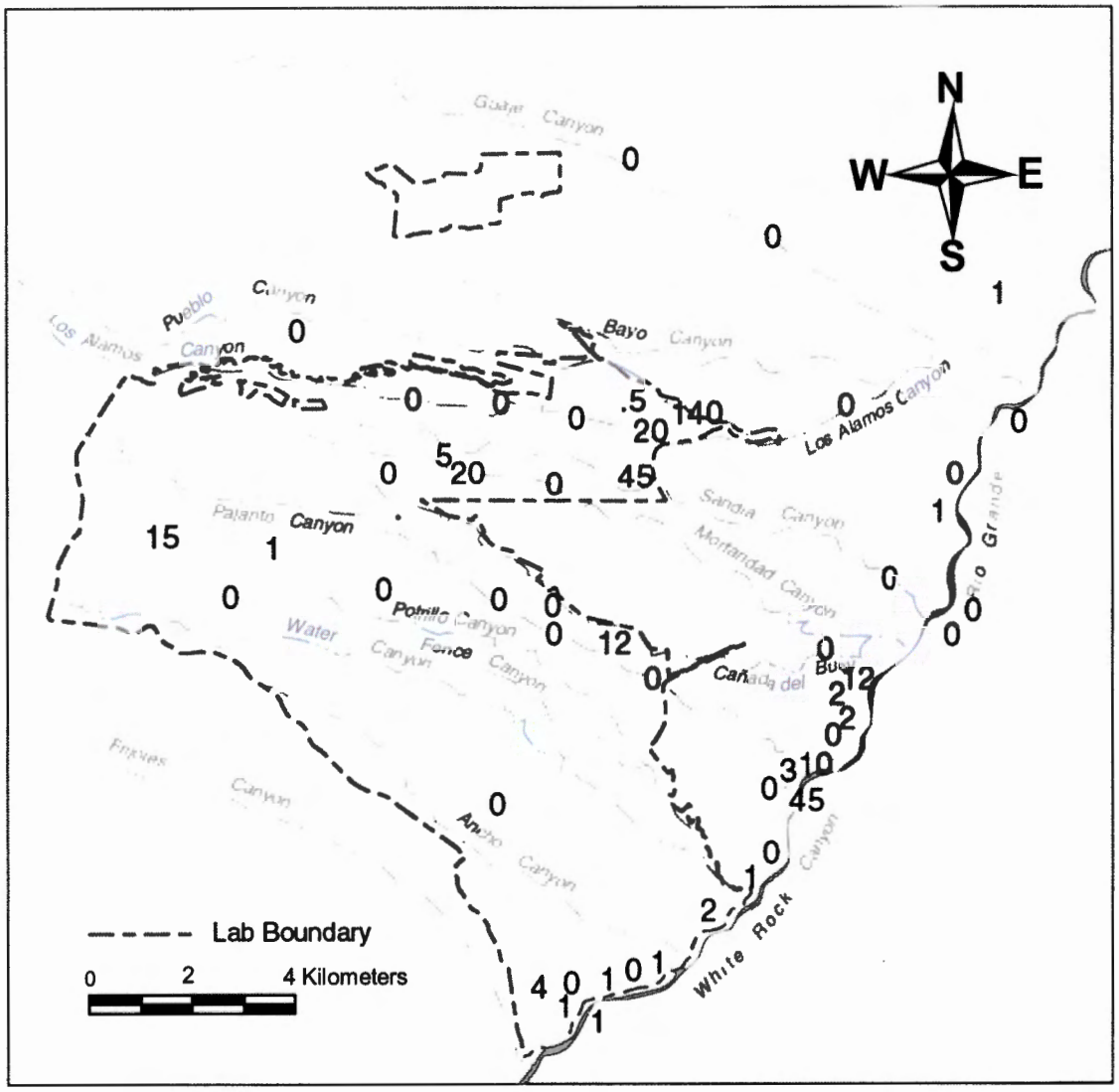


**Figure 3-29.** Low-detection-limit tritium data from wells and springs sampling the regional aquifer. Data are from 2002 to 2004 and do not include borehole data. The highest values occur where effluent discharges have occurred.

Spring 4B. The values, in the range of 45 pCi/L, are similar to data from rainfall and the Rio Grande and may be due to a component of surface water in the spring sample (LANL 2004b).

### 3.2.4 Off-Site Transport

Anthropogenic constituents that reach the regional aquifer will be transported along flow paths that will extend either to pumping wells or to the Rio Grande, the discharge area for the regional aquifer in the Española Basin (Section 2). The travel times along the natural flow paths are quite long (tens of thousands of years), but can be shorter for flow paths leading to pumping wells (Section 4).

As discussed in Section 3.2.1, the most mobile contaminants would be the first to appear in any of the regional aquifer discharge points. Appendix 3-A contains descriptions of canyons and the constituents that have been detected in the regional aquifer. Highly mobile groundwater contaminants including chloride, nitrate, perchlorate, and tritium have migrated into the regional aquifer near LANL. Monitoring data suggest that these constituents may also be discharging in some White Rock Canyon springs. Nitrate, chloride, and sulfate have increased gradually during the past 20 years in Spring 3 and Spring 3A (Figure 3-30). Tritium values in the springs are either in the range of regional aquifer values (less than 3 pCi/L) or up to 45 pCi/L, which could indicate either Laboratory impact or a component of precipitation (tritium in precipitation is 30–450 pCi/L). Perchlorate measured at low levels in some springs appears to be naturally occurring because it is within the range of regional background levels.

Four alternative pathways have been articulated to explain the presence of anthropogenic constituents in White Rock Canyon springs. One potential source is effluent discharged from the county's sewage treatment plants. McQuillan et al. (2004) noted that Los Alamos County water supply well Otowi-1 produces water with above-background nitrate, and detectable perchlorate and tritium, as do some of the springs. The calcium-bicarbonate groundwater at Spring 2B is chemically similar to that in regional aquifer well TW-1 in lower Pueblo Canyon. Although the Spring 2B major ion chemistry is consistent with the upgradient geochemical data from TW-1 in lower Pueblo Canyon, TW-1 is located approximately 4 miles away from Spring 2B. The White Rock Sewage Treatment Plant is very close to the springs. Both TW-1 and Spring 2B are located near (separate) municipal sewage discharges and the common sewage signature could yield similar water chemistries at both sites. Nitrate and chloride are common contaminants associated with sewage effluent.

McQuillan et al. (2004) suggest rapid transport in the regional aquifer from Pueblo Canyon to White Rock Canyon. Contaminants released in Acid Canyon, after having reached the regional aquifer, traveled rapidly through the regional aquifer in an easterly, then southerly path line starting at about Otowi-1 and TW-1, discharging in several springs along White Rock Canyon. However, these flow paths are inconsistent with the gradients in the regional aquifer, based on the latest potentiometric data. This pathway also requires rapid transport through the regional aquifer, contrary to evidence (carbon-14 data) that suggests slow transport through the regional aquifer (Sections 2.7.7 and 4). Water from lower Pueblo Canyon would need to travel many miles through the regional aquifer to Spring 2B with minimal mixing or dispersion in order to account for the observed concentrations.

One further geochemical argument, which suggests that water in Spring 2B does not originate near O-1 and TW-1 in Pueblo Canyon, is the high uranium concentration in Spring 2B water. Uranium concentrations in Spring 2B are sharply anomalous compared to adjacent springs. There have been no high uranium concentrations measured in regional groundwater beneath LANL or Pueblo Canyon (Gallaher et al. 2004) that are comparable to those in Spring 2B. However, high natural uranium concentrations are known to exist throughout the Pojoaque Valley, in the well field in lower LA Canyon, and in the nearby Buckman wellfield. The natural levels have been shown to vary in response to pumping in the old LA wellfield, and delayed impacts may appear in Springs 1 and 2.

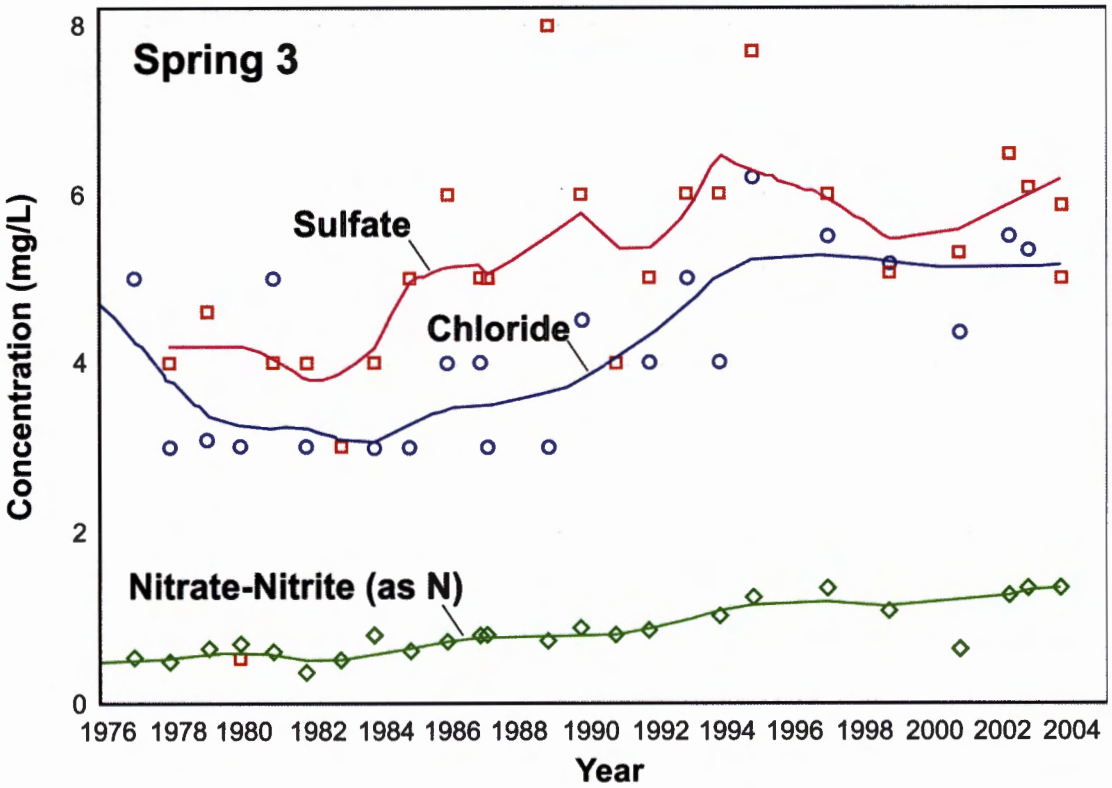


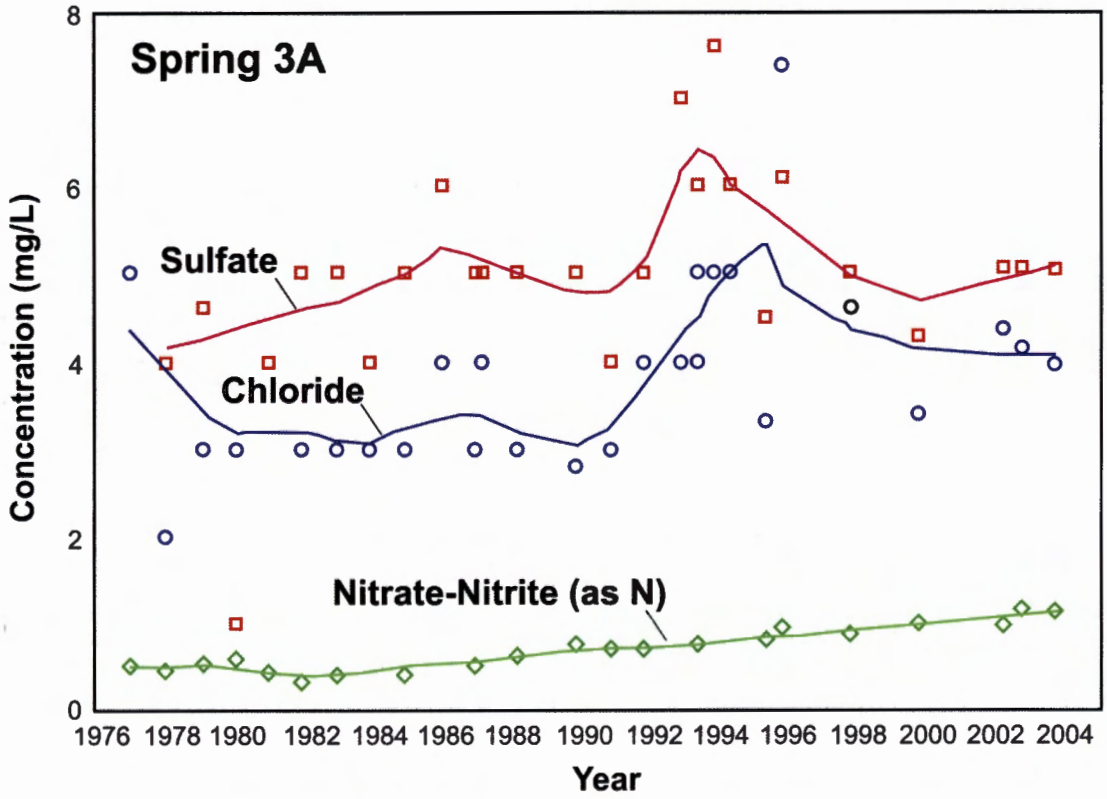


**Figure 3-30.** Anion concentrations in Springs 3 and 3A. Solid lines are best fit smooths to the data using loess methods (Cleveland 1979).

A second hypothesized pathway is a local source for contaminants present in the springs. Spring 2B chemistry is consistent with effluent from the White Rock Sewage Treatment Plant (located on the White Rock Canyon rim above Spring 2B). The decades-long increases in nitrate and chloride concentrations in Springs 3 and 3A suggest a sustained source such as an effluent discharge. Surface flows from the plant pass near these springs.

The third potential pathway is near-surface transport of contaminants to the White Rock Canyon springs. LANL contaminants are hypothesized as being transported in surface water and/or shallow groundwater along Pajarito Canyon from TA-9 to White Rock, followed by infiltration near the springs and a relatively short transit through the vadose zone to the regional aquifer. Such fast, shallow paths are more plausible and consistent with available information than fast transport through the regional aquifer. The major ion chemistry in the springs near Pajarito Canyon is generally consistent with that of groundwater along this flow path. Some fast regional aquifer transport would still need to occur for the contaminants to reach the springs.

The fourth possible pathway is transport via alluvial groundwater and fractural basalt. This pathway involves Laboratory contaminants reaching the springs via shallow and deep pathways in which transport is dominated by movement through fractural basalts. Fast transport through the basalts is more plausible than fast transport in the regional aquifer within the Puye Formation or the Santa Fe Group. The basalt-dominated pathway would likely be fast through the vadose zone as well. Drilling to date has not located any major contamination zones in basalt, but such zones could be isolated and difficult to encounter.

If any of the hypothesized alternative fast pathways invoked to explain the possible presence of LANL-derived constituents in springs exist, groundwater beneath LANL may travel more rapidly to downstream wells or springs than previously recognized, but the overall water quality changes would be anticipated to be relatively minor. Faster travel in the regional aquifer likely would result in less natural attenuation (for example, adsorption, radioactive decay, mixing) of any LANL-derived contamination. The monitoring history to date, however, has revealed minor impacts on the regional aquifer beneath the Laboratory. Continued LANL-wide groundwater monitoring is the most effective mechanism for identifying potential off-site transport of contaminants. See Appendix 3-D for discussion of other alternative conceptual transport models.

### 3.2.5 Summary of Contaminant Distribution and Transport

The impacts to groundwater at the Laboratory have occurred mainly where effluent discharges have increased local infiltration rates and volumes. The depth to which chemical constituents move in the subsurface is determined partly by their chemical behavior: non-reactive constituents move readily with groundwater, while reactive or adsorbing constituents move a shorter distance.

In most cases where effluent sources have been eliminated, groundwater concentrations of non-reactive discharged contaminants have decreased far below past levels (e.g., RDX, nitrate, tritium, and perchlorate) in alluvial groundwater. These mobile contaminants readily move through the subsurface and are detected within perched intermediate zones and at the regional water table beneath several canyons, including Pueblo Canyon, Los Alamos Canyon, Sandia

Canyon, Mortandad Canyon, and Cañon de Valle. In the case of reactive or adsorbing chemicals, the concentrations may remain elevated above background levels for long periods of time after elimination of discharges or other contaminant source terms (e.g., excavation and removal of contaminated sediments). These include constituents such as strontium-90 and the actinides (americium-241, plutonium-238, and plutonium-239, -240).

# 4.0 NUMERICAL MODELS

The conceptual models of the hydrogeologic system beneath the Pajarito Plateau, as well as the supporting data and information, were described in Sections 2 and 3. Numerical modeling is an analytical tool that can be used to integrate and synthesize the sometimes widely spaced point hydrogeologic field data and that allows prediction of how the hydrologic system will behave at different times and under different conditions in the future. However, before models can be used for prediction, they must be shown to adequately reproduce current conditions. A caveat is that different model representations (assumptions, boundary conditions, structural features, dimensionality) can in many cases provide equally good fits to available data. This fact, sometimes called equifinality in the hydrologic literature, implies that different model representations may result in significantly different model predictions. In this section we have selected representative model structures that are most consistent with the available information, while acknowledging that conceptual uncertainties also exist. This section describes the site-scale vadose zone and regional aquifer models that have been developed, including the underlying assumptions, hydrologic processes, calibration, and predictions for flow and transport.

## 4.1 Site-Wide Vadose Zone Flow and Transport Model

Hydrologic modeling of the vadose zone has been conducted to understand the key factors influencing the transport of contaminants from the ground surface to the regional aquifer, and to quantify uncertainties. The main goal of the site-wide vadose zone flow and transport model is to identify regions at the Laboratory where deep migration of contaminants is most likely. These analyses have been useful for guiding and prioritizing site characterization activities and can be used to support risk and performance assessments.

The following summary describes the underlying assumptions and hydrologic processes, and presents numerical modeling predictions of the travel times from the ground surface to the top of the regional aquifer across the Pajarito Plateau. Simulation of travel time of traced water is a necessary first step in predicting the velocities and concentrations of contaminants through the vadose zone. For a modeling analysis that includes predictions of tritium concentrations, see the presentation of a numerical model for Los Alamos Canyon in Section 4.1.3.2.

### 4.1.1 Model Development

Transport of water and dissolved chemicals through the vadose zone beneath the Pajarito Plateau has been the subject of numerous laboratory and field investigations and numerical model development efforts. The characterization and modeling of vadose zone systems requires knowledge of the water supply, percolation rates and the hydrologic properties of rocks and soils under unsaturated conditions. Such an understanding, at a basic level, has been acquired for the Bandelier Tuff underlying much of the Pajarito Plateau. In the past, that knowledge has been used to develop geometrically complex numerical models to investigate in detail the influence of dipping stratigraphy, rugged topography, and manmade alterations to the natural system (see Section 4.1.3 for examples).

Due to the complexity and computational demands of vadose zone models, they typically cover only a small portion of the Laboratory property, and thereby provide only a local picture of the vadose zone system. This section describes a site-wide model for performing first-order analysis of travel time through the vadose zone across the entire Pajarito Plateau. By foregoing some of the complexities in favor of a simpler representation of the flow physics, this model can be extended to include all locations of interest on the LANL property.

The following subsections present the modeling inputs, assumptions, and methodology in more detail.

#### 4.1.1.1 Flow and Transport Processes

Despite the potential complexities associated with vadose zone systems, many basic processes are amenable to characterization and numerical simulation. In the Bandelier Tuff, when the percolation rate is lower than the saturated hydraulic conductivity $K_{sat}$ of the matrix rock, the fluid saturation in the partially water-filled pores modulates itself in order to transmit the fluid under unit-gradient conditions associated with gravity-driven flow. Section 2.6.3 included data suggesting that under most conditions, water percolates through the Bandelier Tuff matrix, and the role of fractures is minor, except for the uppermost units of the Tshirege Member, present only in the westernmost portion of the Laboratory. In these locations, units with very low hydraulic conductivity induce lateral flow, probably through fractures. This phenomenon leads to shallow zones of saturation in which water travels laterally and issues at springs in Cañon de Valle and Water Canyon, from which it flows vertically downward through the rest of the Bandelier Tuff in matrix flow. In contrast, flow through the basaltic and dacitic rocks is assumed to be controlled by fractures. The practical consequence of these conceptual models for travel times will be established in the numerical modeling results. Finally, flow through the Puye Formation is probably also matrix-dominated, although the hydrogeology is complicated and the possibility of channelized, heterogeneous flow must be considered.

In spite of the inherently three-dimensional nature of flow in the vadose zone, an appropriate approximation for estimating travel time is to assume one-dimensional downward percolation of water and migration of contaminants. Intermediate perched groundwater observed in several wells across the Plateau indicates the possibility of lateral diversion (see Section 2.7), but the influence of such groundwater on vadose zone travel time can be assessed in a bounding manner, as is illustrated in Section 4.1.2.3.

#### 4.1.1.2 Infiltration Rate

As the upper fluid flow boundary condition, infiltration is one of the most important inputs for a vadose-zone model. Infiltration is known to depend, often in a complex way, on the local surface hydrologic conditions, topography, microclimatic conditions, evapotranspirative (ET) conditions (including vegetation type), and the presence or absence of impermeable layers such as thin clay layers within and at the base of the alluvium. The water that escapes ET and surface runoff is assumed to percolate through the remainder of the vadose zone to the regional aquifer, carrying with it any aqueous chemicals such as contaminants or dissolved minerals. The percolation rate below the zone of evapotranspiration is the direct input to the vadose zone numerical models. Although this rate undoubtedly changes with time due to storm transients, seasonal variations, and climatic variability, it is assumed that such effects are buffered by the hydrologic processes

that redistribute water in the surface water, alluvial groundwater, and unsaturated rocks of the vadose zone, so that an equivalent constant percolation rate can be assigned. The infiltration rate is also spatially variable at scales ranging from the width of fractured zones to the length of individual canyons.

The methodology for estimating infiltration rates across the Pajarito Plateau is to classify canyons or portions of canyons with a numerical designator, called the Net Infiltration Index (NII). Then, for applying infiltration in the numerical model, each NII would have associated with it an infiltration rate. For the mesas, a uniform infiltration rate of 1 mm/yr was assumed. Appendix 4-A presents the development of the NII values across the Pajarito Plateau; the results are depicted in Figure 4-A-1. Table 4-1 lists, for each NII, the descriptive characteristics of each infiltration class, and the infiltration rates associated with each of the model runs.

#### 4.1.1.3 Numerical Model Implementation

To predict travel time, the FEHM computer code (Zyvoloski et al. 1997) was used to simulate the two-phase, air-water flow problem. For the vertical stratigraphy predicted by the site geologic model, a one-dimensional grid was constructed with 10 evenly spaced numerical grid points within each layer. Hydrologic properties of each unit were assigned based on laboratory measurements and results of previous vadose-zone modeling efforts, and the percolation rate was assigned based on the infiltration map (Figure 2-34). The calculation consists of two steps: first, a steady-state one-dimensional fluid flow calculation is executed to establish the fluid water contents and water velocities through the stratigraphic column from the surface to the water table. Then, this steady-state flow model is used to compute a travel time using particle tracking. After performing the calculation at numerous locations across the Plateau, a site-wide description of vadose zone travel times is assembled in the form of travel-time maps.

To conduct these calculations, several steps of the process were automated within a GIS-based data assembly and querying system. At a given location, the one-dimensional vertical stratigraphy from the site-scale geologic model was used to generate a numerical grid for flow and transport calculations. The point distribution for the one-dimensional models consisted of a high density of points close to drainages across the Pajarito Plateau, and a coarser resolution on the mesas. Regions corresponding to the drainages, where relatively large infiltration is applied, were converted to a high-resolution grid (cell size of 128 ft) with each point located in the center of the cell. On the mesas, a coarser point distribution of 512 ft was taken. This resulted in a total of 30,577 points across the plateau at which one-dimensional transport times were calculated.

**Table 4-1.**
**Determination of Net Infiltration Index and Net Infiltration Rates Used in the Model**

| Net Infiltration Index (NII) | Headwaters or Source | Surface Water | Alluvial Water | Net Infiltration Estimate (mm/yr) | |
|---|---|---|---|---|---|
| | | | | Base Case | High Infiltration Scenario |
| 1 | Plateau | Ephemeral or Intermittent | Not Saturated | 1 | 10 |
| 2 | Mountain or Small Anthropogenic Source | Ephemeral or Intermittent | Not Saturated | 10 | 30 |
| 2 | Plateau | Ephemeral or Intermittent | Sometimes Saturated | 10 | 30 |
| 2 | Plateau | Perennial | Not Saturated | 10 | 30 |
| 3 | Plateau or Small Anthropogenic Source | Ephemeral or Intermittent | Saturated | 100 | 300 |
| 3 | Mountain | Ephemeral or Intermittent | Sometimes Saturated | 100 | 300 |
| 4 | Plateau | Perennial | Saturated | 300 | 1000 |
| 4 | Mountain or Anthropogenic Source | Ephemeral or Intermittent | Saturated | 300 | 1000 |
| 5 | Mountain or Large Anthropogenic Source | Perennial | Saturated | 1000 | 3000 |

### 4.1.2 Model Results

Numerical modeling results are presented for a "base-case" model for canyons and mesas, after which uncertainty in infiltration rate and the impact of perched water conceptual uncertainty are studied.

#### 4.1.2.1 Base-Case Results

A full-scale map of predicted travel times of a water molecule in the vadose zone (from ground surface to the water table of the regional aquifer) is shown in Figure 4-1. Along each canyon with NII other than 1, travel times are predicted to be less than 1000 years. Although the results in canyons are the main focus of this study, results for the mesas are described first. On mesas, the predicted travel times are variable, but for the most part are greater than 1000 years, ranging from 1000-5000 years on the eastern portions of the Laboratory to 20,000 to 30,000 years in the western region.

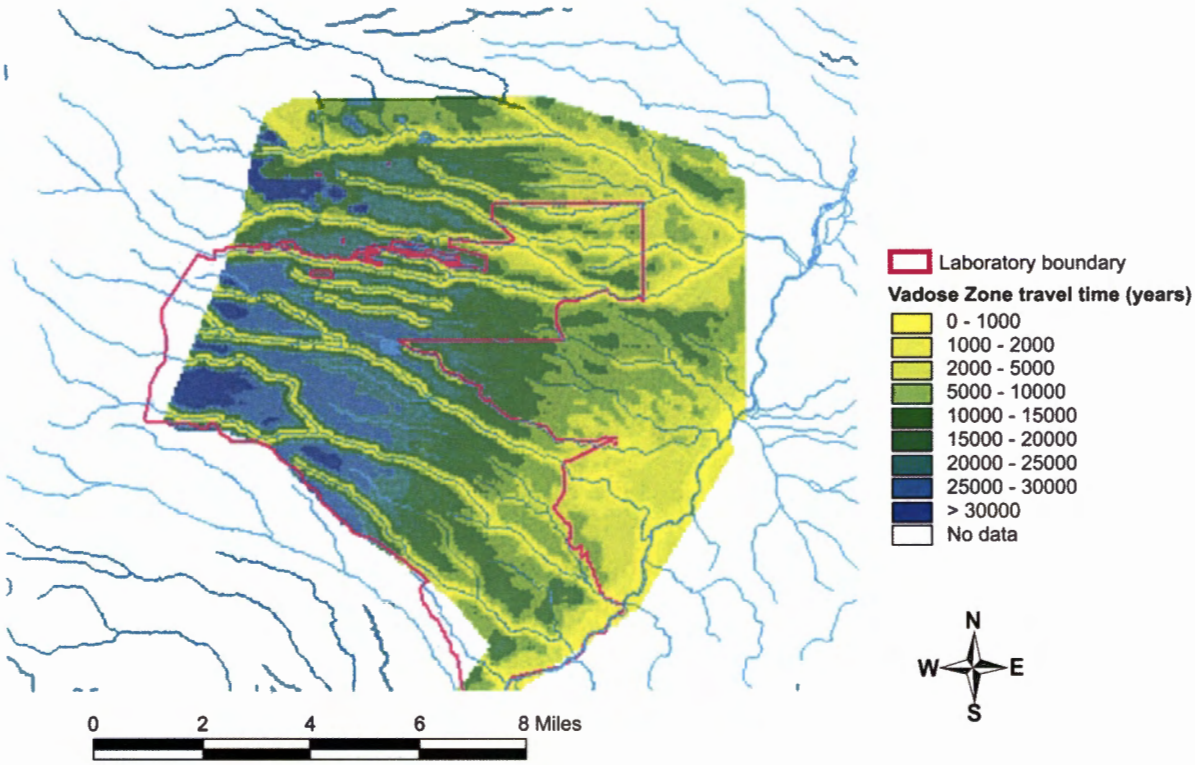


**Figure 4-1.** Predicted vadose zone travel times (years) to the water table: Base case, full scale of travel times.

To a first approximation, travel times from mesa tops are controlled by the thickness of the Bandelier Tuff. Because the Bandelier Tuff exhibits matrix percolation, the travel times on the mesas are controlled by slow percolation at a flux of 1 mm/yr through these units. Other units between the ground surface and the water table are the Cerros del Rio basalts, the Puye Formation, and the Tshicoma dacites. The basalts and dacites are modeled with an extremely low porosity (0.01) to capture the conceptual model feature of flow through these units controlled by fast pathways such as fractures or other heterogeneities. Therefore, most of the travel time to the water table is within the Bandelier Tuff, and the travel time map is therefore dominated by the tuff thickness.

Identification of rapid travel times to the water table from canyon bottoms is important to determine if they are in locations likely to have experienced Laboratory-derived groundwater contamination. Figure 4-2a shows the base-case model result presented in Figure 4-1, except that the travel-time scale ranges from 0 to 100 years (all points with values greater than 100 years are shown in gray). The model predicts that regions of relatively rapid travel times are present in the following canyons: Pajarito Canyon near White Rock, a portion of Cañon de Valle, Mortandad Canyon at the Radioactive Liquid Waste Treatment facility, middle and lower Los Alamos Canyon, large portions of Pueblo Canyon, and Guaje Canyon.

Two factors control these results: infiltration rate and hydrostratigraphy. Generally, travel times less than 100 years are predicted in the portions of canyons with NII values of 4 or 5 (300 mm/yr and 1000 mm/yr, respectively), especially in locations where the Bandelier Tuff is thin. Clearly, canyons with high infiltration rates are locations in which travel times through the vadose zone are likely to be relatively short. In addition, Los Alamos and Pueblo Canyons have regions in the vicinity of their confluence in which the Bandelier Tuff is thin or non-existent. Water infiltrates directly onto basaltic rocks or the Puye Formation, thereby yielding rapidly downward flow through fractures or preferential flow channels. The predicted travel times are especially short (5 to 10 years) in these locations.

#### 4.1.2.2 Uncertain Infiltration Rate

The infiltration rates associated with the NII are uncertain, and therefore must be varied to investigate the uncertainty in the model predictions. Figure 4-3a shows the same vadose zone travel time map as in Figure 4-2a, but for the high infiltration rate scenario (NII = 4-5). As expected, travel times are shorter at the same location in any particular canyon at the higher infiltration rate. As a result, greater stretches of canyons are predicted to exhibit travel times to the regional aquifer water table of less than 100 years. Specifically, in the high flux scenario, most of Pajarito Canyon, much longer stretches of Mortandad and Los Alamos Canyons, Cañon de Valle/Water Canyons from the west to the central portion of the Laboratory, and all of Pueblo Canyon in the vicinity of the Laboratory are predicted to have travel times that are less than 100 years.

This analysis highlights a key uncertainty in the model: the lack of precision in predicting the percolation rate from canyon bottoms. Because contaminants have been introduced into the groundwater in canyons, it is likely that the percolation rate will be one of the key uncertainties that detailed site characterization may address, possibly in conjunction with sensitivity analyses.

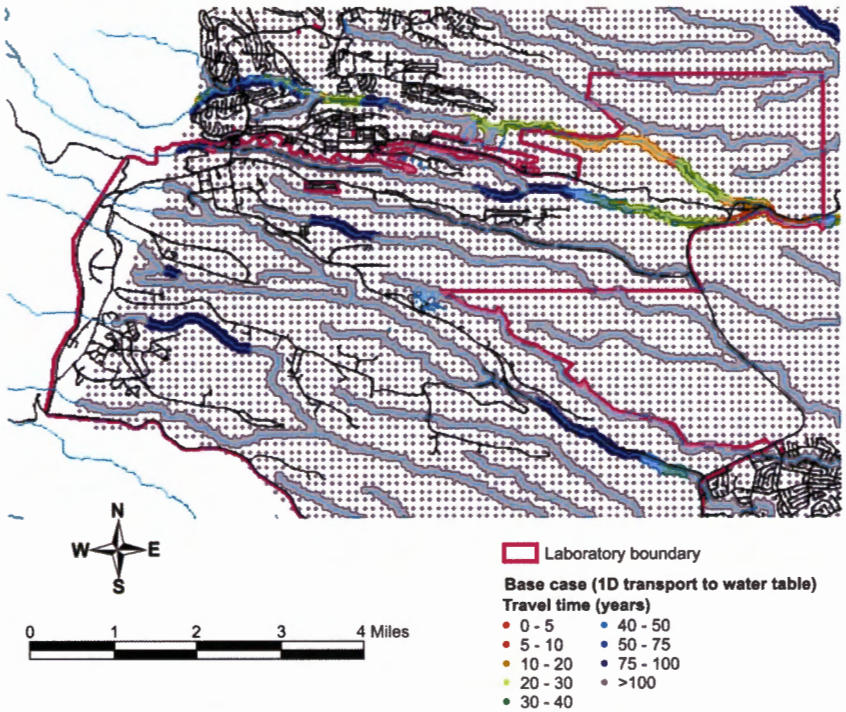


**(a)**

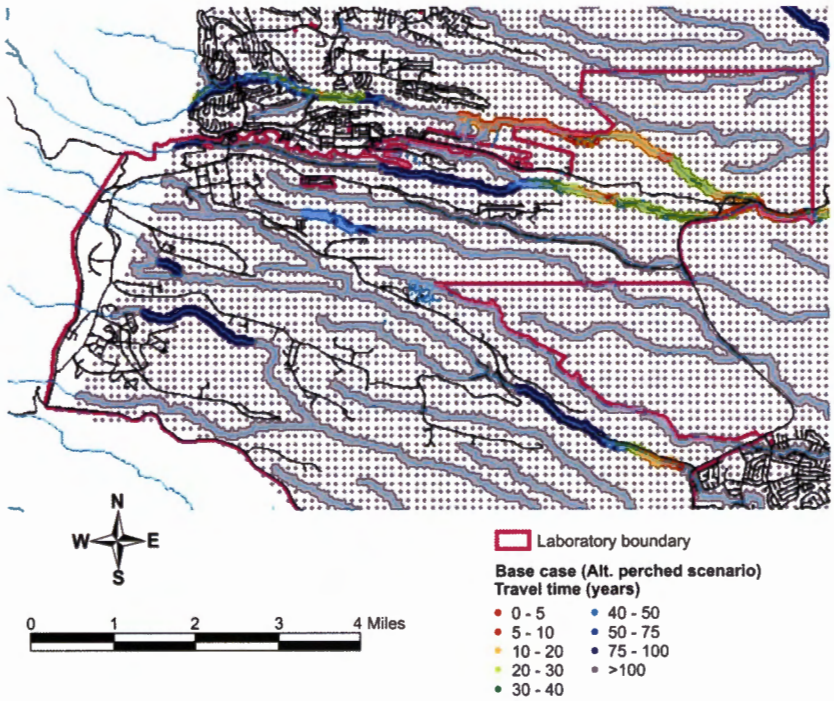


**(b)**

**Figure 4-2.** Predicted vadose zone travel times (years) to the water table, showing only travel times of 100 years or less. Base case percolation scenario: (a) 1-D transport to the water table; (b) alternate perched water model.

#### 4.1.2.3 Perched Water Conceptual Uncertainty

The one-dimensional, vertical transport model assumption is an approximation that may not be valid, given the presence of intermediate groundwater at various locations around the Laboratory. As presented in Section 2.7, zones of saturation have been located directly beneath canyons, where infiltration rates are highest. There is little or no evidence that connected groundwater pathways exist over large areal distances beneath mesas. Given the limitations of the data, the approach taken in the present study is to bracket the range of travel times to the water table that would be predicted assuming "end-member" conceptual models for perched water discussed in Section 2.7:

- Low velocity, virtually stagnant fluid
- High velocity, laterally migrating fluid

For the case of stagnant fluid, the one-dimensional pathway approach presented above is an appropriate model. For this case, the calculations already presented are representative. However, the lateral diversion model explicitly violates the one-dimensional assumption, and therefore a bounding approximation is required. In these analyses, it is assumed that the travel time from the surface to the elevation of perching is the same as was modeled previously, but the travel time from the perched water zone to the water table is minimal. This approach yields the shortest overall possible travel time, and therefore is useful for assessing the impact of this conceptual uncertainty. Note that this analysis assumes that lateral displacement of water and contaminants in perched zones is relatively small compared to lateral displacement in alluvial groundwater systems that are the source of deep percolation.

To perform these calculations, regions were identified within the canyons where intermediate groundwater has been observed, and it was assumed that the vadose zone pathway terminates at that location. This allows travel times to be bounded without explicitly modeling transport from the perching horizon to the regional aquifer. Figures 4-2b and 4-3b show the results of the travel time simulations for the alternate perched water conceptual model for each percolation scenario. Comparing these figures to their counterparts for the one-dimensional downward flow cases (Figures 4-2a and 4-3a), the differences in travel time are quite subtle. The regions with vadose zone travel times of less than 100 years remain approximately the same, and the travel times at the same location are only mildly impacted by the perched water conceptual model. For example, for the base-case infiltration scenario, travel times are shorter by about 15-20 years for the alternate perched water model, and for the high flux scenario, these differences are even smaller.

To understand this result, note that transport from the ground surface to the water table in the one-dimensional model is dominated by percolation through the matrix of the Bandelier Tuff. Therefore, terminating the transport pathway at the base of the tuff, as in the alternate perched water scenario, eliminates a relatively small portion of the total travel time to the regional aquifer. Of course, despite this insensitivity of travel time, the arrival location at the water table is potentially quite different for the two cases: this factor should be considered in specific cases of contaminant transport predictions.

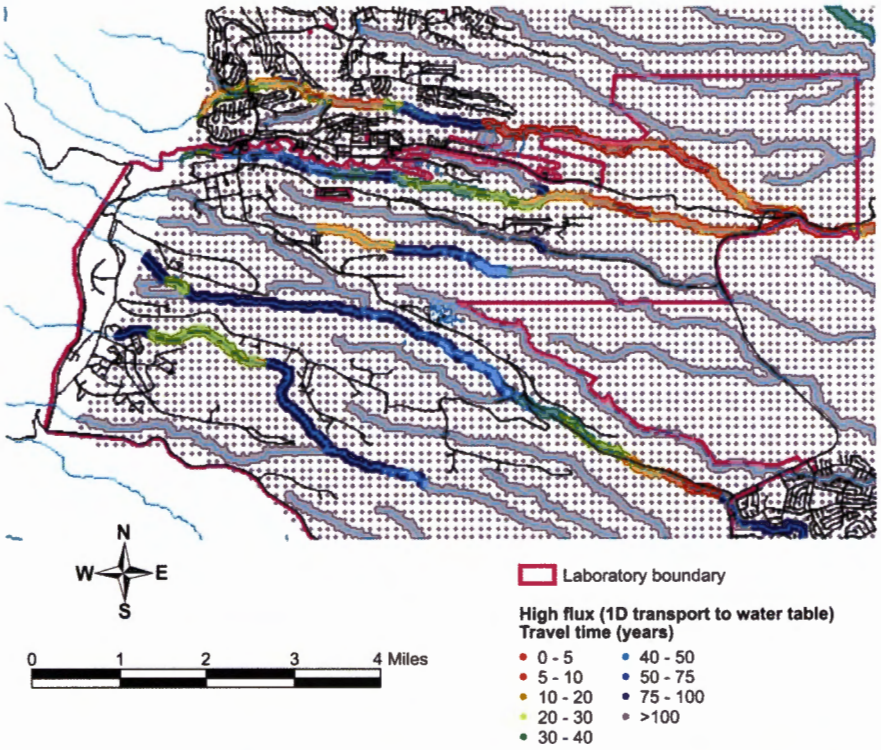


**(a)**

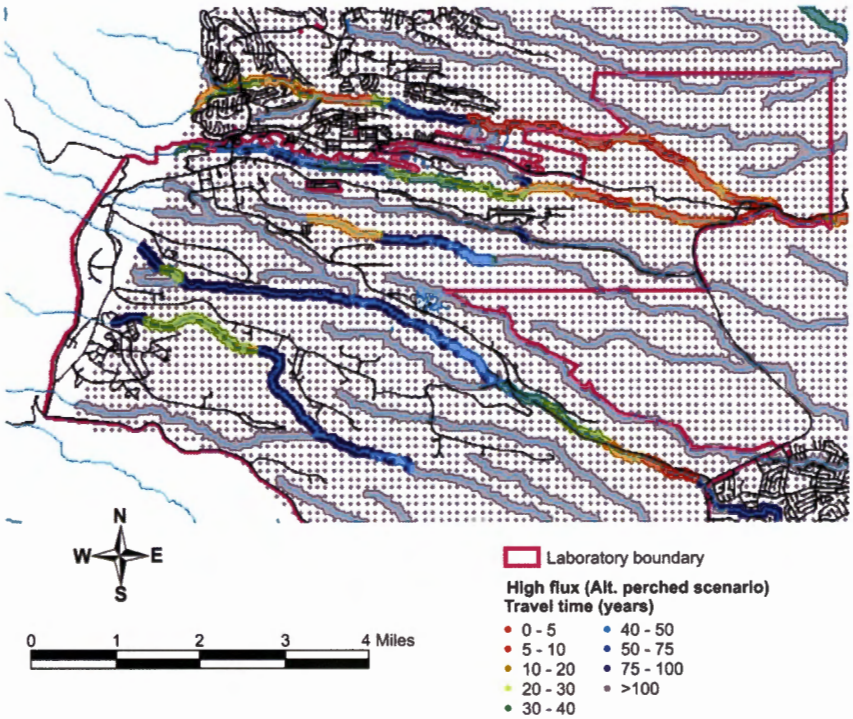


**(b)**

**Figure 4-3.** Predicted vadose zone travel times (years) to the water table, showing only travel times of 100 years or less. High percolation flux scenario: (a)1-D to the water table; (b) alternate perched water model.

### 4.1.3 Contaminant Transport Model Predictions—Representative Canyon and Mesa Sites

This section presents an overview of modeling studies focusing on two representative LANL sites. The first example models contaminant transport from a relatively dry mesa top, while the other addresses a canyon bottom.

#### 4.1.3.1 MDA G Model

This section highlights the model developed for the Material Disposal Area G (MDA G) performance assessment. A detailed description of the model is provided in Appendix 4-B. A performance assessment (PA) is required to site and authorize permanent disposal facilities for radioactive waste. The purpose of the PA is to demonstrate that performance metrics related to protection of human health and the environment are not likely to be exceeded for a specified period of time. Performance objectives and periods of compliance vary according to the characteristics of the radioactive waste being disposed, but groundwater protection for U.S. sites is always explicitly required for at least 1000 years. This study was designed to predict the groundwater pathway dose in support of the PA of MDA G, an active, low-level, solid radioactive waste site located at LANL, as shown in Figure 4-4 (Fig. 1 of Birdsell et al. 2000).

The three-dimensional unsaturated-zone flow and transport model captures the complex hydrogeology and topography of the site and yields radionuclide flux estimates to the regional aquifer. Within the unsaturated-zone model, the source release of radionuclides is computed for 38 waste disposal pits and four shaft fields, as shown in Figure 4-5 (Figure 3 of Birdsell et al. 2000), each contributing to the total inventory. The continued migration of radionuclides through the aquifer is calculated by using a three-dimensional model designed to maintain the temporally and spatially varying distribution of radionuclide flux from the unsaturated zone.

Due to uncertainty of model parameters, the results of these transport simulations contain intrinsic uncertainty. The greatest uncertainties associated with predicting aquifer-related doses from the site, according to Birdsell et al. (2000), are related to understanding of the mechanisms that control flow and transport within the unsaturated zone and the ability to model these mechanisms. To accommodate both parameter and conceptual model uncertainties, large parameter ranges are used to ensure that the range of calculations captures the behavior of the actual system. However, predicted doses using parameters from the most conservative ends of the uncertain ranges are still well below those that would cause concern.

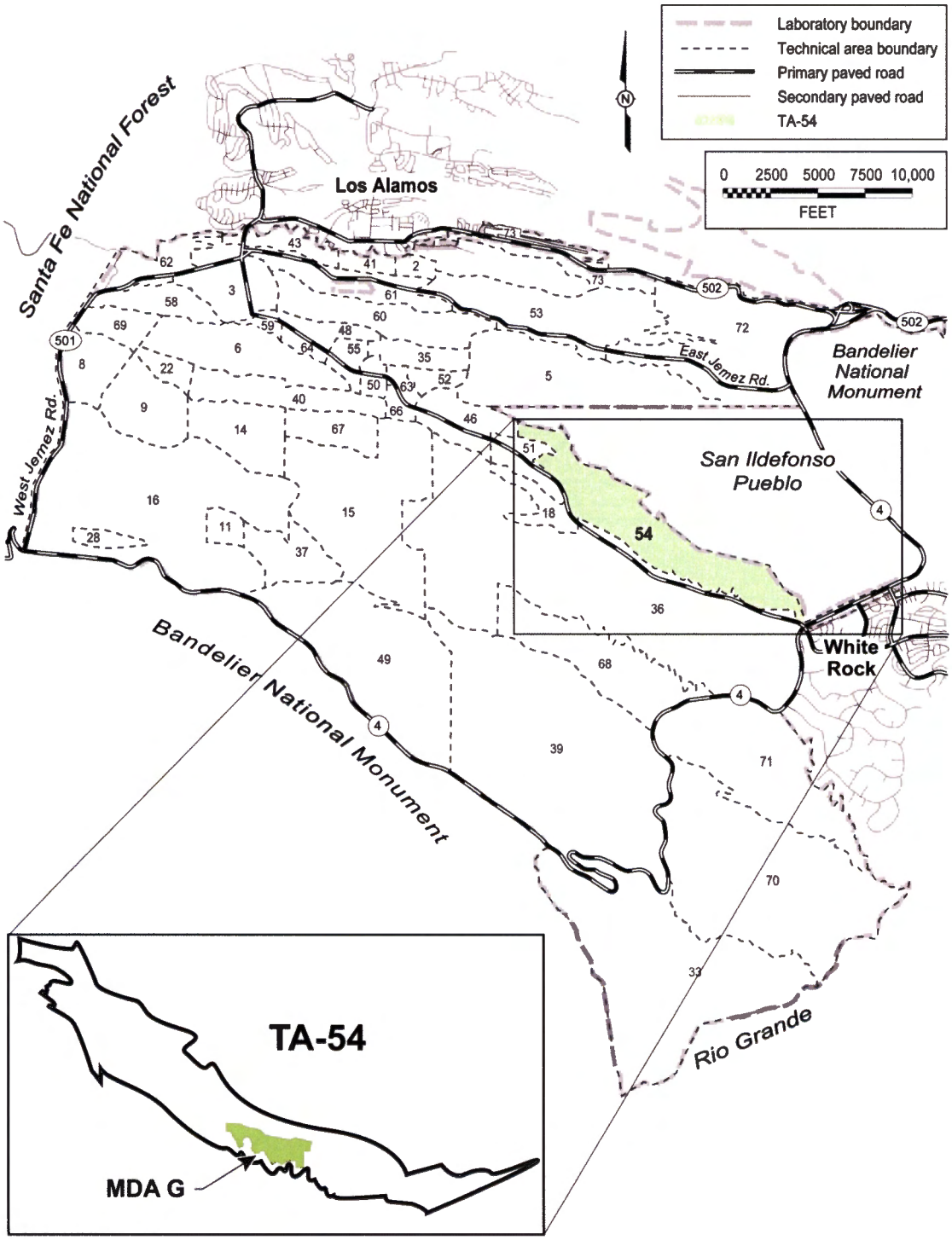


**Figure 4-4.** Study area for the performance assessment of MDA G, an active low-level, solid radioactive waste site located at LANL (from Birdsell et al. 2000).

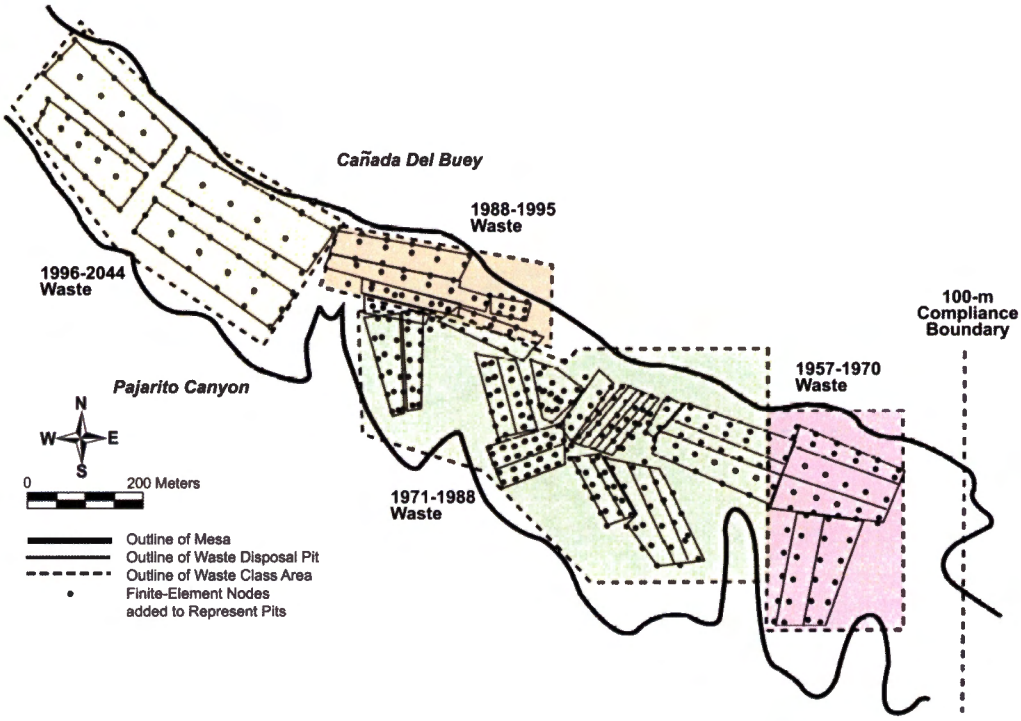


**Figure 4-5.** Approximate locations of the four waste classes and the 100-m compliance boundary used for the MDA G performance assessment. Also shown are the pit boundaries, internal pit nodes, and the outline of the mesa edge for the three-dimensional unsaturated-zone grid (Figure 3 of Birdsell et al. 2000).

The results recorded by Birdsell et al. (2000) indicate that the mesa-top infiltration rate has the greatest impact on the simulated migration of waste through the unsaturated zone. For the current conceptual and numerical models, it controls both the source release rate and subsequent downward solute migration. This uncertainty was bounded by considering a base-case flow field and high- and low-flow cases. A variation in mesa-top infiltration rate from 1 to 10 mm/yr (Appendix 4-B and Table 4-2) results in a range of six orders of magnitude in the 1000-year groundwater-related doses. Clearly, a good understanding of this key parameter is important to the dose assessment. However, because doses are so much less than the performance objectives, conservative yet realistic infiltration rates seem adequate for the MDA G site.

**Table 4-2.**
**Infiltration Rates (mm/year) Used as Upper Boundary Conditions for MDA G Performance Assessment Simulations (fom Birdsell et al. 2000)**

| | Mesa Top | Cañada del Buey | Pajarito Canyon |
|---|---|---|---|
| **1_1_20 (lowest flow case)** | 1 | 1 | 20 |
| **5_1_20** | 5 | 1 | 20 |
| **5_1_50 (base case)** | 5 | 1 | 50 |
| **10_1_20** | 5 | 1 | 20 |
| **10_5_100 (highest flow case)** | 10 | 5 | 100 |

Another source of uncertainty is related to flow in the deeper unsaturated-zone units for which few hydrologic data are available. The simulations take virtually no credit for transport times through the Cerros del Rio basalts, which make up more than 50% of the unsaturated zone. The transport results are based on the steady-flow assumption and on the use of matrix hydrologic properties for all tuff units at the site. Understanding of the response of this fractured system to transient flow events remains uncertain. Transient calculations (Birdsell et al. 1999) indicate that the steady-flow assumption is adequate because fluctuations in both saturation and contaminant flux rates dampen with depth, even when including fractures in the upper two units. Fracture infiltration studies (Soll and Birdsell 1998) lead to the conclusion that fracture flow is difficult to initiate and is short-lived in the upper two tuff units at the observed low field saturations. In addition, only Unit 2 and the uppermost portion of Unit 1v-u of the Tshirege Member, Bandelier Tuff, show evidence of significant fracturing (Krier et al. 1997), and these are excavated during disposal operations to depths where the tuff is poorly fractured. Therefore, the waste should not migrate through any highly fractured units until reaching the basalts. These observations help justify the use of the matrix hydrologic properties for the calculations.

In summary, travel times to the regional aquifer from locations on mesas are expected to be large (e.g., > 1000 yr) due to low infiltration rates and matrix-dominated flow. Calculations in this performance assessment model were deliberately conservative and therefore predicted travel times that were an order of magnitude shorter than the base case model presented in Section 4.1.2.1. Exceptions to this general conclusion are in the western portion of the Laboratory (see Section 4.1.1.1) and in locations where the natural mesa-top conditions have been disturbed by Laboratory activities.

#### 4.1.3.2 Los Alamos Canyon Model

This section highlights the model developed for Los Alamos Canyon RCRA Facility Assessment investigations. A detailed description of the model is provided in Appendix 4-C. Los Alamos Canyon, as shown in Figure 4-6, is one of the most complex sites at the Laboratory. A number of technical areas have been or are currently located in or adjacent to the canyon, resulting in multiple release locations along the canyon. This study examined, through a synthesis of available data and the development of numerical models, fluid flow and contaminant transport in the vadose zone beneath Los Alamos Canyon. Modeling of the subsurface hydrology and transport in the vadose zone is also a challenging activity, given the wide range of infiltration rates, the presence of perched water, and the introduction of a host of contaminants of different chemical properties. Because the canyon serves as a collector of a wide range of contaminants, it was necessary to develop a model at the scale of the canyon, rather than at a smaller scale. The specific goals of the model are to

- Synthesize the available data and conceptual understanding of the vadose zone hydrology beneath Los Alamos Canyon;
- Produce a "base-case" numerical model of the subsurface vadose zone hydrology that ultimately can be used to predict contaminant migration rates and concentrations in fluids reaching the regional aquifer beneath the canyon;

- Quantify the uncertainties associated with those predictions by establishing the bounds on system behavior through a suite of possible models, all of which are consistent with the available data, but which bracket the range of possible behavior;
- Provide a simulation tool for predicting the fate and transport of contaminants in Los Alamos Canyon under different assumed hydrologic and ER stewardship scenarios; and
- Demonstrate a model development methodology that can be used in studies of other canyons on the Pajarito Plateau.

This work focuses on the hydrology beneath Los Alamos Canyon, as a first step toward developing a predictive tool that can be used to simulate contaminant migration in the canyon. Since water is the carrier fluid for the contaminants of interest, constructing a realistic flow model that captures the most important hydrologic processes of the vadose zone is an essential first step in the development of a reliable model. Although the study primarily restricts attention to flow issues, tritium transport in the vadose zone is also modeled. Tritium, in the form of tritiated water, is an excellent tracer for groundwater, and hence is included in this modeling study as a constraint on the flow model.

Figures 4-7 and 4-8 show a full three-dimensional view of fluid saturation and a series of two-dimensional vertical slices through the three-dimensional model. As expected, the figure shows wet conditions in the canyon, dry conditions in surrounding mesas. As with the two-dimensional model, this model result shows the overriding importance of the stratigraphy in controlling the water contents in the rock. The local infiltration rate also exerts a strong control on the results. Directly beneath the canyon, fluid saturation is much higher within a given stratigraphic unit than in other parts of the model domain, a reflection of the high infiltration in the canyon.

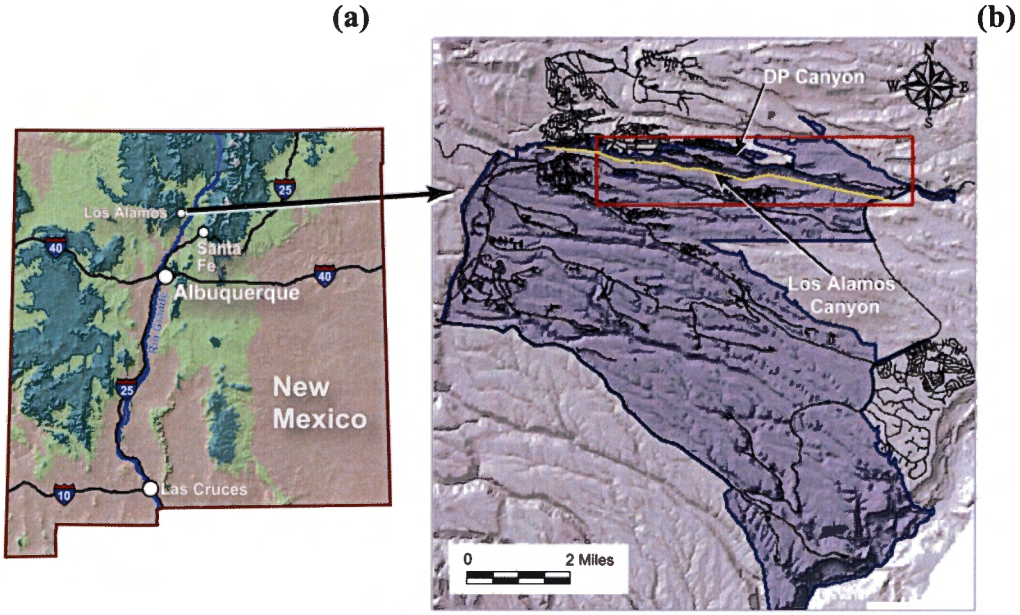


**Figure 4-6.** Location of Los Alamos, New Mexico (a), Los Alamos Canyon study area, and the flow and transport model domain (b). The shaded blue area is the LANL property; the red box indicates the areal extent of the three-dimensional model domain; and the yellow line is the trace of the two-dimensional model domain.

Volumetric water content is the primary measurement used to evaluate the model results because adequate data on water content are available from virtually all vadose zone characterization wells. The fits to the data are presented for three different levels of infiltration rates, i.e., the base-case infiltration map, a map with infiltration scaled down by a factor of three from the base map, and a map with infiltration scaled up by a factor of three (Figures 4-C-7 and 4-C-8). It is evident from the following comparisons that the model is able to capture the general features of data:

- The base infiltration map does an adequate job of jointly matching the water content profiles in these wells, despite the different stratigraphy and position relative to the canyon bottom.
- Good fit for LADP-4 illustrates the adequacy of the model in capturing the fluid saturations in the Tshirege Member (not present in the two-dimensional model), as well as in a region where infiltration rates are taken to be significantly lower than in Los Alamos Canyon at LADP-3.
- The need to apply significantly lower infiltration near LADP-4 is best understood by comparing the water content model and data for these two wells. The significantly wetter conditions in LADP-3 are simulated in the three-dimensional model through the setting of high infiltration in the canyon.

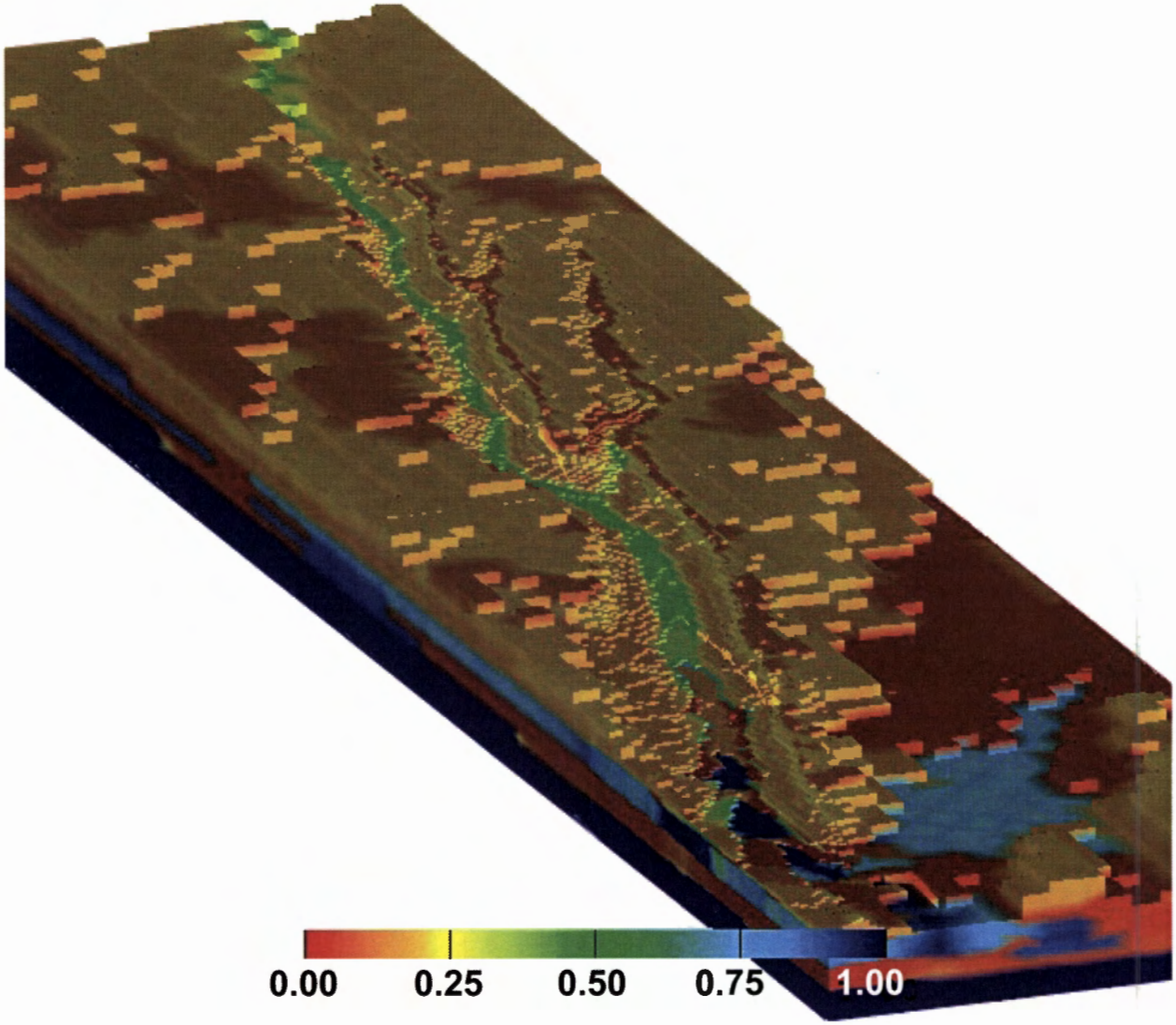


**Figure 4-7.** Three-dimensional flow model results, showing fluid saturation predictions (%) through the model domain (full model view).

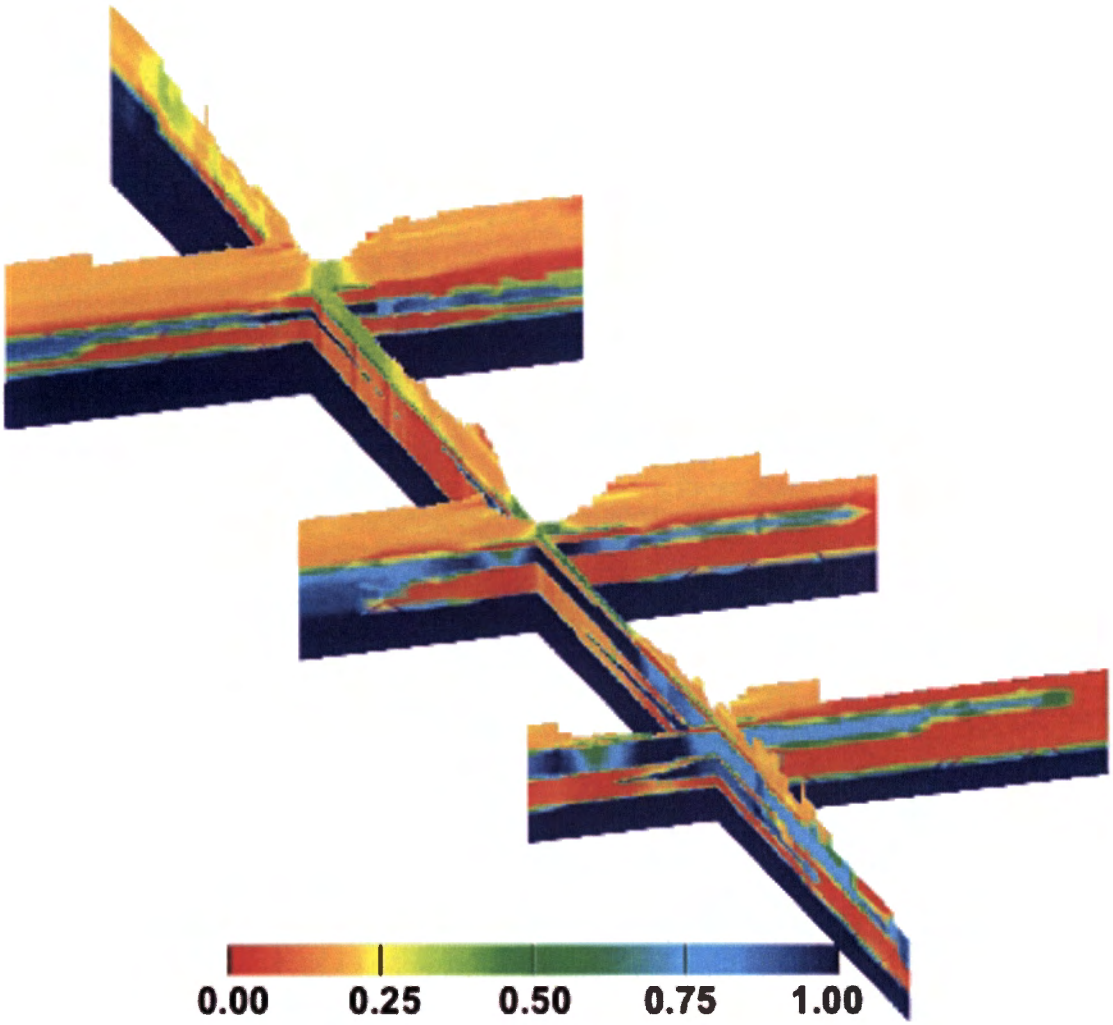


**Figure 4-8.** Fence diagram showing fluid saturation predictions (%) along one north-south and three east-west cross-sections.

Tritium transport model results are presented to further demonstrate the validity of the model and to explore important processes occurring in the vadose zone. Figure 4-9 is the three-dimensional model prediction of the tritium concentration of fluid reaching the water table in the year 1999. The model results are consistent with the available field data, indicating that regional aquifer fluid collected in well R-7 has undetectable levels of tritium, whereas TW-3 and R-9 show that tritium has reached the regional aquifer. Determining the ability of the model to reproduce the field data more quantitatively is difficult because of mixing of the tritium percolating from the vadose zone with regional aquifer fluid and the subsequent mixing of contaminated and clean fluid in the wellbore itself. The latter difficulty is especially acute for the water supply wells, which may draw water from hundreds of feet of screened length.

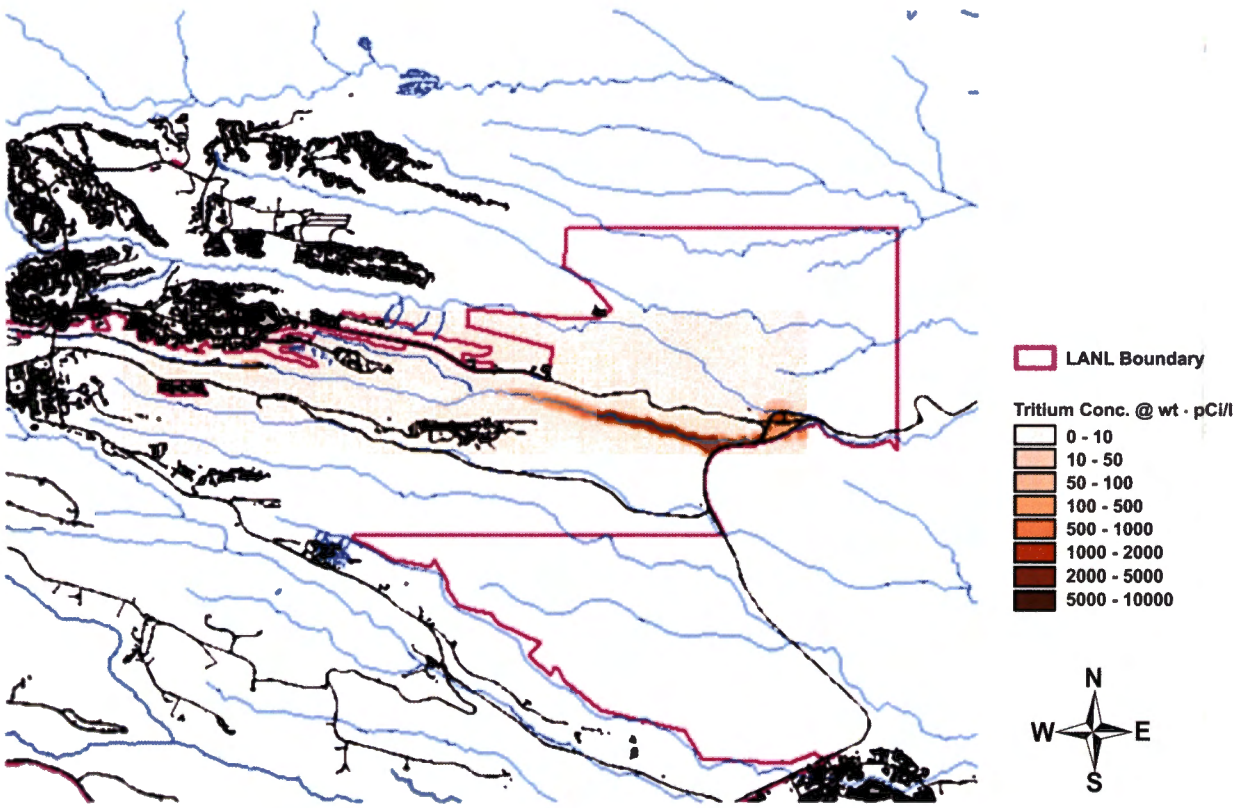


**Figure 4-9.** Three-dimensional model predictions of the tritium concentration of fluid reaching the water table in the year 1999. Significant, above background concentrations are predicted along the canyon at locations downstream of where the Bandelier Tuff is not present in the canyon bottom.

As a final comparison to the available data, we contrast the model results with regional aquifer water supply well O-1. However, because contaminant transport sources from Pueblo Canyon (north of Los Alamos Canyon) were not included in this model, the conclusions related to O-1 are more qualitative. For this comparison, monitoring information published in LANL (2001) is used. Contaminants tritium, perchlorate, and nitrate are all thought to be nonsorbing in this system, and thus the combined results of all three contaminants are used in this interpretation. Well O-1 has been found to contain measurable levels of perchlorate at about a 5 ppb level, nitrate levels higher than at other regional aquifer wells in the area, and consistent, above-background levels of tritium in the 30-40 pCi/L range. All observations point to both Laboratory-derived contaminants and effluent discharges from Los Alamos County. Past releases in Los Alamos and Pueblo Canyons have traversed the entire vadose zone. The present model explains these observations as a consequence of the hydrostratigraphy along the canyon, with rapid travel times at locations where the Bandelier Tuff is thin or non-existent.

Contrast these results with the transport model for MDA G presented in Section 4.1.3.1. Most important, travel times through the vadose zone are predicted to be orders of magnitude larger

for this mesa site than for transport from the bottom of a wet canyon. These travel-time results are consistent with the site-wide vadose zone results presented in Section 4.1.2. Infiltration rates, which directly impact transport velocities, are much larger in a canyon setting, in which all water in a catchment is channeled to the canyon bottom. A significant percentage of that water will escape evapotranspiration and percolate into the deep subsurface along the canyon. In contrast, a mesa top typically provides opportunity for water to run off as surface water or to be lost as evapotranspiration. Moreover, mesa sites have thick sequences of tuff with exceptionally low matrix flow rates. Therefore, percolation rates are much lower.

## 4.2 Numerical Models of Flow and Transport in the Regional Aquifer

The first numerical model for the regional aquifer was developed in 1998 in support of the LANL Groundwater Protection Program (LANL 1998). A number of related models have been developed since then, in support of both the Groundwater Protection Program and the Environmental Restoration Program, at a variety of spatial and temporal scales according to the requirements of the particular model application. In general, there have been three goals for these modeling studies:

- Integrate and interpret 3-D site-wide hydrologic and hydrostratigraphic data, to provide a quantitative basis for developing and testing site-wide conceptual models.
- Predict fate and transport of contaminants in the regional aquifer, in order to optimally place monitoring wells and inform risk assessment studies.
- Provide guidance in prioritization of data collection activities, highlighting the importance of those data that could most reduce numerical and conceptual model uncertainty.

As the Hydrogeologic Workplan has progressed, the data sets supporting the modeling studies have been steadily expanding. Updating the model with larger data sets has identified weaknesses in the modeling approaches and prompted changes in the methodology. This iterative process of data collection and model update and evaluation has significantly increased our understanding of the regional aquifer.

### 4.2.1 Previous Numerical Models

Two models have previously been developed by the USGS for the regional aquifer of the Española Basin, the aquifer system which provides drinking water to Los Alamos, Santa Fe, and Rio Arriba counties, as well as numerous pueblos. In contrast to the LANL modeling effort, these models were developed primarily to address water supply issues—particularly impacts of pumping on streamflow. The first was developed by Hearne (1985), using a computer code he wrote himself. The second was developed by McAda and Wasiolek (1988) (and later refined by Frenzel (1995), using the MODFLOW code (McDonald and Harbaugh 1988). At present, various local and state agencies continue to refine and apply both of these models to water supply issues in this basin.

In many ways, these two models are based on a similar conceptual model of the basin aquifer. Key elements of this conceptual model are as follows: (1) most inflow to the basin occurs as recharge in the mountains flanking the basin and along stream channels within the basin, and

(2) most discharge occurs to the Rio Grande and the lower reaches of its tributaries. A smaller portion of the total inflow and outflow occurs through lateral boundaries (i.e. up to 20% discharges to the Albuquerque Basin), due to structural and topographic features that limit inter-basin flow. The conceptual models of aquifer properties assume that hydraulic conductivity is strongly anisotropic, due to laterally discontinuous bedding features in the Santa Fe Group. The aquifer behaves as confined or leaky-confined, although no large-scale confining beds or low-permeability zones have been identified.

The lateral boundaries of the two models, shown in Figure 4-10, roughly coincide with the extent of basin-fill rocks in the southern portion of the basin (south of Española). Both models use specified flux boundaries to represent losing stream channels. Recharge is applied as specified flux, either at lateral boundaries (representing mountain block recharge) or along the upper model surface (representing recharge along stream channels or areal recharge). Discharge is to the Rio Grande and lower elevations of its major tributaries (specified head and head-dependent boundaries) and to the Albuquerque Basin (specified head in the case of the McAda model).

The conceptual model shared by these models is one of a complex transition from unconfined to leaky-confined conditions at depth, caused by relatively fine-scale bedding features in the rocks that provide resistance to vertical flow. Exact numerical implementation of this complexity is virtually impossible. The Hearne and Frenzel models treat the upper surface of the aquifer as a water table condition. Aquifer properties change from unconfined (top layer) to confined (lower layers); no discrete confining layer is present. Resistance to vertical flow is represented by anisotropy factors ($Kx/Kz \sim 100 - 1000$).

One significant difference between the models is the representation of large-scale heterogeneity. The Hearne model (which only includes the Santa Fe Group aquifer) treats the aquifer as homogeneous and anisotropic, with the numerical grid aligned in parallel with the dip of the beds in the Santa Fe Group. This approach allows the model to reproduce vertical upward head gradients measured in several wells in the eastern basin. The McAda and Frenzel models apply a somewhat ad hoc zonation of aquifer properties, based loosely on pump test results and the need to achieve an adequate model calibration to the data.

Appendix 4-D, Section 3, presents a comparison of inflows and outflows (steady-state, predevelopment) between the two models, as well as more recent estimates of inter-basin flow derived from USGS studies in the Albuquerque Basin.

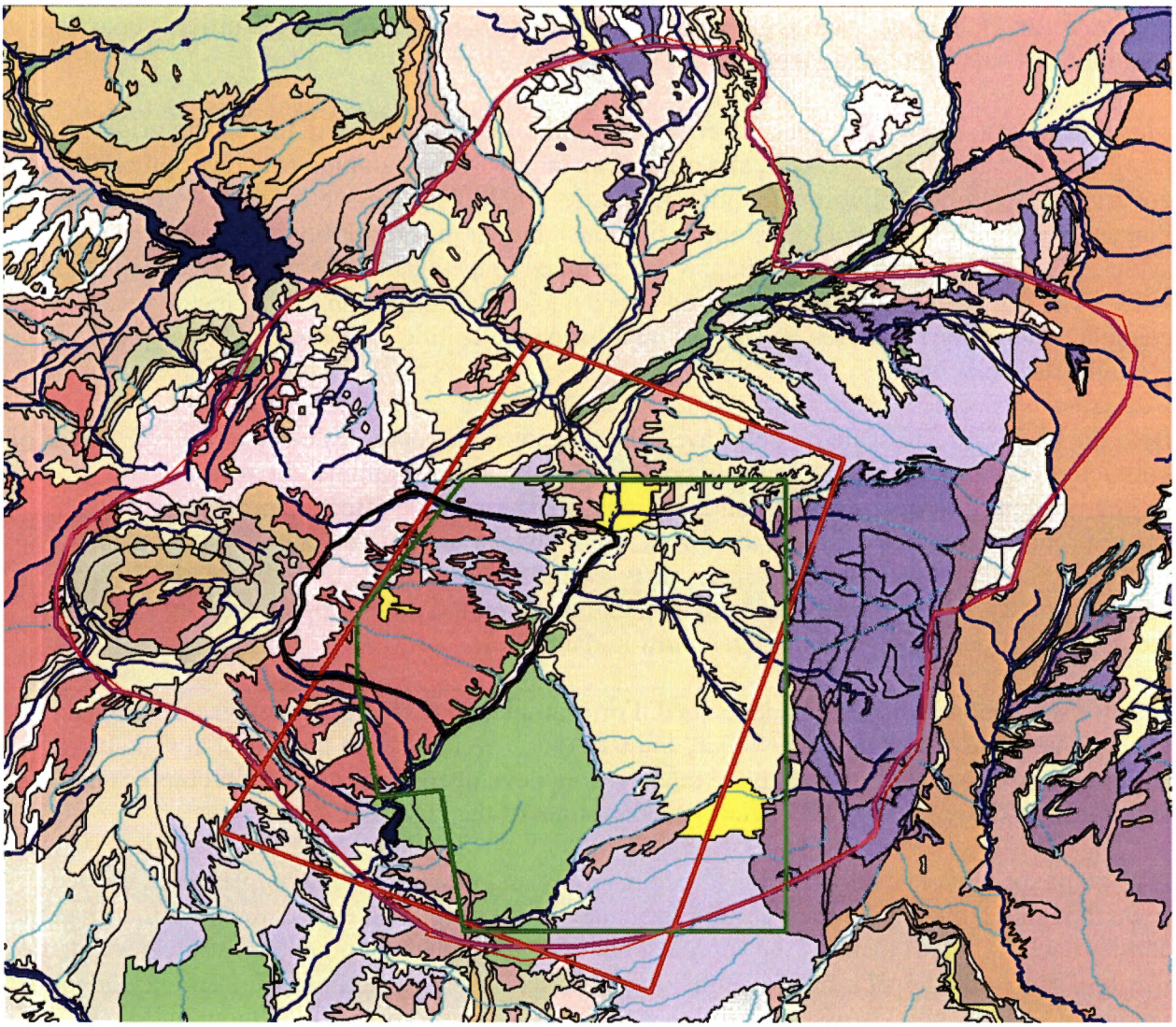

**Figure 4-10.** Geologic map of the Española Basin. Model outlines: green – McAda-Wasiolek model; red – Hearne model; pink – LANL basin-scale; black – LANL site-scale.

### 4.2.2 Overview of LANL Model Development

Unfortunately, both the USGS models of this aquifer system place a model boundary along the western edge of LANL; therefore, use of these models for the LANL site would be compromised by boundary effects (Anderson and Woessner 1992). To ensure that all model boundaries were far from the area of interest (LANL) and to incorporate the possible influences of regional flow on local conditions, a new flow model for the basin was developed. This model not only extends the western boundary farther than the existing models, to minimize boundary effects on site-scale simulations, but it also includes the major recharge areas for the basin. The inclusion of the recharge areas for the basin allows for a more comprehensive approach to estimating fluxes of water through the aquifer, as will be discussed below. The basin-scale model has been used to estimate aquifer properties, to estimate fluxes through the aquifer, to examine the possible influences of pumping in the Buckman wellfield on groundwater beneath the plateau

(and vice versa), to understand regional trends in groundwater quality, and to provide boundary conditions to small, site-scale models.

This initial basin-scale model has undergone several revisions, including increasing grid resolution in the vicinity of LANL and improving the hydrostratigraphic framework model that governs the spatial distribution of aquifer properties. In 2000, a site-scale model for the Pajarito Plateau (see Figure 4-10) was developed with much higher grid resolution than could be achieved with the basin-scale model, and was coupled to the basin-scale model (Keating et al. 2003). The site-scale model has been used to provide contaminant transport calculations, to conduct capture zone analyses, to support monitoring well siting decisions, and to estimate groundwater velocities.

Both the basin and site-scale models have been developed to address site-scale (several to tens of kilometers) issues and this has driven model development. For example, the methods of estimating aquifer properties (Section 2.8) emphasize large-scale effective properties of rocks. These properties may be different than what might be measured at very small scales, such as injection/recovery tests over small intervals in characterization wells or borehole geophysics-based estimates. These models (and model parameters) would not be appropriate for simulating the details of fine-scale (sub-kilometer) flow and transport.

Smaller-scale models have been developed. For example, a 2-D radial model was developed to evaluate the utility of using an R-well as an observation well during a pump test at O-1. In addition, a suite of 2-D and 3-D "box" models were developed to test conceptual models of flow and transport through the highly heterogeneous strata of the Puye Formation.

A principle of model development is to begin simply and gradually add complexity as needed. Even though the models, in their current form, are quite complex, they are much simpler than the aquifer itself. A major focus of the approach has been to implement numerical strategies that are flexible, so that the impacts of conceptual model uncertainty and parameter uncertainty on model predictions can be quickly assessed within a single modeling framework, without building entirely new models.

It should be emphasized that these models are for the regional aquifer only, and therefore do not include alluvial or perched groundwaters. The current versions of the models do not explicitly include springs, so pathways and travel times to springs have not been simulated.

### 4.2.3 Numerical Framework

All of the LANL models have employed the FEHM code (finite element heat and mass transfer) (Zyvoloski et al. 1997), publicly available software. Underlying this code is a sophisticated grid generating software, LaGrit (Trease et al. 1996) which can capture the details of complex hydrostratigraphy known to exist at this site. For conditions of saturated flow and transport (i.e. the regional aquifer), FEHM solves the same set of equations as do other more widely used codes, such as MODFLOW. The choice of this software for the LANL models was driven by the need to couple saturated zone simulations with vadose zone simulations (which use FEHM), to represent complex hydrostratigraphy, and to eventually investigate complex geochemistry and thermal effects (ongoing work). FEHM is well suited to these types of problems, since

temperature and density dependent fluid properties can be accurately accounted for. Some of the more simple simulations presented here do not utilize the specialized capabilities of FEHM and LaGrit; these simulations could easily be repeated using a code such as MODFLOW and one would expect the results to be identical (assuming grid resolution and boundary conditions were identical).

Figure 4-10 illustrates the lateral boundaries of the LANL models. In the basin model, boundaries were located such that they were far from the LANL site and coincided with either hydrologic features or structural boundaries. The northern and southern boundaries coincide with major structural transitions between the Española Basin and basins to the south and to the north, where the thickness of the Santa Fe Group aquifer declines from several thousand feet (in the center of the basin) to near zero at the basin margins (Shomaker 1974) (Cordell 1979). The basin is separated from the Albuquerque and Santo Domingo basins to the south by a structural high, a prong of older sedimentary rocks, and several major fault zones. The site-scale model boundaries coincide with a surface water divide (to the west), and surface water courses to the north (Santa Clara Creek), to the east (the Rio Grande), and to the south (Rio Frijoles).

Figure 4-11 illustrates generalized flow directions within the basin and locations of inter-basin flow along model boundaries. Stream gage locations are also indicated; these data are described more in Appendix 4-E.

The LaGrit software (Trease et al. 1996) was used to develop numerical meshes for the basin and site-scale models. A grid refinement algorithm was used that allows extra detail to be placed where needed in the mesh, such as in the vicinity of LANL. The most refined grid, the site-scale model, has a horizontal resolution of 125m × 125m and a vertical resolution of 12.5m in the shallow layers of the aquifer beneath LANL.

### 4.2.4 Hydrostratigraphy

In contrast to previous models of the basin aquifer, the LANL models define aquifer heterogeneity on the basis of a separate 3-D hydrostratigraphic framework model. This model was developed with surface geologic maps, published cross-sections, geophysical studies, and numerous well logs (see Section 2 and Carey et al. 1999). It is based on structure and lithology, rather than hydrologic data. The degree of detail present in the model is much greater beneath the Pajarito Plateau than for other portions of the basin. This is primarily because there are many more deep characterization wells on the plateau than elsewhere in the basin, but also because of the more complex volcanic and sedimentary stratigraphy of the plateau compared with most other portions of the basin (e.g., Buckman wellfield, entirely within Santa Fe Group sediments).

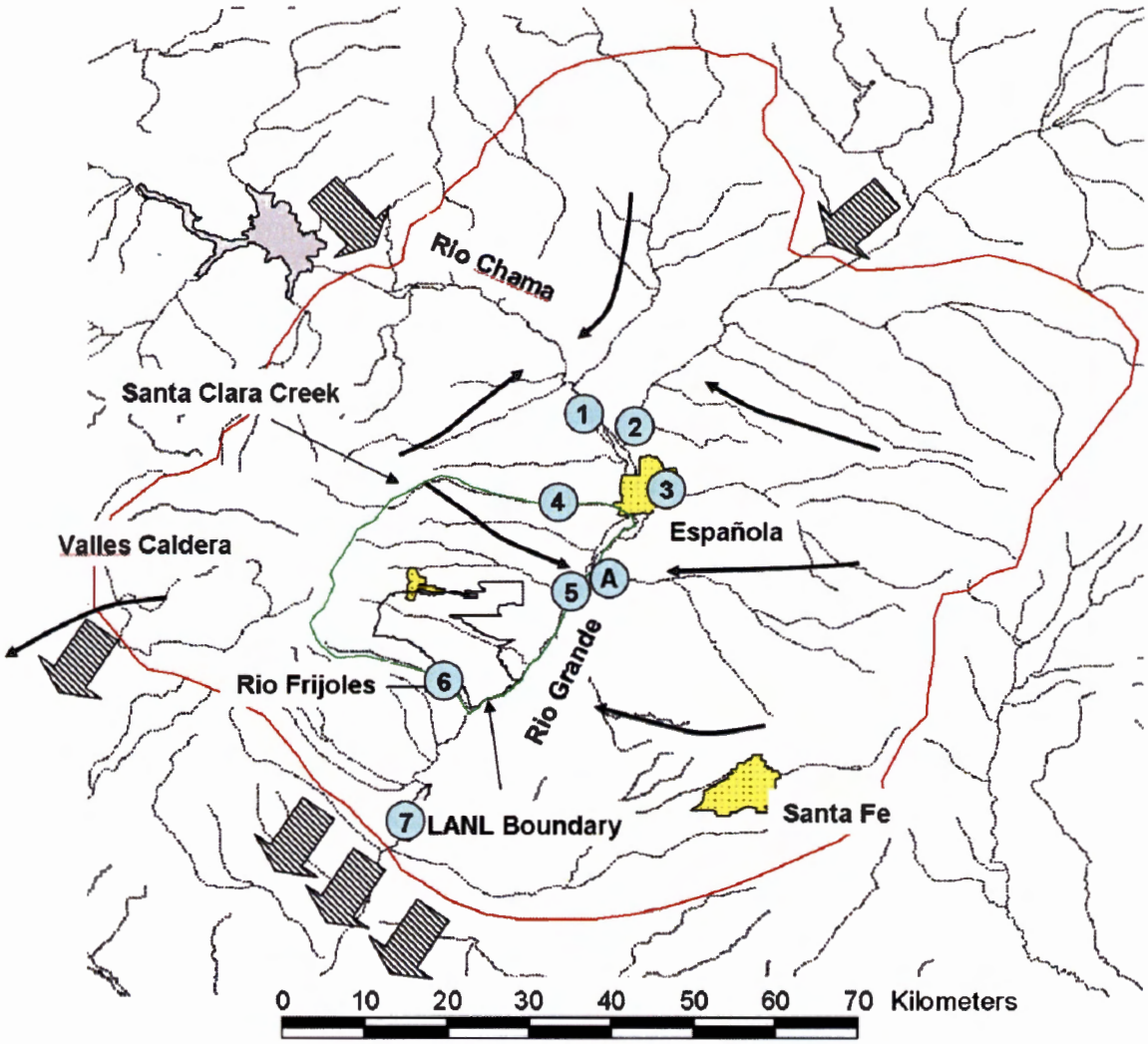


**Figure 4-11.** The Española Basin, with the basin-scale numerical model outline shown in red, and the site-scale model outline shown in green. Black arrows are generalized groundwater flow directions, based on regional water level data (Keating et al. 2003). Striped arrows indicate groundwater flow between this basin and adjacent basins. Circled numbers refer to USGS stream gages: (1) Rio Chama at Chamita; (2) Rio Grande at San Juan; (3) Santa Cruz River; (4) Santa Clara Creek; (5) Rio Grande at Otowi; (6) Rio Frijoles; (7) Rio Grande at Cochiti. The circled "A" indicates the mouth of Pojoaque Creek (see Appendix 4-E).

The process of overlaying the framework model on the numerical mesh for the flow and transport models has been described in Keating et al. (1999). This process assigns every node in the numerical mesh to one of the defined hydrostratigraphic units (see Appendix 4-D, Section 1). The high vertical resolution in the site-scale model is important to the representation of thin basalt flows and thin gravel beds within sedimentary units known to exist in this aquifer. The current model (September 2004) does not contain the latest update to the 3-D site-wide geologic model, which will include additional mapping from 2003 through 2005, drilling, and characterization data.

### 4.2.5 Boundary Conditions

The upper boundary of the model domain represents the top of the saturated zone; these nodes are either no-flow (no recharge), specified flux (recharge), or constant head (river nodes which may either recharge or discharge to the aquifer) (see Figure 4-12). Generally, the lower boundary of the model (no-flow) is the contact between the Precambrian basement and younger rocks. An exception to this is locations where the Precambrian basement crops out (such as in the Sangre de Cristos); in these areas we sub-divide the basement into a shallow, permeable block and a lower, impermeable block.

In the current model formulation, the entire thickness of the aquifer is assigned properties consistent with leaky-confined or confined conditions ($Ss = 10^{-3.3} - 10^{-4.5}\ m^{-1}$). In the current numerical framework, unconfined conditions can be approximated by assigning the shallow layers a relatively high value of specific storage. However, changes in the thickness of the aquifer due to changes in the water table elevation are ignored. This approximation is reasonable for flow simulations in the vicinity of LANL, due to the large thickness of the aquifer (>3000 m) relative to measured changes in heads with time (30–50 m over 50 years). However, transport simulations may be sensitive to this approximation and the model is currently being modified accordingly.

### 4.2.6 Recharge

Recharge from the unsaturated zone is represented as a specified flux boundary condition along the top of the model. The spatial distribution of recharge across the plateau and in the larger basin is complex and inherently uncertain, since recharge rates cannot be measured directly. The model uses a simple approach to represent the spatial distribution of recharge. The advantage of this approach is that it can be easily manipulated to approximate a wide variety of recharge conditions; this flexibility allows for exploration of uncertainty in model predictions due to the inherent uncertainty of any recharge estimate. The disadvantage of this approach is that it does not capture very fine-scale detail. At present, the models have assumed that recharge is constant in time.

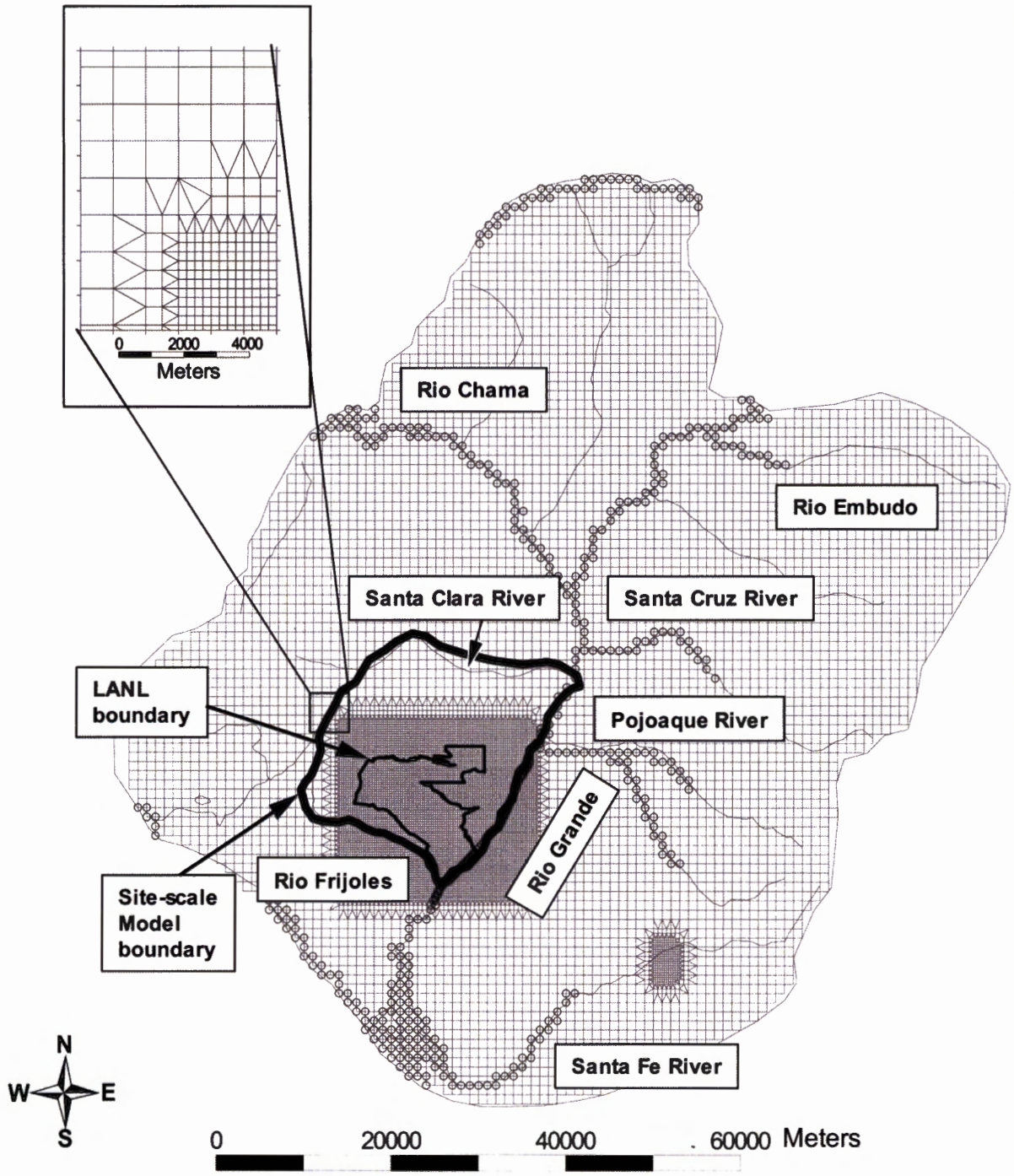


**Figure 4-12.** Basin model grid (plan view) with site-model boundaries indicated. The inset shows the northwest corner of the octree mesh refinement region. The circles show the locations of specified head nodes along rivers and basin margins.

There are three types of recharge accounted for in our model: areal recharge (which occurs mostly in the mountains), perennial stream channel recharge (for major streams in the basin), and ephemeral stream channel recharge (for many of the channels on the plateau). Areal recharge is determined as a function of precipitation (which is, in turn, determined by the surface elevation and long-term average precipitation trends in the basin). The details of the recharge model are presented in Appendix 4-D, Section 2. This numerical framework can be used to generate multiple possible models of recharge. Several examples are shown for the site-scale model in Figure 4-13; these different models all impart the same total flux to the aquifer. Table 4-3 shows the parameters used for these examples. For a more extensive discussion of regional and plateau recharge distributions, see Section 2.7.3.1.

### 4.2.7 Discharge at Rivers and Interbasin Flow

The Rio Grande, its lower tributaries, and locations where inter-basin flow occurs (upper Rio Chama, upper Rio Grande, lower Rio Grande, and Jemez River) are modeled as specified head nodes. Model-predicted fluxes at these boundaries are described in later sections. Heads at the surface are determined using digital elevation model (DEM) data for the basin. Heads at depth along the Española Basin/Albuquerque Basin are specified in accordance with estimates of the water table elevation at this boundary and are constant with depth to the Precambrian boundary. The assumption of "specified head" along the Rio Grande is an approximation suitable for flow and transport calculations far from the river. This simplification is inadequate for addressing the details of stream/aquifer interactions at the Rio Grande and is currently being addressed.

### 4.2.8 Lateral Boundaries of the Site-Scale Model

The locations of the lateral boundaries of the site-scale model were selected with the expectation that fluxes across the boundaries (which are uncertain) will be small relative to the total flux through this portion of the aquifer. The basin model is used to estimate these fluxes, with estimates of corresponding uncertainty (Keating et al. 2003). Fluxes across these lateral boundaries are explicitly mapped, node by node, onto site-scale model boundaries. That analysis showed that uncertainty in fluxes into the site-scale model (from the north) and out of the site-scale model (to the south) due to basin model parameter uncertainty was relatively small. In contrast, flux uncertainty across the western and eastern boundaries was relatively large. These results are described in more detail below.

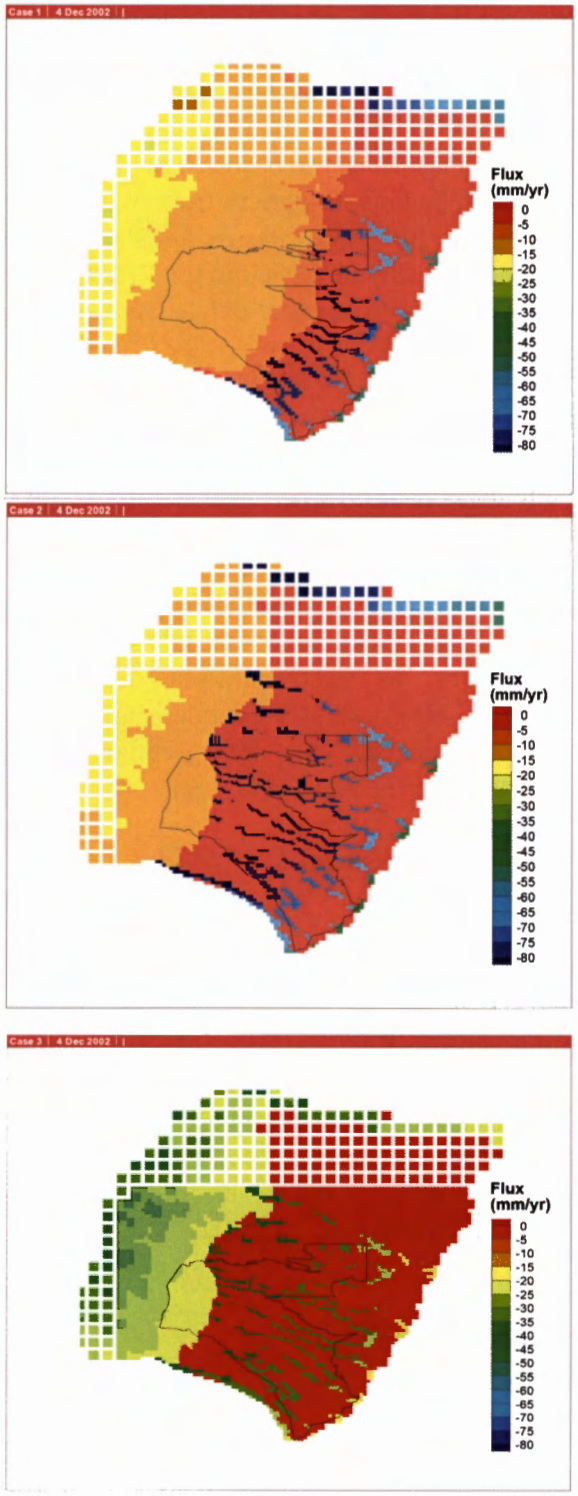


**Figure 4-13.** Examples of three recharge models, all imparting the same total flux. Model parameters are shown in Table 4-3.

**Table 4-3.**
**Example Recharge Models, Shown in Figure 4-13.**

| | Case 1 | Case 2 | Case 3 |
|---|---|---|---|
| Total recharge (kg/s) | 200.3 | 200.3 | 200.3 |
| Diffuse | 122.3 | 70.6 | 145.2 |
| Canyon-focused | 78.0 | 129.7 | 55.1 |
| Zmin (m) | 2000 | 2200 | 2200 |

### 4.2.9 Data Used in Model Development and Testing

The datasets used in model development and testing are as follows: water level data, well construction and location data, water supply production data, hydrostratigraphy, stream channel location and elevations, hydrologic and structural boundaries for the basin, stream gage data, and selected geochemical data. The water level data, well construction and location data, water supply production data, precipitation data, stream gage data, and geochemical data are tabulated in Keating et al. (2005). Hydrologic divides (used to define model boundaries) and stream channel location and elevations were derived from USGS DEM data. Structural and geologic transitions used to define lateral basin boundaries were derived from Kelly (1978) and Shomaker (1974).

### 4.2.10 Flow Model Parameters

Model inputs are recharge rates, aquifer properties (permeability, specific storage), and stress (water supply production rates). Model outputs are heads and aquifer discharge (at constant head nodes along the Rio Grande, Rio Chama, and its tributaries, the Jemez River, and lateral boundaries). Other quantities such a travel times, flow directions, and well capture zones can also be derived from the model output.

As is the case in most groundwater systems, model outputs (heads and aquifer discharge) can be measured with much greater accuracy than model inputs (recharge rates and aquifer properties). This study employs the standard techniques of inverse analysis to derive model inputs (recharge rates and aquifer properties) from model outputs (heads and aquifer discharge). This is the same procedure widely used to derive aquifer properties from pump test data. The application of this method is somewhat unusual in that it acknowledges uncertainty in recharge, a complication that is usually neglected. This analysis provides information on aquifer properties and recharge, with quantified uncertainty, which can then be used to drive forward models and produce predictions.

The methodology used for inverse analysis is described in detail in Keating et al. (2000) and Keating et al. (2003). The three sets of calibration data are (1) pre-development heads (little or no impact from pumping), (2) transient heads (1946–2003), and (3) pre-development estimates of aquifer discharge to rivers. The data are listed in Keating et al. (2005). The details of the inverse analysis have changed over time, and the calibration data set has expanded as new wells have been drilled, computational resources have improved, and the hydrostratigraphic framework model has evolved. The aquifer properties derived from this process should represent larger spatial scales than those derived from short-term pump tests (days), since the transient data set

used represents a long period of time (55 years) and a widely spaced data set (several kilometers).

Table 4-4 illustrates several representative results for inverse analyses conducted using the basin- and site-scale models. See Keating et al. (2003; 2004) for details of these analyses. It is striking that the estimate for the lower Santa Fe Group is so much lower than pump tests conducted in the Los Alamos wellfield (completed entirely within the Santa Fe Group). This may be due to large-scale features, such as north-south trending faults, which would lower the effective permeability of the aquifer. Or this may be due to errors in the analysis or supporting datasets, such as a too low estimate of total recharge to the system. More detailed discussion of the hydrologic properties can be found in Section 2.8.

Figure 4-14 illustrates the degree of match between measured and simulated heads and fluxes at the basin scale, using the parameters shown in Table 4-4 (parameter set 1). Figure 4-15 shows the degree of match between measured and simulated hydrographs in the vicinity of LANL (parameter set 3). The magnitude of measured head response to 60 years of pumping (about 15 m in the central plateau, about 40 m to the east in the Los Alamos wellfield) is adequately reproduced, as is the recovery of heads in the Los Alamos wellfield after the cessation of pumping in 1975). Agreement between simulated and measured heads in water supply wells on a year-to-year basis is less accurate. Possible reasons for this, listed in detail in Keating et al. (2005) include both model errors and measurement errors. Improved fits would require explicit consideration of sub-annual variations in both water production and in measured water level responses.

### 4.2.11 Transport Model Methods and Parameters

The FEHM transport code employs one of two primary methods to simulate solute transport. The first is a particle-tracking methodology. This method can be used to simulate advection-only transport, which produces path lines and travel times that would be expected to represent the mean behavior of a conservative (non-reactive) solute plume. This method can also be used to simulate advective-dispersive transport, where thousands of particle paths are simulated and the number of particles present in any location represents solute concentrations. The second method is a direct solution of the advection-dispersion equation. This method can be used to simultaneously calculate the migration of multiple solutes, concentrations as a function of time and space, and a full suite of reactions with liquid, solid, and gas phases.

## Table 4-4.
## Regional Aquifer Model Parameters

| | | Basin Model | | Site Model (2003) | | Site Model (2004)A | | Site Model (2004)B | |
|---|---|---|---|---|---|---|---|---|---|
| | | Value | +/- | Value | +/- | Value | +/- | Value | +/- |
| **Recharge** | | | | | | | | | |
| | Zmin [m] | 2195.0 | 177.0 | 2214.0 | 362.0 | 2156.1 | 14.0 | 2259.8 | 77.5 |
| | Recharge volume [$m^3$] | 3844.6 | 511.9 | 218.5 | NA | 253.7 | NA | 263.3 | 57.9 |
| | α | NA | NA | NA | NA | 0.1 | NA | 0.1 | NA |
| | κ | NA | NA | NA | NA | 0.0 | NA | 0.1 | NA |
| **Pemeabilities (log10[m2])** | | | | | | | | | |
| Crystalline rocks | Deep Basement (pC) | -15.6 | 8.6 | -15.6 | 305.9 | -18.0 | NA | -18.0 | NA |
| | Paleozoic/Mesozoic | -15.0 | 3.2 | -15.1 | 41.0 | -13.7 | NA | -13.7 | NA |
| | Shallow Sangres | -12.6 | 0.2 | na | NA | NA | NA | NA | NA |
| | Fractured pC | -13.1 | 0.6 | na | NA | NA | NA | NA | NA |
| | Tschicoma Formation | -13.0 | 0.2 | -13.0 | 5.8 | -15.3 | NA | -14.6 | 1.0 |
| Keres Group | Tk (shallow) | NA | NA | NA | NA | -12.7 | NA | -12.7 | NA |
| | Tk (deep) | NA | NA | NA | NA | -13.7 | NA | -13.7 | NA |
| basalts | lumped | -12.2 | 0.2 | -11.9 | 0.6 | NA | NA | NA | NA |
| | Tb4 | NA | NA | NA | NA | -16.1 | 6.5 | -14.9 | 1.7 |
| | Tb1 | NA | NA | NA | NA | -12.1 | NA | -13.5 | 0.4 |
| | Tb2 | NA | NA | NA | NA | -12.2 | NA | -12.2 | 0.4 |
| Puye Formation | (lumped) | -14.2 | 1.4 | -14.4 | 2.7 | NA | NA | NA | NA |
| | Tpt | NA | NA | NA | NA | -12.7 | NA | -11.9 | 0.7 |
| | Tpt-z | NA | NA | NA | NA | -12.7 | NA | -17.5 | 3.2 |
| | Tpp | NA | NA | NA | NA | -16.8 | 1.1 | -11.9 | 0.3 |
| | Tpf | NA | NA | NA | NA | -13.1 | 0.2 | -12.9 | 0.7 |
| | Tpf-z | NA | NA | NA | NA | -15.2 | NA | -15.9 | 0.5 |
| | Tpp-z | NA | NA | NA | NA | NA | NA | -11.0 | 71.9 |
| Santa Fe Group | Tsf-fang[1] | -13.2 | 0.3 | -13.4 | 0.4 | -11.1 | 0.3 | -19.0 | 75.0 |
| | vertical | -15.5 | 0.9 | -15.6 | 1.6 | -11.4 | NA | -18.4 | 0.6 |
| | Tsf -sandy | -13.2 | 0.2 | -13.1 | 0.3 | -13.3 | 0.1 | -13.4 | 0.1 |
| | vertical | -15.0 | 0.4 | -15.5 | 0.9 | -14.2 | 0.1 | -13.5 | 0.2 |
| | East, Pojoaque | -14.1 | 0.4 | NA | NA | NA | NA | NA | NA |
| | Airport | -12.6 | 0.8 | NA | NA | NA | NA | NA | NA |

## Table 4-4.
## Regional Aquifer Model Parameters (continued)

| | | Basin Model | | Site Model (2003) | | Site Model (2004)A | | Site Model (2004)B | |
|---|---|---|---|---|---|---|---|---|---|
| | | Value | +/- | Value | +/- | Value | +/- | Value | +/- |
| **Recharge** | | | | | | | | | |
| | North | -13.4 | 0.5 | NA | NA | NA | NA | NA | NA |
| | Ojo Caliente sandstone | -13.3 | 0.2 | NA | NA | NA | NA | NA | NA |
| | Peñasco embayment | -12.4 | 0.3 | NA | NA | NA | NA | NA | NA |
| | deep | NA | NA | NA | NA | -16.0 | NA | -16.0 | NA |
| | Ancha formation | -12.3 | 0.5 | NA | NA | NA | NA | NA | NA |
| Pajarito fault zone | | -15.3 | 0.8 | -15.3 | 27.1 | -15.0 | NA | -13.9 | 1.3 |
| Specific Storage | (Ss) log10[m-1] | -3.9 | 0.4 | -3.6 | 0.5 | -4.3 | 0.1 | -3.8 | 0.3 |

[1]referred to as Tsf-uv in earlier models
NA = not applicable

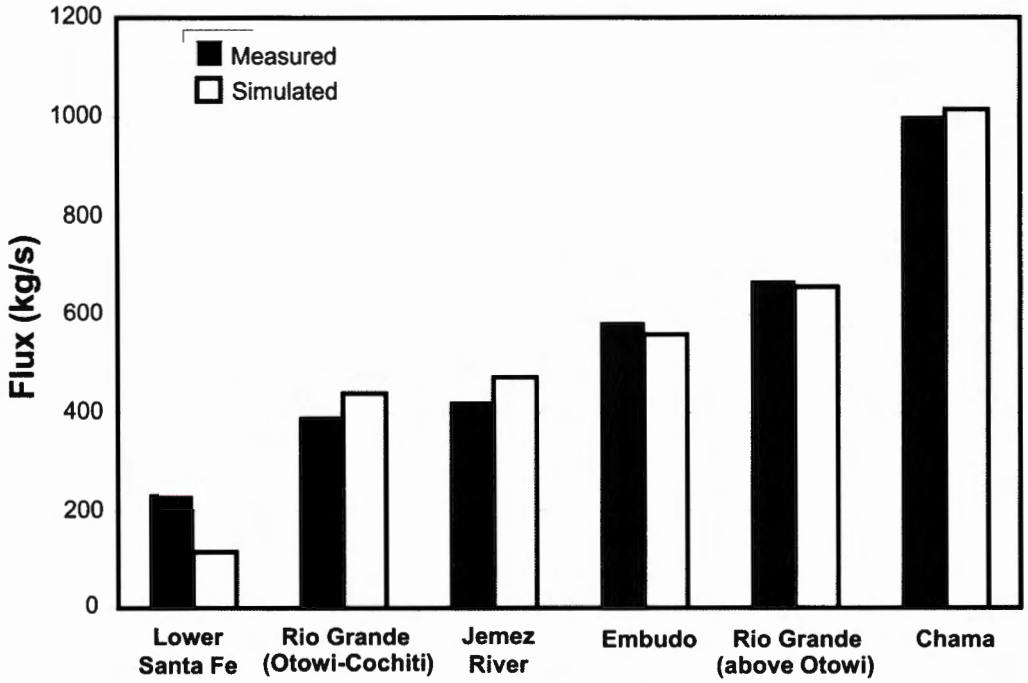


(a)

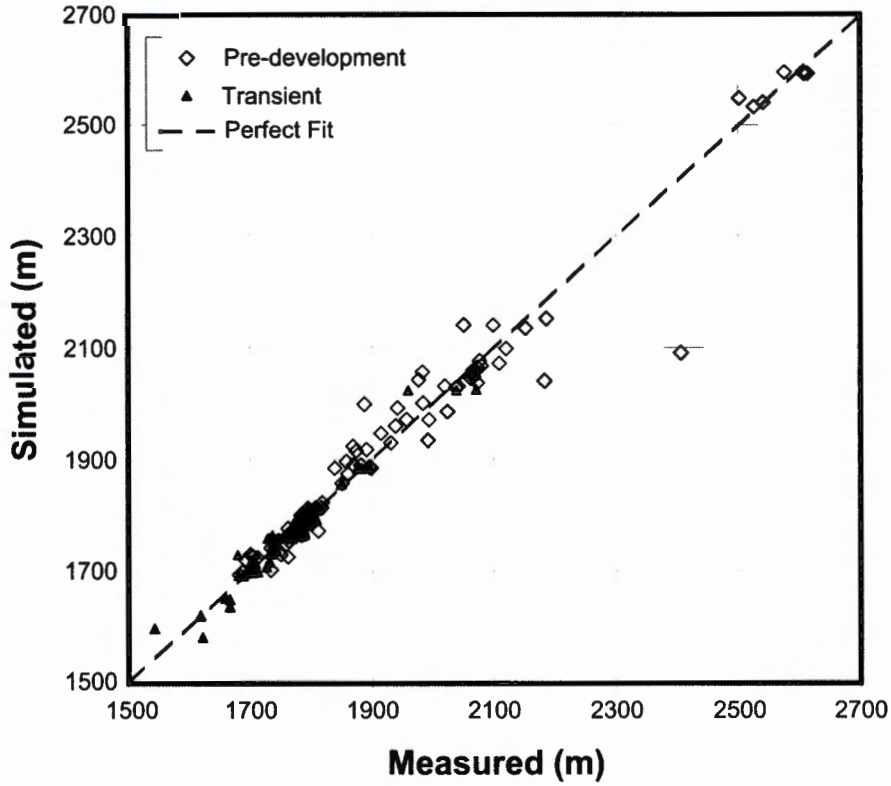


(b)

**Figure 4-14.** For the basin-scale model, comparison between measured and simulated (a) fluxes; (b) heads.

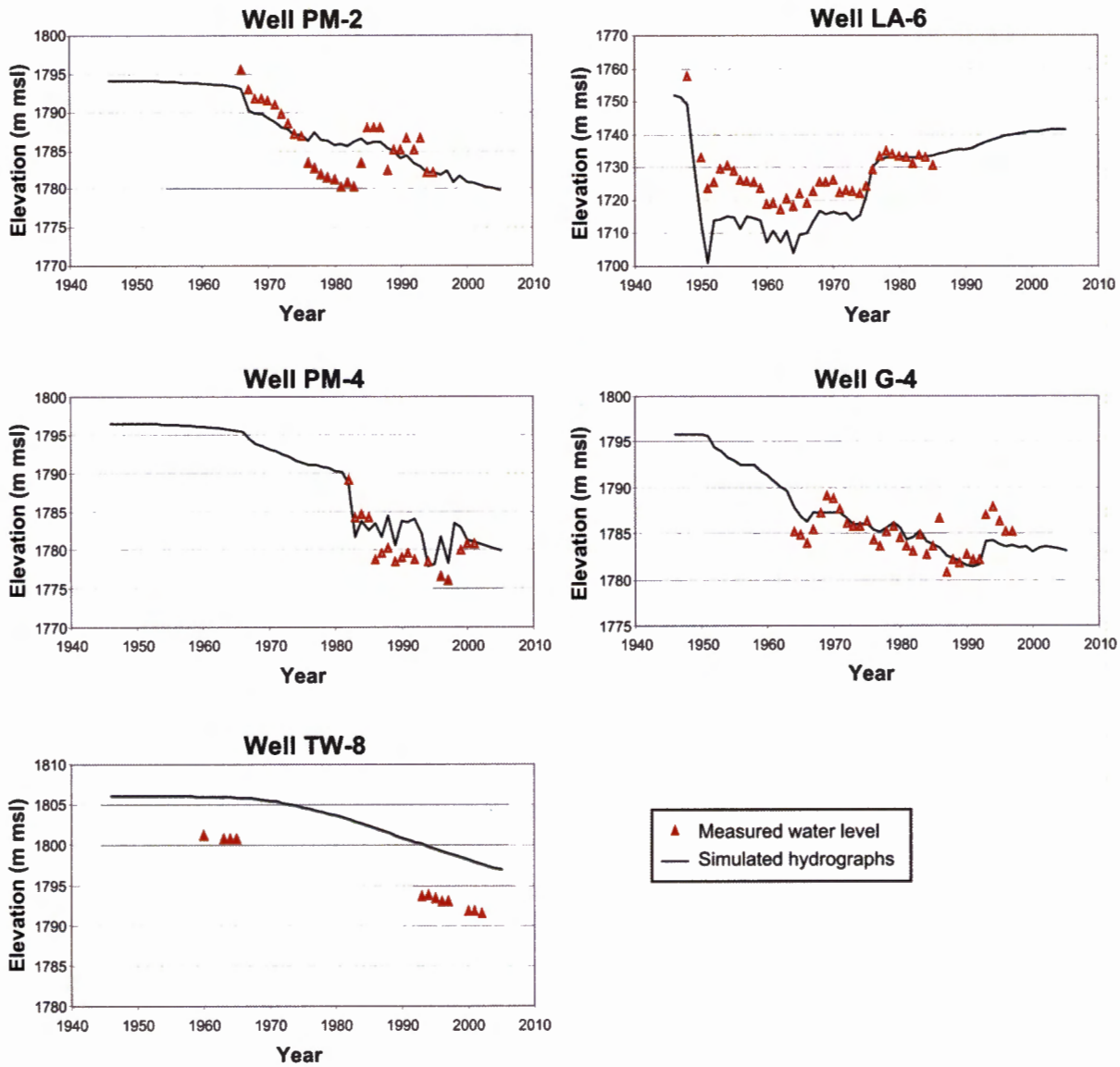


**Figure 4-15.** Comparison of simulated and measured hydrographs for representative wells on the plateau.

For nonreactive chemistry simulations, the particle-tracking methodology is preferable because it avoids the problem of numerical dispersion. Most of the analyses presented here use this method. One important limitation of this method is that the solution is invalid in portions of the numerical grid where elements are nonorthogonal (see Appendix 4-D, Section 1, Figure 4-D-2). However, in these calculations we restrict our analysis of particle-tracking paths to the fine-grid region at the site scale, thereby avoiding the problem.

Two critical parameters for nonreactive transport simulations are rock porosity (which is linearly proportional to travel time) and dispersivity (which controls the degree of spreading and mixing). Neither of these types of data has been collected in this aquifer at scales meaningful for site-scale transport simulations. Therefore, the model uses literature-derived values appropriate for the types of rocks present in this aquifer.

### 4.2.12 Model Applications

There have been three broad categories of model applications. The following subsections present brief examples of modeling studies for each category.

#### 4.2.12.1 Category A: Integrate and interpret 3-D site-wide hydrologic and hydrostratigraphic data, to provide a more quantitative basis for testing site-wide conceptual models than was previously possible.

Many of the fundamental issues pertaining to the regional aquifer are questions that cannot be answered using data collection alone. Where are the predominant recharge areas? How much water is flowing through the aquifer? What are the large-scale hydraulic properties of the aquifer rocks? In what direction is water flowing? What is the pore water velocity of the groundwater? What effect has pumping had in the past and what effect will it have in the future? A great deal of characterization data has been collected over the past few years to address these questions, and the numerical models have been used as a framework for interpreting these data and providing at least partial answers to these questions.

**1. Large scale fluxes.** Keating et al. (2003) demonstrated the use of inverse and predictive analysis to examine the range of possible fluxes and recharge distributions that could explain the measured head data and stream gage data at the basin-scale. This approach acknowledges the uncertainty in aquifer properties and recharge rates, and attempts to determine to what extent quantitative estimates can be made. The aquifer property estimates that resulted from this approach, with uncertainty, are presented in Table 4-4 (parameter sets 1 and 2); the degree of agreement between measured and simulated heads and base flow gains are presented in Figure 4-14.

As shown in Figure 4-14, this analysis demonstrates that the basin-scale model provides a reasonable fit to measured head gradients and discharge to river reaches. The estimated elevation above which significant areal recharge occurs (2195 m, shown as a red line in Figure 4-16) matches almost exactly the location of the transition proposed by Wasiolek (1995). In addition, the estimated percent of precipitation that becomes recharge in the mountains (8%) falls within, although close to the low end of, the range of watershed study results (Appendix 4-E). The predicted outflow to the Albuquerque Basin of 5,801 acre feet per year (afy) is less than previous USGS studies of the Española Basin (McAda and Wasiolek 1988) and more recent studies of the Albuquerque Basin (14,300 afy) (Plummer et al. 2004). This value could be increased by increasing the percent of precipitation that becomes recharge and still be within the range of reasonable values. These results generally support the conceptual model of total basin-scale recharge and discharge fluxes (tabulated in Appendix 4-D and Appendix 4-E), as well as the generalized spatial distribution of fluxes simulated with the recharge model described in Appendix 4-D, Section 2. It also demonstrates the value, at least at large scales, of the 3-D hydrostratigraphic framework model.

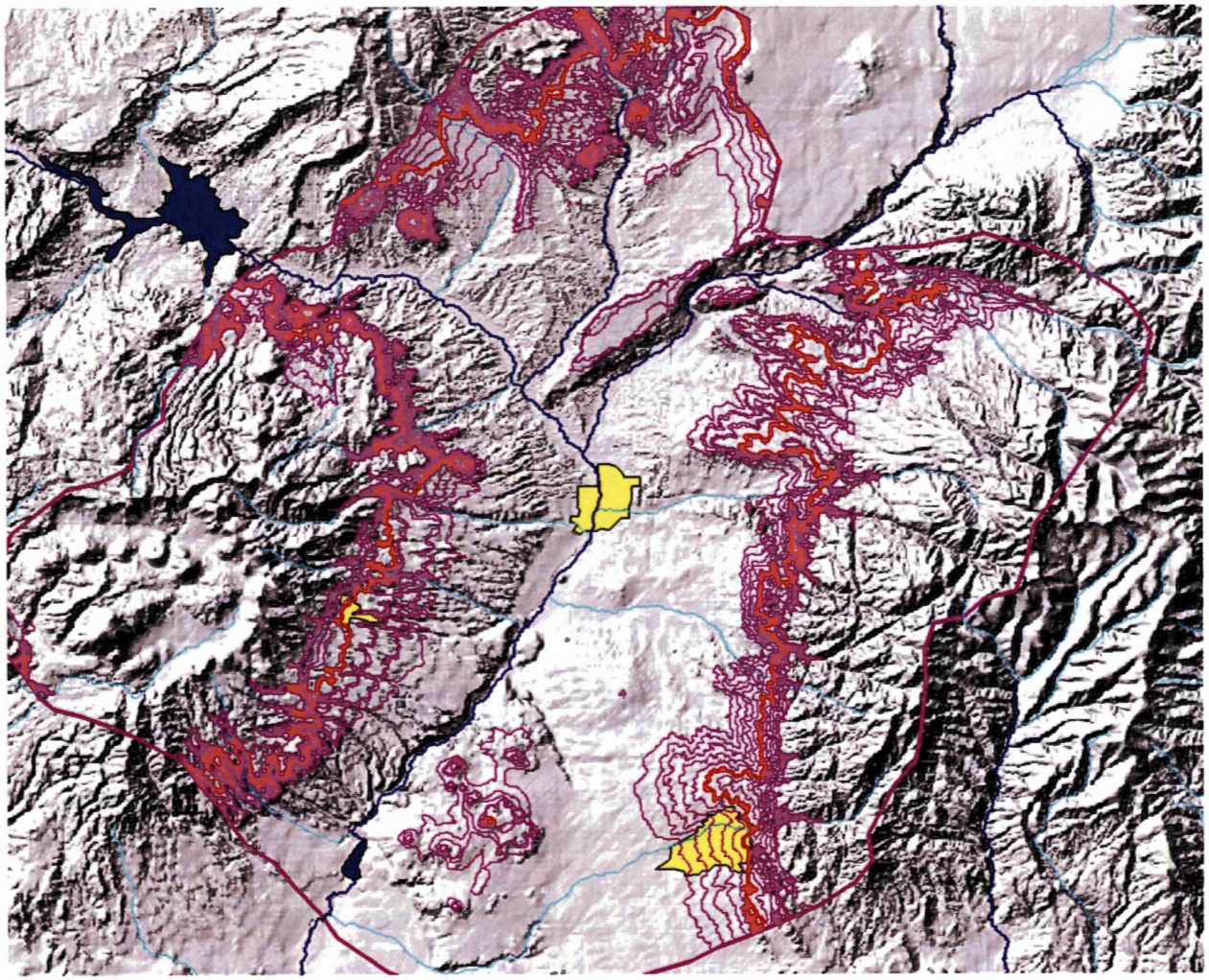

**Figure 4-16.** Location of predicted transition between significant areal recharge and negligible areal recharge (2195 m), and uncertainty bounds. Pink contours span the elevation uncertainty range.

The results of the basin-scale inverse analysis were used to estimate fluxes across the lateral boundaries of the site-scale model, with uncertainty. Figure 4-17 shows the results of this analysis. Fluxes perpendicular to flow (north and south) were calculated to be relatively small and showed much less uncertainty than fluxes parallel to flow (east and west). Significant flux is predicted to cross both the western and eastern boundaries; the high uncertainty of these estimates, however, means that this uncertainty should be explicitly considered when doing transport calculations that might be affected by these fluxes.

All these results depend on the streamflow analyses being reasonably accurate, the 3-D geologic model capturing the most important large-scale hydrologic features in the aquifer, and the method of inverse analysis fully exploring parameter uncertainty. This technique only explores the impact of numerical model parameter uncertainty; overall uncertainty in recharge and fluxes, which would include conceptual model errors, is undoubtedly larger.

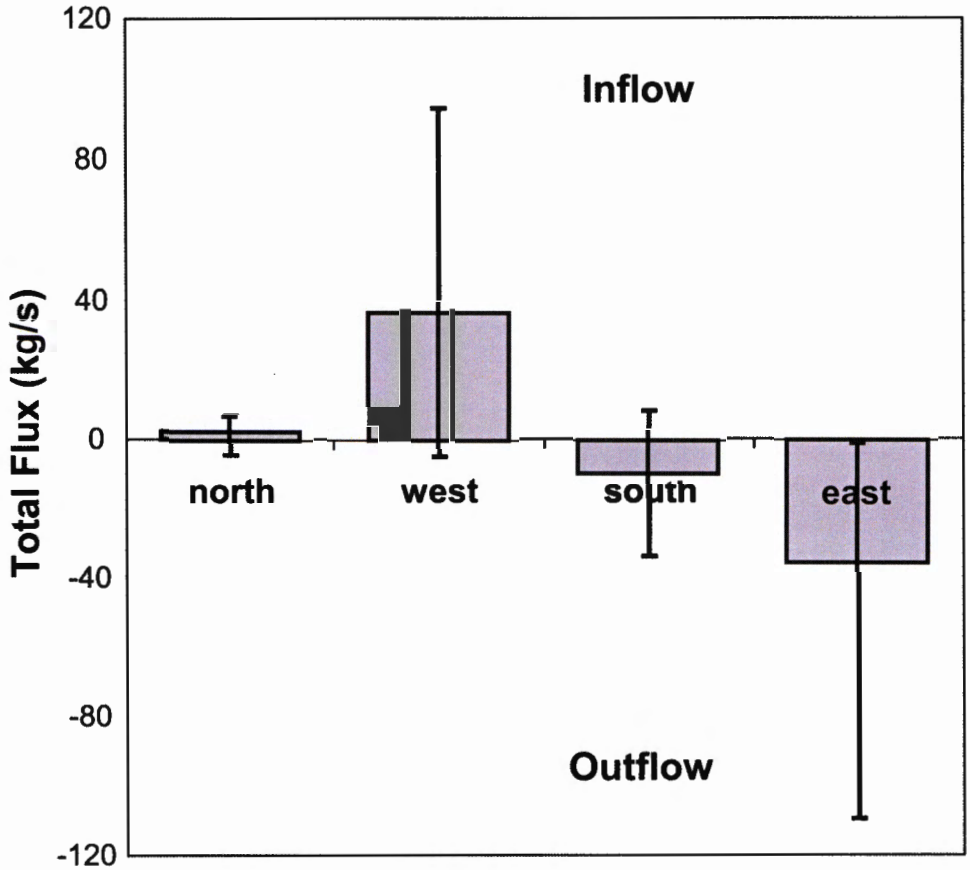


**Figure 4-17.** Fluxes across lateral site-model boundaries predicted by the calibrated basin model. Error bars represent the 95% nonlinear confidence intervals of estimates.

**2. Small-scale fluxes, downgradient of LANL.** A more recent study, Keating et al. (2004), used similar techniques to explore not only the question of uncertainty of total flux through the aquifer, but also uncertainty in fluxes through shallow portions of the aquifer immediately downgradient of LANL. This analysis is pertinent to estimates of contaminant transport away from the site. Figure 4-18 shows that parameter uncertainty in the site-scale model (including uncertainty in recharge rates and aquifer properties) contributes significantly to estimates of total recharge for the aquifer, but that the flux through the shallow portion of the aquifer immediately downgradient of the site is more certain. More detailed study of this result did highlight the large uncertainty in fluxes through a single basalt unit, however. Uncertainty in transport parameters, such as porosity, would produce a much larger impact on total velocity uncertainty; therefore, this study suggests that better measurement of fluxes and recharge would be of far less value than collecting site-specific estimates of porosity.

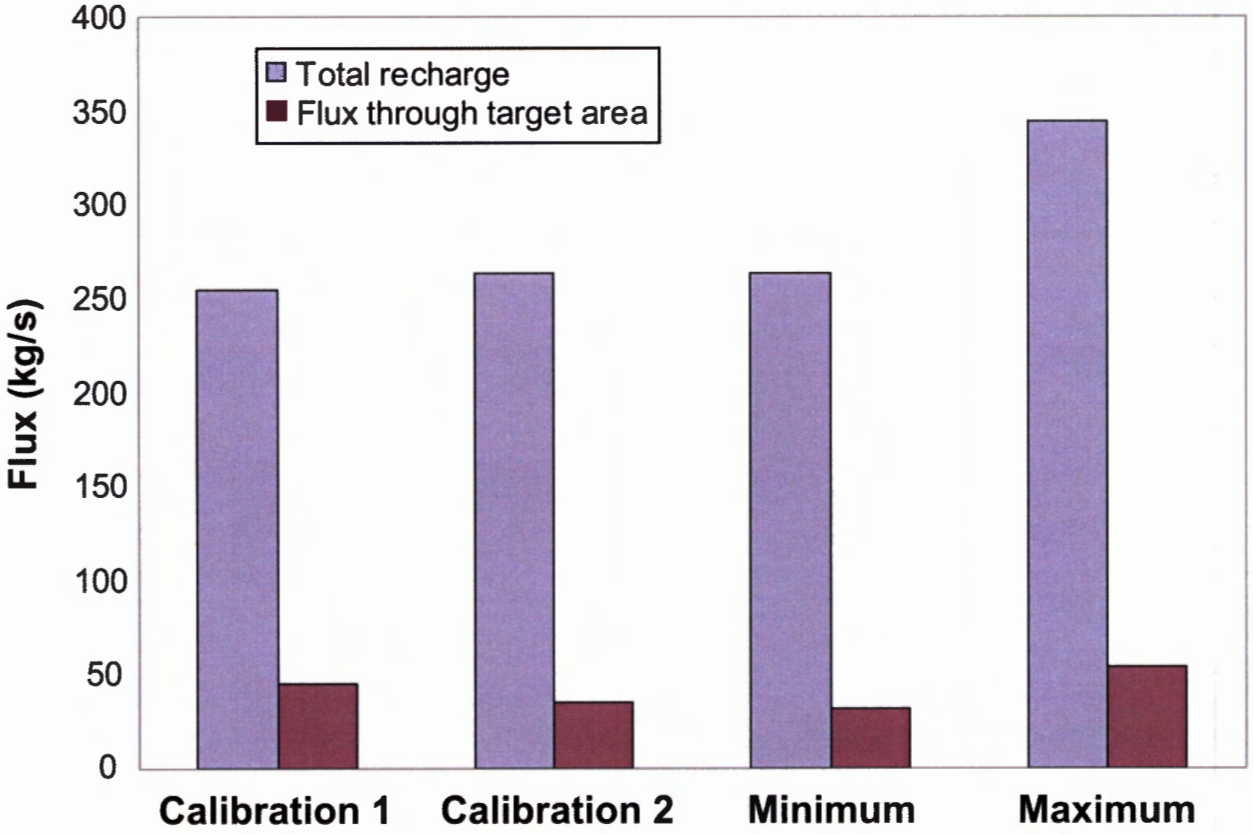


**Figure 4-18.** Results of predictive analysis, compared to two calibrated models. Blue bars indicate total recharge into the aquifer; red bars indicate flux through the shallow plane east of LANL.

**3. Pore-water velocity.** Pore-water velocities in the regional aquifer are very poorly constrained. Through modeling techniques described in this report, flow directions and fluxes can be surmised reasonably well, but velocities are very difficult to infer from hydrologic data alone. Contaminant distributions within the regional aquifer have been useful for identifying the location of fast pathways through the vadose zone, but since the exact location and timing of contaminant entry to the water table is highly uncertain, these observations do not constrain velocities in the regional aquifer. The best method for determining velocities is tracer tests.

The LANL model was used to produce a map of velocities at the water table (see Figure 4-19). These velocities are highly uncertain and are used only to illustrate a few key points. First, given the heterogeneous nature of the aquifer, groundwater velocity is likely to vary considerably over short distances. In this map, the fastest velocities are in the basalts where fracture flow (very low matrix porosity) is assumed. Second, flow on the eastern portion of LANL is predicted to be very slow. This is due to the very low permeability of the Santa Fe Group, which is prevalent at the water table east of LANL (see Table 4-4, Figure 2-10, and related discussion in Section 2.8.7).

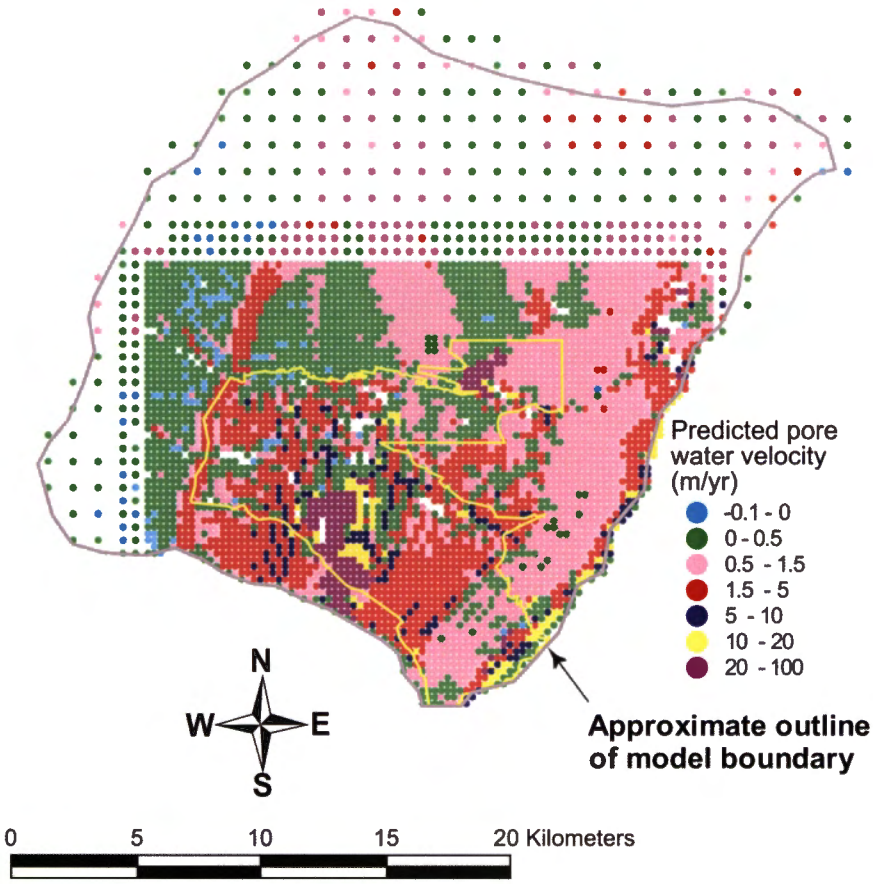


**Figure 4-19.** Model-predicted horizontal component of pore-water velocity at the water table, in m/yr.

The very slow velocities predicted by the model are consistent with $^{14}C$ data presented by Rogers et al. (1996a,b). These data are collected in both water supply wells (screened over the upper 2000 ft of the aquifer) and more shallow wells (DT5A, east side and west side artesian). Figure 4-20 shows a comparison of model predicted $^{14}C$ and measured $^{14}C$ presented by E. Kwicklis in Keating et al. (2000). One interesting aspect of this comparison is that the model underpredicts the age of the very old waters present near the Rio Grande.

In stark contrast to these predictions, Purtymun et al. (1984) produced a generalized map of pore-water velocity in the regional aquifer. His estimates assumed a uniform hydraulic gradient of 0.01 m/m, a uniform porosity of 0.1, and 1-D lateral flow. Using a 1-D version of Darcy's Law and hydraulic conductivity estimates from local pump tests, his resulting velocities ranged from 20 ft/yr (Los Alamos wellfield) to 345 ft/yr (DT wells). Assuming the high velocity estimate of 345 ft/yr, this would represent a travel time of 134 years across LANL from west to east (~9 miles). McQuillan (2003) used the chemistry data from White Rock Canyon Springs and TW-1 and an assumption of 1-D lateral flow to derive a velocity estimate of 358 ft/year (59 year travel time, ~4 miles). More recently, a report by Rice (2004), concurred with these earlier estimates.

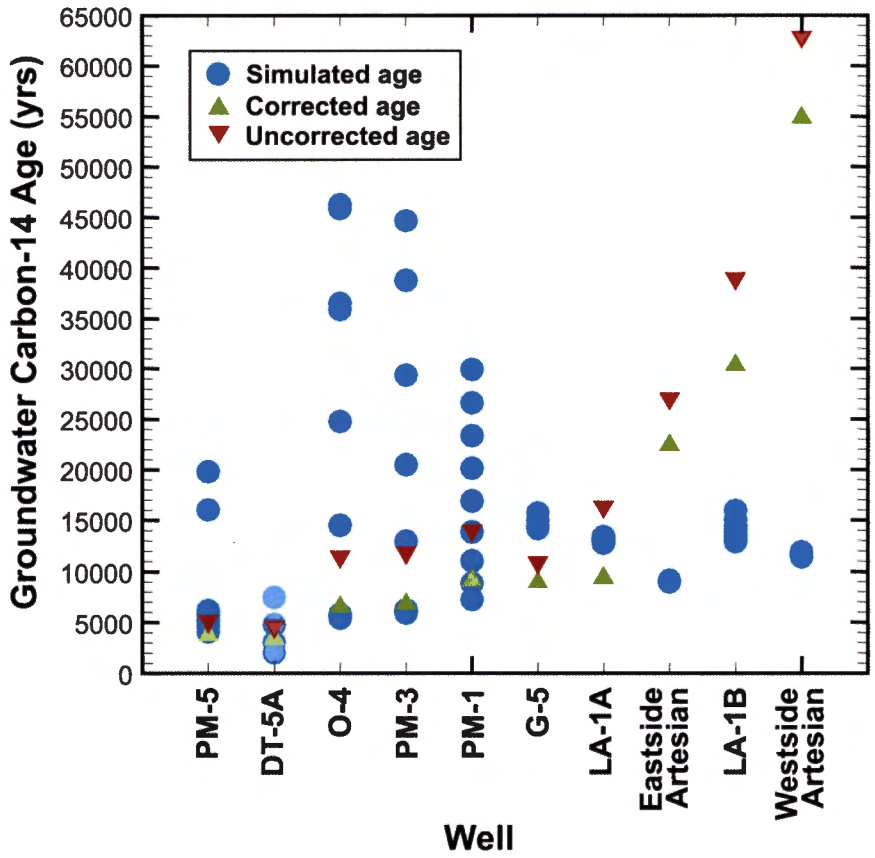


**Figure 4-20.** Comparison of simulated groundwater carbon-14 ages at nodes within the screened depths of wells with the corrected and uncorrected groundwater ages estimated from measured carbon-14 activities.

At present, it is impossible to compare the McQuillan and Rice calculations to the published LANL regional model predictions, because in the model (as configured for past applications) the springs are above the top of the model and therefore flow to the springs cannot be simulated. This is a subtle but very important distinction because the top of the model at present is entirely within the low-permeability Santa Fe Group in the vicinity of the Rio Grande, whereas slightly higher elevations (which include the springs) are within the more permeable units of the Puye Formation. Some springs also issue from the base of the Cerros del Rio lavas. If transport calculations to the springs are required in the future, minor adjustments to model boundaries will suffice to address this issue.

A more difficult question is that of measured hydraulic head gradients and lateral continuity of highly permeable rocks. The model honors measured gradients (in 3-D), the 3-D hydrostratigraphic framework model, and large-scale effective properties of rock units (see Table 4-4). At present, neither the measured 3-D hydraulic heads nor the permeability/hydrostratigraphy information supports the hypotheses presented by McQuillan and Rice. In such a complex aquifer, however, it is entirely possible that their hypotheses could be correct.

## 4. Effect of water supply well production

**Capture zones.** Understanding the influence of water supply production on the aquifer is important from the perspectives of both water supply and contaminant transport. From a water supply perspective, it is very important to know if the current rates of withdrawal are sustainable. From a contaminant transport perspective, an understanding of capture zones is critical to placement of a "sentry" well to protect a production well and to identification of which receptors are most at risk of contamination.

The LANL models have been used to evaluate the impact of water supply production in a number of studies. The philosophy of this approach has been to start simply and gradually add complexity only when needed. In a sense, all of these studies have illustrated the shortcomings of applying "simple" textbook methods of capture zone analysis to this site. Therefore, this is very much an ongoing study.

Using a relatively simple approach, Vesselinov et al. (2002a) calculated capture zones for the Buckman wellfield and all the Los Alamos wells. The motivation for this study was to determine if the LANL aquifer was within the capture zone for the Buckman wells, either at present or (possibly) in the future. This analysis was based on the standard "steady-state" assumption. The results, shown in Figure 4-21, demonstrated that a significant portion of the aquifer beneath LANL could eventually be captured by the Buckman wells. These results also showed the zones of influence of Los Alamos County water supply wells.

The assumptions inherent in this analysis are that current rates of production in water supply wells continue indefinitely until steady state is reached. Given the characteristics of this aquifer, this is not expected to occur for several hundred years from the present. Some wells in the Guaje field and some wells in the Pajarito field (PM-2, -4, and -5) appear to be stabilizing with respect to pumping; the assumption of steady-state may be applicable to these wells. However, given the dramatic fall of water levels in the Buckman wellfield over the past two decades, steady-state is far in the future. Given the uncertainties of water production over the next few decades (e.g. City of Santa Fe is expected to rest the Buckman field beginning in 2009, the steady-state approximation is questionable for this wellfield. It does, however, show one possibility that should be considered for planning purposes.

Vesselinov and Keating (2003) investigated the impact of dispersion and transients on capture zones analyses. Figure 4-22 shows the predicted capture zones when both dispersion (spreading of the plume) and transients (changes in source term and changes in water supply production) are included in the analysis. These authors concluded that significant errors were incurred when dispersion and/or transients were neglected in the analysis. The importance of transients (changing flow field in response to changing water production rates) highlights the importance of identifying when and where contaminants might reach the water table. For the same point of entry to the water table (for example, beneath Ten Site Canyon), a contaminant reaching the aquifer in 1960 might be captured by PM-1, whereas a contaminant reaching the aquifer in 1990 might be captured by PM-5.

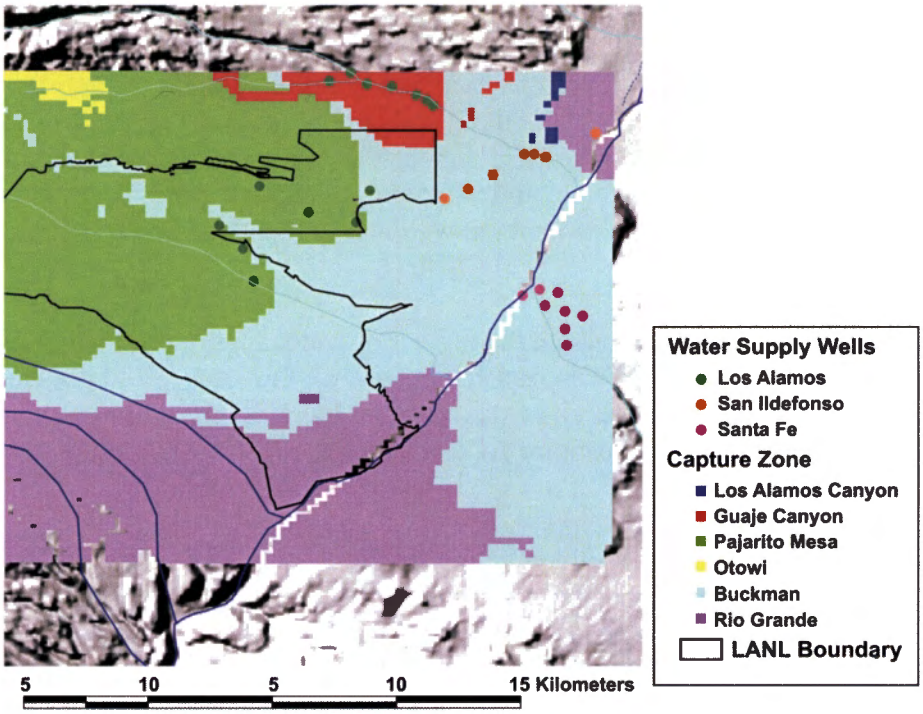


**Figure 4-21.** Predicted steady-state capture zones for wellfields in the vicinity of Los Alamos (from Vesselinov et al. 2002a).

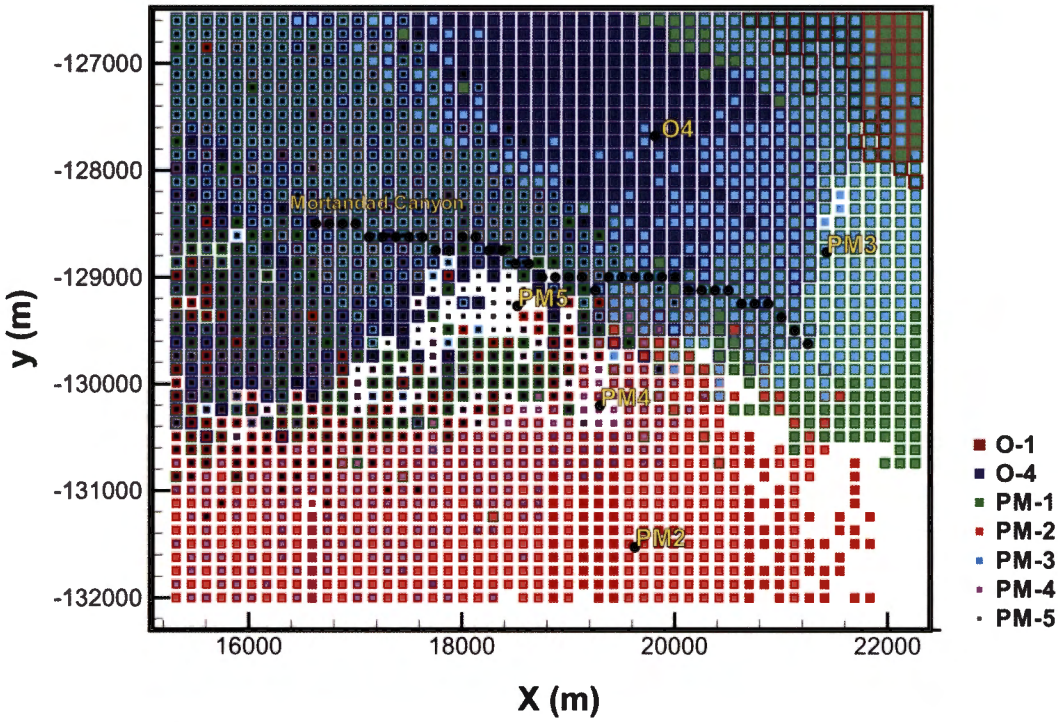


**Figure 4-22.** Predicted transient capture zones for wellfields in the vicinity of Los Alamos from Vesselinov and Keating (2003).

**Effect on streamflow.** In a basin such as the Española Basin, where surface water flow depends to a large degree on groundwater discharge, any water supply production will affect aquifer storage immediately and surface water flow eventually. When the aquifer reaches equilibrium with respect to pumping, the only continued impact will be on surface water flow. Wells drilled near the point of discharge will have a significant effect on surface water flow sooner than wells drilled far from the point of discharge.

Based on parameters shown in Table 4-4 (parameter set 3), the site-scale model was used to predict the percentage of produced water coming from storage and captured streamflow (or recharge) over the past 50 years. Figure 4-23 shows these results, demonstrating that the aquifer is still far from steady-state and that most produced water is still coming from storage.

**5. Hydrostratigraphy.** All of the studies listed above rely on the 3-D hydrostratigraphic framework model to define heterogeneity within the aquifer, according to the spatial distribution of approximately 15 units. Of course, with relatively sparse boreholes on the plateau there is uncertainty in the exact spatial extent of these units (Section 2.4.4). There also may be important heterogeneities within the hydrostratigraphic units as defined by the 3-D model.

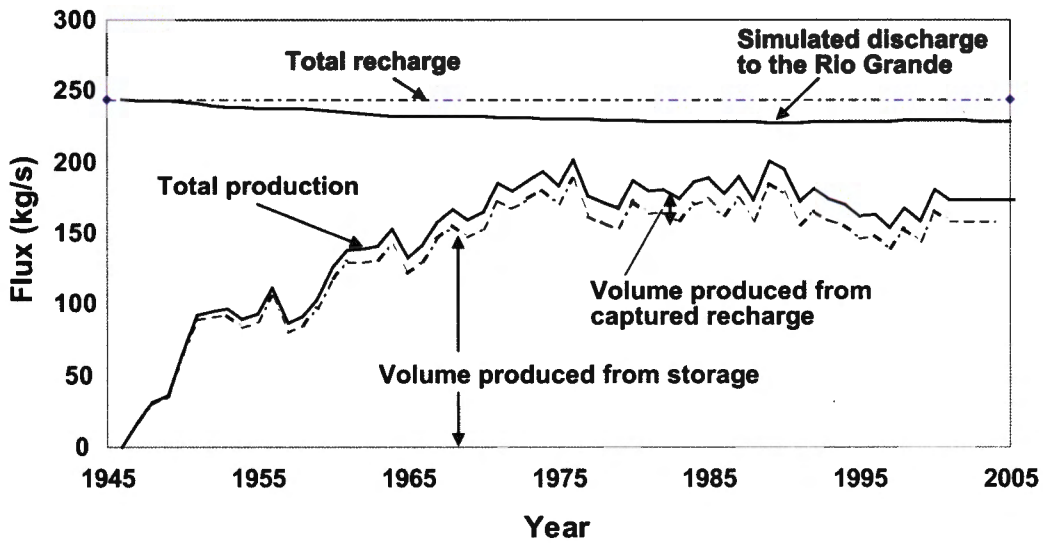


**Figure 4-23.** Simulated discharge to the Rio Grande, and estimated proportion of production in local wellfields that originates as storage and as captured recharge.

This study has devoted considerable effort to modeling heterogeneity within the Puye Formation at scales smaller than the 3-D hydrostratigraphic framework model. The Totavi Lentil is of particular interest, since it is characterized by beds of gravel which may be highly permeable. (Note: In situ hydraulic tests have been equivocal on this issue.) The current hydrostratigraphic framework model defines the Totavi Lentil as a continuous sheet of rock at the base of the Puye Fanglomerate; therefore model predictions that assign this unit a high permeability will be conservative (fastest travel times over long distances). Reneau and Dethier (1995) proposed a very different model of the Totavi Lentil, as a series of discontinuous north-south trending ribbons, separated from each other by terraces left behind as the Rio Grande downcut and moved westward over geologic time. Stochastic methods are appropriate for representing this type of heterogeneity, since the exact location of each of these narrow ribbons could never be known. Figure 4-24 illustrates one realization of a stochastic model of the Totavi Lentil, using Markov-chain transition probabilities based on data collected from geologic maps and measured outcrops (Carle 1996; Fogg 1989). This approach, and the data set that underlies it, are described in detail in Keating et al. (2000).

The Santa Fe Group (Tsf) has some intercalated Miocene basalts (Tb2; see cross-sections in Figures 2-12 to 2-19). To examine two extreme end-members, one might consider hypothetical cases where the deeper unit is either 100% Tsf or 100% Tb2. In 2002 a version of the framework model was created that explicitly identified zones that were uncertain, due to sparse borehole control. Figure 4-25 illustrates one such zone, which might be either a basalt or the Santa Fe Group. Figure 4-26 shows the resulting capture zone predictions, first assuming that zone is a basalt and then assuming that zone is the Santa Fe Group. By comparing the two figures, one can determine the impact of uncertainty of the hydrostratigraphy in this zone.

The Puye Fanglomerate also has beds of sand and gravel which, although of limited spatial extent, may be important in contaminant transport. Using textural descriptions from lithologic logs in R-wells, two different stochastic models of this type of heterogeneity were developed, as shown in Figures 4-27 and 4-28. Both of these methods show promise for use in future simulations.

The model calibration process itself can provide useful information about hydrostratigraphy. For example, if the conceptual model is that unit A is high permeability and unit B is low permeability, through the process of model calibration one can determine whether or not that conceptual model is consistent with large-scale head and flux data. This principle was used to test the conceptual model of a north-south trending high-permeability trough within the upper Santa Fe Group, proposed by Purtymun (1995). Carey et al. (1999) formulated this trough within the 3-D framework model as a fairly narrow feature (Figure 4-29a). Through the model calibration process, it was determined that this geometry was consistent with site-wide hydrologic data. Later, in a 2002 update of the 3-D framework model, this feature was significantly enlarged (Figure 4-29b). It was not possible to calibrate a model that assigned a high permeability to this large feature, so this model was discarded. These results suggest that the high permeability trough is likely to either be small, such as shown in Figure 4-29a, or exist as small, discontinuous patches.

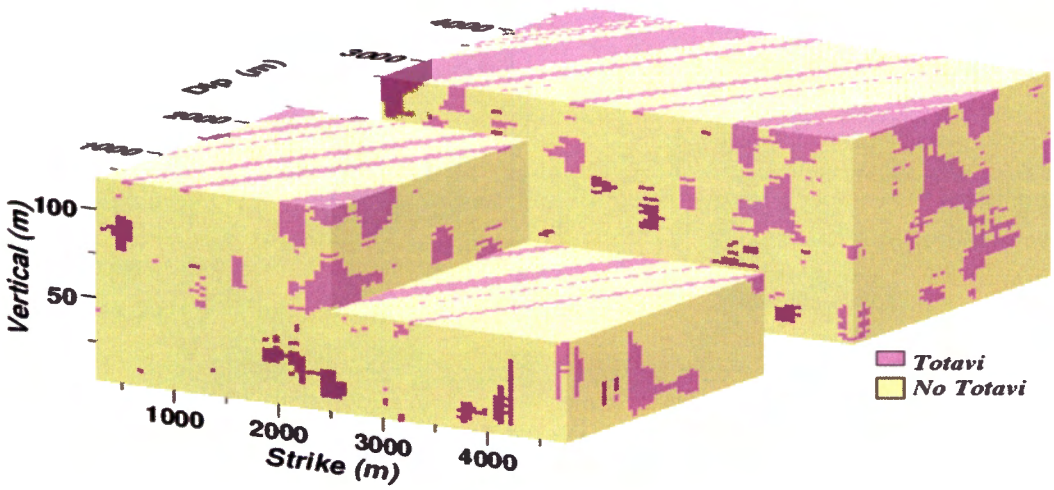


**Figure 4-24.** Heterogeneity within the Puye Formation; one realization of a stochastic Markov-chain model of the Totavi Lentil (dark pink). Model parameters are based on surface geologic maps and measured outcrops.

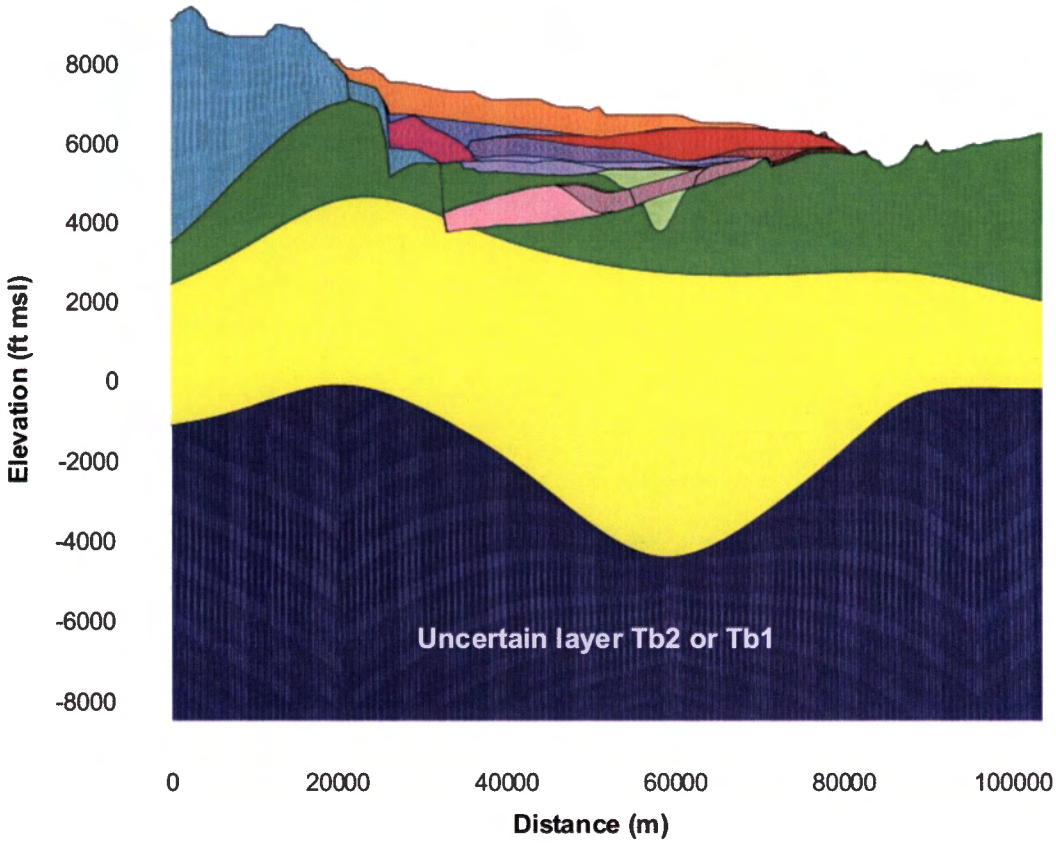


**Figure 4-25.** Cross section through hydrostratigraphic framework model, showing location of layer selected to perform a sensitivity analysis exploring the uncertainty in the geologic framework. The uncertain zone in pink was assumed to be either Tb2 or Santa Fe Group for the purpose of examining sensitivity.

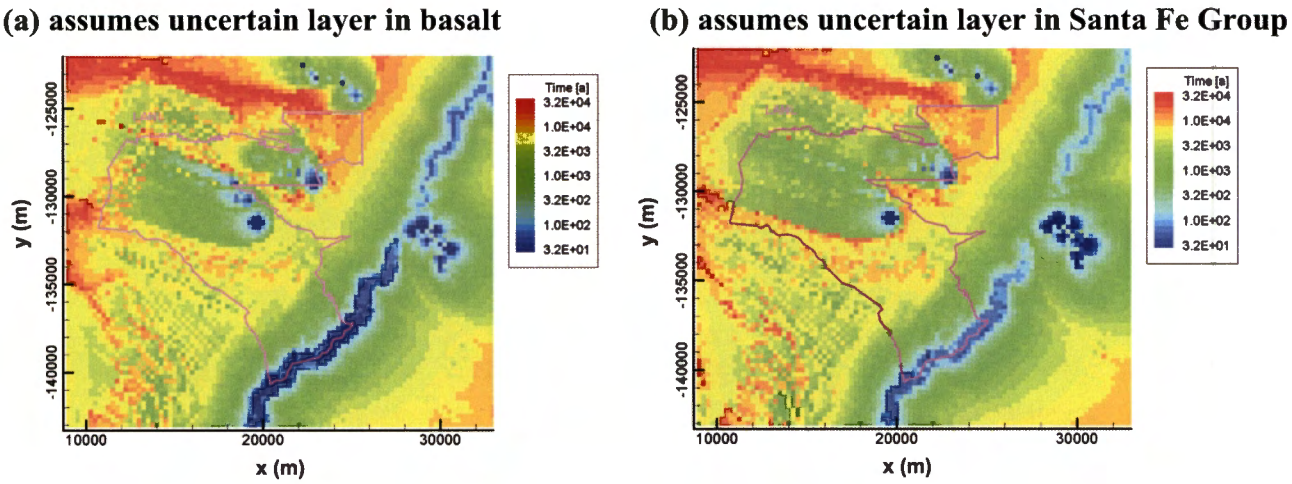


**Figure 4-26.** Predicted steady-state capture zones for wellfields in the vicinity of Los Alamos, using two different alternative models of hydrostratigraphy.

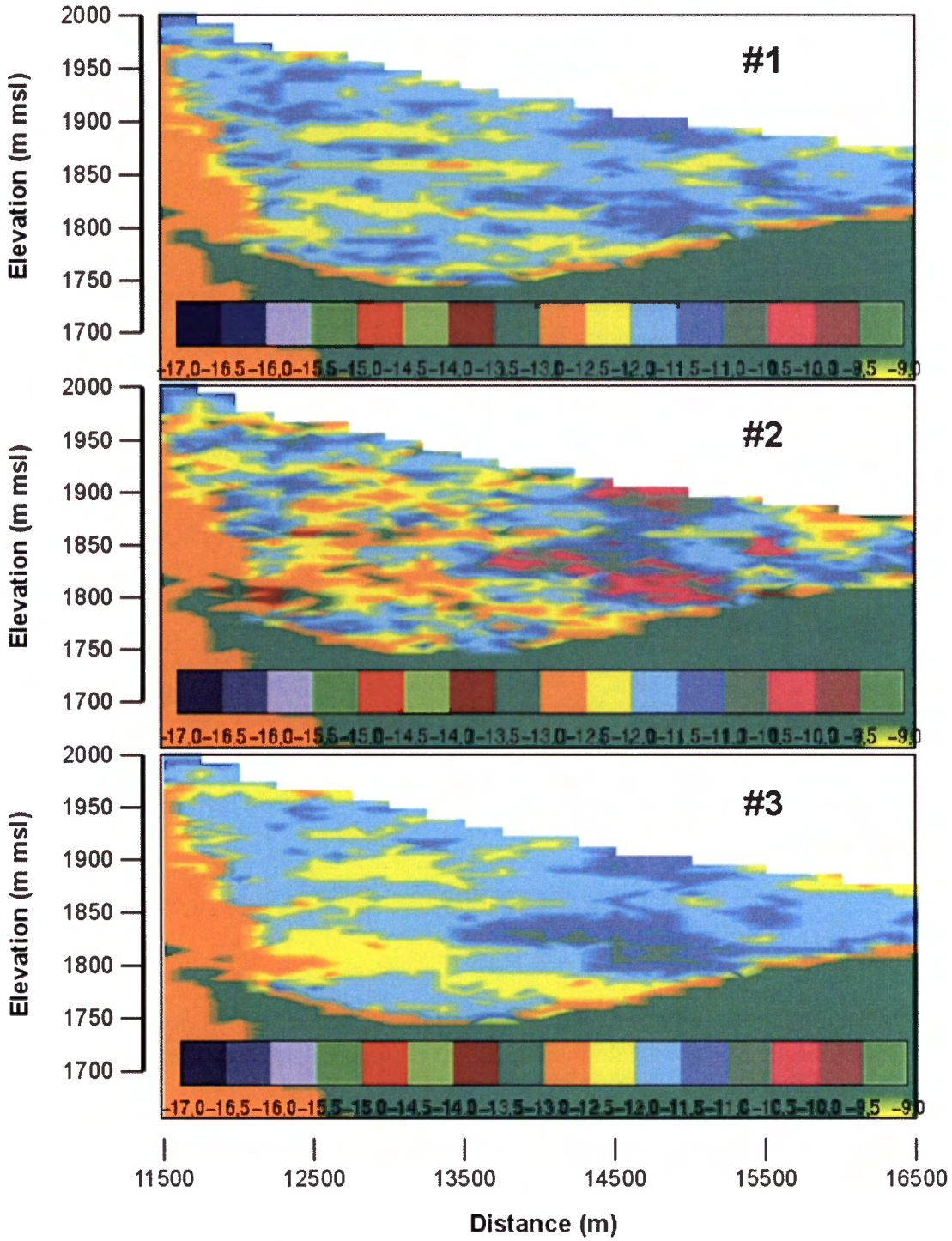


**Note:** 5X Vertical exaggeration. Color scale represents K in $m^2$.

**Figure 4-27.** Heterogeneity within the Puye Formation; three realizations of a stochastic Gaussian model.

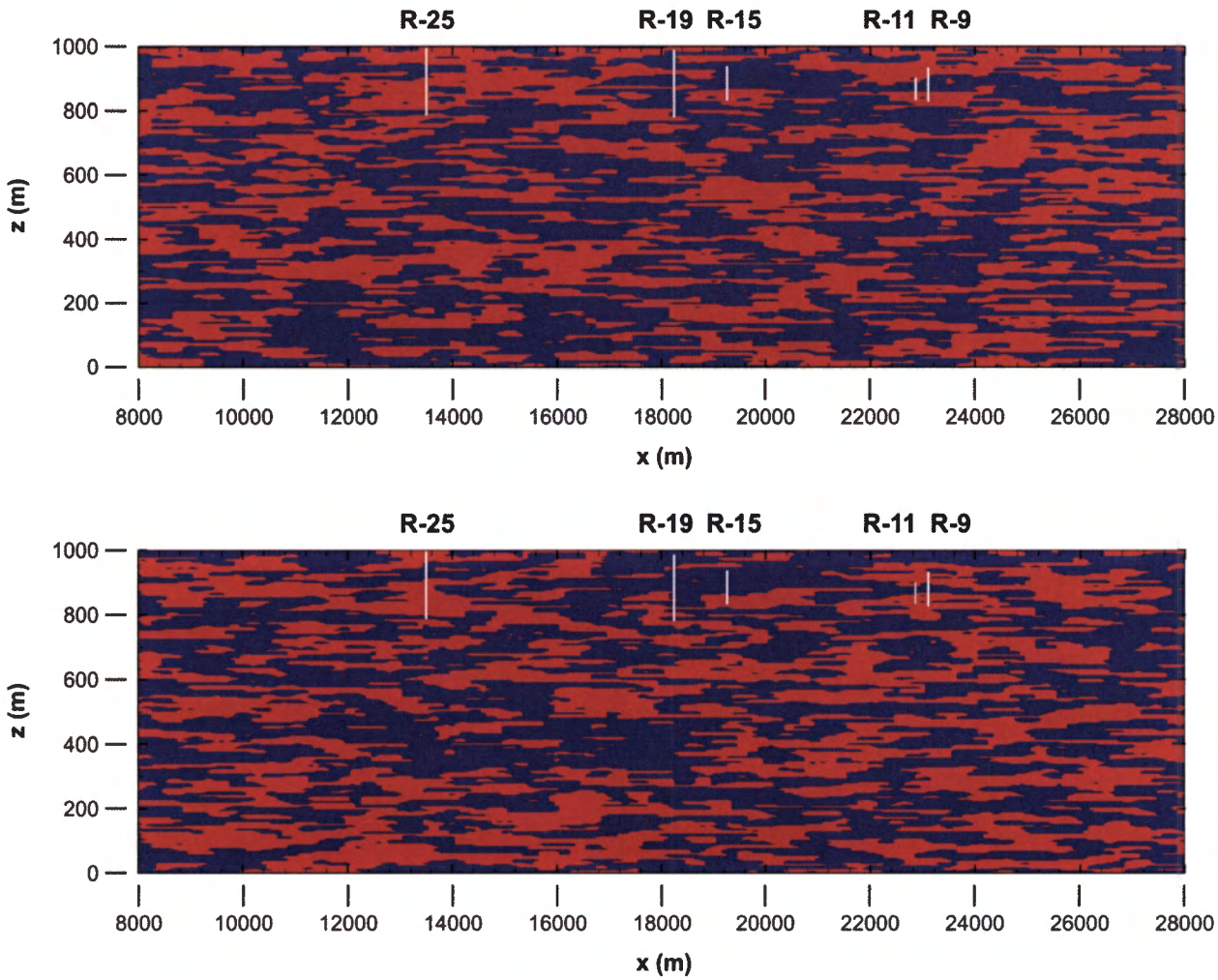


**Notes:** Examples of Markovian realizations conditioned at well data.
Coarse (blue) 55.2%, fine (red) 44.8%
Mean thickness- coarse: 23m, fine: 18m
Mean length- coarse: 1150 m, fine: 900m

**Figure 4-28.** Heterogeneity within the Puye Formation, fanglomerate; two realizations of a stochastic Markov-chain model. Model parameters are based on lithologic logs from R-wells.

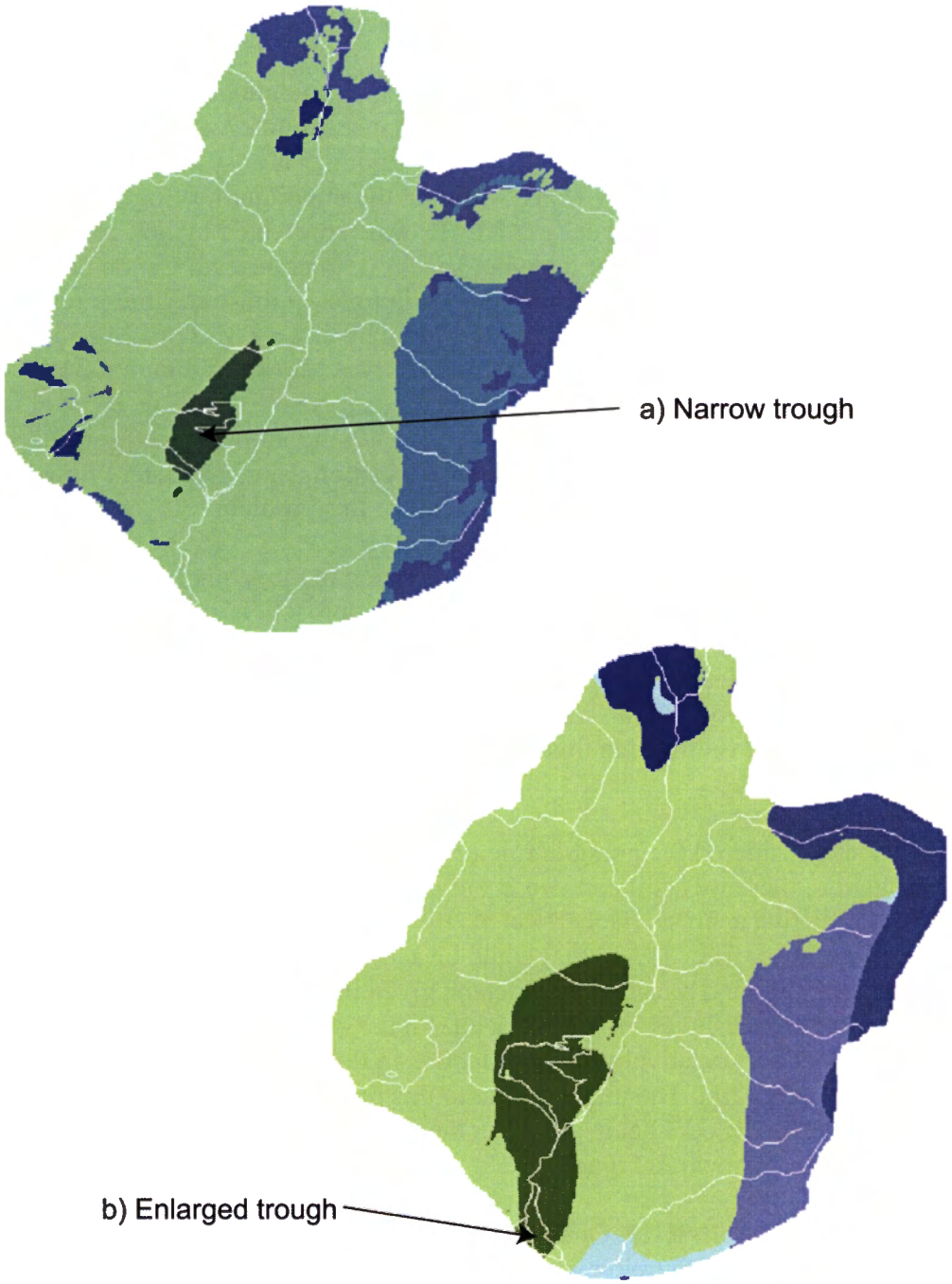


**Figure 4-29.** Two representations of the north-south trending trough in the upper Santa Fe Group.

#### 4.2.12.2 Category B: Predict fate and transport of contaminants in the regional aquifer, in order to optimally place monitoring wells and inform risk assessment studies.

**1. HE transport from TA-16.** The first contaminant transport simulations were conducted in response to the discovery of high explosives (HEs) in the upper saturated zone at R-25. The first model predictions were based on a simple premise: that the aquifer is at steady-state (with current rates of production in water supply wells), and that the important heterogeneities were defined by the 3-D hydrogeologic framework model. HE was represented by non-reactive particles in the model, released at the water table both at TA-16 and beneath Cañon de Valle (assuming rapid downstream transport in the alluvium). Figure 4-30 illustrates these results, which show all the contamination eventually being captured by either PM-2 or PM-4. Travel is predominantly within the Puye Formation. Breakthrough curves, shown in Figure 4-31, suggested that travel times would be on the order of hundreds of years. These slow travel times are consistent with the observation that no HE has been found in monitoring wells drilled since this study, at distances relatively close to R-25. A later simulation using a transient flow field demonstrated that the steady-state analysis was sufficient for this problem.

This study was repeated in 2000 with a more realistic approach to modeling heterogeneity within the Puye Formation (see Figure 4-27). By using a stochastic approach, it was hoped to identify possible fast pathways that could significantly change our earlier result. Table 4-5 illustrates the results of this study, for ten different realizations of the Puye Formation. This result showed that given this model of heterogeneity, first arrivals of contaminants could appear at PM-4 in less than 100 years. The shorter travel times in this study are due to preferential transport through a heterogeneous medium.

None of these analyses considered the possible role of model parameter uncertainty on transport predictions. In particular, there was still concern about possible easterly-southeasterly pathways away from TA-16. Predictive analysis (Doherty et al. 1994) was used to explore the range of possible flow directions away from TA-16 that could be achieved by assigning a large number of combinations of permeability and recharge parameters, given the constraint that any model must still match measured heads and fluxes reasonably well. Figure 4-32 shows the results of this analysis, which found that only relatively small variations in flow directions were possible under variable model calibration criteria. The major caveat to this result is that it depends on the hydrostratigraphic framework model being accurate; the "true" uncertainty in flow directions is undoubtedly larger than that shown in Figure 4-32.

**2. Siting a characterization well, R-13.** One objective for R-13 was that it could eventually be used to monitor possible off-site migration within the regional aquifer of contaminants originating below Mortandad Canyon. Based on the similarity between $^{3}H$ data in alluvial and perched aquifer wells in Mortandad Canyon and in wells due east in Sandia Canyon (R-9, R-12, and O-1), a due easterly pathway had been proposed earlier. Numerical simulations, shown in Figure 4-33, suggested a slight southerly bend to flow directions due to pumping by PM-3, PM-4, and PM-5. This results in a steady-state flow field, which will tend to exaggerate the effects of pumping over what might be the effects of pumping at present. Based, in part, on these results, R-13 was sited along the LANL boundary, south of the due easterly flow path suggested by geochemical results.

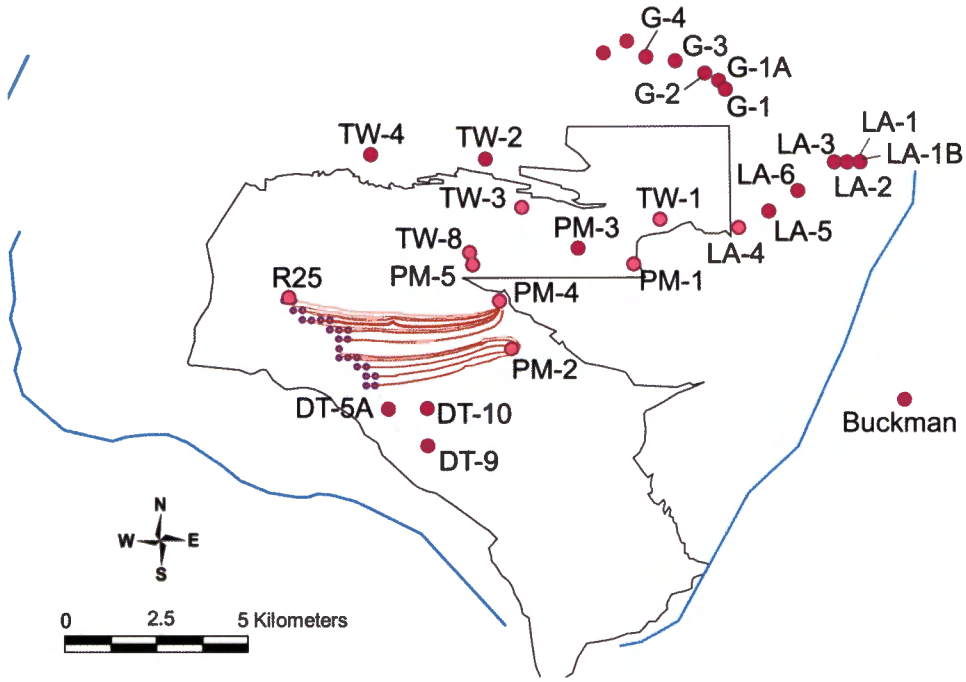


**Figure 4-30.** Predicted paths for particles released at TA-16 and beneath Cañon de Valle and captured at PM-4 and PM-2.

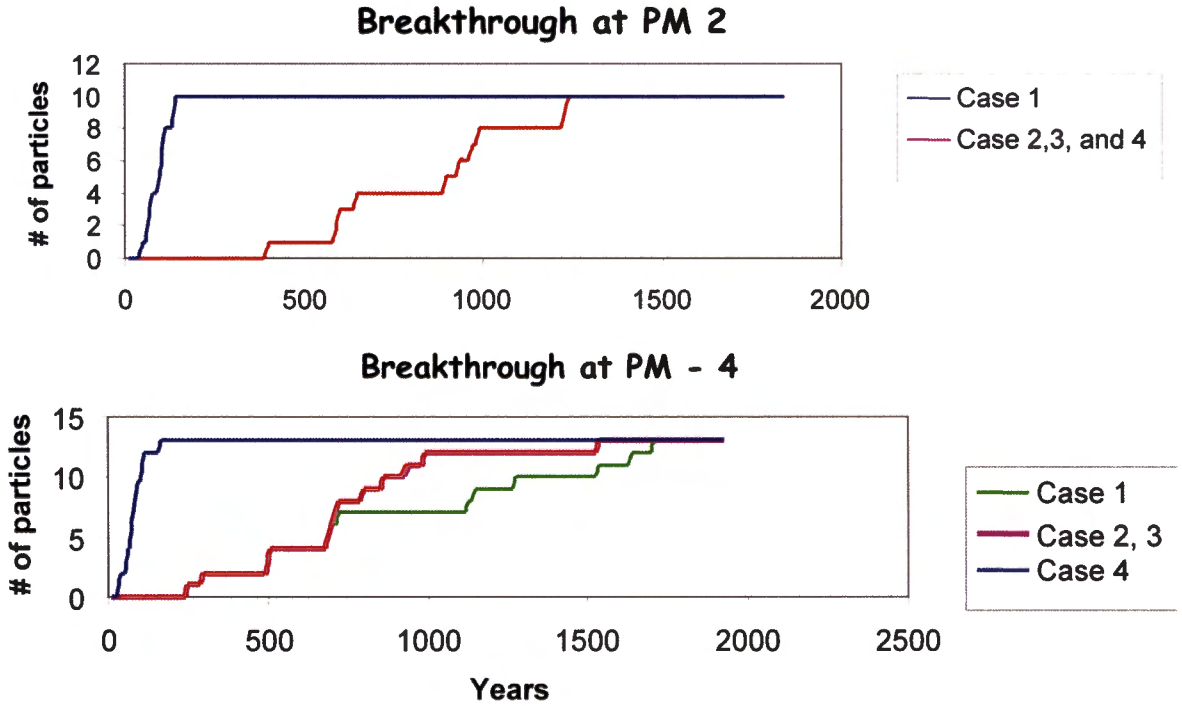


Note: Cases 1–4 represent different realizations of hydraulic conductivity.

**Figure 4-31.** Breakthrough curves for particles released at TA-16 and beneath Cañon de Valle at PM-4 and PM-2.

**Table 4-5.**
**Travel Times Calculated Using Ten Different Models of Hydraulic Conductivity within the Puye Formation**

| | | Case 0 | Case 1 | Case 2 | Case 3 | Case 4 | Case 5 | Case 6 | Case 7 | Case 8 | Case 9 | Case 10 |
|---|---|---|---|---|---|---|---|---|---|---|---|---|
| First Arrivals (yrs) | RG | 420 | 320 | 390 | 340 | 340 | 350 | 360 | 370 | 650 | 840 | 920 |
| | PM-2 | N/A | 250 | 120 | 110 | 200 | NA | NA | 200 | NA | 430 | NA |
| | PM-4 | 120 | 100 | 100 | 90 | 80 | 100 | 90 | 100 | 150 | 180 | 210 |
| Mean Arrivals (yrs) | RG | 730.8 | 825.2 | 901.9 | 935.7 | 794.4 | 688.6 | 675.2 | 928.6 | 1229 | 1626 | 1569.6 |
| | PM-2 | NA | 269.9 | 205.7 | 259 | 304.2 | NA | NA | 249.9 | NA | 430 | NA |
| | PM-4 | 139.1 | 157.4 | 170.9 | 226.9 | 151.6 | 135.9 | 127.9 | 163.8 | 234 | 310 | 318.1 |
| Standard Deviations of Arrivals | RG | 201.7 | 254.8 | 312.7 | 379.7 | 226.1 | 211.1 | 213.1 | 247.7 | 345.6 | 478 | 392.6 |
| | PM-2 | NA | 20 | 62.2 | 81.1 | 79.6 | NA | NA | 69.5 | NA | 0 | NA |
| | PM-4 | 5.7 | 21.5 | 22.7 | 50.7 | 32.1 | 12.8 | 14.8 | 25 | 32.2 | 42.7 | 23.9 |
| Percentage of Particles Captured (%) | RG | 88.4 | 6.8 | 28.3 | 25.5 | 4.3 | 21.4 | 10.9 | 9 | 7 | 7.7 | 7.6 |
| | PM-2 | 0 | 0.02 | 6.6 | 33.8 | 0.1 | 0 | 0 | 0.1 | 0 | 0.02 | 0 |
| | PM-4 | 11.6 | 93.2 | 65.5 | 40.9 | 95.6 | 79.6 | 89.3 | 91 | 93 | 92.3 | 92.4 |

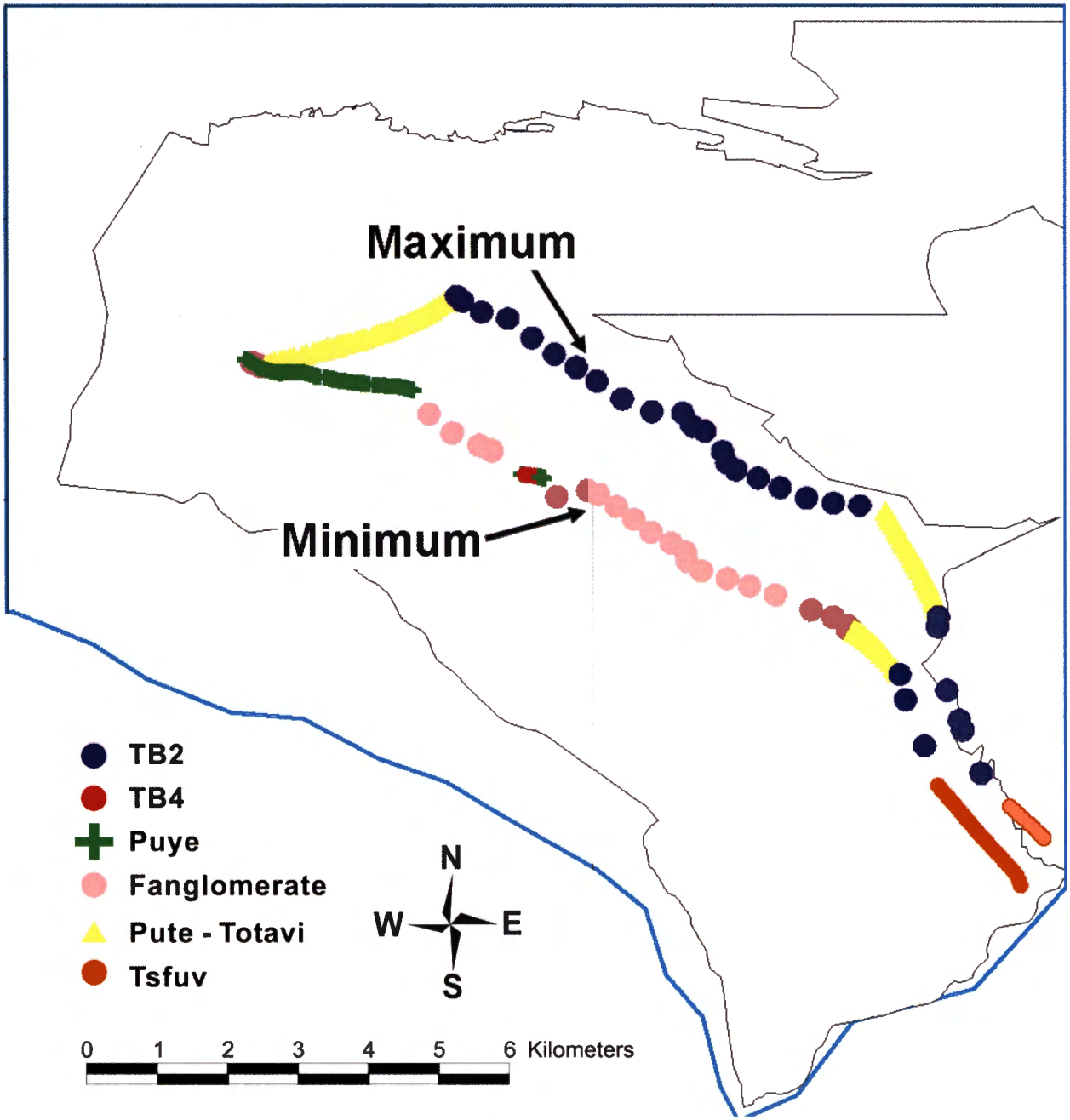


**Figure 4-32.** Results of predictive analysis, showing the possible range of flow directions (farthest northward and farthest southward) for sources at TA-16. Colors represent hydrostratigraphic units through which the water is flowing.

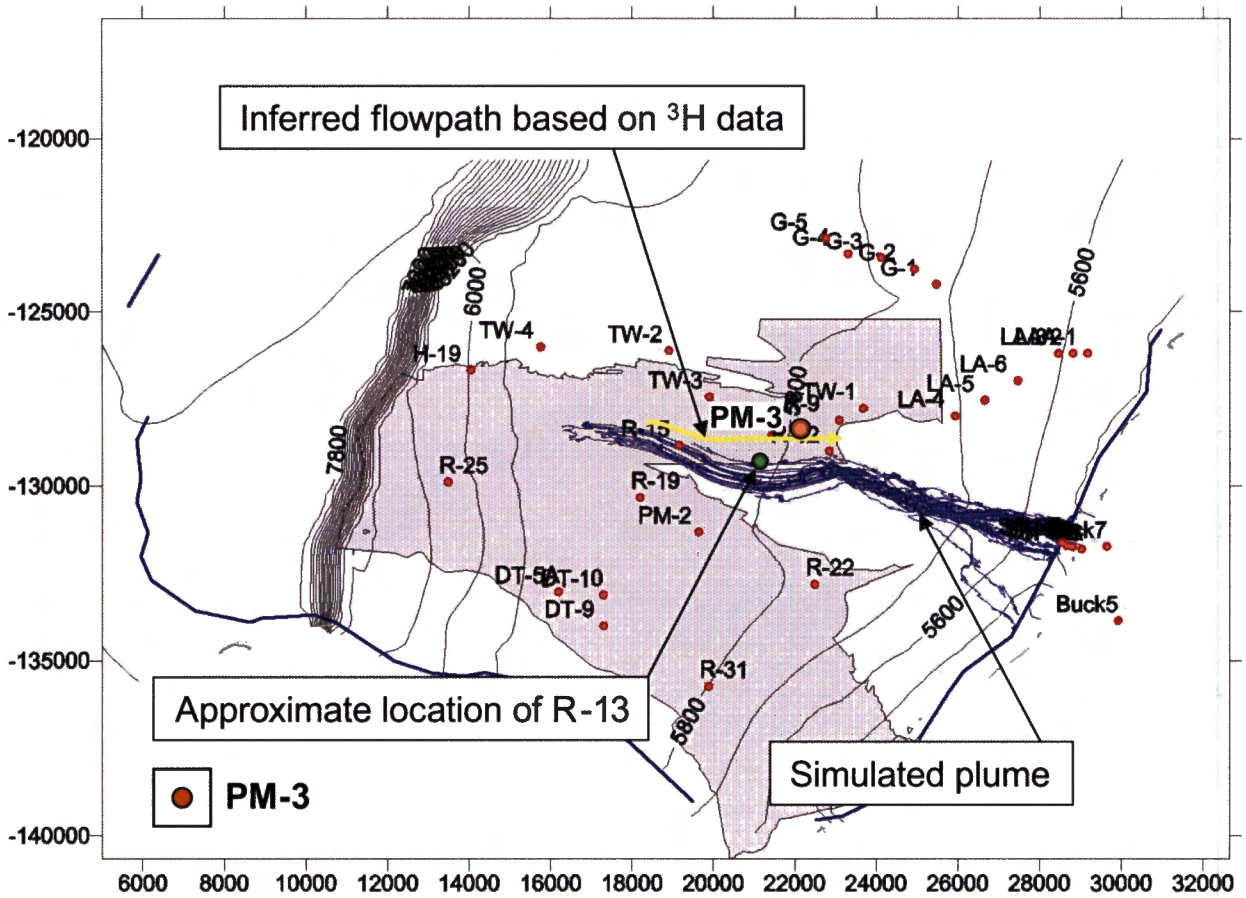


**Figure 4-33.** Predicted plume migration for sources released at the water table below Mortandad Canyon, based on a steady-state, with pumping, flow field.

Recent analyses of transient capture zones in the vicinity of Mortandad Canyon highlight the fact that flow directions and ultimate point of discharge change both in time and distance along the canyon. Solutes reaching the water table at early times (pre-1970s) and at easterly locations along the canyon probably moved to the east, under natural flow conditions and the pull of PM-1. Solutes reaching the water table at later times and further to the west will likely be drawn to the south. If the location and timing of contaminants reaching the water table is uncertain, the optimal monitoring network therefore will include both easterly and south-easterly monitoring locations.

**3. Naturally occurring contamination.** Some groundwaters in the Española Basin, including waters in the vicinity of LANL, are contaminated by naturally occurring arsenic, uranium, and flouride (McQuillan and Montes 1998; Purtymun 1977). Data collected in lower Los Alamos Canyon suggest that long-term pumping in water supply wells may increase concentrations of naturally occurring uranium (Gallaher et al. 2004).

Ongoing modeling studies, using the basin-scale model coupled with new water chemistry data collected in cooperation with Santa Fe County and the New Mexico Environment Department,

are attempting to understand the geochemical mechanisms that enhance dissolution of trace metals in aquifer rocks and the hydrologic mechanisms that may cause groundwater extraction to exacerbate the problem. Figure 4-34 illustrates an example model simulation, which simulates the spatial distribution of total dissolved solids in the basin. The prediction of a large area of high-salt water in the vicinity of Santa Fe has possible implications for water resource planning for that community, i.e., the cost of treating the high-salt water or finding alternate resources.

#### 4.2.12.3 Category C: Provide guidance in prioritization of data collection activities, highlighting the importance of those data that could most reduce numerical and conceptual model uncertainty.

**1. Reducing uncertainty in transport predictions away from TA-16.** After the analysis shown in Figure 4-32 was completed, the model was used to determine how new monitoring wells might reduce the uncertainty in flow directions and travel times. Hypothetical wells were added with head data at five different locations near the particle path lines (shown in Figure 4-35) to determine the value of the head data in reducing pathway uncertainty. When the analysis was conducted, head data from R-25 were not yet available; therefore, head data at this well were not included in the analysis. Interestingly, of the five potential well locations, it was head data at R-25 that had the most benefit. The reason for this result is that information about the vertical component of the 3-D head field at R-25 helped the model determine the extent to which flowpaths are horizontal (fast) or three-dimensional (much slower).

**2. Capture zone of PM-5.** A similar methodology was used to determine the type of data that would be of most benefit to reducing uncertainty in the ability to predict the capture zone of PM-5 (Vesselinov et al. 2002b). A conceptual particle plume was released at a single location at the water table beneath Mortandad Canyon to simulate the transport away from the site. The calibrated model predicted that the particles traveling along the mean pathway would arrive at PM-5 (orange line, Figure 4-36). This model predicted that ~80% of the particles would arrive at PM-5. By varying recharge parameters and aquifer properties in a large number of possible combinations, within calibration constraints, a wide range of possible model predictions was generated. This analysis showed that parameter uncertainty was sufficiently great so that either 0% or 100% capture was also possible (blue and green lines, respectively, on Figure 4-36). Figure 4-37 illustrates the full plume migration in the 0% capture scenario. The analysis determined that better information on recharge rates in Mortandad Canyon would have the most benefit to reducing predictive uncertainty. The caveats to this study include the following: (1) possible recharge rates were not constrained to be within the bounds provided by existing studies of recharge, and (2) the method of modeling recharge probably overestimates the impact of local recharge on local head gradients.

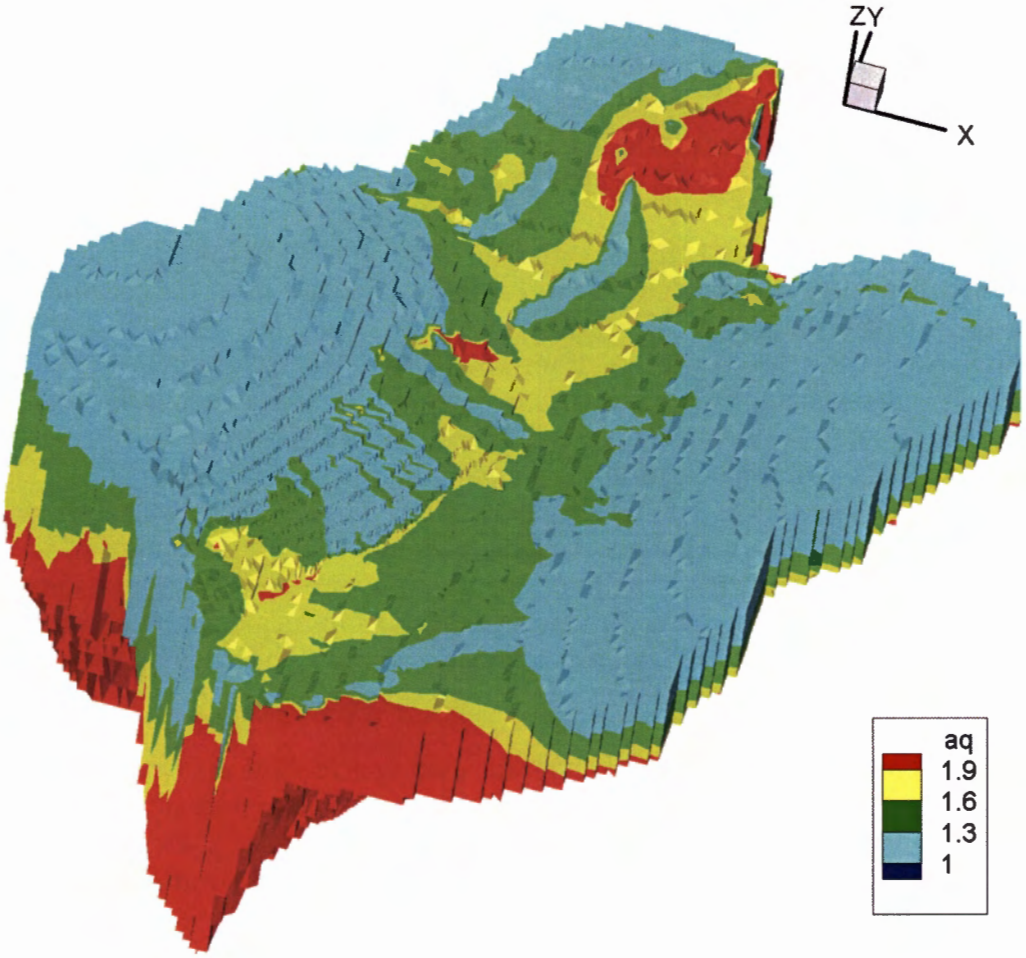


**Figure 4-34.** Predicted total dissolved salts in the groundwater at steady state, using a simple model of mineral dissolution. Red areas show the zones of relatively old water that are not mixing with fresh water.

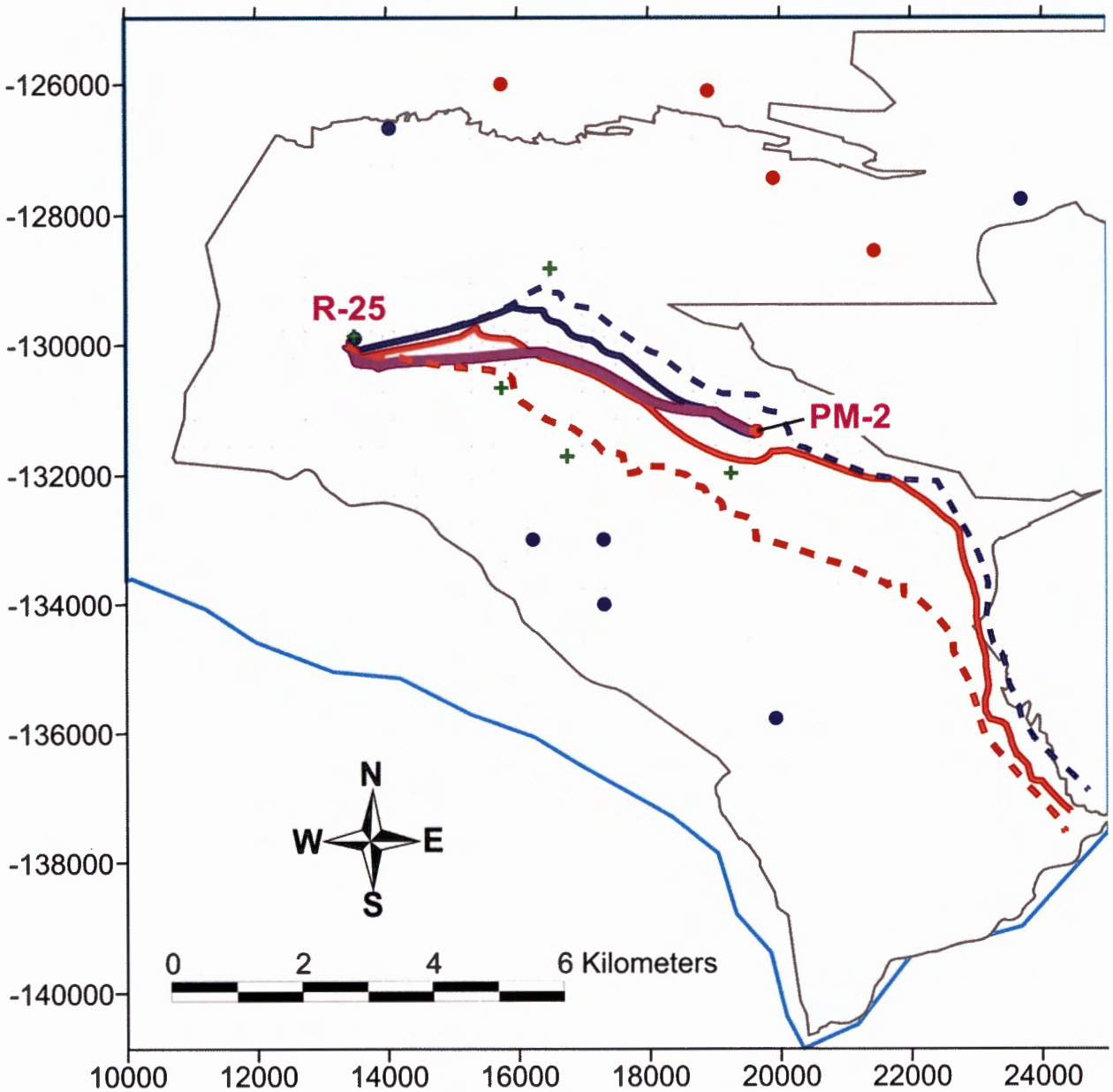


Note: The Purple line is the "calibrated" model result
The blue and red lines are min/max:
The dotted lines are most southern and most northern trajectories;
The solid lines are most shallow and most deep trajectories

- Well with steady-state water level observation
- Well with steady-state and water level and drawdown observations
- Potential location for new data (we assume that each well has multiple screens)
- Plane along which Y is calculated for predictive analysis

**Figure 4-35.** Location of hypothetical wells (green crosses) used to evaluate the potential value of head data in reducing uncertainty in flow directions. Solid and dotted lines show range of uncertainty in flow direction (north/south) and flow depth.

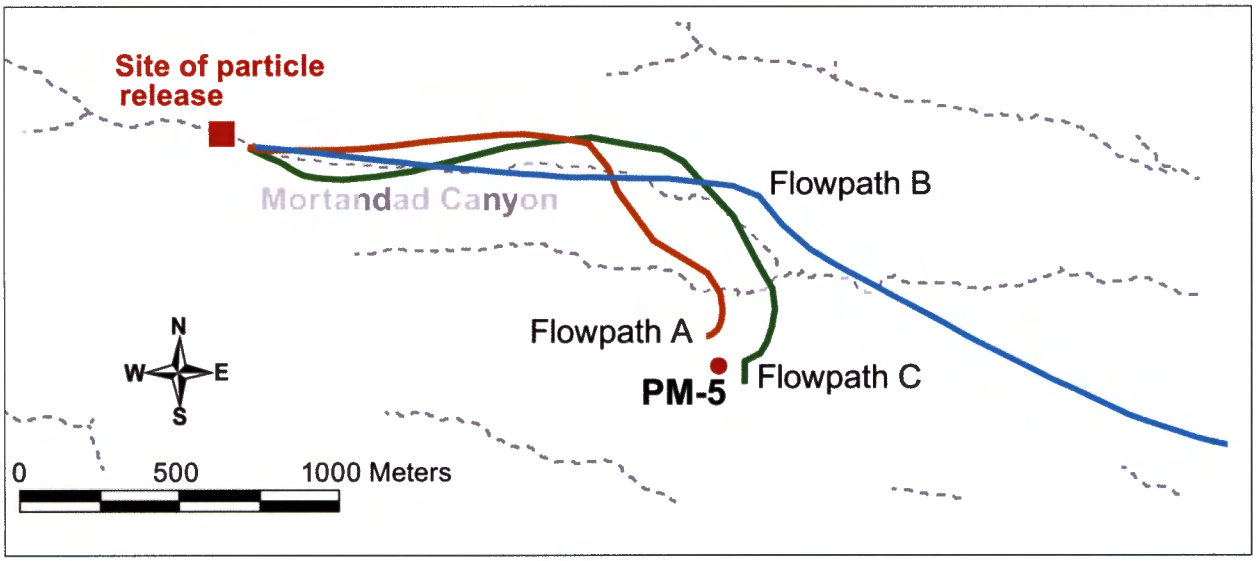


**Figure 4-36.** Mean flowpath for three simulations of plume migration away from Mortandad Canyon: orange-best calibrated model; green – maximum capture by PM-5; blue – minimum capture by PM-5.

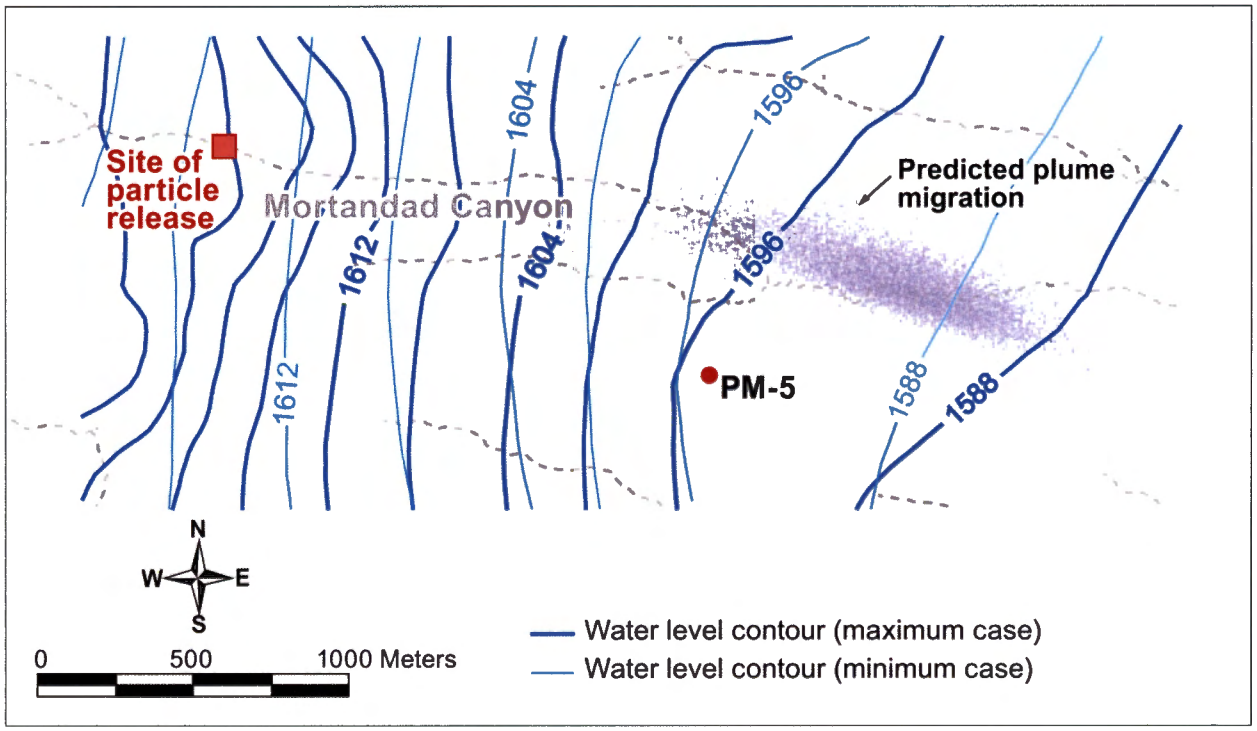


**Figure 4-37.** Illustration of plume migration for minimum capture by PM 5 (0%). Also shown are the two water table elevations predicted by the minimum and maximum cases.

**3. Proposed pump test at O-1.** The best way to characterize the hydraulic properties of the aquifer is to conduct a pump test with one or more monitoring wells. It was proposed that characterization well R-5 be drilled very close to O-1 so that a pump test could be conducted. A 2-D radial model was used, with the 3-D geologic model interpolated onto the grid to represent aquifer heterogeneity, to determine the optimal distance the characterization well should be drilled from O-1. Figure 4-38 shows the radial grid, and the predicted drawdowns as a function of distance from O-1, using a variety of model assumptions and parameters (8 cases). The range of suggested distances from the well that came from this analysis was 100–400 m. Ultimately, the well was sited at a greater distance for other purposes and no pump test was conducted. This test will be feasible when well R-3 is constructed closer to O-1.

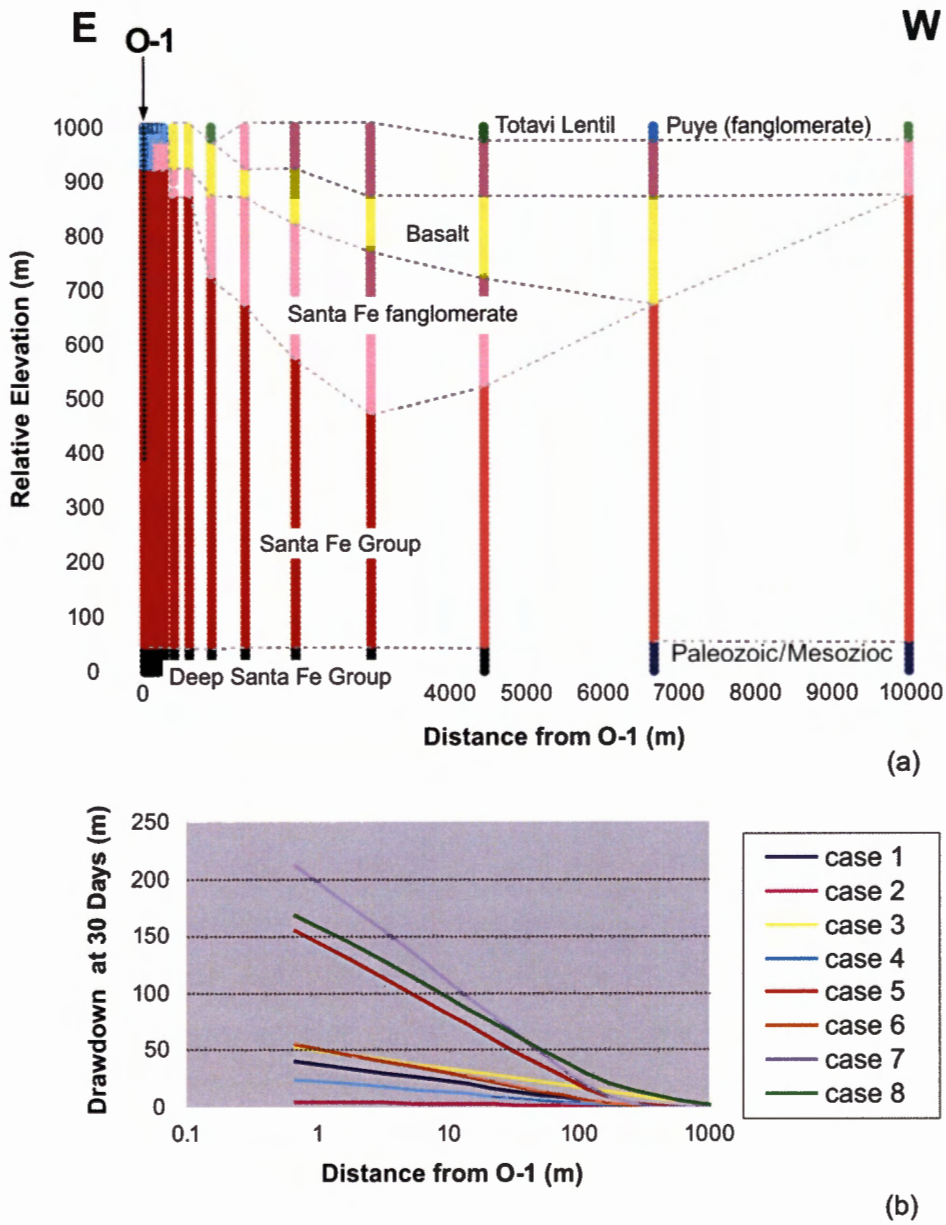


**Figure 4-38.** (a) Hydrostratigraphic units in the vicinity of well O-1, interpolated onto radial grid; (b) Predicted drawdowns at the top of the aquifer, for eight cases.

# 5.0 CONCLUSIONS

## 5.1 Summary

This report has described the geology, hydrology, and geochemistry of the Pajarito Plateau, based on empirical observations and modeling analyses. The purpose of this description is to provide a basis for evaluating and, and if necessary, designing an enhanced monitoring network capable of detecting contaminants. In order for a monitoring system to detect contaminants, an understanding of how contaminants reach groundwater and how contaminants move through groundwater is required. This section draws together the information present in the previous sections to establish a conceptual model of contaminant transport through the hydrogeologic system. This conceptual model is the basis for relating the work to evaluation of risk (Section 5.2) and the monitoring implications described in Section 5.3.

In overview, the contaminant transport conceptual model is one in which contaminants reach points of potential exposure in the regional aquifer only if the following conditions are met:

- Mobile contaminants have been released to the environment
- There are natural or anthropogenic water inputs to carry contaminants downward
- Vadose zone hydrogeologic controls are present, including enhanced infiltration and lateral pathways
- Flow-field modifications are present to influence transport of contaminants in the regional aquifer.

The following subsections draw together the observations and analyses that explain and support these conditions for contaminant transport.

### 5.1.1 Presence of Contaminants

Imprinted on the natural variations in chemistry is the presence of contaminants historically released since the early 1940s when Laboratory operations commenced. While the contaminants are at concentrations largely below regulatory standards or risk levels, they demonstrate the presence of pathways for groundwater flow and contaminant transport from the surface to deeper groundwater. The impacts to groundwater at the Laboratory have occurred mainly where effluent discharges have caused increased infiltration of water. The depth to which chemical constituents move in the subsurface is determined partly by their chemical behavior: nonreactive constituents move readily with groundwater, while reactive or adsorbing constituents move a shorter distance.

In most cases where effluent sources have been eliminated, groundwater concentrations of non-reactive discharged contaminants have decreased far below previous levels (e.g., nitrate, tritium, and perchlorate) in alluvial groundwater. These mobile contaminants move readily through the subsurface and are detected within perched intermediate zones and at the regional water table beneath several canyons, including Pueblo Canyon, Los Alamos Canyon, Sandia Canyon, Mortandad Canyon, and Cañon de Valle. In the case of reactive or adsorbing chemicals, the concentrations in the alluvial groundwater remain elevated significantly above background levels

after elimination of discharges or other contaminant source terms (e.g., excavation and removal of contaminated sediments). These include constituents such as strontium-90 and the actinides (americium-241, plutonium-238, and plutonium-239, 240) (Section 3.1.2).

Lateral flow and transport through surface water and in the alluvial systems are rapid with respect to other subsurface hydrologic processes on the plateau. Rates of lateral transport are even higher during surface flow events, which occur more frequently in the larger wet watersheds than in other areas of the plateau. Sorbing species transport slowly in alluvial waters and more commonly migrate down the canyon floor by sediment transport (LANL, 2004a; Lopes and Dionne, 1998; Solomons and Forstner, 1984; and Watters et al., 1983). Since some of the wet canyons that cross Laboratory land have received liquid-waste discharges from outfalls, the alluvial systems act as line sources for both water and contaminants to the deeper vadose zone beneath such canyons (Section 2.5.2.2).

Data for conservative (nonreactive) constituents (tritium, nitrate, perchlorate) in alluvial groundwater support the conceptual model that this groundwater has a short residence time and conservative contaminants do not accumulate in alluvial groundwater. The time-trend pattern for these contaminants shows a high level when they were being released, followed by a sharp decline in concentration to nearly nondetectable levels when the source was eliminated. Past values of tritium and nitrate in alluvial groundwater in DP, Los Alamos, Pueblo, and Mortandad Canyons exceeded the 20,000 pCi/L mean concentration level (MCL) (Rogers 1998). Because of improvement in effluent quality, values this high do not occur today in these locations (Section 3.2.3.1).

Data for adsorbing constituents (strontium-90, plutonium-239, 240) illustrate the conceptual model of contaminant adsorption onto alluvial sediments. The time- trend pattern for the adsorbing contaminants shows a decline in concentration when the source is cut off, followed by maintaining a fairly constant low concentration in the groundwater due to cation exchange. The highest measured strontium-90 activity was approximately 500 pCi/L in Acid Canyon surface water in 1960. With no present source, levels have dropped dramatically and strontium-90 is now consistently detected at low activities, below 1 pCi/L in alluvial groundwater (Section 3.2.3.1).

Data showing low levels of tritium activity in intermediate perched groundwater support the conceptual model that alluvial groundwater affected by effluent discharges is a principal source of recharge and contaminants for the intermediate perched groundwater. The highest values of tritium in intermediate perched groundwater are found where effluent discharges have occurred. Tritium time-series data also support a conceptual model that groundwater in the intermediate perched zones may have short residence time. In the absence of effluent discharge from TA-45 as a tritium source in Pueblo Canyon, tritium in the intermediate perched zone sampled by well TW-2A fell rapidly during the 1980s (Figure 3-13). This suggests that tritium associated with the former TA-45 treatment plant infiltrated the canyon floor and migrated vertically, at least to the depth of the intermediate perched zone at TW-2A, but had no continuing source when the TA-45 treatment plant was shut down (Section 3.2.3.2).

The distribution of tritium in the regional aquifer supports the conceptual model that surface effluent discharges have caused the instances where Laboratory contaminants are found at depth.

In most cases, the highest regional aquifer tritium values are found near where effluent discharges have occurred, but are much lower than values observed in overlying alluvial or intermediate perched groundwater. Elevated 3H in regional aquifer samples has been observed at wells O-1, TW-1, TW-3, TW-8, LA-1A and LA-2 (Rogers et al. 1996b), as well as in several wells drilled during the hydrogeologic characterization program (Section 2.7.3.1.1).

The fundamental condition that contaminants should have been released for groundwater contamination to occur is illustrated by the distribution of conservative (that is, nonreactive) groundwater contaminants. Generally, compounds like RDX, tritium, perchlorate, and nitrate move readily with the groundwater because chemical reactions do not retard the movement of these compounds or decrease their concentrations, although the activity of tritium does decrease due to radioactive decay. Semireactive constituents (uranium, strontium-90, barium, some HE compounds, and solvents) whose movement is slowed or their concentrations are decreased by geochemical processes and strongly reacting constituents (americium-241, plutonium, and cesium-137) that are nearly immobile are not found above background levels in intermediate perched groundwater or the regional aquifer (Section 3.2.1).

### 5.1.2 Water Inputs

Sufficient water input in a canyon system is a critical condition for transporting anthropogenic constituents. In most cases where Laboratory anthropogenic constituents are found at depth, the setting is either:

- Canyons where natural water input is high (Pajarito, Water, and Cañon de Valle)
- Canyons where anthropogenic water input is high (Pueblo, Los Alamos, Sandia, Mortandad)
- Mesa-top sites where large amounts of liquid effluent have been discharged (such as retention ponds or outfalls) (Cañon de Valle and Water canyons) (Section 3.2.2).

Wet canyons receive large runoff volumes, either through channeling of precipitation or through wastewater discharges. This runoff, in turn, creates surface-water flow along canyon bottoms, which subsequently infiltrates to form near-surface, alluvial water bodies (Section 2.4.2.1). The highest net infiltration rates are estimated to occur in canyons, especially those that head in the mountains, with magnitudes of up to a few hundred millimeters per year caused by channelized runoff. In contrast, much lower net infiltration rates occur across mesas and in the smaller canyons that head on the plateau (Section 2.4.2.1).

The infiltration rate estimates from canyon-bottom alluvium and mesa-top sites are consistent with the estimated infiltration rates inferred from moisture content profiles. In Section 4.1.3.2, numerical models for wells LADP-3 and LADP-4 in Los Alamos canyon are presented showing that moisture profiles reflect the conceptual model of high infiltration in canyons and low infiltration on mesas. That analysis also shows that the uncertainties associated with such estimates are quite high (in the range of a factor of 3). However, by combining moisture content, tracer or contaminant profiles, and water budget information, a more constrained estimate has been achieved (Section 2.5.1). The resulting net percolation rates beneath the alluvial systems of

wet canyons to the underlying unsaturated zone are expected to be among the highest across the plateau, approaching meters per year (100–1000 mm/yr) (Kwicklis et al. 2005) (Section 2.5.2.2).

The alluvial groundwater present in several canyons has a small volume relative to the annual volume of runoff or effluents, does not extend beyond the LANL boundary, and is generally completely refreshed by recharge on a time scale of about a year (Section 3.2.3.1). The Kwicklis et al. (2005) study shows that about 23% of the infiltration occurs from canyon bottoms on the plateau at lower elevations, including 14% of the total in streams that flow at least partly within LANL boundaries.

Although relatively small volumetrically compared to mountain recharge to the west, aquifer recharge occurring locally on the plateau is important to the assessment of flow paths of potentially contaminated water. Tritium data confirms that relatively young water is present in the aquifer (Rogers et al. 1996b), indicating fast pathways through the vadose zone beneath LANL. Kwicklis et al. (2005) used vadose zone occurrences of $^{3}H$ to estimate the time-dependent transport velocities from which they derived the infiltration rates to the regional aquifer. They found that, in Mortandad Canyon, infiltration rates as high as 2000 mm/yr during periods of large volumes of effluent discharge decreased to 100–200 mm/yr when effluent discharge flow rates were reduced. These observations and analyses confirm that local recharge in canyons is an important component of the recharge distribution for the plateau (Section 2.7.3.1.1).

The presence of water, either natural or from the discharge of effluents to canyons or mesa-top locations in the Laboratory's semiarid setting, initiates or increases downward percolation of water. Even under unsaturated flow conditions, this percolation may move significant volumes of water to the regional aquifer within a few decades.

### 5.1.3 Vadose Zone Hydrogeologic Controls

The third condition that controls the distribution of groundwater contaminants is the presence of vadose zone hydrogeologic controls. The controls considered most important in influencing contaminant distribution and transport are: near- surface circumstances that enhance infiltration, potential pathways in the vadose zone (e.g., basalts), and transport through intermediate perched groundwater.

Infiltration rate affects the movement of anthropogenic constituents from the surface to groundwater. As described in Section 2.5.3, undisturbed Bandelier Tuff has a very low infiltration rate. On mesas, the predicted travel times are variable, but for the most part are greater than 1000 years, ranging from 1000 to 5000 years on the eastern portions of the Laboratory to 20,000 to 30,000 years in the western region. Areas that have other geologic units (particularly basalt units or Puye Formation) or fractured units exposed in the canyon bottom have higher, or enhanced, infiltration rates. In addition, the vadose-zone thickness decreases with increasing distance down canyon, due to thinning of the Bandelier Tuff (Section 2.2.9). Where the Otowi Member of the Bandelier Tuff is thick, infiltration rates are quite low. However, on the eastern side of the plateau, the Otowi Member thins to 0 to 100 feet, reflecting both the general thinning of the Otowi Member away from its caldera source and thinning of the ash-flow

tuffs over the Cerros del Rio highland on the east side of the plateau (Section 2.2.9.1). The eastern portions of canyons with thinned or absent Otowi Member have enhanced infiltration. Infiltration rates of 1500 to 2000 mm/yr are estimated for the confluence of Los Alamos and Pueblo Canyons, a consequence of infiltration directly onto Puye fanglomerates or fractured basalts (Section 2.7.3.1.1.).

Enhanced infiltration is especially true for the eastern portion of deep wet canyons because their canyon bottom elevations are 45 to 60 m lower than smaller canyon systems on the plateau. Thus, the deepest canyons extend to stratigraphic horizons having higher infiltration rates because of increased fracture flow. Contaminants transported down canyon via surface flow or through the alluvial groundwater system often percolate through a geologic column consisting primarily of basalt and Puye Formation fanglomerate with little or no overlying tuff. Downward percolation is believed to be more rapid in the basalt than through moderately welded tuff (Section 2.2.8). Thus, these wet canyons have thinner vadose zones and a smaller portion of the flow path with matrix-dominated flow. Los Alamos and Pueblo Canyons have regions in the vicinity of their confluence in which the Bandelier Tuff is thin or nonexistent. Water infiltrates directly onto basaltic rocks or the Puye Formation, thereby yielding rapidly downward flow through fractures or preferential flow channels. The predicted travel times are especially short (5 to 10 years) in these locations (Section 4.1.2.1).

Other instances of enhanced infiltration include the Cañon de Valle and Water Canyon, where rates up to 1000 mm/yr are estimated for areas associated with the Pajarito fault zone. Anthropogenic alterations can also enhance infiltration, for example sediment ponds in Mortandad Canyon and ponds in Cañon de Valle.

In contrast to the Bandelier Tuff, the basaltic rocks clearly exhibit rapid flow through fractures and other fast pathways, so that the permeability of the matrix rock is essentially irrelevant to the rates of water percolation (Stauffer and Stone 2005). Fracture flow occurs because of the orders-of-magnitude lower matrix permeabilities of these rocks, compared to the Bandelier Tuff (Section 2.4.1). The upper surface of the Cerros del Rio basalt is irregular, with a broad highland that extends from north to south under the east-central portion of the Laboratory, largely buried beneath the Bandelier Tuff. The presence of the Cerros del Rio basalt in the vadose zone provides potential lateral fast pathways in the vadose zone (Section 2.2.8). These hydrogeologic factors, compounded by the relatively high deep-percolation rate in wet canyons, likely yield the fastest vadose-zone travel times for contaminants from the land surface of the plateau to the regional aquifer. Transport to the regional aquifer beneath wet canyons is predicted to be on the order of decades to hundreds of years (Section 2.5.2.2).

The water-quality impacts by effluent releases on alluvial groundwater extend in a few known cases to intermediate perched groundwater at depths of a few hundred feet beneath these canyons. Since the contaminated alluvial groundwater bodies are separated from the intermediate perched groundwater by hundreds of feet of dry rock, pathways within the vadose zone are likely present in those canyons. There are two end-member conceptual models for flow within an intermediate perched water zone:

- *Low-velocity, virtually stagnant water resting in a perching horizon within a local structural or stratigraphic depression.* Water percolates very slowly out the bottom of

this zone or spills over the sides of the depression. This configuration views perching horizons as barriers that slow the downward percolation of water. In several wells, intermediate saturated zones thought to represent perched groundwater were screened but failed to produce significant water. These occurrences may represent cases where zones of limited extent were substantially drained when the perching horizon was penetrated during drilling. Once the stagnant water is depleted in an initial round of sampling, there is insufficient recharge upstream to keep the zone saturated.

- *High-velocity, laterally migrating water that travels on top of the perching horizon.* This conceptualization suggests that once groundwater reaches a perched zone, it rapidly percolates laterally along high-permeability pathways until the perching horizon pinches out or is breached by high-permeability features, such as fractures or lateral changes in lithology. In this scenario, water could move in stair-step fashion from one perching horizon to another. There are no confirmed instances of large-scale, lateral vadose zone pathways beneath the Pajarito Plateau at depths greater than the alluvial groundwater. However, the case of lateral flow through the wet, mountain-front mesas at TA-16 suggests that this possibility does exist at greater depths. Although the TA-16 observations are categorized as shallow for the purposes of this discussion because they discharge via springs in the local canyons, it could be argued that deep pathways with flow geometries similar to those of the mountain-front mesa or today's alluvial groundwater zones are evidence for the possibility of deeper fast pathways elsewhere (Section 2.6.2.4).

The site-wide vadose zone transport model predicts that regions of relatively rapid travel times are present in the following canyons: Pajarito Canyon near White Rock, a portion of Cañon de Valle, Mortandad Canyon at the Radioactive Liquid Waste Treatment facility, middle and lower Los Alamos Canyon, large portions of Pueblo Canyon, and Guaje Canyon (Section 4.1.2.3).

Hydrogeologic controls influence movement of anthropogenic constituents through the vadose zone. The presence of geologic units that enhance infiltration, that act as pathways, or are conducive to perching groundwater and forming intermediate perched groundwater appears to be an important condition for groundwater contaminants to be transported to the regional aquifer.

### 5.1.4 Regional Aquifer Transport

Relatively little contamination reaches the regional aquifer from the alluvial groundwater bodies, and water quality impacts on the regional aquifer, though present, are low. Flow field modification is considered important in controlling anthropogenic constituent distribution in the regional aquifer. Anthropogenic constituents that enter the regional aquifer near pumping wells are predicted to have much shorter travel times than those outside the influence of pumping.

The LANL regional aquifer model was used to produce a map of velocities at the water table. These velocities are *highly uncertain* and are used only to illustrate a few key points. First, given the heterogeneous nature of the aquifer, groundwater velocity is likely to vary considerably over short distances. There are two areas with relatively high permeability ($K > 3$ m/day): the north-central aquifer beneath LANL (wells TW-2, R-4, TW-3, R-11, R-28, and R-13) and the south-central aquifer beneath LANL (R-19, screen 6, DT-10, DT-9) (Section 2.4.2.3).

The fastest velocities are in the basalts where fracture flow (very low porosity) is assumed. Basalt straddles the water table in two areas. The most extensive is located in the south-central part of the plateau, where as much as 195 ft of saturated Pliocene Cerros del Rio basalt occurs at the top of the regional zone of saturation in well DT-10 and 290 ft occurs in well R-22 (Figure 2-10). A smaller region of older Miocene basalts straddles the water table in a north-trending zone extending between wells R-12 to R-5.

Second, flow on the eastern portion of LANL is predicted to be *very* slow. This is due to the very low permeability of the Santa Fe Group, which is prevalent at the water table east of LANL (Section 4.2.12.1). The Tesuque Formation is the primary rock unit making up the regional aquifer in the eastern part of the plateau and in the Buckman wellfield east of the Rio Grande. Bedding within the Santa Fe Group and the Puye Formation is likely to cause higher permeability parallel to the beds than perpendicular to the beds. Large vertical head gradients measured in R wells are evidence of anisotropy. The beds within the Puye Formation range from centimeters to meters in thickness. Most are very low angle, dipping to the east. In contrast, beds within the pumiceous volcaniclastic rocks tend to dip to the southwest (R-20, R-2, R-7, R-19, and R-33). Beds within the Santa Fe Group exposed on the western margin of the plateau dip approximately 2–5° to the west (Golombek et al. 1983). Data from R-16 suggest that shallow layers are very low-angle, but deeper layers dip as much as 25° to the west. Hydrologic modeling and pump test analysis suggests that vertical permeability is 100 to 1000 times lower than horizontal permeability in the Santa Fe Group (Hearne 1985; McAda and Wasiolek 1988; Keating et al. 2003). (Section 2.4.2.3)

The regional aquifer conceptual model incorporates data from recent large-scale (30-day) pumping tests. Individual drawdown and recovery water levels in responsive wells demonstrate that the regional aquifer surrounding PM-2 is vertically anisotropic with pronounced resistance to vertical propagation of drawdown at shallower depths. Hydraulically, the aquifer behaves like a semiconfined aquifer at depth with leaky units located above (and perhaps below) a highly conductive layer (Section 2.7.5). It appears that there are water-table conditions near the water table, but leaky-confined aquifer behavior deeper down, although the degree to which the uppermost phreatic zone and the deeper, leaky-confined aquifer are hydrologically connected is unknown. The regional aquifer can be thought of as a compartmentalized aquifer with water from plateau recharge traveling laterally in the phreatic zone as the upper compartment and a lower compartment, which contains deeper groundwater flow as the leaky-confined aquifer that is isolated to some degree from the overlying compartment.

The contaminant pathways in the regional aquifer depend heavily on the strength of the hydrologic separation of the two compartments, which translates into how efficiently the pressure drawdown caused by the pumping wells propagates to the water table. Two conceptual alternatives are end members on a spectrum of potential configurations and thus capture the total potential variability.

- Weak hydraulic separation between the shallow (phreatic; water-table) and deep (leaky-confined; pumped) zones does allow pumping drawdown to reach the water table. Hydraulic gradients in the phreatic zone are affected by the pumping and contaminants

are drawn toward the wells. Contaminants are primarily predicted to arrive at water supply wells with a travel time of less than 50 years.

- Strong hydraulic separation between the shallow (phreatic; water-table) and deep (leaky-confined; pumped) zones does NOT allow the pumping drawdowns to reach the water table. Hydraulic gradients in the phreatic zone are NOT affected by the pumping. Contaminants are predicted to bypass the water supply wells and will arrive at the springs with travel time of about 200 years.

Compartmentalized flow with variably separated shallow and deep zones is supported by observations. The recent pumping tests suggest strong hydraulic separation exists, as described in the "strong separation" regional aquifer conceptual alternative. However, it is likely that some downward movement of water and contaminants does occur due to pumping of water supply wells at depth. Occurrences of tritium and perchlorate in O-1 illustrate the point that flow paths between the shallow and deep aquifer water can exist during production. This observation supports deeper pathways near water supply wells, conforming to the "weak separation" regional aquifer conceptual alternative. However, the extent of vertical transport is undoubtedly a function of the local permeability structure between the water table and the pumping interval in the water supply well, which may vary spatially across the plateau.

It is unclear whether it is important to monitoring goals to distinguish between these two alternatives. The first priority is to enable prediction of contaminant transport velocities sufficiently accurately to design an enhanced monitoring network and interpret the results. Either alternative results in lateral transport of contaminants reaching the water table, especially at locations relatively unaffected by municipal water well pumping. It is possible that the more strongly compartmentalized, two-zone aquifer conceptualization might yield more rapid contaminant transport near the water table, with transport pathways that are more lateral and less influenced by municipal water supply well pumping than the weak separation, more uniformly anisotropic case.

## 5.2 Relation of Hydrogeologic Workplan Results to Risk Assessment

The data, conceptual models, and numerical models resulting from work performed during implementation of the Hydrogeologic Workplan will be used, in combination with data gathered by the Environmental Restoration Program, to perform groundwater risk assessments for LANL-contaminated sites. The risk assessments will synthesize information (and uncertainty) about source term, vadose-zone flow and contaminant transport, and saturated-zone flow and contaminant transport to predict future health effects at receptor locations. They will be performed using a probabilistic approach that incorporates parameter uncertainty and variability, as well as conceptual model uncertainty. Data sets and site information gathered thus far will be used to define uncertainties in the form of parameter distributions and well-defined alternative conceptual models of groundwater flow and contaminant transport. These uncertainties will be propagated through groundwater models and then used in a risk-based decision analysis to identify and rank alternative actions to protect people from potential impacts of groundwater contamination from various release sites.

To construct the probabilistic risk assessment and associated decision analysis, several steps are employed. When using these steps we assume that we have already acquired general knowledge about the site. This assumption is, in general, valid for the main contamination issues on the plateau, based on background information gained during the Hydrogeologic Workplan and Environmental Restoration activities of the past 10 years.

1. *Define the question to be answered.* Examples of the questions might be, "What is the potential, future health risk for water users of municipal supply wells associated with historic effluent releases in canyon X? How can these risks be decreased?"
2. *Define input parameters and construct parameter distributions.* Estimates in the range of model input parameters are made based on field data, historic records and expert judgment. Example distributions might include uncertainty in contaminant masses released as a function of time in geologic and/or in hydrologic properties.
3. *Define conceptual models.* These could be related to source release, to vadose zone and groundwater flow, and to contaminant transport.
4. *Construct numerical models based on information from Steps 1 through 3.* Such models will generally include a vadose-zone and a saturated-zone model.
5. *Sample parameter sets to be used as input for a series of Monte Carlo simulations that capture the ranges of model and parameter uncertainties defined.*
6. *Run probabilistic flow and transport simulations using the numerical models and the parameter sets.*
7. *Use output from flow and transport simulations to calculate health effects or to answer other questions defined in Step 1.*
8. *Perform sensitivity analyses to determine parameters or conceptual models that produce model results indicating potential adverse health effects.*

Steps 2, 3 and 4 rely extensively on work performed for the Hydrogeologic Workplan. Predicted results are compared to field data (concentrations, heads, water content) to verify that model results are reasonable. In addition, in order to create regulator and stakeholder trust in this process and its results, stakeholder input concerning parameter distributions and conceptual models is encouraged.

Based on the sensitivity analysis described in Step 8 above, decision analysis is applied to define the optimal course(s) of action at a particular contaminated site. Such actions may include some combination of cleanup, stabilization, additional characterization, and monitoring. If additional characterization is identified as an action that can reduce risk, the sensitivity analysis yields information not only about which parameters should be better characterized, but also to what degree the uncertainty or variability in a specific parameter should be reduced. If the uncertainty were reduced to within the defined limits through characterization, then an updated risk assessment would calculate reduced risk. The decision analysis may help decrease the cost of future characterization by identifying parameters that do not need to be better characterized. Also, if experts feel that further characterization will not result in decreased uncertainty in a parameter identified in the sensitivity analysis, then that characterization effort might be rejected and an action with a higher probability of success may be pursued instead.

The generic process outlined above will be implemented on a canyon-by-canyon, or site-by-site basis in the future, using information learned from the Workplan and ER activities as a foundation. The conceptual, and for certain sites, numerical models will be formulated based on the knowledge gained and described in Sections 2 and 4 of this report. Thus, the past work becomes the springboard for future risk assessment and decision analysis activities related to groundwater at the LANL site.

## 5.3 Implications of Hydrogeologic Workplan Findings for Monitoring

The principal motivation for embarking on the Hydrogeologic Workplan was to provide the underlying scientific basis needed to make informed decisions regarding monitoring, remediation, or other actions to provide assurance that the groundwater beneath the Laboratory is protected. The site-wide approach taken in the investigation, both in terms of field-based characterization and modeling, has filled in many gaps in our understanding of the groundwater behavior and pathway directions and rates of migration of contaminants. Characterization wells were drilled for a range of objectives, from the collection of basic hydrogeologic information about the regional aquifer to serving as contaminant-specific and unit-specific sampling wells.

This investigation has led to a vastly improved conceptual understanding of the groundwater systems of the Pajarito Plateau: new concepts have been developed, and previous hypotheses have been confirmed or refined. Although wells have been drilled in a manner that does not preclude their being used in an enhanced monitoring network, the goal was to gather general information required to confirm or refine our conceptual models for groundwater flow and transport. Additional information may be necessary to predict contaminant transport in a particular setting: all sites are unique and require site-specific measurements to reduce uncertainties. However, armed with the improved understanding gained from the Hydrogeologic Workplan activities, we are now able to develop improved groundwater monitoring strategies or conduct more cost-effective detailed studies of individual canyons where initial studies have suggested that groundwater risk may exist.

In this section, we place the results of the findings of the Hydrogeologic Workplan into context by discussing the impact of the conceptual model elements learned in the study to the following questions: How does a particular conceptual model element impact -

- the design of an enhanced groundwater monitoring plan?
- the conduct of a detailed contaminant nature and extent study?
- the application of a remediation strategy?

### 5.3.1 Alluvial Groundwater

The alluvial system potentially provides a significant pathway for lateral transport at high velocity over great distances. Travel times on the order of a few years are expected in some canyons for contaminants to travel several kilometers from the release location. Tracer tests in Mortandad Canyon and contaminant migration measurements in Los Alamos and Mortandad canyons illustrate this point. A corollary is that within a few years of reducing the source term (reducing the effluent concentration, removing a solid source through remediation, etc.), concentrations of nonsorbing contaminants decrease due to flushing of the alluvial groundwater. These contaminants can enter the underlying vadose zone. Some contaminants such as Sr-90 travel much more slowly in the alluvial system due to retardation resulting from sorption. The contaminant inventory for these constituents is expected to reside mainly in the alluvial groundwater and on sediments (see Section 3).

A number of attenuation processes act to slow or impede the movement of contaminants, but ultimately the spatial extent of contamination within the canyon is limited by the distance traveled by surface and subsurface water. This distance varies seasonally with rainfall and runoff variability, and can be significantly changed from natural conditions by the input of anthropogenic water sources such as LANL effluent discharges or municipal water treatment facilities.

Alluvial groundwater is the potential source for water and contaminants to the deeper vadose zone. Percolation rates to the deeper vadose zone are temporally and spatially variable. Zones of preferential percolation exist, and it is difficult to predict their locations a priori. These zones are probably controlled by the nature of the hydrogeologic properties at the base of the alluvium, topographic conditions of the canyon, and the degree of fracturing of the underlying basement rock. For example, relatively high recharge is thought to be associated with fractures in Los Alamos Canyon near the Guaje Mountain Fault zone and in locations in the vicinity of the low-head weir, where water infiltrates directly into fractured basalts.

Implications of this conceptual model for nature-and extent studies, groundwater monitoring strategies, and remediation are:

- Long-term monitoring of the alluvial groundwater should focus on nonsorbing contaminants such as tritium, perchlorate, and aqueous HE compounds.
- To monitor changes in contaminant concentrations in response to changes in operations or after remediation, frequent samples must be taken to track progress.
- The absence of a contaminant known through historical records to have been introduced into a canyon likely means that the contaminant resides deeper in the system, and has been flushed out of the shallow system once the release was terminated.
- A relatively complete mass balance of released sorbing contaminants can be achieved by focusing on the alluvial sediments and groundwater.
- If a nonsorbing contaminant has been released for many years into a canyon, most of the inventory probably resides in strata below the alluvial system, so remediation techniques

such as permeable reactive barriers in the alluvial system will be addressing only a small fraction of the inventory.

- Sorbing contaminants are accessible to remediation technologies applied to the alluvial system. Technologies requiring a flux of contaminant, such as a permeable reactive barrier, are likely to work slowly, but may be useful, should some type of vadose zone remediation be required.
- In nature-and-extent studies for nonsorbing contaminants, zones of enhanced infiltration must be located using hydrologic studies to understand the different terms in the water budget. Surface water flow data, piezometric measurements of alluvial groundwater heads, and shallow borings that penetrate the underlying bedrock are useful to identify these zones.
- Numerical models of the surface-water/alluvial groundwater system are useful for constraining the estimates of percolation rates to the deeper vadose zone.

### 5.3.2 Vadose Zone

Transport velocities for nonsorbing contaminants in the deeper vadose zone (below the alluvial systems) are much larger in canyon bottoms than on mesa tops, suggesting that effluent discharges into canyons are the principle threats to the deep groundwater. Localized zones of high water flux from mesas are possible, such as in locations where the surface has been disturbed by human activities, or in faulted regions in close proximity to the Pajarito fault zone. However, most mesas show little, if any, evidence of transport of large quantities of contaminants to great depths. Numerical models of unsaturated zone transport in mesas are consistent with this observation.

Transport of contaminants from the alluvial groundwater zones to the deeper vadose zone can occur in two main rock types: Bandelier Tuff and basalts. Water percolates principally through the matrix pores in the Bandelier Tuff, but drains quickly through fractures and other open void space in the basalts. Fractures in the Tshirege Member of the Bandelier Tuff at the base of the alluvial systems probably serve as preferential pathways for downward percolation, but water quickly imbibes into the rock matrix, and matrix flow is even more likely in the more homogeneous Otowi Member. The subsurface location of contaminants in the vadose zone is controlled by the local percolation rate from the alluvial system. Although contaminants might be present in the rock pores along the entire reach of a contaminated canyon, the greatest quantities of nonsorbing contaminants will likely be present in zones of enhanced percolation. As discussed in the previous subsection, the locations of these zones are difficult to predict in the absence of detailed studies of the alluvial system.

Where Bandelier Tuff is present, travel times to the regional aquifer are controlled by the percolation flux and the total thickness of the underlying tuff units. Travel times through the tuff units probably range from a few decades to several hundred years. This means that most of the inventory of nonsorbing contaminants probably still resides in the vadose zone. In many vadose zone wells, the location of the contaminant front in the vadose zone has been located in the Bandelier Tuff. However, even where a well defined front exists, contamination is also found in deeper perched zones in the same well or in nearby wells. This suggests that a zone of higher percolation flux supplies the zone, and some lateral flow occurs. This lateral flow may be along

the canyon, but it is just as likely that the well is located nearby, but offset from the zone of highest percolation, and the lateral transport occurs a short distance perpendicular to the strike of the canyon.

Where infiltration occurs directly onto basalts, higher percolation rates are expected, along with much more rapid transport of contaminants to depth. Travel times through the basalts are expected to be a few years. Beneath the basalts and the Bandelier Tuff, the Puye Formation represents a highly heterogeneous vadose zone medium in which preferential pathways are likely. Travel times through the Puye Formation are therefore likely to be small for nonsorbing contaminants.

Sorbing contaminants are rarely detected at depths below the alluvial groundwater, even in locations where they were released coincident with nonsorbing contaminants that are found at depth. Retardation due to sorption is a key delay mechanism in the system. Detailed sampling has not been conducted in the few feet of rock immediately below the alluvial groundwater zone, but it is likely that any sorbing contaminants that have escaped the alluvial system have only migrated a very short distance into the bedrock.

Perched water is commonly found beneath naturally wet canyons or canyons with significant water input from anthropogenic sources. Generally, the perched water is not found to flow underneath the adjacent mesas, although data are somewhat limited. Perching is caused by low-permeability horizons: the downward percolation rate exceeds the saturated hydraulic conductivity of the perching horizon, and water collects or is diverted laterally. The degree of lateral flow within perched zones is uncertain. Lateral diversion will force contaminants to reach the water table at a different location than it entered the deeper vadose zone, but it is unlikely that this location will fall significantly outside the uncertainty zone defined by the alluvial groundwater zone. Travel times are not dramatically affected by the nature of flow in the perched zone. Travel times are controlled by percolation through the Bandelier Tuff, and the details of the flow path beneath these units are relatively unimportant in determining the total travel time to the regional aquifer. Finally, perching horizons provide a convenient means for monitoring the extent of transport of contaminants in the vadose zone.

Implications of this conceptual model for nature-and extent studies, groundwater monitoring strategies, and remediation are:

- Monitoring of the performance of waste sites located on mesas will probably turn up little contamination at great depth: sampling ports located in the vadose zone directly beneath the waste are probably required to detect contaminants. Given that regional aquifer monitoring to ensure the validity of this conclusion will probably be required, we should attempt to combine monitoring with characterization or other goals to maximize the utility of the well.
- Wet canyons with contaminants are the locations to focus monitoring.
- In zones where contaminants percolate directly into basalts, contamination has traversed the vadose zone, and characterization efforts should focus on the regional aquifer. Further characterization of nature and extent in the basalts of the vadose zone will not yield as

useful information in locations where contaminants have already reached the regional aquifer.

- Long-term monitoring of the intermediate groundwater should focus on nonsorbing contaminants such as tritium, perchlorate, and aqueous HE compounds.
- Sorbing contaminants can be checked on a less frequent basis because to date they have not traveled to significant depths, making the rapid breakthrough of high concentrations to the perched zones or the regional aquifer very unlikely.
- Given the range of travel times through the vadose zone, it is critical, if risk-based approaches are taken, that decision makers settle on the time period of regulatory interest. Without this definition, studies will not be appropriately focused, and misplaced characterization activities are likely to be the result.
- Although downward migration along the entire length of a wet canyon may occur, unequal percolation rates along the canyon lead to zones where greater depths of penetration of contaminated water has occurred, including all the way to the water table. Uncontaminated regional aquifer water at one location does not guarantee that the regional aquifer is clean at another location in the same canyon.
- Monitoring wells should be located near or downgradient of zones of preferential percolation determined from alluvial and vadose zone studies. In canyons posing significant risk, a higher density of shallow intermediate wells should be considered to pinpoint the preferential transport pathways than in canyons with lower risk potential.
- Given that the lateral displacement of contaminants in perched zones will not add large additional uncertainty to the location of contaminant arrivals at the water table, nor will travel times be much affected, there is no compelling reason to study in detail the nature of flow and transport in the perched zones if the regional aquifer water is ultimately of greatest interest for groundwater protection. Characterization of pathways closer to the surface is more cost effective and definitive, and should bound the lateral extent of transport above the regional aquifer.
- Contaminant inventories are likely to be small in most perched zones compared to the thick, unsaturated regions in which contaminated water is held in the matrix pores. Therefore, the perched zones are not good candidates for remediation by pump-and-treat methods because only a small fraction of the inventory will be accessed. An exception might be the large perched zone containing HE contamination at TA-16. If such a technique is attempted, better hydrologic characterization of the intermediate zones are required than we have obtained to date.
- Perched zones are targets of opportunity for acquiring contaminant concentration data, making them useful in nature and extent studies.
- Remediation of contaminants in the unsaturated rock of the vadose zone is not likely to be successful using available technologies. Water residing in matrix pores cannot be pumped, and most contaminants of interest are not volatile. Gas-phase nutrients could possibly be delivered to increase biological activity and induce bioremediation of organic contaminants, but the large spatial extent of contamination in the vadose zone probably renders such concepts impractical unless a single zone of preferential flow and transport is discovered.

### 5.3.3 Regional Aquifer

The regional aquifer represents the most likely groundwater accessible to humans via the municipal water supply wells and the springs that discharge at the Rio Grande in White Rock Canyon. The focus of this summary is on the elements of the conceptual model most directly connected to the migration of contaminants in the regional aquifer. Aquifer processes and measurements in the broader regional context were established in Section 2.7 and models were presented in Section 4.2.

Local recharge on the plateau on Laboratory property is a relatively small fraction of the total recharge, but is critical to understand for its implications for contamination from historical and current Laboratory operations. Some of the recharge focused along canyons contains contaminants from the Laboratory. This water potentially represents a source term for regional aquifer contamination.

To date, several observations have been made of contaminants reaching the regional aquifer. Conditions facilitating possible rapid downward migration to the regional aquifer are described in the previous subsections. High percolation rates, typically enhanced by anthropogenic water sources, and/or relatively thin or non-existent Bandelier Tuff at the surface are the conditions most likely to result in present-day regional aquifer contamination of nonsorbing constituents. Future contamination at additional locations is expected over a period of decades to centuries as more of the contaminant inventory reaches the water table.

There are no definitive observations of sorbing contaminants having reached the regional aquifer via a groundwater pathway. This fact further supports the concept of retardation due to sorption as the principal retardation mechanism for many contaminants.

Measured concentrations of nonsorbing contaminants in the regional aquifer are much lower than their concentrations in the effluent discharges or in the alluvial groundwater. This is the case even for samples collected near the top of the regional aquifer, where it might be expected that dilution due to dispersive mixing with regional aquifer water would not have taken place to as great a degree as further downgradient and at greater depth. Significant dilution of these plumes has occurred, assuming that samples are representative of the maximum concentrations and are not affected by mixing in the borehole. Borehole mixing and dilution is expected in municipal water supply wells, but is likely to be less prevalent in characterization-well samples with short screens.

Lateral flow directions in the regional aquifer are defined by the potentiometric surface constructed on the basis of new measurements in the shallow regional aquifer in characterization wells drilled during the characterization program. Flow directions are generally west to east or southeast across the plateau. Detailed gradients at scales smaller than the distance between wells are more uncertain, and might be affected by local recharge conditions and pumping of nearby water supply wells. Deeper in the aquifer, gradients and flow directions are uncertain due to lack of deep wells. Different conceptual models lead to either (1) easterly flow paths with water upwelling and discharging at the Rio Grande, or (2) more southerly flow

paths with water leaving the Española Basin via interbasin flow to the Albuquerque Basin. Data to distinguish between these two mechanisms are lacking.

Heads decrease with depth in most characterization wells on the plateau, and this condition is probably magnified by pumping of municipal water supply wells, whose screens are located well below the water table. While this condition might imply that contaminants at the water table should move downward, the hydrodynamics of the system are a function of the rock properties as well as the gradient. At some locations we find significant resistance to flow in the vertical direction, leading to compartmentalized zones that are connected only weakly to each other. Phreatic (unconfined water-table) conditions are present near the water table, whereas the aquifer exhibits behavior consistent with leaky-confined conditions at greater depths. The common observation of water-table conditions on the plateau, the depth-dependent response to pumping during multiple-well hydrologic tests, and the persistent head declines in the deeper aquifer in response to pumping are evidence of this behavior. More information is needed to determine if this is a ubiquitous feature of the aquifer.

This conceptual model means that contaminant transport pathways are not necessarily downward in the regional aquifer. In the extreme, a ubiquitous low-permeability barrier separating the phreatic zone from the deeper zone would render the downward component of the gradient meaningless: downward flow would be negligible, and contaminants hitting the regional aquifer would travel laterally along the streamlines defined by the potentiometric surface. The reality is almost certainly more complex, with thin (in the vertical), laterally discontinuous, low-permeability heterogeneities creating increasingly confined conditions with depth. In such a situation, pathways to the depths of water supply well screens are also likely.

Linear transport velocities are a function of the effective porosity of the medium as well as the groundwater flux. Porosity estimates are best made using interwell tracer tests, but these tests have not yet been conducted in the regional aquifer. Heterogeneous flow at larger scales will tend to result in lower effective porosity estimates than what is measured in cores or with borehole logging tools due to preferential flow. All else being equal, lower effective porosity leads to higher velocities and shorter travel times.

Implications of this conceptual model for nature-and extent studies, groundwater monitoring strategies, and remediation are:

- Contaminant detections in the regional aquifer are spatially variable, with detects and non-detects in the same canyon. Given that contamination has probably arrived at the regional aquifer only at a few locations, contaminant monitoring locations in the regional aquifer must be selected using an approach that integrates information of alluvial, vadose zone, and regional aquifer.
- More detailed investigations along canyons with risk-significant contamination are needed to pinpoint the spatial locations of the fastest pathways to the regional aquifer. Locations within or downgradient of these zones are good locations for contamination monitoring. The concept that the canyons are a line source of recharge is a good starting point, but more detailed information is needed to place monitoring wells.

- Contaminant detections in the regional aquifer will probably continue to be at low concentrations, and changes in time of these values will be gradual. Sampling frequency can thus be relatively long without missing important information.
- Long-term monitoring of the regional aquifer groundwater should focus on non-sorbing contaminants such as tritium, perchlorate, and aqueous HE compounds.
- Sorbing contaminants can be checked on a less frequent basis because to date they have not been detected with certainty in the regional aquifer.
- Contaminants reaching the regional aquifer most likely will travel laterally from their point of entry into the aquifer at the water table. Tortuous pathways to greater depths are also possible, with perhaps only a fraction of the contaminant taking this deeper path, and the rest continuing to travel laterally. Sampling screens in the shallowest portion of the regional aquifer are thus most likely to be well placed to detect contamination. Permeable zones within the first 100 ft or so of the regional aquifer should be the targets for monitoring locations.
- If the water discharging the regional aquifer at the springs in White Rock Canyon is principally water that recharged locally on the plateau, then continued monitoring of these springs for contamination is appropriate. Changes in concentrations are expected to be very gradual, so relatively infrequent sampling is sufficient.
- The extent of downward contaminant migration induced by water supply well pumping is uncertain, ranging from capture of the plume by the supply wells to a shallow, laterally migrating plume unaffected by pumping. Observations at O-1 prove that capture by a water supply well can occur. However, at other locations, weak or non-existent pressure responses in the shallowest screens to pumping from the deeper aquifer suggest that pathways may not exist that connect the shallow and deeper system.
- Given this variability and uncertainty, the concept of a "sentinel well," that is, a well designed to provide advanced warning of supply well contamination, will be difficult to implement. A shallow screen would miss a contaminant transport pathway in which the vertical downward migration occurs upstream of it, whereas a screen at the elevation of the producing zone might miss a vertical pathway located downstream of the monitoring well (including a situation in which the supply well itself is a pathway).
- Monitoring wells designed to be used as sentinel wells must attempt to provide coverage for both types of flow paths. Shallow screens will probably be the best sampling locations for water ultimately discharging at the Rio Grande.
- If pump-and-treat is proposed for a contaminant in the regional aquifer, the system should focus on the uppermost portion of the aquifer, where regional aquifer contaminants are known to reside. More detailed measurements of the hydrologic conditions in the shallow regional aquifer are required to better design monitoring or remediation systems.
- Pumping tests using the water supply wells to induce the pressure response are extremely informative, and should be continued as opportunities present themselves. Each pumped well provides information in the vicinity of that well, so to gain the site-wide knowledge needed, continued testing is required. The tests are not duplicative or redundant: rather, each test provides unique information.

- Tracer tests are the best way to determine the effective porosity of the medium at the field scale. This parameter is needed to convert groundwater flux estimates to a contaminant transport velocity estimate. The Puye Formation and the Cerros del Rio basalts are the most important units in which to conduct these tests, since these are the units encountered at the water table in regions where Laboratory contamination is a concern.
- The regional aquifer flow and transport model must continue to be improved by incorporating new data and concepts. Use of the model to interpret the hydrologic response of the system, to design and interpret the results of the future monitoring program, and in contaminant transport predictive studies requires that models keep up with the new data that will be collected. In the shorter term, available data sets not used in the model development to date, including the pumping tests discussed above, geochemical data, and thermal data, should be incorporated into updated versions of the model.
- For all modeling, including the regional aquifer model, continued exploration of alternative hypotheses should be continued. This statement applies for all aspects of the groundwater model, including those elements not obviously tied to questions of contaminant transport. Groundwater model development is a process in which feedbacks of changes in one portion of the system can affect model performance in unforeseen ways. A philosophy of continuous model improvement should continue to be used to enable higher fidelity predictions as improvements are made.
- Future studies should go beyond current approaches to include a data collection and modeling processes that make the greatest use of opportunities to investigate large portions of the aquifer. These opportunities may include: (1) passive monitoring of aquifer pressures in response to inputs (recharge) and withdrawals (supply well pumping) that occur as a matter of course; (2) incorporation of that information into refined versions of the regional aquifer model; and (3) increasing use of remote data that provides information on large-scale aquifer conditions and properties, including INSAR, airborne electromagnetic data, or gravity data, if initial investigations demonstrate that these techniques provide useful information.

# 6.0 REFERENCES

Abrahams, J.H., J.E. Weir and W.D. Purtymun. 1961. Distribution of Moisture in Soil and Near-Surface Tuff on the Pajarito Plateau, Los Alamos County, New Mexico. U.S. Geological Survey, Professional Paper 424-D, pp. D142-D145.

Allison, J. D., D. S. Brown, and K. J. Novo-Gradac, March 1991. "MINTEQA2/PRODEFA2, A Geochemical Assessment Model for Environmental Systems: Version 3.0 User's Manual," EPA/600/3-91/021, Office of Research and Development, Athens, Georgia. (Allison et al. 1991, 49930)

American Society for Testing and Materials (ASTM), 2000a. Standard Guide for Use of Direct Air-Rotary Drilling for Geoenvironmental Exploration and the Installation of Subsurface Water-Quality Monitoring Devices, ASTM Standard D5782-95.

American Society for Testing and Materials (ASTM), 2000b. Standard Guide for Use of Dual-Wall Reverse Circulation Drilling for Geoenvironmental Exploration and the Installation of Subsurface Water-Quality Monitoring Devices, ASTM Standard D5781-95.

American Society for Testing and Materials (ASTM), 2000c. Standard Guide for Use of Direct Rotary Wireline Casing Advancement Drilling Methods for Geoenvironmental Exploration and the Installation of Subsurface Water-Quality Monitoring Devices, ASTM Standard D5876-95.

American Society for Testing and Materials (ASTM), 2000d. Standard Guide for Use of Direct Rotary Drilling with water-Based Drilling Fluid for Geoenvironmental Exploration and the Installation of Subsurface Water-Quality Monitoring Devices, ASTM Standard D5783-95.

Anderholm, S.K., 1994. Ground-water recharge near Santa Fe, north-central New Mexico, Water Resources Investigations Report 94-4078, U.S.Geological Survey, 68 pp.

Anderson, M., and W.W. Woessner, 1992. Applied groundwater monitoring. Academic Press, Inc., San Diego, 381 pp.

Aubele, J.C. 1978. Geology of the Cerros del Rio volcanic field, Santa Fe, Sandoval, and Los Alamos counties, New Mexico. MS thesis. University of New Mexico. 136 p.

BAER (Burned Area Emergency Rehabilitation), 2000. "Cerro Grande Fire Burned Area Emergency Rehabilitation (BAER) Plan," Interagency Burned Area Emergency Rehabilitation Team. (BAER 2000, 72659)

Bagtzoglou, A. C., 2003a. Perched water bodies in arid environments and their role as hydrologic constraints for recharge rate estimation: Part 1. A modeling methodology, Environ. Forensics, 4, 1, 39-46.

Bagtzoglou, A. C., 2003b. Perched water bodies in arid environments and their role as hydrologic constraints for recharge rate estimation: Part 2. The case of Yucca Mountain, Environ. Forensics, 4, 1, 47-62.

Bailey, R.A., R.L. Smith, and C.S. Ross. 1969. Stratigraphic Nomenclature of Volcanic Rocks in the Jemez Mountains, New Mexico. Bull. 1274-P. US Geol. Survey, Washington. 19 p.

Ball, T., M. Everett, P. Longmire, D. Vaniman, W. Stone, D. Larssen, K. Greene, N. Clayton, and S. McLin. 2002. Characterization well R-22 completion report. Rept. LA-13893-MS. Los Alamos Natl. Lab., Los Alamos. 41 p.

Balleau Groundwater, I., 1995. Buckman alluvial aquifer yield analysis, Balleau Groundwater, Inc., Albuquerque, NM.

Baltz, E.H., J.H. Abrahams, and W.D. Purtymun, March 1963. "Preliminary Report on the Geology and Hydrology of Mortandad Canyon Near Los Alamos, New Mexico, with Reference to Disposal of Liquid Low-Level Radioactive Waste," US Geological Survey Open File Report, Albuquerque, New Mexico. (Baltz et al. 1963, 8402)

Bernhard, G., G. Geipel, T. Reich, V. Brendler, S. Amayri, and H. Nitsche, 2001. Uranyl(VI) carbonate complex formation: Validation of the $Ca_2UO_2$ $(CO_3)_3$(aq.) species. Radiochim. Acta, vol. 89, 511-518 pp.

Biehler, S., J. Ferguson, W.S. Baldridge, G.R. Jiracek, J.L. Aldern, M. Martinez, R. Fernandez, J. Romo, B. Gilpin, L.W. Braile, D.R. Hersey, B.P. Luyendyk, and C. Aike. 1991. A geophysical model of the Española Basin, Rio Grande Rift, New Mexico. Geophysics. 56:340-353.

Birdsell, K.H., W.E. Soll, N.D. Rosenberg and B.A. Robinson, 1995. "Numerical modeling of unsaturated groundwater flow and radionuclide transport at MDA G", Los Alamos National Laboratory report LA-UR-95-2735.

Birdsell, K.H., W.E. Soll, K.M. Bower, A.V. Wolfsberg, T. Orr, and T. A. Cherry, 1999. Simulations of groundwater flow and radionuclide transport in the vadose and saturated zones beneath Area G, Los Alamos National Laboratory, Los Alamos National Laboratory manuscript LA-13299-MS.

Birdsell, K. H., A. V. Wolfsberg, D. Hollis, T. A. Cherry, and K. M. Bower, 2000. Groundwater flow and radionuclide transport calculations for a performance assessment of a low-level waste site, J. Contam. Hydrol., 46, 99-129.

Birdsell, K. H., B. D. Newman, D. E. Broxton, and B. A. Robinson, 2005. Conceptual models of vadose-zone flow and transport beneath the Pajarito Plateau, Los Alamos, New Mexico, Vadose Zone Journal 2005, 4, p. 620-636.

Bishop, C.W., 1991. Hydrologic Properties of Vesicular Basalt. Masters thesis. University of Arizona.

Bitner, K.A., D. Broxton, P. Longmire, S. Pearson, and D. Vaniman, 2004. Response to Concerns About Selected Regional Aquifer Wells at Los Alamos National Laboratory, Los Alamos National Laboratory Report LA-UR-04-6777, Los Alamos, NM.

Blake, W. D., F. Goff, A. I. Adams, and D. Counce, 1995. Environmental Geochemistry for surface and subsurface waters in the Pajarito Plateau and outlying areas, New Mexico, Los Alamos National Laboratory: LA-12912-MS, Los Alamos National Laboratory, Los Alamos, New Mexico.

Bowen, B. M. 1990. Los Alamos Climatology. Los Alamos National Laboratory Report LA-11735-MS, Los Alamos, New Mexico.

Broxton, D and D. Vaniman, 2005. Geologic framework of a groundwater system on the margin of a rift basin, Pajarito Plateau, North-Central New Mexico, Vadose Zone Journal, 2005, 4, pp. 522-550.

Broxton, D., D. Vaniman, P. Longmire, B. Newman, W. Stone, A. Crowder, P. Schuh, R. Lawrence, M. Everett, R. Warren, N. Clayton, D. Counce, E. Kluk, D. Bergfeld. 2002a. Characterization well MCOBT-4.4 and borehole MCOBT-8.5 completion report. Rept. LA-13993-MS, Los Alamos Natl. Lab., Los Alamos. 80 p.

Broxton, D.E., R. Warren, P. Longmire, R. Gilkeson, S. Johnson, D. Rogers, W. Stone, B. Newman, M. Everett, D. Vaniman, S. McLin, J. Skalski, D. Larssen, 2002b. Characterization Well R-25 Completion Report, ER 2001-0697 and LA-13909-MS, Los Alamos National Laboratory, Los Alamos, New Mexico.

Broxton, D., R. Gilkeson, P. Longmire, J. Marin, R. Warren, D. Vaniman, A. Crowder, B. Lowry, D. Rogers, W. Stone, S. McLin, G. WoldeGabriel, D. Daymon, and D. Wycoff, May 2001a. "Characterization Well R-9 Completion Report," Los Alamos National Laboratory Report LA-13742-MS, Los Alamos, New Mexico. (Broxton et al. 2001a, 71250)

Broxton D., D. Vaniman, W. Stone, S. McLin, M. Everett, and A. Crowder. 2001b. Characterization well R-9i completion report. Rept. LA-13821-MS. Los Alamos Natl. Lab., Los Alamos. 16 p.

Broxton, D., R. Warren, D. Vaniman, B. Newman, A. Crowder, M. Everett, R. Gilkeson, P. Longmire, J. Marin, W. Stone, S. McLin, and D. Rogers. 2001c. Characterization well R-12 completion report. Rept. LA-13822-MS. Los Alamos Natl. Lab., Los Alamos. 72 p.

Broxton, D., D. Vaniman, W. Stone, S. McLin, J. Marin, R. Koch, R. Warren, P. Longmire, D. Rogers, and N. Tapia, May 2001d."Characterization Well R-19 Completion Report," Los Alamos National Laboratory Report LA-13823-MS, Los Alamos, New Mexico.

Broxton, D.E., P.A. Longmire, P.G. Eller, and D. Flores. 1995. Preliminary drilling results for boreholes LADP-3 and LADP-4. p. 93-11. In D.E. Broxton and P.G. Eller (eds.) Earth Science Investigations for Environmental Restoration—Los Alamos National Laboratory Technical Area 21. Rept. LA-12934-MS. Los Alamos Natl. Lab., Los Alamos.

Buske, N., 2003. Early Warning: A Radioactive Rio Grande. The RadioActivist Campaign, Belfair, Washington. http://www.radioactivist.org/LANLweb.pdf

Carey, B., G. Cole, C. Lewis, F. Tsai, R. Warren, and G. WoldeGabriel, 1999. Revised site-wide geologic model for Los Alamos National Laboratory, LANL report LA-UR-00-2056, Los Alamos, New Mexico.

Carle, S.F., 1996. A transition probability-based approach to geostatistical characterization of hydrostratigraphic architecture, Ph.D. dissertation, Univ. of Calif., Davis, Davis, CA 182 pp.

Cather, S.M. 1992. Suggested revisions to the Tertiary tectonic history of north-central New Mexico. NM Geol. Soc. Guidebook, 43th Field Conference. New Mexico. p. 109-122.

Cather, S.M. 2004. Laramide orogeny in central and northern New Mexico and southern Colorado. In G.H. Mack and K.A. Giles (eds.). The Geology of New Mexico, a Geologic History. NM Geol. Soc. Special Publication 11. New Mexico. p. 203-248.

Cavazza, W. 1989. Sedimentation pattern of a rift-filling unit, Tesuque Formation (Miocene), Española Basin, Rio Grande Rift, New Mexico. Jour. of Sed. Petrol. v. 59, No. 2, p. 287–296.

Clark, I. D., and Fritz, P., 1997. Environmental Isotopes in Hydrogeology, Lewis Publishers, New York, New York. (Clark and Fritz 1997, 59168)

Cleveland, W.S., 1979."Robust Locally Weighted Regression and Smoothing Scatterplots," Journal of the American Statistical Association, Vol. 74, 829-836.

Coon, L.M. and Kelly, T.E., 1984. Regional hydrogeology and the effect of structural control and the flow of ground water in the Rio Grande trough, Northern New Mexico, NM. Geological Society Guidebook, 35th Field Conference, Rio Grande Rift: Northern NM., pp. 241-244.

Cooper, J.B., W.D. Purtymun, and E.C. John. 1965. Record of Water Supply Wells Guaje Canyon 6, Pajarito Mesa 1, and Pajarito Mesa 2, Los Alamos, New Mexico, Basic Data Report. U.S. Geological Survey Open-File Report. 77p. (Cooper et al. 1965, ER ID 8582)

Cordell, L., 1979. Gravimetric expression of graben faulting in Santa Fe Coutry and the Española Basin, New Mexico, New Mexico Geologic Society Guidebook, 30th Field Conference, Santa Fe County, pp. 59-64.

Cushman, R.L., 1965. An evaluation of aquifer and well characteristics of municipal well fields in Los Alamos and Guaje Canyons, near Los Alamos, New Mexico, Water-Supply Paper, 1809-D, U.S. Geological Survey, 50 pp.

Dander, D. C. 1998. Unsaturated groundwater flow beneath upper Mortandad Canyon, Report LA-UR-98-4759, Los Alamos National Laboratory, Los Alamos, New Mexico.

Daniel B. Stephens & Associates, Inc., 1994. Santa Fe County water resource inventory. Daniel B. Stephens and Associates Inc. Santa Fe, New Mexico.

Davis, T. S., S. Hoines, and K. T. Hill, July 1996. "Hydrogeologic Evaluation of Los Alamos National Laboratory," NMED-HRMB-96/1, Hazardous and Radioactive Materials Bureau, New Mexico Environment Department, Santa Fe, New Mexico. (Davis et al. 1996, 55446).

Dethier, D.P. 1997. Geology of White Rock quadrangle, Los Alamos and Santa Fe counties, New Mexico. Geologic Map 73, scale 1:24000. New Mexico Bureau of Mines & Mineral Resources, New Mexico Institute of Mining & Technology, Socorro, New Mexico.

Dethier, D.P. 2003. Geologic map of the Puye Quadrangle, Los Alamos, Rio Arriba, Sandoval, and Santa Fe counties, New Mexico. Misc. Field Studies Map MF-2419. US Geol. Survey, Denver.

Devaurs, M., and W. D. Purtymun, 1985. "Hydrologic Characteristics of the Alluvial Aquifers in Mortandad, Cañada del Buey, and Pajarito Canyons," Los Alamos National Laboratory Report LA-UR-85-4002, Los Alamos, New Mexico. (Devaurs and Purtymun 1985, ER ID 7415)

Devaurs, M., November 1985. "Core Analyses and Observation Well Data from Mesita del Buey Waste Disposal Areas and in Adjacent Canyons," Los Alamos National Laboratory Report LA-UR-85-4003, Los Alamos, New Mexico. (Devaurs 1985, ER ID 7416)

DeVries. J.J. and I. Simmers. 2002. Groundwater recharge; An Overview of Processes and Challenges. Hydrogeology J. 10:5-17.

Doherty, J., L. Brebber, et al. (1994). {PEST}: Model Independent Parameter Estimation. Brisbane, Australia, Watermark Computing.

Duffy, C. J. 2004. Semi-Discrete Dynamical Model for Mountain-Front Recharge and Water Balance Estimation, Rio Grande of Southern Colorado and New Mexico. in F. M. Phillips, J. F. Hogan, and B. R. Scanlon (eds.), Groundwater Recharge in a Desert Environment: The Southwestern United States. AGU Water Science and Application Series Volume 9.

Dunne, T., and L. Leopold, 1998. Water in Environmental Planning, W. H. Freeman and Co., San Francisco, California. (Dunne and Leopold 1998, 84459)

Emelity, L. A. 1996. "A History of Radioactive Liquid Waste Management at Los Alamos," Los Alamos National Laboratory document LA-UR-96-1283.

Environmental Protection Agency, 1994. Guidance for the Data Quality Objective Process, EPA QA/G-4, Quality Assurance Management Staff, US Environmental Protection Agency, Washington, DC, Final, September, 1994.

External Advisory Group, 2002. Semi-Annual Report to the Groundwater Integration Team of the Los Alamos National Laboratory Report submitted to Hydrogeologic Characterization Program, Los Alamos National Laboratory, June 2002.

External Advisory Group, 2001a. Semi-Annual Report to the Groundwater Integration Team of the Los Alamos National Laboratory Report submitted to Hydrogeologic Characterization Program, Los Alamos National Laboratory, June 2001.

External Advisory Group, 2001b. Semi-Annual Report to the Groundwater Integration Team of the Los Alamos National Laboratory Report submitted to Hydrogeologic Characterization Program, Los Alamos National Laboratory, December 2001.

External Advisory Group, 2000a. Semi-Annual Report to the Groundwater Integration Team of the Los Alamos National Laboratory Report submitted to Hydrogeologic Characterization Program, Los Alamos National Laboratory, June 26, 2000.

External Advisory Group, 2000b. Semi-Annual Report to the Groundwater Integration Team of the Los Alamos National Laboratory Report submitted to Hydrogeologic Characterization Program, Los Alamos National Laboratory, December 5, 2000.

External Advisory Group, 1999a. Semi-Annual Report to the Groundwater Integration Team of the Los Alamos National Laboratory Report submitted to Hydrogeologic Characterization Program, Los Alamos National Laboratory, July 20, 1999.

External Advisory Group, 1999b. Semi-Annual Report to the Groundwater Integration Team of the Los Alamos National Laboratory Report submitted to Hydrogeologic Characterization Program, Los Alamos National Laboratory, December 23 1999.

External Evaluation Group, 1998. Semi-Annual Report, Groundwater Integration Team Report submitted to Hydrogeologic Characterization Program, Los Alamos National Laboratory, October 31, 2000.

Faybishenko, B., C. Doughty, M. Steiger, J. Long, T. Wood, J. Jacobsen, J. Lore, and P. Zawislanski. 2000. Conceptual model of the geometry and physics of water flow in a fractured basalt vadose zone. Water Resour. Res. 36(12):3499–3520.

Ferguson, J.F., Baldridge, W.S., Braile, L.W., Biehler, S., Gilpin, B., and Jiracek, G.R. 1995. Structure of the Española Basin, Rio Grande Rift, New Mexico, from seismic and gravity data. NM Geol. Soc. Guidebook, 46th Field Conference. p. 105-110.

Flint, A.L., L.E. Flint, E.M. Kwicklis, G.S. Bodvarsson, and J. Fabryka-Martin. 2002. Estimating Recharge at Yucca Mountain, Nevada, USA: Comparison of Methods. Hydrogeology J. 10:180-204.

Freeze, R. A. and J. A. Cherry, 1979. Groundwater. Englewood Cliffs, New Jersey, Prentice-Hall, Inc.

Fogg, G.E., 1989. Emergence of geologic and stochastic approaches for characterization of heterogeneous aquifers. NWWA Conference, National Well Water Association, Dallas, Texas.

Frenzel, P.F., 1995. Geohydrology and simulation of groundwater flow near Los Alamos, north central New Mexico, U.S. Geological Survey Water Resources Investigations Report, 95-4091.

Gable, C.W., T. Cherry, H. Trease, and G.A. Zyvoloski, 1995. GEOMESH Grid Generation. Los Alamos National Laboratory document LA-UR-95-4143

Gallaher, B., 1995. "Groundwater velocities in Los Alamos Canyon," Los Alamos National Laboratory memorandum, ESH-18/WQ&H-95-409, Los Alamos, New Mexico. (Gallaher 1995, 49679)

Gallaher, B.M., D.W. Efurd, R.E. Steiner, 2004. "Uranium in Waters near Los Alamos National Laboratory: Concentrations, Trends, and Isotopic Composition through 1999," Los Alamos National Laboratory report LA-14046 (March 2004).

Galusha, T., and J.C. Blick, 1971. Stratigraphy of the Santa Fe Group, New Mexico. Bull. of the Amer. Mus. Nat. Hist. Vol. 144, Article 1. New York. 128 p.

Gardner, J.N. and F. Goff, 1996. Geology of the northern Valles caldera and Toledo embayment, New Mexico. NM Geol. Soc. Guidebook, 47th Field Conference. New Mexico. p. 225-230.

Gardner, J.N., and F. Goff, 1984. Potassium-argon dates from the Jemez volcanic field: Implications for tectonic activity in the north-central Rio Grande Rift. NM Geol. Soc. Guidebook, 35th Field Conference, Rio Grande Rift, Northern New Mexico, University of New Mexico, Albuquerque.

Gardner, J.N., and L. House, 1987. Seismic hazards investigations at Los Alamos National Laboratory, 1984 to 1985. Rept. LA-11072-MS. Los Alamos Natl. Lab., Los Alamos.

Gardner, J.N., F. Goff, S. Garcia, and R.C. Hagan. 1986. Stratigraphic relations and lithologic variations in the Jemez volcanic field, New Mexico. Jour. Geophy. Res. 91:1763-1778.

Gardner, J.N., A. Lavine, G. WoldeGabriel, D. Krier, D. Vaniman, F. Caporouscio, C. Lewis, P. Reneau, E. Kluk, and M.J. Snow. 1999. Structural geology of the northwestern portion of Los Alamos National Laboratory, Rio Grande Rift, New Mexico: Implications for seismic surface rupture potential from TA-3 to TA-55. LA-13589-MS. Los Alamos Natl. Lab., Los Alamos. 112 p.

Gardner, J.N., S.L. Reneau, C.J. Lewis, A. Lavine, D. Krier, G. WoldeGabriel, and G. Guthrie, 2001. Geology of the Pajarito fault zone in the vicinity of S-site (TA-16), Los Alamos National

Laboratory, Rio Grande Rift, New Mexico. LA-13831-MS. Los Alamos Natl. Lab., Los Alamos. 86 p.

Gardner, J.N., T. Kolbe, and S. Chang, 1993. Geology, drilling, and some hydrologic aspects of Seismic Hazard Program boreholes, Los Alamos National Laboratory, New Mexico. Rept. LA-12460-MS. Los Alamos Natl. Lab., Los Alamos. 19 p.

Gardner, J.N., W.S. Baldridge, R. Gribble, K. Manley, K. Tanaka, J.W. Geissman, M. Gonzalez, and G. Baron, 1990. Results from seismic hazards trench #1 (SHT-1). Rept. EES-1-SH90-19, Los Alamos Natl. Lab., Los Alamos.

Glasco, T., 2000. Personal communication from T. Glasco, Los Alamos County Utility Department, to David Rogers, April 5, 2000.

Glatzmaier, T.G., 1993. "RFI Work Plan for Operable Unit 1157, Environmental Restoration Program," Los Alamos National Laboratory document LA-UR-93-1230 (July 1993).

Goff, F., 1995. Geologic map of Technical Area 21. p. 7–18. In D.E. Broxton and P.G. Eller (eds.) Earth Science Investigations for Environmental Restoration—Los Alamos National Laboratory Technical Area 21. Rept. LA-12934-MS. Los Alamos Natl. Lab., Los Alamos.

Goff, F. and J.N. Gardner, 2004. Late Cenozoic geochronology of volcanism and mineralization in the Jemez Mountains and Valles caldera, north central New Mexico. In G.H. Mack and K.A. Giles (eds.). The Geology of New Mexico, a Geologic History. NM Geol. Soc. Special Publication 11. New Mexico. p. 295-312.

Goff, F., and S. Sayer, 1980. "A Geothermal Investigation of Spring and Well Waters of the Los Alamos Region, New Mexico," Los Alamos National Laboratory Report LA-8326-MS, Los Alamos, New Mexico. (Goff and Sayer, 73686)

Goff, F., C.J. Goff, E, Phillips, P. Kyle, W. McIntosh, S. Chipera, and J.N. Gardner, 2003. Megabreccias, early lakes, and duration of resurgence recorded in Valles caldera, New Mexico, EOS, Transactions American Geophysical Union. Fall Meeting, San Francisco (Dec. 8-12). 84(46):F1649-1650.

Goff, F., J.N. Gardner, and G. Valentine, 1990. Geology of St. Peter's dome area, Jemez Mountains, New Mexico. Geologic Map 69, scale 1:24000. New Mexico Bureau of Mines & Mineral Resources, New Mexico Institute of Mining & Technology, Socorro, New Mexico.

Goff, F., J.N. Gardner, and S.L. Reneau, 2002. "Geology of Frijoles 7.5-min. quadrangle, Los Alamos and Sandoval counties, New Mexico". Open-file Geologic Map OF-GM 42. scale 1:24000. New Mexico Bur. Mines and Mineral Res., Socorro.

Golombek, M. P., G. E. McGill, et al., 1983. "Tectonic and geologic evolution of the Española Basin, Rio Grande Rift: structure, rate of extension, and relation to the state of stress in the western United States." Tectonophysics 94: 483-507.

Gray, R.N., 1997. "Hydrologic budget analysis and numerical simulation of groundwater flow in Los Alamos Canyon near Los Alamos, New Mexico," M.S. Thesis Vol. 1 and 2, University of New Mexico, Albuquerque, New Mexico. (Gray, 1997, 58208)

Gray, R.N., 2000. "Los Alamos Canyon water balance modeling study,"prepared for Los Alamos National Laboratory Environmental Restoration Project, Canyons Focus Area, Los Alamos, New Mexico. (Gray, 2000, 85218)

Griggs, R. L., 1964. "Geology and Ground-Water Resources of the Los Alamos Area, New Mexico," with a section on "Quality of Water" by John D. Hem, U.S. Geological Survey Water-Supply Paper 1753, Washington, D.C. (Griggs 1964, 8795)

Griggs, R.L., 1955. Geology and Ground Water Resources of the Los Alamos Area, New Mexico, US Geological Survey Open-File Report to the US Atomic Energy Commission. 219 p.

Griggs, R. L. and J. D. Hem, 1964. Geology and groundwater resources of the Los Alamos Area, New Mexico, U.S. Geological Survey: 107.

Hawley, J.W., C.S. Haase, and R.P. Lozinsky, 1995. An underground view of the Albuquerque Basin. p. 37-55. In C.T. Ortega-Klett (ed.) The Water Future of Albuquerque and the Middle Rio Grande Basin. NM Water Resources Research Institute Report 290. Las Cruces, NM.

Hearne, G. A., 1985. Mathematical model of the Tesuque aquifer system underlying Pojoaque River basin and vicinity, New Mexico, U.S. Geological Survey: 75.

Hearne, G.A., 1980. Simulation of an aquifer test on the Tesuque Pueblo grant, New Mexico, Open-file Report 801922, U.S. Geological Survey.

Heiken, G., K. Wohletz, R.V. Fisher, and D.P. Dethier, 1996. Part II: Field guide to maar volcanoes of White Rock Canyon. In S. Self, G. Heiken, M. Sykes, K. Wohletz, R. Fisher, and D. Dethier (eds.) Field Excursions to the Jemez Mountains, New Mexico. New Mexico Bureau of Mines & Mineral Resources Bull. 134, Socorro, New Mexico. p. 52-76.

Izett, G.A., and J.D.Obradovich, 1994. $^{40}Ar/^{39}Ar$ age constraints for the Jaramillo normal subchron and the Matuyama-Brunhes geomagnetic boundary. Jour. Geophy. Res. 99:2925-2934.

Justet, L., 1996. The geochronology and geochemistry of the Bearhead Rhyolite, Jemez volcanic Field, New Mexico. M.S. Thesis. University of Nevada. Las Vegas. 152 p.

Keating, E. H., B. A. Robinson, and V. V. Vesselinov, 2005. Development and application of numerical models to estimate fluxes through the regional aquifer beneath the Pajarito Plateau, Vadose Zone Journal 2005, 4, pp. 653-671.

Keating, E. H., V. V. Vesselinov, et al., 2003. "Coupling Basin- and Local-Scale Inverse Models of the Española Basin." Groundwater 41(2): 200-211.

Keating, E.H., et al., 2000. A regional flow and transport model for groundwater at Los Alamos National Laboratory, a progress report submitted to the Hydrogeologic Characterization Program, LA-UR-01-2199, Los Alamos National Laboratory.

Keating, E.H., E. Kwicklis, M. Witkowski, and T. Ballantine, 1999. A simulation model for the regional aquifer beneath the Pajarito Plateau, LA-UR-00-1029, Los Alamos National Laboratory, 76 pp.

Kelley, V.C., 1978. Geology of Española Basin, New Mexico. Geologic Map 48. New Mexico Bur. Mines and Mineral Res., Socorro.

Kelley, V.C., 1952. Tectonics of the Rio Grande depression of central New Mexico. NM Geol. Soc. Guidebook, 3rd Field Conference. New Mexico. p. 92-105.

Kempter, K.A. and S. Kelley, 2002. Preliminary geologic map of Guaje Mountain 7.5 minute quadrangle, Los Alamos and Sandoval counties, New Mexico. Geologic Map 55, scale 1:24000.

New Mexico Bureau of Mines & Mineral Resources, New Mexico Institute of Mining & Technology, Socorro, New Mexico.

Kernodle, J. M., D. P. McAda, et al., 1995. Simulation of ground-water flow in the Albuquerque Basin, central New Mexico, 1901-1994, with projections to 2020. USGS Water-Resources Investigation Report 94-4251.

Kersting, A.B., D.W. Efurd, D.L. Finnegan, D.J. Rokop, D.K. Smith, and J.L. Thompson, 1999. "Migration of Plutonium in Ground Water at the Nevada Test Site," Nature, Vol. 397, January 1999, pp. 86-89.

Kingsley, W. H., February 20, 1947. "Survey of Los Alamos and Pueblo Canyon for Radioactive Contamination and Radioassay Tests Run on Sewer-Water Samples and Water and Soil Samples Taken From Los Alamos and Pueblo Canyons," Los Alamos Scientific Laboratory Report LAMS-516, Los Alamos, New Mexico. (Kingsley 1947, 4186)

Kleinfelder, 2004a. Final Well Completion Report Characterization Well R-4, Los Alamos National Laboratory, March 23, 2004.

Kleinfelder, 2004b. Final Well Completion Report Characterization Well R-2, Los Alamos National Laboratory, April 5, 2004.

Kleinfelder, 2004c. Final Well Completion Report Characterization Well R-11, Los Alamos National Laboratory, March 19, 2004.

Kleinfelder, 2004d. Final Well Completion Report Characterization Well R-28, Los Alamos National Laboratory, April 28, 2004.

Kleinfelder, 2004e. Final Well Completion Report Characterization Well R-1, Los Alamos National Laboratory.

Kleinfelder, 2004f. Final Well Completion Report Characterization Well R-26, Los Alamos National Laboratory.

Kleinfelder, 2003. Final Well Completion Report Characterization Well R-21, Los Alamos National Laboratory.

Koch, R. J., and D. B. Rogers, 2003. "Water Supply at Los Alamos, 1998-2001", Los Alamos National Laboratory report LA-13985-SR (March 2003).

Koch, R. J., D. B. Rogers, N. J. Tapia, and S. G. McLin, 2004. "Manual and transducer groundwater levels from test wells at Los Alamos National Laboratory, 1992-2003", Los Alamos National Laboratory report LA-14132 (April 2004).

Koch, R.J., P. Longmire, D.B. Rogers, and K. Mullen, 1999. Report of testing and sampling of municipal supply well PM-4. Rept. LA-13648. Los Alamos Natl. Lab., Los Alamos. 40 p.

Koening, E., and Guevara, D., 1992. Slug testing of alluvial wells in Los Alamos and Mortandad Canyons, Los Alamos County, New Mexico. (Koening, 1992, 87473)

Koning, D., Broxton, D., Vaniman, D., and WoldeGabriel, G., 2005. Upper Miocene clastic deposits adjacent to the northeastern and eastern flanks of the Jemez Mountains, north-central New Mexico -- Preliminary results, Proceedings, New Mexico Geological Society Annual Meeting, April 15, 2005, Socorro, NM, p. 30, LA-UR-05-2620.

Koning, D.J. and F. Maldonado, 2001. Geology of the Horcado Ranch 7.5 minute quadrangle, Santa Fe County, New Mexico. Open-file Geologic Map OF-GM 44. New Mexico Bureau of Geology & Mineral Resources, New Mexico Institute of Mining & Technology, Socorro, New Mexico. 33 p., Map scale 1:24,000.

Kopp, B., A. Crowder, M. Everett, D. Vaniman, D. Hickmott, W. Stone, N. Clayton, S. Pearson, and D. Larssen, 2002. Well CdV-R-15-3 Completion Report, LA-13906-MS, Los Alamos National Laboratory Report, Los Alamos, NM.

Kopp, B., M. Everett, J.R. Lawrence, G. WoldeGabriel, D. Vaniman, J. Heikoop, W. Stone, S. McLin, N. Clayton, and D. Larssen, 2003. Well CdV-R-37-2 Completion Report, LA-14023-MS, Los Alamos National Laboratory Report, Los Alamos, NM.

Krier, D., P. Longmire, R.H. Gilkeson, and H.J. Turin, 1997. Geologic, geohydrologic, and geochemical data summary of MDA G, TA-54, Los Alamos National Laboratory, Los Alamos National Laboratory document LA-UR-95-2696.

Kwicklis, E. M., M. Witkowski, K. Birdsell, B. Newman, and D. Walther, 2005. Development of an infiltration map for the Los Alamos area, New Mexico, Vadose Zone Journal 2005, 4, pp. 672-693.

Langmuir, D., 1997. Aqueous Environmental Geochemistry, Prentice-Hall, Inc., Upper Saddle River, New Jersey. (Langmuir 1997, 56037)

LANL (Los Alamos National Laboratory), May 1981. "Formerly Utilized MED/AEC Sites Remedial Action Program, Radiological Survey of the Site of a Former Radioactive Liquid Waste Treatment Plant (TA-45) and Effluent-Receiving Areas of Acid, Pueblo, and Los Alamos Canyons, Los Alamos, New Mexico," Los Alamos National Laboratory Report LA-8890-ENV (DOE/EV-0005/30), Los Alamos, New Mexico. (LANL 1981 06059.2).

LANL, 1991. RFI Work Plan for Operable Unit 1106, Los Alamos National Laboratory Report LA-UR-91-962, May 1991.

LANL, 1992a. RFI Work Plan for Operable Unit 1079, Los Alamos National Laboratory Report LA-UR-92-850, May 1992, ER ID 7668.

LANL, 1992b. RFI Work Plan for Operable Unit 1129, Los Alamos National Laboratory Report LA-UR-92-800, May 1992.

LANL, 1992c. RFI Work Plan for Operable Unit 1078, Los Alamos National Laboratory Report LA-UR-92-838, May 1992.

LANL, 1992d. RFI Work Plan for Operable Unit 1122, Los Alamos National Laboratory Report LA-UR-92-925, May 1992.

LANL, 1992f. RFI Work Plan for Operable Unit 1144, Los Alamos National Laboratory Report LA-UR-92-900, May 1992, ER ID 7670.

LANL, 1992g. RFI Work Plan for Operable Unit 1071, Los Alamos National Laboratory Report LA-UR-92-810, May 1992, ER ID 7667.

LANL, 1992h. RFI Work Plan for Operable Unit 1147, Los Alamos National Laboratory Report LA-UR-92-969, May 1992.

LANL, 1993a. RFI Work Plan for Operable Unit 1130, Los Alamos National Laboratory Report LA-UR-93-1152, June 1993, ER ID 15313.

LANL, 1993b. RFI Work Plan for Operable Unit 1132, Los Alamos National Laboratory Report LA-UR-93-768, June 1993.

LANL, 1993d. RFI Work Plan for Operable Unit 1082, Los Alamos National Laboratory Report LA-UR-93-1196, July 1993, ER ID 15316.

LANL, 1993e. RFI Work Plan for Operable Unit 1086, Los Alamos National Laboratory Report LA-UR-93-3968, July 1993, ER ID 20946.

LANL, 1993f. Installation Work Plan for Environmental Restoration, Revision 3, Volume 2, Los Alamos National Laboratory Report LA-UR-93-3987, November 1993.

LANL, 1994a. RFI Work Plan for Operable Unit 1085, Los Alamos National Laboratory Report LA-UR-94-1033, May 1994, ER ID 34755.

LANL, 1994b. RFI Work Plan for Operable Unit 1100, Los Alamos National Laboratory Report LA-UR-94-1097, May 1994.

LANL, October 25, 1995a. "Groundwater Protection Management Program Plan" Draft, Los Alamos National Laboratory, Los Alamos, New Mexico.

LANL, 1995a. "Task/Site Work Plan for Operable Unit 1049: Los Alamos Canyon and Pueblo Canyon," Los Alamos National Laboratory document LA-UR-95-2053, Los Alamos, New Mexico. November 1995 (LANL 1995, 50290).

LANL, 1995b. "Task/Site Work Plan for Operable Unit 1049: Los Alamos Canyon and Pueblo Canyon," Los Alamos National Laboratory document LA-UR-95-2053, Los Alamos, New Mexico. November 1995 (LANL 1995, 50290).

LANL, 1996. "Environmental Surveillance at Los Alamos during 1994," Environmental Protection Group Los Alamos National Laboratory Report LA-13047-ENV, Los Alamos, New Mexico. July (1996, ER ID 54769).

LANL, January 31, 1996a. "Groundwater Protection Management Program Plan," Rev. 2.0 (Final), Los Alamos, New Mexico. (LANL 1996, 70215)

LANL, September 11, 1996b. Letter to New Mexico Environment Department from Subject:

LANL, September 1997. "Work Plan for Mortandad Canyon," Los Alamos National Laboratory document LA-UR-97-3291, Los Alamos, New Mexico. (LANL 1997, 56835)

LANL, May 22, 1998. "Hydrogeologic Workplan", Los Alamos National Laboratory, Los Alamos, New Mexico (LANL, 1998, 59599).

LANL, September 1998a. "Work Plan for Pajarito Canyon," Los Alamos National Laboratory report LA-UR-98-2550, Los Alamos, New Mexico. (LANL 1998, 58820).

LANL. 1998b. RFI Phase II Report for Solid Waste Management Unit 16-021(c)-99. Los Alamos National Laboratory report LA-UR-98-4101, Los Alamos, New Mexico.

LANL, 2000a. "Environmental Surveillance at Los Alamos during 1999," Environmental Surveillance Program Los Alamos National Laboratory document LA-13775-ENV, UC-902, Los Alamos, New Mexico. December 2000 (LANL 2000a, 68661).

LANL, 2000b. "Addendum to RFI Report for Field Unit 1, SWMU 3-010(a)," Los Alamos National Laboratory Report, Los Alamos, New Mexico. (LANL 2000b, ER 2000-0553)

LANL, 2001a. "Environmental Surveillance at Los Alamos during 2000," Environmental Surveillance Program Los Alamos National Laboratory Report LA-13861-ENV, Los Alamos, New Mexico. October 2001 (LANL 2001a, 71301).

LANL, 2002a. "Environmental Surveillance at Los Alamos during 2001," Environmental Surveillance Program Los Alamos National Laboratory report LA-13979-ENV, Los Alamos, New Mexico. December 2004 (LANL 2002, 73876).

LANL, February 2002b. "Los Alamos and Pueblo Canyons Work Plan Addendum, Surface Water and Alluvial Groundwater Sampling and Analysis Plan," Los Alamos National Laboratory document LA-UR-02-759, Los Alamos, New Mexico. (LANL 2002, 70235).

LANL, September 2003a. "Phase III RFI Report for Solid Waste Management Unit 16-021(c)-99," Los Alamos National Laboratory document LA-UR-03-5248, Los Alamos, New Mexico. (LANL 2003, 77965).

LANL, August 2003a. "Mortandad Canyon Groundwater Work Plan " Los Alamos National Laboratory document LA-UR-03-6221, Los Alamos, New Mexico.

LANL, 2003a. Characterization well R-5 completion report, Rept LA-UR-03-1600, Los Alamos Natl. Lab., Los Alamos. 21 p.

LANL, 2003b. Characterization Well R-8 Completion Report, LA-UR-03-1162; GPP-03-021 Los Alamos National Laboratory Report, Los Alamos, NM.

LANL, 2003c. Characterization Well R-13 Completion Report, LA-UR-03-1373; GPP-03-023 Los Alamos National Laboratory Report, Los Alamos, NM.

LANL, 2003d. Characterization Well R-14 Completion Report. LA-UR-03-1644; GPP-03-030 Los Alamos National Laboratory Report, Los Alamos, NM.

LANL, 2003e. Characterization Well R-16 Completion Report, LA-UR-03-1841; GPP-03-031 Los Alamos National Laboratory Report, Los Alamos, NM.

LANL, 2003f. Characterization Well R-20 Completion Report, LA-UR-03-1839; GPP-03-032 Los Alamos National Laboratory Report, Los Alamos, NM.

LANL, 2003g. Characterization Well R-23 Completion Report, LA-UR-03-2059; GPP-03-042 Los Alamos National Laboratory Report, Los Alamos, NM.

LANL, 2003h. Characterization Well R-32 Completion Report, LA-UR-03-3984; GPP-03-071 Los Alamos National Laboratory Report, Los Alamos, NM.

LANL, 2004a. "Environmental Surveillance at Los Alamos during 2003," Environmental Surveillance Program Los Alamos National Laboratory report LA-14162-ENV, Los Alamos, New Mexico.

LANL (Los Alamos National Laboratory), 2004b, Los Alamos and Pueblo Canyons Investigation Report: Los Alamos National Laboratory report LA-UR-04-2714, Los Alamos, New Mexico.

LANL, 2005a. Groundwater Background Investigation Report, ER2005-0156, Los Alamos, New Mexico.

LANL, 2005b. Groundwater Level Data Submittal to NMED, LA-UR-05-0457, January 27, 2005.

LASL (Los Alamos Scientific Laboratory), June 6, 1963. "DDT and the Spruce Budworm," LASL News, Los Alamos, New Mexico. (LASL 1963, 64879)

Lavine, A., C.J. Lewis, D.K. Katcher, J.N. Gardner, and J. Wilson. 2003. Geology of the north-central to northeastern portion of the Los Alamos National Laboratory, New Mexico. Rept. LA-14043-MS. Los Alamos Natl. Lab., Los Alamos. 44 p.

Lewis, C., A. Lavine, S.L. Reneau. J.N. Gardner, R. Channell, and W. Criswell. 2002. Geology of the western part of the Los Alamos National Laboratory (TA-3 to TA-16), Rio Grande Rift, New Mexico. Rept. LA-13960-MS. Los Alamos Natl. Lab., Los Alamos. 98 p.

Lindsay, W. L., 1979. Chemical Equilibria in Soils, Wiley and Sons, New York City, New York.

Loeffler, B.M., D.T. Vaniman, W.S. Baldridge, and M. Shafiqullah, 1988. Neogene rhyolites of the northern Jemez volcanic field, New Mexico. Jour. Geophys. Res. 93:6157–6167.

Longmire, P., 2005. Characterization well R-25 geochemistry report, Los Alamos National Laboratory report, LA-14198-MS. (ER 2004-0072).

Longmire, P., 2002a. Characterization Well R-15 Geochemistry Report, LA-13896-MS, Los Alamos National Laboratory, Los Alamos, New Mexico. (Longmire 2002, 72614)

Longmire, P., 2002b. Characterization Wells R-9 and R9i Geochemistry Report, LA-13927-MS. Los Alamos National Laboratory, Los Alamos, New Mexico. (Longmire 2002, 72713)

Longmire, P., June 2002c. "Characterization Well R-12 Geochemistry Report," Los Alamos National Laboratory Report LA-13952-MS, Los Alamos, New Mexico. (Longmire 2002, 72800)

Longmire, P., June 2002d. "Characterization Well R-19 Geochemistry Report," Los Alamos National Laboratory Report LA-13964-MS, Los Alamos, New Mexico. (Longmire 2002, 73282)

Longmire, P., September 2002e. "Characterization Well R-22 Geochemistry Report," Los Alamos National Laboratory Report LA-13986-MS, Los Alamos, New Mexico. (Longmire 2002, 73676)

Longmire, P. and Goff, F., 2002. Characterization Well R-7 Geochemistry Report, LA-14004-MS, Los Alamos National Laboratory, Los Alamos, New Mexico.

Longmire, P., D. Counce, M. Dale, S. Chipera, and M. Snow, 2002. "Conceptual Model of Mineralogical and Hydrochemical Impacts from the Cerro Grande Fire, Los Alamos, New Mexico," in Effects of Landscape Disturbance on Ecohydrologic Systems, Chapman Conference on Eco-Hydrology of Semiarid Landscapes: Interactions and Processes, Los Alamos National Laboratory document LA-UR-02-5613, Los Alamos, New Mexico. (Longmire et al. 2002, 71274)

Longmire, P.A., D. Broxton, W. Stone, B. Newman, R. Gilkeson, J. Marin, D. Vaniman, D. Counce, D. Rogers, R. Hull, S. McLin, and R. Warren. 2001. Characterization well R-15 completion report, Rept LA-13749-MS, Los Alamos Natl. Lab., Los Alamos. 85 p.

Longmire, P., S. L. Reneau, P. M. Watt, L. D. McFadden, J. N. Gardner, C. J. Duffy, and R. T Ryti, May 1996a. "Natural Background Geochemistry, Geomorphology, and Pedogenesis of

Selected Soil Profiles and Bandelier Tuff Los Alamos, New Mexico," Los Alamos National Laboratory report LA-12913-MS, Los Alamos, New Mexico. (Longmire et al. 1996, 48818)

Longmire, P. A., S. Kung, J. M. Boak, A. I. Adams, F. Caporuscio, and R. N. Gray, 1996b. "Aqueous Geochemistry of Upper Los Alamos Canyon, Los Alamos, New Mexico," The Jemez Mountains Region, New Mexico Geological Society Guidebook, 47th Field Conference, New Mexico, pp. 473-480. (Longmire et al. 1996, 54168).

Lopes, T. J., and S. G. Dionne. 1998. A Review of Semivolatile and Volatile Organic Compounds in Highway Runoff and Urban Stormwater. US Geological Survey Open-File Report 98-409.

Manley, K., 1979. Stratigraphy and structure of the Española Basin, Rio Grande Rift, New Mexico. p. 71–86. In R.E. Rieker (ed.) Rio Grande Rift – tectonics and magmatism. Amer. Geophys. Union, Washington.

Martin, B., 1993. "RFI Work Plan for Operable Unit 1082, Environmental Restoration Program," Los Alamos National Laboratory document LA-UR-93-1196 (July 1993).

Marty, R. C., D. Bennett, and P. Thullem, 1997. Mechanism of plutonium transport in a shallow aquifer in Mortandad Canyon, Los Alamos National Laboratory, New Mexico, Envir. Sci. and Tech., 31, 7, 2020-2027.

Mayfield, D. L., A.L. Stoker, and J. Ahlquist, 1979. Formerly Utilized MED/AEC Sites Remedial Action Program, Radiological Survey of the Bayo Canyon, Los Alamos, New Mexico, Los Alamos Scientific Laboratory, DOE\EV-0005\15, ER ID 11717, June 1979.

McAda, D. P., and P. Barroll, 2002. Simulation of ground-wter flow in the middle Rio Grande basin between Cochiti and San Acacia, New Mexico. Water-Resources Investigations Report 02-4200. Albuquerque, N.M., U.S. Geological Survey: 81.

McAda, D. P., and M. Wasiolek, 1988. Simulation of the regional geohydrology of the Tesuque aquifer system near Santa Fe, New Mexico., U.S. Geological Survey: 71.

McIntosh, W.C., and J. Quade. 1995. $^{40}Ar/^{39}Ar$ geochronology of tephra layers in the Santa Fe Group, Española Basin, New Mexico. NM Geol. Soc. Guidebook, 46th Field Conference. p. 279-287.

McDonald, M.G., and A.W. Harbaugh, 1988. Simulation of the regional geohydrology of the Tesuque aquifer system near Santa Fe, New Mexico. Water Resources Investigations Report, 87-4056, U.S. Geological Survey, 71 pp.

McLin, S.G., 2005. Analyses of the PM-2 aquifer test using multiple observation wells, Los Alamos National Laboratory report, LA-14225-MS.

McLin, S.G., 2004. Aquifer test analysis for well R-15. Los Alamos National Laboratory, report LA-14074-MS, Los Alamos, NM.

McLin, S.G., and W. J. Stone, 2004. Hydrologic tests at characterization wells R-9i, R-13, R-19, R-22, and R-31, Revision 1, Los Alamos National Laboratory, report LA-14121-MS, Los Alamos, NM.

McLin, S.G., Purtymun, W.D., Stoker, A.K. and Maes, M.N., 1996. Water supply at Los Alamos during 1994, LA-13057-PR, Los Alamos National Laboratory, Los Alamos, N.M.51 pp.

McQuillan, D., and R. Montes, 1998. Groundwater geochemistry, Pojoaque Pueblo, New Mexico, NMED/GSB/98-1, New Mexico Environment Department, Santa Fe, New Mexico, 34 pp.

McQuillan, D., M. Dale, J. Young, and K. Granzow, 2003. Ground-Water Quality Atlas for Los Alamos County, N.M. http://www.nmenv.state.nm.us/gwb/GWQ%20Atlas/Los_Alamos_County.html

McQuillan, D., M. Dale, J. Young, and K. Granzow, 2004. "Ground-Water Quality Atlas for Los Alamos County, N.M.," New Mexico Environment Department, Accessed 22 Dec. 2004 at: http://www.nmenv.state.nm.us/gwb/GWQ%20Atlas/Los_Alamos_County.html

Meyer, C., and G.A. Smith, 2004. Petrographic analysis of cuttings from Yates #2 La Mesa well and Tertiary tectonic history of Española Basin. In M. Hudson (ed.) Proceedings of the 3rd Annual Española Basin Workshop, Santa Fe, New Mexico, March 2-3, 2004, U.S. Geological Survey Open-File Report 2004-1093. p. 21.

Mott, D., 1999. Water Resources Management Plan, Bandelier National Monument, New Mexico, U. S. Department of the Interior, National Park Service, 165 pp., November 1999.

Neeper, D. A., 2002. Investigation of the vadose zone using barometric pressure cycles, J. Contam. Hydrol., 54, 59-80.

Neeper, D.A. and R.H. Gilkeson, 1996. The Influence of Topography, Stratigraphy, and Barometric Venting on the Hydrology of Unsaturated Bandelier Tuff. New Mexico Geological Society Guidebook, 47th Field Conference, Jemez Mountains Region, pp. 427-432.

New Mexico Environment Department (NMED), 1995a. Letter to Mr. Larry Kirkman, Acting Area Manager, Department of Energy from Benito J. Garcia, Chief, Hazardous and Radioactive Materials Bureau, New Mexico Environment Department. Subject: Denial of Los Alamos National Laboratory's Ground-Water Monitoring Waiver Requests. Date: May 30, 1995.

New Mexico Environment Department (NMED), 1995b. Letter to Mr. Larry Kirkman, Acting Area Manager, Department of Energy from Ed Kelley, Director, Water and Waste Management Division, New Mexico Environment Department. Subject: Comments Concerning Ground-water Contamination and Protection at Los Alamos National Laboratory (LANL), Los Alamos, New Mexico. Date: August 17, 1995.

New Mexico Environment Department (NMED), 1999. Letter, Subject: Hydrogeologic Workplan Data Quality Objectives Los Alamos National Laboratory NM0890010515, September 10, 1999.

New Mexico Environment Department (NMED), 2005. State of New Mexico, Environment Department, in the matter of The United States Department of Energy and the Regents of the University of California, Los Alamos National Laboratory Los Alamos County, New Mexico, respondents, Compliance Order on Consent, proceeding under the New Mexico Hazardous Waste Act Section 74-4-10 and the New Mexico Solid Waste Act, Section 74-9-36(D), March 1, 2005.

Newman, B. D., 2003. Vadose zone pore water perchlorate data from Los Alamos National Laboratory boreholes. Electronic data file, LA-UR-03-3435.

Newman, B.D., 1996. Vadose Zone Water Movement at Area G, Los Alamos National Laboratory, TA-54: Interpretations Based on Chloride and Stable Isotope Profiles. Los Alamos National Laboratory report LA-UR-96-4682, Los Alamos, New Mexico.

Newman, B.D., R.H. Gilkeson and B.M.Gallaher, 1997b. Vadose zone water movement at TA-49, Los Alamos National Laboratory: Interpretations based on chloride and stable isotope profiles. Los Alamos National Laboratory report LA-UR-96-4682, Los Alamos, New Mexico.

Nitao, J.J., and T.A. Buscheck, 1991. Infiltration of a liquid front in an unsaturated, fractured porous medium, Water Resour. Res., 27, 8, 2099-2112.

Nyhan, J.W., B.J. Drennan, W.V. Abeele, M.L. Wheeler, W.D. Purtymun, G. Trujillo, W.J. Herrera, and J.W. Booth, 1985. "Distribution of Plutonium and Americium beneath a 33-yr-old Liquid Waste Disposal Site." *Journal of Environmental Quality, 14,* (4), pp. 501-509.

Nylander, C.L., Bitner, K.A., Cole, G. Keating, E.H., Kinkead, S., Longmire, P., Robinson, B., Rogers, D.B., and Vaniman, D., 2003. Groundwater Annual Status Report for Fiscal Year 2002, LA-UR-03-0244, Los Alamos National Laboratory, Los Alamos, New Mexico.

Nylander, C.L., Ball, T.T., Bitner, K.A., Henning, K., Keating, E.H., Longmire, P., Robinson, B., Rogers, D.B., Stone, W.J., and Vaniman, D., 2002. Groundwater Annual Status Report for Fiscal Year 2001, LA-13931-SR, Los Alamos National Laboratory, Los Alamos, New Mexico.

Nylander, C.L., Bitner, K.A., Broxton, D.E., Henning, K., Hull, R., Johnson, A.S., Keating, E.H., LaDelfe, C., Longmire, P., Newman, B.D., Robinson, B., Rogers, D.B., and Vaniman, D., 2001. Groundwater Annual Status Report for Fiscal Year 2000, LA-13820-SR, Los Alamos National Laboratory, Los Alamos, New Mexico.

Nylander. C.L., K.A. Bitner, K. Henning, A.S. Johnson, E.H. Keating, P. Longmire, B.D. Newman, B. Robinson, D.B. Rogers, W.J. Stone, and D. Vaniman, 2000. Groundwater Annual Status Report for Fiscal Year 1999. LA-13710-SR, March 2000. Los Alamos National Laboratory, Los Alamos, New Mexico.

Nylander, C.L., Bitner, K.A., Broxton, D.E., Cole, G.L., Gallaher, B.M., Johnson, A.S., Katzman, D., Keating, E.H., Longmire, P., McLin, S.G., Mullen, K.I., Newman, B.D., Rogers, D.B., Stoder, A.K., and Stone, W.J., 1999. Groundwater Annual Status Report for Fiscal Year 1998, LA-13598-SR, Los Alamos National Laboratory, Los Alamos, New Mexico.

Nylander, C.L., K.A. Bitner, D.E. Broxton, B.M. Gallaher, P. Longmire, McLin, S.G, B.D. Newman, D.B. Rogers, 1998. Groundwater Annual Status Summary Report FY97 Hydrogeologic Characterization Program, Los Alamos National Laboratory, Los Alamos, New Mexico.

Penrose, W. R., W. L. Polzer, E. H. Essington, D. M. Nelson, and K. A. Orlandini, 1990. Mobility of plutonium and americium through a shallow aquifer in a semiarid region, Envir. Sci. and Tech., 24, 2, 228-234.

Peters, R.R., and E.A. Klavetter, 1988. A continuum model for water movement in an unsaturated fractured rock mass. Water Resour. Res. 24, 3, p. 416-430.

Phillips, F.M., Peters, L.A., Tansey, M.K. and Davis, S.N., 1986. Paleoclimatic inferences from an isotopic investigation of groundwater in the Central San Juan Basin, New Mexico. Quat. Res., 26: 179-193.

Plummer, L.N., L.M. Bexfield, S.K. Anderholm, W.E. Sanford, and E. Busenberg, 2004. Hydrochemical tracers in the middle Rio Grande Basin, USA: 1. Conceptualization of groundwater flow. Hydrogeology Journal, 12(4): 359-388.

Purtymun, W. D., 1977. Hydrologic characteristics of the Los Alamos wellfield, with reference to the occurrence of arsenic in well LA-6, Los Alamos National Laboratory: 63.

Purtymun, W. D. and A. K. Stoker, 1987. Environmental status of Technical Area 49, Los Alamos, New Mexico, 31 pp., Los Alamos National Laboratory Report LA-11135-MS, November 1987.

Purtymun, W. D. and A. K. Stoker, 1990. "Perched Zone Monitoring Well Installation", Los Alamos National Laboratory report LA-UR-90-3230 (December 1990).

Purtymun, W. D. and D.B. Rogers, 2002. Geohydrology of the Pajarito Plateau, with reference to quality of water, 1949-1972, 362 pp., Los Alamos National Laboratory Report LA-UR-02-4726, original report published December 1975, 2002.

Purtymun, W. D. and H. Adams, 1980. Geohydrology of Bandelier National Monument, New Mexico, 15 pp., Los Alamos National Laboratory Report LA-8635-MS, July 1980.

Purtymun, W. D. and S. Johansen, 1974. General geohydrology of the Pajarito Plateau. Ghost Ranch (Central-Northern N.M.): 347-349.

Purtymun, W. D., 1995. "Geologic and Hydrologic Records of Observation Wells, Test Holes, Test Wells, Supply Wells, Springs, and Surface Water Stations in the Los Alamos Area," Los Alamos National Laboratory report LA-12883-MS, Los Alamos, New Mexico.

Purtymun, W. D., J. R. Buchholz, and T. E. Hakonson, 1977. Chemical quality of effluents and their influence on water quality in a shallow aquifer, J. Environ. Qual., 6, 29-32.

Purtymun, W. D., R. J. Peters, and J. W. Owens, 1980. Geohydrology of White Rock Canyon from Otowi to Frijoles Canyon, 25 pp., Los Alamos National Laboratory Report LA-8461-MS, December 1980.

Purtymun, W.D., 1966. Geology and hydrology of White Rock Canyon from Otowi to the confluence of Frijoles Canyon, Los Alamos and Santa Fe Counties, New Mexico, U.S. Geological Survey Open-File Report, 27 pp.

Purtymun, W.D., 1974. Dispersion and movement of tritium in a shallow alluvial aquifer in Mortandad Canyon at the Los Alamos Scientific Laboratory, LA-5716-MS

Purtymun, W.D., 1984. Hydrologic Characteristics of the Main Aquifer in the Los Alamos Area: Development of Ground Water Supplies, Los Alamos National Laboratory Report, LA-9957-MS pp.

Purtymun, W.D., E.A. Enyart, and S.G. McLin, 1989. Hydrologic characteristics of the Bandelier tuff as determined through an injection well system. Report LA-11511-MS, Los Alamos National Laboratory, Los Alamos, New Mexico.

Purtymun, W.D., S. McLin, and A. Stoker, 1990. Water supply at Los Alamos during 1990, LA-12471-PR, Los Alamos National Laboratory.

Purtymun, W.D., S. McLin, and A. Stoker, 1995a. Water supply at Los Alamos during 1992, LA-12926-PR, Los Alamos National Laboratory.

Purtymun, W.D., A.K. Stoker, and S.G. McLin, 1995b. Water supply at Los Alamos during 1993, LA-12951-PR, Los Alamos National Laboratory.

Purtymun, W.D., W.R. Hansen, and R.J. Peters, 1983. "Radiochemical Quality of Water in the Shallow Aquifer in Mortandad Canyon 1967-1978," Los Alamos National Laboratory report LA-9675-MS, Los Alamos, New Mexico. March 1983 (Purtymun et al. 1983, 6407).

Reiland, L.J., and F.C. Koopman, 1975. Estimated availability of surface and groundwater in the Pojoaque River drainage basin, Santa Fe County, New Mexico, Open-file report 74-151, U.S. Geological Survey. 35 pp.

Reneau, S.L. and D.P. Dethier, 1995. Pliocene and Quaternary history of the Rio Grande, White Rock Canyon and vicinity, New Mexico. In: F. Goff (editor), NM Geol. Soc. Guidebook, 47th Field Conference, Jemez Mountains Region, NM Geological Society, pp. 317-324.

Reneau, S. L., and G. Kuyumjian, 2005. Rainfall-runoff relations in Pueblo Canyon, New Mexico, after the Cerro Grande fire: Los Alamos National Laboratory report LA-UR-04-8810, December 2004.

Reneau, S. L., and E. V. McDonald, 1996. Landscape history and processes on the Pajarito Plateau, northern New Mexico: Rocky Mountain Cell, Friends of the Pleistocene, Field Trip Guidebook, Los Alamos National Laboratory report LA-UR-96-3035, Los Alamos, New Mexico, 195 p. (ER ID 55538)

Reneau, S. L., D. P. Dethier, and J. S. Carney, 1995. Landslides and Other Mass Movements Near Technical Area 33, Los Alamos National Laboratory, Los Alamos National Laboratory report LA-12955-MS (June 1995).

Reneau, S.L., J.N. Gardner, S.L. Forman. 1996. New evidence the age of the youngest eruptions in the Valles caldera, New Mexico. Geology 24:7-10.

Rice, G. (2004). New Mexico's Right to Know: The Potential for Groundwater Contaminants from LANL to Reach the Rio Grande *August 19, 2004,* http://www.nuclearactive.org/docs/RGWIindex.html.

Robinson, B. A., G. Cole, J. W. Carey, M. Witkowski, C. W. Gable, Z. Lu, and R. Gray, 2005a. A vadose zone flow and transport model for Los Alamos Canyon, Los Alamos, New Mexico, Vadose Zone J., 4, 729-743.

Robinson, B.A., S.G. McLin, and H.S. Viswanathan, 2005b. Hydrologic Behavior of Unsaturated, Fractured Tuff: Interpretation and Modeling of a Wellbore Injection Test, Vadose Zone Journal, 2005, 4 p. 694-707.

Robinson, B.A., and G.Y. Bussod, 2000. Radionuclide transport in the unsaturated zone at Yucca Mountain: numerical model and field validation studies, Geophysical Monograph 122, Witherspoon Volume, AGU, Washington, D.C., 323-336.

Rogers, D. B., 1998. Impact of tritium disposal on surface water and groundwater at Los Alamos National Laboratory through 1997, Los Alamos National Laboratory Report LA-13465-SR, July 1998.

Rogers, D.B., 1994. Expanded Los Alamos area isohyetal map, Los Alamos National Laboratory, unpublished memo.

Rogers, D. B., and B. M.Gallaher, 1995. The Unsaturated Hydraulic Characteristics of the Bandelier Tuff, Los Alamos National Laboratory report LA-12968-MS, Los Alamos, New Mexico.

Rogers, D.B., 2001. "Impact of Strontium-90 on Surface Water and Groundwater at Los Alamos National Laboratory through 2000," Los Alamos National Laboratory Report LA-13855-MS (December 2001).

Rogers, D.B., B.M. Gallaher, and E.L. Vold, 1996a. Vadose zone infiltration beneath the Pajarito plateau at Los Alamos National Laboratory. New Mexico Geological Society Guidebook, 47th Annual Field Conference, Jemez Mountains Region, 413-420.

Rogers, D.B., A.K. Stoker, S.G. McLin, and B.N. Gallaher, 1996. Recharge to the Pajarito Plateau regional aquifer system, p. 407 – 412. In F. Goff et al. (ed.) NM Geol. Soc. Guidbook, 47th Field conference, Geology of the Los Alamos Jemez Mountains Region, LANL Report LA-UR-96-486,, New Mexico Geological Society, Las Cruces, NM.

Rogers, M.A., 1995. Geologic Map of the Los Alamos National Laboratory Reservation. prepared by Mara, Inc., Los Alamos, New Mexico.

Sanford, W., 2002. Recharge and groundwater models: an overview. Hydrogeology J. 10:110-120.

Sanford, W. E., L. N. Plummer, et al., 2004. "Hydrochemical tracers in the middle Rio Grande Basin, USA: 2. Calibration of a groundwater flow model." Hydrogeology Journal 12: 389-407.

Scanlon, B. R., R. W. Healy, and P.G. Cook. 2002. Choosing appropriate techniques for quantifying groundwater recharge, Hydrogeology J. 10:18-39.

Schuman, R., 1997a. Radioactive waste inventory for the TA-54, Area G performance assessment and composite analysis. Rogers and Associates Engineering Report, RAE-9629-91B-2.

Seager, W.R., M. Shafiqullah, J.W. Hawley, and R.F. Marvin. 1984. New K/Ar dates from basalts and the evolution of the southern Rio Grande Rift. Geol. Soc. Amer. Bull. 95:87-99.

Self, S., F. Goff, J.N. Gardner, J.V. Wright, and W.M. Kite, 1986. Explosive rhyolitic volcanism in the Jemez Mountains: vent locations, caldera development, and relation to regional structure. Jour. Geophy. Res. 91:1779–1798.

Shomaker, J.W., 1999. Well report: construction and testing, Guaje replacement wells GR-1, GR-2, GR-3, and GR-4, Santa Fe County, New Mexico.

Shomaker, J.W., 1974. Interpretation of well logs in Buckman wellfield, and general limits of Tesuque Formation aquifer, prepared for Black and Veatch Consulting Engineers, Albuquerque, NM.

Smith, G.A., 2001. Development of a pyroclastic apron adjacent to rhyolite domes in a subsiding basin: upper Miocene Peralta Tuff, Jemez Mountains, New Mexico. p. 85-96. In L.S. Crumpler and S.G. Lucas (eds.) Volcanology in New Mexico. Bull. 18. NM Mus. Nat. History and Sci., Albuquerque.

Smith, G.A., 2004. Middle to late Cenozoic development of the Rio Grande Rift and adjacent regions in northern New Mexico. In G.H. Mack and K.A. Giles (eds.). The Geology of New Mexico, a Geologic History. NM Geol. Soc. Special Publication 11. New Mexico. p. 331-358.

Smith, G.A., W. McIntosh, A. J. Kuhle, 2001. Sedimentologic and geomorphic evidence for seesaw subsidence of the Santo Domingo accommodation-zone basin, Rio Grande Rift, New Mexico. Geol. Soc. Amer. Bull. 113:561–574.

Smith, R.L., 1960a. Ash Flows. Geol. Soc. Amer. Bull. 71:795–842.

Smith, R.L., 1960b. Zones and zonal variations in welded ash flows. Prof. Paper 354-F. US Geol. Survey, Washington. p. 149–159.

Smith, R.L., and R.A. Bailey, 1966. The Bandelier Tuff: A study of ash-flow eruption cycles from zoned magma chambers. Bull. Volcanologique, 29:83-104.

Smith, R.L., R.A. Bailey, and C.S. Ross, 1970. Geologic map of the Jemez Mountains, New Mexico. Misc. Geol. Inv. Map I-571, scale 1:125,000. US Geol. Survey, Washington.

Soll, W. and K. Birdsell, 1998. The Influence of Coatings and Fills on Flow in Fractured, Unsaturated Tuff Porous Media System. Water Resour. Res. 34:193-202.

Solomons, W., and U. Forstner, 1984. Metals in the Hydrocycle, Springer-Verlag, Berlin, Germany.

Sophocleous, M., 2002. Interactions between groundwater and surface water: The State of the Science. Hydrogeology J. 10:52-67.

Spell, T. and T.M. Harrison, 1993. "$^{40}Ar/^{39}Ar$ geochronology of post-Valles caldera rhyolite, Jemez volcanic field, New Mexico." Jour. Geophy. Res. 98:8031-8051.

Spell, T. L., I. McDougall, and A.P. Doulgeris, 1996. Cerro Toledo Rhyolite, Jemez volcanic field, New Mexico: $^{40}Ar/^{39}Ar$ geochronology of eruptions between two caldera-forming events. Geol. Soc. Amer. Bull. 108:1549–1566.

Spell, T.L., T.M. Harrison, and J.A. Wolf, 1990. $^{40}Ar/^{39}Ar$ dating of the Bandelier Tuff and San Diego Canyon ignimbrites, Jemez Mountains, New Mexico: Temporal constraints on magmatic evolution. Jour. Volcan. and Geotherm. Res. 43:175-193.

Spiegel, Z., and B. Baldwin, 1963. Geology and Water Resources of the Santa Fe area, New Mexico. Water Supply Pap. 1525. US Geol. Survey, Albuquerque, 258 p.

Springer, E., 2005. Statistical Exploration of Matrix Hydrologic Properties for the Bandelier Tuff, Los Alamos, New Mexico, Vadose Zone Journal, 2005, 4, pp. 505-521.

Stauffer, P. H., and W. J. Stone, 2005. Surface water/groundwater connection at the Los Alamos Canyon weir site Part II. Modeling of tracer test results, Vadose Zone Journal, 2005, 4, pp. 718-728.

Stauffer, P. H., K. H. Birdsell, M. S. Witkowski, and J. K. Hopkins, 2005. Vadose zone transport of 1,1,1-trichloroethane: conceptual model validation through numerical simulation, Vadose Zone Journal 2005, 4, pp. 760-773.

Stimac, J., D. Hickmott, R. Abell, A. C. L. Larocque, D. Broxton, J. Gardner, S. Chipera, J. Wolff, and E. Gauerke, 1996. "Redistribution of Pb and other volatile trace metals during

eruption, devitrification, and vapor-phase crystallization of the Bandelier Tuff, New Mexico," Journal of Volcanology and Geothermal Research, vol. 73, 245-266 pp.

Stoker, A.K., S.G. McLin, W.D. Purtymun, M.N. Maes, and B.G. Hammock, 1992. Water supply at Los Alamos during 1989. Rept. LA-12276-PR. Los Alamos Natl. Lab., Los Alamos, 51 p.

Stoker, A.K., W.D. Purtymun, S.G. McLin, and M.N. Maes, 1991. "Extent of Saturation in Mortandad Canyon," Los Alamos National Laboratory report LA-UR-91-1660.

Stone, W.J., 1996. Some fundamental hydrologic issues pertinent to environmental activities at Los Alamos National Laboratory, New Mexico, in F. Goff, B.S. Kues, M.A. Rogers, L.D. McFadden, and J.N. Gardner (editors), New Mexico Geological Society, Guidebook to the Jemez Mountains, 47th Annual Field Conference. New Mexico Bureau of Mines and Mineral Resources, Socorro, NM, pp. 449-453.

Stone, W.J., G. Cole, W. Carey, and M. Jones, 2001. Expanded hydrogeologic atlas for Los Alamos National Laboratory. Los Alamos National Laboratory report LA-UR-01-70, Los Alamos, NM.

Stone, W., D. Levitt, P. Stauffer, D. Wykoff, P. Longmire, D. Newell, C. Jones, A. Groffman, and R. Roback, 2004. "Results of Monitoring at the Los Alamos Canyon Low-Head Weir, 2002-2003," Los Alamos National Laboratory report LA-14103-MS, Los Alamos, New Mexico, March 1994.

Stone, W., D. Vaniman, P. Longmire, D. Broxton, M. Everett, R. Lawrence, and D. Larssen, 2002. Characterization well R-7 completion report. Rept. LA-13932-MS. Los Alamos Natl. Lab., Los Alamos. 107 p.

Stone, W.J. and D.L. Newell, 2002. Installation of the monitoring site at the Los Alamos Canyon low-head weir. Rept. LA-13970-MS. Los Alamos Natl. Lab., Los Alamos. 31 p.

Stone, W.J., and S.G. McLin, 2003. Hydrologic tests at characterization wells R-9i, R-13, R-19, R-22, and R-31. Rept. LA-13987-MS. Los Alamos Natl. Lab., Los Alamos. 46 p.

Swanson, D.A., T.L. Wright, P.R. Hooper, and R.D. Bentley, 1979. Revisions in the stratigraphic nomenclature of the Columbia River Basalt Group. Bull. 1457-G. US Geol. Survey, Washington, 59 p.

Theis, C.V. and C.S. Conover, 1962. Pumping tests in the Los Alamos Canyon wellfield near Los Alamos, New Mexico, Geological Survey Water-Supply Paper, 1619-I. 24 pp.

Thurman, E.M., 1985. Organic geochemistry of natural waters: Martinus Nijhoff, Dr. W. Junk publishers, Boston, MA

Toyoda, S., F. Goff, S. Ikeda, and M. Ikeya. 1995. ESR dating of quartz phenocrysts in the El Cajete and Battleship Rock Members of the Valles Rhyolite, Valles caldera, New Mexico. Jour. Volcan. and Geotherm. Res. 67:29-40.

Trease, H., et al., 1996. The X3D grid generation system. In: B.K. Soni, J.F. Thompson, H. Hausser and P.R. Eiseman (editors). Numerical grid generation system in computational fluid dynamics and related fields, Mississippi State University, p. 1129.

Turbeville, B. N., 1991. "The influence of ephemeral processes on pyroclastic sedimentation in a rift-basin, volcaniclastic-alluvial sequence, Espanola basin, New Mexico." Sedimentary Geology 74: 139-155.

Turbeville, B.N., D.B. Waresback, and S. Self, 1989. Lava-dome growth and explosive volcanism in the Jemez Mountains, New Mexico: Evidence from the Plio-Pliestocene Puye alluvial fan. Jour. Volcan. and Geotherm. Res. 36:267-291.

Turin, H.J., 1995. Subsurface transport beneath MDA G: a conceptual model. Los Alamos National Laboratory document LA-UR-95-1663.

U.S. Department of Justice and New Mexico State Engineer Office, 1996. Selection of a hydrogeologic model for water-rights administration in the Pojoaque River Basin Santa Fe County, New Mexico.

U.S. Geological Survey, 1997. WATSTORE database.

U.S.Geological Survey, 2001. Surface-Water Data for USA, http://water.usgs.gov/nwis/sw

Van Genuchten, M.T., 1980. A closed-form equation for predicting the hydraulic conductivity of unsaturated soils. Soil Sci. Soc. Am. J. 44, 892-898.

Vaniman, D., G. Cole, J. Gardner, J. Conaway, D. Broxton, S. Reneau, M. Rice, G. WoldeGabriel, J. Blossom, and F. Goff, 1996. Development of a site-wide geologic model for Los Alamos National Laboratory, Los Alamos National Laboratory, LA-UR-00-2059.

Vaniman, D., J. Marin, W. Stone, B. Newman, P. Longmire, N. Clayton, R. Lewis, R. Koch, S. McLin, G. WoldeGabriel, D. Counce, D. Rogers, R. Warren, E. Kluk, S. Chipera, D. Larssen, W. Kopp, 2002. Characterization Well R-31 Completion Report, LA-13910-MS, Los Alamos National Laboratory, Los Alamos, New Mexico.

Vaniman, D., and K. Wohletz, 1990. Results of geologic mapping/fracture studies: TA-55 area. Report EES-1-SH90-17, Los Alamos National Laboratory, Los Alamos, New Mexico.

Vuataz, F.D., F., Goff, C. Fouillac, and J.Y., Calvez, 1986. Isotope geochemistry of thermal and nonthermal waters in the Valles Caldera, Jemez Mountains, northern New Mexico. J. Geophysics Res., 91: 1835-1853.

Vesselinov, V.V., and E. H. Keating, 2002a. "Analysis of Capture Zones of the Buckman Wellfield and of a Proposed Horizontal Collector North of the Otowi Bridge," Los Alamos National Laboratory document LA-UR-02-2750, Los Alamos, New Mexico.

Vesselinov, V.V., and E.H. Keating, 2002b. Analysis of model sensitivity and predictive uncertainty of capture zones in the Española Basin regional aquifer: northern New Mexico, ModelCARE 2002 Calibration and reliability in groundwater modeling: a few steps closer to reality, Prague, Czech Republic, pp. 496-500.

Vesselinov, V.V., and Keating, E.H., 2003. On transient capture zone analysis: The importance of dispersion, AGU Meeting, EOS Trans., 84(46), San Francisco, CA, December 8-12, 2003.

Vilks, P., and D.B. Bachinski, 1996. "Characterization of Organics in Whiteshell Research Area Groundwater and the Implications for Radionuclide Transport," Applied Geochemistry, Vol. 11, No. 3, pp. 387-402. (Vilks and Bachinski 1996, 71515)

Vold, E.L., and R. Schuman, 1996. Phase two of the source release modeling for the Los Alamos Area G Disposal Facility performance assessment. Los Alamos National Laboratory document, LA-UR-96-4786.

Waresback, D. B., J. G. McPherson, et al., 1984. "Volcanogenic Alluvial Fan Sedimentation, Puye Formation, New Mexico." AAPG Bull. 68(4): 537.

Wasiolek, M., 1995. Subsurface recharge to the Tesuque Aquifer system from selected drainage basins along the western side of the Sangre de Cristo mountains near Santa Fe, New Mexico, Water-Resources Investigations Report, 94-4072, U.S. Geological Survey.

Watters, R. L., T. E. Hakonson, and L. J. Lane, 1983. The Behavior of Actinides in the Environment. Radiochimica Acta 32:89–103.

Whelan, J.A., and M.F. Reed, 1997. Geostatistical analysis of regional hydraulic conductivity variations in the Snake River Plain aquifer, eastern Idaho. Geol. Soc. Amer. Bull. 109:855-868.

Whiteman, K.J., J.J. Vaccaro, J.B. Gonthier, and H.H. Bauer, 1994. The hydrogeologic framework and geochemistry of the Columbia Plateau aquifer system, Washington, Oregon, and Idaho. Prof. Paper 1413-B. US Geol. Survey, Washington, 73 p.

WoldeGabriel, G., A.W. Laughlin, D.P. Dethier, and M. Heizler, 1996. Temporal and geochemical trends of lavas in White Rock Canyon and the Pajarito Plateau, Jemez volcanic field, New Mexico, USA. NM Geol. Soc. Guidebook, 47th Field Conference. New Mexico. p. 251-262.

WoldeGabriel, G., R.G. Warren, D.E. Broxton, D.T. Vaniman, M.T. Heizler, E.C. Kluk, and L. Peters, 2001. Episodic volcanism, petrology, and lithostratigraphy of the Pajarito Plateau and adjacent areas of the Española Basin and the Jemez Mountains. p. 97-129. In L.S. Crumpler and S.G. Lucas (eds.) Volcanology in New Mexico. Bull. 18. NM Mus. Nat. History and Sci., Albuquerque.

Zyvoloski, G.A., Robinson, B.A., Dash, Z.V. and Trease, L.L., 1997. Summary of the Models and Methods for the {FEHM} Application --- A Finite-Element Heat- and Mass-Transfer Code, LA-13306-MS, Los Alamos National Laboratory.

# APPENDIX 1-A. REGULATORY FRAMEWORK

## 1-A-1. Hydrogeologic Workplan Background

The Hydrogeologic Workplan was intended to collect data necessary to comprehensively address DOE, federal, and state groundwater requirements. The groundwater requirements are for characterization and monitoring. The intent of the Hydrogeologic Workplan was to characterize the hydrogeologic setting to the degree necessary to evaluate the existing monitoring network and design an enhanced network, if necessary.

### 1-A-1.1. DOE Orders

LANL, in compliance with DOE Order 5400.1, published a Groundwater Protection Management Program Plan (GWPMP) on March 6, 1995 (LANL 1995a). A subsequent draft of the plan including revisions and dated January 31, 1996, was approved by DOE/AL on March 15, 1996 (LANL 1996a). The GWPMP provides background information on the hydrologic setting and programs in place at LANL; describes groundwater issues and solutions; and lays out business and implementation plans. The GWPMP concluded that the number and distribution of wells was insufficient to monitor the groundwater beneath LANL. The Hydrogeologic Workplan (LANL 1998) was intended in part to address the monitoring network issue by collecting data necessary to design an enhanced monitoring network.

### 1-A-1.2. RCRA Permit and HSWA Requirements

In 1986, the Environmental Protection Agency (EPA) authorized the State of New Mexico to operate a hazardous waste management program under the RCRA. The New Mexico Environment Department (NMED) issued a Hazardous Waste Facility Permit (Permit NMD890010515) to the Laboratory on November 8, 1989. At that time, both EPA and NMED retained administrative authority for the permit: EPA for the portions of the permit that were affected by the RCRA Hazardous and Solid Waste Amendments (HSWA) enacted in 1984, and NMED, for the parts of the permit that were unaffected by HSWA. In March 1990, the EPA issued a HSWA module to LANL's permit (known as Module VIII) and, in January of 1996, authorized NMED to act as administrative authority for that module. Thus in 1996 NMED became the sole administrative authority for the Laboratory's Hazardous Waste Facility permit.

The activities described in the Hydrogeologic Workplan support the appropriate Resource Conservation and Recovery Act (RCRA) and the New Mexico Hazardous Waste Act monitoring and corrective action decisions that have yet to be made at LANL. This investigation phase comes before and provides the basis for formal RCRA monitoring that may be warranted. The general RCRA requirements for characterization and monitoring are provided in the following sections.

### 1-A-1.3. RCRA Monitoring Requirements

LANL is currently in compliance with RCRA groundwater monitoring requirements. The monitoring requirements under RCRA are different for "regulated units" and for other "solid

waste management units" (SWMUs). This discussion will address both types of monitoring requirements.

**RCRA Monitoring Requirements for Regulated Units**

"Regulated units" are surface impoundments, waste piles, land treatment units, and landfills that received hazardous waste after July 26, 1982. The "regulated units" that remain at LANL and have not undergone clean closure (all hazardous waste residues and contamination have been removed) are

- Area G in Technical Area 54 (TA-54),
- Area H in Technical Area 54 (TA-54), and
- Area L in Technical Area 54 (TA-54).

(Note: Open Burning/Open Detonation units in the High Explosives corridor at LANL, although not considered "regulated units", once permitted may be subject to similar groundwater monitoring requirements as "regulated units" if they pose a threat to groundwater).

The monitoring requirements for regulated units are described in the RCRA regulations in sections 40 CFR 264.90 to 40 CFR 264.100. The monitoring for regulated units is divided into three structured, sequential monitoring programs: (1) a program for detection, (2) a program for compliance, and (3) a corrective action program. The requirements of these monitoring programs are summarized generally in Table 1-A-1. According to the regulations, monitoring of these units may be waived under the following conditions:

- The unit presents no potential impact to groundwater.
- The unit has been clean closed.
- The regional administrator/state director has granted a groundwater monitoring waiver.

Groundwater-monitoring waiver demonstrations for all of LANL's "regulated units" (including those that had not yet been clean-closed) were submitted to NMED in the 1980s and early 1990s. In May 1995, the NMED issued a letter to LANL indicating that there was insufficient information on the hydrogeologic setting upon which to base approval of the groundwater-monitoring waiver demonstrations, and the waiver demonstrations were denied (NMED, 1995a). By letter dated August 17, 1995 NMED required that a site-wide hydrogeologic characterization be completed that would satisfy both the RCRA "regulated units" and the HSWA module requirements. (Section III. A. 1 of the HSWA portion of the RCRA permit requires that the hydrogeologic setting be characterized) (NMED, 1995b). Thus, groundwater monitoring requirements for LANL's "regulated units" can be addressed by the completion of the site-wide hydrogeologic characterization described in the Hydrogeologic Workplan.

In response to the NMED letters, the Laboratory submitted the Hydrogeologic Workplan to NMED in 1996 and received NMED approval on May 22, 1998. The Hydrogeologic Workplan describes a 7-year characterization effort for groundwater on a Lab-wide basis with the objective of developing sufficient understanding of the hydrogeology to design an adequate detection monitoring network or to resubmit waiver demonstrations for some or all of the units.

**Table 1-A-1.**
**RCRA Groundwater Monitoring Programs for Regulated Units**

| Monitoring Program | Triggered by | Purpose | Requirements | Definition | Result |
|---|---|---|---|---|---|
| Detection (40 CFR 264.98) | Required for all owners/operators of facilities that treat, store, or dispose of hazardous waste 40 CFR 264.91(4), unless exempt by waiver | Detect releases that are a threat to human health or the environment | Monitor for indicator parameters, constituents, or reaction products. Monitoring to be based on the type, quantity, and concentration of waste constituents in the unit; mobility, stability, and persistence in unsaturated zone; detectability in groundwater; and concentration in background | "Detected" defined as statistically significant evidence of contamination based on comparison of groundwater quality upgradient and unaffected by unit to groundwater that passes beneath the unit measured at the point of compliance | If "detected", institute compliance monitoring program |
| Compliance (40 CFR 264.99) | Whenever hazardous constituents to which the ground water protection standard applies are detected at a compliance point 40 CFR 264.91(1) | Document that a release from a unit is above a standard. Determine compliance with ground water protection standard | To determine whether regulated units are in compliance with the groundwater protection standard by monitoring constituents and their associated concentrations specified in the permit at the POC for the prescribed period. The groundwater protection standard specifies: list of constituents; concentration limits; point of compliance; period of compliance | "Exceeded" defined as statistically significant evidence of increased contamination | If ground water protection standard concentration limits are being exceeded, institute corrective action program |
| Corrective Action (40 CFR 264.100) | Whenever the groundwater protection standard is exceeded 40 CFR 264.91(2) & (3) | To ensure that corrective action has successfully brought regulated units into compliance with the groundwater protection standard | Requires action taken to prevent hazardous constituents from exceeding concentration limits and a groundwater monitoring program established to demonstrate effectiveness | Same as for Compliance Monitoring Program | If concentrations are being exceeded, re-evaluate corrective action |

**Monitoring Requirements for Solid Waste Management Units**
The applicability of RCRA groundwater monitoring requirements to units not defined as "regulated units" at 40CFR264.90 (or subpart X units that pose a threat to groundwater) is described at 40 CFR 264.101. For these types of solid waste management units (SWMU), there are no specific monitoring requirements; however, preamble language suggests that repetitive monitoring may be necessary to determine the efficacy of a remedy in the event a release is determined to be a threat to human health or the environment. In addition, characterization to determine if a release to groundwater has occurred and to what extent, if any, such release threatens human health or the environment may be necessary. LANL's ENV-ERS Project conducts the investigations necessary to determine if releases have occurred and if a release represents an unacceptable risk to human health and the environment.

There is a requirement for hydrogeologic characterization at Section III.A.1 of the HSWA module of the RCRA operating permit. The work conducted under the Hydrogeologic Workplan was intended to fulfill this requirement for characterization, in addition to the requirements for "regulated units".

In summary, there are no RCRA monitoring requirements for SWMUs that are not "regulated units", unless a release requiring corrective action is identified through characterization. LANL was in the process of characterizing the hydrogeologic setting, identifying releases, determining the extent of any releases, and evaluating the risk posed by any releases through activities associated with the HWP and Module III of the HSWA module.

In 2005, NMED, DOE, and UC signed a Compliance Order on Consent (NMED 2005). The order replaces the site-wide characterization requirements of the Hydrogeologic Workplan with wells intended to investigate the nature and extent of contaminant releases from sources. The data and information gained through implementation of the Hydrogeologic Workplan are invaluable to planning and implementing the site-specific corrective action investigations required by the Order on Consent (NMED 2005).

## 1-A-2. Technical Objectives of the Hydrogeologic Workplan

As previously stated, the Hydrogeologic Workplan was developed in response to NMED letters requiring a better understanding of the hydrogeologic regime in order to evaluate the need for groundwater monitoring. Specifically, NMED identified four issues that needed to be resolved (NMED 1995b):

- Individual zones of saturation beneath LANL have not been adequately delineated and the "hydraulic interconnection" between these is not understood.
- The recharge area(s) for the regional and intermediate aquifers and any associated effects of fracture-fault zones with regard to contaminant transport and hydrology have not been identified.
- The groundwater flow direction(s) of the regional aquifer and intermediate aquifers, as influenced by pumping of production wells, are unknown.
- Aquifer characteristics cannot be determined without additional monitoring wells installed within specific intervals of the various aquifers beneath the facility.

In addition, the Hydrogeologic Workplan was intended to satisfy the characterization requirements in the HSWA module. Table 1-1 is a crosswalk of HSWA module requirements, how they have been addressed, and which sections of this report contain that information. The technical objectives of the Hydrogeologic Workplan were intended to be comprehensive with respect to groundwater regulatory requirements for characterization and potential future monitoring.

The questions posed by the NMED were large-scale hydrogeologic questions that were open-ended – it was unclear how much data would be required to resolve them. To address this issue, the Hydrogeologic Workplan focused the hydrogeologic investigations on information needed to understand potential contaminant transport and exposure from "aggregates": groups of potential release sites (PRS) that are geographically close and had similar waste-generating processes. The Data Quality Objective (DQO) process was employed to develop the data collection and analysis portions of the Hydrogeologic Workplan. The DQO process was developed by the Environmental Protection Agency to ensure that data collected are adequate for decision-making (EPA, 1994). The first step in applying the DQO process was developing a decision flow chart that specified the decisions for which data were necessary (Figure 1-A-1). The decision statements were in answer to the following questions:

- Are the alluvial groundwaters and uppermost subsurface waters at contaminant concentrations greater than a regulatory limit or risk level?
- Is the intermediate perched zone groundwater at contaminant concentrations greater than some regulatory limit or risk level?
- Is the regional aquifer, as affected by canyon systems, impacted by contaminant concentrations greater than some regulatory limit or risk level?
- What are the pathways for exposure to contaminants from sediments associated with alluvial groundwater and uppermost subsurface water?
- Are there sufficient source terms to cause contamination if moved along pathways to the regional aquifer within a compliance time frame?

The first three decisions are used to determine whether groundwater <u>currently</u> exceeds standards. The last two decisions establish whether pathways exist that may allow contamination to occur <u>in the future.</u> Each decision had several subordinate questions that required some data to answer. The decisions cannot be resolved until data sufficient to answer each subordinate question is available. For example, for the decision: "what are the pathways for exposure to contaminants from alluvial sediments and uppermost subsurface water?" the subordinate questions are as follows:

- Does significant recharge occur from near surface to underlying groundwater bodies?
- Do we know the hydraulic properties of the alluvium?
- What are the retardation factors of alluvial sediments?
- Do we understand groundwater movement from alluvial water to intermediate perched zones?

- Do we understand groundwater movement from intermediate perched zones to the regional aquifer?
- Are fractures and faults important contaminant transport pathways for liquids in canyons?

Although there were numerous subordinate questions and decisions, the data needed to resolve them were primarily water quality information from alluvial, intermediate, and regional aquifer groundwater, hydrologic properties, and geochemistry. Modeling tools were identified as critical to analyzing the data collected and to guide further data collection.

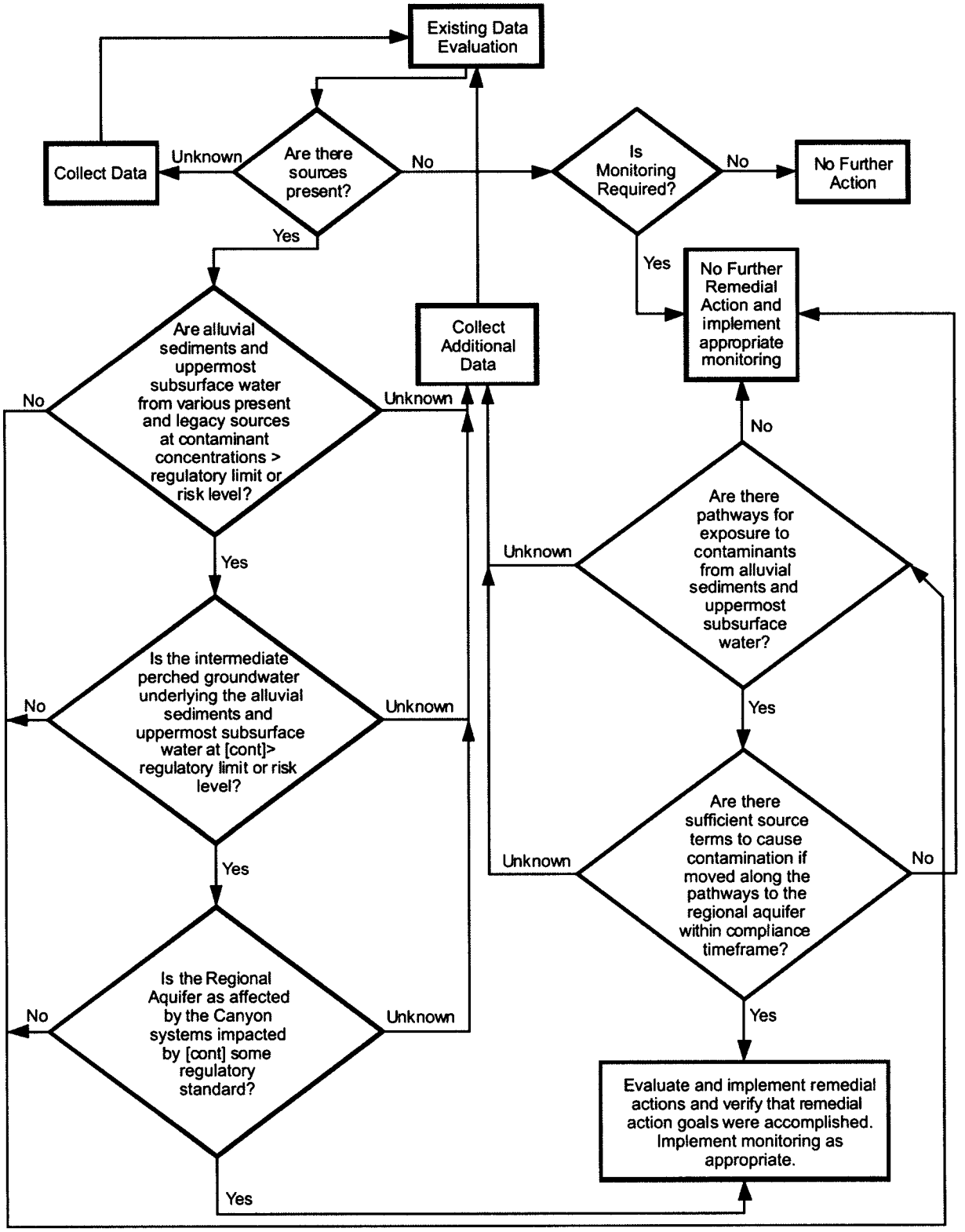


**Figure 1-A-1.** Flow chart used for hydrogeologic characterization decisions (LANL, 1998).

## 1-A-3. Hydrogeologic Workplan Data Collection Approach

The data collection approach described in the Hydrogeologic Workplan utilized an iterative approach that incorporated new information and data into the site conceptual model as it became available. This method enabled effective decision-making for aggregates to occur in the characterization process on a step-by-step basis. This approach was developed, in part, to resemble EPA's concept of the limit of the waste management area as described in the definition of the point of compliance. In this definition, it is acceptable to circumscribe several units with an imaginary line when locating the point of compliance, a vertical surface at the hydraulically downgradient limit of the waste management area at which the groundwater protection standards apply (New Mexico Annotated Code, Title 20, Chapter 4, Part 1, (20 NMAC 4.1) Subpart VI, 264.95(2)). The aggregate approach bounded similar areas in a manner that supported not only logical hydrogeologic characterization but process and regulatory application as well.

Eight aggregates were defined and data collection locations were selected to resolve the subordinate questions and decisions. In aggregates where there were existing data and known contaminant sources, wells were placed where they were most likely to encounter contaminants and to assess contaminant transport pathways. In aggregates with little existing hydrologic data and known contaminant sources, wells were located proximal and down gradient from contaminant sources. In aggregates where there were little existing data and small or no contaminant sources, wells were placed to reduce uncertainties in the hydrologic setting and to confirm the assumption of no groundwater impact.

The original Hydrogeologic Workplan proposed to characterize the hydrogeologic setting by drilling, logging, installing, and sampling wells to the regional aquifer without installing separate intermediate-depth wells. This approach was expected to provide the greatest amount of characterization data and was agreed to by NMED, as documented in a letter sent to NMED (LANL 1996b). This approach was formulated based on the following technical rationale:

- The presence of intermediate zone(s) is controlled by geologic structure and the geology across LANL is extremely variable. Understanding the geologic setting from the surface to the regional aquifer is more important in predicting flow than measurements in individual intermediate zones.
- If a well were installed at the first intermediate zone encountered, there would be a gap in the information between the upper intermediate zone and the top of the regional aquifer. Furthermore, wells installed in the first intermediate zone will not provide any information on the underlying less permeable perching layer. The characteristics of the perching layer must be understood in order to assess the impact to the regional aquifer. The perching layer stratigraphy is as important to evaluating potential pathways as the hydrologic characteristics of the saturated zone itself.
- The data collection described in the Hydrogeologic Workplan is intended to characterize the hydrogeologic setting to a sufficient degree to develop an adequate detection monitoring system or groundwater monitoring waiver, if appropriate. Wells that may be needed to monitor the intermediate zone(s) will be considered as part of the monitoring system design.

### 1-A-3.1 Revision to Hydrogeologic Workplan Data Collection Approach

The characterization approach was modified as the Hydrogeologic Workplan was implemented. A major drilling program change was prompted by an NMED letter (NMED 1999) with two key points: (1) water samples taken from boreholes during the drilling operation would not be adequate for regulatory decisions; and (2) perched zones did not have to be sealed off during drilling, but could be left open until the well was constructed. The practical result of these requirements was that intermediate perched zones could not be characterized by obtaining one sample during drilling. Instead, a dedicated sampling location must be installed to characterize the intermediate perched zones over time. Initially, wells that encountered intermediate perched zones were built with multiple completions. Eventually separate intermediate wells were constructed to be able to monitor the intermediate perched zones. The second point in the 1999 NMED letter, to be able to leave intermediate perched zones open, allowed the wells to be drilled faster because there was no longer a need to telescope down well casing sizes to seal off intermediate perched groundwater zones.

Another modification from the Hydrogeologic Workplan was the use of fluids in drilling. The original Hydrogeologic Workplan called for drilling with no additives in order to collect pristine samples while drilling. The earliest wells were drilled using air-rotary drilling methods with casing advance and the minimal use of fluids other than air. Because of significant problems associated with stuck casing, unstable boreholes, and lost circulation, small amounts of drilling fluids were used to improve lubricity, borehole stabilization, and cuttings circulation. Continuing drilling problems made total reliance on air-rotary drilling with casing advance impracticable for meeting drilling objectives. It became apparent that the depth of the wells and the difficult drilling environment required that more drilling techniques be added to the drilling "tool box" in order to respond to the complex hydrogeologic conditions that characterize the Pajarito Plateau. All of the drilling methods used at LANL are used in standard environmental industry practice and are described by the American Society for Testing and Materials (ASTM). Table 1-A-2 briefly describes the drilling methods used since the beginning of the drilling program.

### 1-A-3.2 Alluvial Groundwater Investigations

Beginning in the mid-1990s, detailed investigations were begun for the ENV-ERS Project, which is driven by the Laboratory's HSWA module to the RCRA operating permit. The first watershed investigation to be implemented was in the Los Alamos and Pueblo Canyon watershed to fulfill request for information requirements presented in the Task/Site Work Plan for Los Alamos and Pueblo Canyons, OU 1049 (LANL 1995b) and the subsequent addendum, Surface Water and Alluvial Groundwater Sampling and Analysis Plan (LANL 2002). The watershed-scale investigations conducted under the ENV-ERS Project are designed to collect data sufficient to evaluate human-health and ecological risk at a watershed scale. In accordance with existing canyons work plans, the Compliance Order on Consent, and the Federal Facility Compliance Agreement for storm water, surface water and alluvial groundwater investigations are conducted in a coupled manner in order to facilitate the development of conceptual models of the relationship between these waters.

## Table 1-A-2. Drilling Methods Used for Hydrogeologic Characterization Wells at Los Alamos National Laboratory

| Drilling Method | Description | Benefits | Drawbacks |
|---|---|---|---|
| Air rotary ASTM D5782-95; D5781-95 (ASTM, 2000a; ASTM, 2000b) | A drill pipe or drill stem is coupled to a drill bit that rotates and cuts through soils, alluvium, and rock. The cuttings produced from the rotation of the drilling bit are transported to the surface by compressed air or by compressed air augmented by municipal water mixed with drilling additives. In conventional air-rotary drilling, the compressed air is forced down the borehole through the drill pipe and returns to the surface up through the annular space. In reverse air rotary, a dual tube drilling system is used and drilling fluids are forced down the outer tube and return up the center tube, where the cuttings are discharged through a cyclone velocity dissipater. The circulation of drilling fluids not only removes cuttings from the borehole but also cools the drill bit. | The air rotary drilling method, employed in an open hole, is the fastest and least expensive drilling method in the unsaturated zone. It is best suited for stable, hard rock formations with good circulation characteristics (in which there is minimal loss of fluids into the formations). Open hole drilling allows for the collection of an extensive suite of geophysical logs for the characterization of hydrogeologic properties. | Experience gained in the early part of the drilling program showed that air rotary drilling in an open hole is not always a suitable method for drilling at depths greater than 150 feet below the regional aquifer water table. The use of municipal water with drilling additives is almost always required to improve borehole stability and circulation of cuttings. Use of these drilling fluids can alter the natural properties of the rocks and it is not possible to collect pristine water samples while drilling. Generation of dust at the surface is a problem unless dust-suppression equipment is used and/or municipal water is added to the circulation fluid. |
| Casing advance ASTM D5876-95 (ASTM, 2000c) | Air-rotary drilling using an under reamer cutting system (rotary bits or downhole hammer) to create a hole large enough for a heavy-walled casing to slide down behind the drill bit. The casing is advanced simultaneously while drilling the hole. Compressed air or compressed air augmented by municipal water mixed with drilling additives is used to remove the cuttings from the bottom of the borehole. When the borehole has reached total depth, the well is constructed inside the heavy walled casing, as the casing is incrementally removed. | The drill casing stabilizes the borehole when drilling through poorly consolidated materials and improves circulation in highly porous or fractured rocks. The cased hole provides a stable environment for the construction of the well. There is relatively little disturbance to the borehole walls and relatively undisturbed samples of rock and water are obtained during drilling. | The heavy-wall casing frequently becomes stuck and is difficult to extract from the borehole. Casing that can not be extracted must be abandoned in the hole, possibly impacting the use of some well screens. The cost is high and drilling rates are often very slow. The use of municipal water with drilling additives is almost always required to provide lubricity between the casing and the borehole wall and to improve borehole stability and the circulation of cuttings. Use of heavy-walled casing severely limits the geophysical methods that can be used for hydrogeologic characterization. |
| Mud rotary ASTM D5783-95 (ASTM, 2000d) | A bit is rotated to cut through the rock while mud is the circulating fluid pumped down through the drill pipe and returned back up the borehole through the annular space. The mud-filled hole stabilizes the borehole wall and cools the drill bit. Circulation of the mud carries the cuttings up to the surface. | Rapid and effective drilling methods. Can be used to maintain borehole stability in poorly consolidated sediments of the saturated zone. Open hole drilling allows for the collection of an extensive suite of geophysical logs for the characterization of hydrogeologic properties. | Does not work well in vadose zone due to lost circulation zones in fractured basalts and in highly porous tuffs and sediments. Masks the recognition of water-bearing zones while drilling. Slow circulation of mud mixes cuttings from throughout the borehole, hampering geologic characterization. Addition of drilling muds and fluids changes the geochemical environment around the borehole. Requires extensive development to remove residual muds and drilling fluids, and to restore the aquifer's hydraulic and geochemical properties to natural conditions. |

The scope of investigation in the Los Alamos/Pueblo watershed (other watershed work plans have similar scope) consisted of 4 sampling rounds collected through one year across a representative range of hydrologic conditions (e.g., higher water levels and more extensive saturation typical of spring snowmelt conditions; and low groundwater levels that commonly occur in the fall), detailed water-level measurements collected using dedicated pressure transducers, measurement of field parameters, a water balance study, and field observations on extent and persistence of surface water. These data were used to develop a conceptual model to describe the occurrence and temporal context of groundwater contamination in support of the risk assessment. The report for the Los Alamos and Pueblo Canyon investigation was submitted to the NMED in April, 2004. The Mortandad Canyon investigation is underway, and the report is scheduled for completion in 2006. Subsequent watershed-scale investigations will be completed in order of priority.

## 1-A-4. Independent Peer Review of the Hydrogeologic Workplan

In 1999, an External Advisory Group (EAG) was formed to provide an independent review of the implementation of LANL's Hydrogeologic Workplan. The EAG consisted of six members with diverse technical and professional backgrounds to provide a broad technical and managerial review of LANL's Hydrogeologic Workplan activities and methods. The EAG was provided semi-annual updates on the program status. The EAG provided a report of findings and observations based on the semi-annual reviews (External Advisory Group 1999a, 1999b, 2000a, 2000b, 2001a, 2001b, 2002; External Evaluation Group 1998). In response, action plans were developed that specified how the recommendations of the EAG were incorporated into the program.

In addition to the semi-annual reviews, the EAG provided technical assistance when requested. In FY99, two EAG members provided invaluable assistance in repairing the well R-25 collapsed screen #3. Numerous problems encountered in the repair process were overcome with the advice and guidance of the EAG members. The "hands on" assistance was critical in completing the characterization well.

## 1-A-5. Outreach Activities

The original Hydrogeologic Workplan (LANL 1998) specified a communications approach that included three quarterly meetings, one annual meeting, and an annual status report to update regulators on the characterization progress. The primary purpose of the quarterly meetings was to report on progress and findings from the previous quarter. The annual meeting was intended to provide more of a synthesis of data collected in the previous year and to allow regulators to provide their input to the planned activities for the coming year. One objective of the annual meeting was to reach a DOE, LANL, NMED consensus on the activities for the following year in time to influence budget requests. The annual report was published as a prelude to the annual meeting and provided the written synthesis of the data collected and interpreted over the year. The first annual meeting was held in March 1998 and participants were limited to representatives of the DOE, LANL, and NMED. Annual meetings were held in 1999, 2000, 2001, 2002, 2003, 2004, and the last annual meeting was held in 2005.

Extensive information has been presented and discussed with regulators and the public in several ways since the Hydrogeologic Workplan was completed in 1997 (Table 1-A-3):

- Three quarterly meetings and one annual meeting held every year (27 documented meetings) with distribution of meeting minutes to an extensive mailing list
- Annual status reports summarizing the work accomplished in the previous year
- Well completion reports
- Geochemistry reports
- Hydrologic testing reports
- Water quality data, which are available over the internet at http://wqdbworld.lanl.gov.
- Annual environmental surveillance reports, which provide the analytical results of surface water and groundwater sampling at LANL and in northern New Mexico.

## Table 1-A-3.
## Documents Relevant to the Hydrogeologic Workplan

| Type of Document | Subject | Reference |
|---|---|---|
| Meeting Minutes | Annual Meeting 3/30/98 | Letter, DOE/LASO file number LAAME 6BK-010 |
| | Annual Meeting 3/29/99 | Letter, LANL file number ESH-18/WQ&H: 99-0162 |
| | Annual Meeting 3/29/00 | Letter, LANL file number ESH-18/WQ&H: 00-0267 |
| | Annual Meeting 3/20/01 | Letter LANL file number ESH-18/WQ&H: 01-126 |
| | Annual Meeting 4/10/02 | Letter LANL file number RRES-DO: 02-25 |
| | Annual Meeting 3/18/03 | Letter LANL file number RES-GPP-03-053 |
| | Annual Meeting 4/12/04 | Letter LANL file number RRES-GPP-04-0023 |
| | Quarterly Meeting 6/29/98 | Letter LANL file number ESH-18/WQ&H: 98-0233 |
| | Quarterly Meeting 10/27/98 | Letter LANL file number ESH-18/WQ&H: 98-0443 |
| | Quarterly Meeting 2/9/99 | Letter LANL file number ESH-18/WQ&H: 99-0066 |
| | Quarterly Meeting 6/23/99 | Letter LANL file number ESH-18/WQ&H: 99-0275 |
| | Quarterly Meeting 10/13/99 | Letter LANL file number ESH-18/WQ&H: 99-0451) |
| | Quarterly Meeting 1/27/00 | Letter LANL file number ESH-18/WQ&H: 00-0056 |
| | Quarterly Meeting 6/22/00 | Letter LANL file number ESH-18/WQ&H: 00-0425 |
| | Quarterly Meeting 10/3/00 | Letter LANL file number ESH-18/WQ&H: 00-0403 |
| | Quarterly Meeting 1/30/01 | Letter LANL file number ESH-18/WQ&H: 01-051 |
| | Quarterly Meeting 6/27/01 | Letter LANL file number ESH-18/WQ&H: 01-284 |
| | Quarterly Meeting 10/16/01 | Letter LANL file number ESH-18/WQ&H: 01-410 |
| | Quarterly Meeting 1/30/02 | Letter LANL file number ESH-18/WQ&H: 02-114 |
| | Quarterly Meeting 7/24/02 | Letter LANL file number RRES-GWPP: 02-03 |
| | Quarterly Meeting 10/29/02 | Letter LANL file number RES-GPP-02-021) |
| | Quarterly Meeting 1/22/03 | Letter LANL file number RES-GPP-03-013 |
| | Quarterly Meeting 10/27/03 | Letter LANL file number RRES-GPP-03-101 |
| | Quarterly Meeting 1/28/04 | Letter LANL file number RES-GPP-04-0023 |
| | Quarterly Meeting 7/13/04 | Letter LANL file number RRES-GWPP:04-0045 |
| | Quarterly Meeting 10/25/04 | Letter LANL file number ENV-GPP:04-0051 |
| | Quarterly Meeting 2/2/05 | Letter LANL file number ENV-GPP:05-0007 |

**Table 1-A-3.**
**Documents Relevant to the Hydrogeologic Workplan (continued)**

| Type of Document | Subject | Reference |
|---|---|---|
| Ground-water Annual Status Reports | Annual Report for FY97 | Nylander, C.L., et al., 1998. |
| | Annual Report for FY98 | Nylander, C.L., et al., 1999. |
| | Annual Report for FY99 | Nylander, C.L., et al., 2000. |
| | Annual Report for FY00 | Nylander, C.L., et al., 2001. |
| | Annual Report for FY01 | Nylander, C.L., et al., 2002. |
| | Annual Report for FY02 | Nylander, C.L., et al., 2003. |
| Well Com-pletion Reports | Well Completion Report for R-1 | Kleinfelder, Well R-1, 2004c. |
| | Well Completion Report for R-2 | Kleinfelder, Well R-2, 2004b. |
| | Well Completion Report for R-4 | Kleinfelder, 2004a, Well R-4, 2004a. |
| | Well Completion Report for R-5 | LANL, Well R-5, 2003a. |
| | Well Completion Report for R-7 | Stone, W., et al., Well R-7, 2002. |
| | Well Completion Report for R-8 | LANL, Well R-8, 2003b. |
| | Well Completion Report for R-9 | Broxton, D.E., et al., Well R-9, 2001a. |
| | Well Completion Report for R-11 | Kleinfelder, Well R-11, 2004c. |
| | Well Completion Report for R-12 | Broxton, D.E., et al., Well R-12, 2001b. |
| | Well Completion Report for R-13 | LANL, Well R-13, 2003a. |
| | Well Completion Report for R-14 | LANL, Well R-14, 2003. |
| | Well Completion Report for R-15 | Longmire, P., et al., Well R-15, 2000. |
| | Well Completion Report for R-16 | LANL, Well R-16, 2003e. |
| | Well Completion Report for R-19 | Broxton, D., et al., Well R-19, 2001d. |
| | Well Completion Report for CdV-R-15-3 | Kopp, B., et al., Well CdV-R-15-3, 2002. |
| | Well Completion Report for CdV-R-37-2 | Kopp, B., et al., Well CdV-R-37-2, 2003. |
| | Well Completion Report for R-20 | LANL, Well R-20, 2003f. |
| | Well Completion Report for R-21 | Kleinfelder, Well R-21, 2003f. |
| | Well Completion Report for R-22 | Ball, T. et al., Well R-22, 2002. |
| | Well Completion Report for R-23 | LANL, Well R-23, 2003g. |
| | Well Completion Report for R-25 | Broxton, D., et al. Well R-25, 2001e. |
| | Well Completion Report for R-26 | Kleinfelder, Well R-26, 2004f. |
| | Well Completion Report for R-28 | Kleinfelder, Well R-28, 2004d. |
| | Well Completion Report for R-31 | Vaniman, D., et al. Well R-31, 2002. |
| | Well Completion Report for R-32 | LANL, Well R-32, 2003h. |

## Table 1-A-3.
## Documents Relevant to the Hydrogeologic Workplan (continued)

| Type of Document | Subject | Reference |
|---|---|---|
| | Well Completion Report for MCOBT-4.4 | Broxton, D., et al., 2002. |
| | Well Completion Report for MCOBT-8.5 | Broxton, D., et al., 2002. |
| | Well Completion Report for R-9i | Broxton, D., et al., 2001c. |
| | Well Completion Report for CdV-16-1(i) | (Completion report not available) |
| | Well Completion Report for CdV-16-2(i) | (Completion report not available) |
| | Well Completion Report for CdV-16-3(i) | (Completion report not available) |
| Geo-chemistry Reports | Geochemistry Report for R-7 | Longmire, P., et al., Well R-7, 2002. |
| | Geochemistry Report for R-9 | Longmire, P., Well R-9, 2002b. |
| | Geochemistry Report for R-9i | Longmire, P., Well R-9i, 2002b. |
| | Geochemistry Report for R-12 | Longmire, P., Well R-12, 2002d. |
| | Geochemistry Report for R-15 | Longmire, P., Well R-15, 2002a. |
| | Geochemistry Report for R-19 | Longmire, P., Well R-19, 2002e. |
| | Geochemistry Report for R-22 | Longmire, P., Well R-22, 2002c. |
| | Geochemistry Report for R-25 | Longmire, P., Well R-25, 2005. |
| Hydro-logic Testing Reports | Hydrologic Testing Report for R-9, R-12, and R-25 | Stone, W. J., Wells R-9, R-12, and R-25, 2000. |
| | Hydrologic Testing Report for R-9i, R-13, R-19, R-22, R-31 | Stone, W.J., et al., Wells R-9i, R-13, R-19, R-22, R-31, 2003. |
| | Hydrologic Testing Report R-15 | McLin, S.G., Well R-15, 2004. |

# APPENDIX 1-B. WELL COMPLETION FACT SHEETS

Location: Upper Mortandad Canyon - TA-5

Description: Brass Marker
Northing: 1769600.84
Easting: 1632354.13
Elevation: 6881.21

Description: Well Casing
Northing: 1769598.84
Easting: 1632355.14
Elevation: 6883.35

Description: Core Hole
Northing: 1769650.6
Easting: 1632227.2
Elevation: 6881.89

Coring:
(0' - 399') Continuous Sampler
(274' - 399') Fluid Assisted

Drilling:
(0' - 90') 13-3/8" Air Rotary Casing Hammer
(90' - 1165') 12-1/4" Mill-Tooth Tri-Cone
(90' - 140') Air Rotary
(140' - 1165') Fluid Assisted Air Rotary

Data Collection:
- Hydrologic Properties:
  Constant Discharge Pumping Test - 1/15/04 - 1/19/04
- Cores/Cuttings submitted for geochemical and contaminant characterization: 19
- Groundwater Samples Submitted
  Perched Groundwater:
  Screening Sample - 11/01/03 (72.6')
  Regional Groundwater:
  Screening Sample - 11/09/03 (1003.3')
  Well Sample - 11/25/03 (1031.1' - 1057.4')
- Geologic Properties:
  Cuttings submitted for:
  Minerology, petrography, and chemistry: 7

Borehole Logs:
- Lithologic: 0' - 1165'
- Video (LANL tool): 0'-782' 11/8/03
  0'-1000' 11/9/03
- Gamma Log (LANL tool): 0-200' 1/05/04
- Schlumberger logs:
  Compensated Neutron Log:
  Cased: 30'-90'; Open Hole: 90'-1165'
  Triple Litho-Density:
  Cased: 30'-90'; Open Hole: 90'-1165'
  Array Induction Imager:
  Cased: none; Open Hole: 90'-1135'
  Elemental Capture Sonde:
  Cased: none; Open Hole: 110'-1156'
  Natural GR Spectroscopy:
  Cased: none; Open Hole: 90'-1142'
  Combinable Magnetic Resonance:
  Cased: none; Open Hole: 110'-1146'
  Fullbore Formation Micro Imager:
  Cased: none; Open Hole: 980'-1165'

Corehole Logs:
- Lithologic: 0' - 399'
- Video (LANL tool): None
- Gamma Ray (LANL Tool): 0-200'

Core Drilling Completed: 12/01/03 - 12/17/03
Rotary Drilling Completed: 10/31/03 - 11/08/03
Contract Geophysics: 11/08/03 - 11/09/03
Well Installation: 11/10/03 - 11/14/03
Well Development Completed: 11/19/03 - 11/25/03

- Casing:
  4.5" ID / 5.0" OD A304 Stainless Steel casing with external couplings
- Number of Screens:
  One (1) 4.46" ID / 5.27" OD, wire wrapped stainless steel, rod based 0.020 slot screen with external couplings.
- Screen Interval: 1031.1' - 1057.4'

Well Development performed by swabbing, bailing, and pumping.
Total Volume Purged: 9,760 gallons
Hydrologic Testing:
Total Volume Removed: 8,912 gallons

Geologic contacts cited are for the R-1 borehole to the regional aquifer. Contacts were determined from cuttings, borehole video, and geophysical logs.

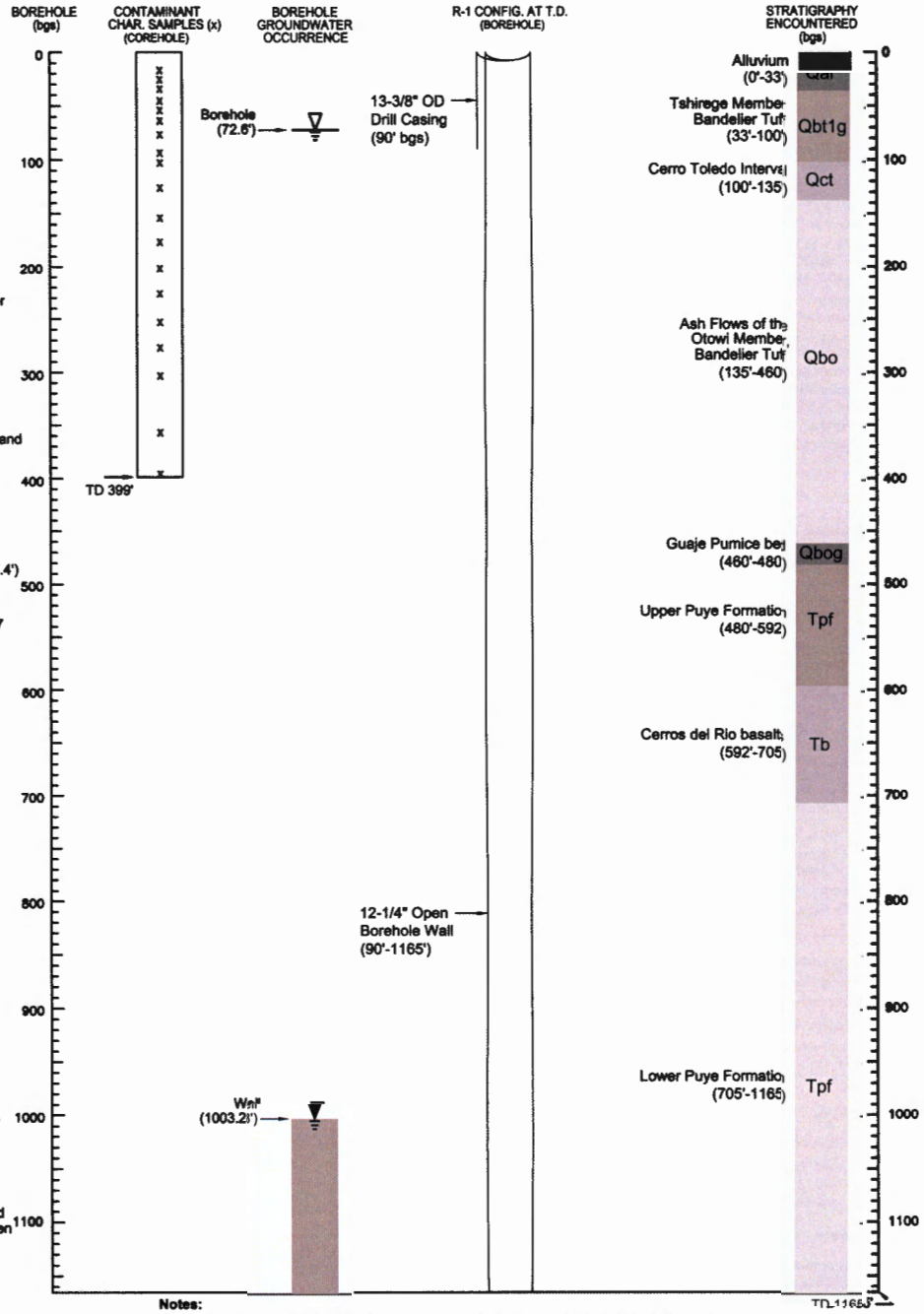


**Notes:**
1. Coordinates - NM State Plane Grid Central Zone (North America) Datum - 1983 (NAD83); expressed in feet.
2. Elevations - National Geodetic Vertical Datum (NGVD 29); expressed in feet above mean sea level.
3. All depths are below ground surface (bgs).
4. Groundwater level measured after well development - 12-20-03.
5. Perched water level measurement in borehole of 72.6' was made with 20' of 13-3/8" drill casing in place on November 1, 2003.
6. Drill casing removed prior to well installation.

**Figure 1-B-1.** Completion diagram for well R-1 (Kleinfelder 2004e).

Location: Upper Pueblo Canyon,
Los Alamos County Property

Description: Brass Marker
Northing: 1778281.56
Easting: 1629519.57
Elevation: 6770.38

Description: Well Casing
Northing: 1778281.63
Easting: 1629521.06
Elevation: 6768.79

Coring:
(0' - 39') Auger with Continuous Sampler
(39' - 241') Auger with Split Spoon

Drilling:
(0' - 40') 13-3/8" Air Rotary Casing Hammer
(40' - 944') 12-1/4" Milltooth Tri-Cone
(40'-143') Air Rotary
(143'-403') Fluid Assisted Air Rotary
(403'-944') Mud Rotary

Data Collection:
- Hydrologic Properties:
  Step - Drawdown Test: 01/10/04
  Constant Rate Pumping Test: 01/11/04 - 01/12/04
- Cores/Cuttings submitted for geochemical and contaminant characterization: 12
- Groundwater Samples Submitted
  Perched Groundwater - none encountered
  Regional Groundwater -
  - Screening Samples: none; mud filled borehole
  - Well Samples: 12/11/03
    01/13/04
- Geologic Properties:
  Cuttings collected for minerology, petrography, and chemistry: 7

Borehole Logs:
- Lithologic: 0' - 944'
- Video (LANL tool): none
- Schlumberger logs: mud filled borehole
  Compensated Neutron Log:
  Cased: 20'-40'; Open Hole: 40'-941'
  Triple Litho-Density:
  Cased: 20'-40'; Open Hole: 40'-941'
  Array Induction Imager:
  Cased: 20'-40'; Open Hole: 40'-936'
  Elemental Capture Sonde:
  Cased: none; Open Hole: 50'-937'
  Natural GR Spectroscopy:
  Cased: 20'-40'; Open Hole: 40'-919'
  Combinable Magnetic Resonance:
  Cased: none; Open Hole: 50'-919'
  Fullbore Formation Micro Imager:
  Cased: none; Open Hole: 50'-937'

Corehole Logs:
- Lithologic: 0' - 241'
- Video (LANL Tool): none

Core Drilling Completed: 9/16/03 - 9/26/03
Rotary Drilling Completed: 10/10/03 - 10/16/03
Contract Geophysics: 10/17/03 & 10/18/03
Well Installation: 10/19/03 - 10/22/03
Well Development Completed: 10/23/03 - 10/28/03
11/17/03 - 11/24/03
12/01/03 - 12/11/03

- Casing:
  4.5" ID / 5.0" OD A304 Stainless Steel casing with external couplings
- Screen Type:
  One (1) 4.46" ID/5.27" OD wire wrapped stainless steel rod-based 0.020 slot screen with external couplings.
- Screen Interval: 906.4' - 929.6'

Well Development performed by airlifting, bailing/swabbing, and aquifer test pumping.
Total Volume Purged: 16,871 gallons

Geologic contacts for R-2 were determined from core samples, cuttings, and geophysical logs.

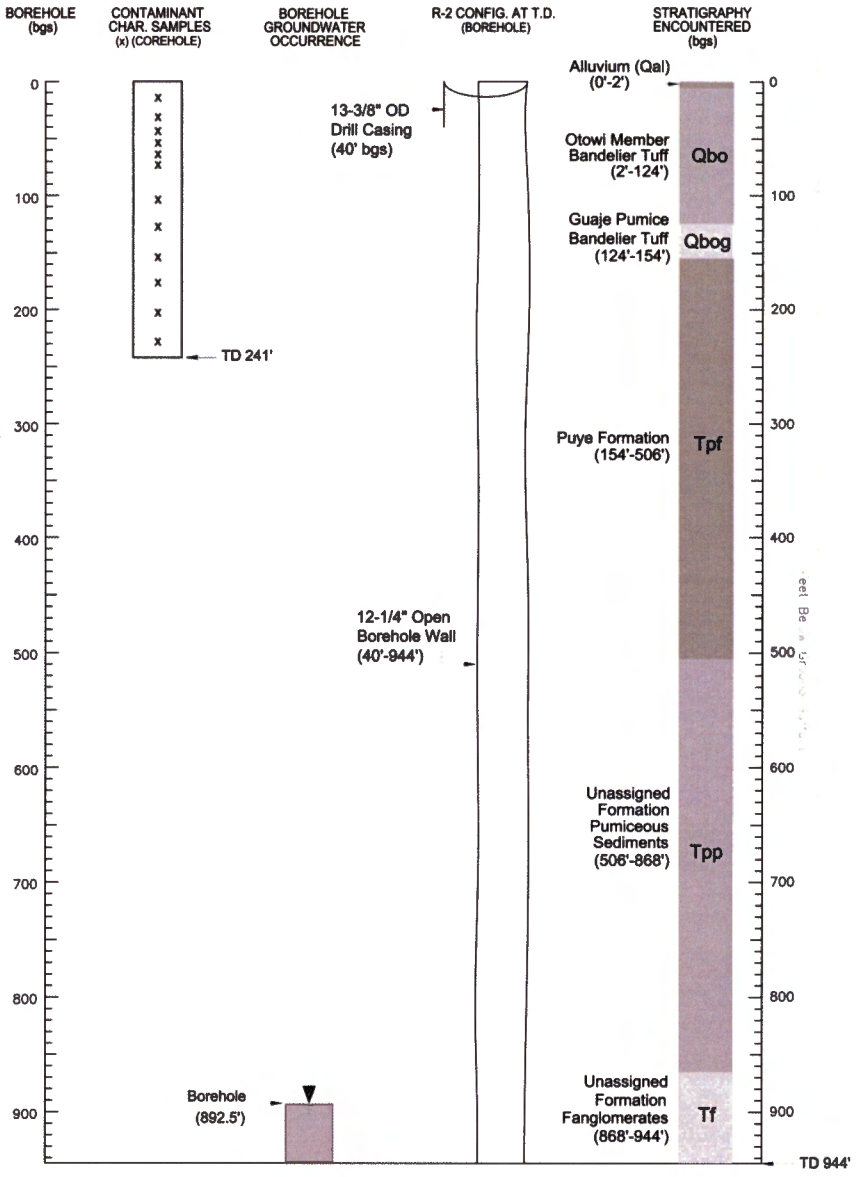


**Keyed Notes:**

1. Coordinates - NM State Plane Grid Central Zone (North America) Datum - 1983 (NAD83); expressed in feet.
2. Elevations - National Geodetic Vertical Datum (NGVD 29); expressed in feet above mean sea level.
3. All depths are below ground surface (bgs).
4. Groundwater level measured after well development - 10-28-03
5. Drill casing removed prior to well installation
6. Three well development intervals were due to scheduling requirements and aquifer characteristics.

**Figure 1-B-2.** Completion diagram for well R-2 (Kleinfelder 2004b).

Location: At inactive emergency Landing Strip in Pueblo Canyon; TA-74

Survey Coordinates / Elevations:
- Coordinates: NAD83
- Elevation: NGVD29

Description: Brass Marker in Concrete Pad
Northing: 1776530.28
Easting: 1639287.98
Elevation: 6577.49

Description: Well Casing
Northing: 1776528.00
Easting: 1639289.98
Elevation: 6579.46

Coring:
(0'-68') Continuous Sampler
(68'-233') Split Spoon

Drilling:
(0'-40') 13-3/8" Air Rotary Casing Hammer
(40'-843') 12.25" Milltooth Tri-Cone
(40'-266') Fluid-assisted Air Rotary
(266'-843') Mud Rotary

Data Collection:
- Hydrologic Properties:
  Constant Discharge
  Pump Test Completed: 01/06/04
- Cores/Cuttings submitted for geochemical and contaminant characterization: 11
- Ground Water Samples Submitted
  Perched Ground Water - 9/9/03 (114'-125')
  Regional Ground Water - 10/10/03 (792.9'-816')
- Geologic Properties: Cuttings submitted for Minerology, petrography, and chemistry: 7

Corehole Logs:
- Corehole: 0'-233'
- Natural Gamma Tool (LANL tool): 0'-230'

Borehole Logs:
- Video (LANL tool): 0'-173'
- Lithologic: 0'-843'
- Schlumberger logs (9/27/03):
  Top of Drilling Fluid at 18' bgs
  Compensated Neutron Tool: 40'-842'
  Triple Litho-Density: 40'-842'
  Array Induction Tool: 40'-836'
  Elemental Capture Spectroscopy: 40'-838'
  Natural Gamma Spectroscopy: 40'-836'
  Combinable Magnetic Resonance: 100'-838'
  Full-Bore Formation Micro Imager: 100'-838'

Core Drilling: 8/28/03 - 9/5/03
Piezometers PZ#1 and PZ#2 completed: 9/5/03
Rotary Drilling: 8/22/03 - 9/26/03
Well Constructed: 9/28/03 - 10/3/03
Well Developed: 10/6/03 - 10/10/03
Well Completion:
- Casing: 4.46" ID / 5.0" OD A304 stainless steel casing with external couplings
- Number of Screens:
  One (1) 4.46" ID / 5.27" OD wire wrapped 0.020" slot stainless steel with external couplings
- Screen Interval: 792.9' - 816' bgs

Well development performed by swabbing, bailing, and pumping.
Total Volume Purged, Including Aquifer Testing: 56,347 gal.
Hydrologic Testing
Total Volume Removed: 42,197 gal.

Geologic contacts for R-4 were determined from core samples, cuttings, and geophysical logs.

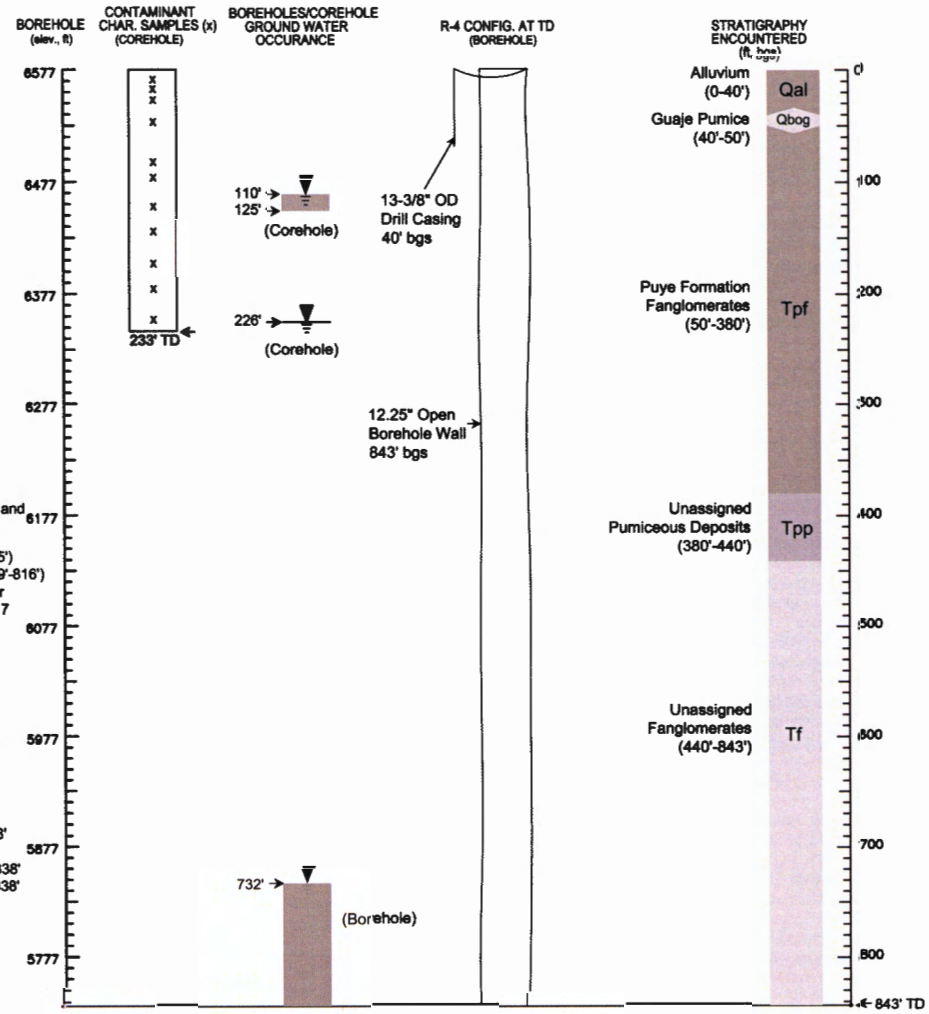


**Keyed Notes:**

1. Coordinates - NM State Plane Grid Central Zone (North America), Datum - 1983 (NAD83); expressed in feet
2. Elevations - National Geodetic Vertical Datum (NGVD29); expressed in feet above mean sea level
3. bgs - below ground surface
4. TBD - to be determined
5. Both piezometers were dry when sounded on 11/25/03.

**Figure 1-B-3.** Completion diagram for well R-4 (Kleinfelder 2004a).

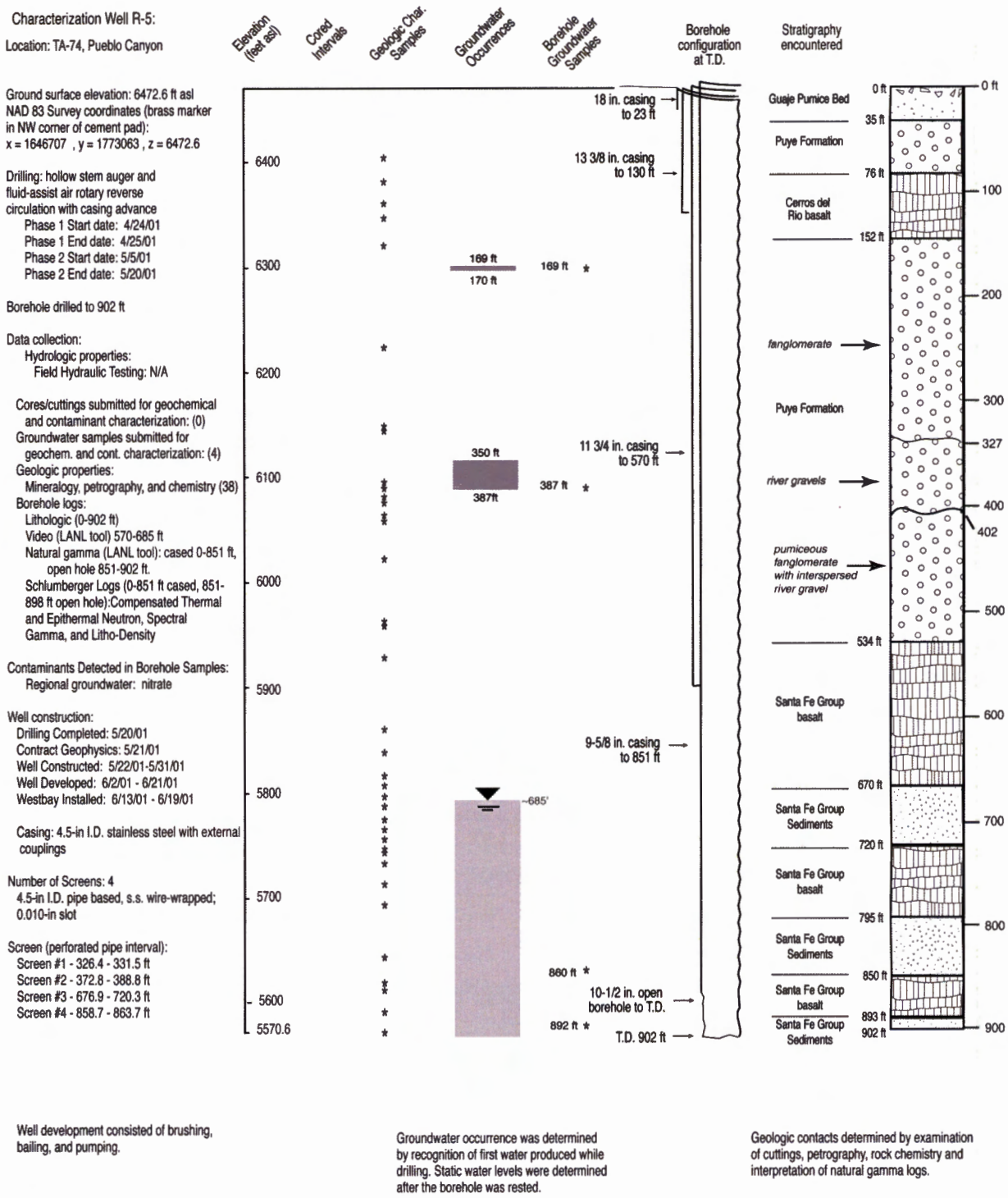


**Figure 1-B-4.** Completion diagram for well R-5 (LANL 2003a).

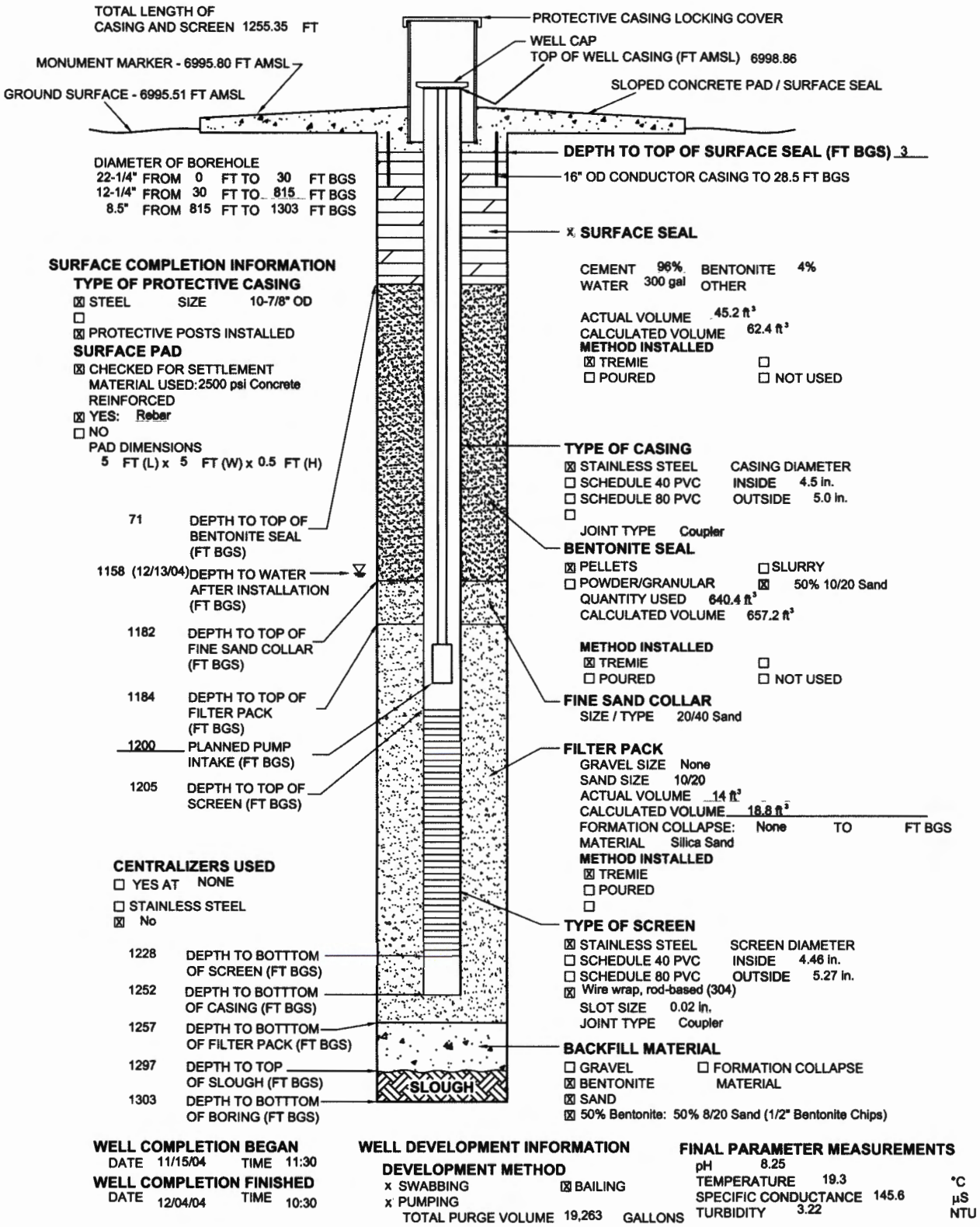


**Figure 1-B-5.** Completion diagram for well R-6 (Note: no report available for R-6).

**Characterization Well R-7:**

Location: TA-53, Los Alamos Canyon, east of Omega West reactor facility.

Survey coordinates (brass marker in NW corner of cement pad):
x: 1631666 E y: 1773653 N (NAD 83 )
z: 6779.2 ft asl (NGVD 29)

Drilling: hollow stem auger and fluid-assist air rotary reverse circulation with casing advance
Phase 1 Start date: 02/22/00
Phase 1 End date: 02/25/00
Phase 2 Start date: 12/11/00
Phase 2 End date: 01/16/01

Borehole drilled to 1097 ft bgs (T.D.)

Data collection:
Hydrologic properties:
Field Hydraulic Testing: No tests were conducted.
Cores/cuttings submitted for geochemical and contaminant characterization: (0)
Groundwater samples submitted for geochem and contaminant characterization: (2)
Geologic properties:
Mineralogy, petrography, and chemistry (27)
Borehole logs:
Lithologic (0-1097 ft)
Video (LANL tool) 0-849 ft and 0-977 ft.
Natural gamma (LANL tool): 0-972 ft, and 0-977 ft. bgs.
Schlumberger Logs (0-290 ft cased, 290-1064 ft open hole): Litho density, Gamma Ray, Caliper, Combinable Magnetic Resonance, Formation Micro Imager, Spectral Gamma, Thermal/Epithermal Neutron, Array Induction, Natural Gamma.
Contaminants Detected in Borehole Samples:
Borehole screening data indicate no contaminants detected above background.

Well construction:
Drilling Completed: 01/16/01
Contract Geophysics: 01/12/01 through 01/13/01, and 01/14/01
Well Constructed: 01/20/01 through 01/31/01
Well Developed: 02/01/01 through 02/08/01
Westbay Installed: 02/21/01 through 02/26/01

Casing: 4.5-in I.D. stainless steel with external couplings

Number of Screens: 3
4.5-in I.D. pipe based, s.s. wire-wrapped; 0.010-in slotted.

Screen (perforated pipe interval):
Screen #1 - 363.2-379.2 ft bgs
Screen #2 - 730.4-746.4 ft bgs
Screen #3 - 895.5-937.4 ft bgs

Well development consisted of wire brushing, bailing, and pumping from Screen #3 and sump. Attempts to pump and bail water from Screens #1 and #2 were unsuccessful because of insufficient water from these zones.

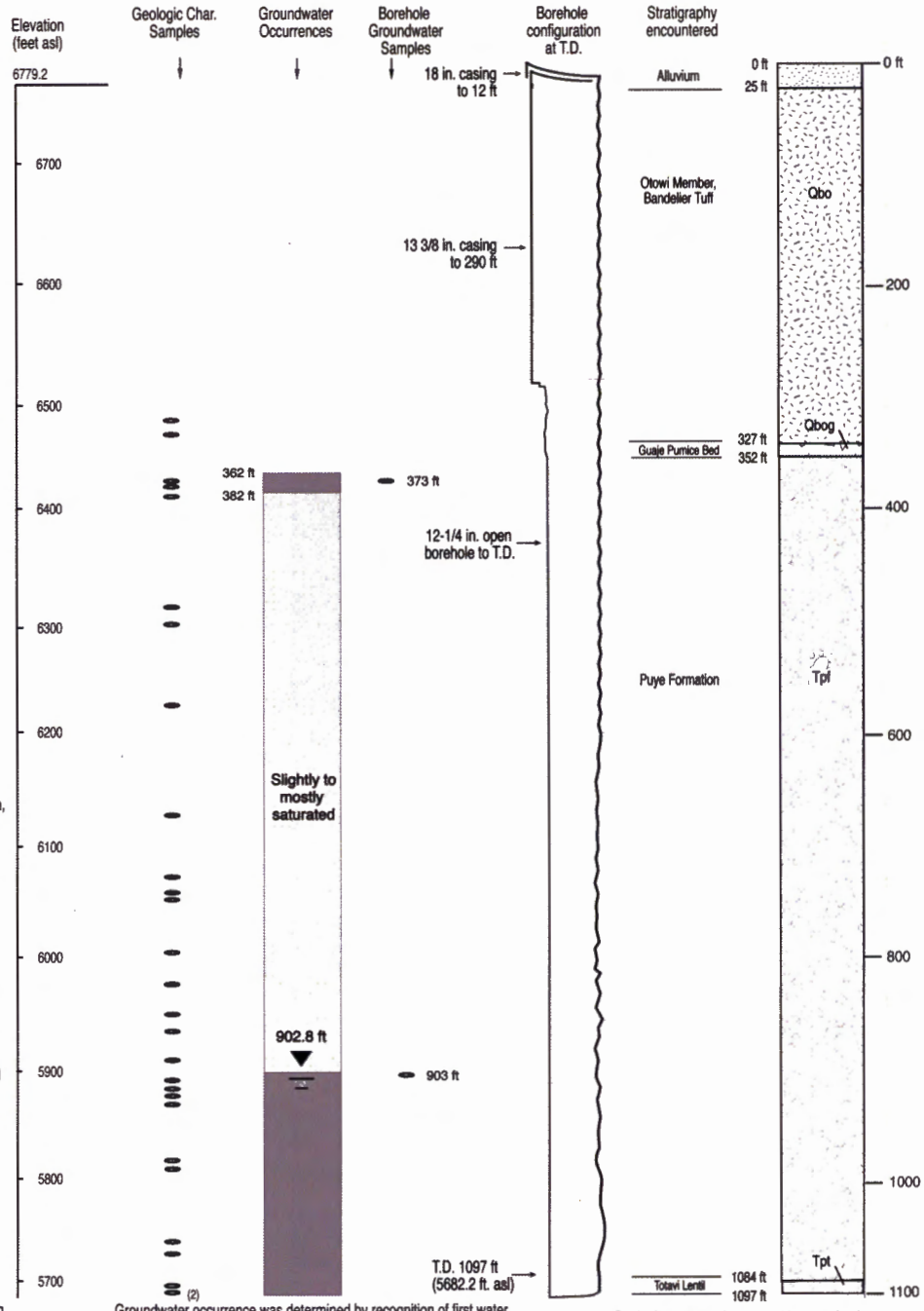


Groundwater occurrence was determined by recognition of first water produced while drilling, by borehole geophysics, and by borehole video. The rocks above the regional water table appeared to be partly to mostly saturated. Screens 1 & 2 were sited to sample the potential saturation above the regional water table. Static water levels were determined after the borehole was rested.

Geologic contacts determined by examination of cuttings and interpretation of natural gamma logs. Contacts may be refined by analysis of geologic samples by petrography and rock chemistry.

**Figure 1-B-6.** Completion diagram for well R-7 (Stone et al. 2002).

**Construction, Stratigraphic, and Hydrologic Information for Hydrogeologic Workplan Characterization Well R-8/8a Rev. B (04/15/02).**

Location: TA-53, Los Alamos Canyon, near confluence with DP canyon.

Survey coordinates (brass marker in NW corner of R-8a cement pad):
x: 1641139 E y: 1772554 N (NAD 83 )
z: 6544.7 ft asl (NGVD 29)
R-8 is 62 ft due east from R-8a at survey coordinates (center of cement plug):
x: 1641195 E y: 1772533 N (NAD 83)
z: 6542.9 ft asl (NGVD 29)

Drilling: air rotary core w/ wireline retrieval and fluid-assist air rotary reverse circulation with casing advance.
R-8 Start date: 09/25/01.
R-8 End date: 12/11/01.
R-8a Start date: 01/09/02.
R-8a End date: 01/27/02.

Borehole R-8 drilled to 1022 ft. bgs. (T.D.).
Borehole R-8a drilled to 880 ft. bgs. (T.D.).

Data collection:
Hydrologic properties:
Field Hydraulic Testing: Falling head test on R-8a screen #2.
Cores/cuttings submitted for geochemical and contaminant characterization: 156/6
Groundwater samples submitted for geochem and contaminant characterization: 1 ( R-8)
Geologic properties:
Mineralogy, petrography, and chemistry: 11
Borehole logs from R-8:
Lithologic: 0-1022 ft.
Video (LANL tool): 0-850 ft. (well casing - R-8A)
Natural gamma (LANL tool): 0-30 ft. and 0-761 ft. (cased); 30-261 ft. and 761-768 ft. bgs. (open hole)
Induction (LANL tool): 0-30 ft. (cased); 30-261 ft. (open hole)
Schlumberger Logs: 0-761 ft. (cased); 761-764 ft. (open hole): Litho density, Spectral Gamma, Elemental Capture, Thermal/Epithermal Neutron, Natural Gamma.

Contaminants Detected in R-8 Water Sample:
Tritium at 15 pCi/l.

Well construction:
Drilling Completed (R-8a): 01/27/02.
Contract Geophysics (R-8): 11/13/01.
Well Constructed (R-8a): 01/28/02 - 02/01/02.
Well Developed (R-8a): 02/04/02 - 02/14/02.
Westbay Installed (R-8a): 02/21/02 - 02/24/02

Casing: 4.5-in. I.D./5.0-in. O.D. stainless steel with external couplings.

Number of Screens: 2
4.5-in. I.D./5.56-in. O.D. pipe based, s.s. wire-wrapped; 0.010-in slotted.

Screen (perforated pipe interval):
Screen #1 - 705.3-755.7 ft. bgs.
Screen #2 - 821.3-828.0 ft. bgs.

Well development consisted of wire brushing, bailing, surging, swabbing, and pumping.

Groundwater occurrence was determined in R-8 by recognition of first water produced while drilling, by borehole geophysics, and by borehole video. Static water levels were determined after the R-8 borehole was rested.

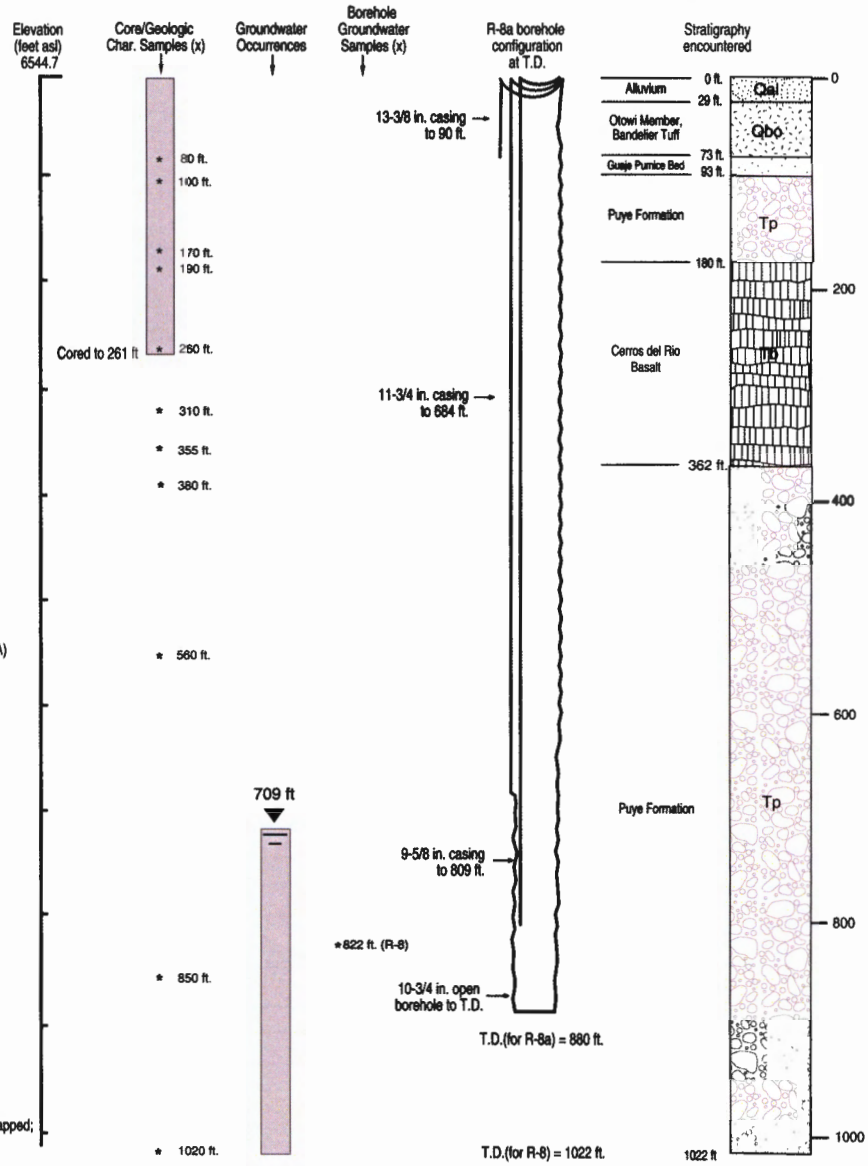


Geologic contacts are from R-8 and were determined by examination of cuttings and interpretation of geophysical logs. Contacts may be refined by analysis of geologic samples by petrography and rock chemistry. No samples collected from R-8a borehole.

**Figure 1-B-7.** Completion diagram for wells R-8 and R-8a (LANL 2003b).

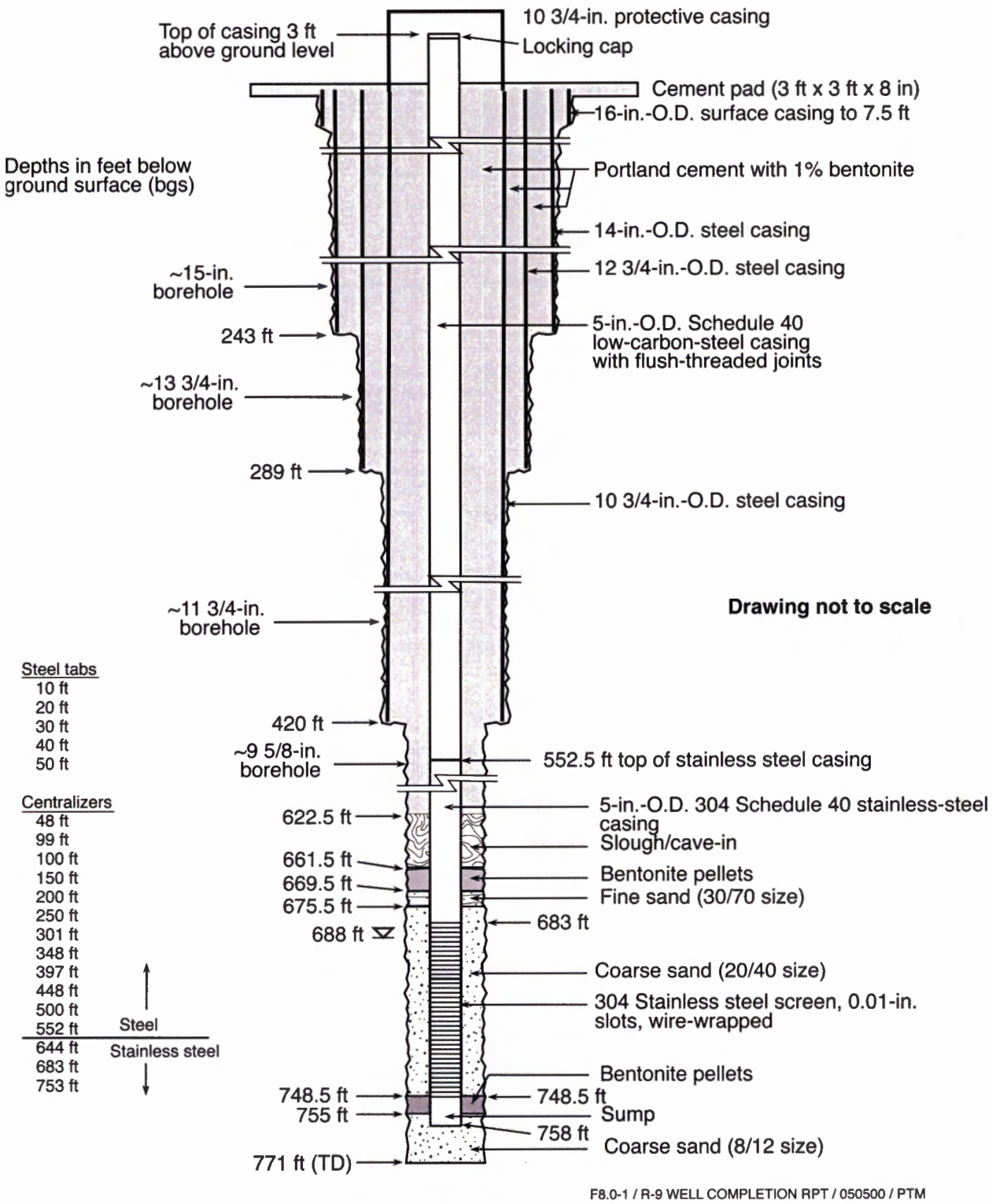


**Figure 1-B-8.** Completion diagram for well R-9 (Broxton et al. 2001d).

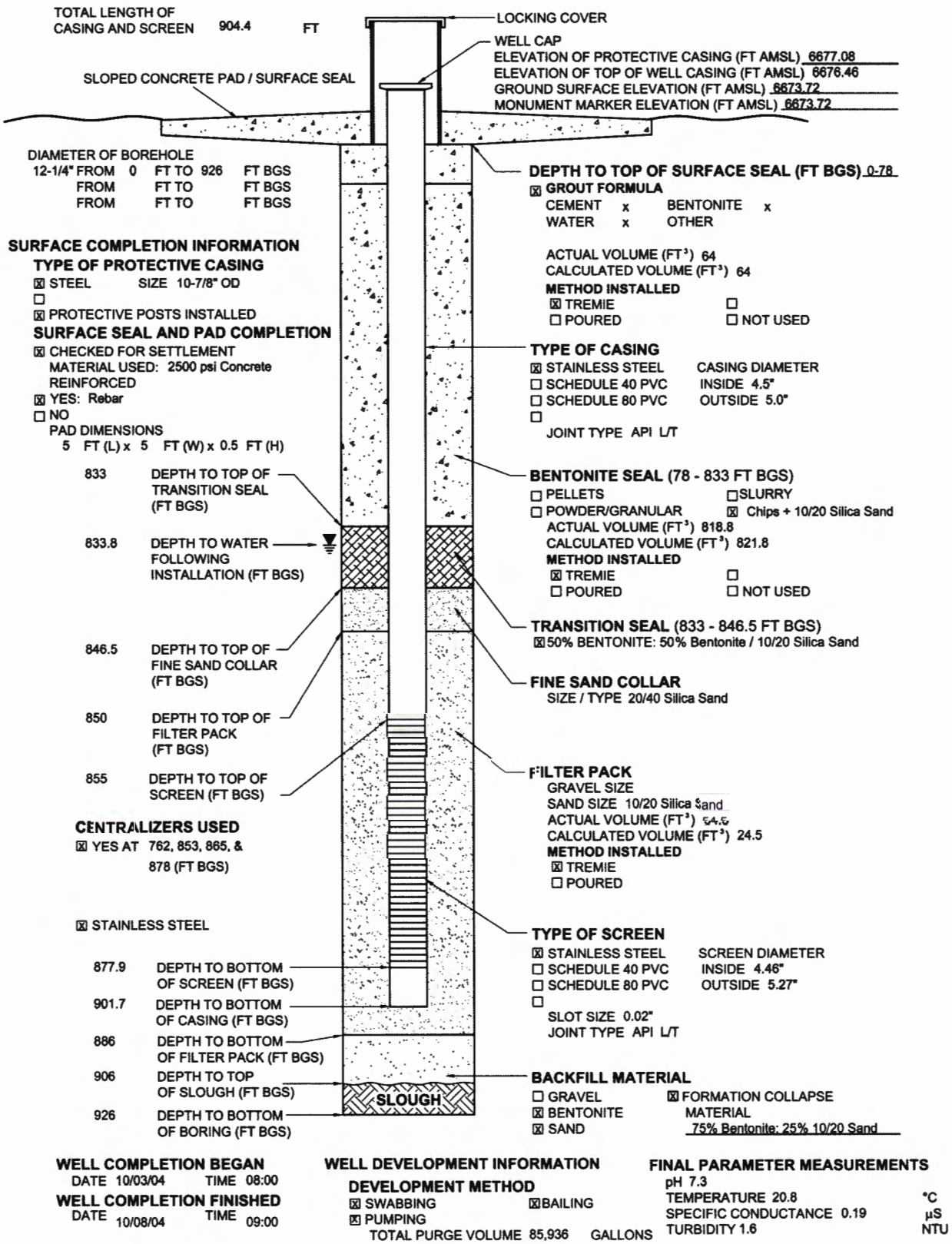


**Figure 1-B-9.** Completion diagram for well R-11 (Kleinfelder 2004c).

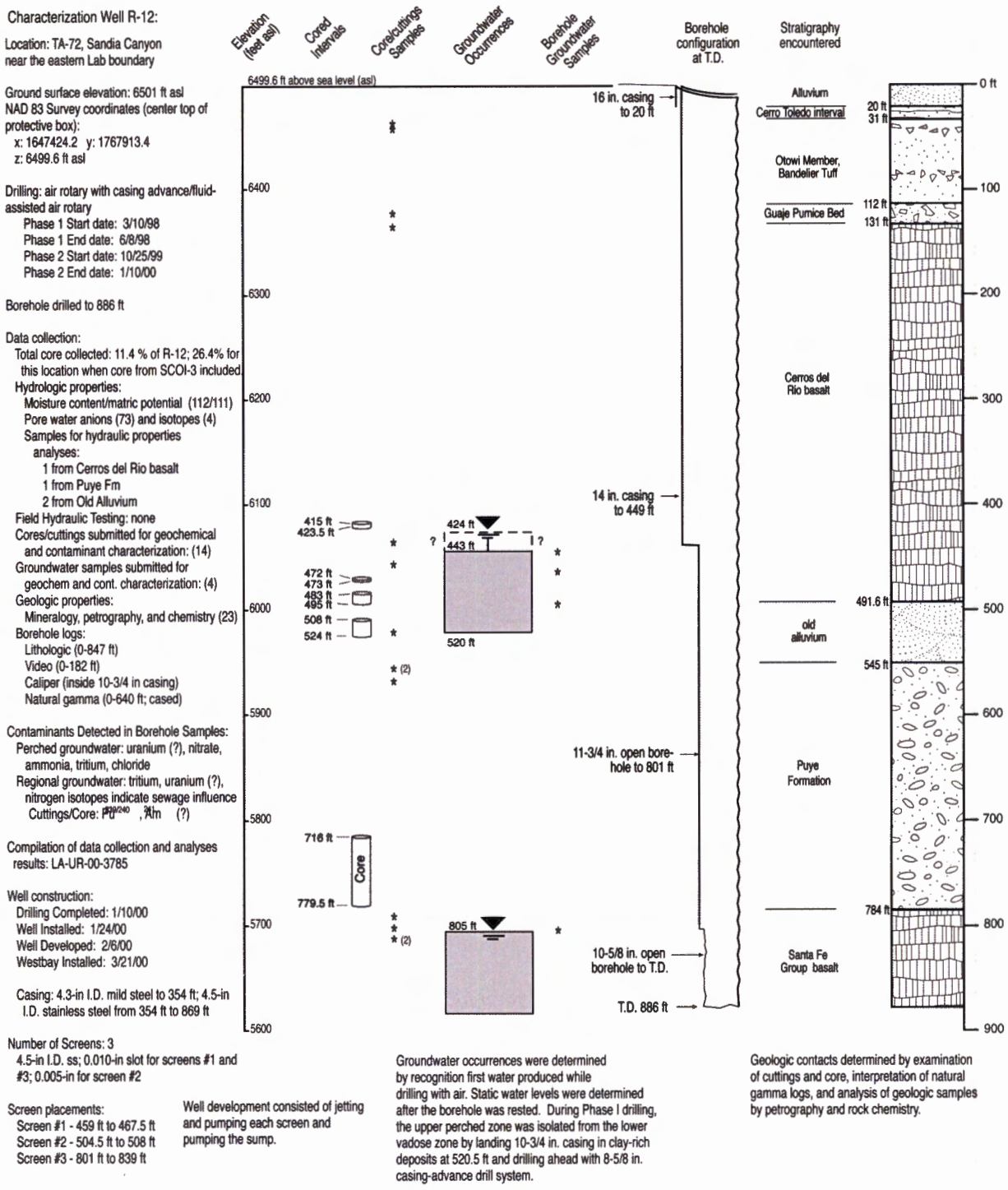


**Figure 1-B-10.** Completion diagram for well R-12 (Broxton et al. 2001b).

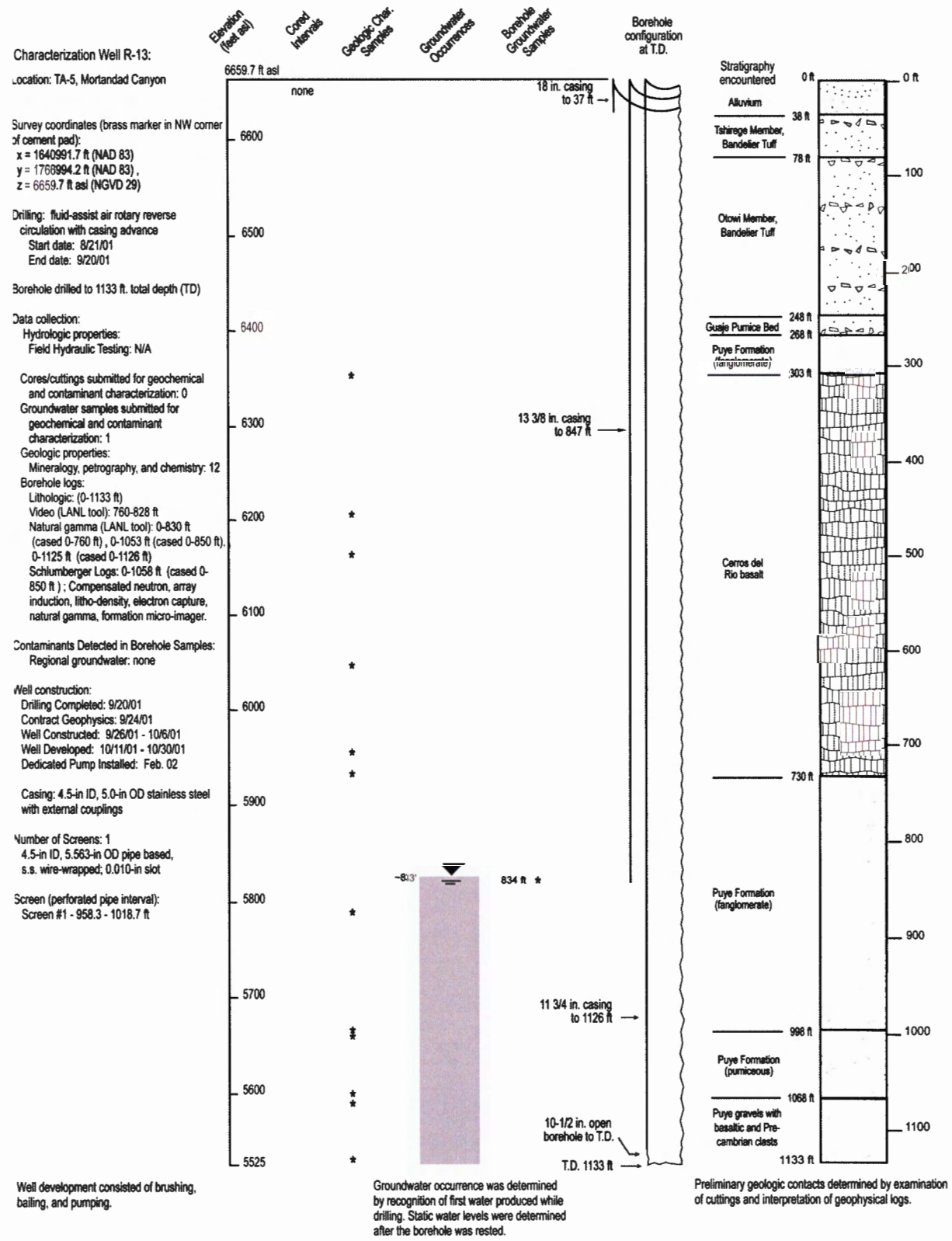


**Figure 1-B-11**. Completion diagram for well R-13 (LANL 2003c).

Location: In Ten Site Canyon, east of the former radioactive liquid waste and septic treatment facilities at TA-35.

Survey coordinates (brass marker in NW corner of R-14 cement pad):
x: 1629855 E y: 1768953 N (NAD 83)
z: 7062.1 ft asl (NGVD 29)

Drilling: air rotary core w/ wireline retrieval, conventional mud drilling, casing advance.
R-14 Start date: 06/02/02.
R-14 End date: 07/02/02.

Borehole R-14 drilled to 1327 ft bgs (TD).

Data collection:
Hydrologic properties: Field hydraulic test: Constant Rate Injection Test on screen #2
Cores/cuttings submitted for geochemical and contaminant characterization: (24)
Groundwater samples submitted for geochem and contaminant characterization: (2)
Geologic properties: (11)
Mineralogy, petrography, and chemistry.

Borehole logs from R-14:
Lithologic: 0-1327 ft
Video (LANL tool): 0-923 ft. and 0-975 ft
Natural gamma (LANL tool): 0-1068 ft and 1046-1325 ft bgs
Schlumberger Logs: 0-12.2 ft (cased), 12.2-1068 ft (open hole): Litho density, Spectral Gamma, Elemental Capture, Thermal/Epithermal Neutron, Combinable Magnetic Resonance, and Natural Gamma.

Contaminants Detected in R-14 Water Samples: none

Well construction:
Drilling Completed: 07/02/02
Contract Geophysics: 06/19/02 - 06/20/02
Well Constructed : 07/04/02 - 07/11/02
Well Developed : 07/19/02 - 11/18/02
Westbay Installed : 11/19/02 - 11/25/02

Casing: 4.5-in I.D. stainless steel with external couplings.

Number of Screens: 2
4.5-in. I D pipe based, s.s. wire-wrapped with 0.010-in. slots.

Screen (perforated pipe interval):
Screen #1 - 1200.6-1233.2 ft. bgs.
Screen #2 - 1266.5-1293.1 ft. bgs.

Well development consisted of wire brushing, bailing, chemical treatments, surging, and pumping.

Groundwater occurrence was determined for R-14 by recognition of first water produced while drilling, by borehole geophysics, and by borehole video. Static water levels were determined after the R-14 borehole was rested.

Groundwater samples collected from packed off screen intervals after well development.

Geologic contacts for R-14 were determined by examination of cuttings and interpretation of borehole video and geophysical logs. Contacts and stratigraphy may be refined by petrographic, geochemical, or mineralogic analysis of geologic samples.

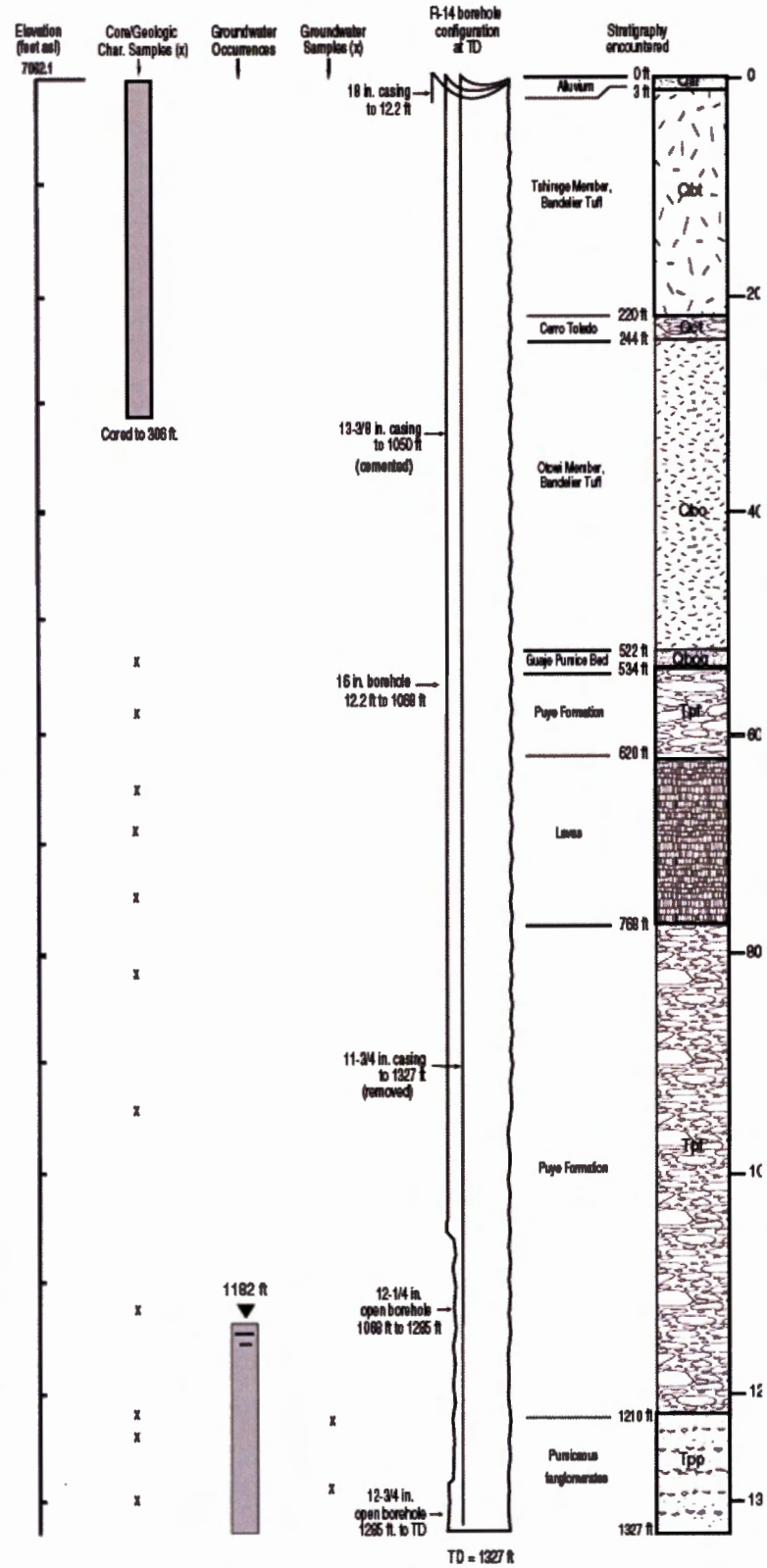


**Figure 1-B-12.** Completion diagram for well R-14 (LANL 2003d).

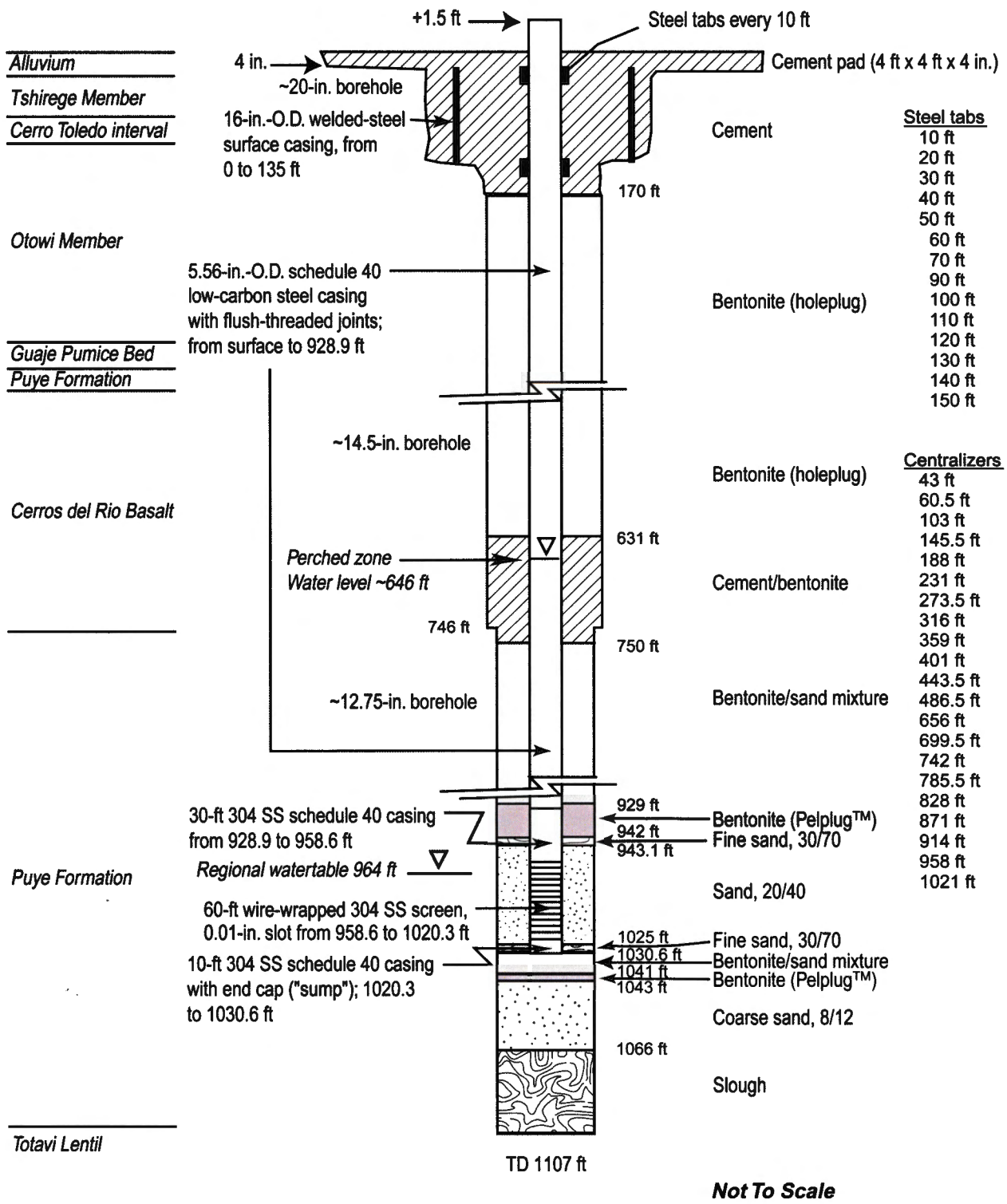


**Figure 1-B-13.** Completion diagram for well R-15 (Longmire et al. 2000).

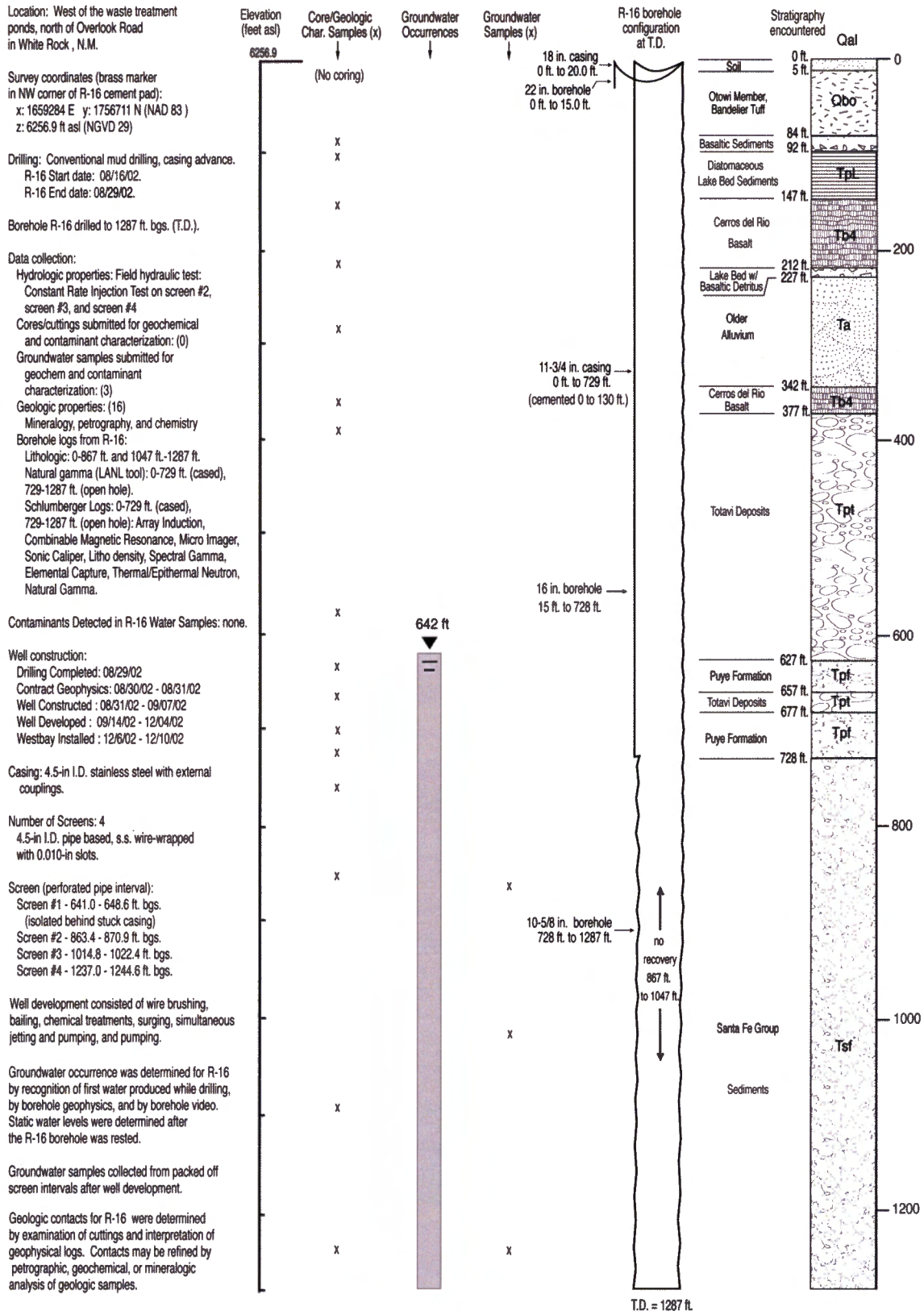


**Figure 1-B-14**. Completion diagram for well R-16 (LANL 2003e).

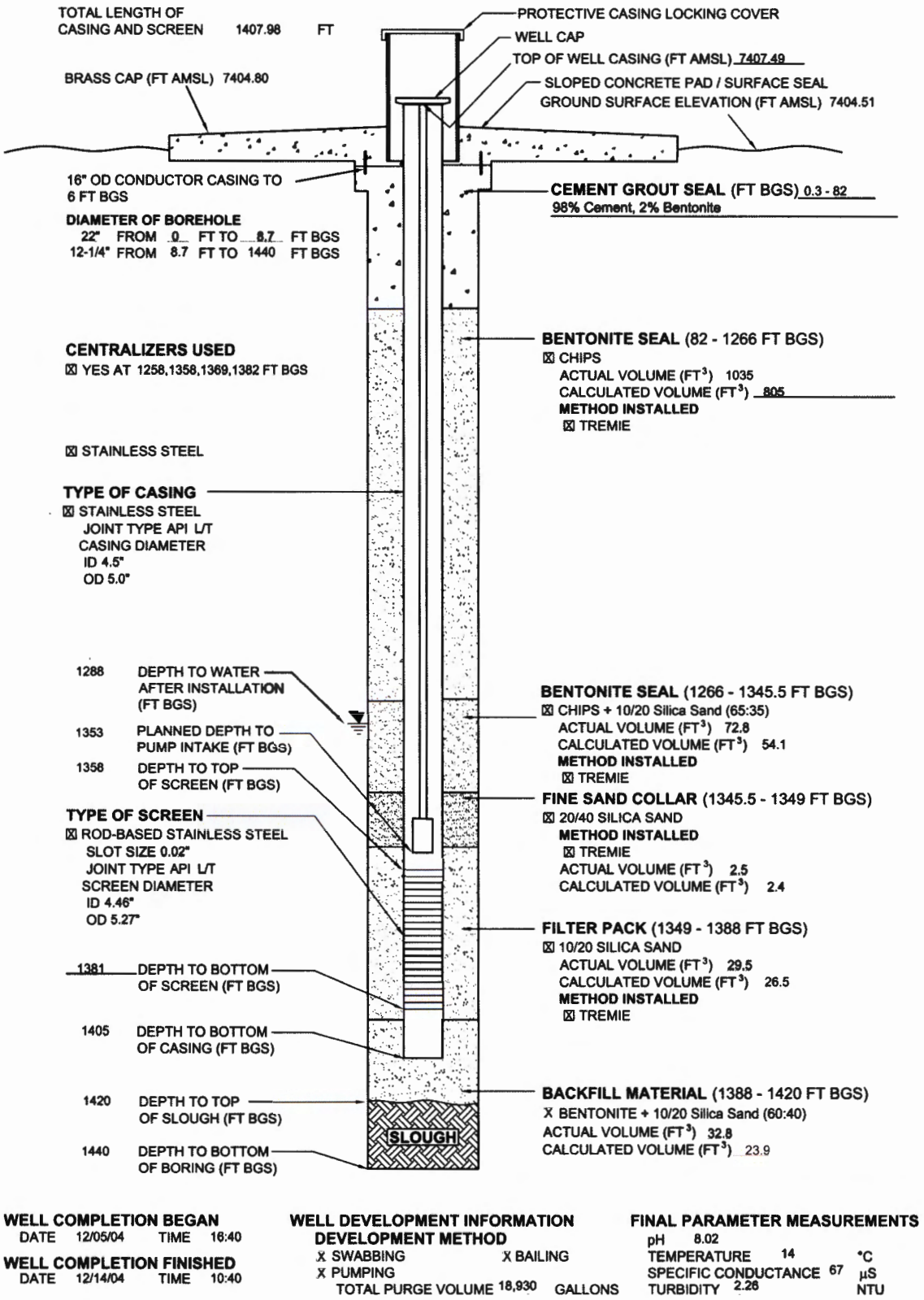


**Figure 1-B-15.** Completion diagram for well R-18 (Note: well completion report not available).

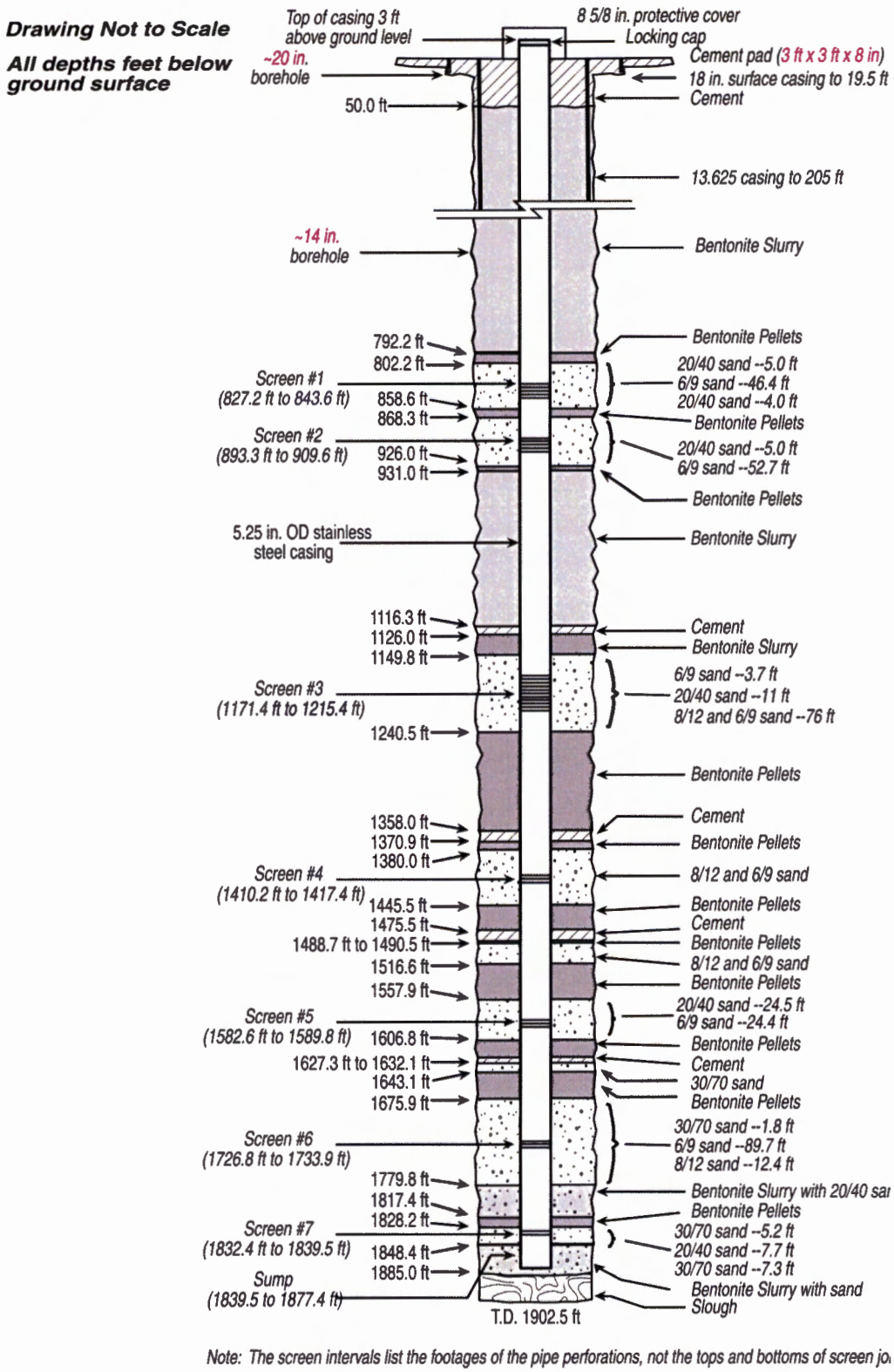


**Figure 1-B-16.** Completion diagram for well R-19 (Broxton et al. 2001d).

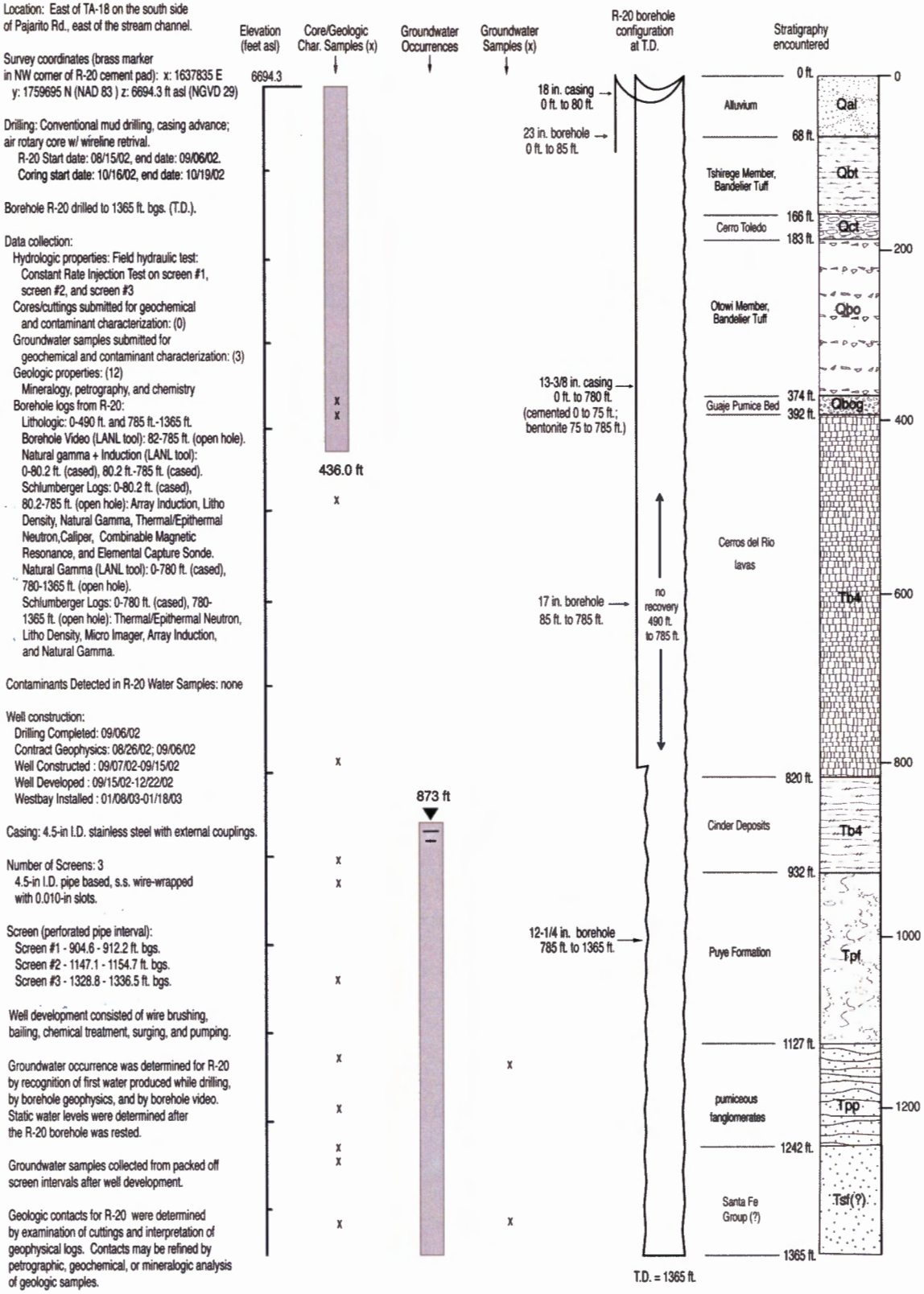


**Figure 1-B-17.** Completion diagram for well R-20 (LANL 2003f).

Location: North of TA-54 in
Canada del Buey Canyon

Survey Coordinates:
(Brass marker in NW corner of R-21 well pad)

Northing: 1759143.0529
Easting: 1641284.1738
Elevation: 6656.24
(New Mexico State Plane Coordinates NAD83, Elevation is NAVD88)

Drilling: 12.25" Mill tooth Tricone, 57'-237'
12.25" Button Bit 237'-244'
12.25" Down hole hammer w/foam 244'-545'
12.25" Button Bit' w/foam 545'-563
12.25" Down hole hammer w/foam 563'-995'

Data Collection:
Hydrologic Properties:
Stepped pumping test (5, 10, and 15 gallons per minute)

Cores/cuttings submitted for geochemical and

contaminant characterization: 11

Geologic Properties:
Mineralogy, petrography, and chemistry: 10

Borehole:
Lithologic: 0'-995'
Video (LANL tool):
0'- 578' bgs (open hole)
Schlumberger logs: All open hole
Compensated Neutron log: 30'-982'
Triple lithodensity: 30'-982'
Array induction imager: 86'-976'
Elemental capture sonde: 30'-930'
Natural GR spectroscopy: 28'-976'
Combinable Magnetic Resonance: 100'-910'
Fullbore formation micro imager: 800'-928'

Core drilling completed: 11/4/02-11/9/02

Rotary drilling completed: 11/14/02-11/17/02

Contract geophysics: 11/18/02 and 11/19/02

Well constructed: 11/19/02-11/26/02

Well developed: 12/4/02-12/5/02

Casing: 6" I.D./6-5/8" O.D. SCH 40
A304 stainless with external couplings.

Number of screens:
One 6" I.D./6-5/8" O.D. wire-wrapped 0.020 slot stainless w/ external couplings.

Screen interval: 888.8'-906.8'.

Well development performed by swabbing, bailing, and pumping.

Geologic contacts for R-21 were determined from core samples, cuttings, borehole video and geophysical logs.

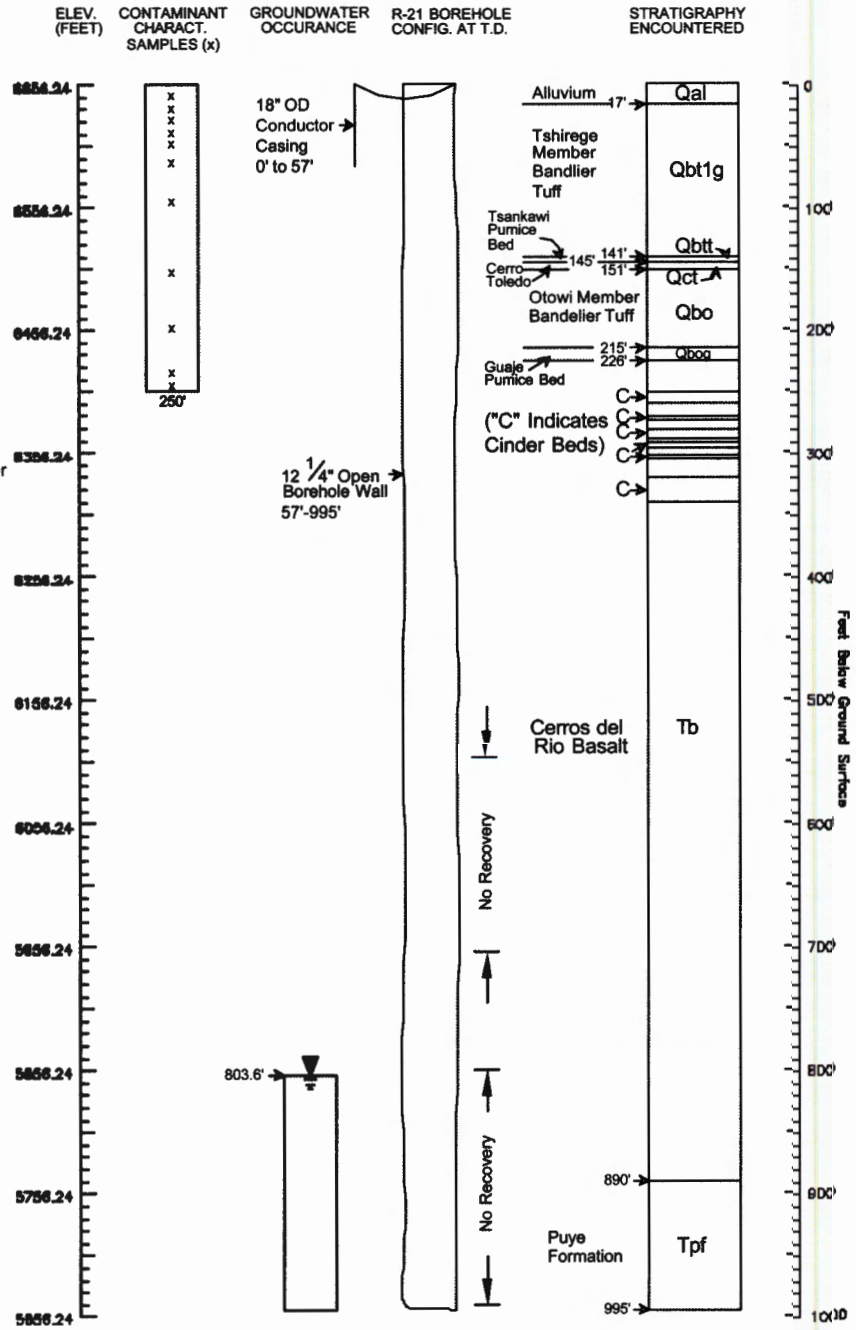


**Figure 1-B-18.** Completion diagram for well R-21 (Kleinfelder 2003f).

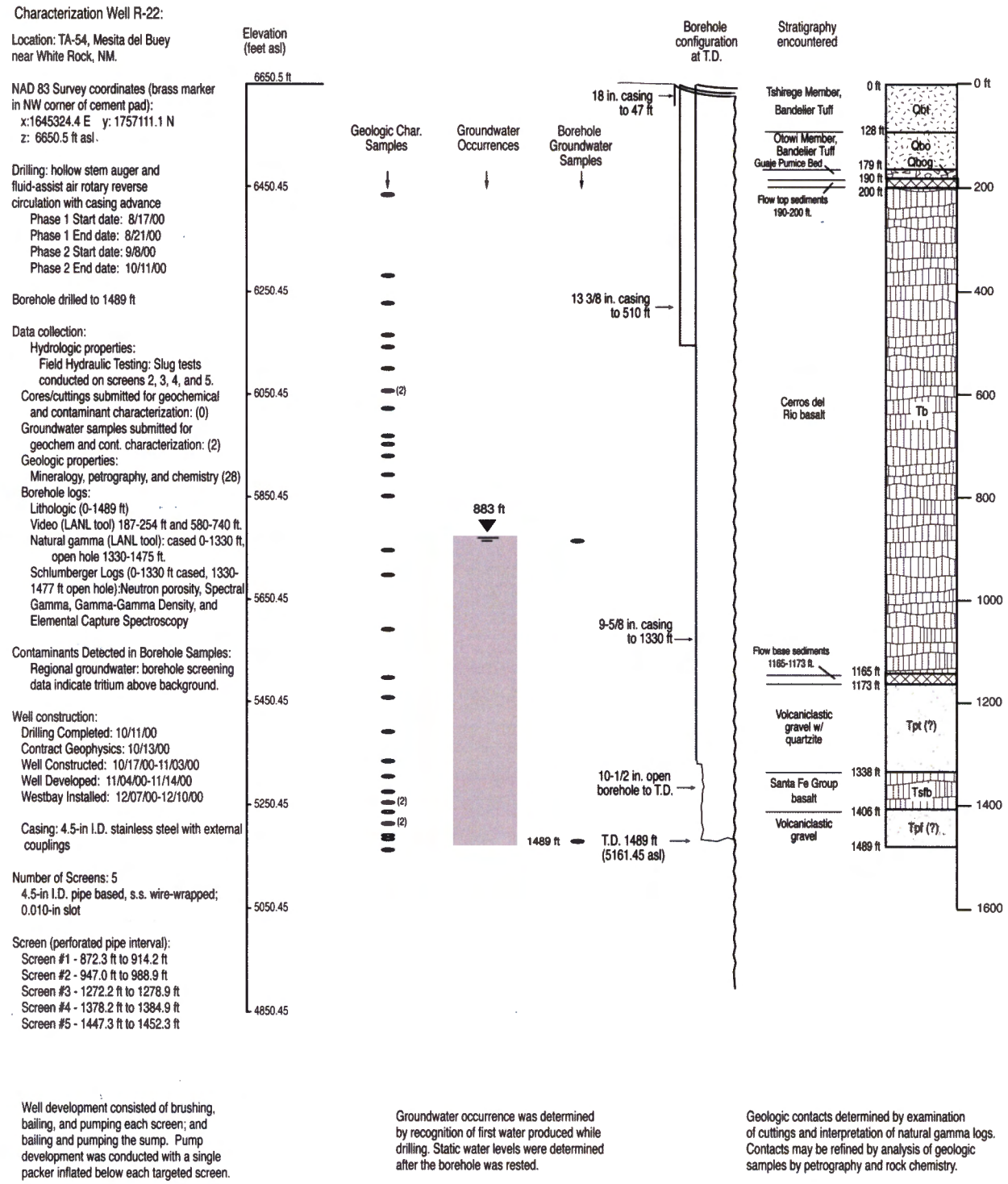


**Figure 1-B-19**. Completion diagram for well R-22 (Ball et al. 2002).

Location: In Pajarito Canyon, just west of the N.M. 4 and Pajarito Road intersection; on the south side of Pajarito Road.

Survey coordinates (brass marker in NW corner of R-23 cement pad):
x: 1647914 E y: 1755165 N (NAD 83 )
z: 6527.8 ft asl (NGVD 29)

Drilling: air rotary drilling, casing advance.
R-23 Start date: 8/17/02
R-23 End date: 9/27/02

Borehole R-23 drilled to 935.0 ft. bgs. (T.D.).

Data collection:
Hydrologic properties: Field hydraulic test: Pump test
Cores/cuttings submitted for geochemical and contaminant characterization: (0)
Groundwater samples submitted for geochem and contaminant characterization: (1)
Geologic properties: (14)
Mineralogy, petrography, and chemistry
Borehole logs from R-23:
Lithologic: 0-935.0 ft.
Video (LANL tool): 0-599 ft. (cased) and 599-826.6 ft. (open hole).
Natural gamma (LANL tool): 0-599 ft. (cased) and 599-840 ft. (open hole).
Schlumberger Logs: 0-599 ft. (cased) and 599-828 ft. (open hole): Litho density, Thermal/Epithermal Neutron, Array Induction, Natural Gamma, Elemental Capture, and Combinable Magnetic Resonance.

Contaminants Detected in R-23 Water Sample: none

Well construction:
Drilling Completed: 09/27/02.
Contract Geophysics: 09/23-24/02.
Well Constructed : 09/27/02-10/02/02.
Well Developed : 10/08/02-02/20/03
Dedicated Pump: 01/06/03-01/08/03

Casing: 4.5-in. I.D. stainless steel with external couplings.

Number of Screens: 1
4.5-in. I.D. pipe based, s.s. wire-wrapped with 0.010-in slots.

Screen (perforated pipe interval):
Screen #1 - 816.0 - 873.2 ft. bgs.

Well development consisted of wire brushing, bailing, surging, and pumping.

Static water level measured on October 8, 2002, in completed and developed well.

Geologic contacts for R-23 were determined by examination of cuttings and interpretation of geophysical logs. Contacts may be refined by petrologic, geochemical, or mineralogic analysis of geologic samples.

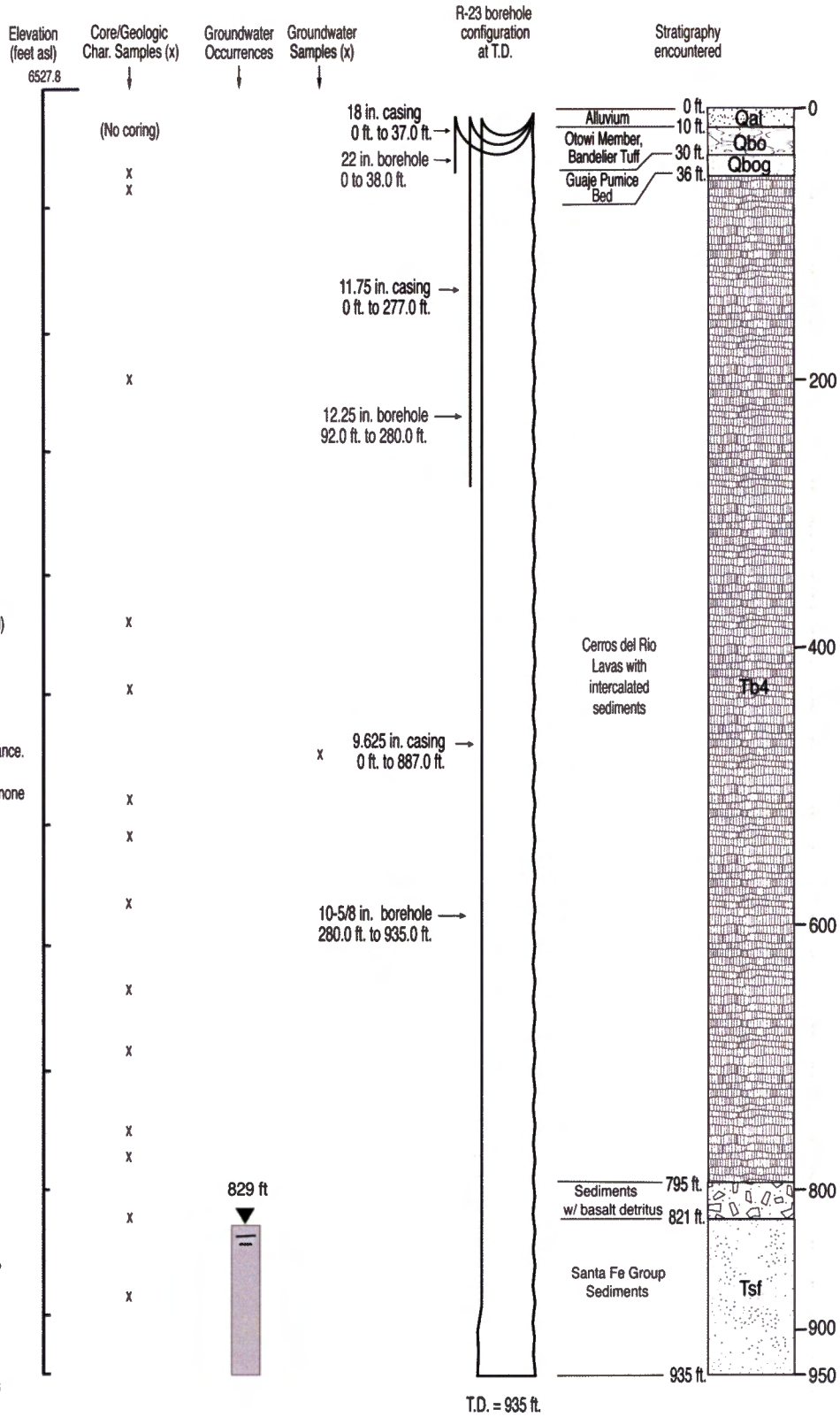


**Figure 1-B-20.** Completion diagram for well R-23 (LANL 2003g).

Characterization Well R-25:

Location: TA-16, South of Canon de Valle

NAD 83 Survey coordinates (brass marker in NW corner of cement pad):
x: 1615178.42 E y: 1764060.50 N
z: 7519.7 ft asl

Drilling: solid stem auger and fluid-assist air rotary reverse circulation with casing advance
Start date: 7/22/98
End date: 2/24/99

Borehole drilled to 1942 ft

Data collection:
Hydrologic properties:
Field Hydraulic Testing: Inconclusive tests.
Matric Potential/Moisture Content (105)
Hydrologic package (5)
Cores/cuttings submitted for geochemical and contaminant characterization: (13) and Anion/Isotope Profile Samples (30)
Groundwater samples submitted for geochem and cont. characterization: (14)
Geologic properties:
Mineralogy, petrography, and chemistry (30)
Borehole logs:
Lithologic (0-1942 ft)
Video (LANL tool) 580-863 ft , 1175-1180 ft, and 1462-1472 ft open borehole
Schlumberger Logs (0-1934.7 ft cased well): Compensated Neutron, Spectral Gamma, Multi-Finger Caliper, hole deviation Cement Bond Log, and Ultrasonic Imager.
LANL Log: Natural gamma.(0-575', 0-980', and 0-1942' cased well)

Contaminants Detected in Borehole Samples: RDX, HMX, TNT, 2 amino 4,6 dinitrotoluene, and 4 amino 2,6 dinitrotoluene

Well construction:
Drilling Completed: 2/24/99
Contract Geophysics: 4/21/99 & 2/10/00
Well Constructed: 3/3/99-5/25/99
Well Developed: 12/6/99-12/13/99, 1/3/00-2/1/00, 4/14/00-4/30/00, 5/4/00-5/8/00, 9/13/00-9/25/00
Westbay Installed: 9/26/00-9/28/00

Casing: 5.625-in O.D. stainless steel with flush threaded couplers.

Number of Screens: 9
5.0-in I.D. flush-threaded s.s.; 0.010-in slot

Screen (perforated pipe interval):
Screen #1 - 737.6 ft to 758.4 ft
Screen #2 - 882.6 ft to 893.4 ft
Screen #3 - 1054.6 ft to 1064.6 ft (damaged)
Screen #4 - 1184.6 ft to 1194.6 ft
Screen #5 - 1294.7 ft to 1304.7 ft
Screen #6 - 1404.7 ft to 1414.7 ft
Screen #7 - 1604.7 ft to 1614.7 ft
Screen #8 - 1794.7 ft to 1804.7 ft
Screen #9 - 1894.7 ft to 1904.7 ft (detached)
Screen #9b - 1871.5 ft to 1875.0 ft

Well development consisted of brushing, bailing, and pumping each screen; and bailing and pumping the sump. Pump development was conducted with a single packer inflated above each targeted screen.

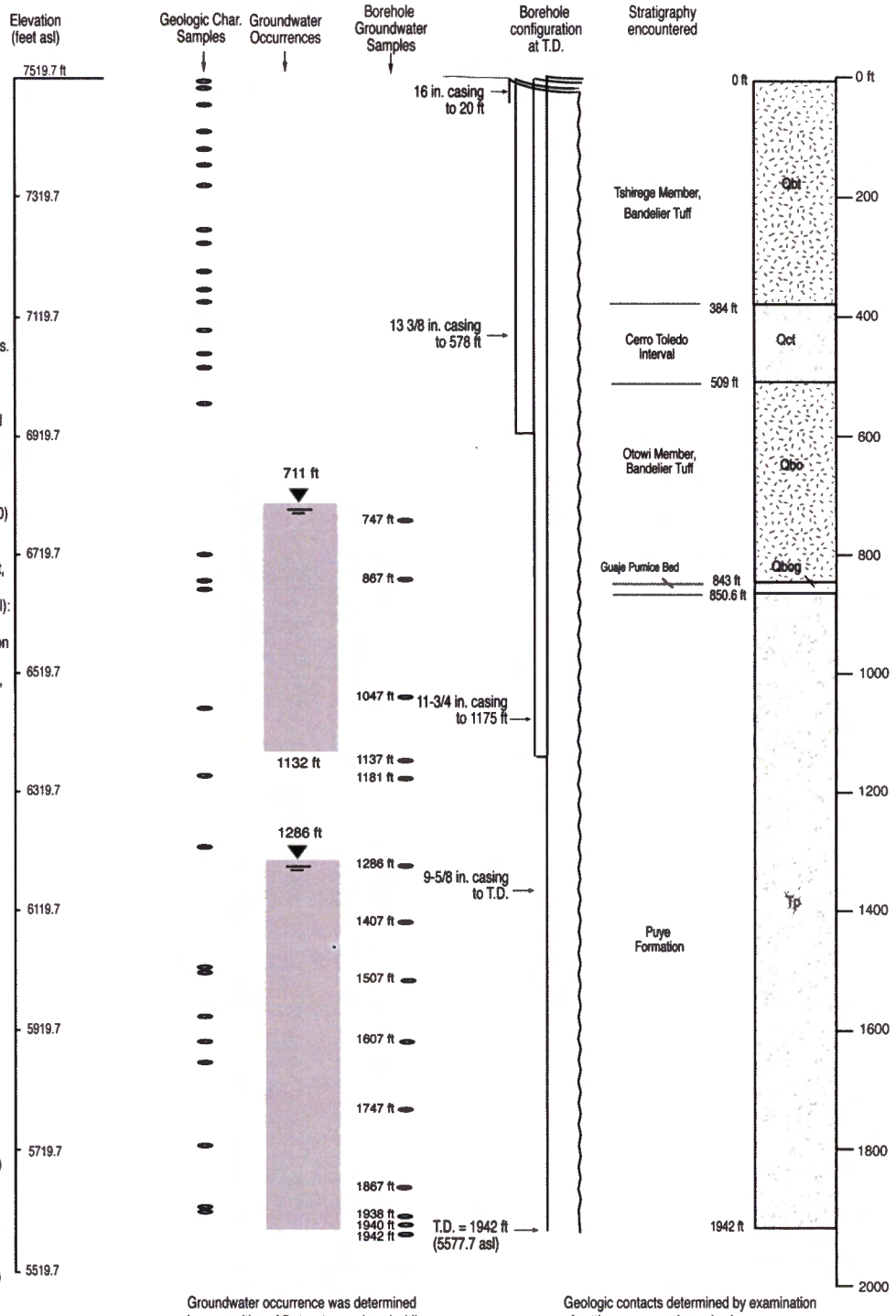


Groundwater occurrence was determined by recognition of first water produced while drilling. Static water levels were determined after the borehole was rested.

Geologic contacts determined by examination of cuttings, core, and geophysics.

**Figure 1-B-21.** Completion diagram for well R-25 (Broxton et al. 2001e).

Location: Mesa South of Cañon de Valle
(on down thrown side of Pajarito Fault) TA-16

Description: Brass Marker
Northing: 1764721.12
Easting: 1610267.33
Elevation: 7641.69

Description: Well Casing
Northing: 1764721.35
Easting: 1610269.56
Elevation: 7643.33

Coring:
(0' - 31') Auger
(31'-55') HQ Coring
(55' - 65') Auger
(65' - 250') HQ Coring

Drilling:
(0' - 77') 13-3/8" Air Rotary Casing Hammer
(77' - 140') 12-1/4" Tri-Cone, Air-rotary
(140' - 205') Air-rotary with water
(205' - 1005') Fluid-assisted (AWQE) air rotary
(1005' - 1490.5') Mud-rotary 8.5" Tri-Cone

Reaming:
(77' - 1005') 14" Roller Reamed - unsuccessful
(1005' - 1490') 10" Reamed - partial success

Data Collection:
- Hydrologic Properties:
  Constant discharge pumping test: 2/11/04 - 2/27/04
- Cores/Cuttings submitted for geochemical and contaminant characterization: 13
- Ground Water Samples Submitted
  Perched Ground Water - 9/18/03 (240') - corehole
  Deep Ground Water -
  Screening Samples: 9/22/03 (604')
  Well Samples: 11/14/03 (1430')
  11/16/03 (660')
- Geologic Properties:
  Cuttings submitted for mineralogy, petrography, and chemistry: 7

Borehole Logs:
- Lithologic: 0' - 1490.5'
- Video (LANL tool): 0' - 717'
- Caliper Logging: 0 - 1475'
- Schlumberger logs:
  Compensated Neutron Log:
  9/28/03: Open Hole: 70'-985'
  10/14/03: Cased: 500'-1005'; Open Hole: 1005'-1481'
  Triple Litho-Density:
  9/28/03: Open Hole: 70'-985'
  10/14/03: Cased: 500'-1005'; Open Hole: 1005'-1481'
  Array Induction Imager:
  9/28/03: Open Hole: 70'-979'
  10/14/03: Cased: 500'-1005'; Open Hole: 1005'-1476'
  Elemental Capture Sonde:
  9/28/03: Open Hole: 70'-981'
  10/14/03: Cased: 500'-1005'; Open Hole: 1005'-1477'
  Natural GR Spectroscopy:
  9/28/03: Open Hole: 70'-979'
  10/14/03: Cased: 500'-1005'; Open Hole: 1005'-1480'
  Combinable Magnetic Resonance:
  9/28/03: Open Hole: 70'-967'
  10/14/03: Cased: none; Open Hole: 1005'-1464'
  Fullbore Formation Micro Imager:
  9/28/03: Open Hole: 450'-965'
  10/14/03: Cased: none; Open Hole: 1005'-1483'

Corehole Logs:
- Lithologic: 0' - 250'
- Video (LANL tool): 0' - 241'
- Gamma Ray (LANL Tool): 0'-245'
- Array Induction (LANL Tool): 0'-245'

Core Drilling Completed: 9/8/03-9/12/03
Rotary Drilling Completed: 9/18/03-10/17/03
Contract Geophysics: 9/28/03 and 10/14/03-10/15/03
Well Installation: 10/17/03-10/21/03
Well Developed: 10/29/03-11/16/03

- Casing:
  4.46" ID / 5.0" OD A304 Stainless Steel casing with external couplings
- Number of Screens:
  Two (2) 4.46" ID wire wrapped stainless steel with external couplings.
  Screen #1 (Upper): 5.53" OD Pipe based 0.010 slot
  Screen #2 (Lower): 5.27" OD Rod based 0.020 slot
- Screen Intervals:
  Screen #1 (Upper): 651.8' - 669.9'
  Screen #2 (Lower): 1421.8' - 1445'

Well Development performed by airlifting, swabbing, bailing, and pumping.
Total Volume Purged: 41,069 gallons

Corehole Temporary Piezometer Completions
- Casing - 1" OD Sched. 40 PVC threaded
- Number of Screens - One (1) 1" OD Sched. 40 PVC 0.010 slotted in each piezometer
- Screen Interval -
  Piezometer 1 - 230'-250'
  Piezometer 2 - 150'-180'

Geologic contacts for R-26 were determined from core samples, cuttings, borehole video, and geophysical logs.

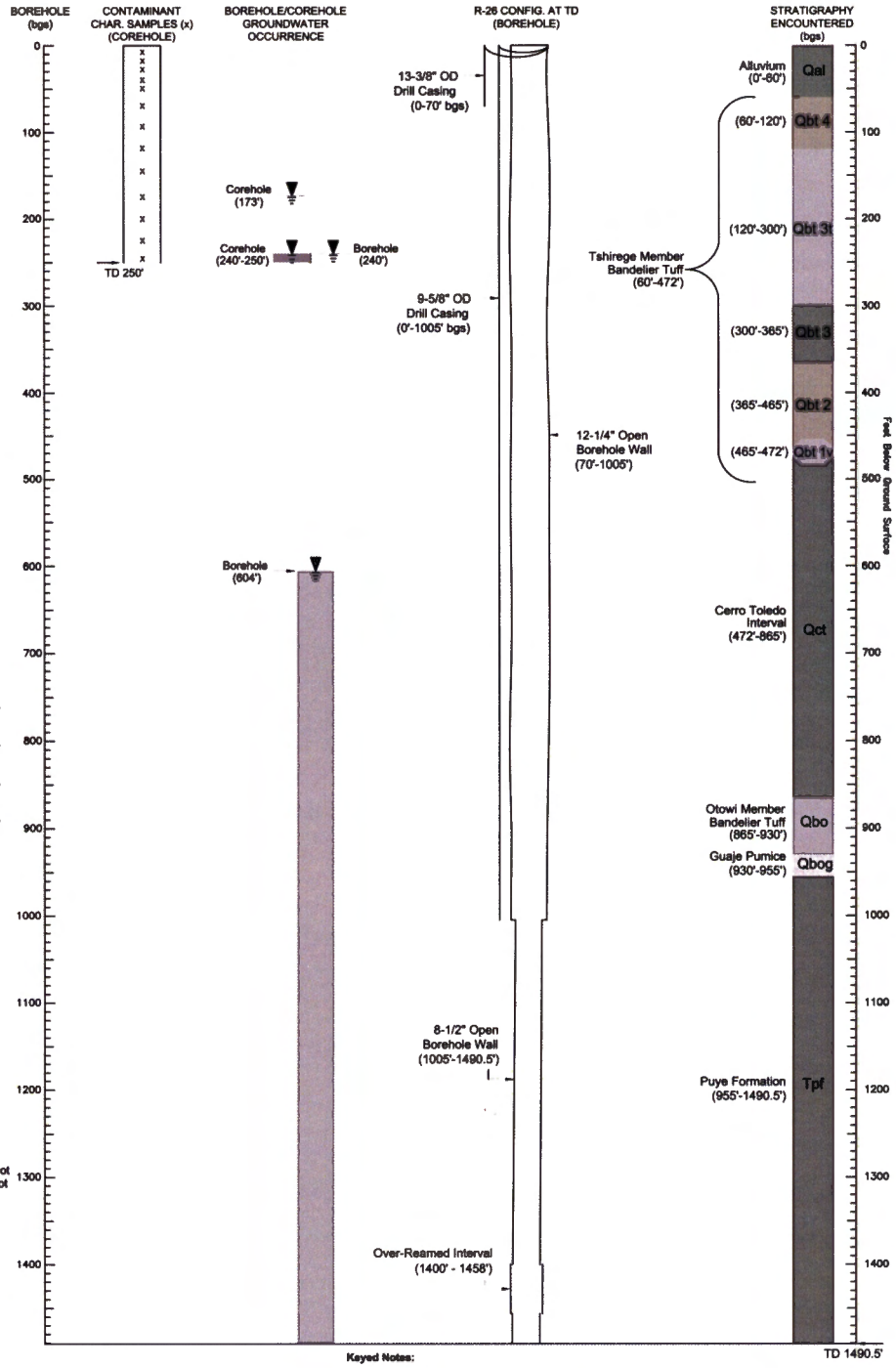


Keyed Notes:

1. Coordinates - NM State Plane Grid Central Zone (North America) Datum - 1983 (NAD83); expressed in feet.
2. Elevations - National Geodetic Vertical Datum (NGVD29); expressed in feet above mean sea level.
3. All depths are below ground surface (bgs).
4. Drill casing removed prior to well installation.
5. Borehole reamed across Screen #2 Interval (1421.8'-1445')
6. Water level measurement in shallow piezometer was 172.97'; the deep piezometer was dry when sounded on 11-25-03.
7. Post-development composite groundwater level measurement recorded on 9-21-03.

**Figure 1-B-22.** Completion diagram for well R-26 (Kleinfelder 2004f).

Location: Upper Mortandad Canyon - TA-5

Description: Brass Marker
Northing: 1768359.0
Easting: 1638988.5
Elevation: 6728.53

Description: Well Casing
Northing: 1768356.8
Easting: 1638989.9
Elevation: 6730.70

Description: Core Hole
Northing: 1768445.3
Easting: 1638997.0
Elevation: 6728.22

Coring:
(0' - 93') Auger with Continuous Sampler
(93' - 95') Auger with Split Spoon
(95' - 129') Coring with Air
(129' - 169') Auger with Split Spoon
(169' - 316.5') Auger with Continuous Sampler
(316.5' - 320') Auger with Split Spoon
(320' - 325') Coring with Air

Drilling:
(0' - 80') 13-3/8" Air Rotary Casing Hammer
(80' - 1005') 12-1/4" Mill-tooth Tri-cone
(80' - 325') Air
(325' - 1005') Fluid Assisted Air Rotary

Data Collection:
- Hydrologic Properties:
  Constant Discharge
  Pumping Test - 2/5/04 - 3/8/04
- Cores/Cuttings submitted for geochemical and contaminant characterization: 16
- Ground Water Samples Submitted
  Perched Ground Water -
  Screening Samples: 12/05/03 (651')
  12/07/03 (707')
  Regional Ground Water -
  Screening Sample: 12/09/03 (889')
  Well Sample: 1/12/04 (947')
- Geologic Properties:
  Cuttings submitted for Minerology, petrography, and chemistry: 7

Borehole Logs:
- Lithologic: 0' - 1005'
- Video (LANL tool): 0' - 888'
- Schlumberger logs:
  Compensated Neutron Log:
  Cased: 30'-80'; Open Hole: 79'-994'
  Triple Litho-Density:
  Cased: 0'-80'; Open Hole: 79'-994'
  Array Induction Tool:
  Cased: none; Open Hole: 79'-986'
  Elemental Capture Sonde:
  Cased: none; Open Hole: 79'-994'
  Natural GR Spectroscopy:
  Cased: none; Open Hole: 79'-971'
  Combinable Magnetic Resonance:
  Cased: none; Open Hole: 79'-994'
  Fullbore Formation Micro Imager:
  Cased: none; Open Hole: 79'-994'

Corehole Logs:
- Lithologic: 0' - 325'
- Video (LANL tool): None
- Gamma Ray (LANL Tool): None

Core Drilling Completed: 11/10/03 - 11/20/03
Rotary Drilling Completed: 11/20/03 - 12/9/03
Contract Geophysics: 12/10/03
Well Installation: 12/12/03 - 12/17/03
Well Development Completed: 1/8/04 - 1/13/04

- Casing:
  4.5" I.D. / 5.0" O.D. A304 Stainless Steel casing with external couplings
- Number of Screens:
  One (1) 4.46" ID/5.27" OD wire wrapped stainless steel rod-based 0.020 slot screen with external couplings.
- Screen Interval: 934.3' - 958.1'

Well Development performed by swabbing, bailing, and pumping.
Total Volume Purged: 17,130 gallons
Hydrologic Properties Testing:
Total Volume Pumped: 10,059 gallons

Geologic contacts are for R-28 deep borehole; contacts were determined from core samples, cuttings, borehole video, and geophysical logs.

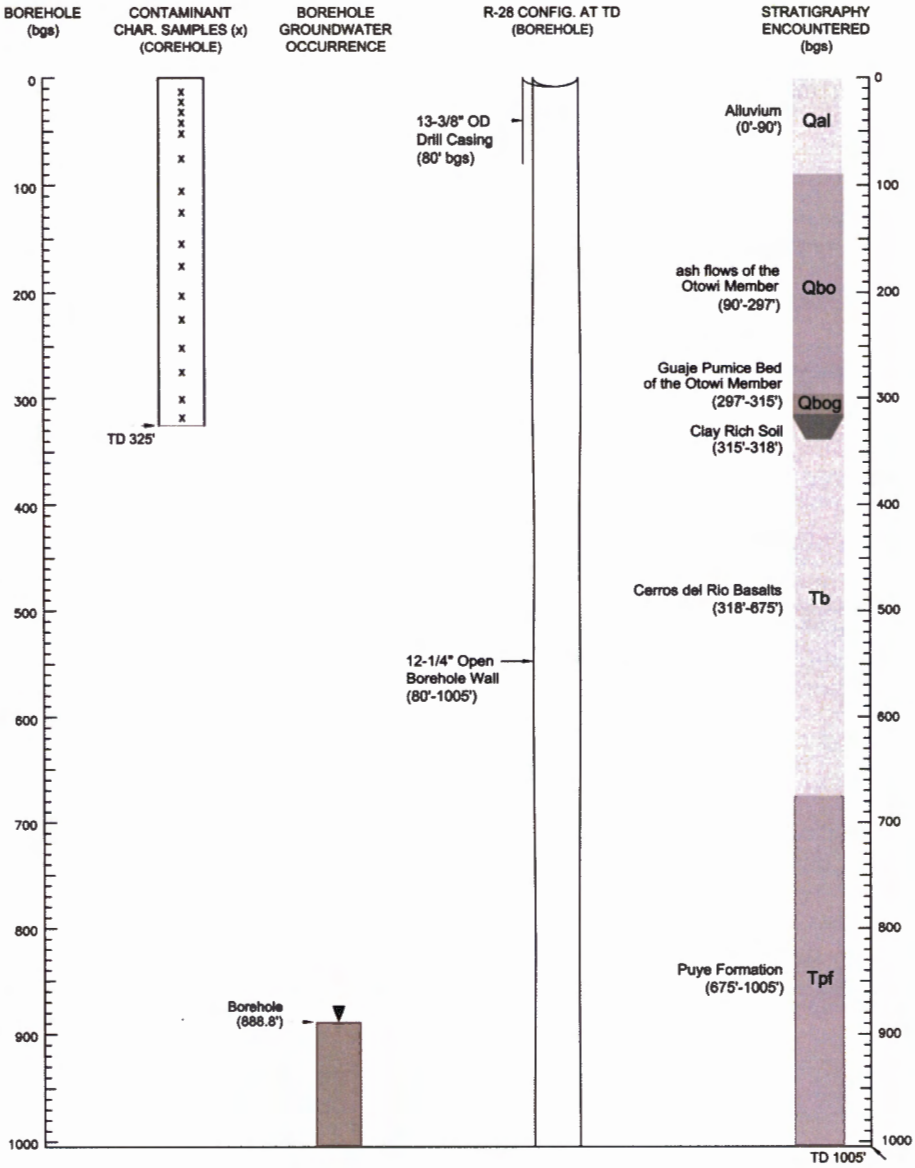


***Legend***

**Qal** = Alluvium
**Qbo** = Otowi Member of Bandelier Tuff
**Qbog** = Guaje Pumice Bed
**Tb** = Cerros del Rio Basalt
**Tpf** = Puye Formation

▼ Water Table

**Notes:**
1. Coordinates - NM State Plane Grid Central Zone (North America) Datum - 1983 (NAD83); expressed in feet.
2. Elevations - National Geodetic Vertical Datum (NGVD 29); expressed in feet above mean sea level.
3. All depths are below ground surface (bgs).
4. Groundwater level measurement recorded on 1-8-04.
5. Drill casing removed during well installation.

**Figure 1-B-23.** Completion diagram for well R-28 (Kleinfelder 2004d).

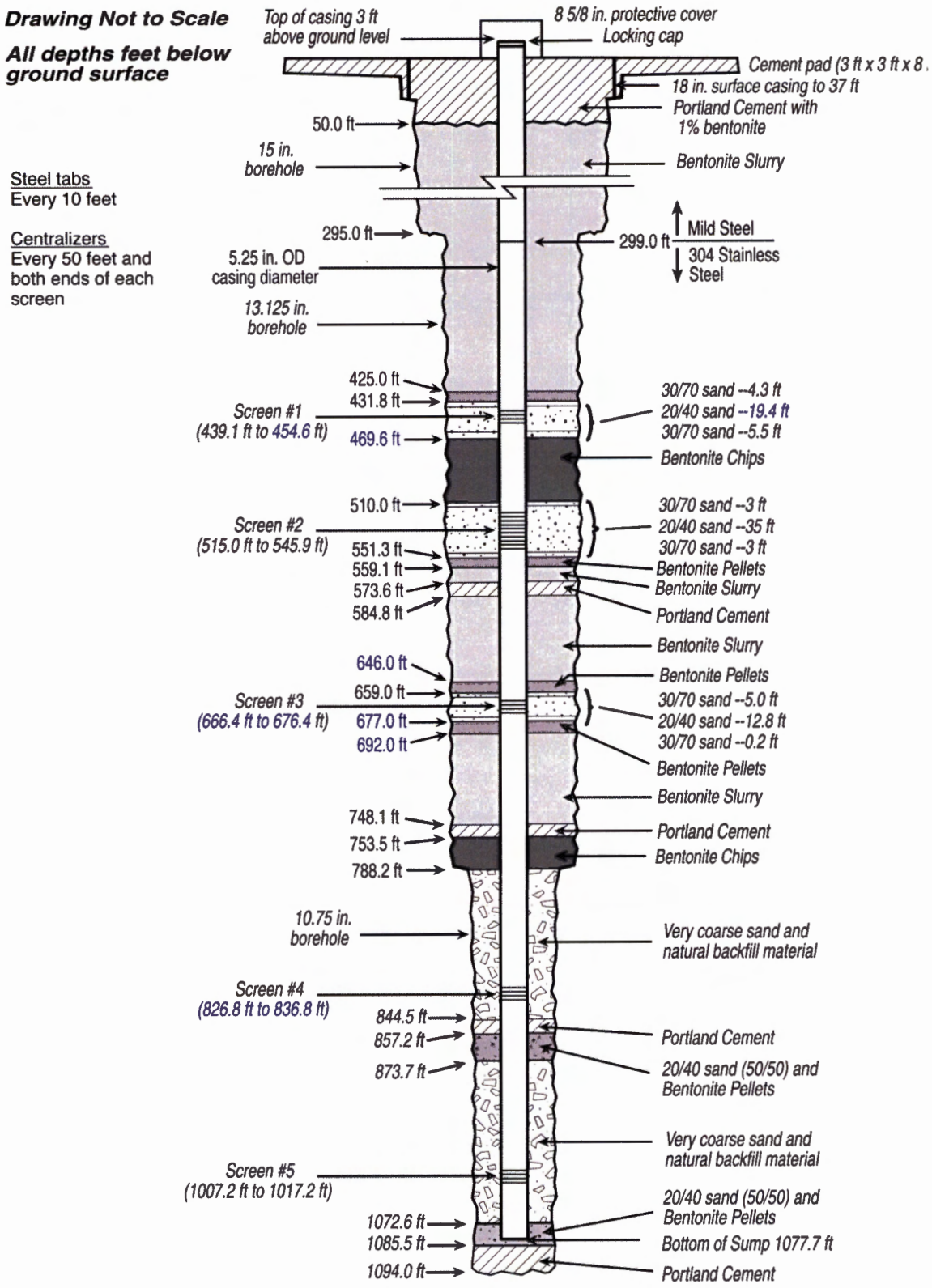


**Figure 1-B-24.** Completion diagram for well R-31 (Vaniman et al. 2002).

Location: In Pajarito Canyon, south of TA-54, along the north side of Pajarito Rd.

Survey coordinates (brass marker in NW corner of R-32 cement pad):
x: 1640798 E y: 1757730 N (NAD 83 )
z: 6637.6 ft asl (NGVD 29)

Drilling: air rotary core w/ wireline retrieval, conventional mud drilling.
R-32 Start date: 07/13/02.
R-32 End date: 08/7/02.

Borehole R-32 drilled to 1008 ft. bgs. (T.D.).

Data collection:
Hydrologic properties: Field hydraulic test: Constant Rate Injection Test on screen #1 and screen #3
Cores/cuttings submitted for geochemical and contaminant characterization: (13)
Groundwater samples submitted for geochem and contaminant characterization: (3)
Geologic properties: (7)
Mineralogy, petrography, and chemistry.
Borehole logs from R-32:
Lithologic: 0-915.5 ft.
Caliper (LANL): 0-1008 ft.
Video (LANL tool): 0-720 ft.
Natural gamma + Induction (LANL tool): 0-808 ft. and 0-1008 ft.
Schlumberger Logs: 0-54.5 ft. (cased), 54.5-808 ft. (open hole): Epithermal Neutron, Litho density, Induction, Combinable Magnetic Resonance, Elemental Capture, Spectral Gamma.

Contaminants Detected in R-32 Water Samples: none

Well construction:
Drilling Completed: 08/07/02
Contract Geophysics: 07/31/02
Well Constructed : 08/09/02 - 08/12/02
Well Developed : 8/18/02 - 11/10/02
Westbay Installed : 11/11/02 - 11/17/02

Casing: 4.5-in I.D. stainless steel with external couplings.

Number of Screens: 3
4.5-in I.D. pipe based, s.s. wire-wrapped with 0.010-in slots.

Screen (perforated pipe interval):
Screen #1 - 867.5 - 875.2 ft. bgs.
Screen #2 - 931.8 - 934.9 ft. bgs.
Screen #3 - 972.9 - 980.6 ft. bgs.

Well development consisted of wire brushing, bailing, chemical treatments, surging, and pumping.

Static water level measured on November 11, 2002, at 783.4 ft in completed and developed well.

Groundwater samples collected from packed off screen intervals after well development.

Geologic contacts for R-32 were determined by examination of cuttings and interpretation of geophysical logs. Contacts may be refined by petrographic, geochemical, or mineralogic analysis of geologic samples.

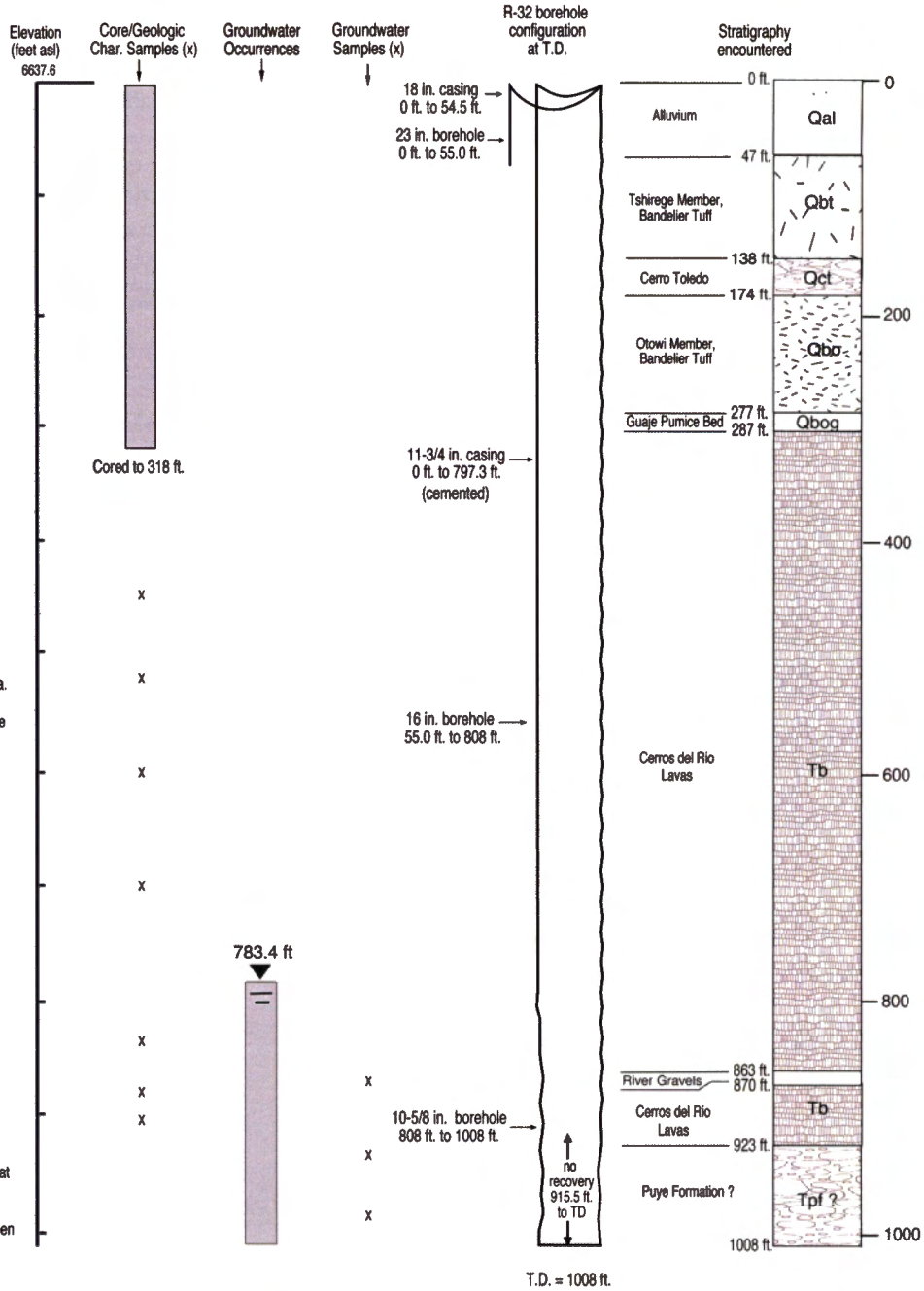


**Figure 1-B-25.** Completion diagram for well R-32 (LANL 2003h).

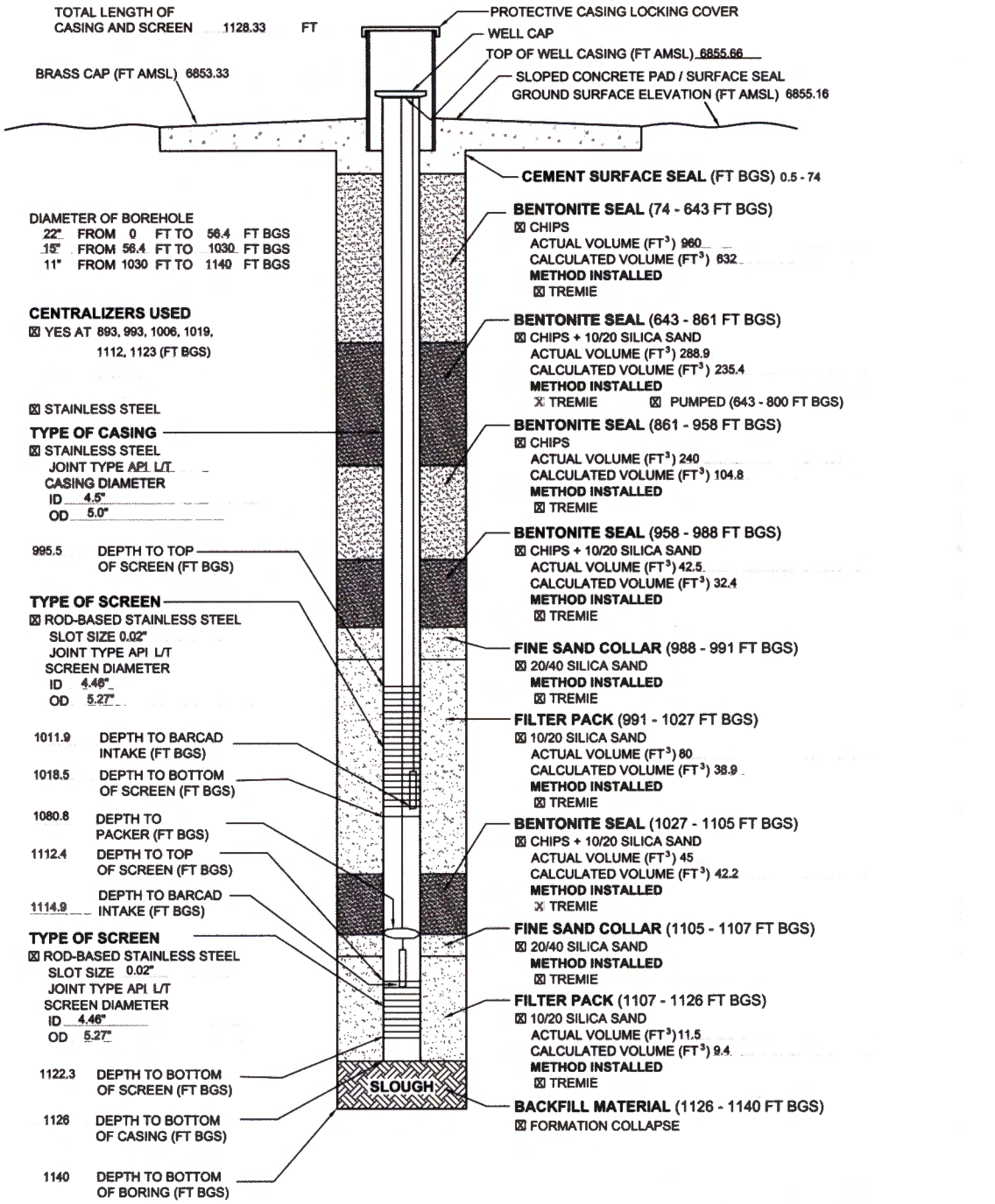


**Figure 1-B-26**. Completion diagram for well R-33 (Note: well completion report not available).

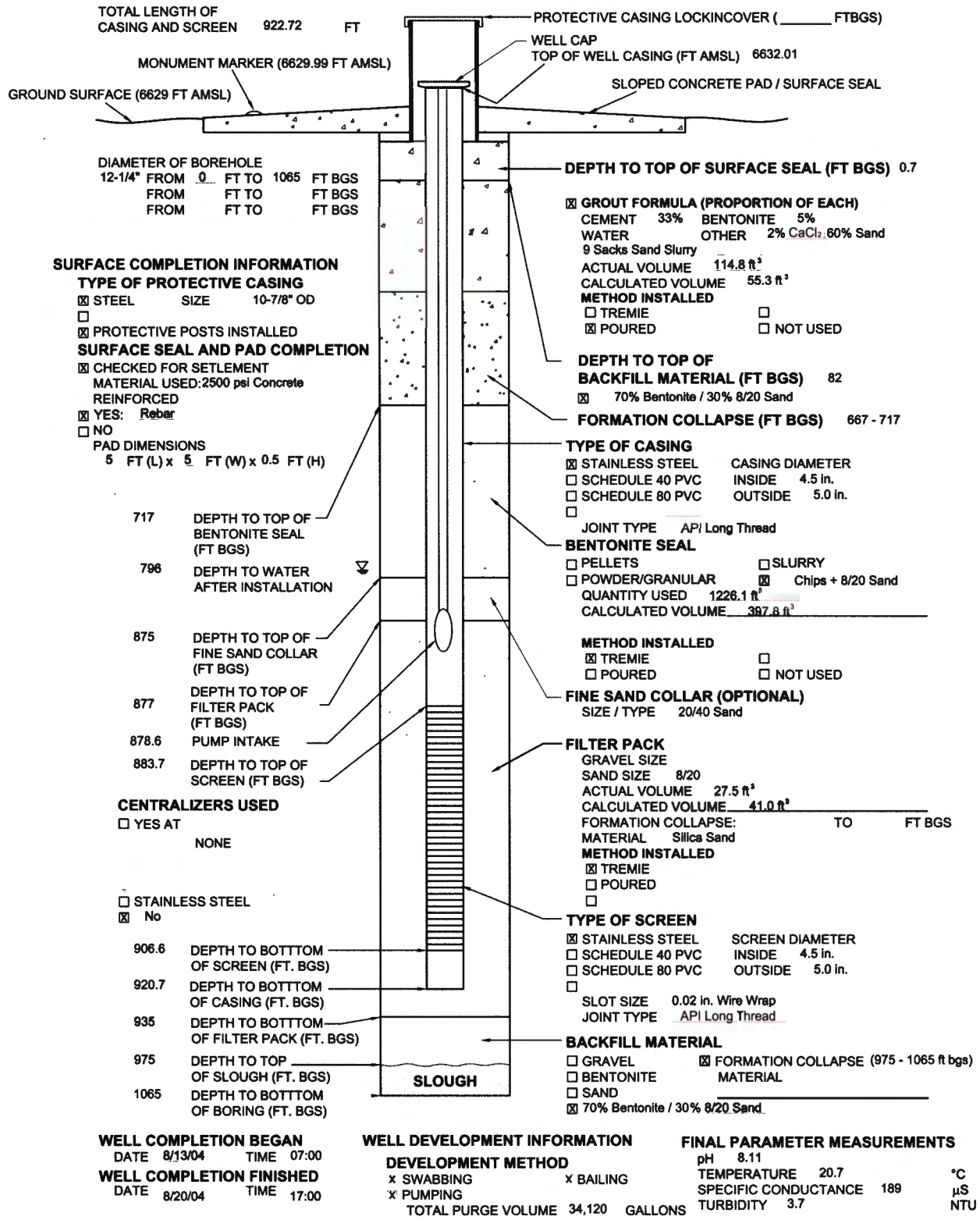


**Figure 1-B-27.** Completion diagram for well R-34 (Note: well completion report not available).

# APPENDIX 2-A. GEOLOGIC INFORMATION USED TO DEFINE THE CONTROLS ON HYDROLOGY

## 2-A-1. Lithologic Information from Cuttings and Core

Drill cuttings and core were collected in all boreholes to meet the regional hydrogeologic characterization requirements described in Section 4.2 of the Hydrogeologic Workplan (LANL, 1998). Cuttings and core provide the most direct evidence for the vertical distribution of hydrogeologic units at each borehole. Correlations of rock units among boreholes are key components of the site-wide 3-D geologic model for the plateau.

Drill cuttings were the most common type of geologic samples produced during the drilling program. Approximately 500 to 700 ml of bulk drill cuttings were collected every 5 ft, as conditions permitted, to the total depth (TD) of each boring. Cuttings were stored in plastic bags labeled with the well name and footage range representing the depth interval at which the cuttings were collected. A subset of unsieved and sieved samples were collected from each cuttings interval and stored in plastic chip trays for geologic examination. The quality and representativeness of cuttings depended on a number of drilling variables including type of circulation fluids used (air, water, foam, mud), circulation type (conventional, reverse), and drill-bit pressure.

Core was collected from dedicated core holes where it was often paired with deeper drill holes. Core was also collected from selected intervals in some regional aquifer boreholes. Core was collected to fulfill a number of characterization objectives, including:

- Geologic characterization of groundwater-bearing zones and aquitards in perched groundwater systems
- Collection of moisture-sensitive samples for hydrologic and chemical analyses of vadose-zone samples (e.g. moisture, anions)
- Collection of intact rock samples to determine hydraulic properties of selected hydrogeologic units.

Rock lithologies, alteration features, and stratigraphic contacts for each borehole are summarized in lithologic logs based on visual examination of cuttings and core. A small subset of core and cuttings was selected for additional characterization to better understand alteration features relevant to rock-water interactions and to aid correlation of rock units between boreholes. The additional characterization primarily consisted of X-ray diffraction for mineralogy, X-ray fluorescence for rock chemistry, thin-section petrography, and $^{40}Ar/^{39}Ar$ age dating. The lithologic logs also incorporated information about stratigraphic contacts and rock properties based on interpretations of borehole geophysical logs.

Core and cuttings are currently archived at the ENV Division Sample Management Facility located at Technical Area 3, building 03-0271-101. All borehole materials are stored in core boxes labeled with the well name, box number, and footage range for the box.

## 2-A-2. Borehole Geophysical Data

Borehole geophysical data were collected to determine the geologic and hydrologic characteristics of the vadose zone, perched saturated zones, and the regional aquifer as specified in Section 4.1.6 of the workplan. A listing of geophysical logs collected during installation of Hydrogeologic Workplan wells is given in the well completion reports associated with those wells. Borehole geophysical data were obtained from two sources. Laboratory/contractor personnel collected caliper, spontaneous potential, single-point resistance and induction, and natural gamma radiation logs using the Laboratory's geophysical logging equipment, usually during breaks in the drilling process when conditions permitted the collection of open-borehole data. A wire-line logging service was contracted to obtain a more extensive suite of borehole geophysical logs once the borehole reached total depth.

The number and types of contracted wire-line geophysical logs varied as a function of borehole condition, the presence or absence of drill or well casing, whether the borehole was air or fluid filled, and technical issues addressed by a particular logging run. Drilling conditions determined whether the borehole was open or cased at the time of logging. Table 2-A-1 gives the typical suites of logs that have been run by wire-line logging services in cased and open boreholes. General logging information and borehole conditions at the time of logging were documented by site personnel.

Preliminary results of geophysical logs were generated in the logging truck at the time the geophysical services were performed. These preliminary logs were used by contractor, DOE, and LANL personnel to help select well screen locations and to evaluate borehole conditions prior to well construction.

The geophysical contractor reprocessed the field measurements to correct for borehole and formation environmental conditions, to perform an integrated analysis of the log measurements so that they were all coherent, and to combine the logs into a single presentation enabling integrated interpretation. The contractor then prepared an interpretive report that was included as an appendix in the well completion reports. The interpretive report includes information about the hydrogeologic characteristics of the rocks penetrated by the boreholes, moisture distributions as a function of depth, the location of the regional water table, borehole diameter, deviation as a function of depth, and degree of drilling fluid invasion. Depending on the suite of logs collected, the interpretive report may include information about

- total and effective water-filled porosity and pore size distribution, from which an estimate of hydraulic conductivity is made,
- bulk density and photoelectric effect, the latter of which is particularly sensitive to lithology,
- electrical resistivity at multiple depths of investigation,
- concentrations of a number of elements,
- spectral natural gamma ray, including potassium, thorium, and uranium concentrations,
- bedding orientation and geologic texture,
- borehole inclination and azimuth, and
- borehole diameter.

## 2-A-3. Borehole Video Logs

Borehole video logs were run in open boreholes to obtain lithologic information and to help determine stratigraphic contacts for the geologic units penetrated, to allow visual examination of borehole walls for evidence of perched saturation, and to document water levels in the boreholes. Video logs also were run when wells were completed to document the as-built condition of installed well components. Additional videos were sometimes run during and after well development to assess the effectiveness of development techniques. Finally, the borehole video logs were used during drilling operations to assess problematic borehole conditions and to guide fishing operations for tools and equipment lost downhole.

One of the principal uses of the borehole video logs was to identify potential groundwater pathways. For example, when used in conjunction with geophysical logs, video logs were an important method for locating highly porous interflow breccias sandwiched between massive basalt flows. These interflow breccias were important for determining the locations of perched zones in some boreholes. The video logs also showed whether the porosity of these interflow breccias was open or modified by deposition of extensive secondary clay minerals. Fractures are potential pathways in the massive flow interiors. Fracture density, fracture dips, and open verses sealed fractures were assessed using video logs.

## 2-A-4. Surface Geophysical Data

Surface geophysical data were used to help constrain the site-wide geologic model. These data include regional gravity data, airborne electromagnetic data, high-resolution resistivity, and magnetotellurics. Gravity data were used to help define regional structure beneath the Pajarito Plateau. Airborne electromagnetic data, high-resolution resistivity, and magnetotelluric data were used to focus groundwater investigations by defining the conductivity structure beneath the plateau. The remainder of this section describes the airborne electromagnetic data in more detail.

An electromagnetic (EM) and magnetic survey was flown over the Pajarito Plateau in early September 2001 by the Fugro Airborne Surveys Corporation on behalf of LANL. A total of 762 line kilometers of MegaTEM® time domain EM data and magnetic data were collected. Flight lines were spaced at 333.3 ft (105 m) within the Laboratory boundaries, and at 666.7 ft (210 m) in buffer zones adjacent to the Laboratory, oriented N20E: with tie lines at an approximate 2000-meter spacing. Because of security constraints stemming from the events of September 11, 2001, flight lines in the western 20% of the Lab, and the two tie lines in the northern portion of the Laboratory were not flown.

The contractor provided maps of Residual Magnetic Intensity (RMI), apparent conductance and conductivity depth slices at various depths, multiparameter profiles with conductivity-depth-transform (CDT) sections for flight lines and digital archives of line and grid data. The digital EM data were analyzed at a later time (end of FY01) by Condor Consulting, Inc. This analysis resulted in two additional models of CDTs along the flight paths. All of the processing assumed a "layered-earth" model, and all of the inversions were restricted to single points/multiple depths (1-D), multiple depths along individual flight lines (2-D), or a constant depth on multiple flight lines (2-D); there was no true 3-D inversion performed on the data set. Data from the existing

3-D geologic model, identifying zones of expected similar hydrologic properties, were provided to Condor and are part of the initial data analysis. Borehole geophysical logs were also provided to Condor to assist in calibrating their models. The results of all three models for each flight line are available. At some future time, a constrained 3-D inversion, utilizing the 3-D hydrogeologic model, may allow better resolution of the conductance inversion results.

Visual correlation of conductance and observed groundwater can be obtained through study of the "multiplots" of the flight lines closest to groundwater occurrences. An effort has been made to allow creation of 3-D conductance models for each of the CDT data sets. Interpolation of flight line data is accomplished through scaled interpolation within an oriented ellipsoid that samples a similar number of points in the directions: vertical, along-flight-line, and between-flight-line. Many 3-D visualization packages are capable of displaying and scaling 3-D grid data. As much of the error/uncertainty of the conductance model occurs in the depth/thickness value, real-time scaling and offsetting the z-axis of the conductance grid can allow correlation with known groundwater locations obtained from drill holes; and thus allow a projection/extrapolation of the groundwater surface beyond the limits of direct observation.

The two tie lines of the survey provide conductance signatures that correlate well with the major faults in the western portion of the Laboratory and could perhaps provide some information regarding their dips. These survey lines indicate other localities with signatures similar to those of the mapped faults, which may indicate buried faults or conductive fracture zones further to the east.

## 2-A-5. Drilling Information

Observations about drilling characteristics by the drillers and on-site geologists contributed to understanding the hydrogeology of the boreholes. These observational data were recorded in field logs, and they provided supplemental information that aided the interpretation of hydrogeologic data from other sources such as cuttings and geophysical logs.

Because of the heterogeneous nature of the rocks beneath the plateau, major lithologic and stratigraphic contacts were commonly marked by significant changes in drill penetration rates. Drilling rates were affected by a number of factors, but chief among them was the competency of the rocks being penetrated. Hard rock units such as strongly welded tuffs, lava flows, and boulder-rich fanglomerate deposits were characterized by slow drilling rates, whereas less competent rocks such as nonwelded tuffs and poorly indurated sands, silts, and clays drilled more rapidly. For example, drill penetration rates normally decreased downhole when going from the nonwelded tuffs at the base of Qbt 3 into the welded tuffs at the top of Qbt 2 and from the Guaje Pumice Bed into Puye Formation and/or Cerros del Rio basalt.

Information about borehole stability and lost-circulation zones also provided important site-specific information about subsurface conditions. For example, open borehole drilling at R-22 was complicated by caving conditions and by difficulty in maintaining free rotation of the drill string though thick sequences of basalt. Normally, the interiors of basalt flows are strongly competent and yield gun-barrel smooth boreholes, but the conditions at R-22 suggested that loose blocks of basalt were caving into the borehole and binding up the drill string. Subsequent

borehole video logs showed that dense networks of fractures intersected the R-22 borehole resulting in an unstable borehole. Similarly, lost circulation zones generally indicated that drilling fluids had escaped into highly porous fractures or scoria zones intersected by the borehole. At R-34, significant zones of lost circulation were associated with thick beds of loose basaltic scoria. Some cavities observed in borehole videos might be small-scale lava tubes or caverns similar to those known to occur in the Cerros del Rio volcanic field east of the Rio Grande.

Important information about water-bearing strata was obtained when drillers noted changes in the drilling fluids circulating through the borehole. Perched water and the top of the regional zone of saturation were readily recognized when water and wet cuttings were returned to the surface using air-rotary drilling methods. Water-bearing zones were identified even when using fluid-assisted air-rotary methods that involved the use of air, municipal water, foam, and other additives for circulation. When using such methods, surplus production of water and thinning of drilling foam often was associated with the intersection of groundwater.

## 2-A-6. Data Generated by Other Projects

Numerous local and regional mapping projects and geological studies have provided important information supporting development of geologic conceptual models and digital realizations of these models. Pioneering work by geologists of the U.S. Geological Survey (USGS) helped define the tectonic setting and the major hydrogeologic units of the region (Smith, 1960a and 1960b, Griggs, 1964; Smith and Bailey, 1966; Bailey et al., 1969; Smith et al., 1970). Regional and local studies of rock unit ages, many of which were supported by the Laboratory, provided a time scale to calibrate the timing of the volcano-tectonic development of the site: faulting and volcanism, and emplacement of the resultant volcanic flows and sedimentary units (Gardner and Goff, 1984, Gardner et al., 1986; Loeffler et al., 1988; Turbeville et al., 1989; Izett and Obradovich, 1994; Spell et al., 1990; Spell and Harrison, 1993; Spell et al., 1996; Toyoda et al., 1995; McIntosh and Quade, 1995; WoldeGabriel et al, 1996; Reneau et al., 1996; Smith, 2001; WoldeGabriel et al., 2001; Goff and Gardner, 2004). Understanding the nature of the evolving tectonic regime allowed development of models to define the conceptual, spatial distribution of hydrogeologic units, as well as explanations of their post-deposition evolution.

The New Mexico state mapping program, supported by the USGS and the New Mexico Bureau of Geology and Mineral Resources, with help from LANL scientists, produced 1:24,000-scale, surface geologic maps and accompanying cross sections for the Frijoles (Goff et al., 2002), White Rock (Dethier, 1997), Puye (Dethier, 2003), and Guaje Mountain (Kempter and Kelley, 2002) quadrangles. These four maps encompass the Laboratory site with a significant buffer zone, allowing the integration of site and regional geologic features. Other geological maps, some with cross sections, covering portions of the LANL include those by Baltz et al., (1963); Goff et al., (1990); Rogers, (1995); Vaniman and Wohletz, (1990); Reneau et al., (1995); Goff, (1995); Lewis et al., (2002); and Lavine et al., (2003).

Española Basin workshops were hosted annually by the Española Basin Technical Advisory Group and sponsored by the U.S. Geological Survey, the New Mexico Bureau of Geology and Mineral Resources, Los Alamos National Laboratory, and the city of Santa Fe. These workshops

were important forums for disseminating results of ongoing technical studies of the hydrogeologic framework of the Española Basin.

The seismic hazards program at LANL was an important source of information about faults and fractures in the vicinity of the Laboratory (Gardner and House, 1987; Gardner et al., 1990, 1993, 1999, 2001; Lewis et al., 2002; and Lavine et al., 2003). Their high-resolution, surface mapping of subunits of the Bandelier Tuff provided new information about the distribution and nature of faulting on the Pajarito Plateau and made estimates about amounts and rates of offset of geologic units. Numerous other Laboratory projects and programs helped to develop geologic information supporting geologic conceptual models. The Environmental Restoration project funded numerous projects as part of its RCRA facilities investigations that provided information about geologic framework of the site and hydrologic properties of geologic units.

Students and their advisors from the graduate programs from the University of New Mexico, New Mexico State University, and New Mexico Institute of Mining and Technology have provided additional hydrogeologic information for the Jemez volcanic field and Española Basin. Studies by graduate students from the University of Texas (e.g., Turbeville et al., 1989) were especially useful for understanding the Puye Formation.

## Table 2-A-1.
## Typical Wire-Line Geophysical Logging Tools

| Cased Hole | Cased Hole | Open Hole | Comments |
|---|---|---|---|
| Array Induction Tool (AIT) | | X | Measures open-hole formation conductivity with multiple depths of investigation at varied vertical resolution |
| Triple Litho Density Tool (TLD) | X | X | Evaluates formation porosity where grain density can be estimated |
| Combinable Magnetic Resonance Tool (CMR) | | X | Provides information on water content and relative abundance of hydrous minerals and capillary-bound versus mobile water |
| Natural Gamma Tool | X | X | Used to distinguish lithologies by their gross gamma signature; also used to calibrate depth of other geophysical tool readings |
| Natural Gamma Ray Spectrometry Tool (also called the spectral gamma tool)[1] | X | X | Used to distinguish lithologies where formations vary in relative and overall concentrations of potassium, thorium and/or uranium |
| Epithermal Compensated Neutron Log (CNL) | X | X | Measures moisture content in unsaturated conditions and porosity in saturated conditions |
| Caliper | | X | Measures rugosity of borehole wall |
| Fullbore Formation Microimager (FMI) | | X | Provides high-quality image of borehole based on electrical properties; used to determine lithologies, bedding attitudes, fracture characteristics, and borehole deviation |
| Elemental Capture Spectrometer (ECS) | X | X | Determines formation lithology from bulk geochemistry; used primarily to determine elemental concentrations of silicon, calcium, iron, titanium, and gadolinium |

[1]A total gamma log was collected with each geophysical suite to correlate separate logging runs within a borehole.

# APPENDIX 2-B. PERCHED WATER OCCURRENCES

This appendix documents the field observations of the 33 occurrences of perched groundwater detected in 29 boreholes across the Pajarito Plateau. Characteristics of deep perched groundwater zones encountered in wells on the Pajarito Plateau are listed in Table 2-B-1.

In the western part of Los Alamos Canyon, perched groundwater occurs at depths of 89 to 137 m (293 to 450 ft) in the Guaje Pumice Bed and in underlying Puye Formation fanglomerate. Saturated thicknesses for these occurrences range from about 6.7 m (22 ft) in the west to about 1 m (3 ft) in the east. These groundwater occurrences in the Guaje Pumice Bed may represent a related groundwater system because of their similar geologic and geographic settings, however, in one well, R-7 (Figure 2-37), perched groundwater occurs immediately beneath the Guaje Pumice Bed, in the underlying Puye Formation. The east-west extent of perched groundwater in the Guaje Pumice Bed is about 5.6 km (3.7 mi). Little is known about the extent of perched groundwater beneath the adjacent mesas, but a dry borehole extending to the Guaje Pumice Bed (borehole 21-2523) suggests that saturation does not extend beneath the mesa north of Los Alamos Canyon. The perched groundwater is free of contamination in the central part of the canyon (e.g. well LAO(I)A-1.1) but contained 3000 pCi/L tritium in 1995 at LADP-3 (Broxton et al, 1995), the easternmost well penetrating this groundwater body. The movement of groundwater in the Guaje Pumice Bed may be controlled by paleotopography on top of the underlying Puye Formation. Structure contours indicate that the down-dip direction for the base of Guaje Pumice Bed beneath Los Alamos Canyon is towards the south and east (Section 2.2.9).

Eastward in Los Alamos Canyon, perched zones are generally thicker and occur at multiple depths. In well R-9 for example, three perched systems were encountered: 1) in the central part of the Cerros del Rio basalt, 2) in the basal part of the Cerros del Rio basalt, and 3) in pumice-rich deposits in the lower part of the Puye Formation. Saturated thicknesses for the top and bottom zones range from about 13.7 to 31.4 m (45 to 103 ft), and the middle zone was 2.1 m (7 ft) thick. The top and middle perched zones in R-9 are also present in well LAWS-1, located 396 m (1300 ft) to the east, but their lateral extent is likely to be much greater. The occurrence of more extensive perched groundwater in the eastern part of Los Alamos Canyon may be due to enhanced infiltration where the canyon floor is underlain by Puye fanglomerate and Cerros del Rio basalt rather than by Bandelier Tuff. Tritium activities of 69 to 246 pCi/L for these perched groundwaters are elevated relative to the cosmogenic baseline of 1 pCi/L, suggesting that these zones contain a component of young water that postdates the advent of atmospheric nuclear testing 60 years ago (Longmire, 2002).

**Table 2-B-1.**
**Characteristics of Deep Perched Groundwater Zones Encountered in Wells on the Pajarito Plateau**

| Watershed | Well Name, Borehole Depth (ft), Surface Elev. (ft) | Depth to Water (ft) | Saturated Thickness (ft) | Groundwater Host Rock | Nature of Perching Layer | Anthropogenic Chemicals Detected | Comments |
|---|---|---|---|---|---|---|---|
| Pueblo Canyon | TW-2a<br>133<br>6646 | 110 | >23 | Puye Fm. fanglomerate | Within Puye Fm. fanglomerate; perching lithology not known | Tritium, nitrate | A single-screen well was installed in this zone (Griggs, 1964, Purtymun, 1995). |
| Pueblo Canyon | R-5<br>902<br>6473 | ~380 | ~37 | Puye Fm. dacitic sands and gravels mixed with 5-15% rounded quartzite and granite river gravels | Within Puye Fm. fanglomerate; perching lithology not known | Nitrate, fluoride, chloride, uranium, and sulphate | A canyon-floor well was installed with four isolated screens (LANL, 2003). Screen #2 is complete in this perched zone. The vertical extent of this zone is poorly known. |
| Pueblo Canyon | TW-1a<br>225<br>6370 | 188-225 (?) | ±37 (?) | Interflow breccia and siltstone in Cerros del Rio basalt | Possibly unfractured massive basalt | Nitrate, phosphate, chloride, boron, and uranium | Groundwater was first encountered near the top of Cerros del Rio basalts in a zone from 212- to 215-ft-deep (Griggs, 1955). Groundwater may be confined because the water level stabilized at 188 ft (Purtymun, 1995). Well screen placed from 215 to 225 ft deep. |
| Pueblo Canyon | POI-4<br>181<br>6372 | 160 | >21 | Cerros del Rio fractured basalt | Confining layer not penetrated | Nitrate, phosphate, chloride, boron, | Groundwater occurs in massive basalt cut by high-angle fractures. A single-screen well was installed in this zone. |

**Table 2-B-1.**
**Characteristics of Deep Perched Groundwater Zones Encountered in Wells on the Pajarito Plateau (continued)**

| Watershed | Well Name, Borehole Depth (ft), Surface Elev. (ft) | Depth to Water (ft) | Saturated Thickness (ft) | Groundwater Host Rock | Nature of Perching Layer | Anthropogenic Chemicals Detected | Comments |
|---|---|---|---|---|---|---|---|
| Los Alamos Canyon | H-19 2000 7172 | 450 | 22 | Porous, well-bedded and well-sorted fall deposits of the Guaje Pumice Bed | Tschicoma Fm. lava flow top | Not sampled | Saturation in this zone was noted while drilling to reach the regional aquifer (Griggs, 1964). The perched zone was not screened, and the regional well was later abandoned. |
| Los Alamos Canyon | LAOI(A)1.1 323 6833 | 289 | 27 | Porous, well-bedded and well-sorted fall deposits of the Guaje Pumice Bed | Top of Puye Formation; possible clay-rich soil horizon – see description for well LADP-3 | None | A single-screen well was installed in this zone. |
| Los Alamos Canyon | R-7 1097 6779 | 373 | 9 | Puye Fm. silty, clayey, and sandy gravels | Clay-rich gravels from 382 to 397 ft deep in the Puye Formation | None | A canyon-floor well was installed with three isolated screens (Stone et al., 2002). Screen #1 in well R-7 is completed in this perched zone. |
| Los Alamos Canyon | R-7 1097 6779 | 744 | ~23 | Puye Fm. sandy gravel with abundant pumice clasts | Puye Fm.; possible perching layer from 767 to 772 ft in silty pebble gravel or from 772 to 777 ft in clayey pumiceous sands. | None | Screen #2 in well R-7 is completed in this zone. Geophysical logs and borehole videos suggest additional perched groundwater zones were encountered when the R-7 borehole was drilled. |
| Los Alamos Canyon | LADP-3 349 6756 | 320 | 9 | Porous, well-bedded and well-sorted fall deposits of the Guaje Pumice Bed | Smectite- and kaolinite-rich soil a few inches thick at top of Puye Formation | Tritium | Soil development occurs at top of the Puye Formation in outcrops and in boreholes elsewhere. A single-screen well was installed in this zone. (Broxton et al., 1995). |

**Table 2-B-1.**
**Characteristics of Deep Perched Groundwater Zones Encountered in Wells on the Pajarito Plateau (continued)**

| Watershed | Well Name, Borehole Depth (ft), Surface Elev. (ft) | Depth to Water (ft) | Saturated Thickness (ft) | Groundwater Host Rock | Nature of Perching Layer | Anthropogenic Chemicals Detected | Comments |
|---|---|---|---|---|---|---|---|
| Los Alamos Canyon | LAOI-3.2a 165.5 ~6620 | 134 | >31 | Basal ash-flow tuffs of the Otowi Member and porous, well-bedded and well-sorted fall deposits of the Guaje Pumice Bed | The perched zone was not fully penetrated during drilling; perching lithology not known | Nitrate, perchlorate, chloride | Perched groundwater was detected while coring through the lowermost part of the Bandelier Tuff. The bottom of saturation was not penetrated by the borehole. A single-screen well was installed in this zone. |
| Los Alamos Canyon | Otowi 4 2806 6639 | ~253 | Not known | Puye Fm. gravels | Within Puye Fm. fanglomerate; perching lithology not known | Not sampled | Saturation in this zone was noted while drilling to install a municipal supply well in the regional aquifer (Stoker et al. (1992). The geologic log notes: "Some perched water was visible in a video log of the 48-in hole at about 253 ft where water cascaded in from a large gravel." This perched zone is not accessed by a well screen in Otowi 4. |
| Los Alamos Canyon | R-6i 660 ~6995 | 592 | 23 | Puye Fm. gravels | Poorly sorted fanglomerate with a silty matrix | Nitrate and perchlorate | This zone occurs at the same elevation and may be related to the perched zone identified by borehole video in nearby supply well Otowi 4 during drilling. A single-screen well was installed in this zone. |

**Table 2-B-1.**
**Characteristics of Deep Perched Groundwater Zones Encountered in Wells on the Pajarito Plateau (continued)**

| Watershed | Well Name, Borehole Depth (ft), Surface Elev. (ft) | Depth to Water (ft) | Saturated Thickness (ft) | Groundwater Host Rock | Nature of Perching Layer | Anthropogenic Chemicals Detected | Comments |
|---|---|---|---|---|---|---|---|
| Los Alamos Canyon | R-9i<br>322<br>6383<br><br>and<br><br>LAWS-01<br>281.5<br>6305 | 137 | 45-99 | Cerros del Rio basalt interflow breccia and highly fractured basalt | Massive basalt with few fractures | Tritium | Groundwater was first encountered at a depth of 180 ft, but the water level quickly rose to 137 ft, indicating possible confinement. At R-9i a canyon-floor well was installed with two isolated screens (Broxton et al., 2001a,b). Screen #1 of R-9i is complete in this zone. In LAWS-01, this zone is sampled via a flexible liner with sampling ports (Stone and Newell, 2002). |
| Los Alamos Canyon | R-9i<br>322<br>6383<br><br>and<br><br>LAWS-01<br>281.5<br>6305 | 275 | 7 | Cerros del Rio basalt brecciated flow base | Clay-rich, stratified, basaltic tephra (maar deposits) from 282 to 289.8 ft | Tritium | Water first encountered at 275 ft. The water level stabilized at 264 ft and may be confined (Broxton et al., 2001a,b). Screen #2 in well R-9i is complete in this zone. In LAWS-01, this zone is sampled via a flexible liner with sampling ports (Stone and Newell, 2002). |
| Los Alamos Canyon | R-9<br>771<br>6383 | 524 | 48 to 103 | Puye Formation sands and gravels | Clay-rich tuffaceous sands and gravels | Tritium | Three stringers of sands and gravels at 579-580.5 ft, 615 ft, and 624-626.8 ft produced perched groundwater (Broxton et al., 2001a). These occurrences probably constitute a single saturated zone because when isolated each yielded the same |

**Table 2-B-1.**
**Characteristics of Deep Perched Groundwater Zones Encountered in Wells on the Pajarito Plateau (continued)**

| Watershed | Well Name, Borehole Depth (ft), Surface Elev. (ft) | Depth to Water (ft) | Saturated Thickness (ft) | Groundwater Host Rock | Nature of Perching Layer | Anthropogenic Chemicals Detected | Comments |
|---|---|---|---|---|---|---|---|
| | | | | | | | depth-to-water of 524 ft. The water-bearing stringers are enclosed by clay-rich tuffaceous sands and gravels that may be confining units or may simply be unproductive. No well screens were installed in this saturated zone. |
| Sandia Canyon | PM-1<br>2501<br>6513 | 450 | Not Known | Cerros del Rio basalt | Not known | Not sampled | During installation of supply well PM-1, the geologic log notes that water was present in brecciated Cerros del Rio basalt at a depth of 450 ft (Cooper et al., 1965). No other information was given about this zone. |
| Sandia Canyon | R-12<br>886<br>6500 | 424 | 76-95 | Fractured Cerros del Rio basalt and underlying fluvial sands and silts, and riverine gravels of the lacustrine facies of the Puye Fm. | Clay-rich lake beds of the lacustrine facies of the Puye Fm. from 519-535 ft | Tritium, nitrate | This is probably the same perched groundwater as that encountered in PM-1. Groundwater was first encountered at a depth of 443 ft, but the water level quickly rose to 424 ft before stabilizing, indicating possible confinement. A well was installed with three isolated screens (Broxton et al., 2001c). Screens #1 and #2 are complete in this perched zone. |

**Table 2-B-1.**
**Characteristics of Deep Perched Groundwater Zones Encountered in Wells on the Pajarito Plateau (continued)**

| Watershed | Well Name, Borehole Depth (ft), Surface Elev. (ft) | Depth to Water (ft) | Saturated Thickness (ft) | Groundwater Host Rock | Nature of Perching Layer | Anthropogenic Chemicals Detected | Comments |
|---|---|---|---|---|---|---|---|
| Mortandad Canyon | I-8<br>745 | 675, water level is at top of well sump | Saturated thickness is unknown, but the zone is probably very thin | Fractured Cerros del Rio basalt | Nature of confining bed is unknown | None | A small amount of water was observed trickling from a fracture at 669 ft bgs in the borehole video. A single-screen well was installed, but only a small amount of water has accumulated in the well sump. |
| Mortandad Canyon | MCOBT-4.4<br>767<br>6836 | 520 | 2-4 currently | Puye Fm. pebble gravel and silty sands | Top of Cerros del Rio basalt | Tritium, nitrate, perchlorate | Initial depth-to-water was 493 ft, but it has since declined to 520 ft. A single-screen well was installed in this zone (Broxton et al., 2002a). |
| Mortandad Canyon | I-4<br>540 | 520 | 2-4 | Puye Fm. pebble gravel and silty sands | Top of Cerros del Rio basalt | Tritium, nitrate, perchlorate | A single-screen well was installed in this zone. This well was installed as a possible replacement well for MCOBT-4.4. |
| Mortandad Canyon | R-15<br>1107<br>6820 | 646 | ~99 (?) | Fractured Cerros del Rio basalt | Clay-rich flow-base rubble or underlying silty basaltic sand (745-746.7 ft) | Tritium, nitrate, perchlorate | Saturation in this zone was noted while drilling to reach the regional aquifer (Longmire et al., 2001). Saturation was first encountered at a depth 646 ft, but a zone of increased water production was noted by the driller from 707-717 ft. It is uncertain whether this occurrence represents one zone or multiple, stacked zones. |

**Table 2-B-1.**
**Characteristics of Deep Perched Groundwater Zones Encountered in Wells on the Pajarito Plateau (continued)**

| Watershed | Well Name, Borehole Depth (ft), Surface Elev. (ft) | Depth to Water (ft) | Saturated Thickness (ft) | Groundwater Host Rock | Nature of Perching Layer | Anthropogenic Chemicals Detected | Comments |
|---|---|---|---|---|---|---|---|
| Mortan-dad Canyon | I-5<br>717<br>6820 | 687 | 20 | Interflow breccia in Cerros del Rio basalt | Possible confining unit in massive basalt in lower part of Cerros del Rio basalt | Tritium, nitrate, perchlorate | This well was installed adjacent to R-15 and targeted the water production zone from 707 to 717 ft that was noted in that borehole. A single-screen well was installed in this zone. It is uncertain whether the perched zone was fully penetrated by the borehole. |
| Mortan-dad Canyon | I-6<br>722<br>6811 | 662 | 43 | Interflow breccia and fractured basalt in Cerros del Rio basalt | Possible confining unit in massive basalt in lower part of Cerros del Rio basalt | Tritium, nitrate, perchlorate | This well is 150 ft north of R-15 and I-5, near the Mortandad Canyon stream channel. A single completion well was installed in this zone. The elevation of the SWL is 16 ft higher than at I-5. It is uncertain whether the perched zone was fully penetrated by the borehole. |
| Pajarito Canyon | R-23<br>935<br>6528 | Not known | Not known | Cerros del Rio basalt | Not known | Not sampled | Perched groundwater was probably encountered while drilling R-23 to the regional aquifer. Water accumulated in the annulus between the drill casing and the borehole wall above a clay-rich bridge. The accumulated water is probably from a perched zone within the Cerros del Rio basalt. The perched zone was not screened. |

**Table 2-B-1.**
**Characteristics of Deep Perched Groundwater Zones Encountered in Wells on the Pajarito Plateau (continued)**

| Watershed | Well Name, Borehole Depth (ft), Surface Elev. (ft) | Depth to Water (ft) | Saturated Thickness (ft) | Groundwater Host Rock | Nature of Perching Layer | Anthropogenic Chemicals Detected | Comments |
|---|---|---|---|---|---|---|---|
| Pajarito Canyon | R-19<br>1902.5<br>7066 | 894 | 18 | Puye Fm. sand and gravel beds | Puye Fm. low-porosity sedimentary deposits. | None | R-19 was installed on the mesa south of Threemile Canyon. A perched zone was encountered in Puye Formation fanglomerate overlying Cerros del Rio basalt. Borehole geophysical logs indicate the perched zone is made up of high-porosity sediments overlying low-porosity sediments. A well was installed with seven isolated screens at this site (Broxton et al., 2001d). Screen #2 is complete in this perched zone. |
| Cañon de Valle | R-25<br>1942<br>7516 | 723 | ~409 | Otowi ash-flow tuff, Guaje Pumice bed, and Puye Fm. fanglomerate | Confining layer occurs in Puye Fm. sedimentary deposits. From 1132 to 1137 ft, cuttings of fine-grained sand and silt are interbedded with gravels and cobbles. Alternating wet and dry sediments occur below this zone to a depth of 1286 ft. | High-explosive compounds and their degradation products, trichloroethene, tetrachloro-ethene | This large saturated zone is separated from the regional aquifer (depth at 1286 ft) by 154 ft of alternating wet and dry fanglomerate deposits. This upper saturated zone is currently interpreted as a perched zone with a leaky confining layer. The top of the same upper saturated zone was penetrated in nearby well CDV-16-1(i) which is located in adjacent Cañon de Valle. A multi-screen mesa-top well was installed at R-25 (Broxton et al., 2002b). Four screens are complete in this thick perched zone. |

**Table 2-B-1.**
**Characteristics of Deep Perched Groundwater Zones Encountered in Wells on the Pajarito Plateau (continued)**

| Watershed | Well Name, Borehole Depth (ft), Surface Elev. (ft) | Depth to Water (ft) | Saturated Thickness (ft) | Groundwater Host Rock | Nature of Perching Layer | Anthropogenic Chemicals Detected | Comments |
|---|---|---|---|---|---|---|---|
| Cañon de Valle | CDV-16-1(i) 683 7382 | 563 | >120 ft; not fully penetrated | Otowi ash-flow tuff | Perching horizon not known; below drill hole depth | High-explosive compounds | Because of the proximity of CDV-16-1(i) and R-25 (~375 ft), the upper saturated zone in these wells is probably laterally connected. The top of the upper saturated zone is 28 ft higher in CDV-16-1(i) (elev. 6821 ft) compared with R-25 (elev. 6793 ft). A single-screen well was installed in this zone. |
| Cañon de Valle | CDV-16-2(i) 1063.1 7467 | 827 (?) | Not known | Puye Fm. fanglomerate | Within Puye Fm. fanglomerate; perching lithology not known | High-explosive compounds | The nature of this perched zone is currently under investigation. Borehole video logs, water level measurements, and the presence of high explosives in groundwater samples indicate that perched water is present. However, efforts to install a well in this zone(s) have not been successful. |
| Cañon de Valle | R-26 1490.5 7642 | 173 | Zones of thin, dis-continuous saturation associated with fractures | Fractured densely-welded tuff in unit Qbt 3t of the Tshirege Member | Water production associated with fractures | Analyses pending | A piezometer was installed in a borehole adjaent to well R-26 to monitor water levels in this perched zone. The piezometer is screened from 175 to 185 ft deep, and the depth to water is 173 ft. Saturation appears to be associated with low-angle platy fractures in the ash-flow tuff. |

**Table 2-B-1.**
**Characteristics of Deep Perched Groundwater Zones Encountered in Wells on the Pajarito Plateau (continued)**

| Watershed | Well Name, Borehole Depth (ft), Surface Elev. (ft) | Depth to Water (ft) | Saturated Thickness (ft) | Groundwater Host Rock | Nature of Perching Layer | Anthropogenic Chemicals Detected | Comments |
|---|---|---|---|---|---|---|---|
| Cañon de Valle | R-26<br>1490.5<br>7642 | About 604 | See comments | Cerro Toledo interval | See comments | Analyses pending | R-26 was recently drilled and interpretation of perched water in this zone is preliminary. Borehole geophysical logs suggest high moisture contents below 575 ft to the top of regional saturation at 954 ft. Perched water appears most likely at depths of 580 to 662 ft and 780 to 827 ft. A water level at 604 ft depth was measured during drilling while the borehole was at a depth of 720 ft. Well R-26 was completed with two isolated well screens with the upper screen placed within the perched zone and the lower screen in the regional zone of saturation. |
| Water Canyon | SHB-3<br>860<br>7608 | 663 | > 197 ft (?), probably not fully penetrated | Otowi ash-flow tuff, Guaje Pumice bed, and Puye Fm. fanglomerate | Confining layer probably not penetrated | None | Saturation occurs in the lower Bandelier Tuff and upper Puye Formation. A temporary mesa-top well was installed in the perched zone (Gardner et al., 1993). |

In Pueblo Canyon perched water was identified in four wells. At wells TW-2a and R-5, perched water occurs within fanglomerate of the Puye Formation and has a saturated thickness of >7 and about 11.3 m (>23 and about 37 ft), respectively. Depth to water is 33.5 m (110 ft) at TW-2a and about 115.8 m (380 ft) at R-5. These perched zones probably represent relatively small, unrelated water bodies because of their distance from one another (4 km [2.5 mi]), the lateral heterogeneity of Puye Formation deposits, and their varying depths beneath the canyon floor. Wells TW-1a and POI-4 encountered perched water at depths of 36 to 48.8 m (118 to 160 ft), respectively, in Cerros del Rio basalt. The saturated thickness is about 11 m (37 ft) at TW-1a and 6.4 m (>21 ft) at POI-4. Saturation is associated with interflow breccia and sediments in TW-1a and with fractured basalt at POI-4.

In Sandia and Mortandad Canyons perched water was found in Cerros del Rio basalt and the Puye Formation. The water quality of these perched zones includes a component of treated waste-water effluent released to the canyons via outfalls (Longmire et al., 2001; Longmire, 2002; Broxton et al., 2002b). Depth to water is also similar, ranging from 129 to 152 m (424 to 500 ft) in Sandia Canyon and 150 to 197 m (493 to 646 ft) in Mortandad Canyon.

In Sandia Canyon, well R-12 encountered perched water from depths of 135 to 158 m (443 to 519 ft). Saturation occurs in the lower part of the Cerros del Rio basalt and extends downward into underlying lacustrine facies of the Puye Formation (Broxton et al., 2001a). The perched water in this zone may be confined because the borehole was dry until a depth of 135 m (443 ft) was reached, but the water level rose to a depth of 129 m (424 ft) once saturation was encountered. The apparent confining layer at the top of this zone is a massive basalt flow with few fractures. An alternative explanation for the observed rise in water level is that the groundwater is unconfined, but water-bearing interconnected fracture systems were not intersected by the borehole until a depth of 135 m (443 ft). The perching layer consists of clay- and silt-rich lacustrine deposits 5 m (16.5 ft) thick. The saturated thickness of this groundwater body is at least 23 m (75 ft), making it one of the thickest perched groundwater bodies identified in the eastern part of the Pajarito Plateau.

In Mortandad Canyon perched water was encountered in three boreholes. At well MCOBT-4.4, the top of perched groundwater zone occurs at a depth of about 150 m (493 ft), within pebble gravel made up of dacitic volcanic detritus in the Puye Formation. The saturated thickness of this zone is between 3 and 6 m (10 and 30 ft). The perching layer includes one or more of the following lithologies: 1) silty sands and gravels in the lower part the Puye sequence (153.3 to 157.6 m [503 to 517 ft]), 2) clay-rich brecciated rubble at the top of Cerros del Rio basalt (157.6 to 159.3 m [517 to 522.5 ft]), or 3) the massive, unfractured interior of the uppermost Cerros del Rio flow (approximately 159.3 to 163.1 m [522.5 ft to 535 ft]). At wells R-15 and I-5, located 347 m (1140 ft) down canyon of MCOBT-4.4, perched water occurs within the lower part of a thick sequence of Cerros del Rio basalts. The depth to water is 197 m (646 ft) in R-15 and 209 m (686 ft) in the adjacent well I-5 which is offset 20 m (66 ft). Saturation in both wells occurs in fractured lava flows and interflow breccias. The variable elevations of the top of perched saturation and varied saturated thicknesses of 30 m (99 ft) in R-15 and 8+ m (26+ ft) in I-5 illustrate the hetergeneous nature of perched bodies located within basaltic rocks. In R-15, the perching horizon is clay-rich flow-base rubble or underlying silty basaltic sands; the perched water at I-5 was not fully penetrated. Because of their different geologic settings, the perched

groundwater at MCOBT-4.4 and R-15/I-5 probably represent unrelated groundwater bodies of limited lateral extent. Other deep boreholes in Mortandad Canyon did not encounter perched groundwater. Based on the distribution of available boreholes, the lateral extent of individual perched groundwater bodies is probably less than 460 m (1500 ft).

Both perched water occurrences in Mortandad Canyon contain elevated tritium, nitrate, and perchlorate. The highest contaminant levels occur in MCOBT-4.4, which contains 14,750 pCi/L tritium, 12.5 mg/L nitrate plus nitrite (as N), and 179 ppb perchlorate (Longmire, 2002, personal communication). Since 1963, these contaminants were released to the canyon as liquid effluent by a waste treatment facility in the upper part of the canyon. The presence of contaminants in perched groundwater beneath Mortandad Canyon indicates that vertical transport through the vadose zone occurs on the timescale of decades.

A large area of complex perched groundwater occurrences is found in the region bounded by Cañon de Valle on the north and Water Canyon on the south in the southwest part of LANL. Five deep boreholes encountered significant zones of groundwater over a 2.6 $km^2$ (1 $mi^2$) area located just east of the Pajarito fault zone. These boreholes included R-25, R-26, CdV-16-1(i), CdV-16-2(i), and SHB-3. Depth to water in these perched zones range from about 183 m (600 ft) just east of the Pajarito fault to about 244 m (800 ft) 2.3 km (1.4 mi) farther east of the fault. Only wells R-25 and R-26 fully penetrate the perched water zones.

At R-26, a water-level measurement of 184 m (604 ft) was obtained when the borehole was 219 m (720 ft) deep. The borehole was eventually completed to a total depth of 454.3 m (1490.5 ft) with the regional water table occurring at a depth of approximately 291 m (954 ft). Borehole neutron, magnetic resonance, and induction logs indicate that high moisture contents occur in rocks below 175 m (575 ft), with perched water most likely at depths of 177 to 202 m (580 to 662 ft) and 238 to 252 m (780 to 827 ft). These perched zones occur within stratified volcaniclastic sediments of the Cerro Toledo interval. Low-permeability sediments within the Cerro Toledo interval probably provide the perching horizons.

R-25, located 1524 m (5000 ft) east of R-26, has two distinct zones of saturation separated by 47 m (154 ft) of partially saturated rocks. The upper zone, which is interpreted as a perched zone, occurs between depths of about 217 to 345 m (711 to 1132 ft) within the Otowi Member and in the upper part of the Puye Formation. An interval of partial saturation occurs below the perched zone from 345 to 392 m (1132 to 1286 ft) depth. Partial saturation was defined by casing off the perched zone and drilling through alternating zones of dry and wet rocks by coring and air-rotary methods. From 392 m (1286 ft) to the total depth of 592 m (1942 ft), continuous saturation representing regional groundwater was encountered within Puye deposits. R-25 was constructed with 9 screens separated by packers using a Westbay™ sampling system. Hydraulic head measurements in isolated screens decrease with depth, indicating downward vertical gradients. Isotopic and water quality data suggest the upper and lower zones of saturation at R-25 represent separate groundwater systems (Longmire, 2003, personal communication).

## Table 3-A-1.
## Guaje Canyon Watershed Description

| Hydrogeologic Element | Characteristic | Description |
|---|---|---|
| Surface Water | Flow | Guaje Canyon heads in the Sierra de los Valles on Forest Service land, enters San Ildefonso Pueblo land, and continues to its confluence with lower Los Alamos Canyon approximately a mile west of the Rio Grande (Figure 3-A-1, Figure 3-A-2). Guaje Canyon is part of the Los Alamos Canyon watershed, but is covered separately because it is a large drainage that is largely unaffected by LANL activities. Guaje Canyon contains an interrupted stream with a perennial reach extending from springs located upstream of Guaje Reservoir to some distance downstream of the reservoir. An intermittent reach extends farther downstream to the confluence with lower Los Alamos Canyon. Snowmelt runoff does not reach the Rio Grande. Rendija Canyon heads on the flanks of the Sierra de los Valles and contains an ephemeral stream. Barrancas Canyon heads on the Pajarito Plateau and has intermittent and ephemeral flow. |
| | Quality | There are no known water quality effects of LANL activities. |
| Springs | Name | No springs have been found in any of these canyons. |
| | Quality | See above. |
| Alluvial Groundwater | Extent | Little or no alluvial groundwater is present in these canyons. Only two alluvial wells have been installed in Guaje Canyon to investigate the presence of alluvial groundwater. These wells were completed in the perennial reach of the canyon and alluvial groundwater was encountered near the stream level. For Rendija Canyon and Barrancas Canyon, no alluvial wells have been installed and no alluvial groundwater is known to exist. |
| | Depth/Thickness | See above. |
| | Quality | No impacts of LANL activities on this water are known. |
| Intermediate Groundwater | Extent/Hydrology | No intermediate groundwater wells have been installed and no groundwater is known to occur in these canyons. Drilling of the water supply wells in Rendija Canyon and Guaje Canyon did not find any intermediate groundwater. |
| | Depth/Thickness | See above. |
| | Quality | No LANL liquid discharges have occurred. |

## Table 3-A-1.
## Guaje Canyon Watershed Description (continued)

| Hydrogeologic Element | Characteristic | Description |
|---|---|---|
| Regional Aquifer | Depth/Hydrology | The regional aquifer occurs in the Puye Formation and the Santa Fe Group in the vicinity of Guaje Canyon. The regional aquifer probably includes rocks of the Tschicoma Formation in the western part of the canyon. The regional aquifer supplies water to the supply wells of the Guaje wellfield. Groundwater flow in the regional aquifer is from the northwest, so no Laboratory contaminant sources are located upgradient of Guaje Canyon sites. The aquifer lies at depths of about 230 to 570 ft in the Guaje wellfield. |
| | Quality | The water is of generally good quality except for high levels of naturally occurring arsenic—up to 40 µg/L in older, now-abandoned wells. The EPA MCL for arsenic is 10 µg/L. |
| Contaminants | Potential Sources | These canyons are located north of the Laboratory, mainly on Forest Service land and on San Ildefonso Pueblo. The primary Laboratory activities in the canyons have involved water supply: the Guaje reservoir is no longer in use, and the Guaje wellfield (now operated by Los Alamos County) currently includes five water supply wells. The wells in this field also extend to lower Rendija Canyon. Rendija Canyon contained a small-arms firing range and several sites used as mortar impact areas. Past Laboratory activities are described in more detail in an RFI Work Plan for the North Canyons and an RFI Work Plan for OU 1071. |
| | Type | |
| References:<br>LANL 2001a; LANL 1992g. | | |

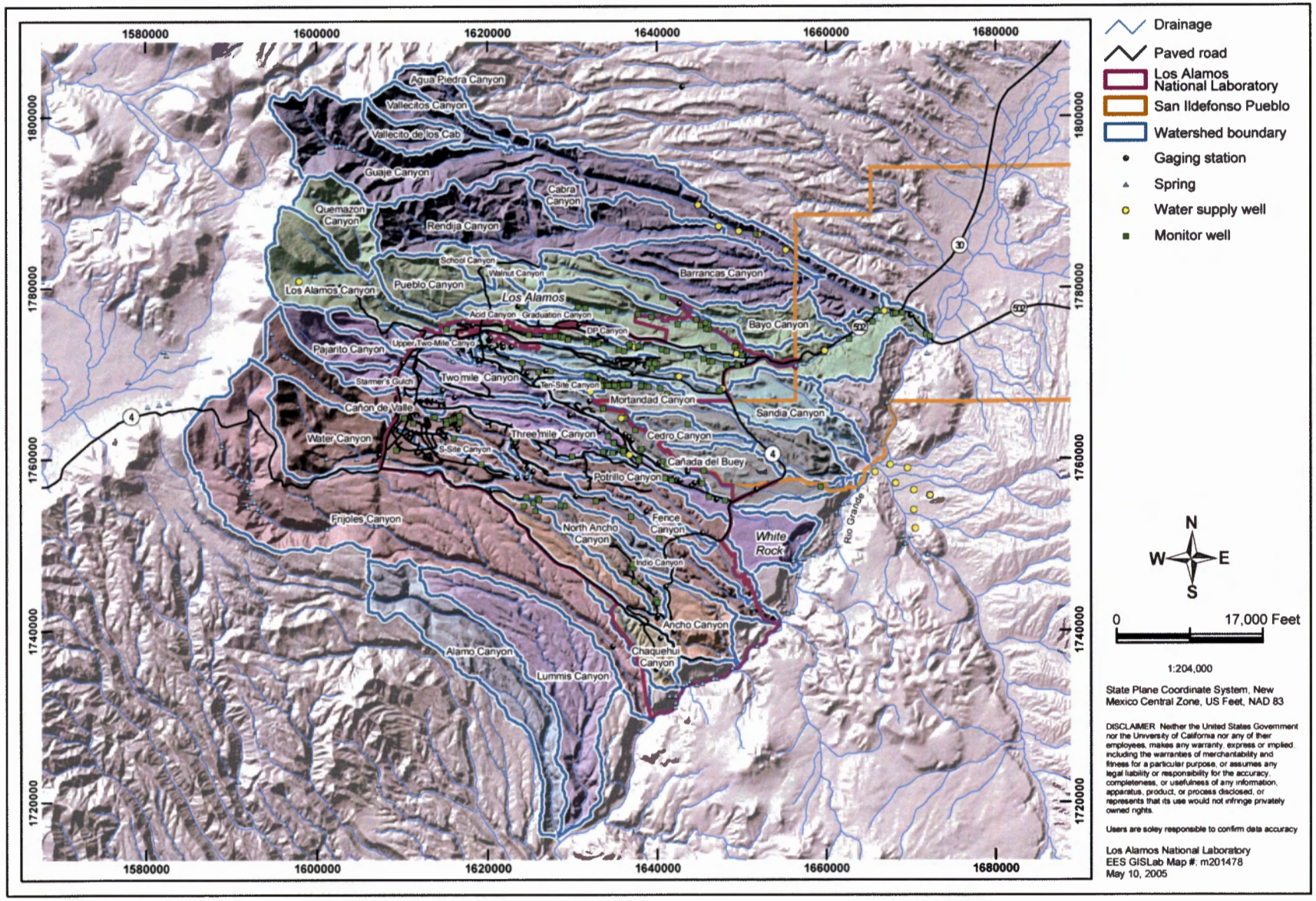


**Figure 3-A-1.** Watersheds on the Pajarito Plateau in the vicinity of Los Alamos National Laboratory.

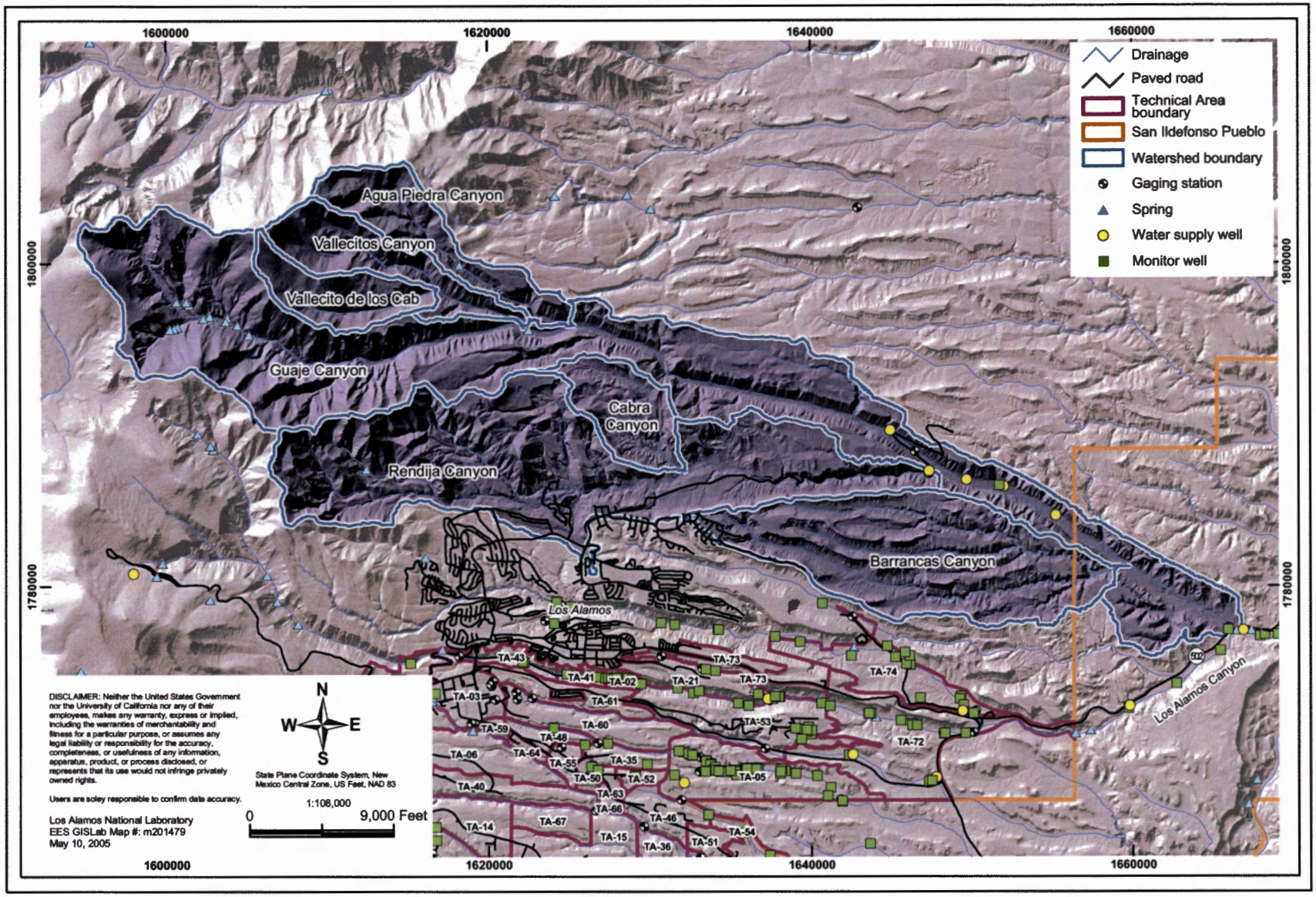


**Figure 3-A-2.** Guaje Canyon watershed.

## Table 3-A-2.
## Los Alamos Canyon Watershed Description

| Hydrogeologic Element | Characteristic | Bayo Canyon | Acid and Pueblo Canyons | DP and Los Alamos Canyons |
|---|---|---|---|---|
| Surface Water | Flow | Bayo Canyon heads on the Pajarito Plateau on land owned by Los Alamos County and extends across the northeast portion of the Laboratory (TA-74), crosses San Ildefonso Pueblo land to the east, and terminates at its confluence with lower Los Alamos Canyon near Totavi (Figure 3-A-1, Figure 3-A-3). The drainage area of Bayo Canyon is about 4 square miles. Surface water flow in Bayo Canyon is ephemeral and intermittent and there are no springs in the vicinity. Stream losses caused by infiltration into the underlying alluvium and evapotranspiration typically prevent surface flow from reaching Los Alamos Canyon.<br><br>No alluvial or intermediate groundwater was encountered during drilling of about 90 boreholes at the TA-10 site in upper Bayo Canyon. Drilling at TA-10 has not found | Pueblo Canyon heads on USFS land, crosses Los Alamos County land, then Laboratory land where it joins Los Alamos Canyon just upstream of the San Ildefonso Pueblo boundary (Figure 3-A-1; Figure 3-A-3). The draingage area of Pueblo Canyon is about 6.5 square miles, including Acid Canyon. Surface water in Pueblo Canyon occurs as ephemeral runoff from precipitation and as perennial flow supported by effluent discharge from the Los Alamos County Sewage Treatment Plant. Generally, ephemeral surface water occurs in the upper portion of Pueblo Canyon following summer rains and snowmelt events, and perennial surface water occurs in the lower portion of Pueblo Canyon because of discharges from the Los Alamos County Sewage Treatment Plant. Surface water in Pueblo Canyon rarely flows across the length of the Laboratory.<br><br>Acid Canyon heads on the Pajarito Plateau in the southwestern portion of the Los Alamos townsite and extends east-northeasterly to its confluence with Pueblo Canyon. The South Fork of Acid Canyon is a short north-trending | Los Alamos Canyon heads on USFS land, crosses Laboratory land, then San Ildefonso Pueblo land before joining the Rio Grande (Figure 3-A-1; Figure 3-A-3). Surface water occurs in Los Alamos Canyon as perennial flow in the upper reaches west of the Los Alamos Reservoir located west of DOE property, and in the lower reaches east of the confluence with Pueblo Canyon. The drainage area of Los Alamos Canyon is about 11.6 square miles, including DP Canyon. Typically, the overflow of water from the reservoir during spring snowmelt results in nearly continuous surface water flow between the western Laboratory boundary and the vicinity of TA-2 for several weeks to several months each year. For most of the year, the only surface flow in Los Alamos Canyon is in lower Los Alamos Canyon due to discharge from the Los Alamos County Sewage Treatment Plant and flow from Basalt and Los Alamos Springs east of the Laboratory boundary.<br><br>Surface water in Los Alamos Canyon rarely flows across the length of the Laboratory except during snowmelt and summer storm events. Most often, surface waters are depleted by infiltration into canyon alluvium creating saturated zones of seasonally variable extent. DP Canyon heads on the Pajarito Plateau in the southeastern portion of the Los Alamos townsite and extends east-southeasterly to its confluence with Los Alamos Canyon. DP Canyon is located entirely within DOE-owned land except for a short segment at the head of the canyon on land owned by Los Alamos County. Surface flow in DP Canyon is generated by rainfall and snowmelt events. DP |

## Table 3-A-2.
## Los Alamos Canyon Watershed Description

| Hydrogeologic Element | Characteristic | Bayo Canyon | Acid and Pueblo Canyons | DP and Los Alamos Canyons |
|---|---|---|---|---|
| | | contamination that extends more than a few feet beneath former release sites. Groundwater in the regional aquifer is as described for Guaje Canyon. | tributary to Acid Canyon. Both of these canyons are entirely within land owned by Los Alamos County. These two canyons drain a surface area that is largely paved and developed. | Spring, located in DP Canyon, discharges continuously except for dry periods, such as during the winter and spring of 1996. |
| | Quality | TA-10 was used as a firing site from 1943 to 1961, for tests with high explosives and radioactive materials. The site included a radiochemistry laboratory. While in operation, the TA-10 sites in Bayo Canyon were investigated for environmental impacts. The site was decontaminated and decommissioned in 1960. TA-10 was the site of an extensive Formerly Utilized Sites Remedial Action Program investigation in 1976. In the mid-1990s the site was studied under a RFI Work Plan for Operable Unit 1079. RFI activities included shrapnel removal and investigation, remediation, or deferred action for several potential release sites. A second RFI work plan was written in 2001. | Key contaminants in Acid Canyon surface water include metals (arsenic, cadmium, manganese, zinc, and cyanide), PAHs (e.g., benzo-a-pyrene, dibenz-a-h-anthracene), and radionuclides (Pu-239, -240, strontium-90, and uranium-234). The metals COPCs are dominated by naturally occurring constituents, or constituents associated with urban runoff. The PAHs are also believed to be associated with runoff from developed areas with the Los Alamos townsite. The radionuclides were detected in bedrock pools in the South Fork of Acid Canyon and are consistent with contaminants found in sediment within the canyon from historical releases from TA-45. The radionuclide contamination generally does not extend beyond the Acid/Pueblo Canyon confluence in detectable concentrations, with the exception of Pu-239, -240 in unfiltered samples. | Key contaminants in upper Los Alamos Canyon surface water include metals (arsenic, manganese, iron, selenium, and cyanide), pesticides, and plutonium-239, -240. The metals are generally considered naturally occurring, although some minor contribution from historical Laboratory releases is possible. The cyanide detects in upper Los Alamos Canyon are believed to be related to combustion of organic matter during the Cerro Grande fire and may also be related to anti-caking and anti-corrosion agents contained in fire retardant. Pesticides are predominantly related to historical use in the Santa Fe National Forest and to use within the Los Alamos townsite. The plutonium-239 is related to outfalls (likely Hillsides 137 and 138) in former TA-1. The Pu-239 is a COPC only for the unfiltered samples indicating the potential that the sample(s) with detections may have contained suspended sediment.<br><br>Key contaminants in DP Canyon surface water and springs include metals (arsenic, copper, lead, manganese, zinc, and cyanide), pesticides, and radionuclides (americium-241, and strontium-90). Chloride is also present. The metals are either naturally occurring or likely related to townsite runoff, since none of the PRSs in DP Canyon are known for metals contamination, the exception |

## Table 3-A-2.
## Los Alamos Canyon Watershed Description

| Hydrogeologic Element | Characteristic | Bayo Canyon | Acid and Pueblo Canyons | DP and Los Alamos Canyons |
|---|---|---|---|---|
| | | | Surface water in Pueblo Canyon above the confluence with Acid Canyon also has metals COPCs and PAHs that are considered to have a source in townsite runoff.<br><br>Surface water in Pueblo Canyon below the confluence with Acid Canyon shows metals COPCs (arsenic, manganese, selenium, and cyanide), and organics COPCs (pesticides and PAHs) that are both likely from townsite, national forest, or Cerro Grande fire sources. Radionuclides include Pu-239, -240, americium-241, and cobalt-60. | being the DP Tank Farm (DPTF, SWMU 21-029) which had lead contamination associated with leaks from the tanks. However, no other of the COPCs from the DPTF are present. The cyanide detections in DP Canyon are from DP Spring and a location at the very head of DP Canyon suggesting a source other than Laboratory operations. The radionuclides are COPCs only for the unfiltered samples indicating the potential that the detections are related to the presence of suspended sediment in the samples. DP Spring consistently shows elevated strontium-90 concentrations related to surface water and alluvial groundwater discharge from Reach DP-2 where strontium-90 is present throughout the sediment due to historical releases from SWMU 21-011(k).<br><br>Key COPCs in surface water and springs in lower Los Alamos Canyon include metals (antimony, arsenic, beryllium, copper, possibly mercury, molybdenum, nickel, selenium, thallium, and cyanide), PAHs (benzo_k_fluoranthene), and pesticides (DDE_4_4_, and DDP_4_4_), and only strontium-90 from unfiltered surface water. The constituents present in lower Low Alamos Canyon appear to be primarily naturally occurring or related to sources other than Laboratory operations. Of the metals identified as COPCs for lower Los Alamos Canyon, only molybdenum (and mercury?) have known Laboratory sources up canyon. The cyanide is believed to be related to the combustion of organic matter during the Cerro Grande fire. Detections of cyanide in the lower canyon are thought to be related to transport of ash from burn areas in the upper watershed during floods. Strontium-90 could be |

## Table 3-A-2.
## Los Alamos Canyon Watershed Description

| Hydrogeologic Element | Characteristic | Bayo Canyon | Acid and Pueblo Canyons | DP and Los Alamos Canyons |
|---|---|---|---|---|
| | | | | from either Los Alamos or Pueblo Canyon, but based on estimated inventories of strontium-90, it is most likely associated with Los Alamos Canyon (specifically SWMU 21-011(k). |
| Springs | Name | There are no springs in Bayo Canyon. | There are no springs in Acid and Pueblo Canyons, | Discharge at DP Spring is highly variable, generally ranging from dry to less than one gallon per minute, and has been observed to respond rapidly to storm-water runoff from upper DP Canyon. Surface water flow generally extends for less than 50 ft down canyon from the point where spring flow joins the stream channel.<br><br>Basalt Spring is recharged by water from the County Sewage Treatment Plant in Pueblo Canyon. It has variable estimated discharge rates from 1 to 10 gallons per minute.<br><br>LA Spring discharges along the south slope of the canyon approximately 300 meters downstream of Basalt Spring. |
| | Quality | See above. | See above. | Chloride, sodium, and manganese, barium, boron, HE, and solvents at concentrations above background. |
| Alluvial Groundwater | Extent | | Two saturated zones are known to occur in the alluvium of Pueblo Canyon. The first is in the upper reach from the headwaters to approximately the Rendija Canyon Fault. The eastern limit of this saturated zone has not been clearly defined and it may extend further down canyon. The second is in the lower reach downstream of the Los Alamos County Sewage Treatment Plant where saturated conditions are supported year-round due to effluent | Two saturated zones are known to occur in the alluvium of Los Alamos Canyon. The first is in the upper part of Los Alamos Canyon and extends eastward from the Los Alamos Reservoir to the vicinity of observation well LAO-4.5 west of State Rte. 4. The second is in the lower part of Los Alamos Canyon and extends from Basalt Spring to the Rio Grande.<br><br>Alluvial groundwater in lower Los Alamos Canyon near Basalt and Los Alamos Springs is chemically similar to surface water flow supported by these springs. The chemistry of the water discharging from Basalt Spring is |

## Table 3-A-2.
## Los Alamos Canyon Watershed Description

| Hydrogeologic Element | Characteristic | Bayo Canyon | Acid and Pueblo Canyons | DP and Los Alamos Canyons |
|---|---|---|---|---|
| | | | releases from the sewage treatment plant. The extent of saturation is variable due to fluctuation in runoff and volume of effluent released during the year. The volume of effluent released into the canyon typically decreases during the spring and early summer months as wastewater from the plant is pumped up canyon for irrigation use on the municipal golf course.<br><br>From 1951 to 1964, surface flow in the mid-reach of Pueblo Canyon was augmented by liquid effluent from the former TA-45 radioactive liquid waste treatment facility via Acid Canyon. In addition, Los Alamos County operated a sewage treatment plant in upper Pueblo Canyon (known as the Pueblo Sewage Treatment Plant) until the current Los Alamos County Sewage Treatment Plant came on-line in 1963. Effluent from these past sources likely supported sustained saturated conditions throughout the mid-reach of Pueblo Canyon as well as shallow bedrock springs such as Hamilton Bend Spring, just west of the current Los Alamos County Sewage Treatment Plant. The sewage treatment plants are sources of boron and nitrate. This | similar to effluent from the Los Alamos County Sewage Treatment Plant. The chemistry of water discharging from Los Alamos Spring may represent an isolated perched system as it does not contain characteristic major ions indicative of sewage effluent.<br><br>Alluvial groundwater in lower Los Alamos Canyon, from the confluence of Guaje Canyon and Los Alamos Canyon to the Rio Grande, shows chemical similarity to both regional aquifer water and surface water from the Rio Grande (LANL, 2004b, 2002, 2001a). |

## Table 3-A-2.
## Los Alamos Canyon Watershed Description

| Hydrogeologic Element | Characteristic | Bayo Canyon | Acid and Pueblo Canyons | DP and Los Alamos Canyons |
|---|---|---|---|---|
| | | | alluvial groundwater may have provided the source for infiltration to intermediate perched zone groundwater or the regional aquifer. Shallow spring flow (including Hamilton Bend Spring) ended following closure of TA-45 and the Pueblo Sewage Treatment Plant. | |
| | Depth/ Thickness | | See above. | In middle and upper Los Alamos Canyon, the saturated thickness in the alluvium varies seasonally from a few feet in the winter months to 25 ft in the spring and summer months when recharge is the greatest. The alluvial groundwater provides recharge to intermediate perched zones by infiltrating along preferential pathways such as faults or permeable bedrock units. |
| | Quality | | Known contaminants at former TA-45 include nitrate, perchlorate, tritium, isotopes of uranium and plutonium, strontium-90, cesium-137, and gross-alpha radiation. The contaminant histories for nitrate, tritium, and strontium-90 illustrate trends in Pueblo Canyon surface water and groundwater. Nitrate has been present from Laboratory radioactive liquid waste effluents and from Los Alamos County Sewage Treatment Plant sanitary effluent. The highest values were found in surface water in the 1950s and 1960s, possibly related to both types of sources. With decommissioning of the radioactive outfall in 1964 and moving | Alluvial groundwater has been found in DP Canyon at wells LAUZ-1 and LAUZ-2, installed for the ER investigation at TA-21. Strontium-90, tritium, and some organic compounds have been detected at LAUZ-1.<br><br>Time series plots of nitrate, tritium, plutonium-239, strontium-90, and molybdenum provide a picture of contaminant trends in Los Alamos Canyon groundwater. Nitrate in discharges into DP Canyon from TA-21 caused surface water and alluvial groundwater concentrations to exceed 100 mg/L (nitrate as nitrogen), or 10 times the MCL, until discharges ceased in 1986. Nitrate concentrations have returned to background since discharges ended.<br><br>TA-21 effluent caused tritium activities in surface water and alluvial groundwater in and downstream of DP Canyon |

## Table 3-A-2.
## Los Alamos Canyon Watershed Description

| Hydrogeologic Element | Characteristic | Bayo Canyon | Acid and Pueblo Canyons | DP and Los Alamos Canyons |
|---|---|---|---|---|
| | | | the sanitary discharge downstream to the Bayo Treatment Plant, less water and less nitrate are present in the upper portion of the drainage in recent years.<br><br>Tritium and strontium-90 histories characterize the radioactive effluent releases into Acid Canyon. Tritium persisted in surface water and alluvial groundwater at fairly high levels for about a decade after effluent releases ceased, but has dropped to background levels since. The highest measured strontium-90 activity was about 500 pCi/L in Acid Canyon surface water in 1960. With no present source, levels have dropped dramatically and strontium-90 is now seen only at low activities, below 1 pCi/L in alluvial groundwater. | to reach values up to 5,000,000 pCi/L or 250 times the MCL. As with nitrate, tritium activities decreased greatly after discharges ceased. In Los Alamos Canyon above the mouth of DP Canyon, the Omega West Reactor cooling line leaked water containing tritium from 1956 to 1993. As a result of this leak, tritium activity in alluvial groundwater remained at values around 10,000 pCi/L or half of the MCL. Once the leak was shut off, tritium levels in Los Alamos Canyon water returned to background.<br><br>Strontium-90 contamination in surface water and alluvial groundwater came from reactor sources at TA-2 and effluent discharges from TA-21. The strontium-90 activity in DP Canyon surface water reached 28,600 pCi/L. There is no present source, and activities of this isotope have dropped greatly after discharges ceased. However, strontium-90 persists in alluvial groundwater at levels above the EPA MCL of 8 pCi/L due to the large inventory in alluvial sediment, providing a source to groundwater. Migration of strontium-90 is considered to be controlled by cation exchange.<br><br>Effects of Manhattan Project releases in upper Los Alamos Canyon cause plutonium-239, -240 activity in alluvial groundwater to remain at about 25% of the DOE 4 mrem drinking water derived concentration guide (DCG) of 1.2 pCi/L. Discharges from TA-21 resulted in plutonium-239, -240 activity in surface water much above the DOE 4 mrem DCG, even exceeding the 100 mrem DCG of 30 pCi/L in the late 1960s. Plutonium activity has decreased substantially with the end of discharges in 1986, but is still |

**Table 3-A-2.**
**Los Alamos Canyon Watershed Description**

| Hydrogeologic Element | Characteristic | Bayo Canyon | Acid and Pueblo Canyons | DP and Los Alamos Canyons |
|---|---|---|---|---|
| | | | | occasionally detected in surface water and alluvial groundwater below the former outfall.<br><br>A short section of alluvial groundwater in Los Alamos Canyon has molybdenum concentrations near or above the New Mexico groundwater standard of 1,000 µg/L. In the early 1990s, molybdenum concentrations in Los Alamos Canyon alluvial groundwater rose sharply above background and exceeded the New Mexico groundwater limit in 2000. The source of this molybdenum is sodium molybdate, a water-treatment chemical commonly used in cooling towers at TA-53. The Laboratory discontinued use of sodium molybdate in June 2002. |
| Intermediate Groundwater | Extent/ Hydrology | | Intermediate perched zones have been identified in two areas beneath Pueblo Canyon. One zone is in the middle reach of Pueblo Canyon where test well (TW)-2A is completed within fanglomerates of the Puye Formation. The perched zone occurs at a depth of about 120 ft. The second is in lower Pueblo Canyon (wells TW-1A and POI-4) within a thick sequence of Cerros del Rio basalts, at a depth of about 188 ft. This intermediate perched zone may be one source of water contributing to the flow from Basalt Spring in Los Alamos Canyon. Fairly rapid communication from Pueblo Canyon surface water and alluvial groundwater to the intermediate perched groundwater was interpreted | Several intermediate perched zones have been encountered in Los Alamos Canyon between TA-2 and State Road 4. A perched zone was encountered at well R-6i east of the facilities at TA-21 on the mesa top. The zone occurs within the Puye Formation at a depth of 593 ft. |

## Table 3-A-2.
## Los Alamos Canyon Watershed Description

| Hydrogeologic Element | Characteristic | Bayo Canyon | Acid and Pueblo Canyons | DP and Los Alamos Canyons |
|---|---|---|---|---|
| | | | by the USGS based on water level measurements and similarities in water quality. | |
| | Depth/Thickness | | See above. | The upper intermediate perched zone occurs within the Guaje Pumice Bed. This zone was encountered in borehole LADP-3 (at 325 ft). This same zone may have been penetrated by test hole H-19, west of the Los Alamos Canyon Bridge. The saturated thickness of this zone decreases from west to east, ranging from 22-ft at LAOI(A)-1.1 to 5-ft at LADP-3. A deeper intermediate perched zone was encountered in LAOI(A)-1.1 in the Puye Formation at about 317 ft. Another hole was drilled from the mesa top at MDA V in TA-21 which is approximately midway between LAOI(A)-1.1 and LADP-3 to investigate the lateral extent of the Guaje Pumice intermediate perched zone under DP Mesa. The MDA V Deep Hole (borehole 21-2523) did not find saturated conditions in the Guaje Pumice Bed at this location, indicating that this intermediate perched zone does not extend northward under DP Mesa. Other intermediate perched zones have been found in the basalt at R-9 near SR-4 at 180 and 275 ft. This well also found three possible saturated zones between depths of 570 and 626 ft, about 100 ft above the regional aquifer. |
| | Quality | | Analysis of water samples from well TW-2A show that this perched zone contains elevated activities of tritium (2,228 pCi/L). This suggests that tritium associated with the former TA-45 treatment plant has infiltrated the canyon floor and migrated vertically, at | Average activities of tritium were 2.98 pCi/L in the perched zone, within the upper Puye Formation at well R-7 east of well LAOI(A)-1.1. Tritium was initially found in LADP-3 at 5500 pCi/L but activity has declined greatly since then, probably related to cessation of the Omega West Reactor cooling line leak in 1993. Average activities of tritium in the two intermediate perched zones at R-9i were 200 pCi/L at |

## Table 3-A-2.
## Los Alamos Canyon Watershed Description

| Hydrogeologic Element | Characteristic | Bayo Canyon | Acid and Pueblo Canyons | DP and Los Alamos Canyons |
|---|---|---|---|---|
| | | | least to the depth of the intermediate perched zone at TW-2A. The tritium history for TW-2A shows a steep decrease the early 1980s, related to the cessation of discharges into Acid Canyon in 1964. Elsewhere in intermediate perched groundwater, tritium has been detected mainly at trace levels. In core from drilling of well R-2, perchlorate was found in more than 50% of the samples.<br><br>Nitrate histories show that concentrations in TW-1A have often been up the 10 mg/L MCL. The high nitrate value in this and other wells in 1994 resulted from a sample preservation error. In about 1980, the Los Alamos County Bayo Sanitary Wastewater Treatment Plant, which discharges into Pueblo Canyon upstream of TW-1, greatly increased discharges. This increase in flow and infiltration apparently resulted in the higher concentrations of nitrate and chloride in TW-1 beginning about 1981. Nitrate (as nitrogen) concentrations in TW-2A, upstream of the Bayo treatment plant, have been 3 mg/L or less. Strontium-90 has not been consistently detected in intermediate perched | 180 ft and 132 pCi/L at 275 ft during characterization sampling.<br><br>Activities of tritium were 3802 pCi/L and concentrations of nitrate (as nitrogen) were 4.20 mg/L. Recharge from DP Canyon is most likely the dominant source of water to this perched intermediate zone.<br><br>Perchlorate has been detected in unsaturated core samples from LADP-3 and R-8. However, perchlorate appears to have a very restricted vertical extent (<15 ft thick) in LA Canyon based on these boreholes. No other perchlorate detections occurred over the 200-350 ft sampling depth in the two boreholes. A similar situation occurs in DP canyon where LAUZ-1 perchlorate is also restricted to a narrow vertical depth range. In this borehole, all but one of the samples were non-detects for perchlorate. Vadose zone cores from DP Mesa boreholes LADP-4 (drilled on a bench above the DP canyon bottom near the former TA-21 radioactive liquid effluent outfall) and borehole 21-2523 (drilled east of MDA V), show a more extensive zone (>200 ft) of perchlorate contamination than occurs in the bottom of Los Alamos or DP canyon. In addition, both of these core holes show co-contamination of chlorate and nitrate. Chlorate has been detected in DP Spring, but chlorate and perchlorate have not been detected in other Los Alamos Canyon surface or groundwater samples. |

## Table 3-A-2.
## Los Alamos Canyon Watershed Description

| Hydrogeologic Element | Characteristic | Bayo Canyon | Acid and Pueblo Canyons | DP and Los Alamos Canyons |
|---|---|---|---|---|
| | | | groundwater. | |
| Regional Aquifer | Depth/ Hydrology | | Depth to the regional aquifer is known in several locations in Pueblo Canyon, including TW-4 in upper Pueblo Canyon, at well TW-2 in the middle reach, and at wells TW-1 and O-1 near the confluence with Los Alamos Canyon. Water level measurements show depths to water to be 1173 ft in 2003 at TW-4, 807 ft in 2001 at TW-2, and 686 ft in 2001 at O-1. Based on Laboratory water-level maps, the general direction of groundwater flow in the regional aquifer is east in the vicinity of Pueblo Canyon.<br><br>East of the Rendija Canyon Fault, the top of the regional aquifer is within the Totavi Lentil of the Puye Formation. | Depth to the regional aquifer is known in several locations in Los Alamos Canyon; at TW-3 and O-4, at O-1 near the confluence with Pueblo Canyon, and at LA-5 and LA-1B in the lower reach. Water level measurements show depths to water to be 784 ft in 2001 at TW-3, 68 ft in 2001 at O-1, 762 ft in O-4 in 1995, and -18 ft (artesian) in 1996 at LA-1B. Based on Laboratory water-level maps, the general direction of groundwater flow in the regional aquifer is east in the vicinity of Los Alamos Canyon. |
| | Quality | | Contaminants have been detected in the regional aquifer, particularly nitrate in TW-1, indicating that the pathways for contaminant migration may be active at least along the lower portion of the canyon. Tritium has been found in TW-1 at up to 360 pCi/L though recent levels are lower at 140 pCi/L. Perchlorate is found within the regional aquifer in Pueblo Canyon, notably in water supply well O-1 at 2.8 ppb using the LC/MS/MS analytical method. Well O-1 | Tritium has been detected in the regional aquifer at up to 80 pCi/L in TW-3 (though recent samples are nondetects) and 24 pCi/L in R-9. In TW-3 nitrate (as nitrogen) values were below 0.3 mg/L prior to 1967, but have averaged above 0.6 mg/L since 1981 with values up to 0.97 mg/L in 1994. Activities of tritium were 181 pCi/L in the regional aquifer at well R-6 during development. Concentrations of nitrate (as nitrogen) were 0.49 mg/L at the well. Concentrations of perchlorate were less than detection (0.0005 ppm) using the ion chromatography method. Because tritium was detected and nitrate concentration is within background, a component of young water containing |

## Table 3-A-2.
## Los Alamos Canyon Watershed Description

| Hydrogeologic Element | Characteristic | Bayo Canyon | Acid and Pueblo Canyons | DP and Los Alamos Canyons |
|---|---|---|---|---|
| | | | also contains a consistent 35-45 pCi/L of tritium and higher nitrate (as nitrogen) than any other regional aquifer well, excluding TW-1. Nitrate (as nitrogen) has been about 1.7 mg/L at well O-1 compared with approximately 0.5 mg/L in other water supply wells.<br><br>Characterization well R-4, west of the Bayo Canyon and Pueblo Canyon confluence, contained 19.49 pCi/L of tritium and 1.39 ppm of nitrate (as nitrogen). These results indicate that the regional aquifer has experienced recent recharge that is most likely the result of past discharges to Acid Canyon to the west of well R-4. | tritium may have originated from a different source other than TA-21. This assumes that tritium, nitrate, and perchlorate were released to the environment at the same time. |
| Contaminants | Potential Sources | | Contaminant sources affecting Pueblo Canyon include two inactive TAs (TA-1 and TA-45). TA-1 included the portion of the present-day Los Alamos townsite where the majority of the theoretical and technical work was accomplished at the Laboratory from 1943–1954. Acid Canyon was the original disposal site for liquid wastes generated by research on nuclear materials for the World War II Manhattan Engineer District atomic bomb project. From 1943 to 1951, Acid Canyon received untreated radioactive industrial effluent from the TA-1 | Several contaminant sources affected upper Los Alamos Canyon. TA-2, located in upper Los Alamos Canyon, was the location of a series of nuclear reactors. The cooling line for the Omega West Reactor leaked water with tritium activity of at least 100,000 pCi/L into the alluvium, probably from 1956 until 1993. TA-21, which is on DP Mesa, north of Los Alamos Canyon, was the site of plutonium processing facilities. The site discharged treated liquid radioactive effluent into DP Canyon from 1952 to 1986 and includes Material Disposal Areas A, B, T, U, and V. TA-41, located in upper Los Alamos Canyon, was used for testing of nuclear weapons components. TA-53, the site of the Los Alamos Neutron Science Center (LANSCE) linear accelerator facility, lies on the mesa south of the canyon. |

## Table 3-A-2.
## Los Alamos Canyon Watershed Description

| Hydrogeologic Element | Characteristic | Bayo Canyon | Acid and Pueblo Canyons | DP and Los Alamos Canyons |
|---|---|---|---|---|
| | | | research activities. The TA-45 treatment plant was completed in 1951 and discharged treated effluents containing residual radionuclides into Acid Canyon from 1951 to 1964. TA-73 is the site of the DOE airport and former landfill, above Pueblo Canyon. Pueblo Canyon also receives sanitary effluent from Los Alamos County Sewage Treatment Plant in Bayo Canyon. The county operated two other sewage treatment plants along Pueblo Canyon in the past.<br><br>More detailed information about these sites can be found in the Task/Site Work Plan for Operable Unit 1049, Los Alamos Canyon and Pueblo Canyon, and the RFI Work Plans for Operable Units 1078, 1079, 1100, and 1106. | Water from National Pollutant Discharge Elimination System (NPDES) permitted outfalls, sanitary treatment, and reactor beam cooling water ponds flowed to Los Alamos Canyon. TA-1 included the portion of the present-day Los Alamos townsite where the majority of the theoretical and technical work was accomplished at the Laboratory from 1943 to 1954. Several facilities discharged untreated chemical waste streams into the canyon. |
| | Type | | Septic tank outfall located on the south rim of Acid Canyon in the 1940s containing plutonium-239, -240 and PCBs. Former Pueblo Canyon WWTP operated from 1951 until 1991. Sludge from the Pueblo Canyon Sewage Treatment Plant contained metals at levels above background. Former Central Sewage Treatment Plant operated from 1947 until 1961. Metals and organic chemicals, including mercury and DDT, were contaminants | TA-1 Hillsides 137, 138, and 140 received discharges from septic tank outfalls from 1943 until the late 1950s. Radionuclides are the primary contaminants at these hillside sites, although some metals contamination is also present).<br>TA-2 housed a series of research nuclear reactors, including the Omega West Reactor, which was a source of tritium releases into alluvial groundwater. Other SWMUs at TA-2 include leach fields for water boiler reactors. Cesium-137 and strontium-90 are primary contaminants associated with the leach fields, and strontium-90 has historically been detected in alluvial groundwater monitoring wells |

## Table 3-A-2.
## Los Alamos Canyon Watershed Description

| Hydrogeologic Element | Characteristic | Bayo Canyon | Acid and Pueblo Canyons | DP and Los Alamos Canyons |
|---|---|---|---|---|
| | | | identified at the outfalls. Outfalls from former TA-1 and former TA-45. TA-45 was the site of the first radioactive liquid waste treatment facility. TA-1 outfalls into Acid Canyon were not treated. These outfalls were the most significant sources of radionuclide and other contamination in Acid and Pueblo Canyons. Plutonium-239,-240 is the primary contaminant, although other radionuclides, metals, and some organic chemicals are also present. | down canyon of the site.<br><br>TA-41 was used for weapons development and long-term studies of weapon subsystems. The primary contaminant sources are a septic system and a sewage treatment plant. Initial data from these SWMUs indicate radionuclides at levels above background, but characterization of TA-41 is incomplete. TA-21 was the site of a plutonium processing plant and polonium and tritium research laboratories. Outfalls were the primary source of radionuclide contaminants in DP and upper Los Alamos Canyons. Radionuclides, particularly cesium-137, and strontium-90, are the primary contaminants discharged from this outfall.<br><br>TA-53 includes a proton accelerator and associated experimental and support buildings used for research with subatomic particles; it is the current site of the Los Alamos Neutron Science Center (LANSCE). The accelerator became fully operational in 1974. Occasional releases occurred from three surface impoundments at the east end of TA-53, referred to as consolidated SWMU 53-002(a)-99, which have contributed contamination to an unnamed tributary drainage to Los Alamos Canyon. The impoundments received sanitary, radioactive, and industrial wastewater from various TA-53 buildings as well as septic tank sludge from other Laboratory buildings. The northern impoundments were active from the early 1970s until 1993. The southern impoundment was active from 1985 until 1998. Inorganic chemicals, organic chemicals, and radionuclide COPCs have been identified at the |

## Table 3-A-2.
## Los Alamos Canyon Watershed Description

| Hydrogeologic Element | Characteristic | Bayo Canyon | Acid and Pueblo Canyons | DP and Los Alamos Canyons |
|---|---|---|---|---|
| | | | | impoundments and in the drainage.<br><br>SWMU 21-018(a), Material Disposal Area (MDA) V, received liquid waste effluent from laundry operations and includes three absorption beds on the south side of DP Mesa that sometimes overflowed into Los Alamos Canyon. Sediment sampling in 1946 documented that plutonium from this source was entering the main channel in Los Alamos. Additional outfalls that discharged off the south rim of DP Mesa include SWMUs 21-023(c), 21-024(b), 21-024(c), 21-024(i), and 21-027(a).<br><br>SWMU 21-029, the DP Tank Farm, was a fuel distribution station with aboveground and underground fuel tanks from 1946 to 1985. Diesel range organic (DRO) and gasoline range organic (GRO) hydrocarbon contamination was identified at two areas of bedrock seeps in the DP Canyon channel and observed to periodically form a sheen in surface water adjacent to the site. The MDAs at TA-21 are not considered to be important from the perspective of releases to the canyons. |

References:

Broxton et al. 1995; Broxton et al. 2001a; Davis et al. 1996; Gallaher 2000; Glasco 2000; Griggs 1964; Kingsley 1947; Kleinfelder 2004a; Koch et al. 2004; Koch and Rogers 2003; LANL 1981; LANL 1991; LANL 1992a; LANL 1992c; LANL 1994b; LANL 1995; LANL 1996; LANL 1998b; LANL 2001a; LANL 2004a; LANL, 2004b; LASL 1963; Longmire 2002a; Longmire and Goff 2002; Mayfield et al. 1979; Newman 2003; Purtymun and Rogers 2002; Rogers 1998.

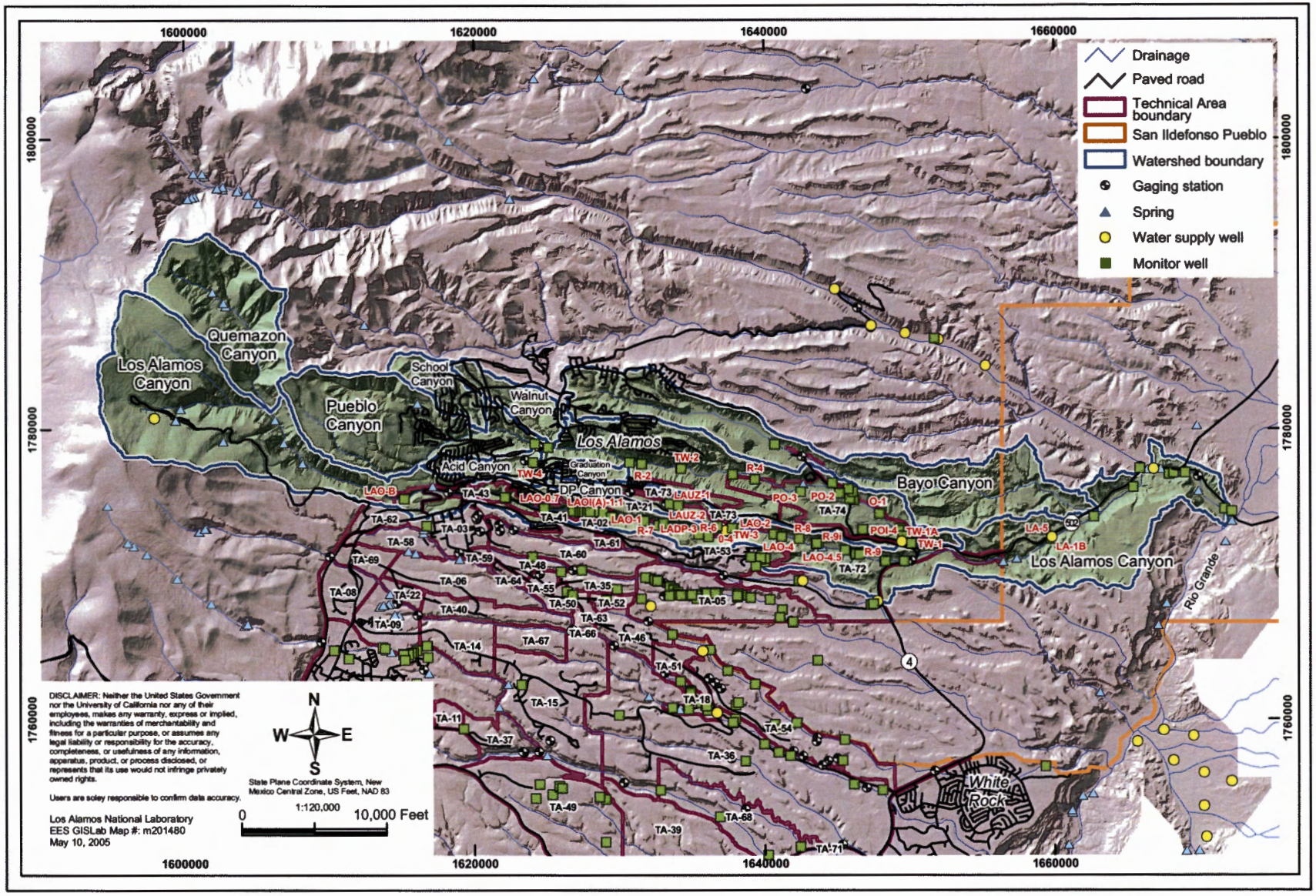


**Figure 3-A-3.** Los Alamos Canyon watershed, including Los Alamos Canyon, Bayo Canyon, Acid Canyon, Pueblo Canyon, and DP Canyon.

## Table 3-A-3.
## Sandia Canyon Watershed Description

| Hydrogeologic Element | Characteristic | Description |
|---|---|---|
| Surface Water | Flow | Sandia Canyon is located on the plateau within the central part of the Laboratory (Figure 3-A-1, Figure 3-A-4). The canyon heads on Laboratory property within TA-3 at an elevation of approximately 7300 ft and trends east-southeast across the Laboratory, Bandelier National Monument, and San Ildefonso Pueblo land, and reaches the Rio Grande in White Rock Canyon at an elevation of 5450 ft. Sandia Canyon has a relatively small total drainage area of about 5.5 $mi^2$.<br><br>Surface water occurs in Sandia Canyon as ephemeral runoff from precipitation and as NPDES-permitted effluent discharge from the Laboratory sanitary wastewater sewage treatment plant and the TA-3 power plant. On a volume basis, baseflow in Sandia Canyon represents one of the largest potential non-natural groundwater recharge sources at the Laboratory. The NPDES outfalls support perennial and intermittent flow within the upper 2.5 miles of the canyon, and a wetland has developed because of the artificial flows. The lower 9.5 miles of channel is ephemeral. |
| | Quality | Surface water quality reflects sewage effluent with nitrate, chloride, and metals slightly above background by approximately 2 to 5 times. Stream sediments contain PCBs and they are detected in surface water at low levels. |
| Springs | Name | Sandia Spring discharges about 1 gpm approximately 0.5 mile from the Rio Grande. |
| | Quality | Contaminant levels are at detection or background levels. |
| Alluvial Groundwater | Extent | Little is known about the occurrence of alluvial groundwater in Sandia Canyon. Most likely, infiltration of surface water creates a saturated zone of seasonally variable extent within the alluvium in the upper reach of the canyon. However, the extent and thickness of alluvial groundwater has not been characterized. Two wells were installed in 1990 to look for alluvial groundwater near the eastern Laboratory boundary as part of the HSWA permit special conditions. Both wells, SCO-1 and SCO-2, were dry at the time of installation. Periodic attempts to sample these wells as part of the Laboratory's annual environmental surveillance activities have found no water in the wells. |
| | Depth/Thickness | See above. |
| | Quality | NA |

## Table 3-A-3.
## Sandia Canyon Watershed Description (continued)

| Hydrogeologic Element | Characteristic | Description |
|---|---|---|
| Intermediate Groundwater | Extent/Hydrology | An intermediate perched zone was found within basalts near SR-4. |
| | Depth/Thickness | The perched zone is at about 440 ft in well R-12. |
| | Quality | The perched zone has tritium above background (60 to 160 pCi/L). In the borehole for R-11, nitrate (as nitrogen) was above background, at about 4.9 mg/L of nitrate (as nitrogen) at a depth of 443 ft bgs. |
| Regional Aquifer | Depth/Hydrology | The regional aquifer lies at about 800 ft depth below Sandia Canyon near SR-4. |
| | Quality | Tritium in well R-12 is about 45 pCi/L, and is above background. Concentrations of nitrate (as nitrogen) were 0.5 ppm at the regional water table during drilling. Characterization well R-11 west of supply PM-3 contained 12.8 pCi/L of tritium and 4.91 ppm of nitrate (as nitrogen), indicating that this well has experienced recent recharge. The $\delta^{15}N_{air}$ of nitrate values were +0.5 and +0.7% for the sample, which suggests that nitrate has not undergone fractionation, and the two values are very consistent with that of nitrate derived from neutralized nitric acid. The most likely source of this unique nitrate at well R-11 is Mortandad Canyon, which has a long history of discharges containing nitrate derived from neutralized nitric acid. |
| Contaminants | Potential Sources | Potential Release Sites (PRS) within the watershed are located at TAs-3, -53, -60, -61, -72, and former TA-20. The Laboratory started use of Sandia Canyon lands during the 1940s. The Laboratory's primary use of Sandia Canyon has been for liquid waste disposal from industrial and sanitary systems, particularly the treated effluents from the TA-46 Sewage Treatment Plant and cooling tower blowdown from the TA-3 power plant. Other sources include discharges from the TA-53 accelerator, the protective force small arms live firing range at TA-72, and a small high explosives firing site near TA-3 (former TA-20). |
| | Type | Nitrate, perchlorate, chromium, copper, PCBs in sediments, HE compounds, tritium, isotopes of uranium and plutonium, lead in surface soils. |

References:
Broxton et al. 2001b; Kleinfelder 2004c; LANL 1996; Longmire 2002c; Purtymun and Stoker 1990.

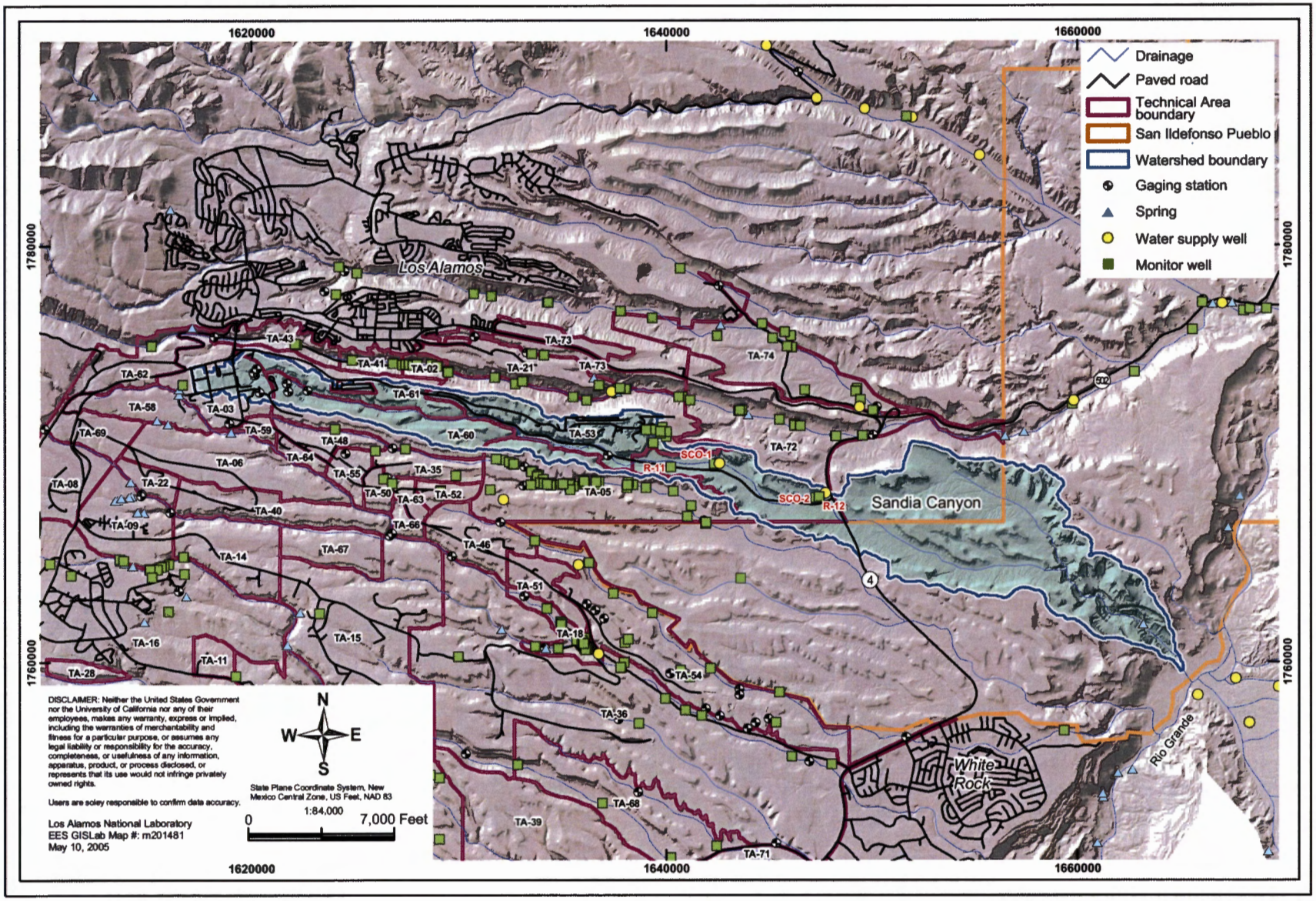


**Figure 3-A-4.** Sandia Canyon watershed.

## Table 3-A-4.
## Mortandad Canyon Watershed Description

| Hydrogeologic Element | Characteristic | Mortandad Canyon | Cañada del Buey |
|---|---|---|---|
| Surface Water | Flow | Mortandad Canyon is an east to southeast trending canyon that heads on the Pajarito Plateau near the main Laboratory complex at TA-3 at an elevation of 7380 ft above sea level (Figure 3-A-1, Figure 3-A-5). The drainage extends about 9.6 mi from the headwaters to its confluence with the Rio Grande at an elevation of 5440 ft asl covering an area of 5 square miles. The canyon crosses San Ildefonso Pueblo land for several miles before joining the Rio Grande. Tributary canyons to the Mortandad Canyon drainage include Effluent Canyon, Ten Site Canyon, Cedro Canyon, and Cañada del Buey.<br><br>Surface water in Mortandad Canyon is ephemeral; however, there are two segments that are effluent-dependent. The ephemeral segments flow only in response to precipitation. Historical Environmental Surveillance Program (ESP) data indicate that persistent surface flow occurs in the effluent-dependent segments at the surface water stations down canyon from the Radioactive Liquid Waste Treatment Facility (RLWTF) outfall (measured at gage E200, Mortandad below Effluent Canyon) and the Los Alamos County sewage treatment plant outfall in White Rock. | Cañada del Buey has a drainage area of 4.2 square miles and within the Laboratory boundary, it is ephemeral in character, based on flow data from three gages: E218 (Cañada del Buey near TA-46), E230 (Cañada del Buey above SR-4), and E225 (Cañada del Buey near MDA G). In the period from 1995 to 2002, the number of days of flow per year ranged from 38 at the gage near TA-46 to zero near MDA G. East of LANL in White Rock, Cañada del Buey has effluent-supported flow from the Los Alamos County sewage treatment plant, which discharges into Cañada del Buey about 2 mi upstream of its confluence with Mortandad Canyon and results in effluent-supported surface flow that regularly extends to the Rio Grande. |
| | Quality | Historically, the following constituents have been detected in Mortandad Canyon surface water at significant levels relative to standards: americium-241, plutonium-238 and plutonium-239, -240, strontium-90, tritium, nitrate, perchlorate, and fluoride. | Operational NPDES-permitted outfalls associated with Cañada del Buey include: 13S associated with the TA-46 SWSC Plant (effluent is sampled at 13S but not discharged; all SWSC effluent is routed to TA-3); and 04A-118 associated with water supply well Pajarito Mesa #4. |

## Table 3-A-4.
## Mortandad Canyon Watershed Description (continued)

| Hydrogeologic Element | Characteristic | Mortandad Canyon | Cañada del Buey |
|---|---|---|---|
| Springs | Name | No springs are present in Mortandad Canyon. However, some wetland areas occur in Pratt Canyon and occur locally downstream. | No springs are present in Cañada del Buey. |
| | Quality | See above. | See above. |
| Alluvial Groundwater | Extent | The extent, quality, and flow of alluvial groundwater in Mortandad Canyon is known from years of investigations. Major recharge to the alluvium occurs from effluent released in the upper canyon. The alluvial groundwater extends about 2 mi downstream from the TA-50 outfall. | Cañada del Buey contains a shallow perched alluvial groundwater system of limited extent, and only two observation wells here have ever contained water. Purtymun (1995) suggested that the primary source of the alluvial water is purge water from supply well PM-4, although storm water and snowmelt runoff augment the alluvial groundwater. However, the presence of water in the alluvium does not correspond to releases from the water supply wells. |
| | Depth/Thickness | The saturated portion of the Mortandad Canyon alluvium is generally less than 10 feet thick and there is considerable variation in saturated thickness depending on the amount of precipitation and runoff in any particular year. Groundwater flow velocity in the alluvium varies from about 60 ft/day in the upper canyon to about 7 ft/day in the lower canyon and has been estimated to be 30 to 40 ft/day between MCO-5 and MCO-8.2. | See above. |
| | Quality | Historically, the following constituents have been detected in alluvial groundwater in Mortandad Canyon at significant levels relative to standards: americium-241; plutonium-238 and plutonium-239, -240; strontium-90; tritium; nitrate; perchlorate; and fluoride. Nitrate (as N) concentrations in alluvial groundwater have generally reflected the concentration in RLWTF effluent. The nitrate concentration in the effluent decreased in 1999 due to improved treatment in the RLWTF, | Some alluvial groundwater samples have contained high levels of gross alpha and gross beta, but have no regular detection of any measured radioisotopes. |

## Table 3-A-4.
## Mortandad Canyon Watershed Description (continued)

| Hydrogeologic Element | Characteristic | Mortandad Canyon | Cañada del Buey |
|---|---|---|---|
| | | and alluvial groundwater concentrations have fallen below the NM groundwater standard of 10 mg/L as a result.<br><br>Perchlorate measurements are available since about 2000. The RLWTF started operating a system for removing perchlorate from the plant effluent on March 26, 2002. Prior to removal, perchlorate was measured in RLWTF effluent at an annual average concentration of 169 ppb in 2001; it has not been detected above 4 ppb since. Alluvial groundwater concentrations have fallen rapidly due to effluent improvement.<br><br>During the last 10 years, tritium has been found above the 20,000 pCi/L EPA MCL at the Laboratory only in alluvial groundwater in Mortandad Canyon. At the end of 2000, the RLWTF adopted a voluntary goal of having tritium activity in its effluent below 20,000 pCi/L, and tritium activity in the effluent dropped below that in 2001 and was 10,400 pCi/L in 2003. Tritium activity in alluvial groundwater downstream has dropped correspondingly with a maximum value of 8,770 pCi/L in 2003.<br><br>The discharge from the RLWTF into Mortandad Canyon creates a localized area of alluvial groundwater where strontium-90 persists at activities above the 8-pCi/L EPA drinking-water MCL. The radionuclides plutonium-238; plutonium-239, -240; and americium-241 are also present above the 4-mrem DOE DCG for drinking water. | |
| Intermediate Groundwater | Extent/Hydrology | Perched groundwater was encountered during drilling of R-15 and MCOBT-4.4 in different stratigraphic zones within the | No intermediate perched groundwater has been found in wells drilled near Cañada del Buey. These wells include |

## Table 3-A-4.
## Mortandad Canyon Watershed Description (continued)

| Hydrogeologic Element | Characteristic | Mortandad Canyon | Cañada del Buey |
|---|---|---|---|
| | | Cerros del Rio basalt. The lateral extent of these intermediate depth perched zones is unknown. | PM-4, R-21, and R-22, as well as numerous wells drilled to investigate conditions beneath MDA L and MDA G. |
| | Depth/Thickness | Intermediate perched groundwater was found at MCOBT-4.4, where a single screen was set in a perched zone within the upper Puye Formation/Cerros del Rio basalt at a depth of 524 ft below ground surface (bgs). In R-15, perched groundwater was encountered at a depth of 646 ft bgs in the lower portion of the Cerros del Rio basalt. | See above. |
| | Quality | Measurements from core samples in several wells indicate that there is a large inventory of perchlorate and nitrate in the unsaturated Bandelier Tuff, extending to distances of 400 feet below the floor of Mortandad Canyon. Preliminary estimates suggest there is 415 to 1250 kg of perchlorate in the upper 300 ft of the vadose zone. Analytical results from groundwater samples collected from MCOBT-4.4 showed 12,797 pCi/L tritium, 13.2 mg/L nitrate plus nitrite (as N), and 142 ppb perchlorate. Perched groundwater encountered during the drilling of R-15 contained 3770 pCi/L tritium and 12 ppb perchlorate.<br><br>Five additional intermediate-depth wells have been drilled and groundwater samples collected from the boreholes near the sediment traps. They contained nitrate, perchlorate, and tritium at concentrations similar to, but less than, those measured at well MCOBT-4.4. | See above. |
| Regional Aquifer | Depth/Hydrology | The regional water table occurs within the Puye Formation in the four wells that encounter the regional aquifer in the Mortandad Canyon watershed. In Ten Site Canyon, approximately 3700 ft west of the confluence with Mortandad Canyon, the regional aquifer was encountered at a depth of | Regional aquifer conditions for Cañada del Buey are covered in the column for Mortandad Canyon and the table for Pajarito Canyon. |

## Table 3-A-4.
## Mortandad Canyon Watershed Description (continued)

| Hydrogeologic Element | Characteristic | Mortandad Canyon | Cañada del Buey |
|---|---|---|---|
| | | 1182 ft in well R-14. In Test Well 8 the regional aquifer occurs at a depth of 994 ft. The regional aquifer was encountered at a depth of 964 ft in R-15, located in Mortandad Canyon approximately 2000 ft east of the confluence with Ten Site Canyon. In well R-13, located approximately 5800 feet ESE of R-15, the regional aquifer was encountered at a depth of 833 ft. Well R-28 lies between R-15 and R-13 and the regional water table occurs at 889 ft. Flow in the regional aquifer is generally west to east; some deviation may be present due to pumping in the Pajarito Mesa well field. Average flow velocity for the regional aquifer in the vicinity of Mortandad Canyon is estimated to be about 95 ft/yr. | |
| | Quality | Wells R-13 and R-14 have not shown contamination in the regional aquifer from samples collected during drilling and/or subsequent characterization. Regional aquifer well R-15 contained 2.4 mg/L nitrate (as N), 18 pCi/L tritium, and up to 4.2 ppb perchlorate in groundwater sampled at a depth of 1019 ft bgs. Well R-28 contains 7.2 mg/L of nitrate (as N) in a borehole sample, and 114 pCi/L of tritium. | Well R-21 contained 0.42 pCi/L of tritium and 0.299 µg/L of perchlorate (using liquid chromatography/mass spectrometry. Well R-21 is not impacted from Laboratory discharges. |
| Contaminants | Potential Sources | The source of contaminants to Mortandad Canyon has been from two liquid waste treatment plants. One is the NPDES-permitted outfall from the TA-50 Radioactive Liquid Waste Treatment Facility. It has been used to treat liquid radioactive waste from Laboratory operations from 1963 to the present. A second radioactive wastewater treatment plant at TA-35 treated wastes from reactor experiments from 1951 to 1963. It did not operate well, and large volumes of wastewater were released into Ten Site Canyon.<br><br>Other mesa-top sites that could impact Mortandad Canyon | Cañada del Buey is bordered on the south by Material Disposal Areas G and L at TA-54. |

## Table 3-A-4.
## Mortandad Canyon Watershed Description (continued)

| Hydrogeologic Element | Characteristic | Mortandad Canyon | Cañada del Buey |
|---|---|---|---|
| | | include MDA C near TA-50 and three waste oil surface impoundments at TA-35 closed in 1989. More information about the history of these sites and planned investigations can be found in the RFI Work Plans for OU 1129 and OU 1147. | |
| | Type | The effluents discharged from TA-3, TA-35, TA-48, and TA-50 have contained a variety of contaminants, including nitrate, perchlorate, tritium, cesium-137, strontium-90, americium-241, and several isotopes of uranium and plutonium. | Past discharges included accidental releases from experimental reactors and laboratories at TA-46. The Los Alamos County sewage treatment plant contributes flow to the lower portion of Cañada del Buey. |

References:

Baltz et al. 1963; Broxton et al. 2002; Kleinfelder 2004d; LANL 1992b; LANL 1992h; LANL 1997; LANL 2000a; LANL 2001a; LANL 2002; LANL, 2003a; Longmire et al. 2001a; Newman 2003; Purtymun et al. 1983; Purtymun 1995.

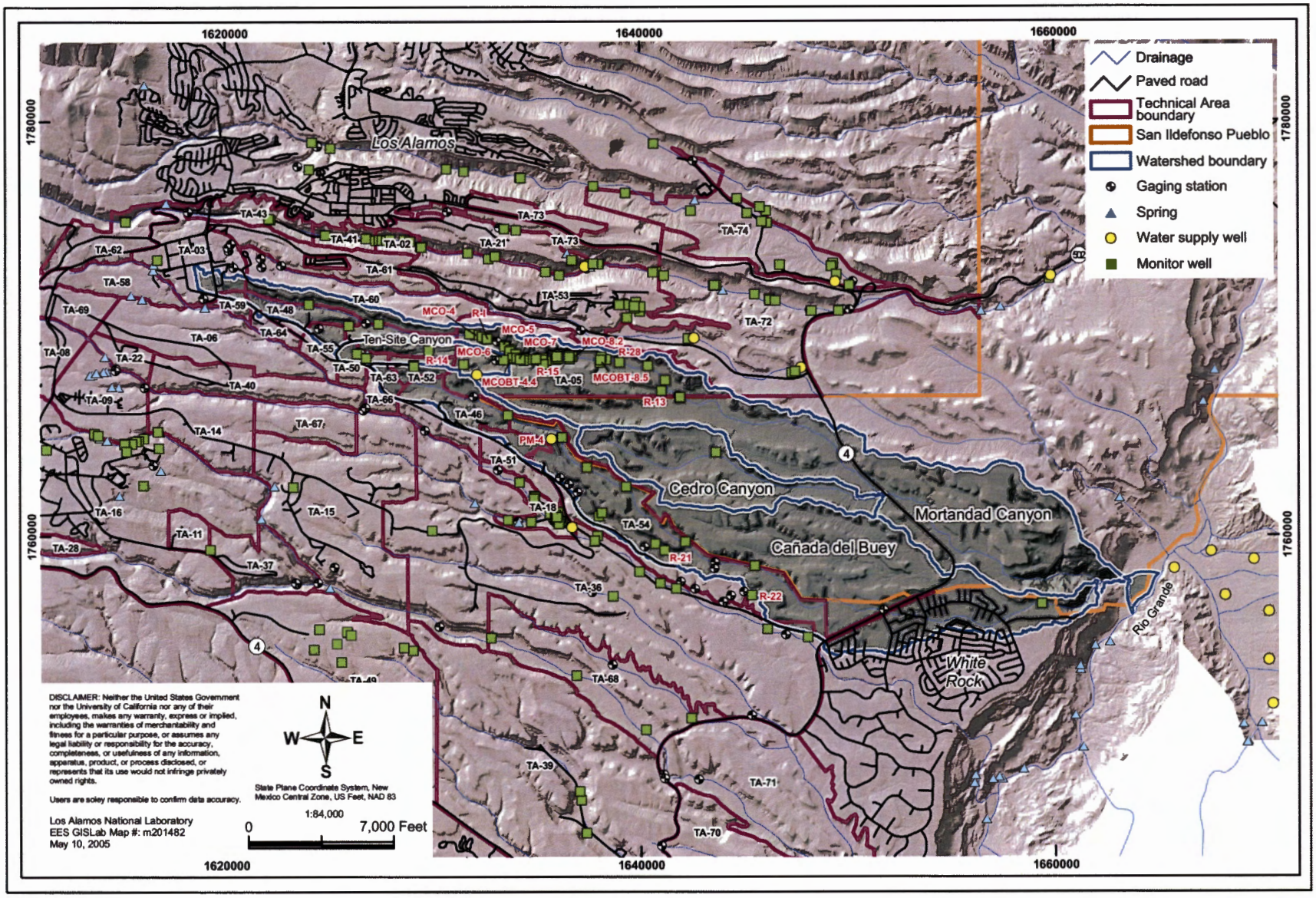


**Figure 3-A-5.** Mortandad Canyon Watershed including Mortandad Canyon and Cañada del Buey.

## Table 3-A-5.
## Pajarito Canyon Watershed Description

| Hydrogeologic Element | Characteristic | Description |
|---|---|---|
| Surface Water | Flow | Pajarito Canyon is located on the Pajarito Plateau in the central part of the Laboratory (Figure 3-A-1; Figure 3-A-6). The canyon heads in the Santa Fe National Forest west of the Laboratory boundary at an elevation of approximately 10,434 ft and trends east-southeast across the Laboratory and Los Alamos County. It empties into the Rio Grande in White Rock Canyon at an elevation of 5422 ft. The drainage area of the Pajarito Canyon watershed is about 12 square miles.<br><br>Surface water occurs in Pajarito Canyon mostly as intermittent flow. Short reaches of perennial flow occur downstream of spring discharges in Starmers Gulch and below Spring 4A in White Rock Canyon. Surface water flow is ephemeral in central Pajarito Canyon between the confluences with Twomile and Threemile Canyons. Flow is also ephemeral through White Rock. In Twomile Canyon, flow is ephemeral west of TA-3 and is possibly intermittent from TA-3 to the confluence with Pajarito Canyon. Three-mile Canyon is ephemeral except for a possible intermittent reach supported by springs above the confluence of Three-mile and Pajarito Canyons. |
| | Quality | High explosive compounds and metals have been detected in surface water in upper and middle Pajarito Canyon. There are no surface water chemistry results for Twomile Canyon except for a small tributary near building SM-30 in TA-3. Samples from the tributary show elevated arsenic and mercury in nonfiltered samples. RDX, SVOCs, and pesticides have been detected in a surface water sample in Threemile Canyon. |
| Springs | Name | Short reaches of perennial flow occur down stream of spring discharges in Starmers Gulch and below Spring 4A in White Rock Canyon. In the western portion of Pajarito Canyon, springs discharge from canyon slopes above the alluvium. The probable source of these springs is groundwater perched within the upper part of the Tshirege Member of the Bandelier Tuff. Typical discharge rates are approximately 1 to 15 gallons per minute. Springs include PC, Homestead, Upper Starmer, Charlies, Garvey, Perkins, Starmer, Josie, Keiling, and Bulldog Springs.<br><br>Springs issue from the canyon floor of upper Twomile Canyon in TA-3 and TA-58. These springs include Hanlon, Anderson, SM-30, SM-30A, and TW-1.72 Springs. There are two springs in the floor of Threemile Canyon (Threemile and TA-18 Springs). |

**Table 3-A-5.**
**Pajarito Canyon Watershed Description (continued)**

| Hydrogeologic Element | Characteristic | Description |
|---|---|---|
| | Quality | HE compounds have been detected in spring water at TA-8 and TA-9. There are no screening data for springs in Twomile Canyon. HE compounds have been detected in Threemile Canyon. |
| Alluvial Groundwater | Extent | There are no alluvial wells in Pajarito Canyon upstream of TA-18. Therefore, information about the nature and extent of alluvial groundwater is limited. Most likely, infiltration of surface water creates a continuous saturated zone within the alluvium that extends from the Pajarito fault zone across the Laboratory to White Rock.<br><br>Alluvial wells have been installed between TA-18 and state road NM4, which demonstrate the presence of alluvial groundwater in this part of Pajarito Canyon. The drilling of seven test holes in 1985 showed that the saturation in lower Pajarito Canyon does not extend laterally under Mesita del Buey near MDAs G and L. Three of the alluvial test holes were completed as groundwater monitoring wells (PCO-1, -2, -3). An additional 20 alluvial wells were installed between 1990 and 1998 by the Environmental Restoration Project as part of the RFI for TA-18. There are no alluvial wells in Twomile Canyon and the extent of alluvial groundwater, if present, is unknown.<br><br>There are no alluvial wells in Twomile Canyon and the extent of alluvial groundwater, if present, is unknown. Alluvial groundwater has been documented in lower Threemile Canyon at 18-BG-1 and 18-MW-8. |
| | Depth/Thickness | Wells PCO-1, -2, and -3 are probably representative of alluvial groundwater between TA-18 and state road NM-4. When installed during 1985, depth to water was 1.3 ft in PCO-1, 6.3 ft in PCO-2, and 3.1 ft in PCO-3. Assuming continuous saturation in the alluvium, the saturated thickness is about 9.7 ft in PCO-1, 2.7 ft in PCO-2, and 8.9 ft in PCO-3. The saturated thickness and presence of water in these wells vary seasonally. Due to drought, these wells have had little water since 2000. At well 18-BG-4 in Threemile Canyon, the water level was 2.5 ft bgs. |
| | Quality | Data indicate the presence of metals, radionuclides, high explosives, VOCs, and anions in alluvial groundwater. Except for VOCs and some radionuclides in wells near TA-18, occurrence of these constituents is irregular and at low levels. There are no water quality data for alluvial groundwater in Twomile Canyon. Alluvial groundwater has been documented in lower Threemile Canyon at 18-BG-1 and 18-MW-8. In lower Threemile Canyon RDX and VOCs have been detected in 18-MW-8. |
| Intermediate Groundwater | Extent/Hydrology | Intermediate perched water is likely to occur beneath Pajarito Canyon, but knowledge of its extent and quality is incomplete. No water quality data for perched intermediate systems are available with current wells. Perched water was suggested during the drilling of PM-2 and SHB-4 in the vicinity of TA-18. At PM-2, a "show of water at 335 ft" was noted in the Otowi Member of the Bandelier Tuff during the cable-tool drilling. In SHB-4, the core tube and core from the top of the |

## Table 3-A-5.
## Pajarito Canyon Watershed Description (continued)

| Hydrogeologic Element | Characteristic | Description |
|---|---|---|
| | | Otowi Member from about 125 ft to 145 ft came out of the hole wet.<br><br>Test Holes 5 and 6 were drilled in 1950 to investigate perched groundwater in Pajarito Canyon south of TA-54. Test Hole 5 was drilled through the Bandelier Tuff and into basalts at a total depth of 263 ft. Test Hole 6 was also drilled through the tuff and into basalts to a total depth of 300 ft. These dry test holes indicate that perched water does not occur in the upper part of the vadose zone in this part of the canyon.<br><br>Between 2000 and 2002 regional wells R-20, R-22, R-23, and R-32 were installed in lower Pajarito Canyon. Perched intermediate water was not identified during the drilling of wells R-20, R-22, and R-32. At R-23, near the eastern Laboratory boundary, there were indications that perched intermediate water may be present in Cerros del Rio basalt. However, R-23 is only screened in the regional aquifer.<br><br>In Twomile Canyon, well 03-MW-1 is a 28-ft-deep mesa top well that samples shallow intermediate perched water near building SM-30 at TA-3. A thin zone of saturation occurs in the upper Tshirege Member. Characterization well R-19, located on the mesa south of Threemile Canyon, had indications of possible perched water at depths of 834 to 840 ft and 894 to 912 ft. Both zones were screened in the completed well, but only the 894 to 912 ft interval (screen 2) in the Puye Formation yields water. |
| | Depth/Thickness | See above. |
| | Quality | Characterization sampling for 03-MW-1 found elevated concentrations of Hg, tritium, and VOCs. A RFI Work Plan is being prepared to determine the extent of this perched zone. Four rounds of characterization sampling for R-19 indicate there are no impacts to the intermediate perched water from Laboratory operations. Less than detection activities of tritium indicate that groundwater in the perched zone pre-dates atmospheric nuclear testing. |
| Regional Aquifer | Depth/Hydrology | Water-level maps indicate that in the vicinity of Pajarito Canyon the general direction of groundwater flow in the regional aquifer is east to southeast. Depth to the regional aquifer is known in Pajarito Canyon at supply well PM-2 and in characterization wells R-20, R-22, R-23, and R-32. The nonpumping water level for PM-2 in 2001 was at a depth of 855 ft. In 2002, the regional water table was at a depth of 826 ft in R-20, 890 ft in R-22, 828 ft in R-23, and 776 ft in R-32. R-23 is completed with a single well screen, R-20 and R-32 have three well screens, and R-22 has five well screens. The regional aquifer probably discharges at Spring 4A and other springs along White Rock Canyon.<br><br>There are no regional aquifer wells associated with Twomile Canyon. Well R-19 is located on the mesa south of Threemile |

## Table 3-A-5.
## Pajarito Canyon Watershed Description (continued)

| Hydrogeologic Element | Characteristic | Description |
|---|---|---|
| | | Canyon. It is down gradient from firing site IJ in TA-36 and is up gradient of TA-18. In addition to two screens in the vadose zone (described above), R-19 has five screens in the regional aquifer. |
| | Quality | Water quality of the regional aquifer beneath eastern Pajarito Canyon shows little, if any, impacts from LANL operations. Four rounds of characterization sampling at R-22 yielded possible detects of Tc-99 in the first sampling round for screens 3 and 4, but it was not detected in any of the screens during subsequent sampling rounds. Tritium was detected above background (~1 pCi/L) in screen 2 (76.6 pCi/L) during the first sampling round, but was at background for subsequent sampling rounds. Tritium activities in screen 5 were slightly elevated relative to background in the four characterization sampling rounds (3.5 to 18.5 pCi/L). Surveillance sampling of PM-2 shows the groundwater meets regulatory standards.<br><br>Wells R-20 and R-32 contained low levels of tritium less than 3 pCi/L (1.98 pCi/L of tritium for well R-20 and 2.84 pCi/L for well R-32). Followup sampling at well R-32 did not confirm the presence of low-level tritium. Low-level perchlorate was not detected at well R-20 and was detected at wells R-23 (0.21 to 0.41 µg/L) and well R-32 (0.21 to 0.29 µg/L). Results for both low-level tritium and low-level perchlorate for these three wells suggest that the regional aquifer is not significantly impacted from Laboratory discharges. The dominant fraction of groundwater in the regional aquifer is greater than 61 years of age, based on the non-detectable tritium.<br><br>Four rounds of characterization sampling at R-19 indicate there are no impacts to the regional groundwater from Laboratory operations. Less than detection activity of tritium at R-19 indicate that the regional groundwater pre-dates nuclear testing. |
| Contaminants | Potential Sources | The primary Laboratory use of Pajarito Canyon watershed has been as the canyon-bottom location for the Los Alamos Critical Experiments Facility (LACEF) at TA-18 and for mesa-top surface and subsurface material disposal areas (MDAs) F at TA-6, Q at TA-8, MDA M at TA-9, and MDAs G, H, J, and L at TA-54. Runoff from firing sites in TA-15 and TA-36 may also be a contaminant source. A detailed description and data summary for Pajarito Canyon potential contaminants is contained within the work plan for Pajarito Canyon. |
| | Type | Pajarito Canyon: metals, radionuclides, HE compounds, VOCs, anions; Twomile Canyon: mercury, tritium, VOCs; Threemile Canyon: HE compounds, VOCs. |

References:
Broxton et al. 2001c; Cooper et al. 1965; Devaurs 1985; Devaurs and Purtymun 1985; Gardner et al. 1993; Griggs 1955; Griggs 1964; LANL 1998a; LANL 2000b; Longmire 2002d; Longmire 2002e; Purtymun 1995.

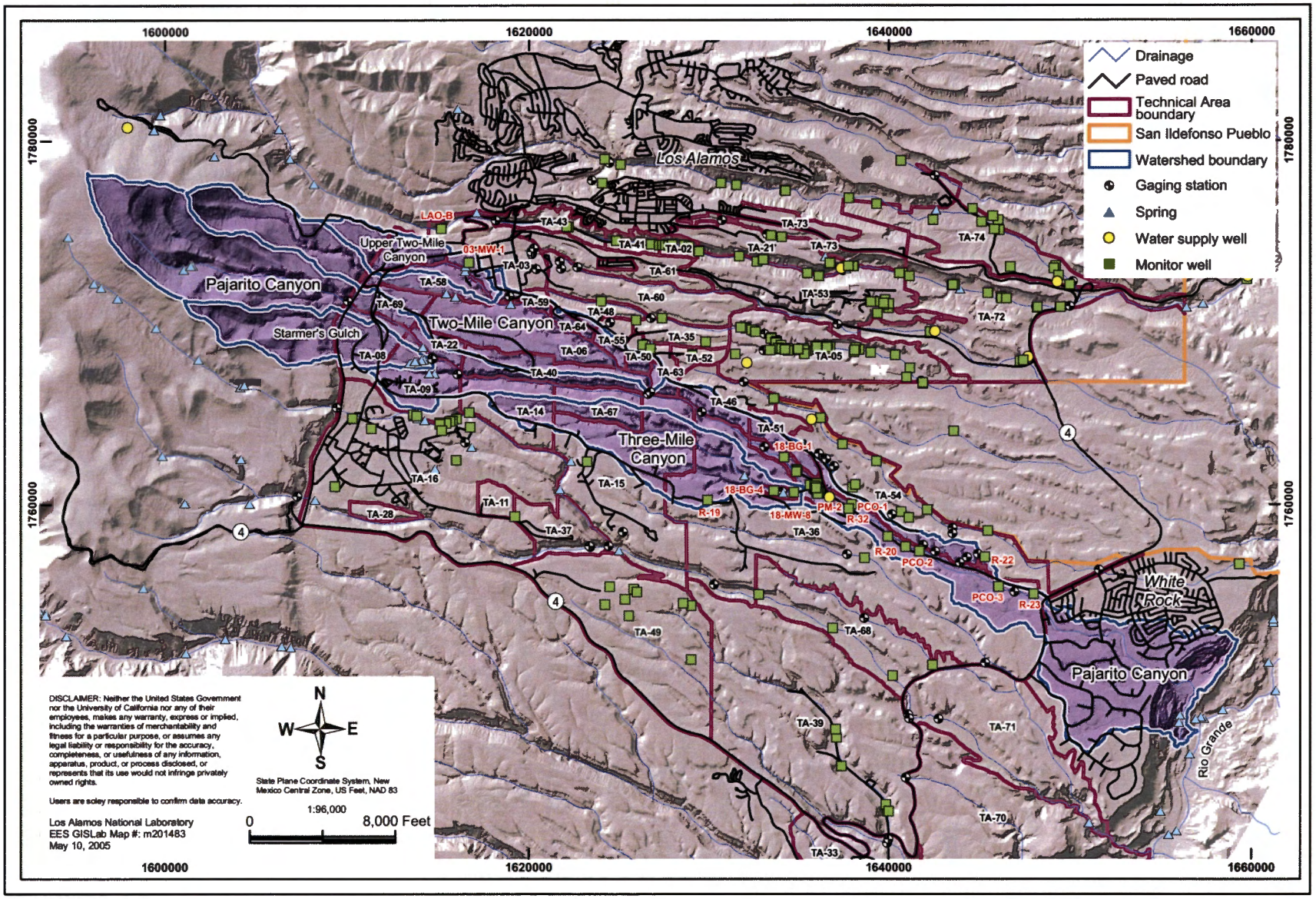


**Figure 3-A-6.** Pajarito Canyon watershed.

## Table 3-A-6.
## Water Canyon Watershed Description

| Hydrogeologic Element | Characteristic | Water Canyon | Cañon de Valle | Potrillo and Fence Canyons |
|---|---|---|---|---|
| Surface Water | Flow | The Water Canyon drainage area is about 6 square miles. Surface water flow in upper Water Canyon is perennial from SR 501 to the eastern edge of TA-28 (Figure 3-A-1, Figure 3-A-7). Intermittent surface water occurs in upper Water Canyon (gage E252, Water above SR-501), primarily in the spring. In middle Water Canyon, flow is ephemeral at gage station E265.2 (Water below SR-4). Lower Water Canyon is ephemeral. | Cañon de Valle has a drainage area of 4 square miles and surface water is perennial from Burning Ground spring to gage E256 (Cañon de Valle below MDA P). Intermittent surface water occurs from natural and anthropogenic sources to gage E262 (Cañon de Valle above Water) Figure 3-A-1, Figure 3-A-7). | The drainage area of Potrillo Canyon and Fence Canyon together is about 4.5 square miles and the surface water flow is entirely ephemeral. |

## Table 3-A-6.
## Water Canyon Watershed Description (continued)

| Hydrogeologic Element | Characteristic | Water Canyon | Cañon de Valle | Potrillo and Fence Canyons |
|---|---|---|---|---|
| | Quality | Except for flow from the Water Canyon Gallery, no surface water quality data are available for upper Water Canyon. In middle Water Canyon, surface water chemistry results show contaminant levels are at detection or background levels. In lower Water Canyon, uranium is significantly greater than background in surface water (>10 ppb) near the firing sites, yet no significant elevation in concentration is seen at State Road 4. | Surface water concentrations of barium are 2-3 mg/L and concentrations of RDX are more than 100 µg/L or ppb. | See above. |
| Springs | Name | Water Canyon Gallery is a spring that issues from the Bandelier Tuff west of LANL in Water Canyon. Spring 5A is in lower Water Canyon. | Several springs issue from the Bandelier Tuff in the upper reaches of Cañon de Valle: Armistead Spring, American Spring (west of LANL) and SWSC, Burning Ground, Martin, and Hollow Springs, and others (in LANL). Note that Martin Spring actually flows into Water Canyon. It is included here because of its close location to the Cañon de Valle springs, and similar contaminant constituents. | There are no springs in Potrillo Canyon or Fence Canyon. |
| | Quality | Water quality data indicate that concentrations of constituents are consistent with other springs within the Sierra de los Valles. | For the on site springs, chloride, sodium, manganese, nitrate, barium, boron, HE compounds, and solvents are at concentrations above background. As in the alluvial system, the main contaminants of concern are HE compounds and barium. HMX, RDX, and TNT concentrations range | See above. |

## Table 3-A-6.
## Water Canyon Watershed Description (continued)

| Hydrogeologic Element | Characteristic | Water Canyon | Cañon de Valle | Potrillo and Fence Canyons |
|---|---|---|---|---|
| | | | up to 32, 330, and 3 µg/L, respectively. Barium concentrations range up to 1310 µg/L. Martin and Fishladder canyons are above 6.1 ppb RDX as well. | |
| Alluvial Groundwater | Extent | In upper Water Canyon, some alluvial groundwater is likely to occur near the headwaters. The occurrence and duration of alluvial groundwater likely decreases down canyon, given limited addition of water, lack of springs and seeps, and rare discharge from tributary canyons. Alluvial groundwater in Martin Canyon (a small tributary canyon to Water Canyon) is intermittent. In middle Water Canyon, alluvial groundwater is present in WCM-1 and WCM-2, but no water is present in WCO-1, WCO-2, and WCO-3. The downstream extent of alluvial groundwater may be between the WCM-2 and WCO-1. | A thin (typically <10 ft thick) alluvial system in Cañon de Valle near SWSC and Burning Ground Springs has perennial saturation. However, alluvial saturation does not extend to the confluence with Water Canyon. The down-canyon extent of saturation is highly variable and fluctuates depending on weather conditions. Saturation is also restricted by the limited extent of alluvium in the canyon. Six alluvial wells are used for water level monitoring and for alluvial water sampling. | In Potrillo Canyon, there is one known occurrence of alluvial groundwater in moisture access hole POTM-2. Several other boreholes have been drilled near this area to define the extent of the groundwater found in POTM-2 but all are dry.<br><br>In Fence Canyon, no occurrences of alluvial groundwater have been documented. However, only one well was installed, well FCO-1, located near State Road 4. Based on physiography, no alluvial groundwater is expected at that location. |
| | Depth/Thickness | The alluvium is typically less than 10 ft thick. | See above. | See above. |
| | Quality | Groundwater quality in Martin Canyon shows primarily barium and high explosives as contaminants but also nitrate, many metals and organics, including values above WQCC standards. | Groundwater quality shows primarily barium and HE compounds including HMX, RDX, and TNT as contaminants. HMX, RDX, and TNT concentrations have been measured up to 610, 759, and 46 µg/L, respectively. High explosive degradation products and perchlorate | See above. |

## Table 3-A-6.
## Water Canyon Watershed Description (continued)

| Hydrogeologic Element | Characteristic | Water Canyon | Cañon de Valle | Potrillo and Fence Canyons |
|---|---|---|---|---|
| | | | have also been detected. Barium concentrations range up to 18,000 µg/L. | |
| Intermediate Groundwater | Extent/Hydrology | No perched water was encountered in any of the holes and all holes have remained dry with the exception of core hole CH-2. DT-5, DT-5P, and four core holes (CH-1, CH-2, CH-3, and CH-4) were drilled to depths of 300 to 500 ft at the main experimental area and more than 50 experimental holes were drilled as deep as 142 ft in Areas 1, 2, 2A, 2B, 3, and 4 from 1959 to 1961. CH-2 may have an undetected natural perched zone; however, this seems unlikely because this recharge pathway apparently developed more than a decade after the hole was completed. | At depths of a few hundred feet, transient zones of perched saturation within the Bandelier Tuff have been identified in two boreholes beneath the TA-16 mesa between Water Canyon and Cañon de Valle. These zones may be related to the perched water that feeds the numerous Cañon de Valle springs. | No perched zones are known in the area of these canyons, although little drilling has been done. |
| | Depth/Thickness | See above. | Wells R-25 and SHB-3 encountered a thick perched zone in the lower Otowi and upper Puye that apparently extends beneath a large portion of the mesa; at R-25 the perched zone extends in depth from 711 to 1132 ft. The lateral extent of this perched zone has not been determined, however. | See above. |
| | Quality | See above. | The transient saturation contains HE and barium contamination and appears to be from former and active HE waste water lagoons on the mesa top rather than to the building 260 | See above. |

**Table 3-A-6.**
**Water Canyon Watershed Description (continued)**

| Hydrogeologic Element | Characteristic | Water Canyon | Cañon de Valle | Potrillo and Fence Canyons |
|---|---|---|---|---|
| | | | outfall. HMX, RDX, and TNT concentrations range up to 21, 2 490, and 1.3 µg/L, respectively. Barium concentrations range up to 1790 µg/L.<br><br>High explosive compounds (for example, 84 µg/L RDX), HE degradation intermediates (2-amino-4,6-dinitro-toluene and 4-amino-2,6-dinitrotoluene), chlorinated solvents, and boron were detected in the perched zone at R-25. The tritium activity in this well is up to 140 pCi/L in the intermediate perched zone, indicating a component of recharge within the last 50 years.<br>The unsaturated soils and tuff that make up the TA-16 mesa, and the alluvial sediments and soils of Cañon de Valle and Martin Canyon contain variable and localized inventories of HE and barium. Core holes in the vicinity of the 260 outfall in particular show detections of these contaminants in the upper few hundred feet of the vadose zone. | |
| Regional Aquifer | Depth/Hydrology | Information on the regional aquifer near Water Canyon is discussed in the table for Ancho Canyon. | Well R-25 encountered the regional aquifer at 1286 ft. | By projecting depths from water supply well PM-2, the regional aquifer lies 730 ft below the bottom of Potrillo Canyon and 620 ft below the bottom of Fence Canyon. |
| | Quality | See above. | High explosives were detected in R-25 although this may have been from | See above. |

**Table 3-A-6.**
**Water Canyon Watershed Description (continued)**

| Hydrogeologic Element | Characteristic | Water Canyon | Cañon de Valle | Potrillo and Fence Canyons |
|---|---|---|---|---|
| | | | cross contamination from the upper saturated zone above, which occurred during drilling (Longmire 2005). High explosives concentrations are decreasing in the regional aquifer samples with time, while they are remaining relatively constant in the upper saturated zone. Tritium activity has decreased during sampling, remaining above 2 pCi/L, suggesting a component of recharge in the past 61 years.<br>Well R-18 located north of well R-25 contained less than -0.32 pCi/L of tritium, less than 0.001 ppm of perchlorate, and concentrations of HE compounds and degradation intermediates were less than detection (0.48 to 1.5 µg/L method detection limit). Well R-18 has not experienced recharges within the past 61 years and the well is not impacted from Laboratory discharges. | |
| Contaminants | Potential Sources | In upper Water Canyon, potential contaminant sources include TA-11, TA-15, and TA-16. Potential contaminants include HE compounds, barium, and solvents. In middle Water Canyon, TA-49 is a potential contaminant source possibly contributing isotopes of uranium and plutonium, lead, beryllium, and HE compounds such as TNT, RDX, HMX, | In Cañon de Valle, potential contaminant sources include TA-8, TA-9, TA-11, TA-14, TA-15, and TA-16. | In Fence Canyon and Potrillo Canyon, firing sites at TA-36 are potential sources of contaminants. |

## Table 3-A-6.
## Water Canyon Watershed Description (continued)

| Hydrogeologic Element | Characteristic | Water Canyon | Cañon de Valle | Potrillo and Fence Canyons |
|---|---|---|---|---|
| | | and barium nitrate. For lower Water Canyon, TA-14, TA-15, and TA-36 are potential sources of high explosives such as TNT, nitrocellulose, trinitramines (RDX), and pentaerythritol tetranitrate (PETN). Metals may also be associated with the explosives (uranium, barium, beryllium, lithium hydride, lead, mercury, copper, and zinc). | | |
| | Type | Soils in several of these operational areas have high levels of uranium contamination. More information for upper Water Canyon may be found in the RFI Work Plan for Operable Unit 1082. For middle and lower Water Canyon, additional detail is contained in the RFI Work Plan for Operable Unit 1144 and RFI Work Plans for Operable Units 1085, 1086, and 1130. | Potential contaminants include HE compounds, barium, nitrate, and solvents. More information may be found in the RFI Work Plan for Operable Unit 1082 and the associated RFI reports. | TNT, nitrocellulose, trinitramines (RDX), and PETN. Metals may also be associated with the explosives (uranium, barium, beryllium, lithium hydride, lead, mercury, copper, and zinc). Soils in several of these operational areas have high levels of uranium contamination. |

References:
LANL 1992f; LANL 1993a; LANL 1993d; LANL 1993e; LANL 1994a; LANL 1998b; LANL 2003b.

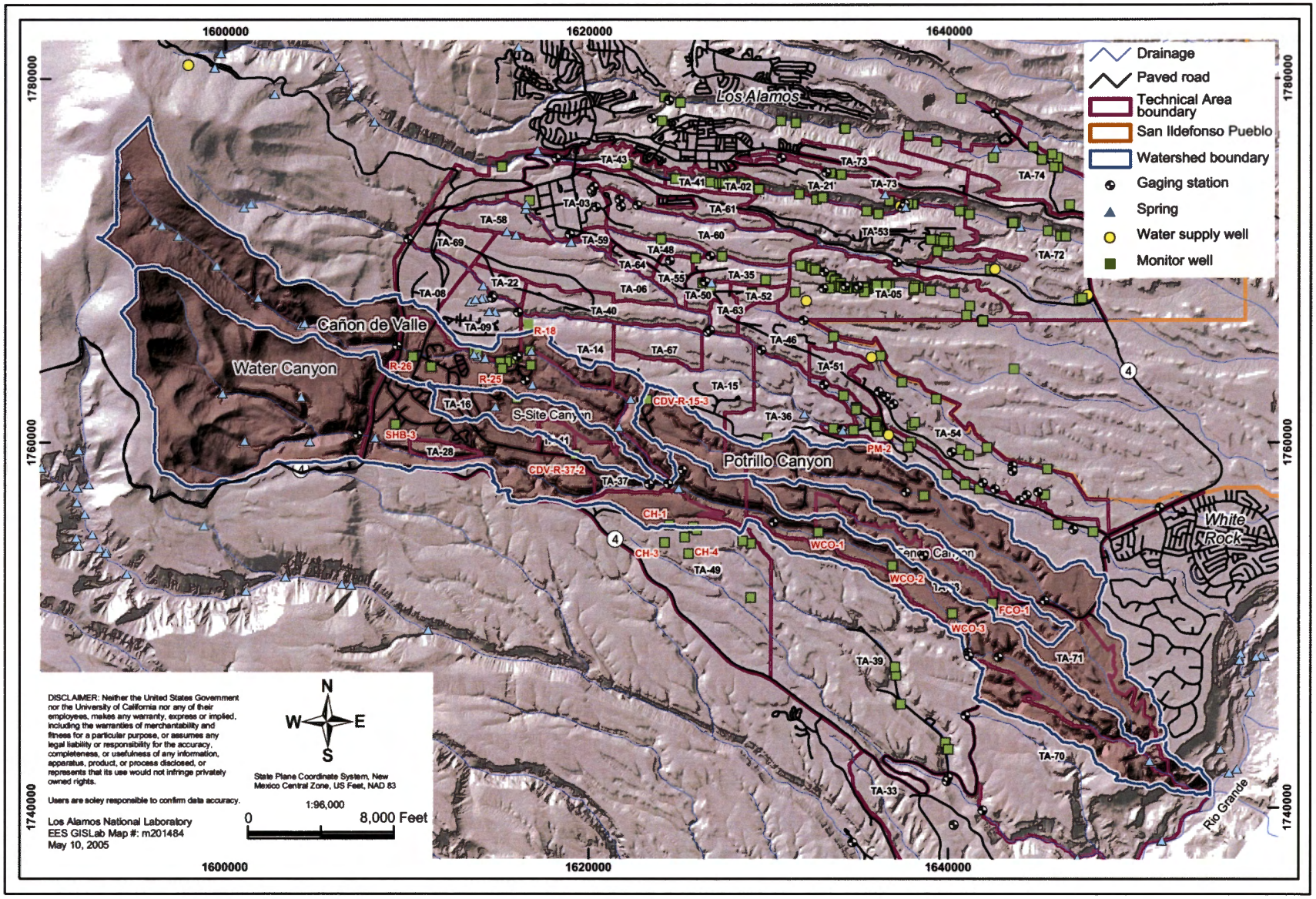


**Figure 3-A-7.** Water Canyon watershed including Pajarito Canyon, Cañon de Valle, Potrillo Canyon, and Fence Canyon.

## Table 3-A-7.
## Ancho Canyon Watershed Description

| Hydrogeologic Element | Characteristic | Description |
|---|---|---|
| Surface Water | Flow | Ancho Canyon lies in the southeastern part of the Laboratory (Figure 3-A-1; Figure 3-A-8) and has a drainage area of 6.7 square miles. Ancho Canyon heads on the Pajarito Plateau and for the most part has ephemeral flow. The canyon has two main branches. Beginning less than a mile above the Rio Grande, flow in Ancho Canyon is perennial, fed by Ancho Spring, a regional aquifer spring. |
| | Quality | |
| Springs | Name | Ancho Spring |
| | Quality | Analysis of water at Ancho Spring by the Environmental Surveillance Program indicates occasional presence of HE compounds and trace levels of depleted uranium. Because the spring issues from the canyon floor, it is uncertain whether these contaminants are being transported by groundwater or if they are being mobilized from sediments in the canyon. Ancho Spring is downgradient of explosives testing sites. |
| Alluvial Groundwater | Extent | Little is known about the presence of alluvial groundwater in Ancho Canyon. Ancho Canyon contains thick alluvium that could host perched groundwater. |
| | Depth/Thickness | Three boreholes (ASC-15, ASC-16, and ASC-18) drilled by the ER Project encountered 4 ft to 9 ft of saturation in alluvium below MDA Y, but no contamination. Several boreholes drilled downgradient of MDA Y did not encounter alluvial groundwater, suggesting that the occurrence of alluvial groundwater in this area is limited in extent. |
| | Quality | See above. |
| Intermediate Groundwater | Extent/Hydrology | No intermediate perched zones have been found beneath Ancho Canyon. ER borehole DMB-1, drilled between building 69 and the Administrative Area at TA-39, penetrated 119 ft of Bandelier Tuff and 5 ft of Cerros del Rio basalts. No intermediate-depth perched water was encountered in this hole, but clay-lined fractures and vesicles in the basalt suggest that the periodic passage of groundwater through these rocks may occur. A test hole (TH-7) drilled 10 ft into basalts in Ancho Canyon below State Road 4 was dry. The hole was drilled in 1950 and has been plugged. |
| | Depth/Thickness | R-31 was drilled in TA-39 in the north fork of Ancho Canyon. A screen was placed from 439 to 454 ft at a possible perched zone, based on water seen in a borehole video. The zone has been dry since and no water samples have been collected from it. |

## Table 3-A-7.
## Ancho Canyon Watershed Description (continued)

| Hydrogeologic Element | Characteristic | Description |
|---|---|---|
| | Quality | See above. |
| Regional Aquifer | Depth/Hydrology | Groundwater flow in the regional aquifer beneath Ancho Canyon is to the east and southeast, towards the Rio Grande. The regional aquifer lies at about 1000 to 1170 ft beneath the mesa at TA-49, and is within the Cerros del Rio basalt, the underlying Puye Fanglomerate, "Totavi" gravels, and possibly the Santa Fe Group (Section 2.3.1). The regional water table, at well R-31 in TA-39, was encountered at about 530 ft within the Cerros del Rio basalt, the underlying Puye Fanglomerate, and "Totavi" gravels. |
| | Quality | Three regional aquifer wells at TA-49 have been sampled since the 1960s to monitor for effects of testing at that site. In general, no contaminants have been consistently found. High metal concentrations (lead, zinc, iron, manganese) in samples are related to metal well casing and fittings. Occasional detections of organic compounds are not supported by follow up sampling. Post-drilling water quality sampling has not been completed at well R-31. |
| Contaminants | Potential Sources | Located south of Ancho Canyon on a mesa near the Rio Grande, TA-33 was used as a firing site and for production of tritium. PRSs include landfills, septic systems, and burn areas. It is situated on a mesa top and is being investigated by the ER Project as OU 1122. TA-39 is located on the floor of middle Ancho Canyon, and it was used for open-air testing of high explosives. PRSs in this technical area include five firing sites, a number of landfills, and septic systems. The ER Project is investigating this technical area as OU 1132. More detailed information about the operational history and the PRSs can be found in the RFI Work Plans for OUs 1122 and 1132.<br><br>TA-49 lies on a mesa in the upper part of the Ancho Canyon drainage. TA-49 was used for underground hydronuclear testing in the early 1960s. The testing consisted of criticality, equation of state, and calibration experiments involving special nuclear materials. The RFI Work Plan for Operable Unit 1144 describes the planned ER investigations that focus on identifying and quantifying migration of contaminants from the shafts. |
| | Type | There are large inventories of radioactive and hazardous materials such as isotopes of uranium and plutonium, lead, beryllium, TNT, RDX, HMX, and barium nitrate. Much of this material was left in shafts drilled into the mesa top. |

References:
LANL 1992d; LANL 1992f; LANL 1993b; Purtymun and Stoker 1987.

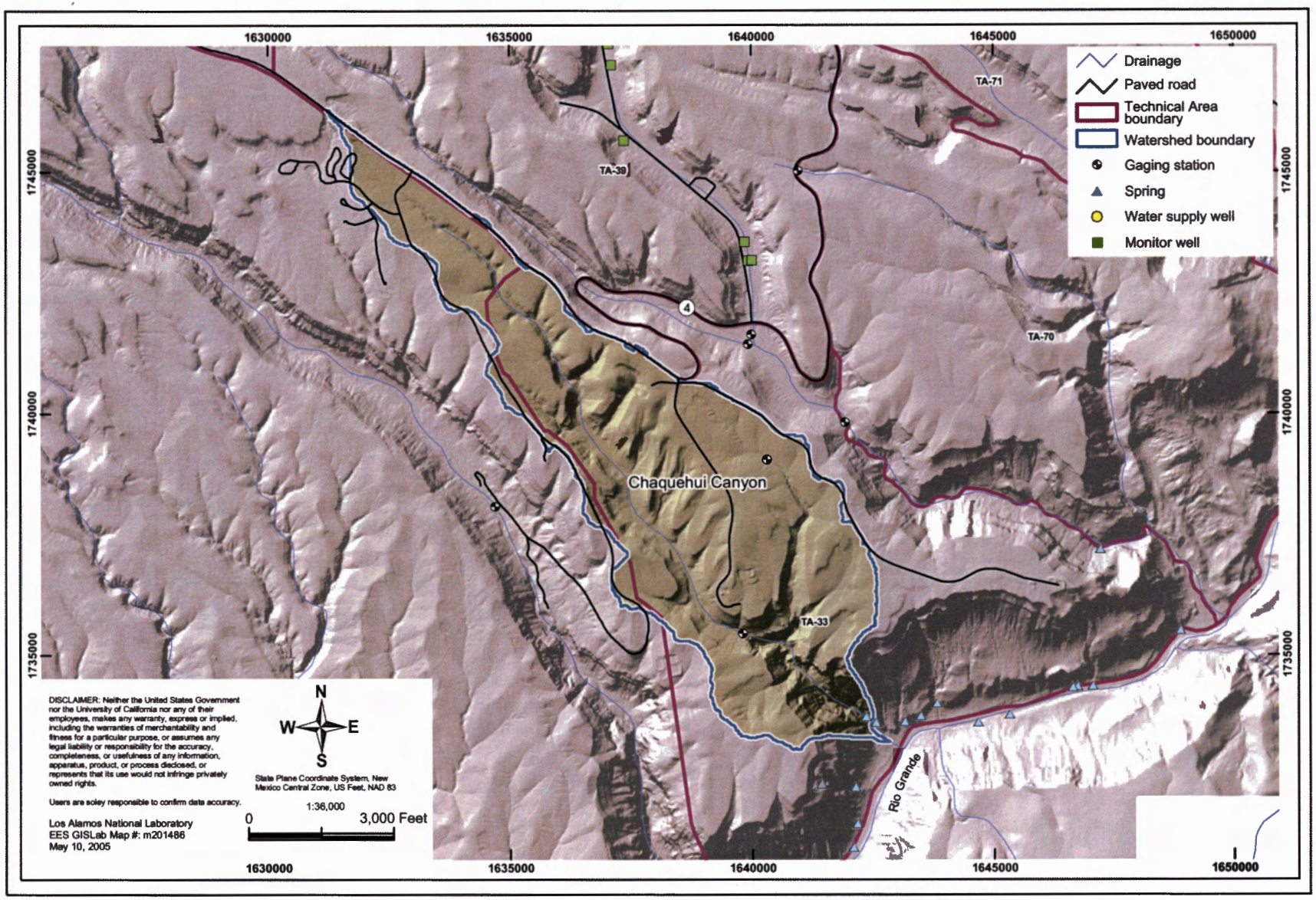


**Figure 3-A-8.** Ancho Canyon watershed.

## Table 3-A-8.
## Chaquehui Canyon Watershed Description

| Hydrogeologic Element | Characteristic | Description |
|---|---|---|
| Surface Water | Flow | Chaquehui Canyon heads on the Pajarito Plateau and has a drainage area of about 2 square miles. It contains an ephemeral stream in its upper portion (Figure 3-A-1, Figure 3-A-9). |
| | Quality | |
| Springs | Name | Springs issue from basalts near the Rio Grande in the area of Chaquehui Canyon (Springs 8A, 9, 9A, 9B, and Doe Spring). These springs are located 130-200 ft above the Rio Grande. About 0.5 mile above the Rio Grande, Doe Spring, a regional aquifer spring, maintains a short perennial reach. Farther down the drainage, Springs 9, 9A and 9B maintain perennial flow that extends 0.25 mile to the Rio Grande. |
| | Quality | |
| Alluvial Groundwater | Extent | Little is known about the presence of alluvial groundwater in Chaquehui Canyon. Much of Chaquehui Canyon is unlikely to contain perched alluvial groundwater because most of its course forms a steep narrow drainage through basalts that are swept free of alluvium by runoff. Purtymun reported that there was water perched locally in the alluvium but provided no basis for this statement. Purtymun probably refers to alluvium downstream of Doe Spring and Springs 9 and 9A. |
| | Depth/Thickness | See above. |
| | Quality | See above. |
| Intermediate Groundwater | Extent/Hydrology | No intermediate groundwater is known in Chaquehui Canyon; however there has been no drilling in the area. |
| | Depth/Thickness | See above. |
| | Quality | See above. |
| Regional Aquifer | Depth/Hydrology | The springs may represent discharge from the regional aquifer in White Rock Canyon. Well R-31 in TA-39 (Ancho Canyon) found the regional aquifer at about 530 ft within the Cerros del Rio basalt, the underlying Puye Fanglomerate, and "Totavi" gravels. |
| | Quality | |
| Contaminants | Potential Sources | Chaquehui Canyon lies south of the mesa occupied by TA-33. TA-33 was used as a firing site and for production of tritium. PRSs include landfills, septic systems, and burn areas. TA-33 is situated on a mesa top and is being investigated by the ER Project as Operable Unit (OU) 1122. |
| | Type | |

References:
LANL 1992d; Purtymun and Rogers 2002.

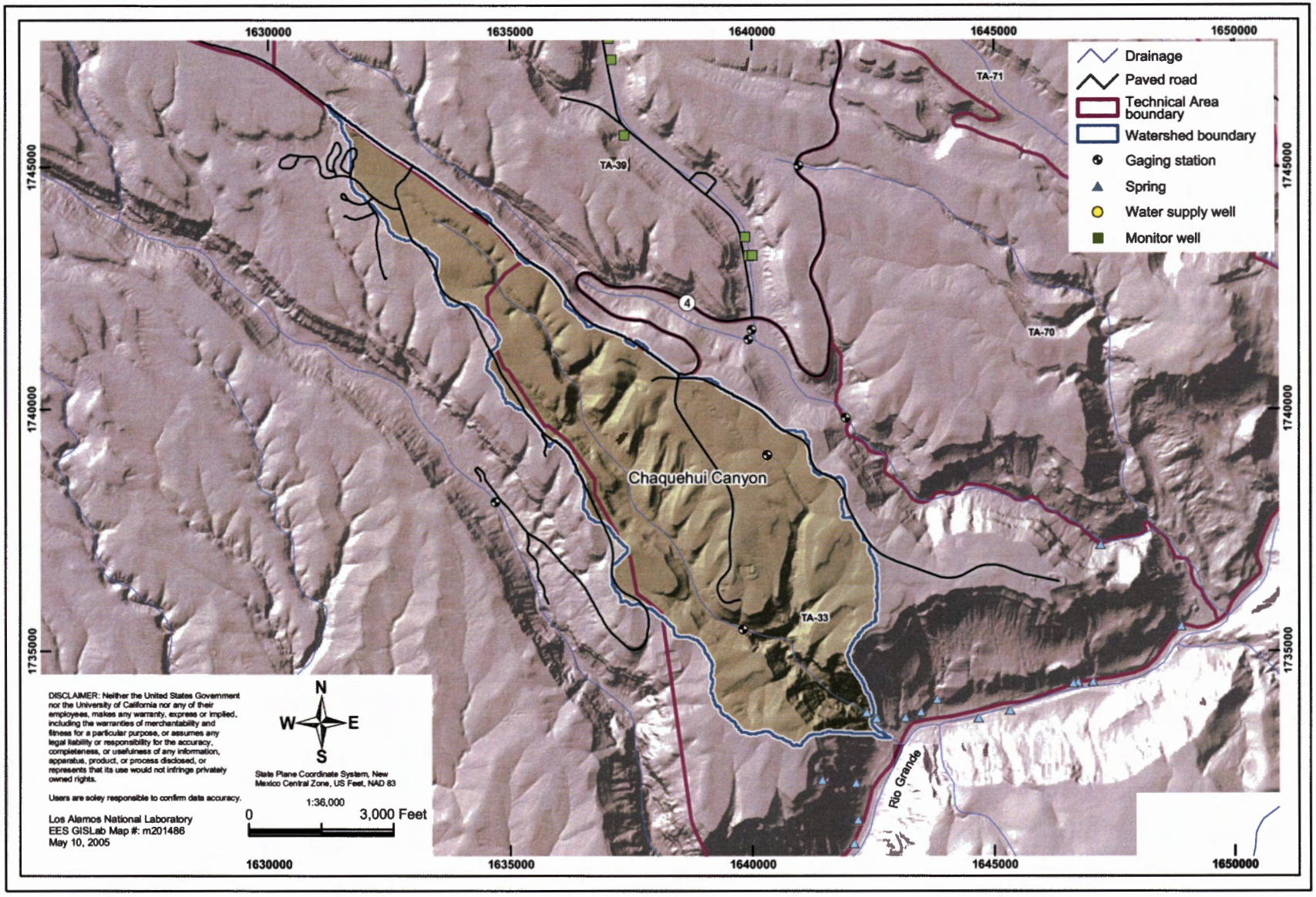


**Figure 3-A-9.** Chaquehui Canyon watershed.

## Table 3-A-9.
## Frijoles Canyon Watershed Description

| Hydrogeologic Element | Characteristic | Description |
|---|---|---|
| Surface Water | Flow | Frijoles Canyon lies on US Forest Service and US Park Service lands south of Laboratory land and heads within the Sierra de los Valles (Figure 3-A-1; Figure 3-A-10) with a drainage area of about 19 square miles. Rito de los Frijoles is a perennial stream that originates in the upper canyon and extends to the Rio Grande. |
| | Quality | The Laboratory has monitored surface water quality at two locations for several decades, one near the park headquarters and one just above the Rio Grande. In general, no Laboratory-derived contamination has been observed. The National Park Service has monitored surface water quality extensively in Frijoles Canyon. High fecal coliform bacteria counts originating from local sanitary sources and horse corrals have been a major issue in surface water quality. |
| Springs | Name | Rito de los Frijoles originates from springs in upper Frijoles Canyon. One regional aquifer spring, Spring 10, discharges at the edge of the Rio Grande south of Frijoles stream. The spring has a very low discharge and is difficult to sample separately from adjacent river water. |
| | Quality | |
| Alluvial Groundwater | Extent | No wells have been drilled into the alluvium in Frijoles Canyon. The presence of perennial surface flow suggests a large extent of alluvial saturation. |
| | Depth/Thickness | The alluvium is probably thin, on the order of 6 m or less. |
| | Quality | See above. |
| Intermediate Groundwater | Extent/Hydrology | No intermediate groundwater is known to exist in the area of Frijoles Canyon; however no wells have been drilled. |
| | Depth/Thickness | See above. |
| | Quality | See above. |
| Regional Aquifer | Depth/Hydrology | No regional aquifer wells are located in Bandelier National Monument. The nearest wells are in Ancho Canyon. |
| | Quality | See above. |
| Contaminants | Potential Sources | Frijoles Canyon lies south of the Laboratory boundary near the Rio Grande, but is separated from TA-33 by Chaquehui Canyon. Local sanitary sources and horse corrals have been potential source of contamination. |
| | Type | There is a high fecal coliform bacteria count in surface water. |

References:
Mott 1999; Purtymun and Adams 1980.

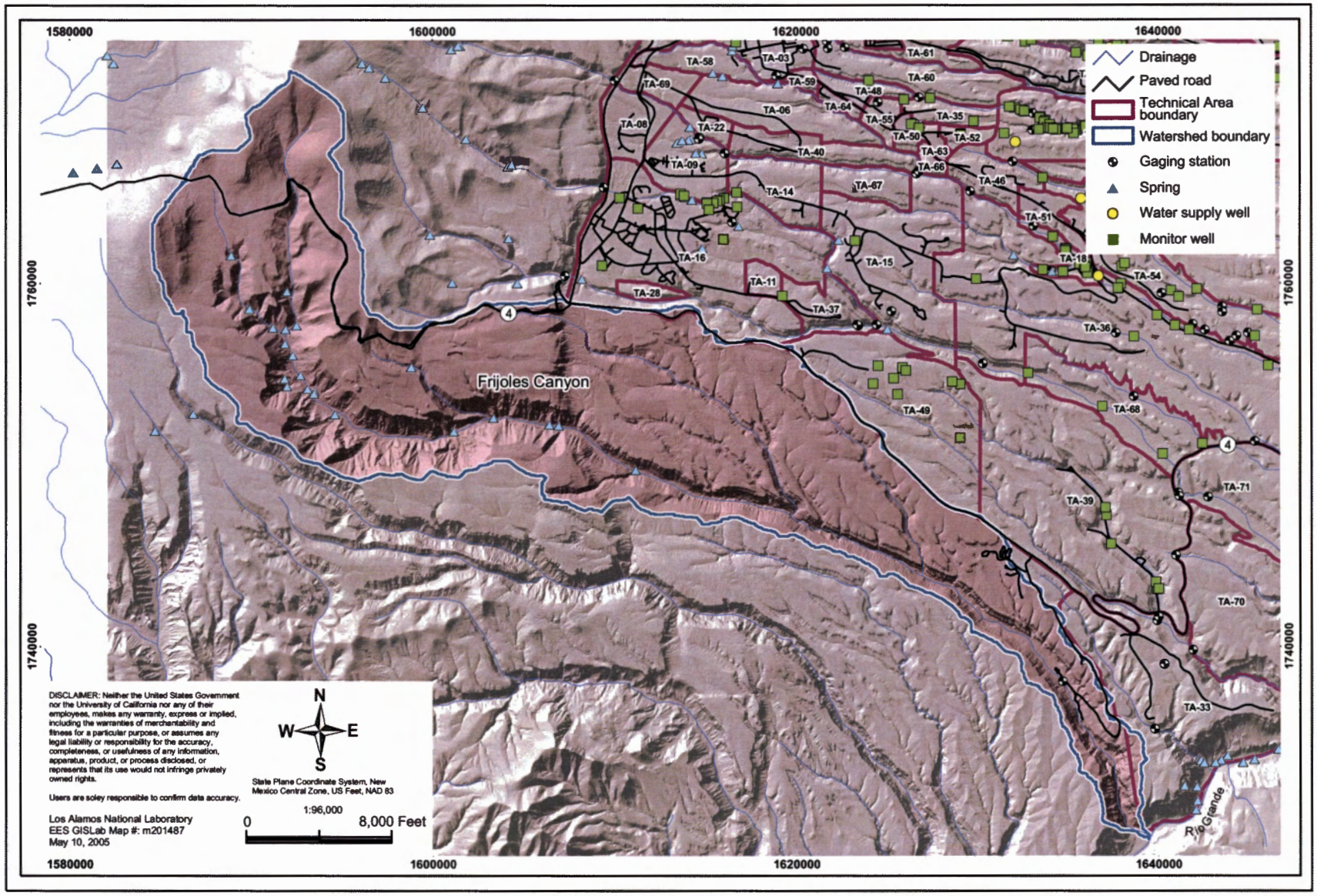


**Figure 3-A-10**. Frijoles Canyon watershed.

## Table 3-A-10.
## White Rock Canyon Watershed Description

| Hydrogeologic Element | Characteristic | Description |
|---|---|---|
| Surface Water | Flow | Flow from regional aquifer springs supports perennial surface water flow in several canyons just above where they reach the Rio Grande: Sandia, Pajarito, Ancho, and Chaquehui canyons (Figure 3-A-1, Figure 3-A-11). Except for Sandia Canyon, these flows reach the Rio Grande.<br><br>The Los Alamos County White Rock Sewage Treatment Plant discharges effluent into Mortandad Canyon just above the river at the northern county boundary. |
| | Quality | The discharge from the White Rock Sewage Treatment Plant is the primary surface water source and has a strong impact on the chemistry of the water that enters the Rio Grande from Mortandad Canyon, leading to higher TDS, nitrate, chloride, sulfate, and some metals. Water quality of the other streams is mainly determined by chemistry of their contributing springs (summarized in the regional aquifer description below). Purtymun (1995) and Purtymun et al. (1980) summarize flow and water quality from the White Rock Canyon springs and surface water. |

## Table 3-A-10.
## White Rock Canyon Watershed Description (continued)

| Hydrogeologic Element | Characteristic | Description |
|---|---|---|
| Springs | Name | Springs near the Rio Grande represent natural discharge from the regional aquifer. The springs discharge from two geologic units, the Tesuque Formation and the Totavi Lentil (the lower part of the Puye Formation). The Tesuque Formation consists of sandstones, siltstones, and interbedded basalts. The Totavi Lentil is a channel fill deposit made up of grain sizes ranging from gravel to boulders.<br><br>Most of the springs discharge close to the elevation of the Rio Grande, though some springs discharge at elevations several tens of feet above the Rio Grande. The springs can be divided into four groups:<br>**Group I springs** discharge from the Totavi Lentil on the west side of the river. The spring water is dominated by calcium bicarbonate with sulfate and chloride of about 4 mg/L and TDS averages 163 mg/L.<br>**Group II springs** discharge from coarse-grained Tesuque Formation sediments on both sides of the river. These springs have sodium bicarbonate water with about 3 mg/L of sulfate and chloride, and TDS averages 183 mg/L.<br>**Group III springs** discharge from fine-grained Tesuque Formation sediments on the west side of the river. These springs also have sodium bicarbonate water with about 10 mg/L of sulfate, 3 mg/L of chloride and TDS averages 215 mg/L.<br>**Group IV springs** discharge from fine-grained Tesuque Formation sediments on the east side of the river near faults and basalt flows. These springs have varied chemistry with higher TDS than the other springs, of 270 to 500 mg/L.<br><br>The springs discharging from the Totavi Lentil (Group I springs) follow the outcrop of this formation, increasing their elevation above the river in a downstream direction. These higher elevation springs generally occur on the flanks of or in the bottom of canyons where erosion has exposed the Totavi Lentil. The elevation of springs above the river could reflect channeling of discharge from the regional aquifer along the higher-permeability Totavi Lentil, combined with the increase in elevation of the water table with distance west of the river.<br><br>An alternative hypothesis about spring origin is that the elevation of some springs (Spring 4A) above the river indicates that they discharge from perched groundwater located above the regional aquifer. As well, the elevation of springs above the river could reflect complex flow paths resulting from local variations in geology and permeability related to numerous large-scale landslides along the canyon walls. |
| | Quality | The US Geological Survey and the Laboratory have monitored chemistry of the White Rock Springs since the 1960s; the springs show no clear impact of Laboratory contamination. Tritium values in the springs are either in the range of regional aquifer values, namely less than 3 pCi/L, or up to 40 pCi/L, which could indicate either Laboratory impact or a component of precipitation. A few springs have relatively high natural uranium. These springs lie mainly on the east side of the river |

## Table 3-A-10.
## White Rock Canyon Watershed Description (continued)

| Hydrogeologic Element | Characteristic | Description |
|---|---|---|
| | | near and north of the Buckman wellfield. Some springs (1, 3, 3A, 4, 5) also show subtle increases in nitrate over 20 years. These increases could be due to the impact of feral cattle grazing near the springs over time as well as to some change in groundwater quality. Perchlorate has been measured at low levels in some springs, but the source is not clear. |
| Alluvial Groundwater | Extent | Alluvial groundwater is not present in the White Rock Canyon area. However, household wells in Los Alamos Canyon (Halladay and Otowi) and household wells nearer the Rio Grande probably draw their water from Santa Fe Group sediments but may draw water in part from alluvium in these drainages. |
| | Depth/Thickness | See above. |
| | Quality | See above. |
| Intermediate Groundwater | Extent/Hydrology | Perched intermediate groundwater may not be present in the White Rock Canyon area. However, an alternative hypothesis about White Rock Canyon spring origin is that the elevation of some springs above the river indicates that they discharge from perched groundwater located above the regional aquifer. |
| | Depth/Thickness | See above. |
| | Quality | See above. |
| Regional Aquifer | Depth/Hydrology | The Rio Grande is the major groundwater discharge zone for the regional aquifer underlying the Pajarito Plateau. The river gains flow through White Rock Canyon, indicating that the local water table (the regional aquifer) lies above the river.<br><br>The City of Santa Fe operates the Buckman wellfield on the east side of the Rio Grande across from White Rock (Figure 3-A-11). The wellfield includes eight pumping wells. These wells draw their water from Santa Fe Group sediments. Vesselinov and Keating (2002) concluded from a modeling study that under long-term steady state conditions, these wells might one day draw perhaps a third of their water from beneath LANL on the west side of the Rio Grande. As a result, LANL has sampled three of the Buckman wells (1, 2, and 8) since 2001 for its Environmental Surveillance Program. Water in these wells is quite old, having passed through the deeper portion of the basin fill sediments where it acquired a higher load of dissolved solutes.<br><br>San Ildefonso Pueblo draws water from more than 10 community and household wells located on both sides of the Rio Grande. Little information on depth or geology for these wells is available. Many of these wells probably draw their water from Santa Fe Group sediments. At least two of the San Ildefonso wells are uncapped artesian wells. |
| | Quality | The US Geological Survey and the Laboratory have monitored chemistry of the White Rock Springs since the 1960s; the springs do not show a definitive impact of Laboratory contamination. Tritium activities in the springs are either in the range |

## Table 3-A-10.
## White Rock Canyon Watershed Description (continued)

| Hydrogeologic Element | Characteristic | Description |
|---|---|---|
| | | of regional aquifer values, namely less than 3 pCi/L, or range from 10 to 50 pCi/L, which could indicate either Laboratory impact or a component of local precipitation—more likely the latter given spring locations. A few springs have relatively high natural uranium. These springs lie mainly on the east side of the river near and north of the Buckman well field. Some springs (1, 3, 3A, 4, 5) also show subtle increases in nitrate over 20 years. These increases could be due to the impact of feral cattle grazing near the springs over time, natural source, and seepage from impoundments within Pajarito Canyon and past effluents released in several canyons. Perchlorate has been measured at low levels in some springs, but the source is not clear. The measured perchlorate values are similar to those found in wells distant from LANL.<br><br>Spring 2B below and east of the White Rock Overlook shows higher concentrations of uranium, chloride, boron, and nitrate than other springs. This spring's chemistry (except for uranium) is similar to the nearby stream in Mortandad Canyon, which is fed by effluent from the White Rock sanitary treatment plant. This similarity in chemistry, along with nitrogen isotope results that indicate a sewage source for both waters, suggests that a large part of the water from Spring 2B comes from the treatment plant effluent in lower Mortandad Canyon. It is possible that natural uranium within the Santa Fe Group sediments has been leached from mineral surfaces in contact with the bicarbonate-rich groundwater. Increasing concentrations of carbonate alkalinity are from the treated sewage effluent discharged upgradient from the spring.<br><br>Some Buckman wells have exceptionally high uranium (up to 230 ppb, compared to the new EPA MCL of 30 ppb). Such naturally occurring uranium is common in the Pojoaque and Tesuque area. The Buckman wells also have high sodium, carbonate alkalinity, and TDS. |
| Contaminants | Potential Sources | TA-33 borders the Rio Grande at the southern end of LANL along White Rock Canyon. The RFI Workplan for OU 1122 describes environmental concerns at TA-33. To the north of TA-33 lies TA-70, a buffer area where no Laboratory activities have occurred.<br><br>Adjoining TA-70 to the north, Los Alamos County land comprises the low to moderate-density residential area of White Rock. Los Alamos County formerly operated sanitary effluent lagoons near the edge of the canyon just south of Pajarito Canyon. A municipal sanitary treatment plant discharges effluent into Mortandad Canyon just above the river at the northern county boundary. This discharge is the main surface water source and has a strong impact on the chemistry of the water that enters the Rio Grande from Mortandad Canyon, leading to higher concentrations of TDS, nitrate, chloride, sulfate, and some metals. To the north of White Rock is undeveloped San Ildefonso property. |

## Table 3-A-10.
## White Rock Canyon Watershed Description (continued)

| Hydrogeologic Element | Characteristic | Description |
|---|---|---|
| | | Los Alamos Canyon lies at the northern end of White Rock Canyon. LANL effluents have moved down Los Alamos Canyon either adsorbed onto sediments or dissolved in stream flow, affecting sediment and shallow groundwater quality in the lower portion of the canyon (Section 2.4). |
| | Type | TA-33 was used as a firing site and for production of tritium. PRSs include landfills, septic systems, and burn areas. It is situated on a mesa top and is being investigated by the ER Project as Operable Unit (OU) 1122. If contaminants are released from TA-33, they may impact Ancho Canyon, Chaquehui Canyon, or the Rio Grande.<br><br>The discharge from the municipal treatment plant is the primary surface water source and has a strong impact on the chemistry of the water that enters the Rio Grande from Mortandad Canyon, leading to higher levels of TDS, nitrate, chloride, sulfate, and some metals. |

References:
LANL 1992d; Purtymun et al. 1980; Purtymun 1995; Vesselinov and Keating 2002; LANL, 2004a.

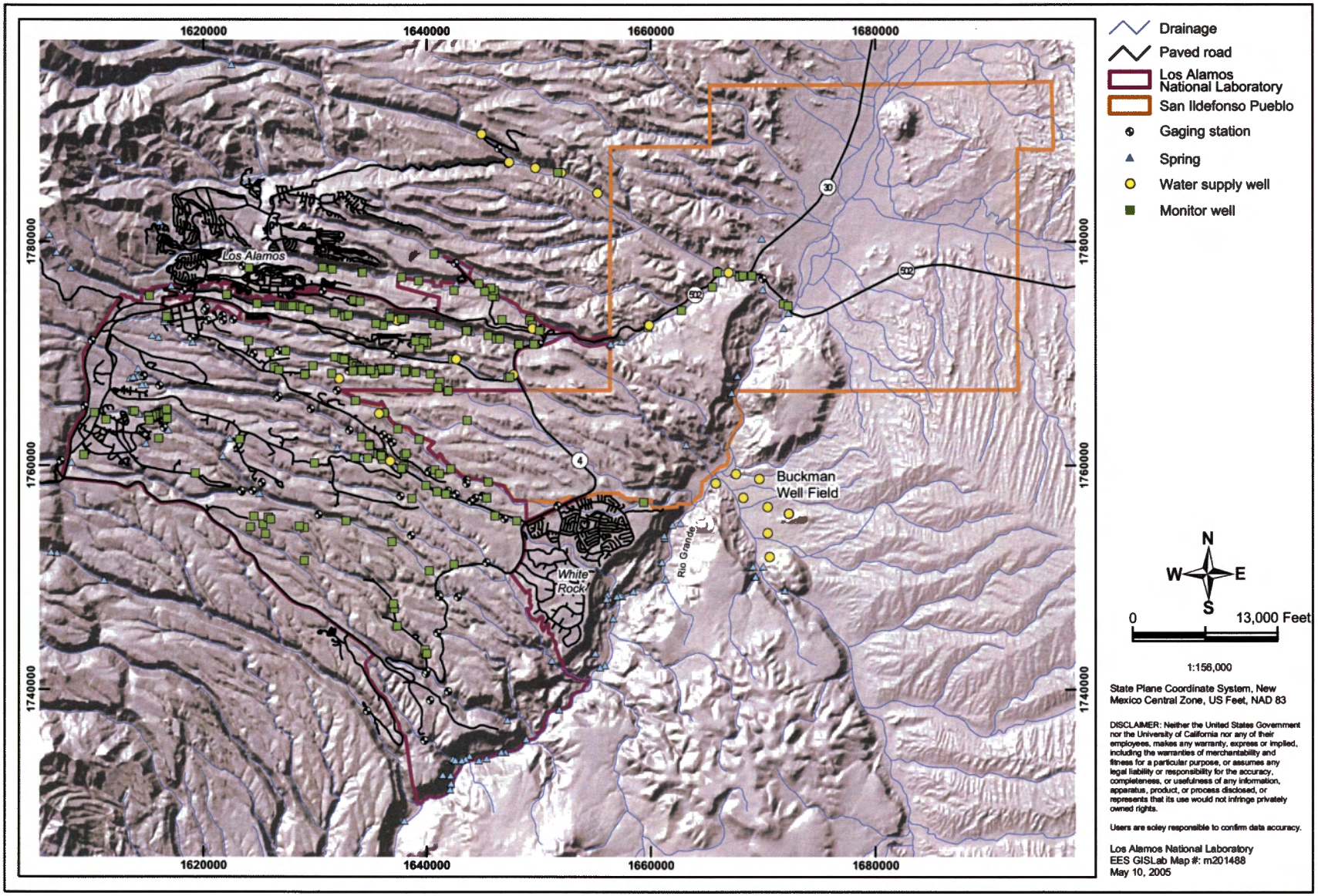


**Figure 3-A-11.** White Rock Canyon.

## 3-B. Alternative Conceptual Models of Contaminant Transport

The purpose of this section is to discuss two alternative interpretations of how water flows and contaminants behave on the Pajarito Plateau. With the uncertainty that is inherent to all subsurface investigations, it is important to examine the strengths and weaknesses of other possible interpretations of the available data. This section explores alternative conceptual models by first providing a description of the alternative model. Second the strengths and limitations of the alternative are summarized. An assessment of how the alternative conceptual model would change the current conceptual model or how risk is assessed is presented. Finally, a discussion of how the alternative conceptual model could be tested is provided.

### 3-B-1. Colloid-Facilitated Transport

The movement of small particles in groundwater flow systems can represent an alternate mechanism for contaminant transport. While generally not as significant overall as the movement of dissolved or immiscible species, the movement of small particles can increase the magnitude of mass transport. This section will focus on colloids, a special class of particles with properties the lie between that of the dissolved state and the solid state.

Historically, researchers have applied the term colloid to particles with a size range of 0.001 to 1 micron (1 micron is 0.001 millimeter). The colloids can be mineral particles, particulate organic matter, biological (for example, bacteria), or even microemulsions of hydrocarbons. The surface area per unit mass is very high for colloids, which greatly affects their mass transport. Contaminants can be transported as colloids resulting in unexpected mobility. This is because the transport of contaminants adsorbed to colloids is determined by the physical/chemical properties of the colloid, rather than properties of the contaminant. Work at the Nevada Test Site suggests that plutonium can be transported over significant lateral distances (~1.3 km) by colloids (Kersting et al. 1999). Predicting colloid transport is extremely difficult, however. Colloid stability and filtration depends on a complex array of factors including density, size, surface chemistry, water chemistry, water flow rates, and pore size distribution of the soil matrix. Table 3-B-1 discusses strengths and weaknesses of a colloid-facilitated transport model.

### 3-B-1.1 Strengths and Limitations of the Colloid-Facilitated Transport Model

**Table 3-B-1.**
**Colloid-Facilitated Alternative Transport Model**

| Strengths | Limitations |
|---|---|
| Since the start of discharges in May 1963, the RLWTF has used the flocculate "calcium hydroxide" and "ferric sulfate" as a part of the treatment process, and it is likely that a continual stream of residual colloids was discharged to the canyon floor. | Bulk of radionuclide inventory appears adsorbed to stream sediments. |
| Work by Penrose et al. (1990) demonstrated the presence of colloids with plutonium and americium along a 3400 m segment of the perched alluvial groundwater system in Mortandad Canyon. The study concluded that the horizontal dispersal of the radionuclides through the groundwater system was due to colloid transport in the subsurface. | That conclusion was challenged, however, by a subsequent review that concluded that the radionuclide transport within the canyon was principally due to surface water, rather than groundwater transport (Marty et al. 1997). |
| At a mesa top site at TA-21, some of these radionuclides occur at much greater depths in the field than expected. Work by Nyhan et al. (1985) suggests that substantial hydraulic loading can enhance the vertical penetration depth. The study examined the distribution of plutonium, americium-241 and water in Bandelier Tuff beneath former liquid waste disposal sites at TA-21. Nyhan et al. (1985) found that after 17 years of migration, the Am-241 was mobilized under heavy hydraulic loading to 30 m. It is possible that the radionuclides are mobilized by other chemicals or possibly by colloid transport in preferential flow paths. | While colloids have been shown to be abundant in the alluvial groundwater, coring has not shown appreciable vertical movement (less than five feet) of plutonium or americium in the vadose zone below the alluvium (Stoker et al. 1991). Studies show that 99% of the plutonium inventory is adsorbed on alluvium and little is in the water column; the colloidal fraction in groundwater represents less than 1 percent of the total plutonium inventory in the canyon (Purtymun et al. 1984; Stoker et al. 1991). These results suggest that vertical transport of the radiocolloids has been minimal in the Bandelier Tuff beneath the canyon floor, even after decades of continual liquid release. |
| Occasional Pu-239, -240 detects in samples from water supply wells (1970s and 1980s mostly) may be colloid related. | No plutonium detects in recent years and earlier detections primarily limited to water supply wells---few in monitoring wells. Unable to validate earlier results because of limitations in existing records. |

### 3-B-1.2 Effect on Current Conceptual Model and Assessment of Risk

Many radionuclides and metals are currently conceptualized to be relatively immobile at the site. If colloid-facilitated transport is significant, the subsurface travel times for these constituents to the accessible environment will be reduced. Health risks from colloid-facilitated transport, however, likely will not be greatly different from the levels presently recognized: sampling of the groundwater systems account for the total contaminant concentrations and already include any colloid contributions, if present. Monitoring of the shallower groundwater at the site, the depths where contaminated colloids should be most abundant, has identified few areas with concentrations above a regulatory standard. Given the vadose zone thickness and likely reduction in contaminated colloid concentrations with depth, contaminant concentrations due to colloid-facilitated transport in the regional aquifer are also expected to meet regulatory standards.

## 3-B-2. Cs-137 "Groundwater Transport" to the Rio Grande

A report written by Norm Buske (2003) for the RadioActivist Campaign (TRAC) and Concerned Citizens for Nuclear Safety (CCNS) in late October 2003 cites samples of aquatic moss from Spring 4A and the Pajarito Stream containing "…consistently low levels of cesium-137 *of LANL* origin [emphasis added]. This is the first confirmed detection of LANL radioactivity from a groundwater pathway." The report also cited moss samples from other sites, as testing positive for Cs-137 and said samples showed Cs-137 "in the range of 0.01 to 6 picocuries/kilogram…Cesium-137…is…at levels far too low to be considered a public health concern." Table 3-B-2 discusses strengths and limitations of a Cs-137 transport model.

### 3-B-2.1 Strengths and Limitations of Cs-137 Groundwater Transport Alternative Model

**Table 3-B-2.**
**Cs-137 Groundwater Transport Alternative Model**

| Strengths | Limitations |
|---|---|
| Detections of tritium and perchlorate in other White Rock Canyon springs support this model. | Levels of these constituents may be within natural ranges. When converted to an equivalent weight basis, the amount of cesium measured by Buske (2003) in the moss samples is within the background concentrations for plants in northern New Mexico. |
| Cesium-137 is a major Laboratory contaminant in Los Alamos and Mortandad Canyons radioactive effluent discharges. | Cesium-137 is a common fallout radionuclide that was distributed globally during atmospheric nuclear tests. It is considerably more probable that the moss accumulated cesium from worldwide fallout rather than from groundwater. Fallout cesium-137 is universally present in surface soils and soil concentrations are one hundred times greater those found in study. |
| | The Buske (2003) results were very close to detection levels, in the range of 0.01 to 6 pCi/Kg wet, and the study did not include control samples (upstream) so that Cs-137 from fallout sources could not be compared. |
| | If Cs-137 traveled through groundwater to a spring along the Rio Grande, several non-adsorbing chemical constituents that usually reflect groundwater contamination, such as nitrate or tritium, likely would accompany and precede Cs-137. Tritium and nitrate values in Spring 4A indicate the spring water reflects background aquifer conditions unaffected by Laboratory discharges. |
| | From 1995 through 2003, LANL has made 121 Cs-137 measurements in White Rock Canyon springs, with only two detections in the data set. Nine of these measurements (with only one detection) were from Spring 4A. Thus, the body of data does not support the presence of Cs-137 in any White Rock spring, at an average detection limit of 3 pCi/L. In addition, Cs-137 is not detectable in regional aquifer monitoring wells upgradient of the springs. |

### 3-B-2.2 Effect on Current Conceptual Model and Assessment of Risk

If real, the groundwater transport of Cs-137 alternative conceptual model would indicate that relatively immobile radionuclides or metals may potentially move through groundwater to the accessible environment at a faster rate than recognized. Assessment of water quality changes at those locations would continue in the future. The current monitoring results from across the regional aquifer do not indicate any location where the concentrations of these constituents are greater than regulatory standards. Given this pattern, it is highly unlikely that concentrations greater than standards would be observed in the future. Contaminant transport models that only take into account sorption and solubility may underestimate the extent a colloid-bound species is able to migrate in groundwater.

A study is being conducted by a LANL team to assess the distribution and concentrations of cesium in moss throughout northern New Mexico. The objective is to collect various moss sample specimens from springs located in northern New Mexico and southern Colorado (a great distance from LANL) and analyze them for Cs-137 activity. This program will collect the data necessary to evaluate whether Cs-137 concentrations near the Laboratory are anomalous. Additional monitoring of wells and springs in the Los Alamos area will continue to look for evidence of rapid movement of cesium (and other contaminants) through the groundwater system.

## APPENDIX 4-A. METHOD FOR ESTIMATING INFILTRATION RATE IN CANYONS

Net infiltration is defined as the flux of water that percolates to depths greater than the zone in which evapotranspiration (ET) processes take place. A complete site-wide study of net infiltration has recently been completed (Kwicklis et al. 2005). That study presents estimates of net infiltration determinations with a variety of estimation techniques, including Darcy's Law, chloride mass-balance and water-balance methods. The study extrapolates these estimates to other areas within the site for which estimates do not exist. Factors used to make this extrapolation include topography, soil type, vegetation, and bedrock type. The Kwicklis et al. (2005) publication was not ready in time to be used in model predictions presented elsewhere in this report. Previous modeling analyses should be updated to include the detail from the site-wide net infiltration study, as appropriate.

Since net infiltration to the vadose zone beneath the plateau is assumed to occur mainly through canyons, the plateau is differentiated topographically as mesa or canyon. For the net infiltration map presented here, the mesa locations are all assigned the same fixed net infiltration rate. For the base-case study, this rate is 1 mm/yr (Section 2.6.1). More variability is added to the map for canyon locations because the canyons are the main source of recharge across the plateau, and also because conditions in canyons across the plateau vary from wet to dry. For these reasons, a ranking scheme was developed to classify portions of canyons by a net infiltration index (NII) that describes the net infiltration rate.

The net infiltration index ranges in value from one to five, with one representing the lowest and five representing the highest infiltration potential. The NII is based on a number of physical factors, as shown in Table 4-A-1:

- The location of the headwaters is the first factor because those canyons that head in the mountains generally have a larger drainage area, and receive more precipitation and run-off than those that head on the plateau. Anthropogenic water sources within the canyons can also yield large surface flows that contribute similarly to headwaters located higher in the mountains. For this reason, anthropogenic sources were included with the first factor.
- The persistence of surface water in the canyon bottom is the next factor used to define the NII. Those canyons with perennial streams are expected to generate higher net infiltration than those with ephemeral or intermittent streams, and therefore receive a higher ranking.
- Observation of alluvial water is the final factor used to define the NII. Some canyons have alluvial groundwater of significant depth while others have limited or no alluvial water. Those canyons with deeper alluvial groundwaters receive a higher net infiltration index than those without.

Note that the factors contributing to the NII are used to define a set of net infiltration indices that may be updated with site-specific observations and data. However, as a general approach for supporting a plateau-wide modeling effort, the NII is a reasonable simplification. In some cases, factors such as persistent surface and alluvial waters may indicate an absence of vadose-zone infiltration rather than a higher net infiltration rate. Examples of this include the surface expression of springs or perching in the alluvium caused by a large contrast in hydraulic conductivity between the alluvium and underlying tuff. Despite these types of alternative

hypotheses, the model assumes a higher NII in the wetter areas, so that it errs on the side of predicting more rapid transport. Once areas with potential fast paths are identified, more site-specific and detailed net infiltration studies can be performed to refine the predictions.

Table 4-A-1 also includes the net infiltration assumed for each NII. These estimates exhibit approximately three orders of magnitude variation in net infiltration between the driest and the wettest canyons. To assess uncertainty in infiltration, different sets of net infiltration estimates are also included in this study.

Once the NII and the associated infiltration rates for each NII have been defined, the next step is to assign net infiltration indices of canyons or portions of canyons across the Pajarito Plateau. This task was accomplished by compiling information from the LANL Hydrogeologic Workplan about the descriptive factors listed in Table 4-A-1. Major canyons from Guaje Canyon, located north of the laboratory, to Chaquehui Canyon, located south of the laboratory, were characterized with respect to the location of their headwaters, anthropogenic sources, and observations of surface and alluvial waters. In most cases, a particular canyon is split into sections because the hydrologic factors change as one moves down the canyon. The characteristics of these canyons or portions of canyons are shown in Table 4-A-1, along with the resulting net infiltration index for each section. The net infiltration index is determined by comparing the characteristics in Table 4-A-1 to the net infiltration factors in Table 4-A-1.

Figure 4-A-1 shows the resulting NII map for the study area with respect to the LANL boundary. Canyons with no portion of their reach inside the site area, in the gray area of this figure, are not assigned a NII as part of this study because laboratory-derived contaminants are not present in these canyons. Infiltration rates converted from the values in Table 4-A-1 were used as the upper water-flux boundary conditions for the series of one-dimensional vadose-zone flow and particle tracking runs.

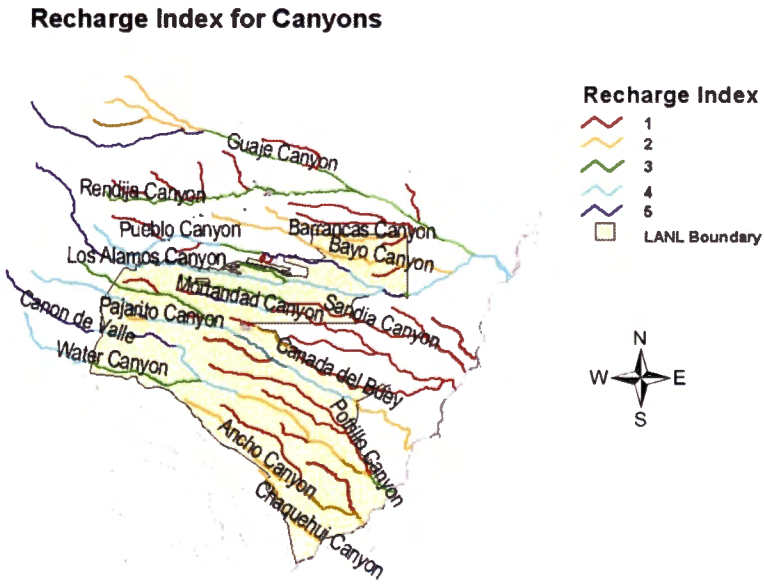


**Figure 4-A-1.** Infiltration on the Pajarito Plateau: result of analysis to determine the Net Infiltration Index (NII) indicator parameter across the Pajarito Plateau and surrounding region of the study area.

## Table 4-A-1.
## Determination of Net Infiltration
## Index for Sections of Canyons on the Pajarito Plateau

| Canyon/ ArcView Identifier | Reach | Headwaters (drainage <5 mi² unless noted) | Surface Water | Alluvial Water | Published Net Infiltration | Notes | NII |
|---|---|---|---|---|---|---|---|
| Pueblo (Pueb1) | From Headwaters to Guaje Mountain Fault | Mountains (drainage >8 mi$^2$) | Ephemeral | Saturated | | LANL (1998) p. 4-41, 4-42 | 4 |
| Pueblo (Pueb2) | Below Guaje Mountain Fault, above sewage treatment plant | Mountains | Ephemeral | May or may not be saturated | | LANL (1998) p. 4-41, 4-42 | 3 |
| Pueblo (Pueb3) | Below sewage treatment plant to halfway across Lab land | Mountains and anthropogenic source | Perennial | Saturated | | LANL (1998) p. 4-41, 4-42 | 5 |
| Pueblo (Pueb4) | Half way across Lab land to confluence with LA Canyon | Mountains | Intermittent | Saturated | | LANL (1998) p. 4-41, 4-42 | 4 |
| Pueblo (Historic) | Mid (below TA-45) and upper (old sewage) canyon | Mountains | Possible historic perennial flow | Possible historic saturated conditions | Previous effluent TA-45 (1951-1964); old sewage plant (pre-1963) | | 4 (historic) |
| Los Alamos (LA1) | West of the reservoir | Mountains (drainage >10 mi$^2$) | Perennial | Saturated | | LANL (1998) p. 4-48 | 5 |
| Los Alamos (LA2) | East of reservoir to TA-2 | Mountains | Continuous during snow melt (weeks to months); otherwise ephemeral | Saturated (thickness varies seasonally from several feet in winter to 25 ft in spring and summer) | All LA Canyon estimates based on Gray, (1997) Table 8<br><br>714, 213, 566, 1076 mm/yr | LANL (1998) p. 4-48 | 4 |
| Los Alamos (LA3) | TA-2 to confluence of Pueblo Canyon | Mountains | Ephemeral | Saturated (same as above) | 222, 408 mm/yr | LANL (1998) p. 4-48 | 4 |

## Table 4-A-1.
## Determination of Net Infiltration
## Index for Sections of Canyons on the Pajarito Plateau (continued)

| Canyon/ ArcView Identifier | Reach | Headwaters (drainage <5 mi² unless noted) | Surface Water | Alluvial Water | Published Net Infiltration | Notes | NII |
|---|---|---|---|---|---|---|---|
| Los Alamos (LA4) | Confluence of Pueblo Canyon to LAO-4.5 | Mountains | Perennial | Saturated | 399 mm/yr | LANL (1998) p. 4-48 | 5 |
| Los Alamos (LA5) | LAO-4.5 to Basalt Spring | Mountains | Ephemeral | Not Saturated | 362 mm/yr | LANL (1998) p. 4-48 | 3 |
| Los Alamos (LA6) | Lower; Basalt Spring to Rio Grande | Mountains | Ephemeral | Saturated | 325 mm/yr | LANL (1998) p. 4-48 | 4 |
| DP (DP) | All | Plateau | Ephemeral, except nearly continuous discharge near DP spring | Saturated conditions observed at wells LAUZ-1, LAUZ-2 (elsewhere ?) | | LANL (1998) p. 4-48 | 3 |
| Sandia (San1) | Headwaters to TA-72 | Plateau with small anthropogenic source | Ephemeral | Not character-ized (likely saturated portions) | Surface water source is precipitation and treatment plant water (not much snow melt) | LANL (1998) p. 4-53 | 3 |
| Sandia (San2) | Below TA-72 | Plateau | Not present | Not character-ized (eastern part near SCO-1 & SCO-2 dry since 1990) | | LANL (1998) p. 4-53 | 1 |
| Cañada del Buey (CdB1) | All else | Plateau | Ephemeral (with snow-melt and thunder-storms) | Not saturated | <0 (Rogers et al. 1996) | LANL (1998) p. 4-59, 4-61 | 1 |
| Cañada del Buey (CdB2) | Between CDBO-6 & CDBO-7 | Plateau | Ephemeral (with snowmelt and thunder-storms) | Sometimes saturated within weathered tuff (near discharge of PM-4) | | LANL (1998) p. 4-61 | 2 |
| Pajarito (Paj1) | West of Homestead Spring | Mountains (drainage >10 mi²) | Occurs as springs above alluvium (1-15 gpm) | Saturated alluvium (perched to ~10 ft depth) | | LANL (1998) p. 4-61, 4-62 | 4 |
| Pajarito (Paj2) | Several 100 yards near Homestead Spring | Mountains | Perennial | Saturated alluvium (perched to ~10 ft depth) | | LANL (1998) p. 4-61, 4-62 | 5 |

## Table 4-A-1.
## Determination of Net Infiltration
## Index for Sections of Canyons on the Pajarito Plateau (continued)

| Canyon/ ArcView Identifier | Reach | Headwaters (drainage <5 mi² unless noted) | Surface Water | Alluvial Water | Published Net Infiltration | Notes | NII |
|---|---|---|---|---|---|---|---|
| Pajarito (Paj3) | Below Homestead Spring to above Three-Mile Canyon | Mountains | Intermittent to ephemeral | Saturated alluvium (perched to ~10 ft depth) | | LANL (1998) p. 4-61, 4-62 | 4 |
| Pajarito (Paj4) | Three-mile Canyon to eastern LANL boundary | Mountains | Ephemeral | Saturated alluvium (perched to ~10 ft depth) | | LANL (1998) p. 4-61, 4-62 | 4 |
| Pajarito (Paj5) | East of LANL boundary to Rio Grande | Mountains | (Not discussed) Assumed ephemeral | Not saturated | | LANL (1998) p. 4-61, 4-62, 4-60 | 2 |
| Ancho (Ancho) | All | Plateau | Ephemeral from precipitation (sometimes severe) | Little known (possible shallow perched zone) | | LANL (1998) p. 4-69 | 2 |
| Chaq-uehui (Cheq1) | Headwaters to 0.5 mile from Rio Grande | Plateau | Ephemeral | Little known (However, observed infiltration into tuff at TA-33, tritium at 100-170 ft) | | LANL (1998) p. 4-74 | 2 |
| Chaq-uehui (Cheq2) | 0.5 miles from/to Rio Grande | Plateau | Perennial for short distance | Little known | | LANL (1998) p. 4-74 | 2 |
| Cañon de Valle (CdV1) | Headwaters to Pajarito Fault | Mountains | Perennial | Saturated | | LANL (1998) p. 4-78, 4-79 | 5 |
| Cañon de Valle (CdV2) | Pajarito Fault to 260 Outfall | Mountains | Intermittent | Saturated | | LANL (1998) 4-78,4-79 | 4 |
| Cañon de Valle (CdV3) | 260 Outfall to MDA P | Mountains and Anthropogenic source | Perennial | Saturated | | LANL (1998) p. 4-78, 4-79 | 5 |
| Cañon de Valle (CdV4) | MDA P to Water Canyon | Mountains | Intermittent | Saturated | | LANL (1998) p. 4-78, 4-79 | 4 |
| Potrillo (Pot1) | Headwaters to POTM-wells | Plateau | Ephemeral (no significant snowmelt, discharge sink at POTM-wells) | Only saturated observance once at well POTM-2 | 0.01 cm/yr (Rogers et al. 1996a) | LANL (1998) p. 4-85 | 1 |

## Table 4-A-1.
## Determination of Net Infiltration
## Index for Sections of Canyons on the Pajarito Plateau (continued)

| Canyon/ ArcView Identifier | Reach | Headwaters (drainage <5 mi² unless noted) | Surface Water | Alluvial Water | Published Net Infiltration | Notes | NII |
|---|---|---|---|---|---|---|---|
| Potrillo (Pot2) | POTM-wells to Water Canyon | Plateau | Rare | Not expected | | LANL (1998) p. 4-85 | 1 |
| Fence (Fen1) | All | Plateau | Ephemeral (no significant snowmelt) | Little known, dry at State Rt. 4 | | LANL (1998) p. 4-86 | 1 |
| Water (Wat1) | Headwaters to west of LANL boundary | Mountains | Mostly perennial | Assumed saturated | | LANL (1998) p. 4-87, 4-79 | 4 |
| Water (Wat2) | Western LANL boundary to Cañon de Valle | Mountains | Unknown | Unknown | | LANL (1998) p. 4-87, 4-79 | 3 |
| Water (Wat3) | Cañon de Valle to well DT-10 | Mountains | Intermittent and Ephemeral | Saturated | | LANL (1998) p. 4-87, 4-79 | 4 |
| Water (Wat4) | DT-10 to spring 5AA | Mountains | Ephemeral | Not saturated | | LANL (1998) p. 4-87, 4-79 | 2 |
| Water (Wat5) | At spring 5AA | Mountains | Short perennial reach | Possibly saturated | | LANL (1998) p. 4-87, 4-79 | 4 |
| Water (Wat6) | Beneath 5AA to Rio Grande | Mountains | Ephemeral | Not saturated | | LANL (1998) p. 4-87, 4-79 | 2 |
| Mortandad (Mort1) | Headwaters to TA-50 outfall | Plateau | Ephemeral and Intermittent | Not saturated | See LANL (1998) p.4-92 for surface water loss estimates | LANL (1998) p. 4-89, 4-91 | 1 |
| Mortandad (Mort2) | Downstream from TA-50 wastewater treatment plant for about 1 mile | Plateau with large anthropogenic source | Perennial for about 1 mile | Saturated (~10 ft thick) | Dander (1998) 4500 mm/yr | LANL (1998) p. 4-89, 4-91 | 5 |
| Mortandad (Mort3) | Downstream from TA-50 wastewater treatment plant (from 1 mile downstream to 2 miles) | Plateau | Ephemeral | Saturated (~10 ft thick); approx. from TA-50 to just above San Ildefonso land | | LANL (1998) p. 4-89, 4-91 | 4 |

## Table 4-A-1.
## Determination of Net Infiltration
## Index for Sections of Canyons on the Pajarito Plateau (continued)

| Canyon/ ArcView Identifier | Reach | Headwaters (drainage <5 mi² unless noted) | Surface Water | Alluvial Water | Published Net Infiltration | Notes | NII |
|---|---|---|---|---|---|---|---|
| Mortandad (Mort4) | From just above boundary with San Ildefonso land to the Rio Grande | Plateau | Ephemeral | Not saturated | | LANL (1998) p. 4-89, 4-91 | 1 |
| Guaje (Guaje1) | Upstream (near springs) to downstream from the Guaje Reservoir | Mountains | Perennial | Saturated | | LANL (1998) p. 4-95 | 5 |
| Guaje (Guaje2) | Downstream from Guaje Reservoir to LA Canyon | Mountains | Intermittent | Possible seasonal saturation | | LANL (1998) p. 4-95 | 3 |
| Rendija (Ren1) | All | Mountains | Ephemeral | Unknown | | | 3 |
| Barrancas (Barr1) | All | Plateau | Intermittent and Ephemeral | Potentially saturated | | LANL (1998) p. 4-96, 4-97 | 2 |
| Bayo (Bayo) | | Plateau | Intermittent and Ephemeral | Potentially saturated (90 boreholes in former TA-10, found no alluvial water) | | LANL (1998) p. 4-97 | 2 |
| Three-Mile (Three) | All | Plateau | ? | ? | | Assume like Potrillo | 1 |
| Two-Mile (Two) | All | Mountain | Assumed ephemeral | Assumed saturated | | LANL, (1998) p. 4-60 | 3 |

# APPENDIX 4-B. MDA G MODEL

This appendix summarizes modeling work previously reported in Birdsell et al. (2000). The purpose of this modeling presentation is to demonstrate the use of the vadose zone concepts outlined in this report and to present representative modeling results for a relatively dry mesa. This system is therefore one end member of the different types of vadose-zone behavior expected for the plateau. A model for the other extreme, a wet canyon, is presented for Los Alamos Canyon in Appendix 4-C.

## 4-B-1. Introduction and Motivation

Performance assessment (PA) is required to site and authorize permanent disposal facilities for radioactive waste. The purpose of the PA is to demonstrate that performance measures related to protection of human health and the environment are not likely to be exceeded for a specified period of time. Performance objectives and periods of compliance vary according to the characteristics of the radioactive waste being disposed, but groundwater protection for U.S. sites is always explicitly required for at least 1000 years. This study presents an integrated case study that predicts the groundwater pathway dose in support of the performance assessment PA of the active, low-level, solid radioactive waste site located at the Laboratory, shown in Figure 4-4 (from Figure 1 of Birdsell et al. 2000). In contrast to the modeling study of Los Alamos Canyon presented in Appendix 4-C, this model illustrates aqueous contaminant transport from a relatively dry mesa, as opposed to a canyon bottom.

The three-dimensional unsaturated zone flow and transport model captures the complex hydrogeology and topography of the site and yields radionuclide flux estimates to the regional aquifer. Within the unsaturated zone model, the source release of radionuclides is computed for 38 waste disposal pits and four shaft fields (Figure 4-5, from Figure 3 of Birdsell et al. 2000), each contributing to the total inventory. The continued migration of radionuclides through the aquifer is calculated by using a three-dimensional model designed to maintain the temporally and spatially varying distribution of radionuclide flux from the unsaturated zone.

## 4-B-2. Hydrostratigraphy and Hydraulic Properties

The strata that underlie the LANL waste site are composed of a series of nonwelded to moderately welded rhyolitic ash-flow and ash-fall tuffs underlain by a thin pumice bed (Guaje Pumice), a thick basalt (Cerros del Rio Basalt), and a fanglomerate (Puye Formation), as shown in Figure 4-B-1 (from Figure 3 of Birdsell et al. 2000). The tuff has eroded to leave a system of alternating finger-shaped mesas and canyons. LANL's low-level waste disposal facility is located atop one such mesa with the waste buried in disposal pits and shafts to a depth of approximately 20 m. The surrounding canyons lie 30 m below the steep-sided mesa, and the water table is located approximately 250 to 300 m below the disposal pits.

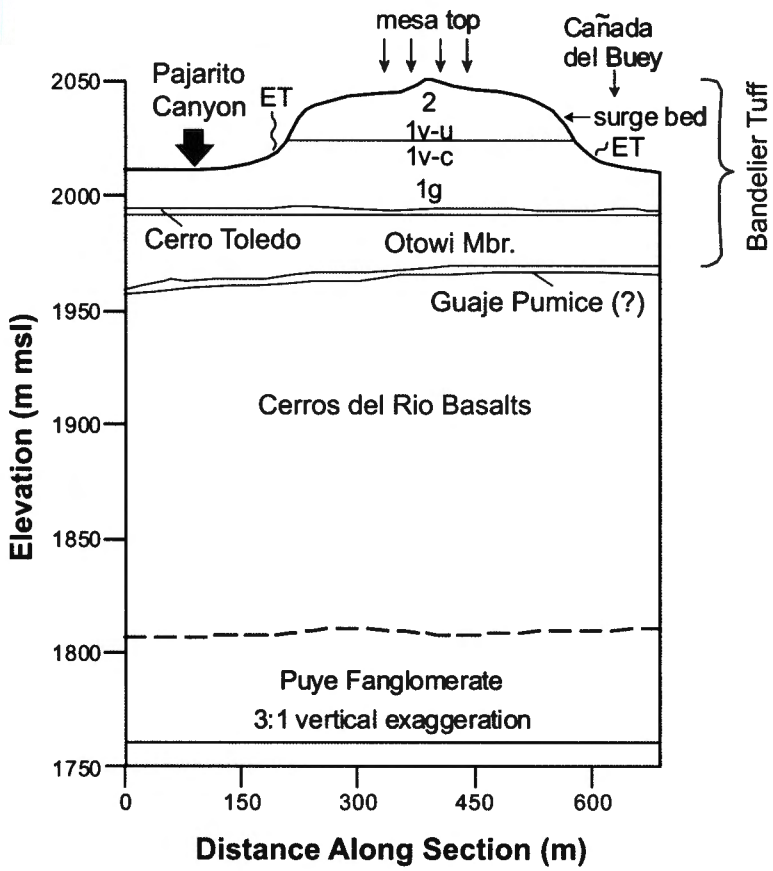


**Figure 4-B-1.** Conceptual model of hydrostratigraphy of the unsaturated zone for the MDA G Performance Assessment Model.

The stratigraphy at this site has several important features. The Bandelier Tuff, which composes the upper six stratigraphic units (See Figure 4-B-1), dips gently and thins toward the eastern end of the site. The top tuff layer, Unit 2, and the upper few meters of the second layer, Unit 1v-u, are extensively fractured and are separated by a thin surge bed (Krier et al. 1997). Fractures in the deeper tuff units have also been observed in outcrop (Krier et al. 1997). In addition, the Cerros del Rio Basalts, which comprise over 50% of the unsaturated zone, display significant variability (Turin, 1995). The basalts range from extremely dense with no apparent porosity, to highly fractured, to so vesicular as to appear scoriaceous. Finally, the Puye Fanglomerate lies at the base of the unsaturated zone and extends into the saturated zone. The fanglomerate consists of cobbles and boulders of volcanic debris in a matrix of silts, clays, and sands (Purtymun, 1995). Clay, silt and pumice lenses, and interbedded Cerros del Rio basalt are also common.

The van Genuchten model (van Genuchten, 1980), is used to represent the moisture retention characteristic curves for all units in the unsaturated-zone model. Birdsell et al. 2000 summarizes the hydrologic parameters used for all of the units in the unsaturated-zone flow and transport model. The parameters for the van Genuchten model (saturated permeability, porosity, inverse air entry pressure, etc.) are fairly well characterized for the six Bandelier Tuff units and for the crushed-tuff backfill but not for the deeper units. The properties for the tuff units (Krier et al.

1997), the crushed tuff, and the Guaje Pumice were measured on core samples of matrix material. Estimated values for the saturated conductivity and porosity of the Puye Fanglomerate (Purtymun 1984) are used, and we assume that the van Genuchten fitting parameters are similar to those of coarse sands.

No hydrologic property data were available for the basalts at the time this study was performed. The basalt is modeled as a composite-continuum medium made up of both fractures and matrix material (Peters and Klavetter 1988). To ensure conservatism, we set the continuum porosity of the basalt to that of the fractures, thus forcing very low residence times of solutes in this unit for which there was no hydrogeologic characterization data.

### 4-B-3. Infiltration

Although the average precipitation rate for the area is 35.6 cm/year (Bowen, 1990), most of this precipitation is lost to runoff and evapotranspiration, resulting in a heterogeneous infiltration pattern that is controlled by the mesa/canyon setting of the site. Infiltration is thought to be seasonal with most occurring during spring snowmelt and, to a lesser extent, during the summer thunderstorm season (Rogers et al. 1996a). Figure 4-A-1 shows the different scales of infiltration across the plateau. Based on measured rock saturations and chloride data, a very low net infiltration rate (same as net infiltration, as used in Appendix 4-A) of 1 to 10 mm/year is thought to exist within the mesa. Pajarito Canyon is wetter with an estimated net infiltration rate of 10 to 100 mm/year, while Cañada del Buey is dry with a net infiltration rate similar to the mesa top. The steep mesa sides represent an evaporative region water sink rather than a source region. The coupling of the fractured units separated by the high-permeability surge bed with the mesa's topographic relief is thought to enhance air circulation and consequently lead to evaporative drying within the mesa interior.

### 4-B-4. Radionuclide Releases

The waste disposal facility occupies about 300,000 $m^2$ atop a finger-shaped mesa with waste buried in pits and shafts to a depth of approximately 20 m (Figure 4-5). Between 1957 and 1995, solid radioactive waste was buried in 34 disposal pits and in almost 200 shafts located in five shaft fields. The waste form buried at the site contains over 60 radionuclides with the majority of the waste being $^{235}U$, $^{238}U$, and $^{232}Th$. Currently, only low-level radioactive waste is accepted, but prior to 1971, transuranic and mixed wastes were also accepted (Schuman 1997a). An expansion area with four large pits and another shaft field is planned for operation through 2044 and is included in this study.

The waste is categorized in terms of four disposal-unit classifications that are determined by the age of the wastes, because different regulations govern wastes disposed of during different time periods and because inventory records have improved with time. Detailed inventory information for the 1971–1988 waste and the 1988–1995 waste are obtained from disposal records. However, detailed inventory data are not available prior to 1971 and are uncertain for future activities. Therefore, the inventory in the 1957–1970 waste is extrapolated backwards based on disposal operations from 1971 to 1977, and the inventory for the 1996–2044 waste is projected based on current operations and expected future operations (Schuman 1997a; Vold and Shuman 1996).

The release of radionuclides from the disposal units is represented by one of two release mechanisms: rapid release or solubility-limited release (Vold and Schuman 1996). The maximum porewater concentration of each nuclide is calculated based on its inventory, its waste volume and the moisture content in the pits. This concentration is then compared to the nuclide's solubility limit to determine which source-release model is appropriate for each nuclide in each disposal unit. That is, if the maximum porewater concentration exceeds the nuclide's solubility limit, the release concentration is held at the solubility limit until that nuclide's inventory has been exhausted. If the porewater concentration does not exceed the nuclide's solubility limit, the rapid-release model is used. Nuclides with very large solubility limits, such as $^{129}I$ and $^{99}Tc$, are controlled by this mechanism throughout the site.

## 4-B-5. Computational Grids

The stratigraphic configuration used for the unsaturated zone model is derived from various sources including the then-current LANL site-wide geologic model (Vaniman et al. 1996), well-log picks, and surface observations. The data set is interpolated with the Stratagraphic Geocellular Modeling SGM Software Stratamodel to generate the three-dimensional geologic framework model. The three-dimensional unsaturated zone grid is generated with the Geomesh/X3D software (Gable et al. 1995) from this geologic framework model. An initial grid is constructed with the 45.7-m spacing of the geologic framework model and then resolved to include the 38 waste disposal pits and to better delineate the mesa sides. The final grid contains 41,542 nodes and 254,614 tetrahedral elements.

The saturated zone model extends from just west of the site to the Rio Grande. The grid is rectangular and oriented perpendicular to groundwater equipotentials. It is 9773 m long, 1280 m wide, and 100 m deep with 19,580 nodes and 102,960 tetrahedral elements. To better model the vertical dispersion of the contaminant plumes entering the aquifer from the unsaturated zone, the vertical element height is refined near the water table. The grid is also refined horizontally beneath the site to approximately 500 m downstream to accurately capture the spatial distribution of the radionuclides as they move toward the downstream compliance regions.

## 4-B-6. Model Implementation

Model implementation issues include how to assign the flow boundary conditions, initial conditions for transient flow, and hydraulic parameters in the model. We will also discuss some assumptions employed in model implementation.

To determine appropriate infiltration rates for the site, Birdsell et al. (2000) ran 5 two-dimensional simulations using different steady mesa-top infiltration rates of 10 mm/year, 1 mm/year, 0.1 mm/year, 0.01 mm/year and 0.0 mm/year, and compared the simulated saturation profiles to site field data. Figure 4-B-2 (adapted from Figure 5 of Birdsell et al. 2000) shows the calculated steady-state saturation profiles at the center of the mesa for the five infiltration rates along with the ranges of in situ saturation data measured in the six Bandelier Tuff units. The shape of the calculated saturation profiles shows the same trend as the data, e.g. saturations

decrease from Unit 2 to Unit 1v-u and then increase again in Unit 1v-c, etc., but no single infiltration rate yields predicted saturation values that fit the entire data set. Based on their study, together with that of Newman (1996), Birdsell et al. (2000) used a range of mesa-top infiltration rates from 1 to 10 mm/year. The bottom boundary for the unsaturated zone model is the water table.

For the saturated-zone model, a steady flow field is calculated by applying a pressure head difference of 101 m (Purtymun 1995) across the east and west sides of the model. No-flow boundaries are used for the top, bottom, north and south sides. Recharge is believed to occur mainly to the west of the site, at higher elevations in the Jemez Mountains. A water-balance estimate shows that the volume of water entering the aquifer from the unsaturated zone at the site is negligible compared to the aquifer volume (Birdsell et al. 1999). Thus, water flowing from the unsaturated zone to the aquifer is not included.

Several assumptions have been made in implementing the simulation model, including steady infiltration rates and an equivalent continuum medium for the Cerros del Rio Basalts. Although the deep percolation is thought to be seasonal with most occurring during spring snow melt and to a lesser extent during the summer thunderstorm season (Rogers et al. 1996a), Birdsell et al. (1999) studied the effects of annual transients in percolation rate on unsaturated zone transport at the site. They found that simulated transient pulses are damped with depth so that the calculated cumulative contaminant flux at the base of the Bandelier Tuff is similar under transient and steady flow fields.

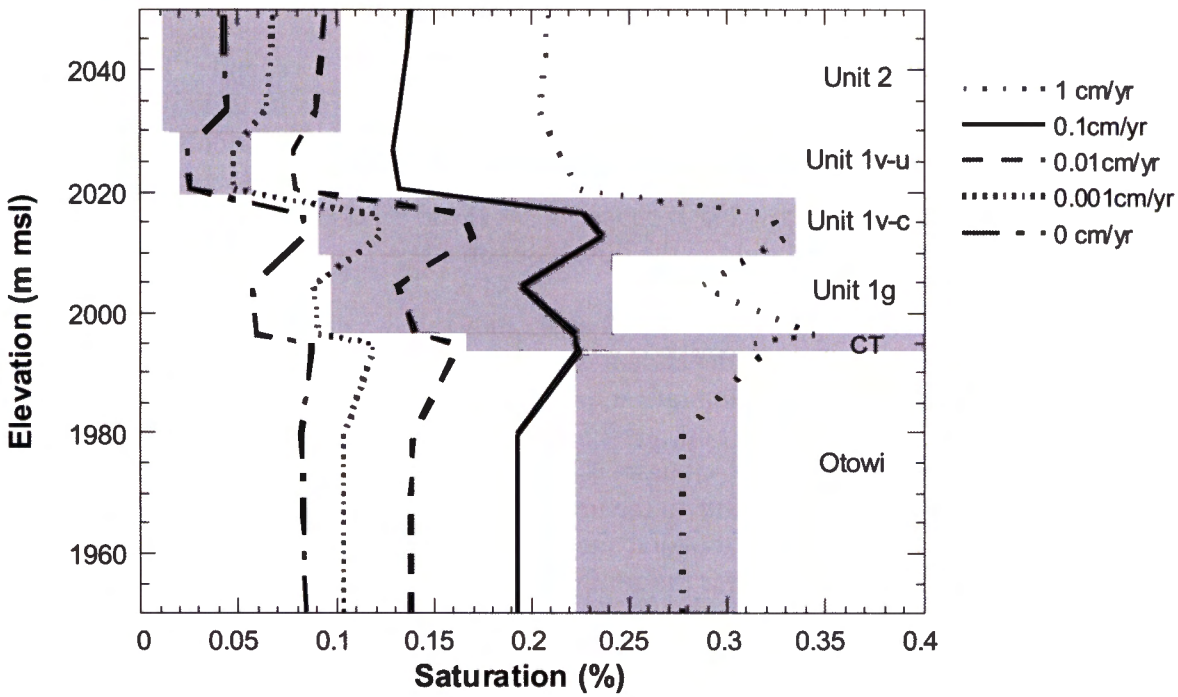


**Figure 4-B-2.** Comparison of site data (gray boxes) to calculated steady-state saturation profiles for several infiltration rates.

Another important assumption is that matrix flow dominates in the unsaturated tuff units at the site. This assumption is justified by considering that the pits are excavated completely through Unit 2, the most highly fractured tuff unit, thus excluding the fracture system and the likelihood of fracture flow through this unit. In addition, numerical studies of fracture flow for the site indicate that flow through fractured tuffs is difficult to maintain in low-saturation, high-capillarity systems (Soll and Birdsell 1998). Because the site in this study is a solid waste site, significant fracture flow through the unsaturated tuff units is unlikely.

Furthermore, the basalt is modeled as an equivalent continuum medium made up of both fractures and matrix material (Peters and Klavetter1988). Matrix properties are derived from analog basalts in Idaho (Bishop 1991). Fracture properties are chosen, through numerical sensitivity studies, so that no lateral diversion occurs at the top of the basalts in the simulations, even when the flow rate exceeds the matrix saturated hydraulic conductivity. The continuum porosity is set equal to the fracture volume fraction, $10^{-4}$, to ensure rapid transport of 1 to 5 years through this unit, hence, foregoing any retardation due to matrix flow or sorption. Notice that this treatment of transport through the basalt yields a conservative result e.g., faster groundwater travel times and higher peak doses than actually expected.

It is evident that there is significant uncertainty in infiltration rates. For the purpose of sensitivity analyses, we defined a base-case set of infiltration rates as a reference, as listed in Table 4-B-1. Variations are made on the base-case infiltration rates to examine the impact of uncertain parameters on the model results.

## 4-B-7. Representative Transport Result

Unsaturated zone transport calculations were run for $^{14}C$, $^{129}I$, $^{237}Np$, $^{99}Tc$, and $^{238}U$ using the base-case, steady flow field, 5_1_50 (nomenclature for these model results is defined in Table 4-B-1). These nuclides were chosen because of their low distribution coefficients, ranging from 0 to 2.43 for most of the unsaturated zone units. Using screening techniques developed by Birdsell et al. (1995), Birdsell et al. (2000) chose $^{14}C$, $^{129}I$, and $^{99}Tc$, and eliminated the remaining nuclides from consideration in the dose assessment.

Figure 4-B-3 (adapted from Figure 8 of Birdsell et al. 2000) shows the simulated $^{129}I$ plumes in the unsaturated zone for the four age-dependent waste classes after 1000 years using the base-case flow field. Although the infiltration rate at each source region is the same (5 mm/year), the four plumes are quite different due to both inventory variations and differences in bed thickness. The inventory distribution in the disposal units is heterogeneous, leading to large variations in radionuclide flux from the disposal units to the unsaturated zone. For example, the 1971–1988 (Figure 4-B-3b) inventory dominates the total site release of $^{129}I$ to the aquifer at 1000 years. Also, the 1988–1995 shafts located near the southern edge of the mesa (Figure 4-B-3c) concentrate nearly 80% of the 1988–1995 $^{129}I$ inventory into a small area. This localized inventory produces a predominant plume at the southern portion of the mesa, while the pits to the north and west produce the less concentrated plumes. The location of the basalt unit and the effect on plume migration of the vertical, fracture-dominated flow through this unit is readily visible in these simulations. Once the solutes reach the basalt, they migrate quickly through the unit. In the 1996–2044 waste scenario (Figure 4-B-3d), only the plume's leading edge reaches the basalt after 1000 years because the Bandelier Tuff units are much thicker beneath this proposed expansion area.

To assess the effect of uncertainty in flow rate on transport results, Birdsell et al. (2000) examined the transport of the 1988–1995 $^{129}I$ inventory using different flow fields and compared the nuclide fluxes through the unsaturated zone. Figure 4-B-4 (from Figure 10 of Birdsell et al. 2000) shows the total flux of $^{129}I$ for the five flow fields described in Table 4-B-1. By comparing the 1_1_20 case, the 5_1_20 case, and the 10_1_20 case, it is seen that increased mesa percolation leads to faster breakthrough and increased solute flux through the unsaturated zone. This flow-rate dependency is compounded by the velocity-dependent rapid-release source term. The solute flux at 1000 years for the lowest flow case, 1_1_20, is five to seven orders of magnitude less than the other cases considered. This case is used to predict the lower-bound dose in the uncertainty analysis. Comparing the 5_1_20 case to the 5_1_50 case shows that additional flow through Pajarito Canyon results in faster breakthrough and increased solute flux to the saturated zone. The 10_5_100 case represents the wettest case and yields the fastest breakthrough and highest flux to the saturated zone and, consequently, the highest dose over the first 1000 years. This case is used to estimate an upper-bound dose for the uncertainty analysis.

**Table 4-B-1.**
**Infiltration Rates (mm/year) Used as Upper Boundary Conditions for MDA G Performance Assessment**

| | Mesa Top | Cañada del Buey | Pajarito Canyon |
|---|---|---|---|
| 1_1_20 (lowest flow case) | 1 | 1 | 20 |
| 5_1_20 | 5 | 1 | 20 |
| 5_1_50 (base case) | 5 | 1 | 50 |
| 10_1_20 | 5 | 1 | 20 |
| 10_5_100 (highest flow case) | 10 | 5 | 100 |

Source: Birdsell et al. (2000).

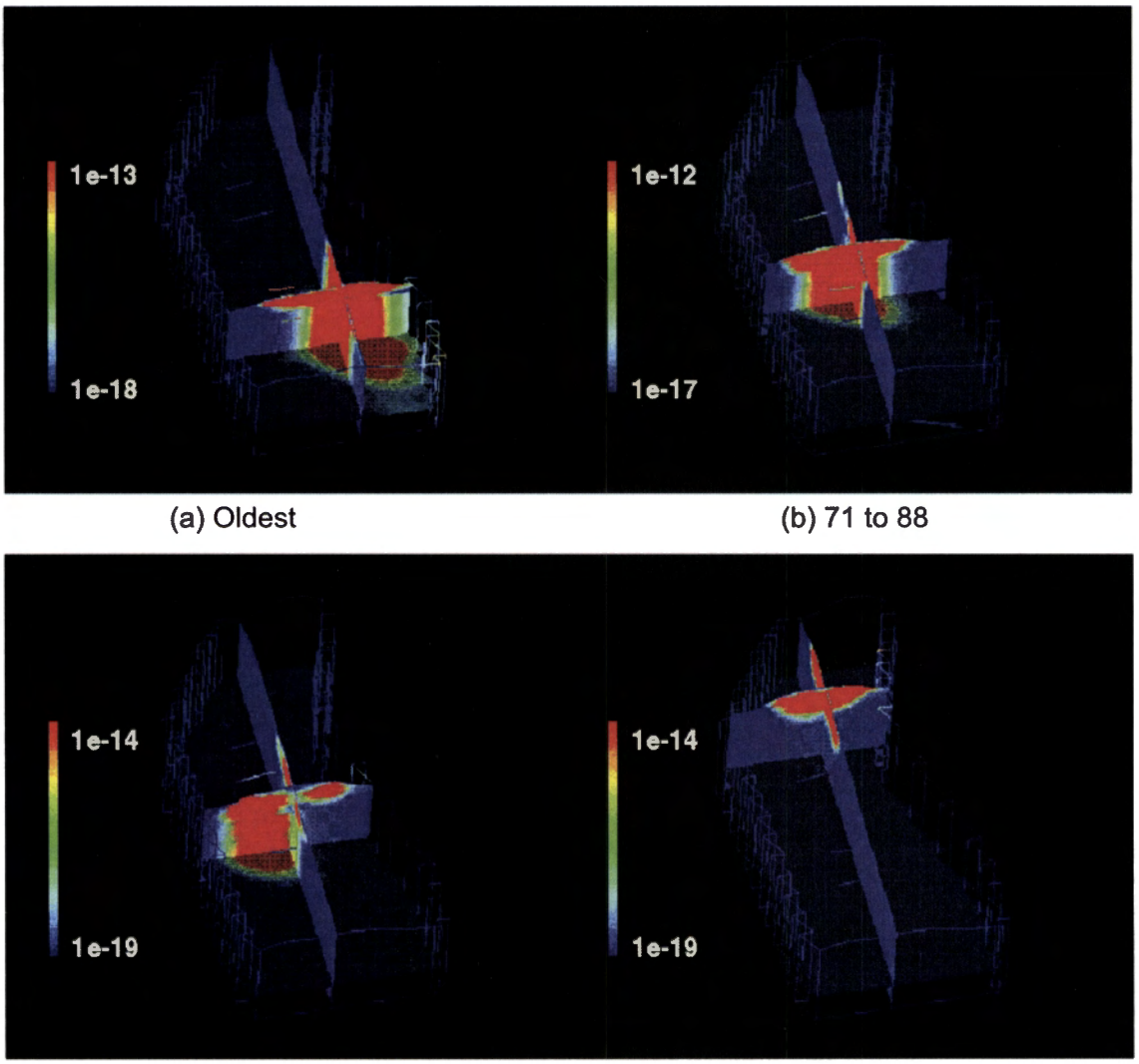


(a) Oldest (b) 71 to 88

(c) Historic (d) Future

**Figure 4-B-3.** Iodine-129 plumes (concentration, moles/liter) in the vadose zone at 1000 years for the four different source regions, base-case flow field.

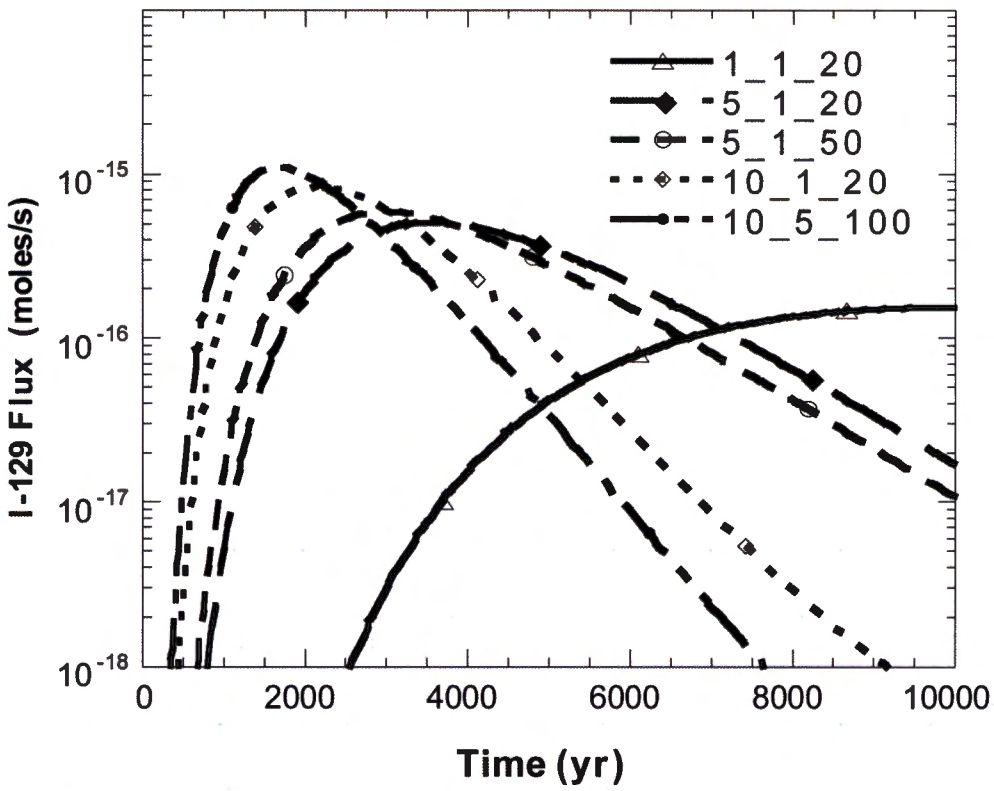


**Figure 4-B-4.** Total flux of the 1988–1995 $^{129}I$ inventory from the unsaturated zone to the saturated zone for various flow cases.

## 4-B-8. Discussion

Due to uncertainty in model parameters, the results of these transport simulations contain intrinsic uncertainty. The greatest uncertainties associated with predicting aquifer-related doses from the site, according to Birdsell et al. (2000), are related to the understanding of the mechanisms that control flow and transport within the unsaturated zone and our ability to model these mechanisms. At this point, they concluded that uncertainty related to the hydrologic processes themselves, i.e., conceptual model uncertainty, dominates the ability to make accurate predictions of transport at the site moreso than uncertainty related to the hydrologic and geochemical properties data. Importantly, however, predicted doses using parameters from the most conservative ends of the uncertain ranges are still well below regulatory concern.

The results of Birdsell et al. (2000) indicate that the mesa-top infiltration rate has the greatest impact on the simulated migration of waste through the unsaturated zone. It controls both the source release rate and subsequent downward solute migration. They bounded this uncertainty by considering a base-case flow field and high- and low-flow cases. As shown in Table 4-B-2, a variation in mesa-top infiltration rate from 1 to 10 mm/year results in a range of six orders of magnitude in the 1000-year groundwater-related doses. Clearly, a good understanding of this key parameter is important to the dose assessment. However, because doses are so much less than the performance objectives developed in Birdsell et al. (2000), conservative yet realistic infiltration rates seem adequate for this site. With respect to travel times, models of dry mesas such as that

associated with MDA G generally predict travel times in the neighborhood of 1000 years or more. This basic result indicates that groundwater pathway risks associated with waste disposed under dry mesa conditions are expected to be risks that will present themselves far into the future, as opposed to there being a significant present-day risk. This result applies only to the groundwater: a complete pathway assessment should be conducted that includes other exposure scenarios in addition to groundwater.

**Table 4-B-2.**
**Maximum Ground Water and**
**All Pathways Doses for the PA and CA Wastes,**
**Base Case Flow Field (mrem/yr) MDA G Performance Assessment.**

| | PA - Ground Water | PA - All Pathways | CA - All Pathways |
|---|---|---|---|
| Performance Objective | 4 | 25 | 100 |
| 1000 yr (Base Case) | $2.4 \times 10^{-7}$ | $6.5 \times 10^{-7}$ | $3.7 \times 10^{-5}$ |
| Peak Dose (Base Case) | $3 \times 10^{-5}$ @ ~4500 yrs | $1 \times 10^{-4}$ @ ~4500 yrs | $2 \times 10^{-3}$ @ ~3000 yrs |
| 1000 yr (high-flow case) | $8.0 \times 10^{-6}$ | $2.2 \times 10^{-5}$ | $1.4 \times 10^{-3}$ |
| 1000 yr (low-flow case) | $9 \times 10^{-12}$ | $2 \times 10^{-11}$ | $1 \times 10^{-10}$ |

Source: Birdsell et al. (2000).

Finally, there are residual uncertainties related to flow in the deeper unsaturated-zone units for which few hydrologic data are available. The simulations take virtually no credit for transport times through the Cerros del Rio basalts, which make up more than 50% of the unsaturated zone. The transport results are based on the steady-flow assumption and on the use of matrix, hydrologic properties for all tuff units at the site. The response of this fractured system to transient flow events is not completely known. Transient calculations (Birdsell et al. 1999) indicate that the steady-flow assumption is adequate because fluctuations in both saturation and contaminant flux rates dampen with depth even when including fractures in the upper two units. Fracture infiltration studies (Soll and Birdsell, 1998) lead to the conclusion that fracture flow is difficult to initiate and is short-lived in the upper two tuff units at the observed low field saturations. These conclusions are supported by modeling studies presented for Los Alamos Canyon in Appendix 4-C, as well as the findings of Robinson et al. (2005b).

# APPENDIX 4-C. LOS ALAMOS CANYON MODEL

## 4-C-1. Introduction and Motivation

Los Alamos Canyon, as shown in Figure 4-6, is one of the most complex sites at the Laboratory. A number of technical areas have been or are currently located in or adjacent to the canyon, resulting in multiple release locations along the canyon. This section examines, through a synthesis of available data and the development of numerical models, fluid flow and contaminant transport in the vadose zone beneath Los Alamos Canyon. The subsurface hydrology and transport in the vadose zone is also a challenging activity, given the wide range of infiltration rates, the presence of perched water, and the introduction of a host of contaminants of different chemical properties. Because the canyon serves as a collector of a wide range of contaminants, we decided that it was necessary to develop a model at the scale of the canyon, rather than at a smaller scale. The specific goals of the model are as follows:

- Synthesize the available data and conceptual understanding of the vadose zone hydrology beneath Los Alamos Canyon;
- Produce a "base-case" numerical model of the subsurface vadose zone hydrology that ultimately can be used to predict contaminant migration rates and concentrations in fluids reaching the regional aquifer beneath the canyon;
- Quantify the uncertainties associated with those predictions by establishing the bounds on system behavior through a suite of possible models, all of which are consistent with the available data, but which bracket the range of possible behavior;
- Provide a simulation tool for predicting the fate and transport of contaminants in Los Alamos Canyon under different assumed hydrologic and ER stewardship scenarios; and
- Demonstrate a model development methodology that can be used in studies of other canyons on the Pajarito Plateau.

This work focuses on the hydrology beneath Los Alamos Canyon, as a first step toward developing a predictive tool that can be used to simulate contaminant migration in the canyon. Since water is the carrier fluid for the contaminants of interest, constructing a realistic flow model that captures the most important hydrologic processes of the vadose zone is an essential first step in the development of a reliable model. Although we primarily restrict attention to flow issues, tritium transport in the vadose zone is also modeled here. Tritium, in the form of tritiated water, is an excellent tracer for groundwater, and hence is included in this modeling study as a constraint on the flow model. Although the work here is restricted to Los Alamos Canyon, we anticipate that the methodology and approach applied here can be used to develop models at other sites at the Laboratory.

## 4-C-2. Hydrostratigraphy

Accurate modeling of groundwater flow and transport in Los Alamos Canyon requires the integration of geologic model information with computational grids. Stratamodel was used to create a three-dimensional geologic framework model for Los Alamos Canyon. The geologic framework model consists of 20 distinct geologic units and is the product of a continuous process of model development and improvement in support of the Hydrogeologic Workplan

(LANL 1998) activities, including the development of numerical flow and transport models such as the present study. The record of model development and improvement is documented in various LANL reports (Vaniman et al. 1996, Carey et al. 1999). The different versions of the geologic models are distinguished based on the fiscal year (FY) in which they were built. Several of the sensitivity analyses were performed with the FY98 version as the geologic basis, while most of simulations are done based on the FY99 version.

The defined stratigraphic units and their accepted designators are listed in Table 4-C-1. Figure 4-C-1 shows a two-dimensional cross section of the geologic model, illustrating the complexity of the current conceptualization of the subsurface. A characteristic of this two-dimensional stratigraphic model that is different than other models developed for sites on the Pajarito Plateau such as MDA G (Birdsell et al. 1999) and Mortandad Canyon (Dander 1998) is the absence of significant thickness of the Tshirege Member of the Bandelier Tuff. Los Alamos Canyon cuts deeply into the Bandelier Tuff such that the Otowi Member is the first unit encountered beneath the alluvium in the canyon bottom over much of the model domain. In the eastern portion of the model, the Otowi is not present, and instead the Cerros del Rio (Tb4) is the first unit encountered. This is the case at R-9, where the stratigraphic section consists only of basalts and the Puye Formation. Figure 4-C-2 depicts the full three-dimensional model stratigraphy, along with the locations of important wells and facilities referred to later.

Table 4-C-2 lists the hydrologic properties used for the Los Alamos Canyon model. Permeability and porosity values used for each unit are listed first, followed by the unsaturated hydrologic parameters for the van Genuchten (1980) formulation used in the present study. It is assumed in this study that hydrologic properties are homogeneous within each individual unit. Although the appropriate hydrologic properties for the various units are thought to be somewhat site dependent, these property values are representative averages of site-wide conditions and can be used as a starting point for vadose zone numerical simulations.

**Table 4-C-1.**
**Stratigraphic Units Present in the Vicinity of Los Alamos Canyon**

| Group/Formation | Unit Name | Symbol |
|---|---|---|
| Tshirege Member of the Bandelier Tuff | Unit 5 | Qbt5 |
| | Unit 4 | Qbt4 |
| | Unit 3 | Qbt3 |
| | Unit 2 | Qbt2 |
| | Vapor-phase altered member of Unit 1 | Qbt1v |
| | Glassy member of Unit 1 | Qbt1g |
| | Tsankawi Pumice | Qbtt |
| Cerro Toledo Interval | Cerro Toledo | Qct |
| Otowi Member of the Bandelier Tuff | Otowi Member ash flow | Qbof |
| | Guaje Pumice bed | Qbog |
| Puye Formation | Puye fanglomerate | Tpf |
| | Totavi Lentil | Tpt |
| Cerros del Rio basalt | Basalt 4 | Tb4 |
| | Basalt 3 | Tb3 |
| | Basalt 2 | Tb2 |
| | Basalt 1 | Tb1 |
| Tschicoma Formation | Tschicoma latite | Tt2 |
| | Tschicoma dacite | Tt1 |
| Santa Fe Group | Chaquehui (volcaniclastic) aquifer unit | Tsfuv |
| | Santa Fe Group undifferentiated | Tsfu |

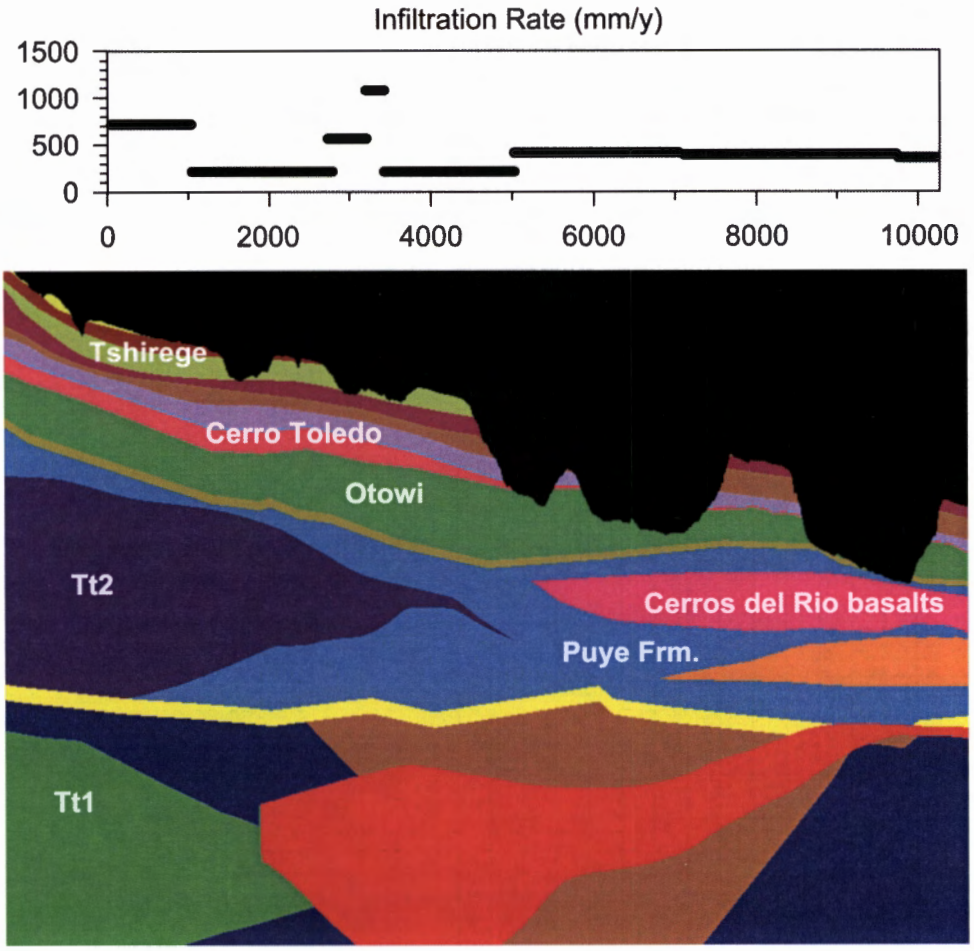


**Figure 4-C-1.** Cross section of stratigraphy in the vicinity of Los Alamos Canyon. Also shown is the infiltration map used along the canyon bottom (derived from water budget study of Gray 1997).

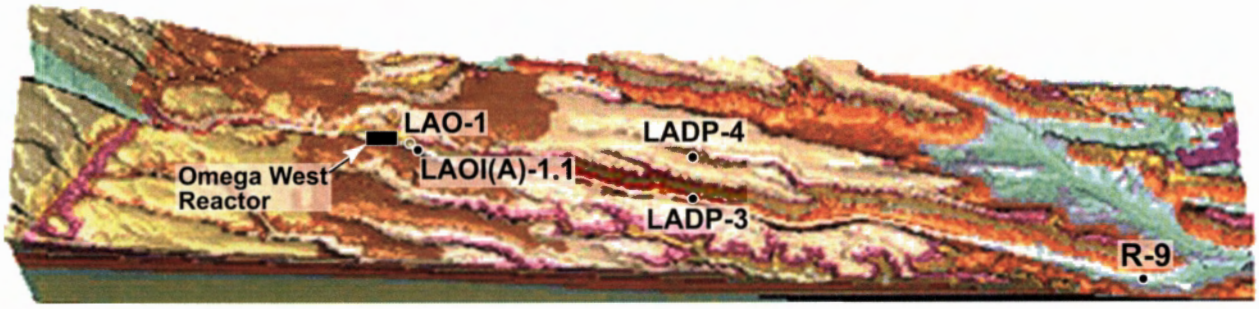


**Figure 4-C-2.** Three-dimensional depiction of the stratigraphic framework model used to construct the flow and transport model for Los Alamos Canyon. Important wells and the site of a nuclear reactor are also shown.

**Table 4-C-2.**
**Hydrologic Property Values in the Los Alamos Canyon Model**

| Hydrogeologic Unit | Geologic Designation | Permeability, $m^2$ | Porosity | Van Genuchten $\alpha$ parameter, $m^{-1}$ | Residual Moisture Content | Van Genuchten $n$ parameter, unitless |
|---|---|---|---|---|---|---|
| Unit 3, Tshirege Member | Qbt3 | 1.01e-13 | 0.469 | 0.29 | 0.045 | 1.884 |
| Unit 2, Tshirege Member | Qbt2 | 7.48e-13 | 0.479 | 0.66 | 0.032 | 2.09 |
| Vitric unit, Tshirege Member | Qbt1v | 1.96e-13 | 0.528 | 0.44 | 0.009 | 1.66 |
| Glassy unit, Tshirege Member | Qbt1g | 3.68e-13 | 0.509 | 2.22 | 0.018 | 1.592 |
| Basal pumice unit, Tshirege Member | Qbtt | 1.01e-12 | 0.473 | 1.52 | 0.01 | 1.506 |
| Cerro Toledo Interval | Qct | 8.82e-13 | 0.473 | 1.52 | 0.01 | 1.506 |
| Otowi Member | Qbof | 7.25e-13 | 0.469 | 0.66 | 0.026 | 1.711 |
| Guaje Pumice Bed | Qbog | 1.53e-13 | 0.667 | 0.081 | 0.01 | 4.026 |
| Cerros del Rio Basalt, Puye Formation | Tb4 | 2.47e-12 | 0.3 | 0.1 | 0.066 | 2. |
| Tschicoma dacites | Tt2 | 2.96e-13 | 0.3 | 0.1 | 0.066 | 2. |
| Miocene basalts, Santa Fe Group | Tb3 | 2.96e-13 | 0.3 | 0.1 | 0.066 | 2. |
| Puye Formation | Tpf | 4.73e-12 | 0.25 | 5. | 0.01 | 2.68 |
| Totavi Lentil | Tpt | 4.73e-12 | 0.25 | 5. | 0.01 | 2.68 |
| Santa Fe Group | Tsfuv | 2.65e-13 | 0.25 | 5. | 0.01 | 2.68 |

## 4-C-3. Infiltration Rates and Water Budget Model

The infiltration rate on the upper surface is one of the most important inputs in simulating flow and transport in the site. For the mesa areas, various hydrologic and chemical techniques have been employed to estimate infiltration rates in various settings. Rogers et al. (1996a) outlined an interpretive technique for estimating local infiltration rates based on measured hydrologic properties and water content values in samples collected from the vadose-zone tuffs. They obtained infiltration rates on mesas as low as 0.06 mm/yr with higher mesa values only found where surface conditions such as ponds were present. In more recent analyses, Birdsell et al. (1999) obtained a value on the order of 1 mm/yr for undisturbed mesa conditions at TA-49, and values estimated from 60-300 mm/yr beneath paved regions. At TA-16, chloride mass balance data collected by Newman (presented in Birdsell et al. 2005) were interpreted using the chloride mass balance method. Infiltration rates slightly higher than 1 mm/yr were obtained in this manner, which is consistent with the analyses of moisture content. Therefore, an infiltration rate of 1 mm/yr is assumed at all locations except the canyon bottom in the current model.

To estimate the infiltration rate along Los Alamos Canyon, we use the study of Gray (1997), who focuses on the water budget and fluid flow in the surface water stream and shallow alluvial aquifer in Los Alamos Canyon. The fundamental model equation used to evaluate the water budget is

$$I = P - R - ET - \Delta S$$

where $I$ is infiltration, $P$ is precipitation, $R$ is runoff, $ET$ is the evapotranspiration term, and $\Delta S$ is the change in fluid storage. Since there was no experimental basis for estimating $\Delta S$, Gray assumes it to be zero, listing it as an uncertainty in his analysis. The water budget calculations employed data from several sources, including stream-flow data from three stream-flow gages that provide estimates of surface water flow rates, and meteorological data from five precipitation measurement stations. These data were used by Gray in both an overall water budget for the canyon and a detailed water budget calculation. Details can be found in Gray (1997).

Figure 15 of Gray (1997) shows the results from the overall water budget performed for Los Alamos Canyon. The key result from this aspect of Gray's work is the estimation of the relative amounts of ET, runoff, and infiltration to the deeper vadose zone. Over the three-year period of that study, Gray found that 71% to 83% of the water introduced into Los Alamos Canyon was lost to evapotranspiration. Gray points out many limitations and uncertainties in this estimate. Given the direct influence of this term in the water budget and indirectly on infiltration rate, a more comprehensive study of the processes is warranted. Most of the rest of the water not undergoing evapotranspiration is estimated to be recharging the deeper vadose zone, whereas runoff was found to be relatively small. Average infiltration rates applicable to the Los Alamos Canyon watershed were found to range from roughly 100 to 200 mm/yr for the period of study. These values are average values for the watershed, and might be expected to be higher locally directly beneath the stream channel.

In addition to the overall water budget, Gray (1997) conducted a detailed study using measured data and a numerical model to further break down the components of the water balance. A calibrated numerical flow model of the alluvial aquifer was developed to analyze the spatial and temporal distributions of infiltration in the canyon. Gray divided the canyon alluvial aquifer model into nine zones that corresponded to locations of the monitoring wells used in the model calibration. The model calibration procedure involved adjusting the drain conductance term that controlled the water flux leaving the alluvial aquifer (and entering the underlying bedrock) to match the water level data. The other terms in the water budget (excepting the storage term) were also included in the model, so that the calibration procedure provides a direct estimate of the spatially dependent infiltration rate along the canyon. Table 4-C-3 summarizes the results of this analysis. The highest infiltration rate of 1076 mm/yr occurs in Gray's Zone 4, corresponding to well LAO-0.8. This well falls near the southern projection of the Guaje Mountain fault zone, and was determined to have a strikingly low water level. This observation, and the numerical model calibrated to it, suggest high infiltration in this zone, perhaps due to an enhanced permeability due to fracturing. Zones 1 and 3 also exhibit higher than average infiltration. Gray postulates that Zone 3 may be higher because of its proximity to the Guaje Mountain fault, and Zone 1 infiltration may be high due to a greater saturated thickness in this portion of the canyon. The rest of the Los Alamos Canyon study area exhibited lower infiltration rates.

## 4-C-4. Contaminant Sources

A host of possible contaminant source sites exist for Los Alamos and DP canyons, resulting from past and present Laboratory operations. The most important of these for our purposes include TA-1 (Townsite), TA-41 (Weapons Development Facility), TA-2 (Omega West Reactor Site), TA-21 (DP Site), and TA-53 (LANSCE). In particular, the Omega West reactor site, located in Los Alamos Canyon, was used since 1943 to house and operate a series of research reactors. Early reactors were fueled by aqueous uranyl solutions, whereas other reactors were fueled by solid fuel elements. A variety of contaminants (mostly radionuclides) are suspected to have been released into the canyon. Most relevant to the present study is tritium, produced from a leak in the primary cooling water system at the reactor. The leak occurred from a break in a weld seam in a section of the delay line running from building TA-2-1 to the surge tank. This leak was discovered in 1993, and tritium was detected within a stretch of canyon corresponding to the southern projection of the Guaje Mountain fault zone. Typical concentrations in the cooling water ranged from $15.7 \times 10^6$ to $20.2 \times 10^6$ pCi/L. The duration of the leak is not documented, but measurements of tritium concentrations in alluvial aquifer well LAO-1 (located at the eastern boundary of TA-2) suggest that the leak may have begun between November 1969 and January 1970. This reactor was permanently shut down in 1994.

In the transport simulations, among all possible contaminants, we choose tritium, which, in the form of tritiated water, is among the simplest chemical constituents to model because its chemical state as a water molecule implies that it is a tracer for water. Other contaminants may undergo sorption, precipitation, and complex speciation processes that complicate the transport simulation.

**Table 4-C-3.**
**Infiltration Rates for Various Portions of Los Alamos Canyon***

| Zone | Location | Infiltration, mm/yr | ET, mm/yr | Downgradient Loss, mm/yr |
|---|---|---|---|---|
| 1 | LA Reservoir to 1100 ft east of bridge | 714 | 464 | 56 |
| 2 | End of Zone 1 to LAO-C | 213 | 167 | 223 |
| 3 | LAO-C to LAO-0.6 | 566 | 158 | 547 |
| 4 | LAO-0.6 to LAO-0.8 | 1076 | 0 | 148 |
| 5 | LAO-0.8 to LAO-1 | 222 | 195 | 93 |
| 6 | LAO-1 to LAO-2 | 408 | 28 | 111 |
| 7 | LAO-2 to LAO-6 | 399 | 93 | 46 |
| 8 | State Rt. 4 to Lab boundary | 362 | 139 | 19 |
| 9 | East of Lab boundary | 325 | 121 | 0 |

* Values from the analysis of Gray (1997)

## 4-C-5. Numerical Grids

To deal most efficiently with issues of computational demands and model accuracy, we have utilized both two- and three-dimensional models for various flow and transport model analyses. A major advantage of two-dimensional grids is the smaller number of nodes and elements. Calculations run very quickly, making the grid appropriate for scoping calculations and sensitivity studies. When very high spatial resolution is required, three-dimensional grids are also necessary. However, since the grid is two-dimensional, there are limitations as to what spatial variability of flow properties can be captured in the model. In two-dimensional simulations, the model domain implicitly assumes that flow is negligible in the direction normal to the grid. This problem is relaxed in the three-dimensional grid, at the cost of greater computational times and a somewhat reduced grid resolution. Computational grids have been built for both the two-dimensional and three-dimensional simulation models.

For the two-dimensional grid, the western boundary of the domain is located at New Mexico state plane coordinates (492916.5, 541257.7), just west of the Omega Bridge. Note that all state plane coordinates are specified in meters. The eastern boundary extends in a one-dimensional fashion from the western boundary to a coordinate location of (502959.6, 539688), just west of the intersection of State Route (SR) 4 and New Mexico State Highway (NMSH) 502. The extent of Los Alamos Canyon in the two-dimensional model is represented by drawing a one-dimensional line as closely as possible down the center of the canyon. To do this, the length of the canyon was traced from the western to the eastern boundary using a digital topographic map as a reference in Stratamodel (See Figure 4-6). The bends in Los Alamos Canyon are also accounted for. The final version of the two-dimensional grid for Los Alamos canyon consists of 57,004 nodes, 111,256 tetrahedral elements, and contains 11 materials.

In the process of selecting the simulation domain for the three-dimensional Los Alamos Canyon grid, we consider the historical information about contaminant releases and important sites along the canyon that may be relevant to contaminant transport issues in the canyon. It is deemed necessary that areas such as TA-21, TA-2 (the Omega West reactor), DP Canyon, and well R-9 be within the domain of the three-dimensional grid. The Los Alamos Canyon model domain is rectangular in shape and encompasses most of Los Alamos Canyon, DP Canyon, and some of the adjacent mesas to the north and south of Los Alamos Canyon. The model domain extends from the topographic surface to a depth of 1650 meters. Within this grid, we capture both the mesas and the canyon in the same grid, so that infiltration boundary conditions and contaminant releases can be applied correctly. One of the major constraints on the grid building process is to keep the total number of nodes as low as possible but, at the same time ensure that there is adequate resolution in the areas of interest. The final grid, shown in Figures 4-C-3 and 4-C-4, is a three-dimensional grid that is composed of 301,436 nodes, 1,688,457 elements, and 14 unique materials.

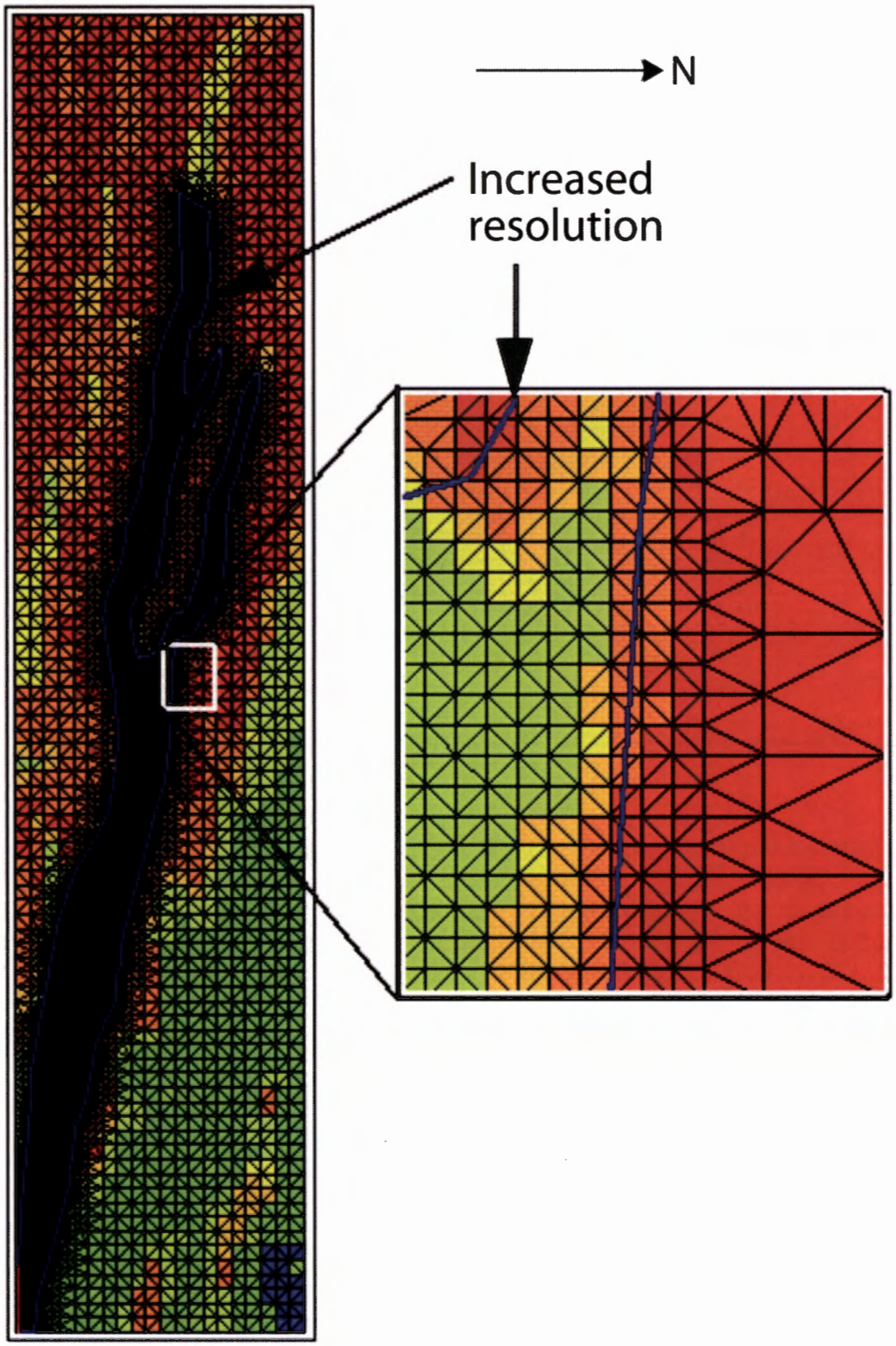


**Figure 4-C-3.** Three-dimensional model grid. Plan view showing the areas of enhanced grid resolution along Los Alamos and DP Canyons.

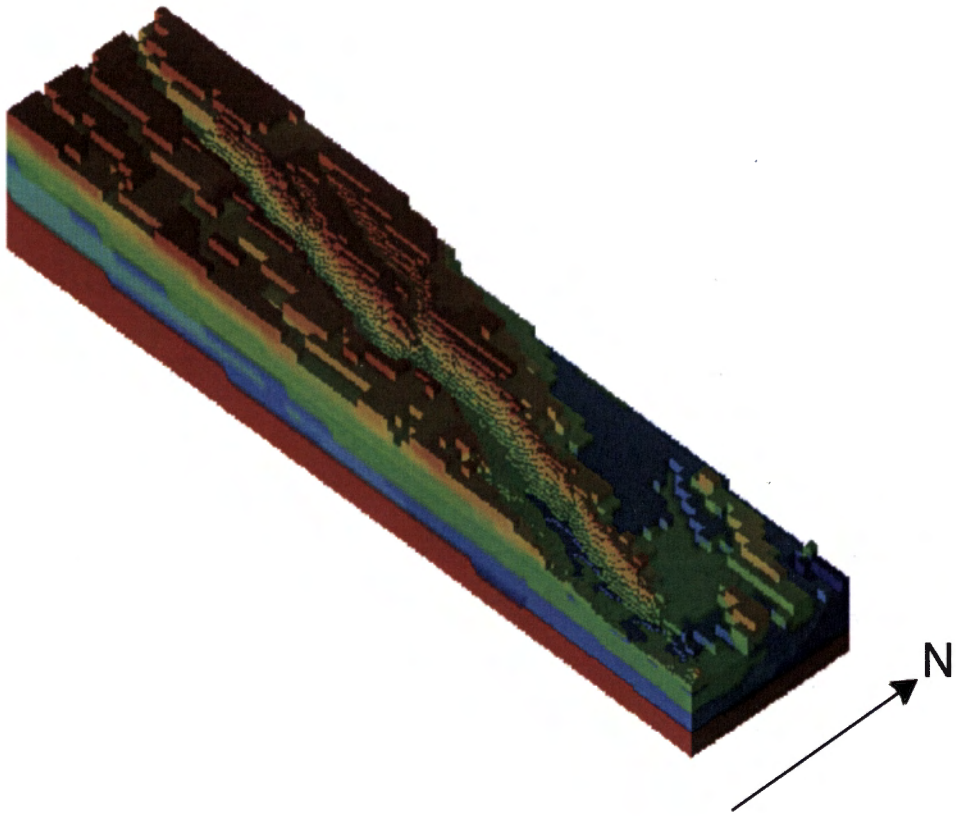


**Figure 4-C-4.** Three-dimensional view of the Los Alamos Canyon model numerical grid.

## 4-C-6. Model Implementation

Model implementation issues include how to assign the flow boundary conditions, initial conditions for transient flow, and hydraulic parameters in the model. We will also discuss some assumptions employed in model implementation.

The infiltration values obtained from Gray (1997) in Los Alamos Canyon were applied directly to the two- and three-dimensional models. In the three-dimensional model, it is relatively straightforward to apply an estimated infiltration rate on all grid nodes identified as representing the interface of the alluvium bottom and the bedrock. In a two-dimensional model, we implicitly assume that there are no variations in infiltration in the third dimension (the horizontal direction normal to the canyon). As a result, the appropriate flux to be input to the two-dimensional model is not necessarily the value along the canyon bottom. Figure 4-C-1 shows the infiltration map above the two-dimensional model domain. The infiltration rates so applied in two dimensions are expected to be maximum values. In this study, it is assumed that the relative flux entering the subsurface at different locations along the canyon remains the same, but the absolute value of infiltration is uncertain. The fluid mass flow rate at each top node is determined upon multiplying the infiltration rate at that node by the nodal area normal to the upper surface of the model (for an assumed 1 m thickness of the two-dimensional model domain).

The bottom boundary condition represents the water table. The water table is estimated from results compiled by Keating (personal communication, 1999). Any node falling below this surface is assigned a value of saturation equal to 0.999 to represent the regional aquifer. Therefore, the vadose zone model domain extends only down to this surface, and the bottom region is simply a boundary condition rather than a calculated result.

The hydrologic properties at each grid node in the two- and three-dimensional models are determined by the properties of the unit in which the node falls. The hydrologic properties used for the Los Alamos Canyon model are listed in Table 4-C-2.

It is evident that there is significant uncertainty in the hydrologic properties and infiltration rates due to, for example, the true variability of medium properties, a limited number of measurements, and measurement errors. For the purpose of sensitivity analyses, we defined a base-case set of hydrologic properties and boundary conditions as a reference. In the base case, the values for the hydrologic properties are taken from Table 4-C-2 and the infiltration rate for the canyon is taken from Table 4-C-3 (1 mm/yr for the mesas). The base case parameter set used the mean values of the hydrologic parameters for all units. This practice has been used in other modeling studies on the Plateau, including Dander (1998) and Birdsell et al. (1999). Variations are made on the base-case parameters to examine the impact of uncertain parameters on the model results.

Once the hydrologic properties and initial and boundary conditions are selected, the flow and transport equations are solved using the finite element heat and mass (FEHM) code that simulates heat conduction, heat and mass transfer for multiphase flow within porous and permeable media, and noncondensible gas flow within porous and permeable media. The code handles model geometries in two or three dimensions, and has a variety of solute transport model options available for use. For details of the fundamental model equations solved by the code, see Zyvoloski et al. (1997).

## 4-C-7. Fluid Saturation Model Results

Figures 4-C-5 and 4-C-6 show a full three-dimensional view of fluid saturation and a series of two-dimensional vertical slices through the three-dimensional model. As expected, the figure shows wet conditions in the canyon, dry in surrounding mesas. As with the two-dimensional model, this model result shows the overriding importance of the stratigraphy in controlling the water contents in the rock. The local infiltration rate also exerts a strong control on the results. Directly beneath the canyon, fluid saturation is much higher within a given stratigraphic unit than in other parts of the model domain, a reflection of the high infiltration in the canyon.

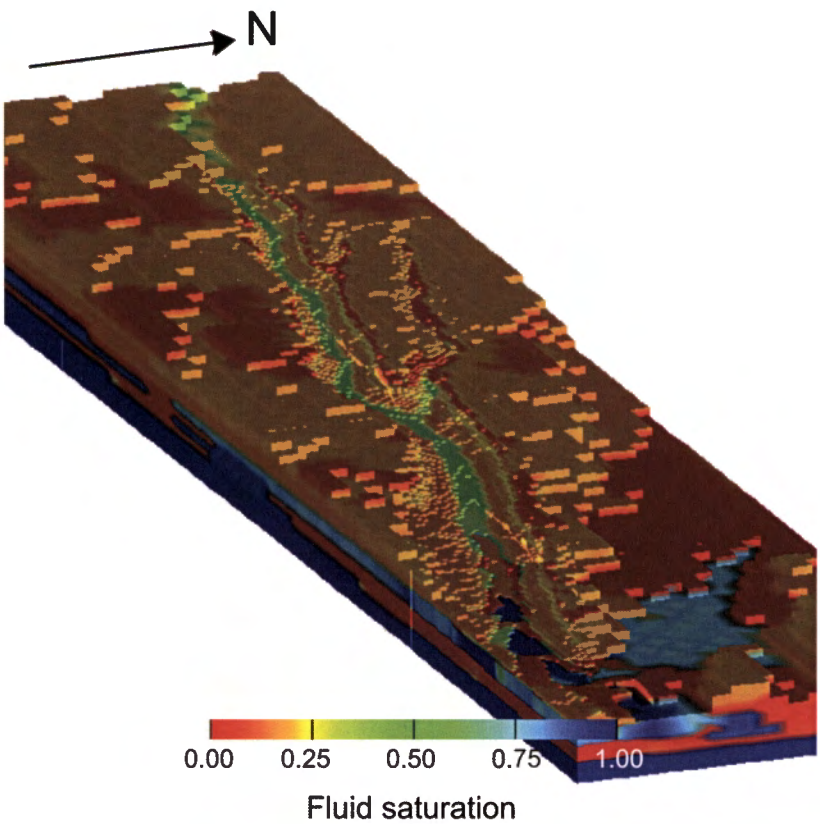


**Figure 4-C-5.** Full model three-dimensional flow results showing fluid saturation predictions through the model domain.

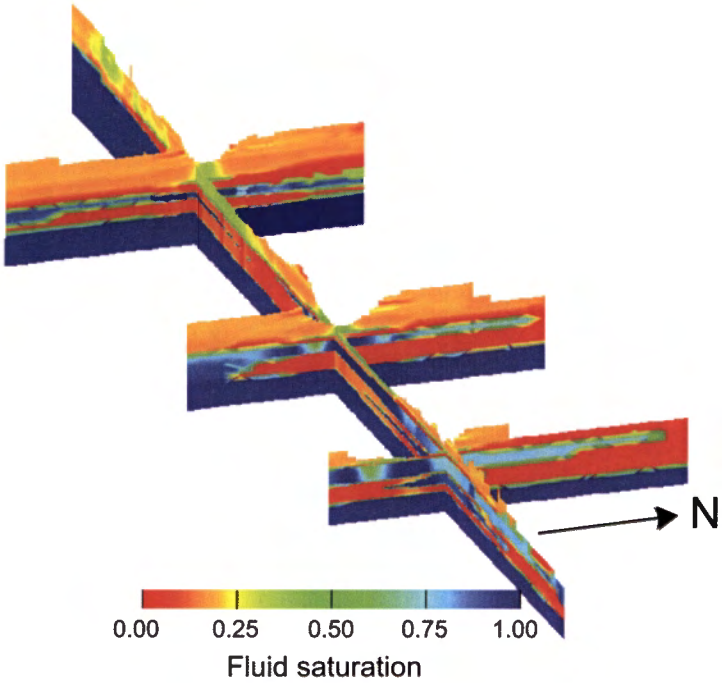


**Figure 4-C-6.** Fence diagram showing one north-south and three east-west cross-sections.

### 4-C-7.1 Moisture Comparisons to Data

We choose volumetric water content as the primary measurement used to evaluate the model results because adequate data on water content is available from virtually all vadose zone characterization wells. Robinson et al. (2005a) presents a detailed analysis of the comparisons of volumetric water contents predicted in the three-dimensional model to measured values in three wells located in Los Alamos Canyon: LADP-3, LAOI(A)-1.1, and R-9. Representative results are shown in Figures 4-C-7 and 4-C-8 for wells LADP-3 and LADP-4, respectively. The fits to the data are presented for three different levels of infiltration rates, i.e., the base-case infiltration map, a map with infiltration scaled down by a factor of three from the base map, and a map with infiltration scaled up by a factor of three. It is seen that the base infiltration map does an adequate job of jointly matching the water content profiles in these wells, despite the different stratigraphy and position relative to the canyon bottom. The good fit for LADP-4 illustrates the adequacy of the model in capturing the fluid saturations in the Tshirege Member (not present in the two-dimensional model), as well as in a region where infiltration rates are taken to be significantly lower than in Los Alamos Canyon at LADP-3. The need to apply significantly lower infiltration near LADP-4 is best understood by comparing the water content model and data for these two wells. The significantly wetter conditions in LADP-3 are simulated in the three-dimensional model through the setting of high infiltration in the canyon. It is evident from these comparisons that the model is able to capture the general features of data.

### 4-C-7.2 Sensitivity Analysis

As was discussed previously, there is significant uncertainty in the hydrologic property values and infiltration rates in the Los Alamos Canyon model. Therefore, it is important to investigate how the deviations of the parameter values from the base case affect the model predictions.

**Sensitivity to flow transients**. In model simulations presented thus far, it is assumed that the infiltration is time-independent. However, infiltration is likely to be a more transient phenomenon. Gray (1997) shows that in Los Alamos Canyon, water levels in alluvial aquifer wells fluctuate with season in response to summer storm events and spring runoff from snowmelt. It is not clear to what extent these transients are damped by the surface and alluvial aquifer flow processes. To test the potential influence on vadose zone water contents, we take a "worst-case" approach to bound the problem. In the first simulation, we test the sensitivity of the model to a very sharp impulse of water corresponding to the entire predicted infiltration of one-half year concentrated in a one-week time period. This bounding case is intended to model the case of all infiltration occurring in a single spring runoff event and a single summer storm event. Figure 4-C-9a shows the predicted water content profiles in LADP-3 in response to such an event. The influence is only felt in the uppermost ten meters or so of the vadose zone. The quantity of water input during the event, though intense, is insufficient to have a significant influence on the water content profile. These events would then be followed by a half-year of no infiltration, which would cause the profile to bounce back to nearly its original state. Therefore, the assumption of steady-state conditions over time scales of years should have no influence on the interpretation of the water content profiles in the observation wells, except possibly very close to the surface (alluvium-bedrock interface).

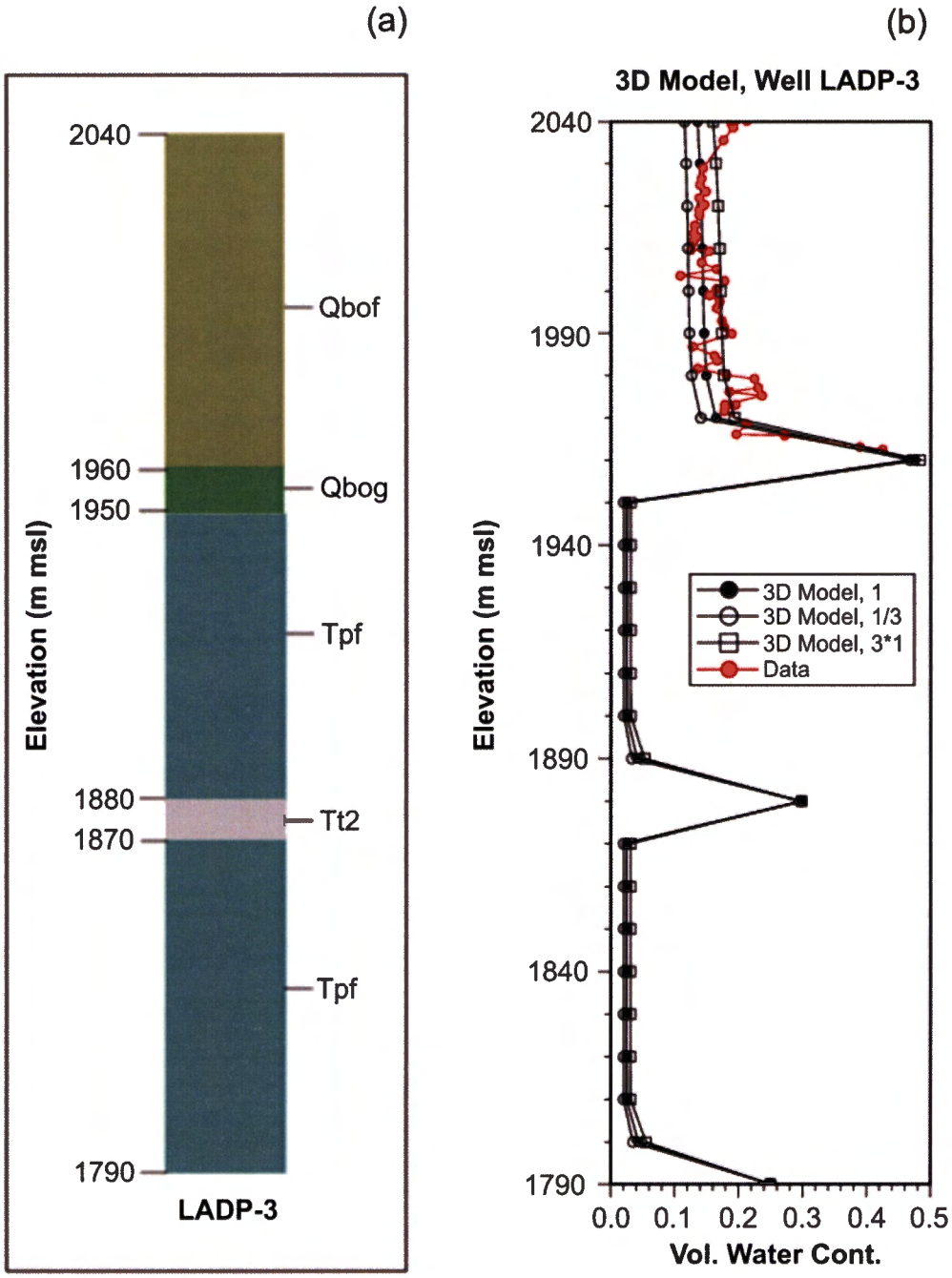


**Figure 4-C-7.** Comparison of data and three-dimensional model predictions for water contents in well LADP-3 (a. stratigraphy; b. data-model comparison).

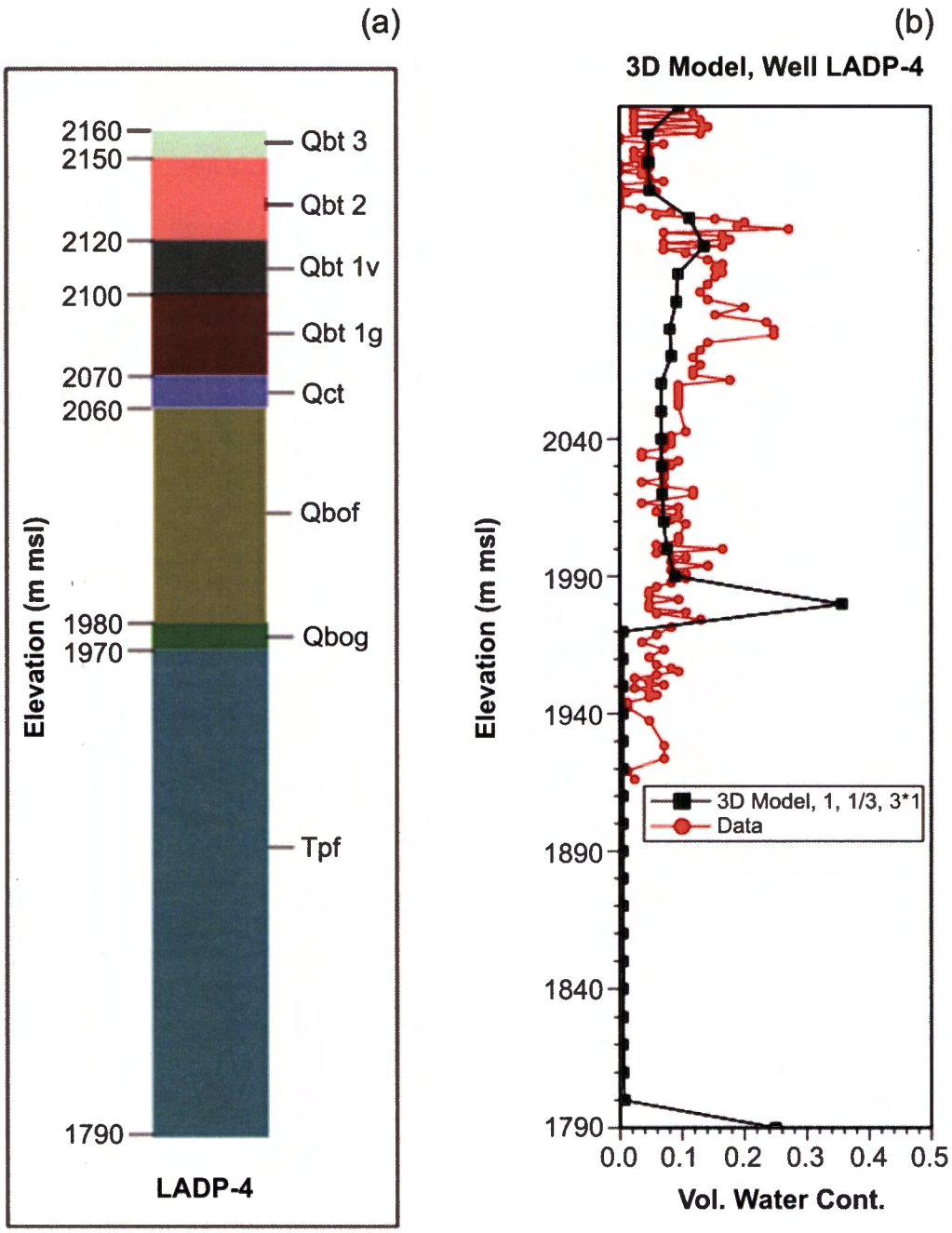


**Figure 4-C-8.** Comparison of data and three-dimensional model predictions for water contents in well LADP-4 (a. stratigraphy; b. data-model comparison).

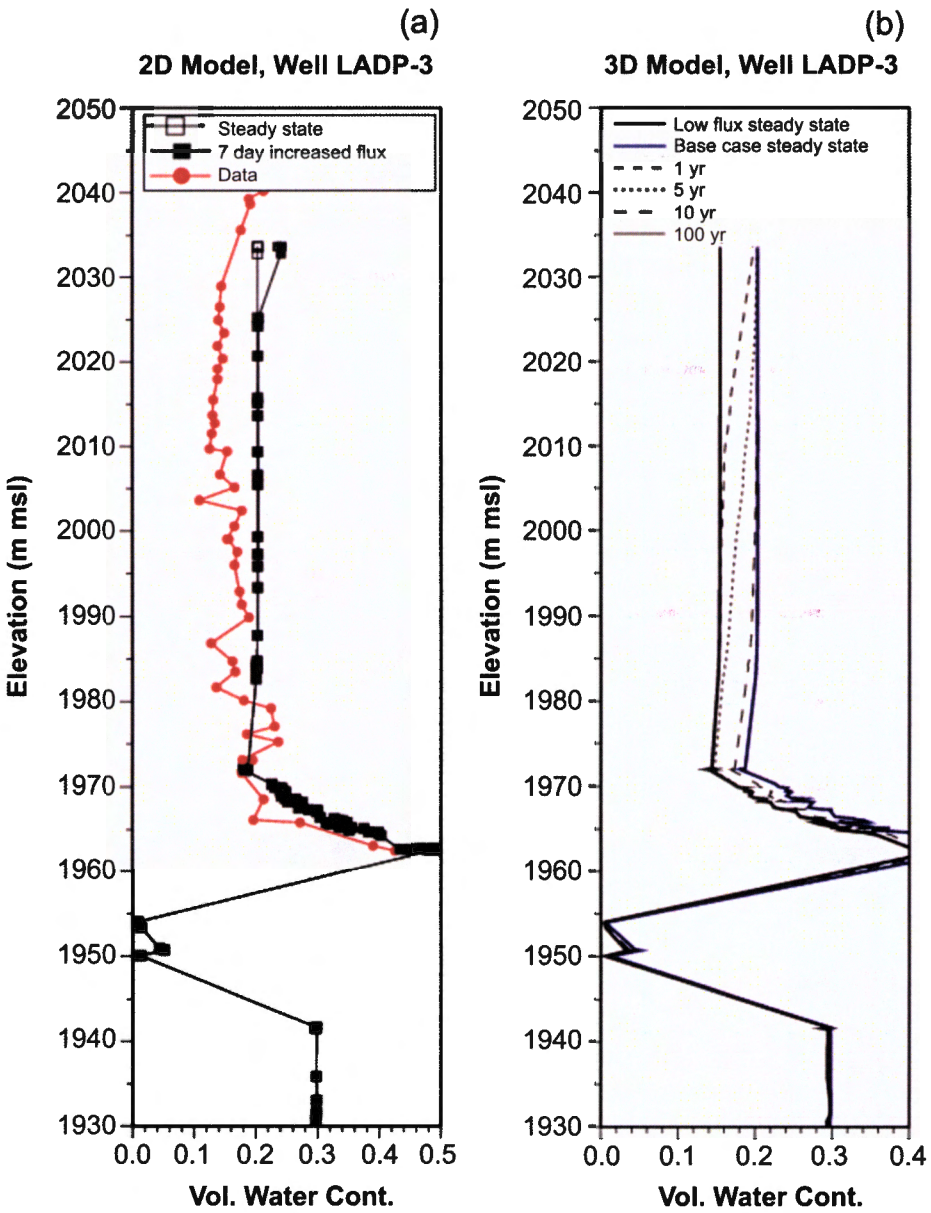


**Figure 4-C-9.** Two-dimensional model predictions for the water content in response to transient episodes of enhanced infiltration. (a) Well LADP-3, single one-week episode of enhanced infiltration. (b) Well LADP-3, prolonged period of enhanced infiltration (infiltration is increased by a factor of five starting at time 0).

Longer-term variability in the infiltration rate over years or decades could also complicate the interpretation of water content measurements, and thus need to be examined. Figure 4-C-9b shows the results of a simulation in which the infiltration steady state is used as an initial condition, and the rate is increased to the base-case infiltration map at time zero. The plot shows that over a time period of a few years, the water contents increase to significant depths. Within about a decade, the profile throughout the entire section of the Otowi Member reflects the new,

higher infiltration rate. At times of one or a few years, the transient water content profile shows curvature similar to that seen in several of the observation wells, including LADP-3. This does not necessarily mean that the curvature is caused by such a transient, but simply that reasonable variability in infiltration rates over years to decades complicates the interpretation of the water content profiles. This simulation is meant to provide a caution against over-interpretation of the details of the water content profiles. Furthermore, it is recognized from this analysis that the match of a steady-state model to the data in Los Alamos Canyon represents the fluid flow characteristics of the system within the previous ten to 100 years leading up to the collection of the water content data. In general, this result is dependent on the hydrologic conditions of the particular model area. Wet canyon systems with high infiltration rates have transient time periods of this order of magnitude, while dry mesas may take upward of thousands of years to attain a new steady-state water content profile when the infiltration rate changes.

## 4-C-8. Tritium Modeling Results

Tritium transport model results are presented to further demonstrate the validity of the model and to explore important processes occurring in the vadose zone. Figure 4-C-10 shows the three-dimensional model predictions of the tritium concentration of fluid reaching the water table in the year 1999. Significant, above-background concentrations are predicted along the canyon at locations downstream of where the Bandelier Tuff is not present in the canyon bottom. An important characteristic of the model is the preferential transport to the water table at locations downstream of the confluence of Los Alamos and DP canyons. The main reason for this result is that the thickness of Bandelier Tuff is much greater at upstream locations in the canyon, whereas in the vicinity of R-9, no Bandelier Tuff is present. Recall that the conceptual model for vadose zone flow consists of matrix flow and transport in the Bandelier Tuff, and preferential fracture flow and transport in the basalt units. Rapid transport to the water table at the downstream locations is due to fracture flow in the basalts and fairly rapid transport through the Puye Formation. Therefore, concentration levels in these locations in the canyon are predicted to be significantly greater than zero (in the thousands of pCi/l) in this portion of model domain.

The wells at which tritium concentrations in the regional aquifer can be compared are the water supply well O-4 and test well-3, both located near the confluence of Los Alamos and DP canyons, and characterization wells R-7 and R-9. Well O-4 results indicate that tritium is predicted to be mostly present in the vadose zone; however, a small but non-zero concentration is predicted to have reached the regional aquifer. Well R-7, located downstream of tritium contaminants but upstream of the Los Alamos-DP Canyon confluence, shows the slowest migration rate of tritium. By contrast, the most rapid transport to the water table is observed at R-9, where the peak concentrations of tritium are predicted to already have reached the water table. These model results are consistent with the available field data. Regional aquifer fluid collected in well R-7 has indetectable levels of tritium, whereas TW-3 and R-9 show that tritium has reached the regional aquifer. Determining more quantitatively the ability of the model to reproduce the field data is difficult because of mixing of the tritium percolating from the vadose zone with regional aquifer fluid and the subsequent mixing of contaminated and clean fluid in the wellbore itself. The latter difficulty is especially acute for the water supply wells, which may draw water from hundreds of feet of screened length.

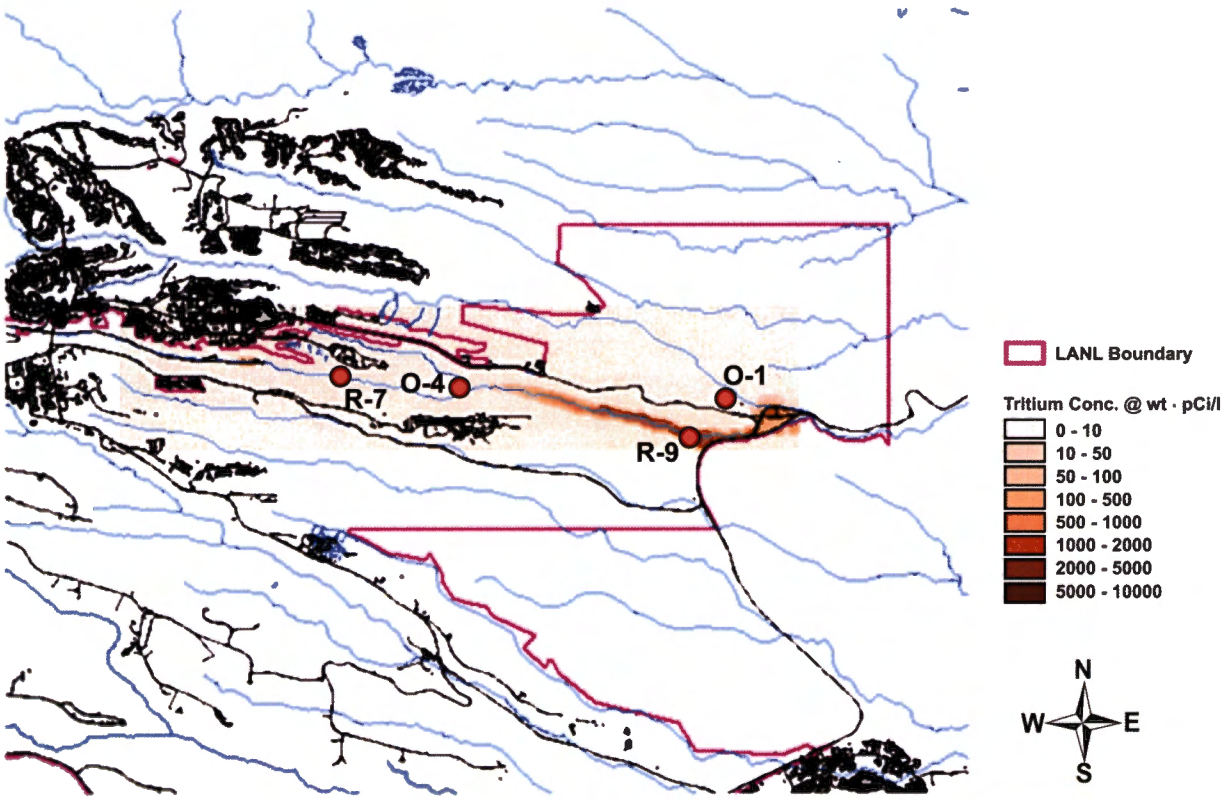


**Figure 4-C-10.** Three-dimensional model predictions of the tritium concentration of fluid reaching the water table in the year 1999. Significant, above background concentrations are predicted along the canyon at locations downstream of where the Bandelier Tuff is not present in the canyon bottom.

As a final comparison to the available data, we contrast the model results with regional aquifer water supply well O-1. However, because contaminant transport sources from Pueblo Canyon (north of Los Alamos Canyon) were not included in this model, the conclusions related to O-1 are more qualitative. For this comparison, monitoring information (LANL 2001) is used. Contaminants tritium, perchlorate, and nitrate are all thought to be nonsorbing in this system, and thus the combined results of all three contaminants are used in this interpretation. Well O-1 has been found to contain measurable levels of perchlorate at about a 5 ppb level, nitrate levels higher than at other regional aquifer wells in the area, and consistent, above-background levels of tritium in the 30-40 pCi/L range. All observations point to both Laboratory-derived contaminants and effluent discharges from Los Alamos County from past releases in Los Alamos and Pueblo Canyons having traversed the entire vadose zone. The present model explains these observations as a consequence of the hydrostratigraphy along the canyon, with rapid travel times at locations where the Bandelier Tuff is thin or non-existent.

Contrast these results with the transport model for MDA G presented in Appendix 4-B. Most important, travel times through the vadose zone are predicted to be orders of magnitude longer for this mesa site than for transport from the bottom of a wet canyon. The reason for this is straightforward. Infiltration rates, which directly impact transport velocities, are much larger in a canyon setting, in which all water in a catchment is channeled to the canyon bottom. A

significant percentage of that water will escape evapotranspiration and percolate into the deep subsurface along the canyon. In contrast, a mesa top typically provides opportunity for water to drain as surface water, evaporate, or transpire. Therefore, percolation rates are much lower,

# APPENDIX 4-D. REGIONAL AQUIFER MODEL DEVELOPMENT

## 4-D-1. Grid Information

Three-dimensional groundwater models have been developed using FEHM (Zyvoloski et al. 1997); computational grids were generated using LaGriT (Trease et al. 1996). The computational grids for both the basin- and site-scale models are shown in Figures 4-D-1 to 4-D-4; grid characteristics are summarized in Table 4-D-1. The structure of the two models are identical, except for the increased vertical resolution of the site-scale model and the smaller lateral extent.

A view of the upper surface of the basin model grid is shown in Figure 4-D-1. Constant head nodes are indicated by circles. Boundary conditions for the basin-scale model are shown in Figure 4-D-2. A view of the upper surface of the site-scale model is shown in Figure 4-D-3. Boundary conditions for the site-scale model are shown in Figure 4-D-4. Horizontal grid resolution varies from 250 m near the margins to 125 m beneath LANL. Vertical resolution varies from 12.5 m in the upper portion of the aquifer to 500 m at depth.

Each node in the computational mesh is assigned to a unit according to its location relative to the 3-D hydrostratigraphic structure defined by the geologic model. Interpolation from the hydrostratigraphic model to the grid nodes is done by defining closed volumes for each hydrostratigraphic unit. Each node of the mesh can be in one and only one of these volumes. The node properties are assigned based on which volume a node resides in. In this relatively simple approach, the location of contacts between hydrostratigraphic units can only be resolved to the degree of discretization in the finite element mesh. The resulting zonation for the basin and site-scale models are shown in Figures 4-D-5 and 4-D-6.

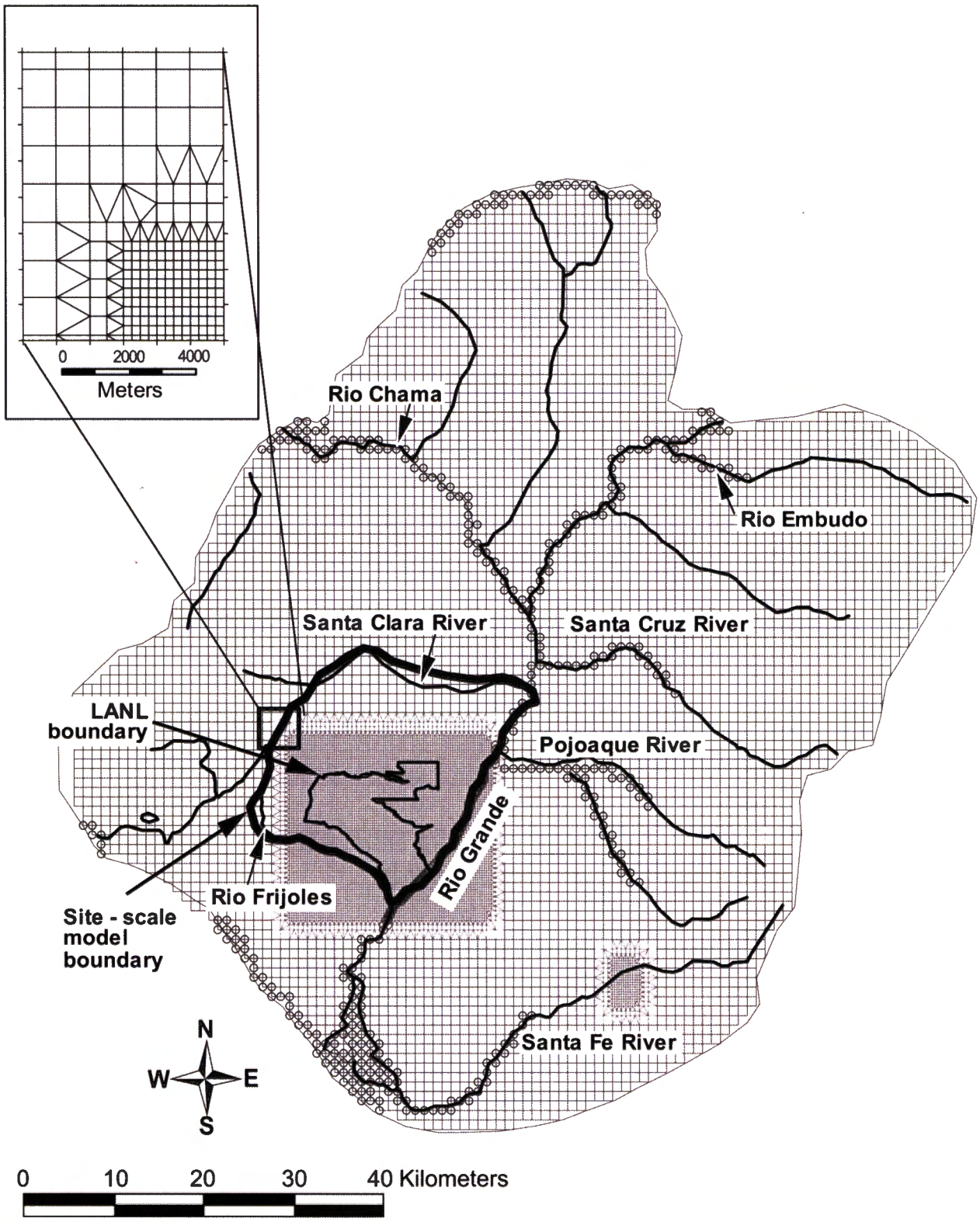


**Figure 4-D-1.** Top view of basin-scale model grid with side view (inset).

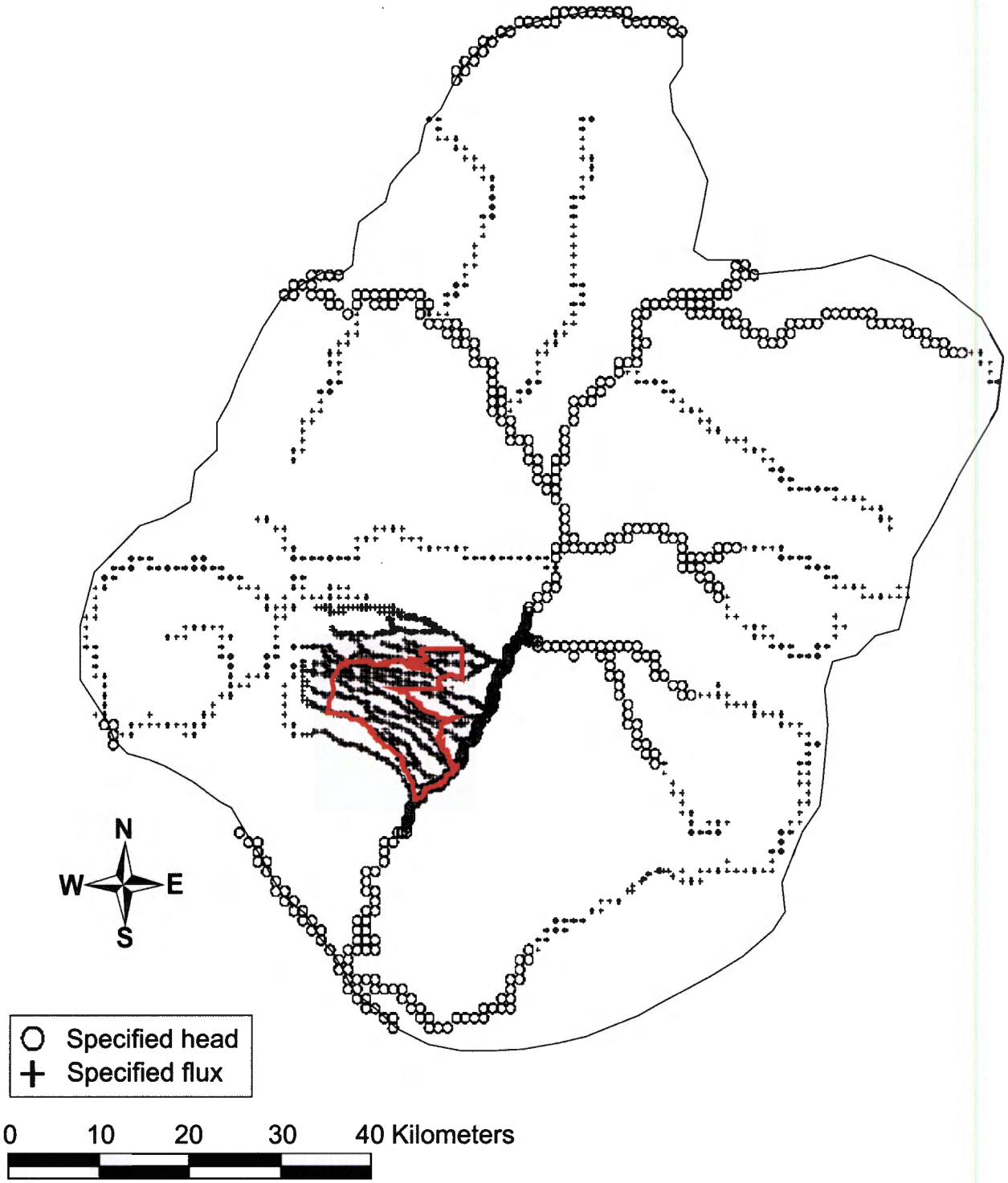


**Figure 4-D-2.** Boundary conditions along top surface of basin-scale model.

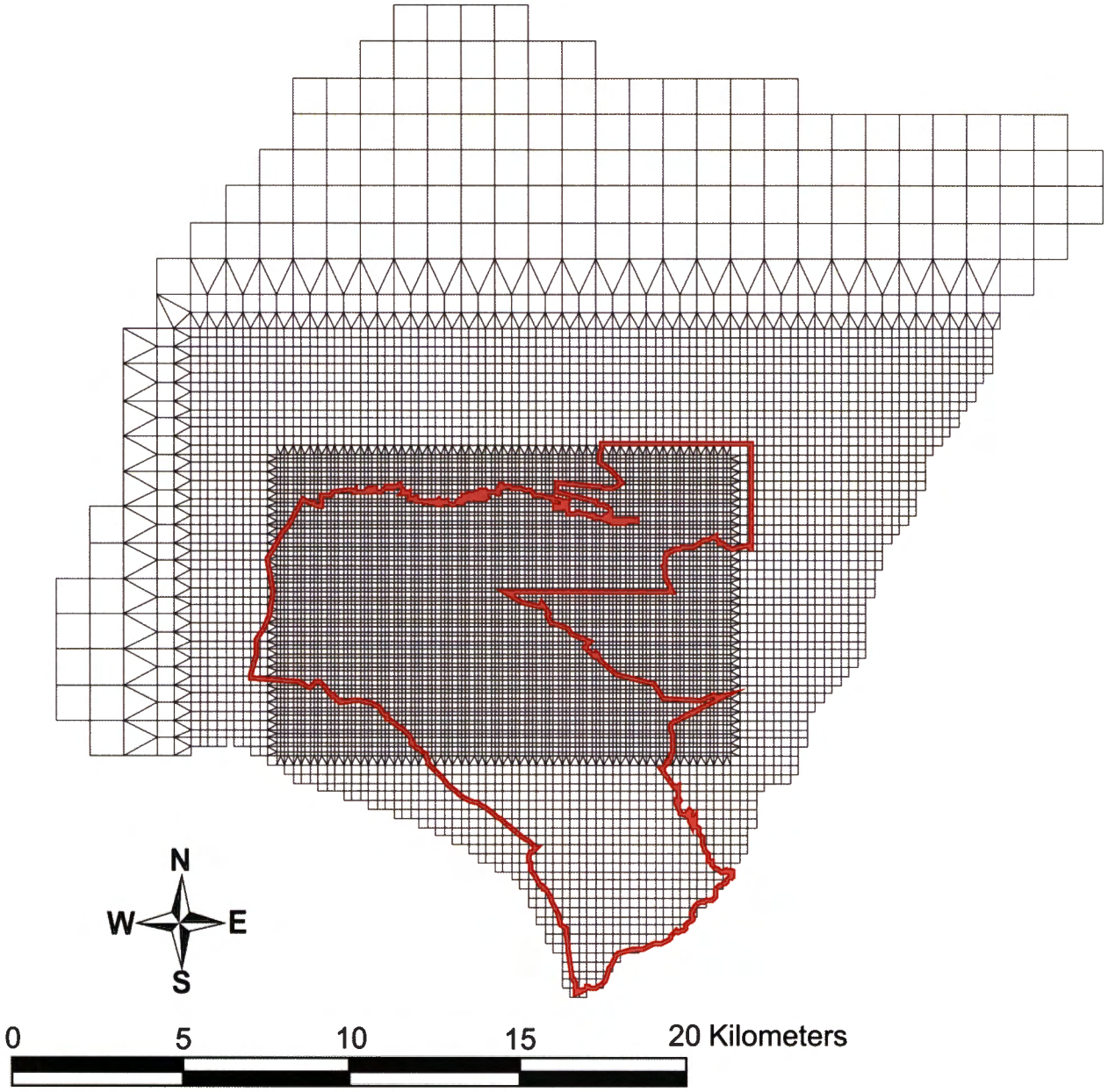


**Figure 4-D-3.** Plan view of the site-scale grid. LANL boundary shown for reference.

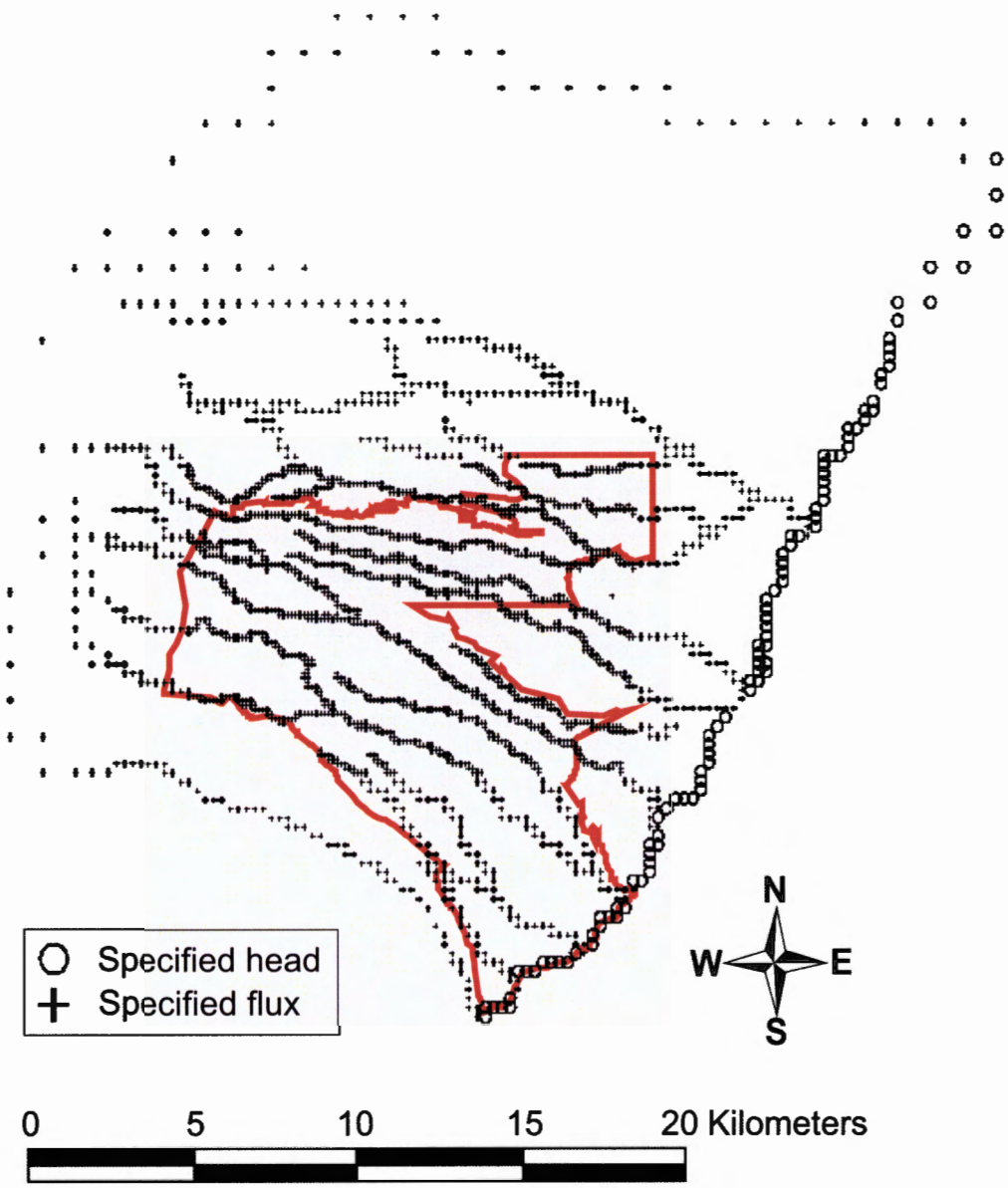


**Figure 4-D-4.** Boundary conditions along top surface of site-scale model.

**Table 4-D-1.**
**Hydrostratigraphic Units in Site-Scale Model**

| Unit | Sub-unit | Abbreviation | Volume (km³) | Fraction of Total |
|---|---|---|---|---|
| PreCambrian | | p€ | 4.50 | 0.005 |
| Paleozoic/Mesozoic | | PM | 273.53 | 0.292 |
| Santa Fe Group | Deep | Tsf-deep | 36.47 | 0.039 |
| | fanglomerate | Tsf-fang | 23.62 | 0.025 |
| | sandy | Tsf-sandy | 457.58 | 0.489 |
| Keres Group | deep | Tk (deep) | 12.59 | 0.013 |
| | shallow | Tk (shallow) | 1.15 | 0.001 |
| Basalts | | Tb1 | 6.19 | 0.007 |
| | | Tb2 | 5.61 | 0.006 |
| | | Tb4 | 2.20 | 0.002 |
| Tschicoma | | Tt | 7.09 | 0.008 |
| Puye Formation | Totavi Lentil | Tpt | 2.02 | 0.002 |
| | Pumiceous | Tpp | 1.96 | 0.002 |
| | fanglomerate | Tpf | 5.45 | 0.006 |
| Uncertain (1) | | Tb2s | 14.02 | 0.015 |
| Uncertain (2) | | Tb4f | 0.45 | 0.000 |
| Pajarito Fault zone | | | 82.04 | 0.088 |
| Total volume | | | 936.51 | 1.000 |

## 4-D-2. Recharge Model

We define groundwater recharge $R$ over the model domain as follows:

$$R(x,y) = \alpha\, \xi(x,y) \cdot P[Z(x,y)], \tag{1}$$

$$\xi(x,y) = \begin{cases} 1 & Z(x,y) > Z_{\max} \\ \frac{Z_{\max} - Z(x,y)}{Z_{\max} - Z_{\min}} & Z_{\min} < Z(x,y) < Z_{\max} \\ 0 & Z(x,y) < Z_{\min} \end{cases}, \tag{2}$$

where $P$ is precipitation, $Z$ is ground-surface elevation defined from the digital elevation model of the region, $\xi$ is a dimensionless weight function which is characterized by parameters $Z_{\min}$ and $Z_{\max}$, $\alpha$ is the fraction of precipitation that becomes recharge above $Z_{\max}$. Note that $Z_{\min}$ defines the elevation below which no recharge occurs, and above elevation $Z_{\max}$ the recharge is equal to $\alpha P$. The total recharge flux $Q$ over the model domain $\Omega$ is defined as

$$Q = \iint_{\Omega} R\,dxdy = \alpha \iint_{\Omega} \xi P\,dxdy = \alpha P'(Z_{\min}, Z_{\max}), \tag{3}$$

where $P'$ is a function of $Z_{\min}$ and $Z_{\max}$ only. We assume $P(Z)$ is a simple linear model with fixed regression parameters, which we derive using annual precipitation data for the region (Bowen, 1992; Spiegel and Baldwin 1963). Thus, there are four unknowns to be estimated ($Q$, $\alpha$, $Z_{\min}$ and $Z_{\max}$) coupled through Equation 3. For example, to calculate $Q$ we need to

estimate $\alpha$, $Z_{min}$ and $Z_{max}$. For our inverse models, we found it to be more computationally efficient to include $Q$, $Z_{min}$ and $Z_{max}$ in the estimation process, and compute $\alpha$ as

$$\alpha = \frac{Q}{P'(Z_{min}, Z_{max})}. \tag{4}$$

Precipitation ($P$) is defined as a function of elevation ($Z$), according to a regression equation derived from regional data (Spiegel and Baldwin 1963) and Pajarito Plateau data (Rogers 1994). Figure 4-D-7 shows these data; the derived regression relationship is

$$P \text{ (in/yr)} = -16.4 + (.004542) * Z \text{ (feet)}, r^2 = 0.9$$

Using a USGS DEM model for the basin, we derive a map of annual precipitation from which the recharge fluxes are derived. We apply focused recharge along the upper reaches of perennial streams in the basin; the ratio of $R_f$ (focused recharge along perennial streams) to $Q$ is an unknown parameter that can be estimated in the inverse analysis. Finally, recharge along ephemeral streams on the Pajarito Plateau is applied in linear proportion to the indices developed by Birdsell (see Nylander 2002). The ratio of this type of recharge to $Q$ is defined as $\kappa$.

Figure 4-D-8 shows an example of a recharge model derived using equations 1-4. Note that this particular example applies the highest rates of recharge in the basin to the streams flowing through LANL (>>35 mm/yr). This approach assures that the maximum possible fluxes of contaminants into the regional aquifer are captured in the models. The model parameters employed to generate this particular recharge map are

$$Q = 6400 \text{ kg/s}; Z_{min} = 2300 \text{ m}; \alpha = 12.5\%; \kappa = 0.03, \text{ and } R_f = 0.2.$$

In summary, the full set of recharge model parameters are $Q$, $Z_{min}$, $Z_{max}$, $R_f/Q$, and $\kappa$. These five parameters can be varied to provide a wide range of recharge conditions, all within the calibration constraints of head and baseflow discharge.

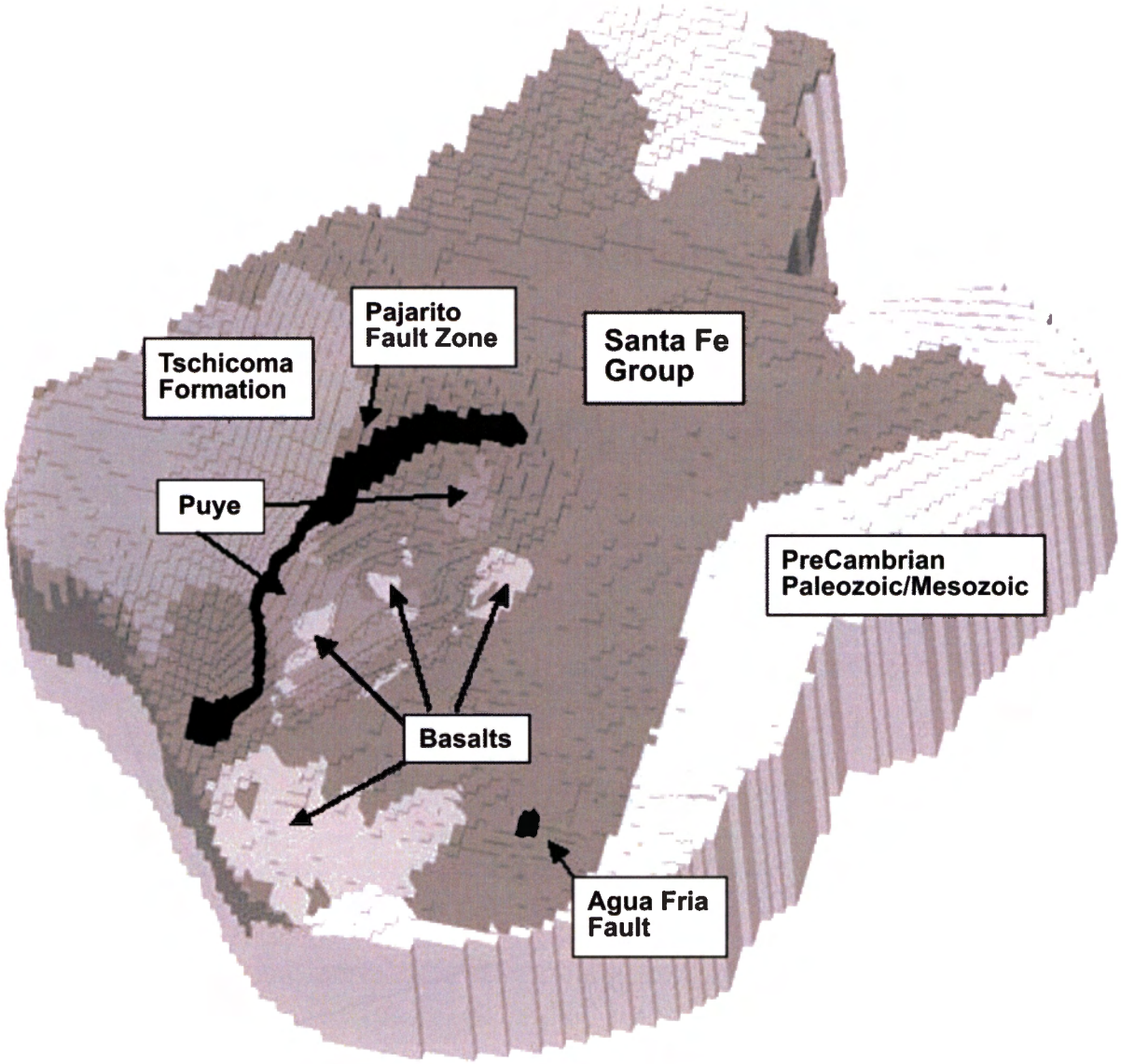


**Figure 4-D-5.** Three-dimensional representation of the major hydrostratigraphic units in the basin-scale model.

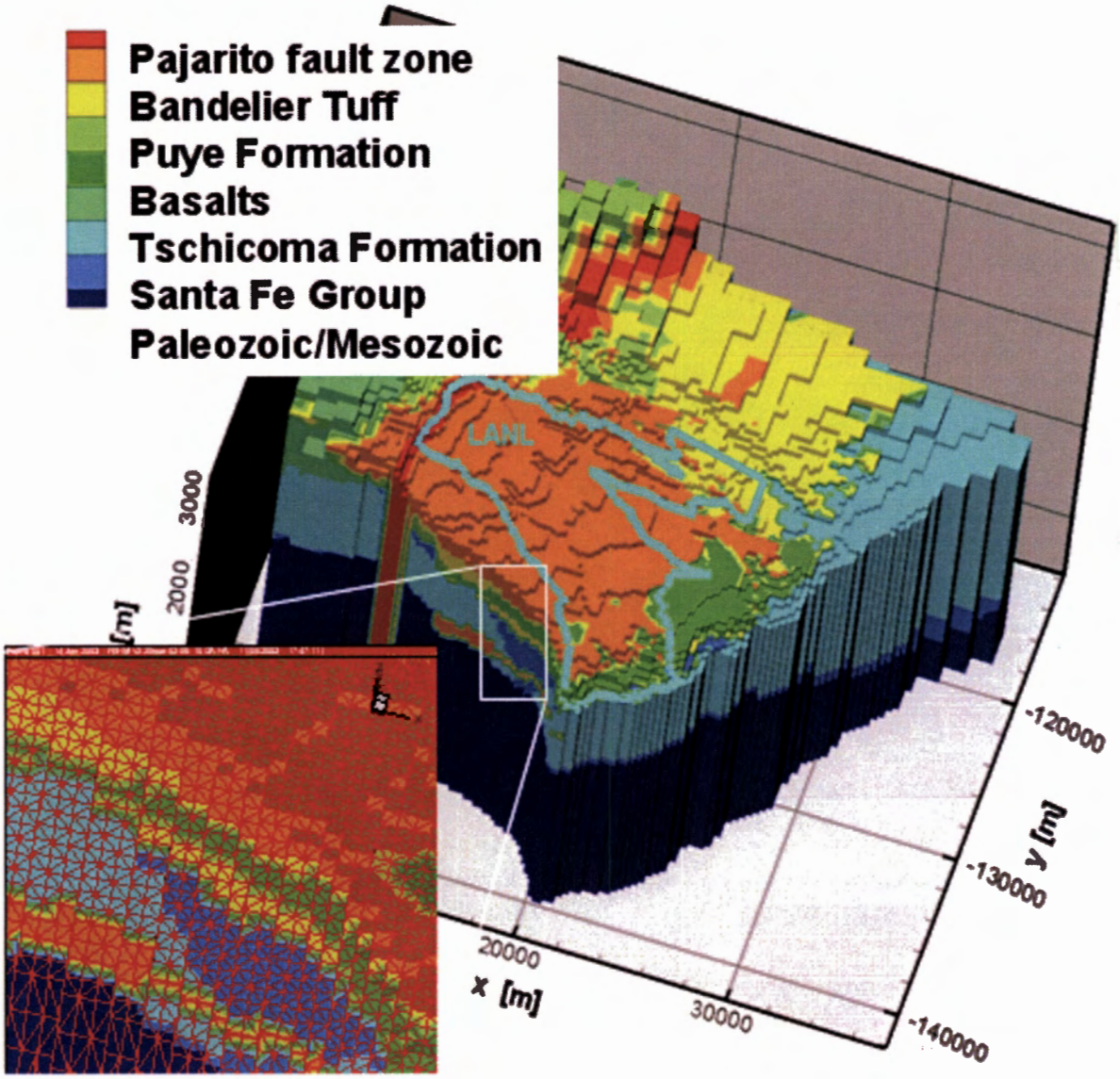


**Figure 4-D-6.** Site-scale model grid, colored according to major hydrostratigraphic units.

## 4-D-3. Flux Estimates.

Table 4-D-2 compares flux estimates from previous models developed for the Española Basin.

**Table 4-D-2.**
**Flux Estimates Derived from Previous Models, in AFY**

| | | cfs/.0014 | 0.0014 | |
|---|---|---|---|---|
| **INFLOW** | | McAda | Frenzel | Hearne |
| | Total Area (km$^2$) | | | |
| | Areal Recharge (cfs) | 7571 | 3429 | 0 |
| **Lateral Boundaries** | | | | |
| Inflow (cfs) rom: | east | 21571 | 14929 | 2693 |
| | west | 7429 | 7214 | 8100 |
| | north | 1429 | 1357 | 971 |
| | south | 1571 | 500 | |
| **Rivers** | | | | |
| Inflow (cfs) rom: | SF River | 5357 | 5357 | 5150 |
| | Poj. River | 0 | 929 | 1261 |
| | RG | 1357 | 0 | 0 |
| | Cochiti | 0 | 0 | 0 |
| | Tesuque | 3071 | 2714 | 1772 |
| | Rio En Medio/Nambe | 2857 | 3000 | 1714 |
| | Arroyo Hondo | 500 | 500 | 0 |
| | Santa Cruz | 0 | 0 | 2936 |
| | Head dependent rivers | 0 | 929 | 0 |
| **TOTAL INFLOW** | | 52714 | 40857 | 24597 |
| | | | | |
| **OUTFLOW** | | | | |
| **Lateral Boundaries** | | | | |
| Outflow[1] (cfs) to: | east | 0 | 0 | 0 |
| | west | 12429 | 8643 | 0 |
| | north | 2143 | 2714 | 243 |
| | south | 214 | 1643 | 0 |
| | | | | |
| **Rivers** | | 0 | 0 | 0 |
| Outflow (cfs) to: | Santa Fe River | 4643 | 0 | 3107 |
| | Pojoaque River | 5214 | | 2766 |
| | Rio Grande | 28071 | 0 | 11293 |
| | Cochiti | 0 | 0 | 4464 |
| | La Cienega | 0 | 4643 | 0 |
| | Tesuque | 0 | 0 | 243 |
| | Rio En Medio/Nambe | 0 | 0 | 0 |
| | Arroyo Hondo | 0 | 0 | 0 |
| | Santa Cruz | 0 | 0 | 1071 |
| | Head dependent rivers | 0 | 23357 | 0 |
| **TOTAL OUTFLOW** | | 52714 | 41000 | 23187 |

[1] Outflow to "west" is outflow to the Albuquerque Basin. For comparison, subsurface inflow to the Albuquerque Basin from the north (including the Española Basin and Jemez Mountains) was estimated to be 19,400 afy (Kernodle et al. 1995), 28,500 afy (McAda and Barroll, 2002), and 2772 afy (Sanford et al. 2004).

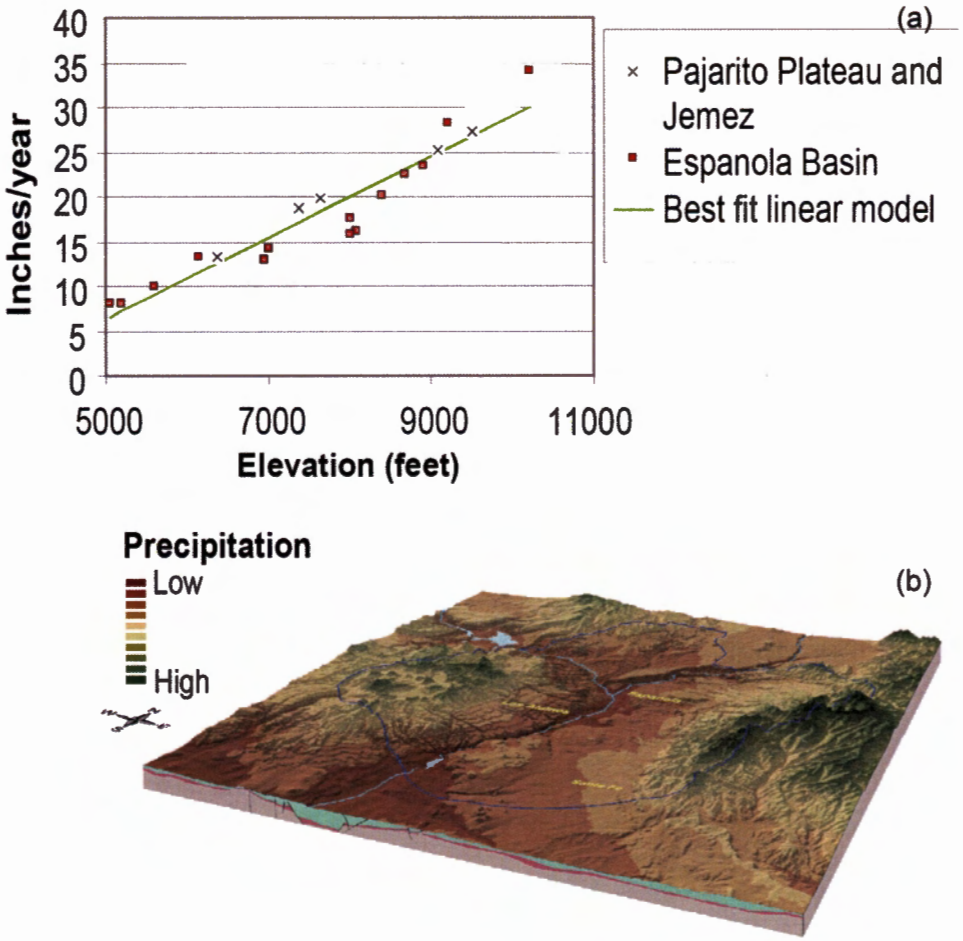


**Figure 4-D-7.** (a) Average annual precipitation in the vicinity of the Española Basin. (b) Regression equation for precipitation applied using USGS DEM.

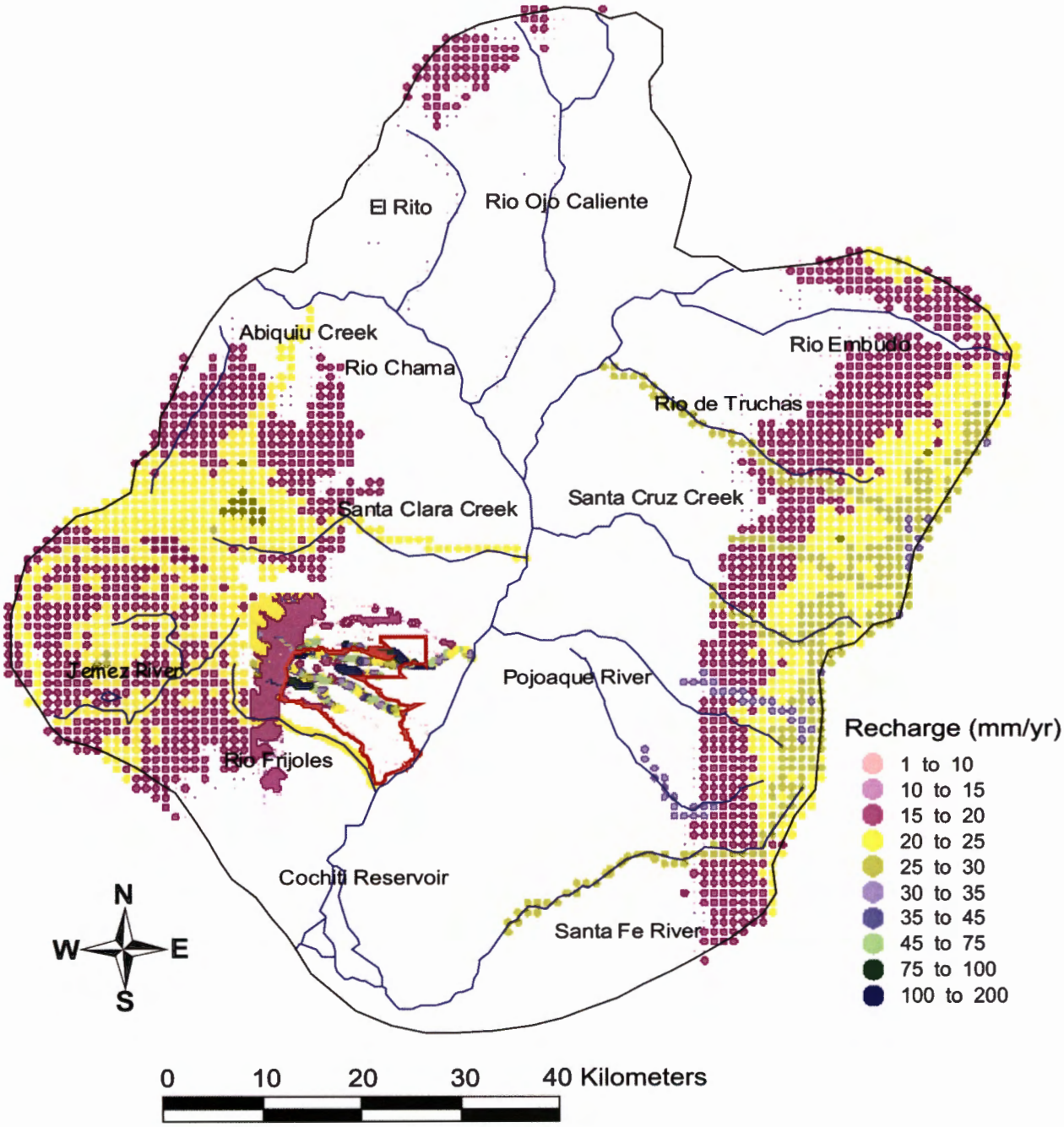


**Figure 4-D-8.** Average annual precipitation verses elevation derived from data of Spiegel and Baldwin (1963) and Rogers (1994).

## APPENDIX 4-E. ESTIMATING AQUIFER DISCHARGE USING STREAMFLOW DATA

The method we use for estimating base flow gain along the Rio Grande is a very simple one, also used by Spiegel and Baldwin (1963), the U.S. Department of Justice (1996), and others. The strategy is to difference measured surface water flow at two gages during January, when other causes of streamflow loss/gain such as evapotranspiration and irrigation withdrawals are likely to be minimal. Because the calculated baseflow gain is generally small compared to total flow in the Rio Grande, small measurement errors in flow at the gages could have large influence on these calculations. The approach applied here assumes that measurement errors are random; therefore, their impact can be minimized by repeating the calculations over a number of years and deriving a long-term mean. Uncertainty in the mean estimate will be an indication of measurement error. Unless the record is much longer than significant temporal trends, temporal trends cannot be ascertained with this method.

We apply this approach to two reaches of the Rio Grande: (1) San Juan Pueblo (828110) to Otowi (8313000) and (2) Otowi (8313000) to Cochiti (8314500). Collectively, these two reaches span the entire length of the Rio Grande that comprises the eastern extent of the Pajarito Plateau, from Santa Clara Creek to Rio Frijoles.

**(1) San Juan Pueblo (828110) to Otowi (8313000).** A major tributary to the Rio Grande, the Rio Chama, enters this reach just downstream from the gage 8290000 (Rio Chama at Chamita). There was a 23-year period during which all three of these gages were operational (1963 to 1985). By comparing this period of record to a much longer period of record at the Otowi gage (1890–2004), it can be seen that flows were normal during the 1963–1985 period, except two unusually high flow years (1973 and 1975). The January flow at Otowi was highly correlated to, and slightly more than, the sum of flows at San Juan Pueblo and Rio Chama at Chamita, suggesting a consistent base flow gain component along this reach. Three minor tributaries, the Santa Cruz River, the Pojoaque River, and the Santa Clara River, contribute to gain along this reach. Insufficient data during the 1963 to 1985 prevents using measured flows for these years; instead, we use a long-term average from other years, shown in Table 4-E-1.

For each of the 23 year period from 1963 to 1985, we calculated base flow gain during January by the following relationship:

Base flow gain = measured flow (RG Otowi – RG San Juan – Rio Chama, Chamita) – long-term average measured flow (Pojoaque + Santa Clara + Santa Cruz).

The 23-average base flow gain calculated using this approach is 41.2 cfs.( +/- 12.8 at the 95% confidence interval). There is a strong trend evident for gain to be higher in years of higher flow; it is unclear whether this trend is real or is related to sources of error such as small ungaged tributaries which may only be significant at high flow. The adequacy of the derived long-term estimate is shown in Figure 4-E-1a.

**(2) Otowi (8313000) to Cochiti (8314500).** These two gages have both been operational since 1926, well before pumping began at the Buckman wellfield below Otowi. January flow at the

two stations is highly correlated ($r^2$=0.96). For most years the data suggest that the reach is gaining; for some years the data suggest a losing reach. One tributary enters the Rio along this reach, Rio Frijoles, which was gaged from 1983 to 1996. We estimate the average January flow at the Rio Frijoles to be 1.2 cfs. Accounting for the inflow from the Rio Frijoles, the gain between these reaches is 13.0 cfs +/- 8.8. The sum of the flow at Otowi and Rio Frijoles and this base flow estimate, compared to the flow at Cochiti, is shown as a yellow line in Figure 4-E-1b.

## Table 4-E-1.
## Comparison of Gain/Loss Calculations to Other Studies

| Reach | Source | Method | Reach Length (km) | Total Gain ($m^3/s$) | Gain/mi ($m^3/s/km$) |
|---|---|---|---|---|---|
| Rio Grande (Otowi to Cochiti) | This report (Table 2-3) | Streamflow analysis | 41.8 | 0.39 | 0.009 |
| | U.S. Department of Justice (1996) | Streamflow analysis | 41.8 | 0.40 | 0.009 |
| | Hearne (1985) | Numerical model | 38.6 | 0.46 | 0.012 |
| | McAda (1988) | Numerical model | 27.4 | 0.63 | 0.023 |
| | Purtymun (1966) | Seepage runs | 18.5 | 0.43 | 0.023 |
| | Griggs (1964) | Seepage runs | 18.5 | 0.37 | 0.020 |
| | Spiegel & Baldwin (1963)[1] | Streamflow analysis | 32.2 | 0.71 | 0.022 |
| Rio Grande (Embudo to Otowi) | This report (Table 2-3) | Streamflow analysis | 51.0 | 0.67 | 0.013 |
| | U.S. Department of Justice (1996) | Streamflow analysis | 51.0 | 1.50 | 0.029 |
| Rio Grande (Española to Otowi) | Hearne (1985) | Numerical model | 33.8 | 0.20 | 0.006 |
| | McAda (1988) | Numerical model | 17.7 | 0.43 | 0.024 |
| | USGS seepage runs | Seepage runs | 27.4 | 0.15 | 0.005 |
| Rio Chama (Abiquiu to Chamita) | This report (Table 2-3) | Streamflow analysis | 39.9 | 1.00 | 0.025 |
| | This report (Table 2-2) | Area relation | 39.9 | 1.19 | 0.030 |
| | Hearne (1985)(lower reach only) | Numerical model | | 0.06 | |
| Santa Cruz River | Hearne (1985) | Numerical model | | 0.04 | |
| | This report (Table 2-2) | Area relation | | 0.33 | |
| | This report (Table 2-3) | Streamflow analysis | | 0.14 | |
| Pojoaque River | Reiland & Koopman (1975) | Streamflow analysis | | 0.40 | |
| | McAda (1988) | Numerical model | | 0.21 | |
| | This report (Table 2-2) | Area relation | | 0.27 | |
| | Hearne (1985) | Numerical model | | 0.09 | |
| Santa Clara River | This report (Table 2-3) | Streamflow analysis | | 0.09 | |
| | This report (Table 2-2) | Area relation | | 0.05 | |
| Santa Fe River | This report (Table 2-3) | Streamflow analysis | | 0.23 | |
| | McAda (1988) | Numerical model | | 0.18 | |
| | this report (Table 2-2) | Area relation | | 0.32 | |
| | Hearne (1985) | Numerical model | | 0.12 | |
| Rio Embudo | This report (Table 2-3) | Streamflow analysis | | 0.58 | |
| | This report (Table 2-2) | Area relation | | 0.30 | |

[1] Their approach includes only those years when the reach was deemed "gaining." ("Losing" years were assumed to be caused by erroneous data and were deleted from the analysis.)

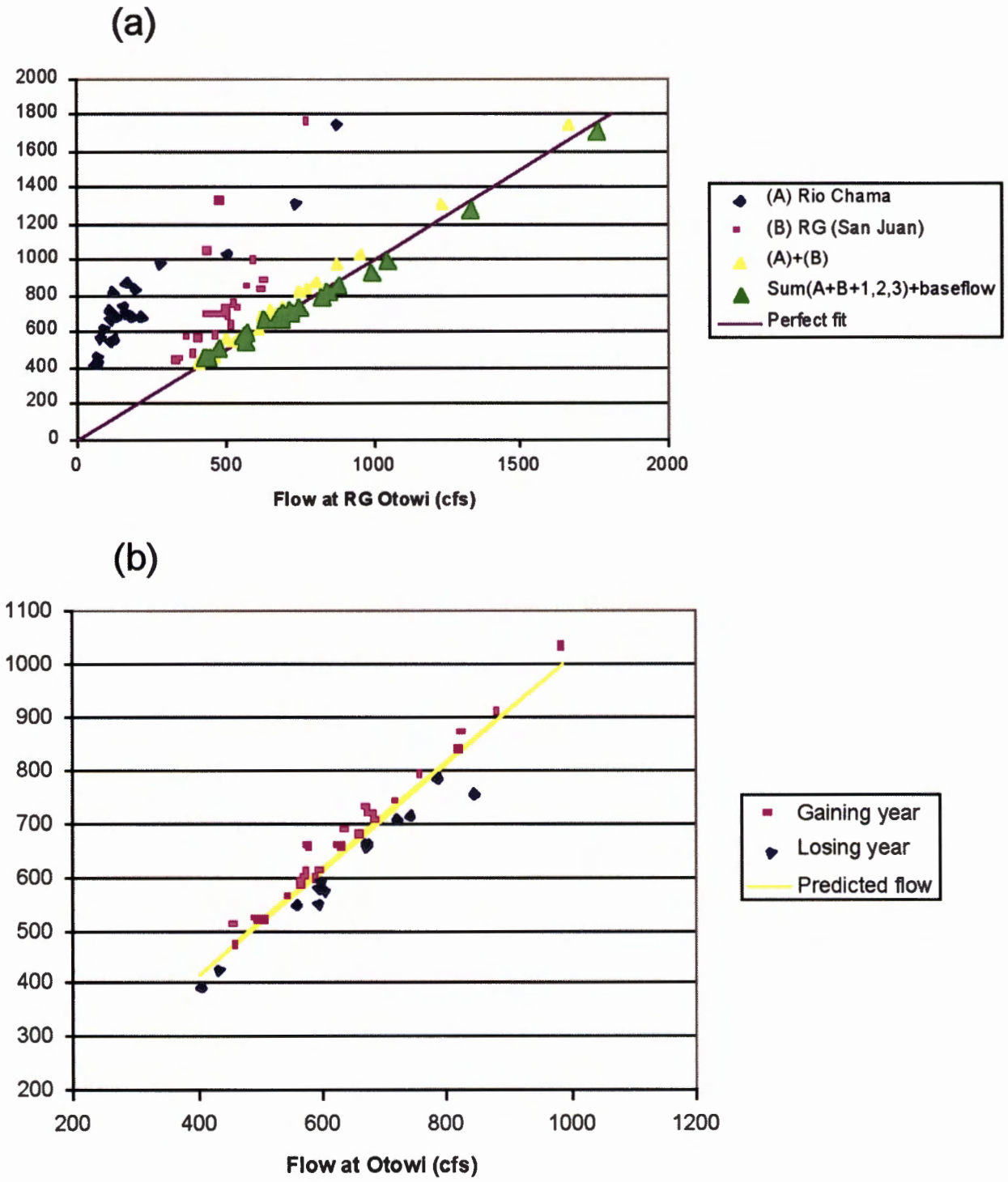


**Figure 4-E-1.** Measured January flow at the Otowi gage, compared to (a) contributing flow at Rio Chama, Rio Grande at San Juan, minor tributaries, and estimated base flow, and (b) measured January flow at the Cochiti gage.

To extrapolate these estimates to a slightly different reach of the Rio Grande, from Santa Clara Creek to Rio Frijoles, we calculate the ratios of stream lengths within each of the estimated reaches above. Santa Clara to the Otowi Bridge gage is approximately 6/10 the distance of RG San Juan to Otowi Bridge; we estimate 24.7 +/- 7.7 cfs gain along this reach. Otowi to Rio Frijoles is approximately $^1/_2$ the distance of Otowi to the Cochiti gage; for this reach we estimate 6.5 cfs +/- 4.4. In total, our baseflow estimate for the Santa Clara to Rio Frijoles reach of the Rio Grande is 31.2 cfs +/- 12.1 or 884 kg/s +/- 343.

**Errors**. Sources of errors in the method include systematic errors in streamflow measurements which do not affect all of the streamflow gages used in the differencing equations and which are persistent for the entire period of overlapping record, systematic departures of tributary flows (Pojoaque + Santa Clara + Santa Cruz) from the long-term averages shown in Table 4-E-2 and and unmeasured surface water inflows/outflows. Water budget components are estimated for watersheds in the Española Basin and are shown in Table 4-E-3.

**Table 4-E-2.**
**Estimates of Long-Term Average Flow at Small Tributaries**

| Gage | | | Data Source | # of Years of Record | Period | Mean January Flow (cfs) |
|---|---|---|---|---|---|---|
| 1 | Pojoaque River, at mouth | Site 6 | Reiland and Koopman (1975) | 38 | 1935–1972 | 4.9 |
| 2 | Santa Clara Creek | 8292000 | USGS | 17 | 1936–1994 | 3.3 |
| 3 | Santa Cruz River | 8291500 | USGS | 10 | 1941–1950 | 5.9 |
| 4 | Rio Frijoles | 8313350 | USGS | 14 | 1983–1996 | 1.2 |

## Table 4-E-3.
## Water Budget Components Estimated for Watersheds within the Española Basin, Expressed as Fraction of Total Precipitation

| | Watershed Area (square miles) | Area-Weighted Average Elevation[a] (feet) | Precipitation[b] (acre-ft/yr) | ET[c] | Runoff | Recharge | Sublimation | Recharge | Source |
|---|---|---|---|---|---|---|---|---|---|
| | | | | Fraction of total precipitation | | | | Inches/yr | |
| **Santa Fe River** | 28.7 | 8989 | 36706 | 0.69 | 0.19 | 0.11 | 0.01 | 2.71 | Wasiolek (1995) |
| **Santa Fe River** | 26.95 | 8989 | 30060 | 0.71<br>0.73[d] | 0.19 | 0.10<br>0.08[d] | --- | 2.02<br>1.61[d] | Anderholm (1994, Table 7) |
| **Little Tesuque Creek** | 7.7 | 8786 | 9370 | 0.72 | 0.09 | 0.19 | 0.00 | 4.41 | Wasiolek (1995) |
| **Little Tesuque Creek** | 7.34 | 8786 | 8,573 | 0.88 | 0.05 | 0.07 | --- | 1.61 | Anderholm (1994, Table 7) |
| **Rio Nambe** | 34.2 | 9325 | 48826 | 0.62 | 0.19 | 0.11 | 0.08 | 3.03 | Wasiolek (1995) |
| **Tesuque Creek** | 11.2 | 9197 | 15288 | 0.65 | 0.20 | 0.10 | 0.05 | 2.45 | Wasiolek (1995) |
| **Tesuque Creek** | 11.84 | 9197 | 13120 | 0.75 | 0.18 | 0.07 | --- | 1.50 | Anderholm (1994, Table 7) |
| **Combined Little Tesuque and Tesuque Creeks** | 19.18 | 9030 | 21693 | 0.89<br>0.93[d] | 0.04 | 0.07<br>0.03[d] | --- | 1.54<br>0.67[d] | Anderhom (1994, Table 7) |
| **Rio en Medio** | 8.7 | 9242 | 11973 | 0.64 | 0.15 | 0.14 | 0.07 | 3.73 | Wasiolek (1995) |
| **Arroyo Hondo** | 8.38 | ? | 8560 | 0.84 | 0.06 | 0.10 | --- | 1.86 | Anderholm (1994, Table 7) |
| **LA Canyon '93** | ? | 8428 | 13694 | 0.71 | 0.03 | 0.26 | 0.00 | 6.52 | Gray (1997) |
| **LA Canyon '94** | ? | 8428 | 12409 | 0.83 | 0.00 | 0.17 | 0.00 | 4.01 | Gray (1997) |
| **LA Canyon '95** | ? | 8428 | 15912 | 0.73 | 0.02 | 0.25 | 0.00 | 7.33 | Gray (1997) |

[a] Average basin elevation was calculated by the authors for drainage basins as defined by Wasiolek (1995). No adjustments were made to the average drainage basin elevations to account for the small differences in drainage basin areas between the Anderholm (1994) and Wasiolek (1995) studies.
[b] Precipitation volumes reported by Wasiolek (1995) for winter and spring had already been adjusted to reflect the effects of sublimation of snow. The precipitation volume estimated to exist before before sublimation was determined using information provided by Wasiolek (1995, p. 18). Calculated fractions for evapotranspiration, runoff, recharge, and sublimation reported here for the Wasiolek study are relative to this pre-sublimation precipitation value.
[c] The authors estimated the evapotranspiration (ET) for Anderholm's study based on Anderholm's estimates for precipition (P), runoff (RO), and recharge (R):
$ET = P - RO - R$
[d] These estimates used the chloride-based recharge estimate corrected for runoff from the basin.